frontiers | Research Topics

Genetics and epigenetics of chronic kidney disease

Edited by
Jia Rao, Duan Ma, Aihua Zhang, Julia Hoefele and Andrew Mallett

Published in
Frontiers in Medicine

ISSN 1664-8714
ISBN 978-2-83251-766-6
DOI 10.3389/978-2-83251-766-6

About Frontiers

Frontiers is more than just an open access publisher of scholarly articles: it is a pioneering approach to the world of academia, radically improving the way scholarly research is managed. The grand vision of Frontiers is a world where all people have an equal opportunity to seek, share and generate knowledge. Frontiers provides immediate and permanent online open access to all its publications, but this alone is not enough to realize our grand goals.

Frontiers journal series

The Frontiers journal series is a multi-tier and interdisciplinary set of open-access, online journals, promising a paradigm shift from the current review, selection and dissemination processes in academic publishing. All Frontiers journals are driven by researchers for researchers; therefore, they constitute a service to the scholarly community. At the same time, the *Frontiers journal series* operates on a revolutionary invention, the tiered publishing system, initially addressing specific communities of scholars, and gradually climbing up to broader public understanding, thus serving the interests of the lay society, too.

Dedication to quality

Each Frontiers article is a landmark of the highest quality, thanks to genuinely collaborative interactions between authors and review editors, who include some of the world's best academicians. Research must be certified by peers before entering a stream of knowledge that may eventually reach the public - and shape society; therefore, Frontiers only applies the most rigorous and unbiased reviews. Frontiers revolutionizes research publishing by freely delivering the most outstanding research, evaluated with no bias from both the academic and social point of view. By applying the most advanced information technologies, Frontiers is catapulting scholarly publishing into a new generation.

What are Frontiers Research Topics?

Frontiers Research Topics are very popular trademarks of the *Frontiers journals series*: they are collections of at least ten articles, all centered on a particular subject. With their unique mix of varied contributions from Original Research to Review Articles, Frontiers Research Topics unify the most influential researchers, the latest key findings and historical advances in a hot research area.

Find out more on how to host your own Frontiers Research Topic or contribute to one as an author by contacting the Frontiers editorial office: frontiersin.org/about/contact

Genetics and epigenetics of chronic kidney disease

Topic editors

Jia Rao — Fudan University, China
Duan Ma — Fudan University, China
Aihua Zhang — Nanjing Children's Hospital, China
Julia Hoefele — Technical University of Munich, Germany
Andrew Mallett — Townsville University Hospital, Australia

Citation

Rao, J., Ma, D., Zhang, A., Hoefele, J., Mallett, A., eds. (2023). *Genetics and epigenetics of chronic kidney disease*. Lausanne: Frontiers Media SA.
doi: 10.3389/978-2-83251-766-6

Table of contents

frontiers | Frontiers in Medicine

TYPE Editorial
PUBLISHED 13 February 2023
DOI 10.3389/fmed.2023.1078300

OPEN ACCESS

EDITED BY
Giuseppe Coppolino,
University Magna Graecia of Catanzaro, Italy

REVIEWED BY
Gema Ariceta,
Vall d'Hebron University Hospital, Spain
Hee Gyung Kang,
Seoul National University, Republic of Korea

*CORRESPONDENCE
Julia Hoefele
✉ julia.hoefele@tum.de
Jia Rao
✉ jiarao@fudan.edu.cn
Andrew J. Mallett
✉ andrew.mallett@health.qld.gov.au

SPECIALTY SECTION
This article was submitted to Nephrology, a section of the journal Frontiers in Medicine

RECEIVED 24 October 2022
ACCEPTED 27 January 2023
PUBLISHED 13 February 2023

CITATION
Hoefele J, Rao J and Mallett AJ (2023) Editorial: Genetics and epigenetics of chronic kidney disease. *Front. Med.* 10:1078300. doi: 10.3389/fmed.2023.1078300

Editorial: Genetics and epigenetics of chronic kidney disease

Julia Hoefele[1]*, Jia Rao[2,3,4]* and Andrew J. Mallett[5,6,7,8]*

[1]Institute of Human Genetics, Klinikum Rechts der Isar, School of Medicine, Technical University of Munich, Munich, Germany, [2]Department of Nephrology, Children's Hospital of Fudan University, National Children's Medical Center, Shanghai, China, [3]Shanghai Kidney Development and Pediatric Kidney Disease Research Center, Shanghai, China, [4]Shanghai Key Laboratory of Birth Defect, Children's Hospital of Fudan University, Shanghai, China, [5]Faculty of Medicine, University of Queensland, Brisbane, QLD, Australia, [6]Institute for Molecular Bioscience, University of Queensland, Brisbane, QLD, Australia, [7]College of Medicine and Dentistry, James Cook University, Townsville, QLD, Australia, [8]Department of Renal Medicine, Townsville University Hospital, Townsville, QLD, Australia

KEYWORDS

kidney genetics, epigenetics, nephrogenetics, genomics, chronic kidney disease

Editorial on the Research Topic
Genetics and epigenetics of chronic kidney disease

Diagnostics, therapy, and care for individuals affected by chronic kidney disease (CKD) are continuing to be better characterized, with increasing recognition of the resultant high health and economic burden worldwide due to CKD. Genetic contributors to CKD are also being better recognized and considered among both adults and children affected by CKD, with more than 500 different genes thus far identified to be associated with CKD. This Research Topic provides a concise overview of the current knowledge and outlook on future developments in diverse hereditary kidney diseases leading to CKD. The focus of this Research Topic is hereditary nephropathies including glomerulopathies (e.g., Alport syndrome and nephrotic syndrome), ciliopathies, tubulopathies, and congenital anomalies of the kidney and urinary tract (CAKUT). Here, we provide a broad overview of the articles included and reflect on the progress still to be made in this important area.

Alport syndrome is characterized by microscopic hematuria and proteinuria leading to end-stage kidney disease until 40 years of age. Male individuals are phenotypically more clearly affected because of X-linked inheritance in the majority of instances, although there is a more strongly emerging understanding of autosomal dominant forms. Female individuals with X-linked Alport syndrome usually show a milder phenotype compared to affected male individuals. CKD can also be observed in these individuals but is less frequent and/or occurs later in life. X-inactivation and other genetic modifiers have been postulated as being causative for the clinical variability. Günthner et al. showed that there is no correlation between the phenotype and X-inactivation, thus leading to the hypothesis that other genetic modifiers shape the phenotype in female individuals. Zhou et al. focused on the very rare occurrence of Alport syndrome with diffuse leiomyomatosis due to contiguous *COL4A5-COL4A6* gene deletions and showed that female individuals are mildly affected compared to male individuals. In addition, extrarenal manifestations, which are known to occur in individuals with Alport syndrome such as hearing impairment or ocular changes, have not been as frequently observed as in female individuals.

Nephrotic syndrome is one of the most frequent causes of glomerulopathy in children and is characterized by proteinuria, hypalbuminemia, and edema. In ∼30% of children with steroid-resistant nephrotic syndrome (SRNS), a monogenic cause can be identified. Rong et al. retrospectively analyzed the genotypes and phenotypes of a Chinese cohort of pediatric individuals with disease-causing variants in *NPHS1*, one of the most mutated genes in individuals with SRNS. Next to the already known phenotypes, this study could identify three disease-causing variants in *NPHS1*, often observed in Chinese patients with congenital nephrotic syndrome implicating potential founder variants. Zhu et al. performed a genotype–phenotype correlation in a Chinese cohort of pediatric individuals and observed that almost 74% carry disease-causing variants in one of the following genes: *WT1*, *NPHS1*, *NPHS2*, and *ADCK4*.

Congenital anomalies of the kidney and urinary tract are an umbrella term for a broad spectrum of symptoms, ranging from mild forms like vesicoureteral reflux to severe forms like bilateral renal agenesis. Li Y. et al. identified that the candidate gene *Gen1* interacts with *Robo2* and that this was observed to be associated with CAKUT in a mouse model. Soraru et al. have then described a research study underway that will seek to identify potential monogenic etiologies in a cohort of patients experiencing kidney failure of uncertain cause. This is important given the concurrent reporting of several key case reports of rare instances of monogenic kidney diseases by Gambino et al., Li Q. et al., and Tian et al..

There have also been key contributions to understanding gene expression and its role in kidney disease phenotypes. Shi et al. reported on the methylomic landscape and CAKUT phenotypes, and this is complemented by Raghubar et al., who demonstrated the spatial transcriptomic landscape in healthy human and mouse kidney tissues.

Individuals with a CAKUT phenotype may occasionally have autosomal dominant polycystic kidney disease (ADPKD). This circumstance is already described as a phenocopy disorder. ADPKD is one of the most frequent causes of end-stage kidney disease in adults. A study by Xu et al. showed abnormalities of methylation in the tissue of individuals with ADPKD, implicating the finding of a biomarker as a prognostic factor for disease progression.

Conceptualizing the space more broadly, Shen et al. identified *IFT144* gene expression as a potential biomarker in lupus nephritis. Li M.-s. et al. reviewed lipoprotein glomerulopathy, which is most commonly associated with variants in *APOE*. Chaudhary et al. undertook a genome-wide association study and identified the interaction between *SMOC2* and *APOL1* in the development of progressive CKD.

The utilization and clinical utility of clinical genetic diagnoses for monogenic kidney disease is an area of substantial interest. Xiao et al. reported on the experiences of preimplantation genetic testing in their center for monogenic kidney disease during the past 20 years, which has the potential to inform real-world practice. The potential applicability of such approaches is further highlighted by the breadth of rare genetic forms of CKD, as indicated by individual case reports by Gambino et al. on a case of *TTC21B*-associated kidney and liver disease, Li Q. et al. on a multi-generational pedigree association of a *WT1* variant with IgA nephropathy, and Tian et al. reporting a *KCNJ1*-associated case of Bartter syndrome type II.

The variety of these contributions to the literature exemplifies the breadth and depth of research that is currently underway in understanding the genetics and epigenetics of kidney disease. There is likely to be a substantial number of additional reports on novel phenotypes to be reported in association with known genes, even as the number of novel genes to be reported is likely to continue to slow. This further highlights the importance of an integrative approach to future research efforts, especially in incorporating research for a better understanding of gene expression and regulation associated with kidney phenotypes as a parallel though related area to germline gene variation.

Author contributions

JH, JR, and AM wrote the original draft and edited the manuscript. All authors reviewed and approved the final manuscript.

Funding

AM was supported by a Queensland Health Advancing Clinical Research Fellowship.

Conflict of interest

The authors declare that the research was conducted in the absence of any commercial or financial relationships that could be construed as a potential conflict of interest.

Publisher's note

frontiers in Medicine

ORIGINAL RESEARCH
published: 25 October 2021
doi: 10.3389/fmed.2021.762848

Identification and Validation of IFI44 as Key Biomarker in Lupus Nephritis

Lingling Shen[1,2,3,4†], *Lan Lan*[1,2,3,4†], *Tingting Zhu*[1,2,3,4], *Hongjun Chen*[1,2,3,4], *Haifeng Gu*[5], *Cuili Wang*[1,2,3,4], *Ying Chen*[1,2,3,4], *Minmin Wang*[6], *Haiyan Tu*[7], *Philipp Enghard*[8], *Hong Jiang*[1,2,3,4*] *and Jianghua Chen*[1,2,3,4*]

[1] *Kidney Disease Center, The First Affiliated Hospital, College of Medicine, Zhejiang University, Hangzhou, China,* [2] *Key Laboratory of Nephropathy, Hangzhou, China,* [3] *Institute of Nephropathy, Zhejiang University, Hangzhou, China,* [4] *Zhejiang Clinical Research Center of Kidney and Urinary System Disease, Hangzhou, China,* [5] *Department of Geriatrics, The First Affiliated Hospital, College of Medicine, Zhejiang University, Hangzhou, China,* [6] *Department of Nephrology, Zhejiang Provincial People's Hospital, Affiliated People's Hospital, Hangzhou Medical College, Hangzhou, China,* [7] *Department of Nephrology, The Second Affiliated Hospital, Zhejiang University School of Medicine, Hangzhou, China,* [8] *Department of Nephrology and Medical Intensive Care, Charité - Universitätsmedizin Berlin, Berlin, Germany*

OPEN ACCESS

Edited by:
Jia Rao,
Fudan University, China

Reviewed by:
Jianhua Mao,
Zhejiang University, China
Daw-Yang Hwang,
National Health Research Institutes, Taiwan
Xu-jie Zhou,
Peking University First Hospital, China

***Correspondence:**
Hong Jiang
jianghong961106@zju.edu.cn
Jianghua Chen
chenjianghua@zju.edu.cn

†These authors have contributed equally to this work and share first authorship

Specialty section:
This article was submitted to Nephrology, a section of the journal Frontiers in Medicine

Received: *23 August 2021*
Accepted: *28 September 2021*
Published: *25 October 2021*

Citation:
Shen L, Lan L, Zhu T, Chen H, Gu H, Wang C, Chen Y, Wang M, Tu H, Enghard P, Jiang H and Chen J (2021) Identification and Validation of IFI44 as Key Biomarker in Lupus Nephritis. Front. Med. 8:762848. doi: 10.3389/fmed.2021.762848

Lupus nephritis (LN) is a common and severe organ manifestation of systemic lupus erythematosus (SLE) and is a major cause of SLE related deaths. Early diagnosis is essential to improve the prognosis of patients with LN. To screen the potential biomarkers associated with LN, we downloaded the gene expression profile of GSE99967 from the Gene Expression Omnibus (GEO) database. Weighted gene co-expression network analysis (WGCNA) was utilized to construct a gene co-expression network and identify gene modules associated with LN. Gene Ontology (GO) analysis was also applied to explore the biological function of genes and identify the key module. Differentially expressed genes (DEGs) were identified and Maximal Clique Centrality (MCC) values were calculated to screen hub genes. Furthermore, we selected promising biomarkers for real-time PCR (qRT-PCR) and enzyme-linked immunosorbent assay (ELISA) validation in independent cohorts. Our results indicated that five hub genes, including IFI44, IFIT3, HERC5, RSAD2, and DDX60 play vital roles in the pathogenesis of LN. Importantly, IFI44 may considered as a key biomarker in LN for its diagnostic capabilities, which is also a promising therapeutic target in the future.

Keywords: lupus nephritis, weighted gene co-expression network analysis, hub genes, biomarker, type-I interferon

INTRODUCTION

Systemic lupus erythematosus (SLE) is an autoimmune disease involving an inappropriate immune response to endogenous nuclear particles, which affects multiple organs and systems (1). Lupus nephritis (LN) is an immune complex glomerulonephritis that develops as one of the most common and severe target-organ manifestations of SLE (2). The treatment of LN is mainly based on glucocorticoids and immunosuppressants, but the effect is not live up to expectations. Approximately 10–30% of LN patients progress to end-stage renal disease (ESRD) within 15 years after diagnosis, which is the major cause of mortality in SLE (3). Thus, it is imperative to further study the pathogenesis of LN to contribute to the diagnosis and treatment of LN and improve the prognosis of patients with LN.

The pathological mechanism of LN is complicated. Recent studies have shown that LN susceptibility genes, which break immune tolerance are involved in the pathogenesis of LN

(4, 5). These genes can enhance the innate immune signaling pathways and promote lymphocytes activation, thus leading to renal damage (4). In addition, autoreactive leukocytes, immune complexes, and complement proteins also play essential roles in LN pathogenesis through various inflammatory mediators (6). However, despite the increased understanding of LN, the genetic and pathogenetic basis of LN remain unclear.

With the rapid development of bioinformatics, microarray data based on high-throughput sequencing has been used to explore the mechanism of diseases at the gene level and identify biomarkers to diagnose diseases or assess prognosis. Weighted gene co-expression network analysis (WGCNA) is a systematics biology method used for integrating gene expression and clinical traits to identify candidate biomarkers and therapeutic targets (7). WGCNA has been widely applied to study various diseases, including cancer (8), autoimmune disease (9), and chronic kidney disease (10). However, there are few studies of WGCNA in LN.

In this study, WGCNA was utilized to construct a gene co-expression network and identify gene modules associated with LN. Gene Ontology (GO) analysis was also applied to explore the potential biological function of genes and identify the key module. Then, we screened five hub genes and verified them by quantitative real-time PCR (qRT-PCR). Furthermore, two promising biomarkers including IFI44 and IFIT3 were selected for enzyme-linked immunosorbent assay (ELISA) validation in an independent cohort. Our findings provide a key biomarker associated with LN pathogenesis and progression, which is helpful for the early diagnosis and treatment of patients with LN.

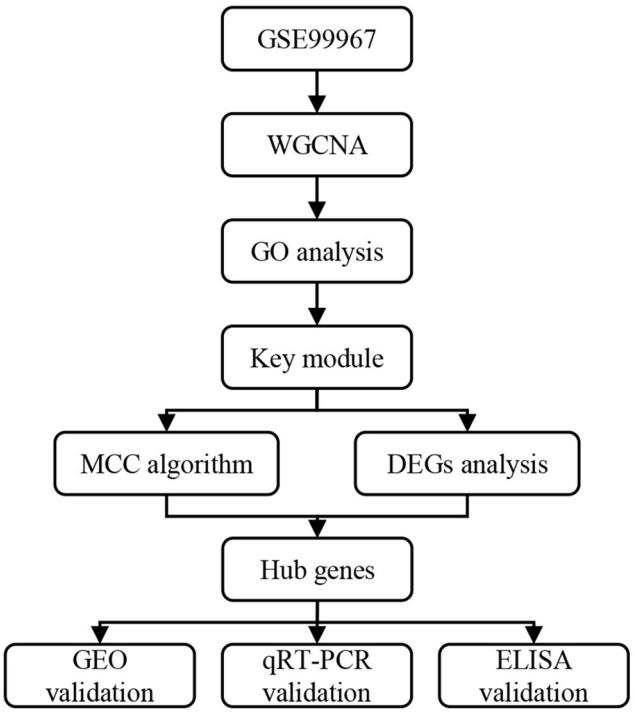

FIGURE 1 | Overall study design. WGCNA, weighted gene co-expression network analysis; GO, gene ontology; MCC, maximal clique centrality; DEGs, differentially expressed genes; GEO, gene expression omnibus; qRT-PCR, quantitative real-time PCR; ELISA, enzyme-linked immunosorbent assay.

MATERIALS AND METHODS

Data Collection

Figure 1 shows the overall study design. We downloaded series matrix files of GSE99967 from the Gene Expression Omnibus (GEO) (https://www.ncbi.nlm.nih.gov/geo) database to identify the hub genes related to LN. The platform of the GSE99967 dataset was GPL21970 (Affymetrix Human Gene 2.0 ST Array). After obtaining the data, one sample GSM2666765 was removed for its inconsistent expression data (**Supplementary Figure 1**). The remaining whole peripheral blood samples from 29 LN patients and 16 normal controls were kept for further analysis (11). The expression data had been $\log_2$ transformed.

Weighted Gene Co-expression Network Analysis

The R package "WGCNA" (7) was utilized to construct the co-expression network of all genes in the GSE99967 dataset. Briefly, we calculated Pearson's correlation to construct a pairwise coefficient matrix and then transformed into a weighted adjacency matrix with an appropriate soft-thresholding power. Next, we converted the adjacency matrix into a topological overlap matrix (TOM), and used hierarchical clustering and dynamic tree cut algorithm to classify genes on TOM-based dissimilarity. Then we calculated the correlations of module eigengene (ME), which represents the first principal component of a module, and merged similar modules with highly correlated eigengenes. In addition, a module-trait relationship was calculated based on the correlation between the gene module and clinical trait. Finally, gene significance (GS) which refers to the correlation between gene expression and the clinical trait was used to identify clinical-related modules.

Functional Enrichment Analysis

To investigate the potential biological function of genes in clinical-related modules, we performed GO enrichment analysis using Database for Annotation, Visualization and Integrated Discovery DAVID (https://david.ncifcrf.gov/). GO terms with $p < 0.05$ were considered statistically significant. The R package "ggplot2" was utilized to show results in the bubble chart.

Differentially Expressed Gene Analysis

The GEO2R online tools (12) were used to identify differentially expressed genes (DEGs) between LN patients and normal controls. Genes with adjusted $p < 0.05$ and $|\log_2$ fold change $(FC)| \geq 1$ were considered as DEGs. The heatmap and volcano plot of all DEGs were made by the R package "pheatmap" and "ggplot2," respectively.

Hub Genes Identification

We used CytoHubba (13), a Cytoscape software (14) plugin to select the hub genes in the key module. The top ten genes with higher maximal clique centrality (MCC) values were screened.

Among these ten genes, five DEGs were identified as hub genes. We investigated the GS and module membership (MM) of the selected hub genes to verify their reasonability.

Validation of Hub Genes in Other Datasets

To validate five hub genes, we downloaded another two datasets GSE72798 (15) and GSE32591 (16) from the GEO database. The dataset GSE72798 consists of 10 LN patients and 10 normal controls and the RNA was extracted from blood samples. In the GSE32591 dataset, the total RNA was extracted from kidney biopsy of 32 LN patients and 14 normal controls.

Patients and Samples Collection

To further verify selected genes, we recruited 78 LN patients, 67 healthy controls (HCs), and 25 patients with IgA nephropathy from the First Affiliated Hospital, College of Medicine, Zhejiang University. Patients or the public provided written informed consent to participate in this study. All LN patients were confirmed by kidney biopsy, and the Systemic Lupus Erythematosus Disease Activity Index (SLEDAI) was calculated, which contains 24 items reflecting disease activity. Active LN was defined as biopsy-proven active nephritis or SLEDAI $\geq$10 and at least two renal elements of the SLEDAI; inactive LN was defined as biopsy-proven pure class V or VI nephritis or SLEDAI <10.

Serum was separated from blood samples and stored at −80°C. Peripheral blood mononuclear cells (PBMCs) were isolated by human PBMCs separation medium (tbdscience, Tianjin, China).

RNA Extraction and qRT-PCR

Total RNA was extracted from PBMCs samples using TRIzol® (Invitrogen, CA, USA) and then reversely transcribed into cDNA by the PrimeScript™ II Reverse Transcriptase (Takara, Shiga, Japan). According to the manufacturer's instructions, reverse transcription was conducted at 37°C for 15 min and 85°C for 5 s. qRT-PCR was performed by SYBR Green on CFX96™ Real-Time PCR Detection Systems (Bio-rad, CA, USA). All primer sequences used were shown in **Supplementary Table 1**. The conditions of qRT-PCR were as follows: 95°C for 30 s, followed by 40 cycles of 95°C for 5 s and 60°C for 31 s, with dissociation at 95°C for 15 s, 60°C for 1 min and 95°C for 15 s. The average threshold cycle (Ct) was calculated for each transcript, which was performed in triplicate. The relative expression of each mRNA was normalized by GAPDH and analyzed using the $2^{-\Delta\Delta CT}$ method [$\Delta\Delta CT$ = (CT of gene) – (CT of GAPDH) – (CT of HC)].

ELISA

The serum levels of IFI44 and IFIT3 were assessed with ELISA kits (G-Biosciences, CA, USA for IFI44, and MyBioSource, CA, USA for IFIT3). Briefly, diluted serum samples were incubated in the microplate. The membrane was then incubated with biotin-labeled antibody after washing twice. Similarly, the membrane was incubated with avidin-labeled horseradish peroxidase (HRP) and then with substrated solution (TMB). Finally, the absorbance values at 450 nm of samples were read, and the concentration of IFI44 and IFIT3 were calculated using standard curves run on each ELISA plate.

Statistical Analyses

Statistical analyses were performed using SPSS 20 (IBM) and GraphPad Prism 8.0 (GraphPad Software, CA, USA). The unpaired *t*-test was used to analyze differences between two groups. Results were expressed as the mean ± standard deviation (SD). The receiver operator characteristic (ROC) curves were drawn and area under curve (AUC) was calculated to assess the diagnostic capability of biomarkers. Logistic regression analysis was performed to create a combined score. $P < 0.05$ was considered statistically significant.

RESULTS

Construction of Weighted Gene Co-expression Network

Samples in the GSE99967 dataset were divided into two groups (29 LN samples and 16 normal controls). Expression data of all genes from GSE99967 were used to conduct WGCNA (**Figure 2**). Based on scale-free topology model fit index and mean connectivity, the soft-threshold power was set as four (**Figure 2A**). Then, we merged similar modules to acquire 12 co-expression modules by setting the cut height of module eigengenes as 0.5 (**Figures 2B,C**). **Figure 2D** showed the cluster dendrogram and adjacency heatmap of eigengenes, which means that 12 modules were primarily separated into two clusters.

Key Module Identification

From the heatmap of module-trait relationships, we found that multiple modules were associated with LN (**Figure 3A**). Then, we calculated the gene significance of all genes in 12 co-expression modules (**Figure 3B**). The results showed that the darkgreen module was most significantly related to LN, followed by the purple module. The correlation between MM and GS in these two modules are shown in **Figure 3C**, which mean that MM was highly correlated with GS for LN in both darkgreen module and purple module (cor = 0.77, p = 5.8e−76, and cor = 0.41, p = 5.2e−15, respectively).

To investigate the potential biological function of genes in the above two modules, we performed GO enrichment analysis. The top 20 significant GO biological process terms of each module were shown in **Figures 3D,E**. We found that genes in the purple module were mainly enriched in defense response to virus, type I interferon signaling pathway, immune response, and inflammatory response, which are highly associated with LN. However, genes in the darkgreen module were mostly distributed in terms like cell diversion and proliferation, mitotic nuclear division, and DNA replication, which mainly play roles in metabolism. Thus, we defined the purple module as the key module related to LN and performed further analysis.

Identification of Hub Genes

Hub genes should be DEGs between LN patients and normal controls. In dataset GSE99967, a total of 137 DEGs were identified, including 84 up-regulated genes

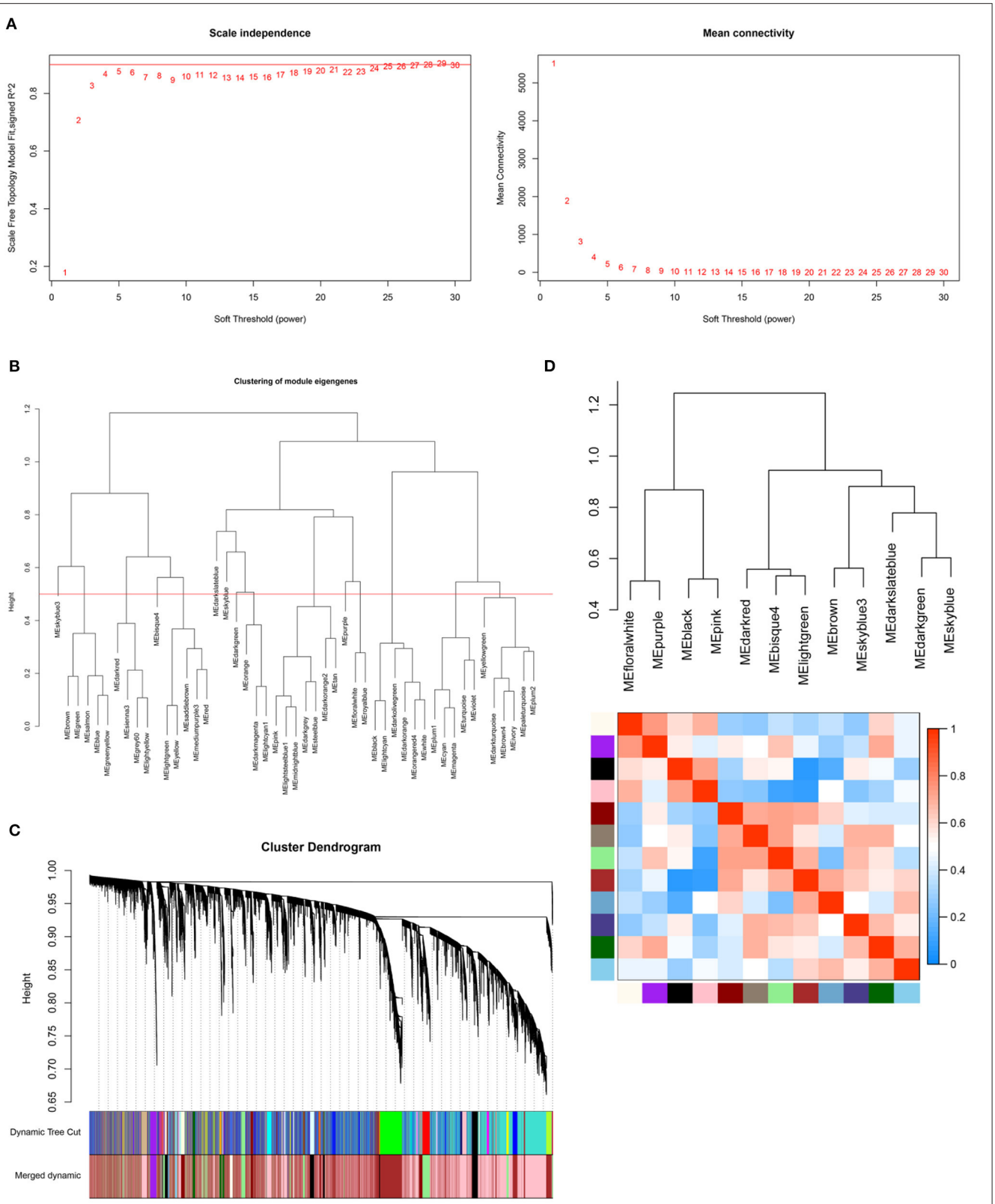

FIGURE 2 | Construction of weighted gene co-expression network. **(A)** Analysis of the scale-free topology model fit index for soft threshold powers (Left) and analysis of the mean connectivity for soft threshold powers (Right). The soft-thresholding power was set as four. **(B)** Clustering of module eigengenes. The red line represents cut height (0.5). **(C)** The cluster dendrogram of genes. **(D)** The cluster dendrogram and adjacency heatmap of eigengenes.

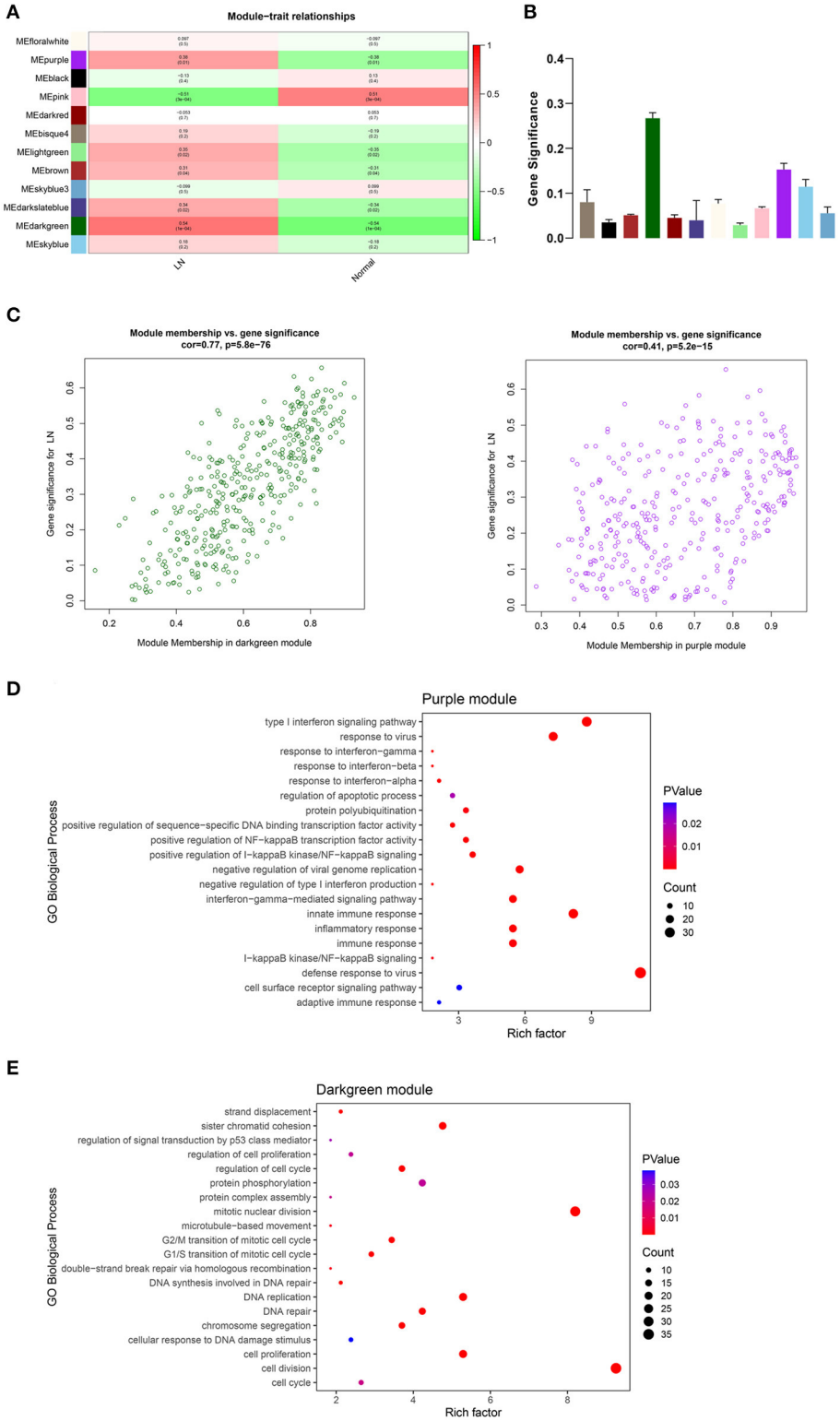

FIGURE 3 | Key module identification. **(A)** Heatmap of module-trait relationships. The correlation coefficients and *p*-value are shown in each cell. Red presents a positive correlation and blue presents a negative correlation. **(B)** Gene significance of all genes in 12 modules related to LN. Different colors of columns present different modules. **(C)** Scatter plot for correlation between module membership and gene significance in darkgreen module (Left) and purple module (Right). The top 20 significant GO terms (biological process) of the purple module **(D)** and darkgreen module **(E)**. The color and size of each point indicate the *p*-value and the number of genes in the corresponding term, respectively. LN, lupus nephritis; GO, gene ontology.

and 53 down-regulated genes (**Supplementary Table 2**). The heatmap and volcano plot of all DEGs are shown in **Supplementary Figures 2, 3**.

To identify hub genes in the key module, we calculated MCC values of genes in the purple module and extracted the top 10 genes with higher scores (**Supplementary Figure 4**). Among these ten genes, 5 DEGs were identified as hub genes, including interferon induced protein 44 (IFI44), interferon induced protein with tetratricopeptide repeats three (IFIT3), HECT and RLD domain containing E3 ubiquitin protein ligase 5 (HERC5), radical S-adenosyl methionine domain containing two (RSAD2), and DExD/H-box helicase 60 (DDX60). The GS and MM value of these genes were all > 0.4 and 0.9, respectively, indicating that hub genes were significantly associated with the key module and LN trait.

Validation of Hub Genes by Other Datasets and qRT-PCR

As expected, the expression levels of hub genes including IFI44, IFIT3, HERC5, RSAD2, and DDX60 were significantly upregulated in LN samples from the GSE99967 dataset (**Figure 4A**). For verifying hub genes, we obtained another two datasets GSE72798 and GSE32591, and analyzed the expression levels of the above five genes between LN patients and normal controls (**Figures 4B,C**). Except for DDX60 in GSE72798, the other four hub genes were markedly increased in LN samples.

In addition, to further validate these four hub genes, we collected nine blood samples from four healthy controls and five LN patients (patient characteristics are shown in **Supplementary Table 3**) to perform qRT-PCR. The results showed that compared with HCs, the mRNA levels of IFI44, IFIT3, HERC5, and RSAD2 were all significantly elevated in LN patients (**Supplementary Figure 5**), meaning that they are expected to be potential biomarkers in identifying LN.

ELISA Validation

Among five hub genes, we selected type I interferon-response genes IFI44 and IFIT3 for further analysis. To detect the serum levels of IFI44 and IFIT3, 124 subjects, including 51 healthy controls and 73 LN patients (patient characteristics are shown in **Supplementary Table 4**) were used to perform ELISA assays (**Figure 5**). As expected, IFI44 and IFIT3 were markedly upregulated in LN patients compared with the healthy controls (**Figure 5A**). Furthermore, ROC curves were used to calculate the sensitivity and specificity of these two biomarkers for identifying LN patients. The AUC values of IFI44 and IFIT3 were 0.811 and 0.758, respectively (**Figure 5B**, **Supplementary Table 5**). Then, we combined these two biomarkers using logistic regression analysis (**Supplementary Figure 6A**, **Supplementary Table 6**). However, the AUC value of combined score (AUC $= 0.811$) was the same as IFI44 (**Supplementary Figure 6B**), indicating that IFI44 had the highest power to distinguish between the two groups. Additionally, we found that IFI44 was significantly elevated in active LN compared with inactive LN patients, while IFIT3 failed to discriminate active LN from inactive ones (**Figure 5C**). And the AUC of IFI44 in differentiating active LN from inactive LN patients was 0.697, which was similar to clinical indicators such as anti-dsDNA (AUC $=$ 0.600), C3 (AUC $= 0.665$), and C4 (AUC $= 0.673$) (**Figure 5D**; **Supplementary Table 7**).

To examine whether serum IFI44 and IFIT3 can reflect the pathological class of kidney biopsy, we classified 73 LN patients into five groups according to LN class. The results showed that they were both elevated in class III($\pm$V), class IV($\pm$V), and class V compared with HCs (**Supplementary Figure 7**), meaning that both IFI44 and IFIT3 can indicate the prognosis of LN.

Moreover, we identified the specificity of IFI44 for LN. An independent cohort of 37 subjects, including 12 healthy controls and 25 patients with IgA nephropathy (patient characteristics are shown in **Supplementary Table 8**), were used for investigation. Interestingly, there was no statistical difference between HCs and patients with IgA nephropathy (**Figure 5E**), indicating that IFI44 is specific for LN.

DISCUSSION

Lupus nephritis is a major cause of morbidity and mortality in SLE, and many patients end in chronic kidney disease (CKD) or ESRD due to limited drug treatment (17, 18). Therefore, it is imperative to develop candidate biomarkers and potential therapeutic targets to improve the prognosis of patients with LN. In this study, we used the GSE99967 dataset to screen the hub genes associated with the pathogenesis of LN. WGCNA was utilized to construct co-expression modules associated with LN, and GO enrichment analysis was applied to explore the biological function of genes in the key module. Five hub genes were obtained using the MCC algorithm, including IFI44, IFIT3, HERC5, RSAD2, and DDX60. qRT-PCR and ELISA assays were performed to validate potential biomarkers in independent cohorts. We found that both IFI44 and IFIT3 have diagnostic accuracy in identifying LN, especially IFI44, which is specific for LN. Our findings may shed light on the pathogenetic basis of LN and provide candidate biomarkers for its treatment.

We found that genes in the key module were mainly enriched in defense response to virus and type I interferon signaling pathway, which are consistent with previous studies (19, 20). Anders HJ et al. indicated that endogenous RNA-related autoantigens can be recognized by Toll-like receptor-7 (TLR7), a viral nucleic acid recognition receptor that triggers antiviral immunity, thus aggravating lupus nephritis (21). In contrast, blockade of TLR7, TLR9, or both attenuates lupus nephritis (22). Additionally, antiviral genes such as ISG15, MX1, and the OAS gene family are involved in the pathogenesis of LN (23). Likewise, type I interferon signaling pathway-related genes, such as IRF5 and STAT4, are associated with the risk of LN (24). Triantafyllopoulou A et al. revealed the role of intrarenal type I IFNs in kidney damage of LN (25). Furthermore, monitoring the peripheral blood type I interferon signature can track the kidney disease activity in patients with SLE (26). Therefore, hub genes we obtained from the key module were confirmed to be highly relevant to LN.

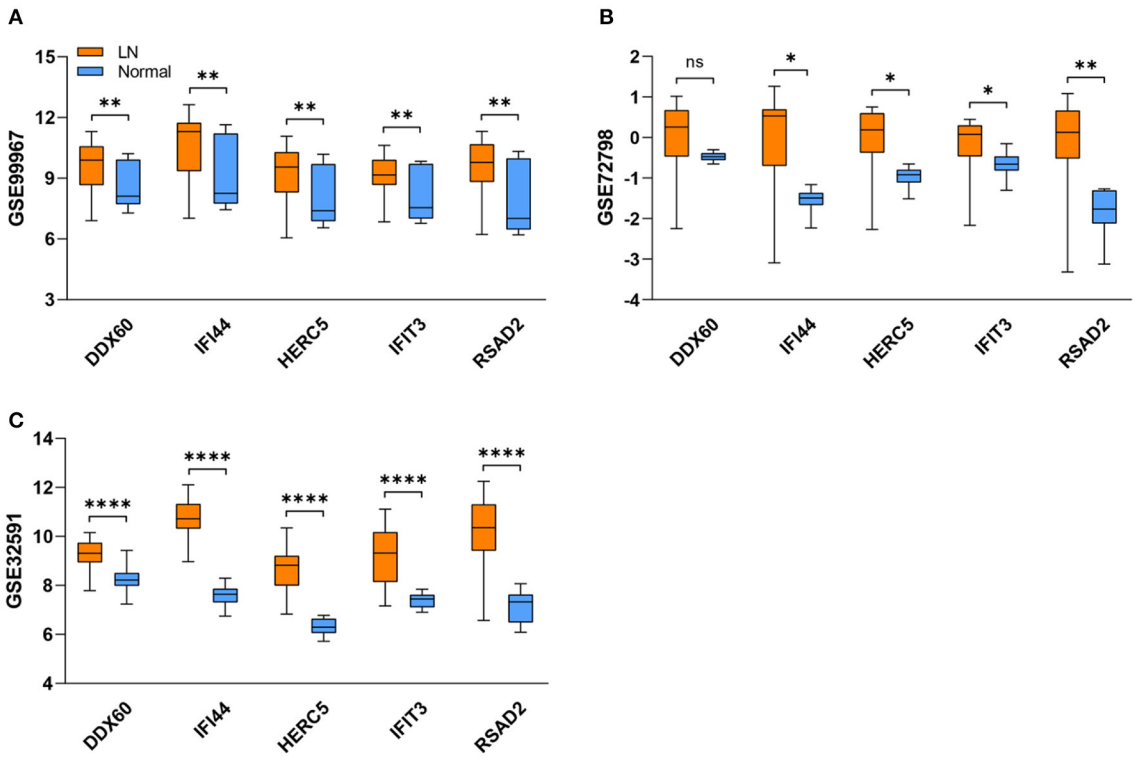

FIGURE 4 | Validation of five hub genes in datasets. **(A–C)** The blue box refers to the normal group and the orange one refers to the LN group. Box represents mean ± SD by an unpaired *t*-test. $^{*}P < 0.05$, $^{**}P < 0.01$, $^{***}P < 0.0001$, ns, no significance; LN, lupus nephritis.

Both IFI44 and IFIT3 are type I IFN signature genes, which may contribute to the pathogenesis of autoimmune diseases (27, 28). In independent cohorts, we found that serum IFI44 and IFIT3 can discriminate LN patients from healthy controls, which may act as candidate biomarkers in identifying LN. Similar to our findings, increased gene expression of IFI44 and IFIT3 was observed in SLE patients compared to HCs (29). What's more, IFI44, as an LN-specific biomarker, can distinguish between active LN patients and inactive ones. Previous studies have shown that patients with class III, IV, or V LN, but not class I or II LN, are at direct risk of CKD progression. What's worse, both class III and class IV LN involve irreversible nephron loss, which shortens kidney lifespan (30). Interestingly, our results revealed that IFI44 and IFIT3 were both elevated in class III(±V), class IV(±V), and class V LN, suggesting that these two biomarkers can indicate the prognosis of LN. Also, IFIT3 may proposed as a novel therapeutic target for blocking the production of type I IFN in patients with SLE (31). In terms of epigenetics, IFI44 and IFIT3 were hypomethylated in comparisons between lupus patients and non-lupus subjects (32, 33). Moreover, both IFI44 and IFIT3 have antiviral activity, meaning that they may be involved in the anti-endogenous nucleic acid response of LN patients (34, 35).

In addition, HERC5, RSAD2, and DDX60 are all interferon induced-genes, which play important roles in antiviral response (36–39). Consistent with our findings, recent studies revealed that the expression level of RSAD2 was markedly increased in the SLE samples compared with controls, which may act as a potential biomarker gene and therapeutic target for the treatment of SLE (40, 41). Similarly, upregulated gene expression of DDX60 was observed in the IFN-I-positive childhood-onset SLE patients (42). Due to the epigenetic susceptibility of lupus, Coit P et al. found that HERC5 is hypomethylated in lupus patients with renal involvement (43). Thus, it is important to clarify the relationship between these five hub genes and the pathogenesis of LN.

Our findings provide new insights into the occurrence, progression of LN patients. Sun G et al. explored the genes genetically associated with LN through bioinformatics analysis (44). They found that LN-related genes were mainly involved in immune and inflammatory responses, which are in agreement with what we found. Likewise, the GSE104948 dataset was analyzed by WGCNA, and CD36 was ultimately screened out as a hub gene of the pathogenesis of LN (45). However, neither of their findings have been validated in LN patients. Moreover, Yao M et al. used dataset GSE32591 to explore the pathophysiological changes in glomeruli and tubulointerstitia of LN patients (46). Consistent with our findings, they found that type I interferon response was highly active in LN and the crosstalk genes, such as IRF7, HLA-DRA, ISG15, PSMB8, and IFITM3 were validated in six samples. However, in our study, after identifying the hub genes, we verified the mRNA expression and serum concentration of them with large sample size, and they are expected to be candidate biomarkers and potential therapeutic targets of LN.

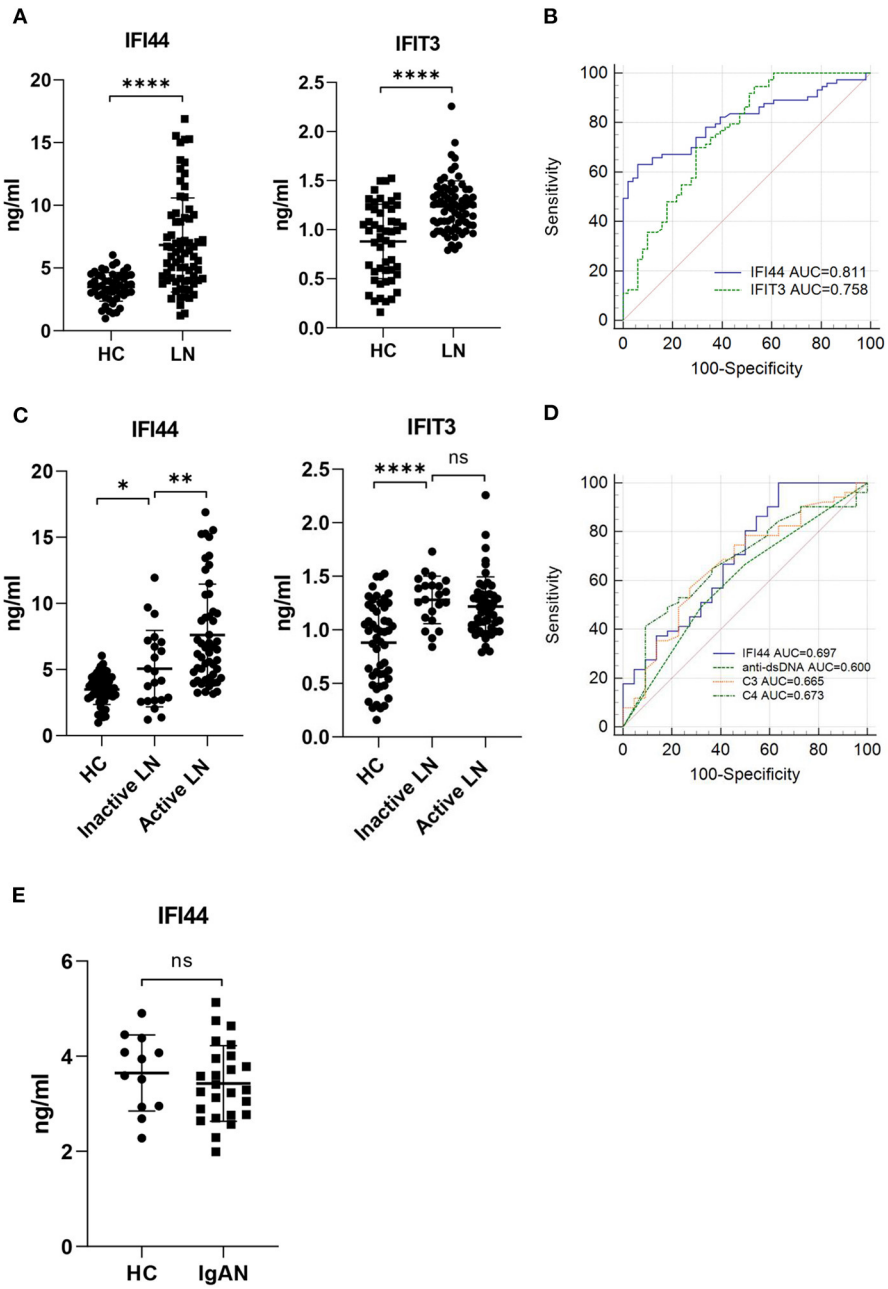

FIGURE 5 | ELISA validation and ROC analysis. **(A)** Serum IFI44 (Left) and IFIT3 (Right) were measured in 51 healthy controls and 73 LN patients by ELISA. **(B)** Receiver operator characteristic (ROC) curves show the diagnostic performance of serum IFI44 (blue) and IFIT3 (green) in identifying LN patients. **(C)** 73 LN patients were divided into two groups (Inactive LN=22, Active LN=51) according to renal biopsy and the Systemic Lupus Erythematosus Disease Activity Index (SLEDAI). **(D)** ROC curves of IFI44, anti-dsDNA, C3, and C4 in differentiating active LN from inactive LN patients. **(E)** Serum IFI44 was tested in 12 healthy controls and 25 patients with IgA nephropathy. Data shown are mean ± SD by an unpaired *t*-test. $^{*}P < 0.05$, $^{**}P < 0.01$, $^{****}P < 0.0001$, ns, no significance; HC, healthy control; LN, lupus nephritis; IgAN, immunoglobulin A nephropathy.

However, our study contains some limitations. First, patients in validation cohorts are composed of Chinese. Hence, our findings may not generalize LN patients from different races and ethnicities. Second, samples for qRT-PCR validation are limited. Thus, more samples are needed to verify the mRNA expression of these hub genes. Third, the exact mechanisms of the identified hub genes in the occurrence and progression of LN need to be further investigated.

In conclusion, based on WGCNA, we identified five hub genes, including IFI44, IFIT3, HERC5, RSAD2, and DDX60, which are highly correlated with LN. GO enrichment analysis revealed that these genes are mainly enriched in defense response

to virus, type I interferon signaling pathway and immune response. In validation cohorts, IFI44 was found to be a candidate biomarker to diagnose diseases or assess prognosis. Our findings provide potential therapeutic targets and shed light on the pathogenetic basis of LN.

DATA AVAILABILITY STATEMENT

The raw data supporting the conclusions of this article will be made available by the authors, without undue reservation.

ETHICS STATEMENT

The studies involving human participants were reviewed and approved by the Research Ethics Committee of the First Affiliated Hospital, College of Medicine, Zhejiang University. The patients/participants provided their written informed consent to participate in this study.

AUTHOR CONTRIBUTIONS

JC, HJ, and LS designed the study. LS and TZ conducted bioinformatics. LS, LL, HC, HG, and PE carried out experiments. YC, MW, and HT performed the statistical analysis. LL and CW wrote the manuscript. All authors contributed to the manuscript and approved the submitted version.

FUNDING

This work was supported by Sino-German center (M-0144).

SUPPLEMENTARY MATERIAL

The Supplementary Material for this article can be found online at: https://www.frontiersin.org/articles/10.3389/fmed.2021.762848/full#supplementary-material

REFERENCES

1. Kaul A, Gordon C, Crow MK, Touma Z, Urowitz MB, van Vollenhoven R, et al. Systemic lupus erythematosus. *Nat Rev Dis Primers.* (2016) 2:16039. doi: 10.1038/nrdp.2016.39
2. Lech M, Anders HJ. The pathogenesis of lupus nephritis. *J Am Soc Nephrol.* (2013) 24:1357–66. doi: 10.1681/ASN.2013010026
3. Mageau A, Timsit JF, Perrozziello A, Ruckly S, Dupuis C, Bouadma L, et al. The burden of chronic kidney disease in systemic lupus erythematosus: a nationwide epidemiologic study. *Autoimmun Rev.* (2019) 18:733–7. doi: 10.1016/j.autrev.2019.05.011
4. Mohan C, Putterman C. Genetics and pathogenesis of systemic lupus erythematosus and lupus nephritis. *Nat Rev Nephrol.* (2015) 11:329–41. doi: 10.1038/nrneph.2015.33
5. Iwamoto T, Niewold TB. Genetics of human lupus nephritis. *Clin Immunol.* (2017) 185:32–9. doi: 10.1016/j.clim.2016.09.012
6. Parikh SV, Almaani S, Brodsky S, Rovin BH. Update on lupus nephritis: core curriculum 2020. *Am J Kidney Dis.* (2020) 76:265–81. doi: 10.1053/j.ajkd.2019.10.017
7. Langfelder P, Horvath S. WGCNA: an R package for weighted correlation network analysis. *BMC Bioinformatics.* (2008) 9:559. doi: 10.1186/1471-2105-9-559
8. Long J, Huang S, Bai Y, Mao J, Wang A, Lin Y, et al. Transcriptional landscape of cholangiocarcinoma revealed by weighted gene coexpression network analysis. *Brief Bioinform.* (2020) 22:1–17. doi: 10.1093/bib/bbaa224
9. Ashton JJ, Boukas K, Davies J, Stafford IS, Vallejo AF, Haggarty R, et al. Ileal transcriptomic analysis in paediatric crohn's disease reveals IL17- and NOD-signalling expression signatures in treatment-naive patients and identifies epithelial cells driving differentially expressed genes. *J Crohns Colitis.* (2021) 15:774–86. doi: 10.1093/ecco-jcc/jjaa236
10. Beckerman P, Qiu C, Park J, Ledo N, Ko YA, Park AD, et al. Human kidney tubule-specific gene expression based dissection of chronic kidney disease traits. *EBioMedicine.* (2017) 24:267–76. doi: 10.1016/j.ebiom.2017.09.014
11. Wither JE, Prokopec SD, Noamani B, Chang NH, Bonilla D, Touma Z, et al. Identification of a neutrophil-related gene expression signature that is enriched in adult systemic lupus erythematosus patients with active nephritis: clinical/pathologic associations and etiologic mechanisms. *PLoS ONE.* (2018) 13:e0196117. doi: 10.1371/journal.pone.0196117
12. Davis S, Meltzer PS. GEOquery: a bridge between the gene expression omnibus (GEO) and bioConductor. *Bioinformatics.* (2007) 23:1846–7. doi: 10.1093/bioinformatics/btm254
13. Chin CH, Chen SH, Wu HH, Ho CW, Ko MT, Lin CY. CytoHubba: identifying hub objects and sub-networks from complex interactome. *BMC Syst Biol.* (2014) 8 Suppl 4:S11. doi: 10.1186/1752-0509-8-S4-S11
14. Shannon P, Markiel A, Ozier O, Baliga NS, Wang JT, Ramage D, et al. Cytoscape: a software environment for integrated models of biomolecular interaction networks. *Genome Res.* (2003) 13:2498–504. doi: 10.1101/gr.1239303
15. Ducreux J, Houssiau FA, Vandepapeliere P, Jorgensen C, Lazaro E, Spertini F, et al. Interferon alpha kinoid induces neutralizing anti-interferon alpha antibodies that decrease the expression of interferon-induced and B cell activation associated transcripts: analysis of extended follow-up data from the interferon alpha kinoid phase I/II study. *Rheumatology.* (2016) 55:1901–5. doi: 10.1093/rheumatology/kew262
16. Berthier CC, Bethunaickan R, Gonzalez-Rivera T, Nair V, Ramanujam M, Zhang W, et al. Cross-species transcriptional network analysis defines shared inflammatory responses in murine and human lupus nephritis. *J Immunol.* (2012) 189:988–1001. doi: 10.4049/jimmunol.1103031
17. Tektonidou MG, Dasgupta A, Ward MM. Risk of end-stage renal disease in patients with lupus nephritis, 1971-2015: a systematic review and bayesian meta-analysis. *Arthritis Rheumatol.* (2016) 68:1432–41. doi: 10.1002/art.39594
18. Almaani S, Meara A, Rovin BH. Update on lupus nephritis. *Clin J Am Soc Nephrol.* (2017) 12:825–35. doi: 10.2215/CJN.05780616
19. Postal M, Vivaldo JF, Fernandez-Ruiz R, Paredes JL, Appenzeller S, Niewold TB. Type I interferon in the pathogenesis of systemic lupus erythematosus. *Curr Opin Immunol.* (2020) 67:87–94. doi: 10.1016/j.coi.2020.10.014
20. Migliorini A, Anders HJ. A novel pathogenetic concept-antiviral immunity in lupus nephritis. *Nat Rev Nephrol.* (2012) 8:183–9. doi: 10.1038/nrneph.2011.197
21. Anders HJ, Krug A, Pawar RD. Molecular mimicry in innate immunity? the viral RNA recognition receptor TLR7 accelerates murine lupus. *Eur J Immunol.* (2008) 38:1795–9. doi: 10.1002/eji.200838478
22. Pawar RD, Ramanjaneyulu A, Kulkarni OP, Lech M, Segerer S, Anders HJ. Inhibition of toll-like receptor-7 (TLR-7) or TLR-7 plus TLR-9 attenuates glomerulonephritis and lung injury in experimental lupus. *J Am Soc Nephrol.* (2007) 18:1721–31. doi: 10.1681/ASN.2006101162
23. Cao Y, Mi X, Wang Z, Zhang D, Tang W. Bioinformatic analysis reveals that the OAS family may play an important role in lupus nephritis. *J Natl Med Assoc.* (2020) 112:567–77. doi: 10.1016/j.jnma.2020.05.006
24. Nghiem TD, Do GT, Luong LH, Nguyen QL, Dang HV, Viet AN, et al. Association of the STAT4, CDKN1A, and IRF5 variants with risk of lupus nephritis and renal biopsy classification in patients in Vietnam. *Mol Genet Genomic Med.* (2021) 9:e1648. doi: 10.1002/mgg3.1648
25. Triantafyllopoulou A, Franzke CW, Seshan SV, Perino G, Kalliolias GD, Ramanujam M, et al. Proliferative lesions and metalloproteinase activity in murine lupus nephritis mediated by type I interferons and macrophages. *Proc Natl Acad Sci U S A.* (2010) 107:3012–7. doi: 10.1073/pnas.0914902107

26. Banchereau R, Hong S, Cantarel B, Baldwin N, Baisch J, Edens M, et al. Personalized immunomonitoring uncovers molecular networks that stratify lupus patients. *Cell.* (2016) 165:551–65. doi: 10.1016/j.cell.2016.03.008
27. Zhao X, Zhang L, Wang J, Zhang M, Song Z, Ni B, et al. Identification of key biomarkers and immune infiltration in systemic lupus erythematosus by integrated bioinformatics analysis. *J Transl Med.* (2021) 19:35. doi: 10.1186/s12967-021-02728-2
28. Maria NI, Brkic Z, Waris M, van Helden-Meeuwsen CG, Heezen K, van de Merwe JP, et al. MxA as a clinically applicable biomarker for identifying systemic interferon type I in primary sjogren's syndrome. *Ann Rheum Dis.* (2014) 73:1052–9. doi: 10.1136/annrheumdis-2012-202552
29. Bodewes ILA, Huijser E, van Helden-Meeuwsen CG, Tas L, Huizinga R, Dalm V, et al. TBK1: a key regulator and potential treatment target for interferon positive sjogren's syndrome, systemic lupus erythematosus and systemic sclerosis. *J Autoimmun.* (2018) 91:97–102. doi: 10.1016/j.jaut.2018.02.001
30. Anders HJ, Saxena R, Zhao MH, Parodis I, Salmon JE, Mohan C. Lupus nephritis. *Nat Rev Dis Primers.* (2020) 6:7. doi: 10.1038/s41572-019-0141-9
31. Wang J, Dai M, Cui Y, Hou G, Deng J, Gao X, et al. Association of abnormal elevations in IFIT3 with overactive cyclic GMP-AMP synthase/stimulator of interferon genes signaling in human systemic lupus erythematosus monocytes. *Arthritis Rheumatol.* (2018) 70:2036–45. doi: 10.1002/art.40576
32. Coit P, Jeffries M, Altorok N, Dozmorov MG, Koelsch KA, Wren JD, et al. Genome-wide DNA methylation study suggests epigenetic accessibility and transcriptional poising of interferon-regulated genes in naive CD4+ T cells from lupus patients. *J Autoimmun.* (2013) 43:78–84. doi: 10.1016/j.jaut.2013.04.003
33. Joseph S, George NI, Green-Knox B, Treadwell EL, Word B, Yim S, et al. Epigenome-wide association study of peripheral blood mononuclear cells in systemic lupus erythematosus: identifying DNA methylation signatures associated with interferon-related genes based on ethnicity and SLEDAI. *J Autoimmun.* (2019) 96:147–57. doi: 10.1016/j.jaut.2018.09.007
34. Johnson B, VanBlargan LA, Xu W, White JP, Shan C, Shi PY, et al. Human IFIT3 modulates IFIT1 RNA binding specificity and protein stability. *Immunity.* (2018) 48:487–99 e5. doi: 10.1016/j.immuni.2018.01.014
35. DeDiego ML, Nogales A, Martinez-Sobrido L, Topham DJ. Interferon-Induced protein 44 interacts with cellular FK506-binding protein 5, negatively regulates host antiviral responses, and supports virus replication. *mBio.* (2019) 10:e01839–19. doi: 10.1128/mBio.01839-19
36. Giugliano S, Kriss M, Golden-Mason L, Dobrinskikh E, Stone AE, Soto-Gutierrez A, et al. Hepatitis C virus infection induces autocrine interferon signaling by human liver endothelial cells and release of exosomes, which inhibits viral replication. *Gastroenterology.* (2015) 148:392–402 e13. doi: 10.1053/j.gastro.2014.10.040
37. Bernheim A, Millman A, Ofir G, Meitav G, Avraham C, Shomar H, et al. Prokaryotic viperins produce diverse antiviral molecules. *Nature.* (2021) 589:120–4. doi: 10.1038/s41586-020-2762-2
38. Mathieu NA, Paparisto E, Barr SD, Spratt DE. HERC5 and the ISGylation pathway: critical modulators of the antiviral immune response. *Viruses.* (2021) 13:1102. doi: 10.3390/v13061102
39. Oshiumi H, Kouwaki T, Seya T. Accessory factors of cytoplasmic viral RNA sensors required for antiviral innate immune response. *Front Immunol.* (2016) 7:200. doi: 10.3389/fimmu.2016.00200
40. Yu Y, Liu L, Hu LL, Yu LL, Li JP, Rao JA, et al. Potential therapeutic target genes for systemic lupus erythematosus: a bioinformatics analysis. *Bioengineered.* (2021) 12:2810–9. doi: 10.1080/21655979.2021.1939637
41. Fang Q, Li T, Chen P, Wu Y, Wang T, Mo L, et al. Comparative analysis on abnormal methylome of differentially expressed genes and disease pathways in the immune cells of RA and SLE. *Front Immunol.* (2021) 12:668007. doi: 10.3389/fimmu.2021.668007
42. Wahadat MJ, Bodewes ILA, Maria NI, van Helden-Meeuwsen CG, van Dijk-Hummelman A, Steenwijk EC, et al. Type I IFN signature in childhood-onset systemic lupus erythematosus: a conspiracy of DNA- and RNA-sensing receptors? *Arthritis Res Ther.* (2018) 20:4. doi: 10.1186/s13075-017-1501-z
43. Coit P, Renauer P, Jeffries MA, Merrill JT, McCune WJ, Maksimowicz-McKinnon K, et al. Renal involvement in lupus is characterized by unique DNA methylation changes in naive CD4+ T cells. *J Autoimmun.* (2015) 61:29–35. doi: 10.1016/j.jaut.2015.05.003
44. Sun G, Zhu P, Dai Y, Chen W. Bioinformatics analysis of the core genes related to lupus nephritis through a network and pathway-based approach. *DNA Cell Biol.* (2019) 38:639–50. doi: 10.1089/dna.2019.4631
45. Yang H, Li H. CD36 identified by weighted gene co-expression network analysis as a hub candidate gene in lupus nephritis. *PeerJ.* (2019) 7:e7722. doi: 10.7717/peerj.7722
46. Yao M, Gao C, Zhang C, Di X, Liang W, Sun W, et al. Identification of molecular markers associated with the pathophysiology and treatment of lupus nephritis based on integrated transcriptome analysis. *Front Genet.* (2020) 11:583629. doi: 10.3389/fgene.2020.583629

Conflict of Interest: The authors declare that the research was conducted in the absence of any commercial or financial relationships that could be construed as a potential conflict of interest.

The reviewer JM declared a shared affiliation with the authors to the handling editor at time of review.

Publisher's Note: All claims expressed in this article are solely those of the authors and do not necessarily represent those of their affiliated organizations, or those of the publisher, the editors and the reviewers. Any product that may be evaluated in this article, or claim that may be made by its manufacturer, is not guaranteed or endorsed by the publisher.

frontiers in Medicine

ORIGINAL RESEARCH
published: 27 October 2021
doi: 10.3389/fmed.2021.766224

Clinical Manifestations of Alport Syndrome-Diffuse Leiomyomatosis Patients With Contiguous Gene Deletions in *COL4A6* and *COL4A5*

Xi Zhou†, *Jingjing Wang*†, *Jianhua Mao** and *Qing Ye**

The Children's Hospital of Zhejiang University School of Medicine, National Clinical Research Center for Child Health, Hangzhou, China

Alport syndrome-diffuse leiomyomatosis is a rare type of X-linked Alport syndrome resulting from contiguous deletions of 5′ exons of *COL4A5* and *COL4A6*. Studies have suggested that the occurrence of diffuse leiomyomatosis is associated with the characteristic localisation of the *COL4A6* gene deletion break point. An electronic database was searched for all studies accessing AS-DL to analyze the clinical characteristics, gene deletion break points of patients with AS-DL, and the pathogenesis of AS-DL. It was found that the proportion of *de novo* mutations of AS-DL was significantly higher in female probands than male probands (78 vs. 44%). Female patients with AS-DL had a mild clinical presentation. The incidence of proteinuria and ocular abnormalities was much lower in female probands than in male probands, and there was generally no sensorineural hearing loss or chronic kidney disease (CKD), which progressed to Stage 3 in female probands. The contiguous deletion of the 5' exons of *COL4A5* and *COL4A6*, with the break point within the intron 3 of *COL4A6*, was the critical genetic defect causing AS-DL. However, the pathogenesis of characteristic deletion of *COL4A6* that contributes to diffuse leiomyomatosis is still unknown. In addition, characteristic contiguous deletion of *COL4A5* and *COL4A6* genes in AS-DL may be related to transposed elements (TEs).

Keywords: X-linked Alport syndrome, diffuse leiomyomatosis, *COL4A5*, *COL4A6*, gene deletion, DNA analysis

OPEN ACCESS

Edited by:
Jia Rao,
Fudan University, China

Reviewed by:
Oliver Gross,
University Medical Center Göttingen, Germany
Wenyan Huang,
Shanghai Jiao Tong University, China

***Correspondence:**
Qing Ye
qingye@zju.edu.cn
Jianhua Mao
maojh88@zju.edu.cn

†*These authors have contributed equally to this work and share first authorship*

Specialty section:
This article was submitted to Nephrology, a section of the journal Frontiers in Medicine

Received: *28 August 2021*
Accepted: *29 September 2021*
Published: *27 October 2021*

Citation:
Zhou X, Wang J, Mao J and Ye Q (2021) Clinical Manifestations of Alport Syndrome-Diffuse Leiomyomatosis Patients With Contiguous Gene Deletions in COL4A6 and COL4A5. Front. Med. 8:766224. doi: 10.3389/fmed.2021.766224

INTRODUCTION

Alport syndrome is a hereditary glomerular disease characterised by hematuria, progressive nephritis, sensorineural hearing loss, and ocular abnormalities (1, 2). AS is mainly caused by mutation of the gene-encoding type IV collagen in the glomerular basement membrane. Abnormal expression of type IV collagen leads to irregular thickening and thinning of glomerular basement membrane (GBM), lamellation and splitting in lamina densa, podocyte disappearance, glomerulosclerosis with extracellular matrix deposition, renal fibrosis, and finally leads to end-stage renal disease (ESRD). Alport syndrome is a heterogeneous disease with three modes of inheritance, including X-linked Alport syndrome (XLAS), autosomal recessive AS (ARAS), and autosomal AS (ADAS). X-linked Alport syndrome (XLAS, OMIM: 301050) is the most common disease form, accounting for about 80–85% (1, 3). Extensive abnormalities of glomerular basement membrane (GBM) in patients with AS were observed under the electron microscope, including

irregular thinning, thickening, and lamellation, and splitting in lamina dense (2). Absence or incomplete expression of type IV collagen α5 chain can be observed in kidney tissue of patients with XLAS. XLAS is caused by mutation of the *COL4A5* gene-encoding type IV collagen α5 chain (4). Mutations include missense mutations, splice site mutations, truncating mutations, and deletion mutations. These mutations are spread throughout the gene without any identified mutational hot spot. *COL4A5* is located on the X chromosome. Therefore, male patients with hemizygous mutation usually have severe clinical manifestations. Female heterozygote carriers may have a wide range of symptoms, from isolated hematuria to ESRD (5).

COL4A6 gene is paired with *COL4A5* head-to-head, located on chromosome Xq22.3, encoding collagen α6 chain, usually expressed in Bowman's capsule, epidermis, and smooth muscle cells (6). Studies have shown that rare XLAS families, patients with contiguous deletion of *COL4A5* gene, and *COL4A6* gene will be associated with diffuse leiomyomatosis (DL). DL is a benign smooth muscle tumour characterised by abnormal proliferation of well-differentiated smooth muscle cells involving the gastrointestinal tract, tracheobronchial, and female reproductive tract (7). Clinical symptoms commonly include progressive dysphagia, vomiting, or dyspepsia; less frequent, retrosternal pains, dyspnea, cough, or weight loss. Alport syndrome-diffuse leiomyomatosis (AS-DL, OMIM: 308940) is a rare variant of the X-linked Alport syndrome. Up to now, it has been reported that about 30 AS-DL families were found to carry a characteristic contiguous deletion of *COL4A5* and *COLA6* (8, 9). However, not all kinds of deletion of the *COLA6* gene will cause DL (10). This study reports an XLAS case with complete *COL4A6* gene deletion. At the same time, through the summary of reported clinical cases and literature review of related basic research results, the break point of the deletion of *COL4A6* gene in patients with AS-DL was identified, and the hypothesis that caused characteristic contiguous deletion of *COL4A5* and *COL4A6* gene and the possible pathogenesis of DL caused by *COL4A6* gene deletion were summarised.

PATIENTS AND METHODS

Subjects and Clinical Assessment

The proband (III-3) in the pedigree was admitted with proteinuria and haematuria to the Department of Nephrology, The Children's Hospital of Zhejiang University School of Medicine. Clinical information of the family members of the patient was collected during interviews; this included age, gender, symptoms, previous history of the disease, and positive test results. Blood samples from the proband and his mother were collected for genetic screening. Written informed consent was obtained from all the participants before enrolment.

DNA Extraction

The manufacturer extracted genomic DNA from 5 ml of peripheral blood collected from the patient with XLAS and his family members using a QIAamp Blood DNA Mini Kit (Qiagen®, Milano, Italy) instructions. DNA concentrations were determined using a NanoDrop spectrophotometer (Thermo Scientific®, Waltham, USA). DNA samples were stored at −20°C until use.

Whole-Exome Sequencing

Array capture was used to enrich relevant human genes (SeqCap EZ Human Exome Library v2.0, Roche®, Basel, Switzerland), sequenced using the Illumina HiSeq 2000 platform (2016 Illumina, Inc. USA).

Filtering Data

The following steps were taken to prioritise high-quality variants: (i) variants within intergenic, intronic, and untranslated regions (UTRs) and synonymous mutations were excluded from downstream analysis; (ii) variants with a quality score below 20 were excluded; (iii) only a conservation score (phyloP) above three based on comparison of humans and 43 vertebrates was considered; (iv) after this prior selection, the remaining genes were filtered by the function. PolyPhen-2 software (http://genetics.bwh.harvard.edu/pph2/) predicted the possible impact of variants. The final set of selected variants was visually inspected using Integrative Genomics Viewer. Previously described polymorphic variants in public data were investigated and compared with the variations found in the exome of the proband. The selected mutations investigated in this study were not found in previous exome sequences (http://evs.gs.washington.edu/EVS/).

Sanger Sequencing Validation

Sanger sequencing was used to confirm next-generation sequencing of all subjects. DNA from the patient and his family members was subjected to PCR analysis. Polyacrylamide gel electrophoresis was used to determine the size of the amplification products, which were purified using a QIA quick PCR purification kit (Qiagen®, Milano, Italy) and then sequenced using both forward and reverse primers with ABI BigDye Terminator Cycle Sequencing Kit v. 3.1 and an ABI PRISM 3730XL Genetic Analyzer (Applied Biosystems®, Foster

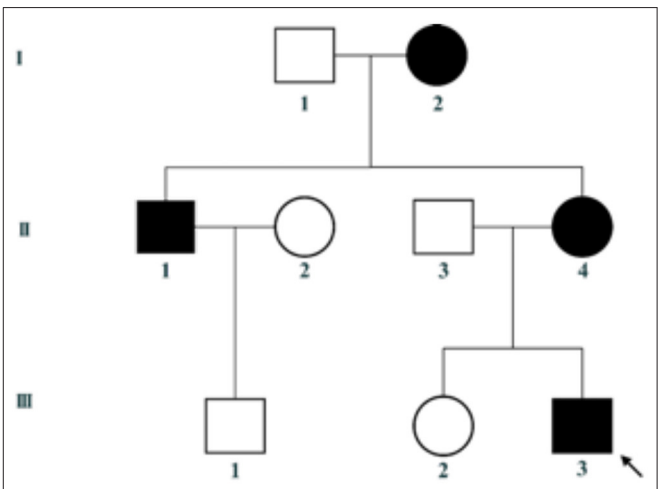

FIGURE 1 | Pedigree of the family. III-3 is the proband.

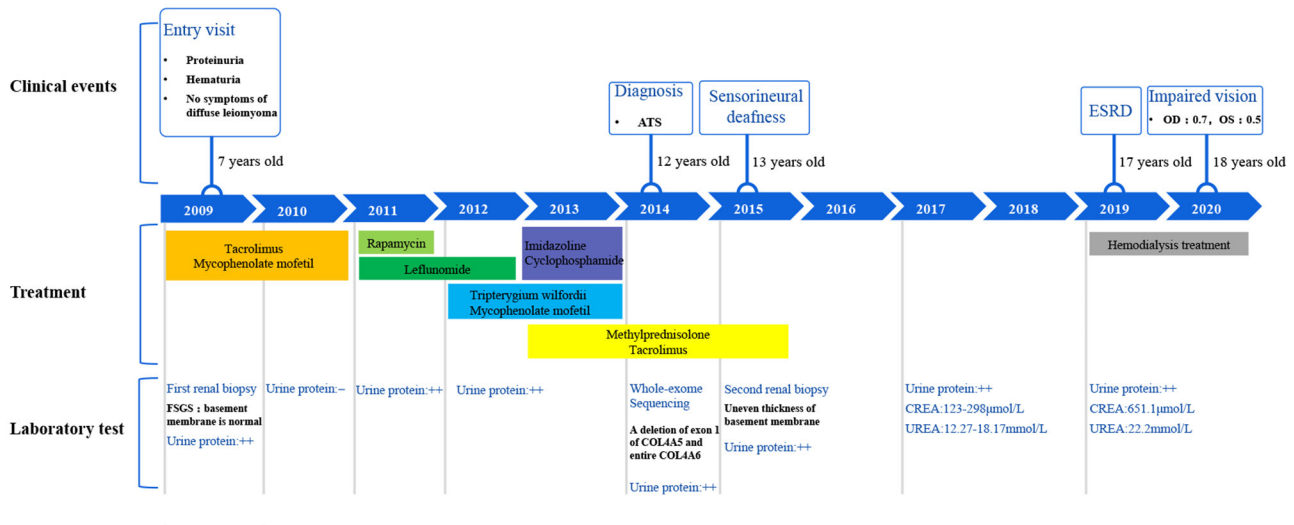

FIGURE 2 | Disease progression of the proband.

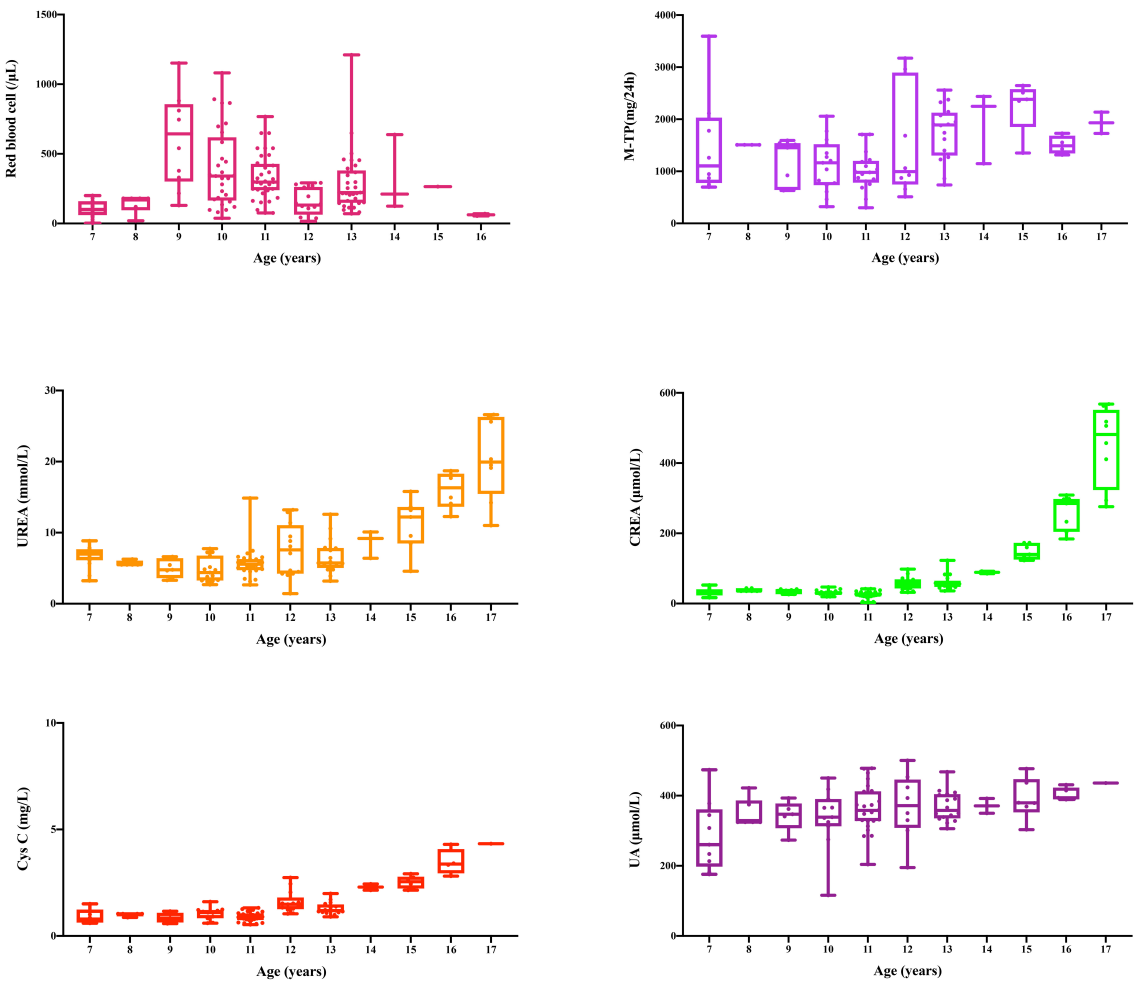

FIGURE 3 | Changes of laboratory indexes during 11 years from diagnosis to progression to uremia.

City, USA). The results were aligned with the reference sequence, and mutations were identified using sequencer software (http://www.genecodes.com). The deletions of the *COL4A5* gene and *COL4A6* gene exons were confirmed by qPCR, PCR, and gel electrophoresis. All primers were designed using the online tool primer 3. The primers of each exon of the *COL4A5* gene and *COL4A6* gene are shown (**Supplementary Table 1**), respectively. The fluorescence quantitative PCR reaction system of *COL4A5* gene exon detection is as follows: 2* KAPA SYBR Fast qPCR Master Mix Universal 10 μl, 10-μM F Primer 0.4 μl, 10-μM R Primer 0.4 μl, DNA templates 1 μl, ROX High 0.4 μl, PCR-grade water 7.8 μl. The reaction system of *COL4A6* gene exon detection is as follows: 5 × buffer A 5 μl, 10-mm dNTP 0.5 μl, 10-m f primer 1.25 μl, 10-m r primer 1.25 μl, DNA templates 1 μl, 0.1 μl DNA polymerase (kapa2g robust hot start PCR kit), 15.9-μl PCR-grade water. PCR cycle conditions: 95°C 3 min, 95°C 3 s, 60°C 30 s, 40 cycles.

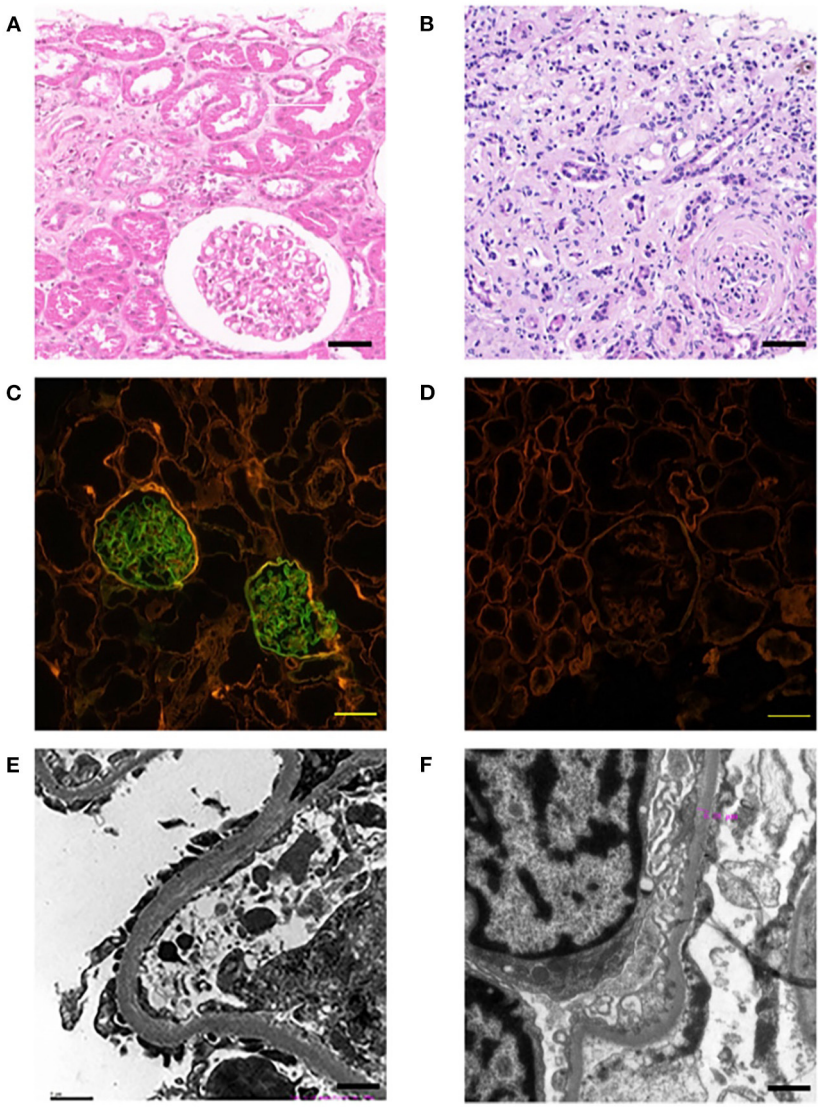

FIGURE 4 | Pathological examination results of probands. The left panel **(A,C,E)** show the results of the first renal biopsy (March 10, 2009), and the right panel **(B,D,F)** show the results of the second renal biopsy (August 28, 2015). **(A)** HE staining is characterised by FSGS. Scale bars, 100 μm. **(B)** HE staining is characterised by AS. Scale bars, 100 μm. **(C)** Immunofluorescence staining of α5 chain (IV) showed that the expression of α5 chain was normal; the immunofluorescence staining was positive, which emitted bright green fluorescence by a confocal laser scanning microscope. Scale bars, 20 μm. **(D)** Immunofluorescence staining of α5 chain (IV) showed the absence expression of α5 chain; the immunofluorescence staining was negative, which showed no emitted bright green fluorescence by a confocal laser scanning microscope. Scale bars, 20 μm. **(E)** The electron microscope examination showed that the basement membrane was normal. Scale bars, 1 μm. **(F)** The electron microscope examination showed that the glomerular basement membrane was uneven in thickness, about 200–500 nm. Scale bars, 1 μm.

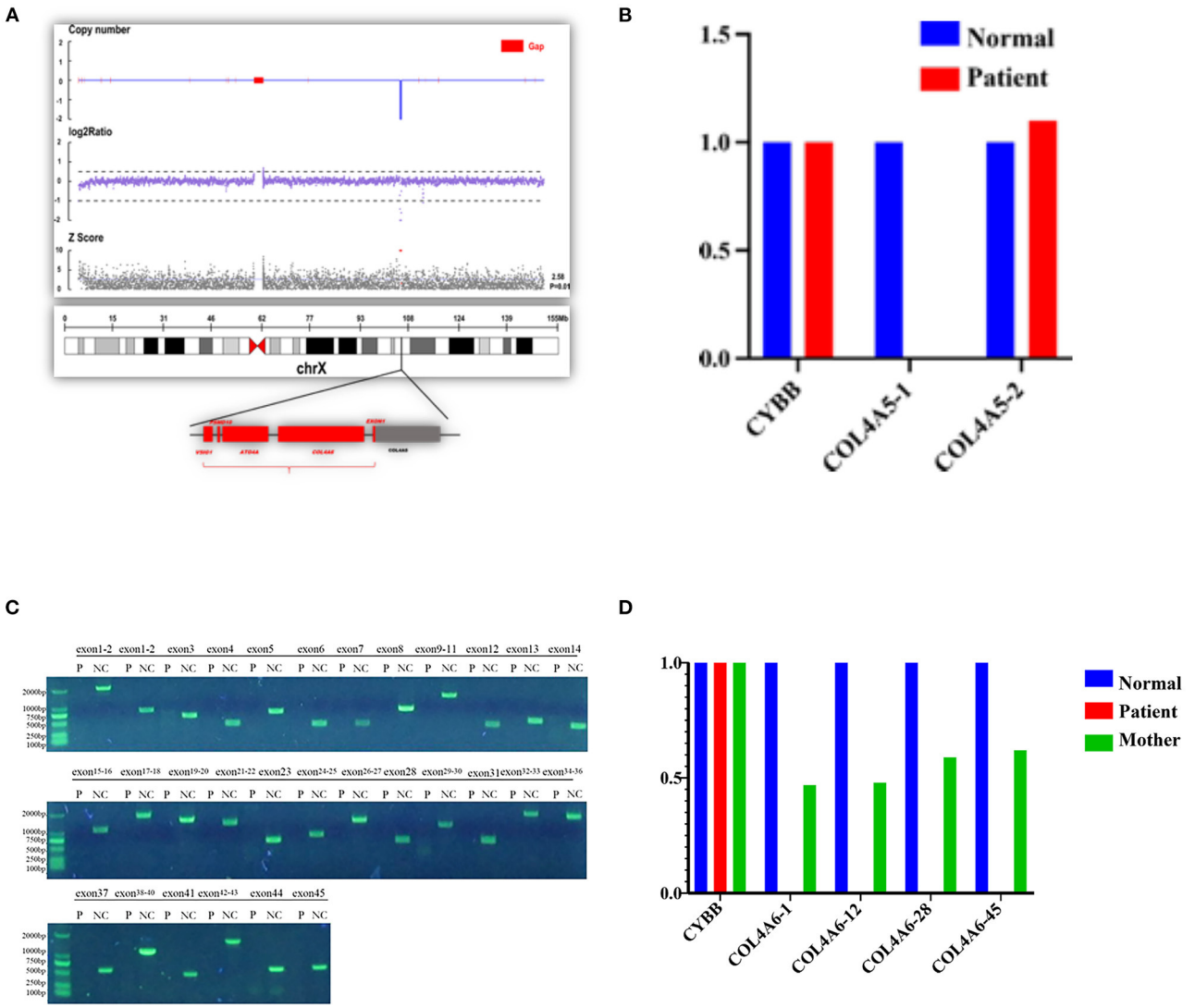

FIGURE 5 | Contiguous gene deletion of *COL4A5* and *COL4A6* in the AS case we reported. **(A)** Whole exon sequencing showed that the *COL4A5-COL4A6* gene was contiguously deleted on the X chromosome of the proband. **(B)** qPCR verification of the exon deletion break point of *COL4A5* gene of the proband. The first exon of the *COL4A5* gene was deleted, and the copy of the second exon was normal. **(C)** Verification of the exon deletion break point of *COL4A6* gene of the proband. Amplifying each exon for the electrophoresis result of PCR in the same group of the normal control sample and the proband sample of the *COL4A6* gene. The fragment size is 1,986 bp, 643 bp, 1,560 bp, 376 bp, 714 bp, 1,354 bp, 568 bp, 796 bp, 1,402 bp, 383 bp, 509 bp, 466 bp, 1,078 bp, 1,776 bp, 1,473 bp, 1,278 bp, and 611 bp. The amplification results of control genes of the proband and normal control samples have obvious specific bands, and the product length is consistent with the design length. It is suggested that the proband *COL4A6* gene may be homozygous deletion. **(D)** qPCR verification of the exon deletion break point of *COL4A6* gene of the proband and mother of the proband. The normal control samples, proband samples, and maternal samples were detected by fluorescence quantitative PCR in the same group, and the copy numbers of exons 1, 12, 28, and 45 (represented by *COL4A6*-1, *COL4A6*-12, *COL4A6*-28, and *COL4A6*-45, respectively) of the target gene were detected by using ALB gene as internal reference gene. The results showed that the *COL4A6* gene of the proband had no amplification signal. That is, no copy of the gene was detected. The ratio of the copy number of each exon of the *COL4A6* gene in the maternal sample to the normal control is about 0.5, suggesting that the proband has a homozygous deletion of the *COL4A6* gene and the maternal sample has heterozygous deletion.

RESULT

An XLAS Family With Contiguous Deletion of the *COL4A5* and *COL4A6*

This family includes an 18-year-old male proband (III-1), his mother (II4), his maternal uncle (II1), and maternal grandmother (I2) (**Figure 1**). This study recorded the progress of the disease (**Figure 2**) and the changes in the laboratory evaluation of the renal function of the proband (**Figure 3**). Urinary abnormalities include proteinuria and hematuria, were detected in the proband at the age of 7 and diagnosed as focal segmental glomerular sclerosis (FSGS) based on the first renal biopsy. The immunofluorescence staining showed normal expression of α5 chain, which was positive in GBM, and the

electron microscopic analysis revealed diffuse fusion of the foot process, normal thickness of basement membrane, and an increased mesangial matrix of GBM of the proband (**Figure 4**). The therapeutic regimen of mycophenolate mofetil (MMF) and tacrolimus (TAC) was used to treat FSGS in the proband from 2009 to 2010. Urine protein turned negative in 2010 when the proband was 8 years old. However, urine protein turned positive in 2011, and repeated use of various immuno suppressants was ineffective. At age 13, he was diagnosed with XLAS based on genetic analysis, typical immunofluorescence staining, and electron microscope findings on a second renal biopsy. The immunofluorescence staining showed negative expression of α5 chain, and the electron microscopic analysis showed irregular thickening of the GBM, with splitting and fragmentation of the lamina densa (**Figure 4**). High-frequency sensorineural hearing loss was diagnosed at the same age. The proband reached ESRD at 17 years old. Ocular abnormalities (OD: 0.7, OS: 0.5) have been presented since the proband was 18 years old. The proband has no symptoms that might be suggestive of DL as he was never reported a history of gastrointestinal or tracheobronchial symptoms, such as dysphagia, postprandial vomiting, retrosternal or epigastric pain, recurrent bronchitis, dyspnea, cough, and stridor. In addition, the mother of the proband, diagnosed with XLAS, has had proteinuria and hypertension since 15 years old. In addition, his mother has no evidence of CKD and DL. The maternal grandmother of the proband has transient (intermittent) proteinuria and no evidence of CKD and DL. The maternal uncle of the proband presented with urinary abnormalities and eventually reached ESRD at age 27 years. The maternal uncle of the proband also shows no DL symptoms.

In order to identify a molecular cause underlying the clinical features of the patient, a genetic analysis of the proband and his mother was conducted. The deletion of entire exons of *COL4A6* and exon 1 of *COL4A5* was detected in the proband by whole-exome sequencing and confirmed by PCR. Genetic testing of blood DNA from the mother of the proband also showed the heterozygous deletion of all exons of *COL4A6* and exon 1 of *COL4A5* (**Figure 5**). The father of the proband did not have AS symptoms and carry the mutation of *COL4A5* or *COL4A6*. Co-segregation was observed in this family.

Clinical Phenotypes of AS-DL Probands With Contiguous Deletion of the *COL4A5* and *COL4A6*

Totaling 15 relevant references were identified by searching the database of PubMed to analyse the clinical characteristics and gene deletion break points of patients with AS-DL (**Table 1** and **Figures 6A–C**). Thirty-one probands had been retrieved, including 11 females and 20 male probands whose ratio of males to females is 1:.55. The initial clinical manifestation related to AS-DL appeared in early childhood, with a median age of 3 years and a general age of no more than 13 years. Among them, the median age of the male proband who had an initial clinical manifestation of AS-DL was 3 years old, while that of the female proband was later, with a median age of 6 years old. Many AS-DL probands have a family history. However, about 56% of probands were *de novo*. The DL of these probands occurred before the age of 25, and the median age of developing DL was 9 years old. There is no significant difference in the occurrence time of DL between different sexes. Among them, the median age of the male proband developing DL was 9.5 years old, and that of female patients was 9 years old. All probands analysed in the article were diagnosed with oesophageal leiomyomas. Oesophagus leiomyomas are a constant finding in families with AS-DL, the initial clinical manifestation in most patients. A few probands were diagnosed as rectal involvement by DL. Only a few probands had respiratory symptoms (dyspnea, wheezing, asthma, and bronchitis). In addition, several female probands had genital leiomyomas with diffuse clitoral and vulvar hypertrophy. Except for DL, the incidence of other clinical symptoms in patients with AS-DL from high to low was hematuria, proteinuria, sensorineural hearing loss, and ocular abnormalities. Hematuria was one of the most common clinical manifestations, which usually occurs earlier, and the incidence of male probands was higher than that of female probands. Hematuria occurred in 97% of patients and was observed in all these male probands. The median onset age of hematuria was 4.5 years. About 91% of female probands also developed hematuria, and their median age of hematuria was 3 years old. Proteinuria was also very common in these probands. About 59% of probands have proteinuria, among which the incidence of proteinuria in male probands was 68%, while that in female probands was about 40%. There was no difference in the median age of proteinuria between male and female probands, and all were 6 years old.

Sensorineural hearing loss usually occurs in older children. About 41% of the probands were found to have sensorineural hearing loss, and they were all male patients with a median age of 11 years. The most common ocular abnormality of probands was cataracts, and there were a few cases with posterior polymorphous corneal dystrophy and retinopathy with severe symptoms. The incidence of ocular abnormalities was 41%; among which, about 50% of male probands and 18% of female probands had ocular abnormalities. The median age of male probands with ocular abnormalities was 6 years old, while female probands had no record of onset age. Of these probands, 34% have advanced to Stage III or above of chronic kidney disease. All of them were male. The median age of occurrence was 25 years old. DL is not specifically associated with the progression of the disease. AS-DL probands have different clinical phenotypes. The most common clinical manifestations were hematuria, proteinuria, and diffuse leiomyoma, accounting for 17%. Second, hematuria and diffuse leiomyoma accounted for 14%. refer to the following figure for more information (**Figures 6D–F**).

In conclusion, the proportion of *de novo* mutations in AS-DL was significantly higher in female probands than in male probands (78 vs. 44%). The clinical manifestations of AS-DL in female probands were relatively few and mild. The incidence of proteinuria and ocular abnormalities was much lower than in male probands, and there was generally no hearing loss or progression to CKD Stage 3.

Probands with AS-DL were found to carry the contiguous deletion of the 5′ exons of *COL4A5* and *COL4A6*, with the break

TABLE 1 | Clinical and genetic characterisation of patients with Alport syndrome–diffuse leiomyomatosis.

Proband	Gender	Age (onset of symptoms)	Age	Phenotype							GBM	Intron deletion	Genotype Deletion		*de novo*	References
				Hematuria	Proteinuria	Hypertension	≥CKD stage3	Diffuse leiomyo-matosis	Hearing loss	Ocular abnormalities			*COL4A5*	*COL4A6*		
1	M	6	19	+(6)	–	–	+	+(8)	–	–	+	Del int.1[*COL4A5*]~del int.2[*COL4A6*]	EX.1	EX.1_2	Y	(11)
2	M	6	30	+(6)	–	–	+(16)	+(21)	+ (24)	+ (21)	+	Del int.1[*COL4A5*]~del int.2[*COL4A6*]	EX.1	EX.1_2	NA	(12)
3	M	11	29	+(11)	–	–	+(25)	+(17)	+(>20)	+(>20)	+	Del int.1[*COL4A5*]~del int.2[*COL4A6*]	EX.1	EX.1_2	N	(12)
4	F	10	13	+(10)	+(10)	–	–	+(10)	–	–	+	Del int.1[*COL4A5*]~del int.2[*COL4A6*]	EX.1	EX.1_2	Y	(13)
5	F	9	23	–	–	–	–	+(9)	–	–	+	Del int.1[*COL4A5*]~del int.2[*COL4A6*]	EX.1	EX.1_2	NA	(14)
6	M	2	26	+(2)	+(7)	+	+	+(25)	+(6)	+(26)	+	Del Int.2~int.51[*COL4A5*]	EX.2–51	/	N	(10)
7	M	13	15	+(15)	+(15)	–	+(15)	+(13)	–	–	+	Del int.1[*COL4A5*]~del int.2[*COL4A6*]	EX.1	EX.1_2	N	(15)
8	M	7	10	+(7)	+(9)	–	–	+(9)	–	–	+	Del int.1[*COL4A5*]~del int.2[*COL4A6*]	EX.1	EX.1_2	Y	(16)
9	F	3	11	+(3)	+(6)	–	–	+(7)	–	–	+	Del int.1[*COL4A5*]~del int.2[*COL4A6*]	EX.1	EX.1_2	N	(16)
10	F	1	15	+(1)	+(3)	–	–	+(6)	–	–	+	Del int.36[*COL4A5*]~del int.2[*COL4A6*]	EX.1_36	EX.1_2	Y	(16)
11	M	1	10	+(1)	+(5)	–	–	+(10)	+	–	+	Del int.4[*COL4A5*]~del int.2[*COL4A6*]	EX.1_4	EX.1_2	N	(16)
12	M	5	38	+(5)	+(5)	–	ESRD (30)	+(11)	+	–	+	Del int.1[*COL4A5*]~del int.2[*COL4A6*]	EX.1	EX.1_2	N	(16)
13	M	5	25	+(11)	–	–	ESRD (25)	+(5)	+	–	+	/	EX.1	EX.1–2	NA	(17)
14	M	2	16	+(20)	–	–	–	+(12)	+	–	+	/	EX.1	EX.1–2	NA	(17)
15	M	13	40	+	+	–	ESRD(40)	+(13)	+	+	+	/	EX.1	EX.1–2	N	(18)
16	M	3	20	+(4)	+	–	+	+(3)	+(6)	–	+	/	EX.1–36	EX.1–2	Y	(19)
17	M	<11	33	+	+	–	–	+(14)	+(11)	+(11)	+	/	EX.1	EX.1–2	N	(19)
18	M	<1	9	+(2)	–	–	–	+(<1)	+(9)	–	+	/	EX.1–7	EX.1–2	Y	(20)
19	F	9	25	+	–	–	–	+(9)	–	+	+	/	EX.1	EX.1–2	Y	(21)
20	M	1	1	+(1)	+(1)	–	–	+(1)	–	+(1)	+	/	EX.1	EX.1–2	N	(22)
21	F	NA	NA	+	–	–	–	+	–	–	NA	/	EX.1	EX.1–2	Y	(23)
22	F	NA	NA	+	–	–	–	+	–	–	NA	/	EX.1	EX.1–2	Y	(23)

(Continued)

TABLE 1 | Continued

Proband	Gender	Age (onset of symptoms)	Age	Phenotype					GBM	Intron deletion	Genotype Deletion		*de novo*	References
				Hematuria	Proteinuria	Hypertension	≥CKD stage3	Diffuse leiomyomatosis	Hearing loss	Ocular abnormalities			*COL4A5* *COL4A6*	
23	F	NA	NA	+	–	–	–	+	–	–	NA	/	EX.1–30 EX.1–2	Y	(23)
24	F	NA	NA	+	–	–	–	+	–	–	NA	/	EX.1–2 EX.1–2	Y	(23)
25	M	3	24	+(3)	+	–	ESRD (16)	+(6)	–	+(6)	+	/	EX.1–3 EX.1–2	Y	(24)
26	M	2	7	+(2)	+(7)	–	–	+(7)	–	+(4)	+	/	EX.1 EX.1–2	Y	(24)
27	M	1	17	+(1)	+(4)	–	–	+(9)	+(17)	+(2)	+	/	EX.1 EX.1–2	N	(24)
28	M	NA	NA	+	NA	NA	NA	+	NA	–	NA	/	EX.1–2 EX.1–2	NA	(24)
29	M	1	14	+	+	–	–	+	–	+(1)	+	/	EX.1 EX.1–2	Y	(24)
30	F	2	5	+	+	–	–	+	–	–	+	/	EX.1 EX.1–2	N	(24)
31	F	NA	NA	+	NA	NA	NA	+	NA	+	NA	/	EX.1 EX.1–2	NA	(24)

GBM, glomerular basement membrane; CKD, chronic kidney disease; F, female; M, male; Del, deletion; NA, data not available; Y, yes; N, no; EX, exon; age at the onset of the phenotype was placed in parentheses.

point located within the intron 3 of *COL4A6*. All of them include the 4.2 kb critical region, containing exon 1 of *COL4A5*, exons 1', 1, and 2 of *COL4A6*, and the common promoter region that regulates the expression of the two adjacent genes.

DISCUSSION

All of the AS-DL families have been found to have a contiguous deletion of 5' exons of *COL4A5* and *COL4A6*. All of them contain 4.2 kb critical regions starting from intron 2 of *COL4A6* and ending at intron 1 of *COL4A5*. At present, all reported cases show that the deletion of exon 1 and exon 2 of the *COL4A6* gene will be affected by DL (10–26) (**Figure 7A**). When the deletion break point of the *COL4A6* gene extends to exon 3, most cases will not be affected by DL. However, in 2011, a case of AS-DL detected with deletion of the *COL4A6* gene extended into intron 3 was reported (19). No AS-DL case was reported with the contiguous deletion of *COL4A5-COL4A6* extended to the exon 4 of *COL4A6* or the whole *COL4A6* gene. Therefore, the break point of the deletion that can cause DL is located in intron 3 of the *COL4A6* gene. Contiguous *COL4A5* and *COL4A6* deletions extending upstream beyond exon 4 of *COL4A6*, or encompassing the entire *COL4A5* and *COL4A6* genes, or deletion mutations involving only *COL4A5*, were identified in patients with X-linked AS, who did not develop DL. In addition, mutation only in *COL4A6* has not been found in patients with AS-DL. However, the report in 2013 mentioned that a *COL4A5* deletion spanning exons 2 through 51, extending distally beyond *COL4A5* but proximally not into *COL4A6*, was detected in an AS-DL family, which segregated with the disease phenotype. The report mentioned that deletion of the 5′ exons of *COL4A6* is not needed to develop diffuse leiomyomatosis in patients with Alport syndrome, contrary to the recognised gene deletion characteristics of patients with AS-DL. However, the author did not detect the α6 (IV) collagen chain. It is impossible to determine whether the *COL4A6* gene is typically expressed (10).

The mechanism of leiomyoma caused by *COL4A6* deletion is not completely clear (**Figure 7B**). A hypothesis is that the partially deleted *COL4A6* gene expresses a truncated α6 (IV) chain, which leads to leiomyoma. However, the α6 (IV) collagen chain was not detected in the basement membrane of oesophageal leiomyoma resected from patients with AS-DL (27). The truncated α6 (IV) chain was absent in leiomyoma, so the truncated α6 (IV) chain may not be related to leiomyoma formation. In the X-AS canine model, the *COL4A5* gene carries unintentional point mutation, and the α6 (IV) chain cannot be assembled with an abnormal α5 (IV) chain to form a heterotrimerand express in the smooth muscle basement membrane. This study found that there was no leiomyoma in dogs lacking the α6 (IV) chain, which shows that the absence of the α6 (IV) chain or the absence of the α6 (IV) chain combined α5 (IV) chain cannot be the primary cause of DL. Therefore, there may be other mechanisms leading to DL (28). Deletion of a 4.2 kb minimal overlap region extending from intron 2 of *COL4A6* and intron 1 of *COL4A5* was observed in all patients with AS-DL. Another hypothesis is that a silencing element

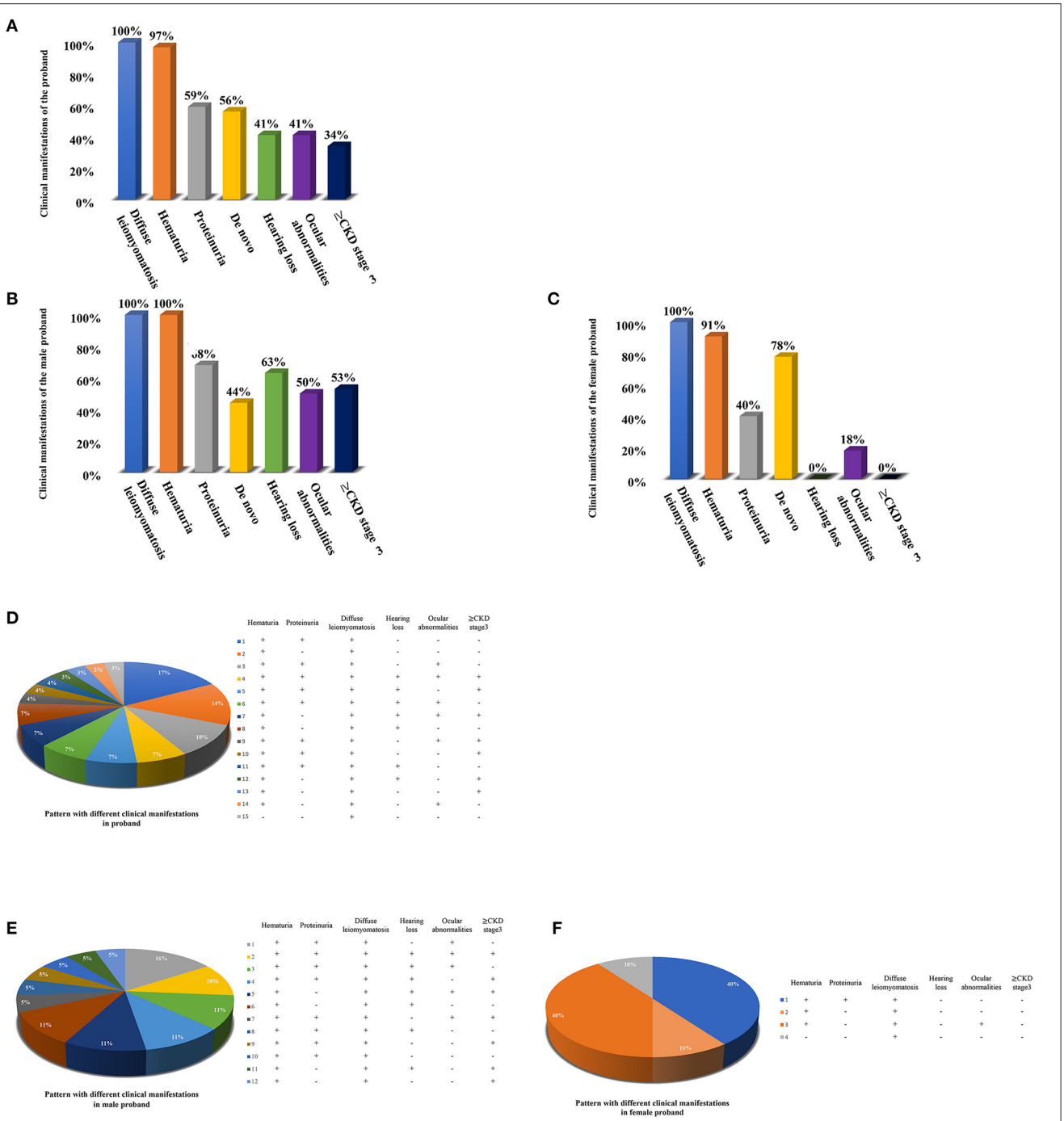

FIGURE 6 | Clinical manifestations of the AS-DL proband and the pattern with different clinical manifestations. **(A)** Clinical manifestations of the total AS-DL proband. **(B)** Clinical manifestations of the male AS-DL proband. **(C)** Clinical manifestations of the female AS-DL proband. **(D)** The pattern with different clinical manifestations. **(E)** The pattern with different clinical manifestations in male probands. **(F)** The pattern with different clinical manifestations in female probands.

in this critical region may include a kind of microRNA and inhibit the expression of genes related to DL. Loss of this critical region contributes to the overgrowth of smooth muscle cells. However, patients with complete *COL4A6* deletion do not show DL, which contradicts this hypothesis. Alternatively, the 4.2-kb region may act as an insulator that protects against smooth muscle overgrowth afforded by inhibiting the distal enhancers and/or neighbouring genes. This deletion may activate a specific enhancer, which leads to smooth muscle cell overgrowth. The enhancer may locate in the undeleted part of intron 3 of *COL4A6*, which is consistent with the phenomenon that patients only show AS without DL when there is deletion extended to exon 4 of

COL4A6. In addition, IRS4, a neighbouring gene of *COL4A5*, is also considered a candidate gene that may be activated (13). *IRS4* is connected with various growth factor receptors with tyrosine kinase activity (such as insulin receptor, IGF1R, and FGFR1) and a complex intracellular signal molecular network containing the SH2 domain. This molecular network plays an essential role in cell growth and proliferation. In addition, the α5 (IV) collagen chain has many binding sites of extracellular matrix (ECM) components; it also interacts with various integrin and non-integrin cell receptors. It is also possible that the absence of α5 (IV) chain or existence of abnormal α5 (IV) chain in the basement membrane leads to changes in the structure or function of other ECM components and/or cell surface receptors, thus leading to the overgrowth of smooth muscle cells (10, 29). However, these assumptions are not entirely satisfactory. The molecular mechanism of AS associated with DL remains to be clarified.

Another interesting question is, why are gene deletions in patients with XLAS concentrated at the junction of *COL4A5* and *COL4A6*? Other studies suggest that transposed elements (TEs) may play an essential role in the contiguous deletion of *COL4A5* and *COL4A6*. Transposed elements can provide new exons, genes, and regulatory sequences that greatly influence exon-intron structure formation and regulation of gene expression. Studies have found that the number of break points in TEs appears to be higher than expected of the general number of TEs of the genomic sequences of *COL4A6* and *COL4A5*. Therefore, TEs may promote the occurrence of non-allelic homologous recombination events, including AS-DL (12, 16, 30).

To sum up, this study reports an XLAS proband with deletion of the complete *COL4A6* gene and exon 1 of *COL4A5*. This case expanded the knowledge of genotype-phenotype correlations of AS. It is worth noting that according to the genotype-phenotype correlations in AS-DL, any woman with manifestations suggestive of DL but does not have any clinical or laboratory evidence of kidney disease should be considered for AS-DL diagnosis as male offspring are at risk for AS-DL. Since the pathogenesis of AS-DL is still unclear, further studies are needed to explore the pathogenesis.

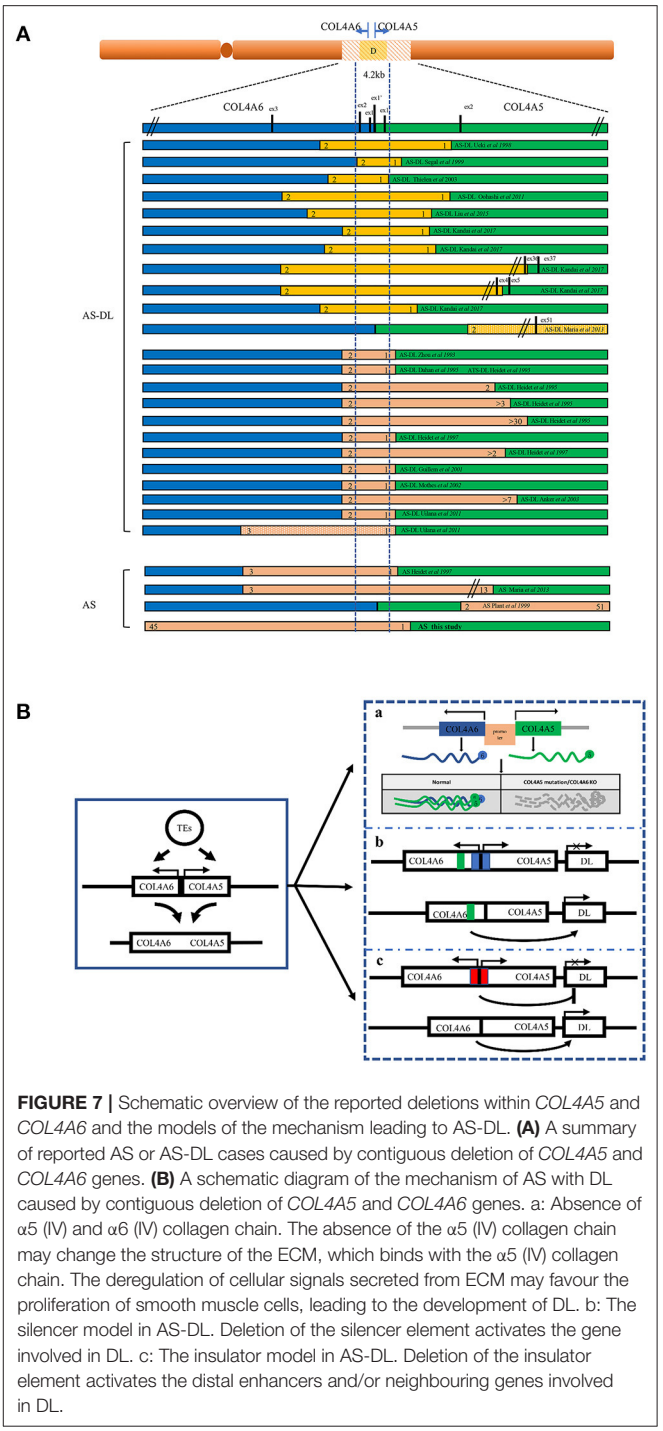

FIGURE 7 | Schematic overview of the reported deletions within *COL4A5* and *COL4A6* and the models of the mechanism leading to AS-DL. **(A)** A summary of reported AS or AS-DL cases caused by contiguous deletion of *COL4A5* and *COL4A6* genes. **(B)** A schematic diagram of the mechanism of AS with DL caused by contiguous deletion of *COL4A5* and *COL4A6* genes. a: Absence of α5 (IV) and α6 (IV) collagen chain. The absence of the α5 (IV) collagen chain may change the structure of the ECM, which binds with the α5 (IV) collagen chain. The deregulation of cellular signals secreted from ECM may favour the proliferation of smooth muscle cells, leading to the development of DL. b: The silencer model in AS-DL. Deletion of the silencer element activates the gene involved in DL. c: The insulator model in AS-DL. Deletion of the insulator element activates the distal enhancers and/or neighbouring genes involved in DL.

DATA AVAILABILITY STATEMENT

The original contributions presented in the study are publicly available. This data can be found at: https://www.ncbi.nlm.nih.gov/sra/, PRJNA759552.

ETHICS STATEMENT

The studies involving human participants were reviewed and approved by the Children's Hospital, Zhejiang University School of Medicine Ethics Committee. Written informed consent to participate in this study was provided by the participants' legal guardian/next of kin. Written informed consent was obtained from the individual(s), and minor(s)' legal guardian/next of kin, for the publication of any potentially identifiable images or data included in this article.

AUTHOR CONTRIBUTIONS

XZ drafted the initial manuscript and contributed to manuscript editing. JW collected the data from patients and contributed to manuscript editing. QY and JM devised the conceptual ideas, contributed to the discussion and interpretation of the results,

and reviewed the final manuscript. All authors approved the final manuscript.

FUNDING

This study was supported by the Key Project of Provincial Ministry Co-construction, Health Science, and Technology Project Plan of Zhejiang Province (WKJ-ZJ-2128), Key Laboratory of Women's Reproductive Health Research of Zhejiang Province (No. ZDFY2020-RH-0006), the National Natural Science Foundation of China (Grant/Award No: U20A20351), and Key Research and Development Plan of Zhejiang Province (Grant/Award No: 2021C03079).

ACKNOWLEDGMENTS

We are grateful to all the patients and their families and the help of all the physicians in the course of the medical treatment. We want to thank the support of the Zhejiang Provincial Key Laboratory of Immunity and Inflammatory Diseases.

SUPPLEMENTARY MATERIAL

The Supplementary Material for this article can be found online at: https://www.frontiersin.org/articles/10.3389/fmed.2021.766224/full#supplementary-material

REFERENCES

1. Williamson DA. Alport's syndrome of hereditary nephritis with deafness. *Lancet.* (1961) 2:1321–3. doi: 10.1016/S0140-6736(61)90899-6
2. Kruegel J, Rubel D, Gross O. Alport syndrome–insights from basic and clinical research. *Nat Rev Nephrol.* (2013) 9:170–8. doi: 10.1038/nrneph.2012.259
3. Flinter FA, Cameron JS, Chantler C, Houston I, Bobrow M. Genetics of classic Alport's syndrome. *Lancet.* (1988) 2:1005–7. doi: 10.1016/S0140-6736(88)90753-2
4. Barker DF, Hostikka SL, Zhou J, Chow LT, Oliphant AR, Gerken SC, et al. Identification of mutations in the COL4A5 collagen gene in Alport syndrome. *Science.* (1990) 248:1224–7. doi: 10.1126/science.2349482
5. Temme J, Peters F, Lange K, Pirson Y, Heidet L, Torra R, et al. Incidence of renal failure and nephroprotection by RAAS inhibition in heterozygous carriers of X-chromosomal and autosomal recessive Alport mutations. *Kidney Int.* (2012) 81:779–83. doi: 10.1038/ki.2011.452
6. Khoshnoodi J, Pedchenko V, Hudson BG. Mammalian collagen IV. *Microsc Res Tech.* (2008) 71:357–70. doi: 10.1002/jemt.20564
7. Garcia Torres R, Guarner V. Leiomyomatosis of the esophagus, tracheobronchi and genitals associated with Alport type hereditary nephropathy: a new syndrome. *Rev Gastroenterol Mex.* (1983) 48:163–70.
8. Zhang X, Zhou J, Reeders ST, Tryggvason K. Structure of the human type IV collagen COL4A6 gene, which is mutated in Alport syndrome-associated leiomyomatosis. *Genomics.* (1996) 33:473–9. doi: 10.1006/geno.1996.0222
9. Miner JH. Alport syndrome with diffuse leiomyomatosis. When and when not? *Am J Pathol.* (1999) 154:1633–5. doi: 10.1016/S0002-9440(10)65417-X
10. Sa MJ, Fieremans N, de Brouwer AP, Sousa R, e Costa FT, Brito MJ, et al. Deletion of the 5'exons of COL4A6 is not needed for the development of diffuse leiomyomatosis in patients with Alport syndrome. *J Med Genet.* (2013) 50:745–53. doi: 10.1136/jmedgenet-2013-101670
11. Ueki Y, Naito I, Oohashi T, Sugimoto M, Seki T, Yoshioka H, et al. Topoisomerase I and II consensus sequences in a 17-kb deletion junction of the COL4A5 and COL4A6 genes and immunohistochemical analysis of esophageal leiomyomatosis associated with Alport syndrome. *Am J Hum Genet.* (1998) 62:253–61. doi: 10.1086/301703
12. Segal Y, Peissel B, Renieri A, de Marchi M, Ballabio A, Pei Y, et al. LINE-1 elements at the sites of molecular rearrangements in Alport syndrome-diffuse leiomyomatosis. *Am J Hum Genet.* (1999) 64:62–9. doi: 10.1086/302213
13. Thielen BK, Barker DF, Nelson RD, Zhou J, Kren SM, Segal Y. Deletion mapping in Alport syndrome and Alport syndrome-diffuse leiomyomatosis reveals potential mechanisms of visceral smooth muscle overgrowth. *Hum Mutat.* (2003) 22:419. doi: 10.1002/humu.9191
14. Oohashi T, Naito I, Ueki Y, Yamatsuji T, Permpoon R, Tanaka N, et al. Clonal overgrowth of esophageal smooth muscle cells in diffuse leiomyomatosis-Alport syndrome caused by partial deletion in COL4A5 and COL4A6 genes. *Matrix Biol.* (2011) 30:3–8. doi: 10.1016/j.matbio.2010.09.003
15. Liu W, Wong JK, He Q, Wong EH, Tang CS, Zhang R, et al. Chinese family with diffuse oesophageal leiomyomatosis: a new COL4A5/COL4A6 deletion and a case of gonosomal mosaicism. *BMC Med Genet.* (2015) 16:49. doi: 10.1186/s12881-015-0189-7
16. Nozu K, Minamikawa S, Yamada S, Oka M, Yanagita M, Morisada N, et al. Characterization of contiguous gene deletions in COL4A6 and COL4A5 in Alport syndrome-diffuse leiomyomatosis. *J Hum Genet.* (2017) 62:733–5. doi: 10.1038/jhg.2017.28
17. Dahan K, Heidet L, Zhou J, Mettler G, Leppig KA, Proesmans W, et al. Smooth muscle tumors associated with X-linked Alport syndrome: carrier detection in females. *Kidney Int.* (1995) 48:1900–6. doi: 10.1038/ki.1995.489
18. Mothes H, Heidet L, Arrondel C, Richter KK, Thiele M, Patzer L, et al. Alport syndrome associated with diffuse leiomyomatosis: COL4A5-COL4A6 deletion associated with a mild form of Alport nephropathy. *Nephrol Dial Transplant.* (2002) 17:70–4. doi: 10.1093/ndt/17.1.70
19. Uliana V, Marcocci E, Mucciolo M, Meloni I, Izzi C, Manno C, et al. Alport syndrome and leiomyomatosis: the first deletion extending beyond COL4A6 intron 2. *Pediatr Nephrol.* (2011) 26:717–24. doi: 10.1007/s00467-010-1693-9
20. Anker MC, Arnemann J, Neumann K, Ahrens P, Schmidt H, Konig R. Alport syndrome with diffuse leiomyomatosis. *Am J Med Genet A.* (2003) 119A:381–5. doi: 10.1002/ajmg.a.20019
21. Guillem P, Delcambre F, Cohen-Solal L, Triboulet JP, Antignac C, Heidet L, et al. Diffuse esophageal leiomyomatosis with perirectal involvement mimicking Hirschsprung disease. *Gastroenterology.* (2001) 120:216–20. doi: 10.1053/gast.2001.20883
22. Sugimoto K, Yanagida H, Yagi K, Kuwajima H, Okada M, Takemura T, et al. Japanese family with Alport syndrome associated with esophageal leiomyomatosis: genetic analysis of COL4A5 to COL4A6 and immunostaining for type IV collagen subtypes. *Clin Nephrol.* (2005) 64:144–50. doi: 10.5414/CNP64144
23. Heidet L, Cohen-Solal L, Boye E, Thorner P, Kemper MJ, David A, et al. Novel COL4A5/COL4A6 deletions and further characterization of the diffuse leiomyomatosis-Alport syndrome (DL-AS) locus define the DL critical region. *Cytogenet Cell Genet.* (1997) 78:240–6. doi: 10.1159/000134666
24. Heidet L, Dahan K, Zhou J, Xu Z, Cochat P, Gould JD, et al. Deletions of both alpha 5(IV) and alpha 6(IV) collagen genes in Alport syndrome and in Alport syndrome associated with smooth muscle tumours. *Hum Mol Genet.* (1995) 4:99–108. doi: 10.1093/hmg/4.1.99
25. Renieri A, Bassi MT, Galli L, Zhou J, Giani M, De Marchi M, et al. Deletion spanning the 5' ends of both the COL4A5 and COL4A6 genes in a patient with Alport's syndrome and leiomyomatosis. *Hum Mutat.* (1994) 4:195–8. doi: 10.1002/humu.1380040304
26. Heiskari N, Zhang X, Zhou J, Leinonen A, Barker D, Gregory M, et al. Identification of 17 mutations in ten exons in the COL4A5 collagen gene, but no mutations found in four exons in COL4A6: a study of 250 patients with hematuria and suspected of having Alport syndrome. *J Am Soc Nephrol.* (1996) 7:702–9. doi: 10.1681/ASN.V75702
27. Heidet L, Cai Y, Sado Y, Ninomiya Y, Thorner P, Guicharnaud L, et al. Diffuse leiomyomatosis associated with X-linked Alport syndrome: extracellular matrix study using immunohistochemistry and in situ hybridization. *Lab Invest.* (1997) 76:233–43.

28. Zheng K, Harvey S, Sado Y, Naito I, Ninomiya Y, Jacobs R, et al. Absence of the alpha6(IV) chain of collagen type IV in Alport syndrome is related to a failure at the protein assembly level and does not result in diffuse leiomyomatosis. *Am J Pathol.* (1999) 154:1883–91. doi: 10.1016/S0002-9440(10)65446-6
29. Heidet L, Boye E, Cai Y, Sado Y, Zhang X, Flejou JF, et al. Somatic deletion of the 5' ends of both the COL4A5 and COL4A6 genes in a sporadic leiomyoma of the esophagus. *Am J Pathol.* (1998) 152:673–8.
30. Belancio VP, Hedges DJ, Deininger P. Mammalian non-LTR retrotransposons: for better or worse, in sickness and in health. *Genome Res.* (2008) 18:343–58. doi: 10.1101/gr.5558208

Conflict of Interest: The authors declare that the research was conducted in the absence of any commercial or financial relationships that could be construed as a potential conflict of interest.

Publisher's Note: All claims expressed in this article are solely those of the authors and do not necessarily represent those of their affiliated organizations, or those of the publisher, the editors and the reviewers. Any product that may be evaluated in this article, or claim that may be made by its manufacturer, is not guaranteed or endorsed by the publisher.

frontiers in Medicine

ORIGINAL RESEARCH
published: 11 November 2021
doi: 10.3389/fmed.2021.771227

Genetic Variations and Clinical Features of *NPHS1*-Related Nephrotic Syndrome in Chinese Children: A Multicenter, Retrospective Study

Liping Rong[1†], Lizhi Chen[1†], Jia Rao[2†], Qian Shen[2†], Guomin Li[2], Jialu Liu[2], Jianhua Mao[3], Chunyue Feng[3], Xiaowen Wang[4], Si Wang[4], Xinyu Kuang[5], Wenyan Huang[5], Qingshan Ma[6], Xiaorong Liu[7], Chen Ling[7], Rong Fu[8], Xiaojie Gao[9], Guixia Ding[10], Huandan Yang[11], Mei Han[12], Zhimin Huang[13], Qian Li[14], Qiuye Zhang[15], Yi Lin[15], Xiaoyun Jiang[1†] and Hong Xu[2*†] on behalf of Chinese Children Genetic Kidney Disease Database (CCGKDD)*

[1] Department of Pediatrics, The First Affiliated Hospital, Sun Yat-sen University, Guangzhou, China, [2] Department of Nephrology, Children's Hospital of Fudan University, Shanghai, China, [3] Department of Nephrology, The Children's Hospital, Zhejiang University School of Medicine, Hangzhou, China, [4] Department of Nephrology and Rheumatology, Wuhan Children's Hospital (Wuhan Maternal and Child Healthcare Hospital), Tongji Medical College, Huazhong University of Science & Technology, Wuhan, China, [5] Department of Nephrology and Rheumatology, Children's Hospital of Shanghai Jiaotong University, Shanghai, China, [6] Department of Pediatric Nephrology, First Hospital, Jilin University, Changchun, China, [7] Department of Nephrology, Bejing Children's Hospital Affiliated to Capital University of Medical Science, Beijing, China, [8] Department of Pediatrics, Puyang Oilfield General Hospital, Puyang, China, [9] Department of Nephrology, Shenzhen Children's Hospital, Shenzhen, China, [10] Department of Nephrology, Nanjing Children's Hospital Affiliated to Nanjing Medical University, Nanjing, China, [11] Department of Nephrology, Xuzhou Children's Hospital, Xuzhou, China, [12] Department of Nephrology, Children's Hospital of Dalian Medical University, Dalian, China, [13] Department of Pediatrics, Affiliated Hospital of Guangdong Medical University, Zhanjiang, China, [14] Department of Pediatric Nephrology, Rheumatism and Immunology, Shandong Provincial Hospital Affiliated to Shandong University, Shandong, China, [15] Department of Pediatrics, Affiliated Hospital of Qingdao University, Qingdao, China

Introduction: Few studies have addressed the genetic spectrum of *NPHS1* variants in Chinese children with nephrotic syndrome. In this multicenter study, the clinical manifestations and features of *NPHS1* variants in Chinese children with nephrotic syndrome were researched.

Method: Genotypical and phenotypical data from 30 children affected by *NPHS1* variants were collected from a multicenter registration system in China and analyzed retrospectively.

Results: The patients were divided into two groups: congenital nephrotic syndrome (CNS [$n = 24$]) and non-CNS (early onset nephrotic syndrome [$n = 6$]). Renal biopsy was performed on four patients in the non-CNS group, revealing minimal change disease in three and focal segmental glomerulosclerosis in one. A total of 61 *NPHS*1 variants were detected, involving 25 novel variants. The "recurrent variants" included c.928G>A(p.Asp310Asn) in eight patients with CNS, followed by c.616C>A(p.Pro206Thr) in four, and c.2207T>C (p.Val736Ala) in three. Steroid treatment was applied in 29.2% (7/24)of the patients in the CNS group and 50% (3/6) of the patients in the non-CNS group. One patient in each group experienced complete remission

OPEN ACCESS

Edited by:
Andrew Mallett,
Townsville Hospital, Australia

Reviewed by:
Peter Trnka,
The University of Queensland, Australia
Judy Savige,
The University of Melbourne, Australia

***Correspondence:**
Xiaoyun Jiang
jxiaoy@mail.sysu.edu.cn
Hong Xu
hxu@shmu.edu.cn

[†]These authors have contributed equally to this work

Specialty section:
This article was submitted to Nephrology, a section of the journal Frontiers in Medicine

Received: *06 September 2021*
Accepted: *05 October 2021*
Published: *11 November 2021*

Citation:
Rong L, Chen L, Rao J, Shen Q, Li G, Liu J, Mao J, Feng C, Wang X, Wang S, Kuang X, Huang W, Ma Q, Liu X, Ling C, Fu R, Gao X, Ding G, Yang H, Han M, Huang Z, Li Q, Zhang Q, Lin Y, Jiang X and Xu H (2021) Genetic Variations and Clinical Features of NPHS1-Related Nephrotic Syndrome in Chinese Children: A Multicenter, Retrospective Study. Front. Med. 8:771227. doi: 10.3389/fmed.2021.771227

but relapsed subsequently. Immunosuppressants were administered to three patients in the non-CNS group, eliciting an effective response. In the CNS group, three patients underwent renal transplantation and six died mainly from infection.

Conclusion: Variants of *NPHS1* cause CNS and early childhood-onset nephrotic syndrome. *NPHS1* variants in Chinese individuals with nephrotic syndrome (NS) were mainly compound heterozygous variants, and c.928G>A(p.Asp310Asn) in exon 8 may act as a recurrent variant in the Chinese population, followed by c.616C>A(p.Pro206Thr) in exon 6. Steroids and immunosuppressants may be effective in selected patients.

Keywords: *NPHS1*, variants, congenital nephrotic syndrome, children, multicenter, steroid resistance

INTRODUCTION

Nephrotic syndrome (NS) is one of the most common glomerular diseases in children. It is generally divided into steroid-sensitive NS (SSNS) and steroid-resistant NS (SRNS), depending on the response of the patient to steroid therapy. SRNS is a challenging clinical disease, in which 50% of the patients progress to end-stage renal disease within 15 years (1, 2). However, in some patients, temporary or sustained remission may be achieved. Some patients exhibit multidrug-resistant phenotypes, even with enhanced immunosuppressive therapy (3). In children with SRNS, there are usually genetic mutations affecting either podocytes or the glomerular basement membrane (4). *NPHS1* is one of the most common genetic SRNS causes, accounting for 13% of the genetic cases (3). The human *NPHS1* gene is located on the long arm of chromosome 19 (19q13.1) and contains 29 exons, whose protein product "nephrin" is a member of the immunoglobulin-like superfamily. *NPHS1* mutations are primarily responsible for CNS of the Finnish type. SRNS caused by mutations in the *NPHS1* gene is manifested by NS but lacks its extrarenal manifestations, and virtually all patients are unresponsive to steroid and immunosuppressant therapy (5). Fortunately, the recurrence rate after transplantation is low. SRNS can be divided into three types according to age: congenital (presenting within the first 3 months of life, most of which are steroid-resistant), childhood, and adulthood (6). As the *NPHS1* variants are not common, it may be difficult to identify them before genetic testing has been carried out in cases with late-onset NS. Furthermore, pediatric clinicians have a relatively insufficient understanding of this condition. To better understand *NPHS1* variants in pediatric patients in China, we present the clinical and genetic data from a pediatric study involving 30 patients, derived from a multicenter registration system. In this research, the gene mutation spectrum and the resultant clinical manifestations in children were analyzed aiming to describe the general situation of *NPHS1* variants in children with NS in China and raise awareness of this disease among clinical pediatricians.

The National Multicenter Registry (Chinese Children Genetic Kidney Disease Database [CCGKDD], www.ccgkdd.com.cn) has assembled the largest genetically screened cohort with pediatric renal disease in China (7). The data was submitted to the CCGKDD registry monthly by the participating centers in the nation. Eligibility criteria for the registration were complete information of phenotype and genotype for each family, and each medical center identified all the eligible patients post standardized training from the "Internet Plus" Nephrology Alliance of National Center for Children's Care. The phenotype data was identified by clinician experts in pediatric nephrology. The data-entry clerks who had only the ID number for the probands were trained to collect the phenotype information for the registration and they checked the birthdate and phenotype for duplication, and finally contacted clinicians to confirm the individual information before the final registry version. We retrospectively collected information regarding the genotype and phenotype of *NPHS1*-associated kidney disease from the registry and investigated the associations between clinical and genetic findings.

MATERIALS AND METHODS

Study Design and Participants

Patients from 0 to 18 years of age diagnosed as NS combined with confirmed *NPHS1* variants, who underwent genetic analysis between January 1, 2014, and December 31, 2020, were retrospectively recruited from the CCGKDD in this cohort. NS was diagnosed according to the following criteria: heavy proteinuria (urine protein > 50 mg/kg/day); hypoalbuminemia (ALB <25 g/L); hypercholesteremia (cholesterol > 5.7 mmol/L); and clinical edema. All patients in this cohort were identified with *NPHS1* variants through genetic testing of the clinical panel (targeted gene sequencing) or whole exome sequence (WES). The information on presenting clinical features, genetic diagnosis, medical management, and status (with native renal function, dialysis, transplantation, deceased) at last follow-up was collected. The collection of data was stopped at 18 years of age. No identifying information was collected about the patients. A retrospective analysis of genotype, phenotype, and renal outcome was performed.

Mutation Analysis

Due to the high cost of genetic testing for WES, targeted gene sequencing was more commonly used before 2017, whereas the application of WES gradually increased after 2018. Therefore, either the clinical panel (targeted genes sequencing) or WES was applied for genetic testing in an individual patient in this retrospective study. The 249 targeted genes included in the

clinical panel (targeted gene sequencing) in this cohort are presented in **Supplementary Table 1**. WES and variant burden analysis were performed by Wuxi NextCODE, Chigene, and MyGenostics, respectively. Genomic DNA was isolated from blood lymphocytes and subjected to exome capture using Agilent SureSelect human exome capture arrays (V5, Life Technologies), NimbleGen, the xGen Exome Research Panel v1.0 (IDT), or MyGenosticsGencapTM capture technology, followed by next-generation sequencing on the Illumina HiSeq sequencing platform. Over 99% of the target sequence was sequenced at a 30× read depth. Reads with adaptors, reads in which unknown bases (Ns) were more than 10%, and low-quality reads were discarded from raw data to generate clean reads. Clean reads were mapped to the human reference genome assembly (NCBI build 37/hg19) with CLC Genomics Workbench (version 6.5.1) software (CLC bio). Variants were annotated for predicted effects on protein function (using ANNOVAR and SnpEff) and allele frequency in public databases (genomAD, dbSNP, the 1000 Genomes Project, and ExAC). For synonymous variants, intronic variants that were more than 15 bp from exon boundaries (which are unlikely to affect messenger RNA splicing) and common variants (minor allele frequency >1%) were discarded. Missense variants were assessed with MutationTaster2, Provean, SIFT, and Polyphen-2. Evidence for disease causality was assessed using ClinVar and the Human Genome Mutation Database, followed by a manual review of the cited primary literature. Variant interpretations were performed by a panel of nephrologists or molecular geneticists with domain expertise in inherited kidney diseases, bioinformaticians, and clinical molecular geneticists using American College of Medical Genetics and Genomics (ACMG) guidelines (8) for clinical sequence interpretation. Diagnostic variants were defined as "pathogenic" or "likely pathogenic" or "variants of uncertain significance (VUS)." The novel variants of VUS in patients included in our study were considered as disease-causing based on the following: the phenotype of the patient or family history is highly specific for NPHS1-related NS; along with a pathogenic variant detected in trans; through clinical discussion combined with genotype and phenotype among nephrologists and molecular geneticists.

Statistical Tests

Continuous variables summarized with median, interquartile range (IQR), and categorical data were summarized with proportions. Fisher's exact test or chi-square test was used to compare proportions depending on the number of cases. The level of significance was determined at $p < 0.05$. Statistical analysis was performed with SPSS version 20.0 statistical package software (IBM Co., Armonk, NY, USA).

Ethics Statement

The present study adhered to the principles of the 1964 Declaration of Helsinki and was approved by the ethics committee of the participating centers. Written informed consent was obtained from the parents or guardians of all the patients for the publication of any potentially identifiable images or data included in this article. The Institutional Review Board (IRB) of the Children's Hospital of Fudan University (Shanghai, China) approved and monitored this study involving participating centers (IRB No. 2018286).

RESULTS

Patient Characteristics and Clinical Phenotypes

In this study, data of 30 children with renal disease putatively caused by *NPHS1 variants* were collected from CCGKDD, which had included the data of 2,297 patients (30/2,297, counting for 1.30%). The median age at the time of onset was 51 days (range 1 day−3.6 years of age), the median age of genetic diagnosis was 2 months (1 month−3.6 years of age), the average duration at the time of genetic diagnosis was 1 month, and the male-to-female ratio was 1:1 (more details shown in **Table 1**). The patients were divided into two groups according to clinical phenotype:congenital NS (CNS[$n = 24$]); and non-CNS (early onset NS[$n = 6$]). There was no significant difference in the sex ratio between the CNS and the non-CNS groups. At the onset of the disease, nephrotic proteinuria and edema were the primary manifestations. Some were accompanied by microscopic hematuria (11/30 [36.7%]), oliguria (7/30 [23.3%]), and hypertension (4/30 [13.3%]). Regarding complications, some of the children suffered mild and moderate anemia (6/30 [20.0%]), congenital heart disease (3/30 [10.0%] including two with atrial septal defects and one with patent ductus arteriosus), congenital hypothyroidism (7/30 [23.3%]), and motor retardation (one case exhibiting an inability to crawl at 9 months). In terms of birth history, 12 premature infants, including five at the gestational age of 32–34 weeks, were associated with no amniotic fluid and placental abnormalities. Prematurity in one infant (32 weeks) was associated with hydramnios and a large placenta. Three patients had hernias (one indirect inguinal hernia and two umbilical hernias). One case was associated with cytomegalovirus infection. All the patients were examined for *NPHS1* variants. Renal biopsy was performed on four patients in the non-CNS group, among whom three exhibited minimal change disease (MCD) and one manifested with focal segmental glomerulosclerosis (FSGS). Serum albumin was lower in the CNS group than in the non-CNS group, and the urinary protein-to-creatinine ratio was higher in the CNS group. There was no significant difference in the levels of serum creatinine and cholesterol between the two groups (refer for more details in **Table 2**).

NPHS1 Variants

Mutation analysis of all *NPHS1* genes was performed on 30 patients from 30 families. Nephrotic panel gene testing (targeted gene sequencing) was done in 20 patients and WES in the remaining 10 patients. Diagnostic variants including VUS combined with "likely pathogenic" (LP) or "pathogenic" (P) were thought to be disease-causing variants through assessment of the genotype and phenotype associations. The patients in our cohort were recruited with the variation of *NPHS1* gene, without the combination of any other genes variations. One patient exhibited a homozygous *NPHS1* variant (c.3110_3166del), and a single

TABLE 1 | Clinical features and treatment for 30 patients with *NPHS1* variants.

ID	Age of onset/ gender	Renal histopathology	Steroid response	Treatment	Extrarenal manifestation	Outcome at the last follow-up
Congenital nephrotic syndrome						
01	42d /M	nd	nd	Conservative treatment	Congenital hypothyroidism	CKD stage 1, NR
02	1mo/F	nd	PR	Steroid, renal replace treatment	Congenital clubfoot,hypertension, cholestasis	renal transplantation
03	2mo/M	nd	nd	Conservative treatment	None	CKD stage 1, NR
04	7d/M	nd	nd	No treatment	Congenital hypothyroidism	CKD stage 1, NR*
05	2mo/M	nd	nd	No treatment	Congenital heart disease (atrial septal defect)	Died of infection 5 months after birth
06	45d/M	nd	NR	Steroid	Hydrocele, umbilical hernia	CKD stage 1, NR
07	2mo/F	nd	nd	No treatment	Congenital hypothyroidism	CKD stage 1, NR*
08	1mo/F	nd	nd	Conservative treatment, renal transplantation	None	Renal transplantation
09	45d/F	nd	nd	No treatment	None	CKD stage 1, NR*
10	73d/F	nd	PR	Steroid	Inguinal hernia	CKD stage 1, NR*
11	3mo/M	nd	nd	No treatment	Congenital hypothyroidism	CKD stage 1, NR*
12	1mo/F	nd	CR	Steroid	None	CKD stage 1, CR
13	52d/F	nd	nd	No treatment	None	Died of infection after discharge
14	1mo/F	nd	nd	No treatment	Cystic lesion in the left frontal lobe	CKD stage 1, NR*
15	1mo/F	nd	nd	No treatment	None	CKD stage 1, NR*
16	2mo/F	nd	nd	Conservative treatment, ACEI	CMV infection; Loss of high-frequency hearing	CKD stage 1, NR
17	1mo/M	nd	nd	Conservative treatment, ACEI	Central hypothyroidism	Renal transplantation
18	1.5mo/M	nd	nd	Conservative treatment, ACEI	None	CKD stage 1, NR
19	1d/M	nd	nd	No treatment	PDA	Died of infection 15 days after birth
20	2d/F	nd	NR	Steroid	Femoral vein thrombosis	Died of infection 2 months after birth
21	1d/M	nd	nd	No treatment	None	Died of infection 11 days after birth
22	1d/F	nd	nd	Conservative treatment, ACEI	ASD	Died of infection 4 months after birth
23	3mo/F	nd	nd	Conservative treatment, ACEI	Ileus, umbilical hernia	CKD stage 1, NR
24	2mo/F	nd	NR	Steroid, ACEI	Umbilical hernia Congenital hypothyroidism	CKD stage 1, NR
Early children onset nephrotic syndrome						
25	8mo/M	FSGS	nd	Steroid, ACEI	None	CKD stage 1,PR
26	3.6y/M	MCD	nd	Steroid, ACEI	None	CKD stage 1, PR
27	2y/M	MCD	CR	Steroid, CsA	None	CKD stage 1, CR
28	1.5y/M	MCD	nd	ACEI	None	CKD stage 1, PR
29	1.5y/M	nd	NR	Steroid, tacrolimus, MMF	None	CKD stage 1, PR
30	3y/F	nd	NR	Steroid, CsA	None	CKD stage 1, PR

*nk, not known; MMF, mycophenolate mofetil; CsA, cyclosporin A; CR, complete remission; PR, partial remission; NR, no remission; CNS, congenital nephrotic syndrome; M, male; F, female; IS, immunosuppressant; FSGS, focal segmental glomerulosclerosis; MCD, minimal change disease; CKD, chronic kidney disease; nd, not done; CMV, cytomegalovirus; PDA, patent ductus arteriosus; ASD, atrial septal defect; NRDS, respiratory distress syndrome of newborn. *The family gave up on treatment for the patient without follow-up since the first hospitalization.*

TABLE 2 | The comparison between CNS group and non-CNS group in patients.

	Total (*n* = 30)	**CNS group (*n* = 24)**	**non-CNS group (*n* = 6)**
Patient No. (*n*, %)	100% (30/30)	80.0% (24/30)	20.0% (6/30)
Male. (*n*, %)	50.0% (15/30)	41.7% (10/24)	83.3% (5/6)
Median age at onset (day)	51 (30∼82)	41 ± 26	771 ± 360
History of premature birth	40.0% (12/30)	50.0% (12/24)	0 (0/6)
Large placenta	13.3% (4/30)	16.7% (4/24)	0 (0/6)
Laboratory result			
Creatinine (umol/L)	20.0 ± 8.6	19.5 ± 9.0	21.7 ± 6.8
Albumin (g/L)	11.0 (10.0∼15.6)	11.6 ± 3.4	24.2 ± 11.1
Cholesterol (mmol/L)	7.2 ± 4.0	6.8 ± 2.3	9.1 ± 8.3
UPCR (mg/mg)	24 (6.3∼59.0)	54.4 ± 49.6	4.7 ± 2.4
Renal biopsy	13.3% (4/30)	0 (0/24)	66.7% (4/6)
Treatment			
Steroid treatment (*n*, %)	33.3% (10/30)	29.2% (7/24)	50.0% (3/6)
CR	20.0% (2/10)	14.3% (1/7)	33.3% (1/3)
PR	20.0% (2/10)	28.6% (2/7)	0 (0/3)
NR	60.0% (6/10)	57.1% (4/7)	66.7% (2/3)
Immunosuppressant (n, %)	10.0% (3/30)	0(0/24)	50.0% (3/6)
TAC+MMF (PR)	3.3% (1/30)	-	16.7% (1/6)
CsA (PR)	3.3% (1/30)	-	16.7% (1/6)
CsA (CR)	3.3% (1/30)	-	16.7% (1/6)
ACEI (n, %)	23.3% (7/30)	16.7% (4/24)	50.0% (3/6)
Outcome			
CKD stage 1	70.0% (21/30)	62.5% (15/24)	100% (6/6)
CKD stage 1, CR	6.7% (2/30)	4.2% (1/24)	16.7% (1/6)
CKD stage 1, PR	16.7% (5/30)	0 (0/24)	83.3% (5/6)
CKD stage 1, NR	46.7% (14/30)	58.3% (14/24)	0 (0/6)
Renal transplantation	10.0% (3/30)	12.5% (3/24)	0 (0/6)
Death	20.0% (6/30)	25.0% (6/24)	0 (0/6)
Type of variant			
Novel variants (n, %)	41.0% (25/61)	44.0% (22/50)	27.3% (3/11)
Missense (*n*, %)	49.2% (30/61)	46.0% (23/50)	63.6% (7/11)
Frameshift (*n*, %)	19.7% (12/61)	20.0% (10/50)	18.2% (2/11)
Splice (*n*, %)	11.5% (7/61)	14.0% (7/50)	0 (0/11)
Nonsense (*n*, %)	13.1% (8/61)	14.0% (7/50)	9.1% (1/11)
Intronic (*n*, %)	3.3% (2/61)	4.0% (2/50)	0 (0/11)
Duplication (*n*, %)	1.6% (1/61)	2.0% (1/50)	0 (0/11)
Nonframeshift deletion (*n*, %)	1.6% (1/61)	0 (0/50)	9.1% (1/11)
Hotspot variants			
c.928G>A	13.1% (8/61)	16.0% (8/50)	0 (0/11)
c.616C>A	6.6% (4/61)	2.0% (1/50)	27.2% (3/11)
c.2207T>C	4.9% (3/61)	4.0% (2/50)	9.1% (1/11)

heterozygous *NPHS1* variant was identified in another, whereas the remaining 28 exhibited compound heterozygous *NPHS1* variants (more details in **Table 3** and **Supplementary Table 2**). A total of 61 variants were detected among all the patients, including 46 different disease-causing *NPHS1* variants, with 25 novel variants that have not been previously reported, mainly in the CNS group. Mutation types consisted of 30 missense, 12 frameshifts, seven splice-site, eight nonsense, one duplication, and one deletion. The recurrent variant was c.928G>A in exon 8 in eight patients, followed by c.616C>A in four, c.2207T>C in three, and c.1394G>A, c.2783C>A, and c.3478C>T in two, respectively. The variants were broadly distributed over the nephrin protein located in exons 2, 3, 4, 6, 8, 10, 11, 13, 16, 18, 19, 20,22, 23, 24, 25, 26, 27, and 28 (**Figure 1**). The variant of c.928G>A was present in the CNS group, whereas c.616C>A was mainly found in the non-CNS group (more details in **Table 2**). The other variants exhibited no significant differences between the two groups. An overview of variants of NPHS1 gene type in

TABLE 3 | Genetic information for 30 patients with *NPHS1* variants (NM_004646.3).

Case	Age of onset/ gender	NHSP1 variants			Type of variant	Hom/Het	Variation origin	ACMG	Reference	MAF	
		Nucleotide change	Aminoacid change	Location						Gome_ALL	Gome_EAS
Congenital nephrotic syndrome											
1	42d /M	**IVS25-2T>A***	/	Intron 25	Splice site	Co-Het	Unknow	VUS	-	-	-
		c.928C>T	p.Asp310Asn	Exon 8	Missense	Co-Het	Unknow	LP	(9)	1.2156×10^{-5}	1.634×10^{-4}
2	1mo/F	c.3325C>T	p.Arg1109Ter	Exon 26	Nonsense	Co-Het	Unknow	P	(10)	1.551×10^{-4}	1.0874×10^{-4}
		c.3312-2A>T*	/	/	/	Co-Het	Unknow	VUS	-	-	-
3	2mo/M	**c.2590C>T***	p.Arg864Cys	Exon 19	Missense	Co-Het	F	LP	-	4.8723×10^{-5}	3.3025×10^{-4}
		c.867G>T*	p.Trp289Cys	Exon 8	Missense	Co-Het	het; p,wt; m,wt	LP	-		
4	7d/M	c.1394G>A	p.Cys465Tyr	Exon 11	Missense	Co-Het	Unknow	P	(11)	-	-
		c.928G>A	p.Asp310Asn	Exon 8	Missense	Co-Het	F	P	(9)	1.2156×10^{-5}	1.634×10^{-4}
5	2mo/M	**c.394G>A***	p.Glu117Lys	Exon 3	Missense	Co-Het	F	VUS	-	-	-
		c.1439A>G*	P.Lys480Thr	Exon 11	Missense	Co-Het	F	VUS	-	-	-
		c.1500_1507del*	p.Gly500fs	Exon 12	Frameshift	Co-Het	Not Available	P	-	-	-
6	45d/M	c.3478C>T	p.Arg1160Ter	Exon 27	Nonsense	Single Het	F	LP	(12)	9.943×10^{-5}	5.4366×10^{-5}
7	2mo/F	**c.2629-c.2630delAAinsT***	p.Lys877Xfs*1	Exon 19	Frameshift	Co-Het	F	P	-	-	-
		c.1315 + 1G>A(-)	/	/	/	Co-Het	M	P	(13)	-	-
8	1mo/F	**c.2205_2206insTGGAC***	p.Val736Trpfs*18	Exon 16	Frameshift	Co-Het	M	P	-	-	-
		c.3478C>T	p.Arg1160Ter	Exon 27	Nonsense	Co-Het	F	LP	(12)	9.943×10^{-5}	5.4366×10^{-5}
9	45d/F	c.3213delG	p.Leu1072Phefs*71	Exon 24	Frameshift	Co-Het	F	LP	(14)	-	-
		c.2663G >A	p.Arg888Thr	Exon 19	Missense	Co-Het	M	P	(15)	4.3654×10^{-6}	0
10	73d/F	c.928G>A	p.Asp310Asn	Exon 8	Missense	Co-Het	M	P	(9)	1.2156×10^{-5}	1.634×10^{-4}
		c.360del C*	p.Pro120fs	Exon 8	Frameshift	Co-Het	F	P	-	-	-
		c.1240.A>G	p.Thr414Ala	Exon 8	Missense	Co-Het	F	VUS	Clinvar:VCV000930198		-
11	3mo/M	c.616C>A	p.Pro206Thr	Exon 6	Missense	Co-Het	M	LP	(16)	3.185×10^{-5}	4.35×10^{-4}
		IVS12-10C>A*	/	Intron 12	Splice site	Co-Het	F	VUS	-	-	-

(Continued)

TABLE 3 | Continued

Case	Age of onset/ gender	NHSP1 variants			Type of variant	Hom/Het	Variation origin	ACMG	Reference	MAF	
		Nucleotide change	Aminoacid change	Location						Gome_ALL	Gome_EAS
12	1mo/F	c.928G>A	p.Asp310Asn	Exon 8	Missense	Co-Het	F	P	(9)	1.2156×10^{-5}	1.634×10^{-4}
		c.2207T>C	p.Val736Ala	Exon 16	Missense	Co-Het	M	P	(17)	-	-
		c.3312-23C>T	/	Intron 25	Missense	Co-Het	M	VUS	(18)	1.0608×10^{-5}	1.5039×10^{-4}
13	52d/F	**c.2928-2A>C(IVS21)***	/	Intron 21	Splice site	Co-Het	M	LP	-	-	-
		c.928G>A	p.Asp310Asn	Exon 8	Missense	Co-Het	F	P	(9)	1.2156×10^{-5}	1.634×10^{-4}
14	1mo/F	c.802C>T	p.Arg268X	Exon 7	Nonsense	Co-Het	F	LP	(19)	2.8512×10^{-5}	0
		c.1528T>C*	p.Ser510Pro	Exon 12	Missense	Co-Het	M	VUS	-	-	-
15	1mo/F	c.2788C>T	p.Gln930X	Exon 20	Nonsense	Co-Het	F	P	(15)	-	-
		c.3442delC	p.Gln1148fs	Exon 27	Frameshift deletion	Co-Het	M	P	(15)	-	-
16	2mo/F	c.2207T>C	p.Val736Ala	Exon 16	Missense	Co-Het	M	P	(17)	-	-
		c.2210A>C*	p.His737Pro	Exon 16	Missense	Co-Het	F	VUS	-	-	-
17	1mo/M	c.2212 + 2_2212 + 3delTG	-	-	Splicing	Co-Het	F	P	(19)	-	-
		c.1409G>A*	p.Gly470Asp	Exon 11	Missense	Co-Het	M	VUS	-	-	-
18	1.5mo/M	c.1440 + 1G>A	-	Intron 11	Splicing	Co-Het	F	P	(20)	-	-
		c.928G>A	p.Asp310Asn	Exon 8	Missense	Co-Het	M	P	(9)	1.2156×10^{-5}	1.634×10^{-4}
19	1d/M	**c.741G>A***	p.Trp247X	Exon 7	Nonsense	Co-Het	M	P	-	-	-
		c.928G>A	p.Asp310Asn	Exon 8	Missense	Co-Het	F	P	(9)	1.2156×10^{-5}	1.634×10^{-4}
20	2d/F	**c.3144delG***	p.Gln1048fs	Exon 23	Frameshift deletion	Co-Het	M	P	-	-	-
		c.514delA*	p.Thr172fs	Exon 4	Frameshift deletion	Co-Het	F	P	-	-	-
21	1d/M	**c.1699T>C***	p.Cys567Arg	Exon 13	Missense	Co-Het	F	VUS	-	-	-
		c.3523_3524del	p.Leu1175ValfsTer2	Exon 28	Frameshift deletion	Co-Het	M	LP	(21)	3.9765×10^{-6}	5.4366×10^{-5}
22	1d/F	**c. 1531C > T***	p.Arg511X,731	Exon 12	Frameshift deletion	Co-Het	F	LP	-	-	-
		c.2071 + 2T>C*	-	-	Splicing	Co-Het	M	P	-	-	-
23	3mo/F	c.2783C>A	p.Ser928X	Exon 20	Nonsense	Co-Het	Unknow	P	(22)	-	-
		c.928G>A	p.Asp310Asn	Exon 8	Missense	Co-Het	Unknow	P	(9)	1.2156×10^{-5}	1.634×10^{-4}
24	2mo/F	c.1219C>T	p. Arg407Trp	Exon 10	Missense	Co-Het	F	P	(23)	-	-
		dup(exon23-28)*	-	Exon 23-28	Duplication	Co-Het	M	LP	-	-	-

(Continued)

TABLE 3 | Continued

Case	Age of onset/ gender	NHSP1 variants			Type of variant	Hom/Het	Variation origin	ACMG	Reference	MAF	
		Nucleotide change	Aminoacid change	Location						Gome_ALL	Gome_EAS
Early children onset nephrotic syndrome											
25	8mo/M	c.616C>A	p.Pro206Thr	Exon 6	Missense	Co-Het	M	LP	(16)	3.185×10^{-5}	4.35×10^{-4}
		c.472G>T*	p.Val158Fhe	Exon 4	Missense	Co-Het	F	VUS	-		
26	3.6y/M	c.2207T>C	p.Val736Ala	Exon 16	Missense	Co-Het	F	P	(17)	-	-
		c.616C>A	p.Pro206Thr	Exon 6	Missense	Co-Het	M	LP	(16)	3.185×10^{-5}	4.35×10^{-4}
27	2y/M	c.C2783A	p.Ser928X	Exon 20	Nonsense	Co-Het	M	P	(22)	-	-
		c.139delG	p.Ala47ProfsTer81	Exon 2	Frameshift	Co-Het	F	LP	(12)	8.1213×10^{-6}	0
28	1.5y/M	c.3250dupG	p.Val1084fs	Exon 24	Frameshift insertion	Co-Het	F	LP	(10)	-	-
		c.2380T>C*	p.Ser794Pro	Exon 18	Missense	Co-Het	M	VUS	-	-	-
29	1.5y/M	c.1394G>A	p.Cys465Tyr	Exon 11	Missense	Co-Het	Unknow	P	(11)	-	-
		c.616C>A	p.Pro206Thr	Exon 6	Missense	Co-Het	Unknow	LP	(16)	3.185×10^{-5}	4.35×10^{-4}
30	3y/F	**c.3110_3166del***	/	Exon 23	Nonframeshift deletion	Hom	hom; F, het; M, het	P	-	-	-

**Novel variants in bold.*

Hom, Homozygous; Het, Heterozygous; Co-Het, compound Heterozygous; MAF, Minor Allele Frequency; P, Pathogenic; LP, Likely Pathogenic; VUS, Variants of uncertain significance; m, month; y, year. D, day. Wt, wild type.

this study is shown in **Figure 2**. The patients were classified into the P+P/LP+P group and P+VUS/LP+VUS group to review the clinical features of patients from the perspective of the features of the variants. The results of the comparison between the two groups with different disease-related pathogenicity are shown in **Table 4**. The comparison of the phenotype and genotype in CNS patients with *NPHS1* variants in this study with the other four cohorts reported in the literature (23–26) is shown in **Table 5**.

Treatment and Follow-Up Information

All 24 patients with CNS received nutritional support, diuretics, albumin infusion, preventive measures, treatment of infection, and other symptomatic support treatment at disease onset. In total, 10 patients were administered steroid therapy, including three with early childhood-onset NS and seven with CNS. In the CNS group, three patients responded effectively, including two with partial remission and one with complete remission. In the non-CNS group, two patients were resistant to steroid therapy and one had complete remission but relapsed frequently. Immunosuppressive therapy, including cyclosporin A (CsA), tacrolimus, and mycophenolate, was administered to the three patients with childhood-onset NS, resulting in effective outcomes, including two with partial remission and one with complete remission. Seven patients were on antiproteinuric therapy with angiotensin-converting enzyme inhibitors, including four in the CNS group, exhibiting no response, and three in the non-CNS group, exhibiting partial response (more details provided in **Table 2**). Due to the poor socioeconomic status of the family or poor prognosis related to hereditary factors, 30.0% (9/30) of patients with CNS phenotypes were left untreated after genetic diagnosis. At the most recent observation, the remaining 70.0% (21/30) of patients were still in stage 1 chronic kidney disease (CKD) and 10.0% (3/30) had undergone renal transplantation. Among those who had received early preemptive kidney transplantation, one patient had undergone repeated transplantation due to allograft failure. All three patients had remained in stage 1 CKD before the first transplantation. Among the patients with stage 1 CKD ($n = 21$), two were in complete remission, five in partial remission, and 14 in no remission at the last observation.

DISCUSSION

The current study was a nationwide, multicenter study, with the largest number of pediatric cases of *NPHS1* gene variants in the country. This research yielded important information regarding the distribution of clinical phenotypes and genotypes in childhood SRNS. The 30 patients were from 30 unrelated families located in 11 provinces and autonomous regions in China. By analyzing the characteristics of clinical manifestations and genotypes, we aimed to enable clinicians to understand better disease-related *NPHS1* variants and optimize decision making.

In this study, most of the *NPHS1* variants were found in the CNS group, accounting for 80.0% (24/30) of cases. They were also found in early childhood-onset NS (age $\leq$ 3 years), accounting for 20.0% (6/30) of the cases. The results of the current study and previous findings confirm that *NPHS1* variants can cause a broader variety of clinical phenotypes in nephrotic syndrome including childhood- and adult-onset focal segmental glomerulosclerosis than CNS (3, 6, 23, 27, 28). The variants of NPHS1 showed no obvious difference between patients with MCD and FSGS. Similarly, the previous study showed the spectrum of renal histologic findings atypical for CNS with NHPS1 variants ranging from MCD to FSGS (6). The histopathological manifestations may be related to podocyte injury and persistent proteinuria caused by NPHS1 variants. Extrarenal manifestations were present in 16 of the 24 patients with CNS in our study, mainly in congenital hypothyroidism, hernia, and congenital heart disease. From the results, there was no considerable difference in variants between patients with and without extrarenal manifestations. Combined with the literature review, we consider that the extrarenal manifestations in our study were possibly secondary to CNS or cooccurring complications along with CNS rather than related to genetic variation.

A previous consensus indicated that patients with NS caused by *NPHS1 variants* exhibit a weak response to steroid therapy (5, 24, 29). In our study, one patient (case 12), responded effectively to initial steroid therapy and maintained an effective response in subsequent nonfrequent relapses. The *NPHS1* variants of this child exhibited three-compound heterozygous variants, namely c.928G>A in exon 8, c.2207T>C in exon 16, and c.3312-23C>T in intron 25. This finding from our study was inconsistent with previous reports and may indicate that steroid therapy can be usefully applied in CNS patients with these variants loci in *NPHS1*. However, it was just an individual observation result from clinical practice in our study. A recent genome-wide association study reported that there are some common risk variants in *NPHS1* that are associated with childhood SSNS (30). However, the steroid-sensitive mechanism remains unclear. We speculate that perhaps the nephrin protein, resulting from these variants, maintains its partial function and shows the response to steroid or immunosuppressive therapy, which may help actin reorganization in the cytoskeleton of podocytes. Further study of its molecular mechanism and long-term follow-up is required. In this study, it was also indicated that some children with early childhood-onset NS caused by *NPHS1* variants may be effectively treated with steroid and immunosuppressive agents. Studies involving greater numbers of patients will be needed to observe the effects of immunosuppressive therapy, along with further mechanism studies to determine the significance of these variants.

The results of *NPHS1* variant analysis in our study revealed that there were mainly compound heterozygous variants, accounting for 93.3% (28/30) of cases, with one homozygous variant. This finding suggests that compound heterozygous variants are the major variation pattern in *NPHS1* in Chinese patients. The most frequent variant was c.928G>A in exon 8 (eight patients), which was present in CNS patients, followed by c.616C>A in four, c.2207T>C in three, and c.1394G>A, c.2783C>A, and c.3478C>T in two, respectively. These findings were, to some extent, different from reports from other Chinese studies (15, 31–33). Our findings indicated that heterozygous

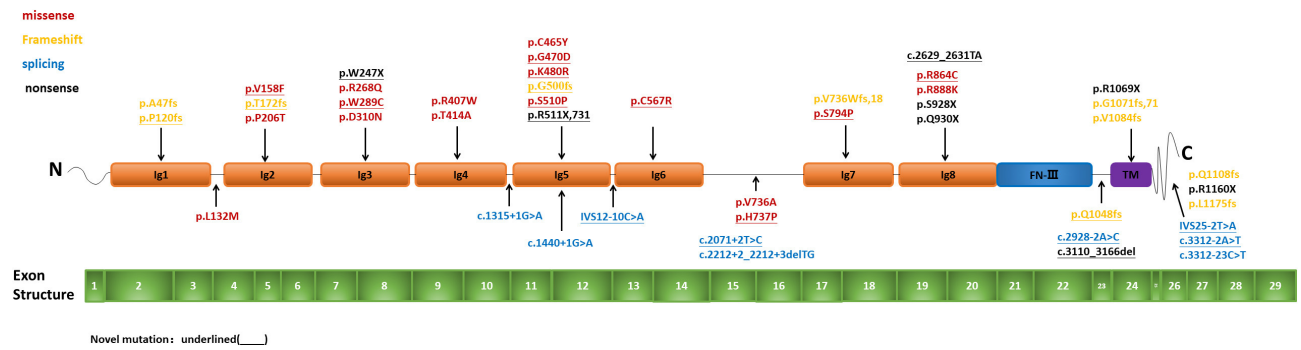

FIGURE 1 | Pattern of variant(s) in the *NPHS1* gene: Exon structure of the *NPHS1* gene and the location of the variants identified in the present study.

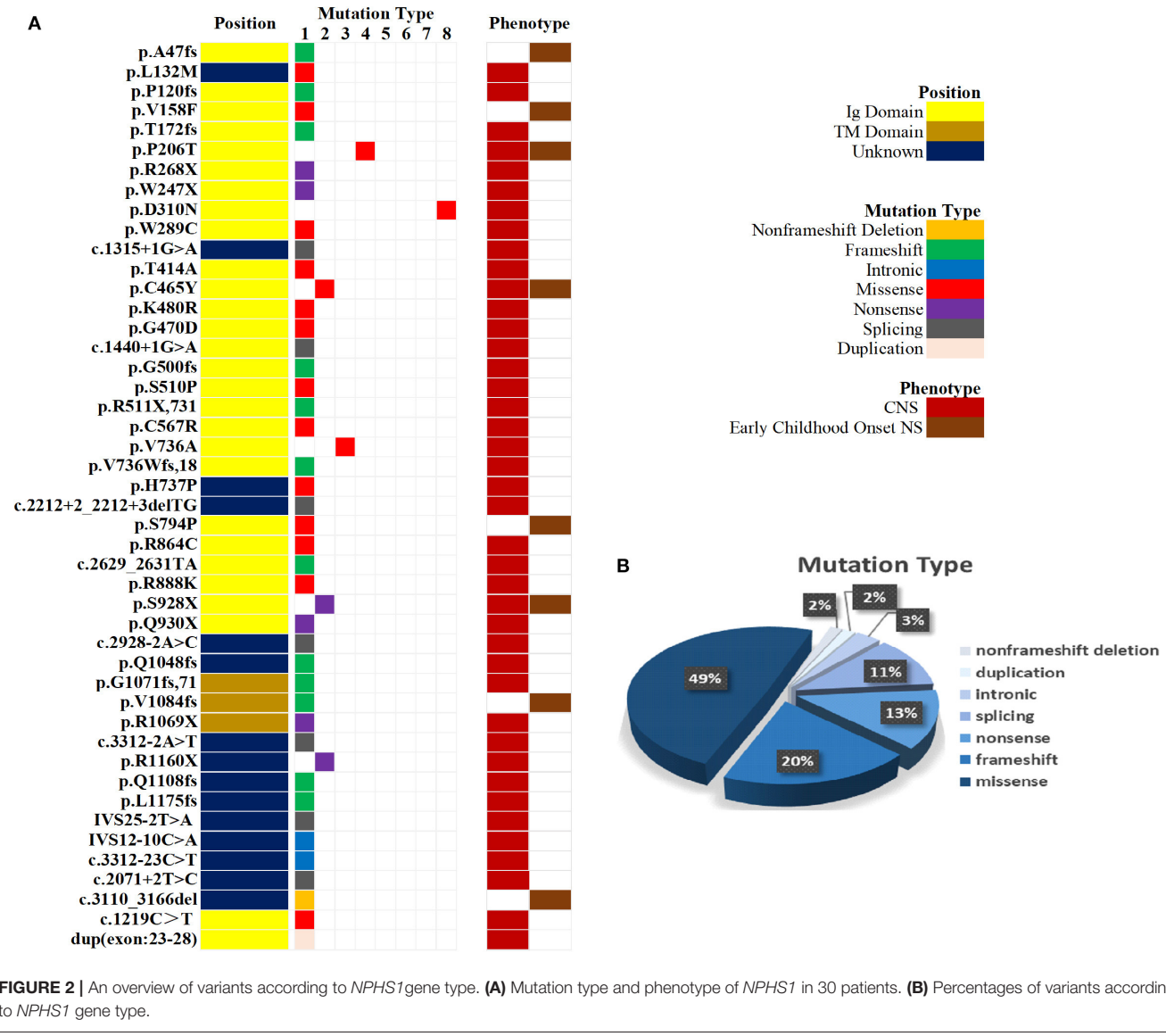

FIGURE 2 | An overview of variants according to *NPHS1*gene type. **(A)** Mutation type and phenotype of *NPHS1* in 30 patients. **(B)** Percentages of variants according to *NPHS1* gene type.

TABLE 4 | The comparison between two groups with different pathogenicity variants.

	P+P/P+LPgroup (*n* = 19)	P+VUS/LP+VUSgroup (*n* = 11)	*p* value
Patient No. (*n*, %)	63.3% (19/30)	36.7% (11/30)	-
CNS (*n*, %)	78.9% (15/19)	81.8% (9/11)	0.380
Non-CNS (*n*, %)	21.1% (4/19)	18.2% (2/11)	0.739
Median age at onset(day)	57(32∼88)	50(19∼59)	0.400
History of premature birth	26.3% (5/19)	63.6% (7/11)	0.052
Renal biopsy	10.5% (2/19)	18.2% (2/11)	0.470
Treatment			
Steroid treatment (*n*, %)	42.1% (8/19)	18.2% (2/11)	0.210
CR	12.5% (1/8)	50% (1/2)	0.378
PR	25.5% (2/8)	0 (0/2)	-
NR	62.5% (5/8)	50% (1/2)	0.667
Immunosuppressant (*n*, %)	15.8% (3/19)	0 (0/11)	0.279
TAC+MMF (PR)	33.3% (1/3)		-
CsA (PR)	33.3% (1/3)		-
CsA (CR)	33.3% (1/3)		-
ACEI (*n*, %)	15.8% (3/19)	36.4% (4/11)	0.200
Outcome			
CKD stage 1	58.3% (14/19)	63.6% (7/11)	0.429
CKD stage 1, CR	14.3% (2/14)	14.3% (1/7)	0.726
CKD stage 1, PR	28.6% (4/14)	0 (0/7)	0.255
CKD stage 1, NR	57.1% (8/14)	85.7% (6/7)	0.127
Renal transplantation	5.3% (1/19)	18.2% (2/11)	0.298
Death	44.4% (4/19)	18.2% (2/11)	0.739
Variant pathogenicity	P/LP	VUS	
Variants (*n*, %)	78.7% (48/61)	21.3% (13/61)	-
Mutation type			
Novel mutation (*n*, %)	29.2% (14/48)	84.6% (11/13)	<0.001
Missense mutation (*n*, %)	41.7%(20/48)	76.9% (10/13)	0.025
Splice mutation (*n*, %)	8.3%(4/48)	23.1% (3/13)	0.159
Frameshift mutation (*n*, %)	25.0%(12/48)	0 (0/13)	0.054
Nonsense mutation (*n*, %)	16.7%(8/48)	0 (0/13)	0.183
Intronic mutation (*n*, %)	4.2%(2/48)	0 (0/13)	1.00
Duplication (*n*, %)	2.1% (1/48)	0 (0/13)	1.00
Nonframeshift deletion (*n*, %)	2.1% (1/48)	0 (0/13)	1.00

P, Pathogenic; LP, Likely Pathogenic; VUS, Variants of uncertain significance; High pathogenicity: P/LP variants. Low pathogenicity, LP or P + VUS variants; CKD, chronic kidney disease.

variants, including c.928G>A and c.616C>A, are "pathogenic recurrent variants" of *NPHS1* in China, whereas c.928G>A is the main genotype of CNS. It is generally believed that recurrent genetic variants occur *via* two mechanisms: one is a founder effect and the other is a mutational hot spot. In our study, the variant 928G>A occurred with high frequency and was rarely reported in other populations, and so we speculated whether it is a founder effect. However, there remains the little specific supporting basis for this speculation since there is little data about researches on *NPHS1* in China, and data in our study was so limited that it was difficult to perform further analysis for the founder effect. The mutation results revealed that missense mutations were the main mutation types in the two groups. Splice mutations, nonsense mutations, and intronic mutations mainly occurred in patients with a phenotype of congenital nephrotic syndrome, similar to previous reports. In the present study, 13 variants were found to be of uncertain significance, accounting for 21.3% of cases, of which 11 variants have not been reported yet. Most of the patients who carried the novel variants, along with a pathogenic variant detected in trans, presented typical clinical features of CNS. Among the 11 novel variants of VUS, eight were located in exons with "damaging" *in silico* predictions. Although the pathogenicity of variants with VUS has not been identified, from the perspective of clinical practice based on factors involved, all of them in this study were thought to be disease-causing variants through fully integrated analyses of the phenotypical manifestations and genotypes. However, the introns and copies of these variants need to be further detected and analyzed to determine their pathogenicity.

TABLE 5 | Phenotype and genotype of CNS patients with *NPHS1* mutation in the literatures and comparison with our cohort.

		CNS patients with *NPHS1* mutation in the Literature and in Our Cohort				
		Worldwide Cohort (23)	**France (24)**	**Saudi Arabia (26)**	**Japan (25)**	**This study**
	Time interval	1996–2008	2000–2014	2008–2017	Nationwide survey in 2016	2014–2020
Phenotype	Patient number	36	36	9	33	30
	Male. (*n*, %)	NA	52.6% (19/36)	55.5% (5/9)	45.4%(15/33)	50.0% (15/30)
	CNS	100%	100%	88.9% (8/9)	100%	80.0% (24/30)
	Child onset NS (*n*, %)	0	0	11.1% (1/9,)	0	20.0% (6/30)
	Median age at onset(day)	NA	0.5 (0–13)	2.4 (0.1–6), month	0.0 (0.0–2.0),month	51.0 (30.0∼82.0)
	History of family	NA	Consanguinity 46%	Consanguinity 100%	NA	0
	Large placenta	NA	12/17	-	30/30	13.3% (4/30)
	Extra-renal anomalies	NA	NA	Right pulmonary artery stenosis; Seizure disorder; Recurrent chest infection; Recurrent chest infection	Malformation; Epilepsy; Mental retardation	Congenital hypothyroidism, congenital clubfoot, hernia, CMV infection, Loss of hearing, ASD, PDA
	Renal biopsy	10/36	8/36	None	13/30	4/30
Treatment	Steroid treatment (*n*, %)	20.8%	None	NA	3/29 (nR, 3)	33.3% (10/30)
	IS (*n*, %)	4 in CsA(NR,4)	None	NA	3/28 (CSA, NR, 2; PR, 1)	10.0% (3/30)
Outcome	CKD stage 1	NA	NA	NA	NA	70.0% (21/30)
	RRT	10 in renal transplantation	68% (25/37)	2 with PD	26/33 in PD; 1/33 in HD; 17/33 in renal transplantation	10.0% (3/30) in renal transplantation
	Death	NA	16% (6/37)	70.1% death in CNS	NA	20.0% (6/30)
Mutation type	Homozygous (*n*, %)	26/36	61.1% (22/36)	100%	NA	3.3% (1/30)
	Co-het (*n*, %)	10/36	38.9% (14/36)	0	NA	96.7% (29/30)
	Novel mutation (*n*, %)	19/37	7/31	NA	NA	41.0% (25/61)
	Hotspot variants	c.1760T>G, 10.8% (4/37) c.3243_3250insG, 8.1% (3/37) c.3478C>T, 8.1% (3/37)	c.139 del; 13.9% (5/36) c.1379 G>A; 22.2% (8/36)	NA	NA	c.928G>A, 13.1% (8/61) c.616C>A, 6.6% (4/61) c.2207T>C, 4.9% (3/61)

A, not applicable; CsA, cyclosporin A; CR, complete remission; PR, partial remission; NR, no remission; CNS, congenital nephrotic syndrome; RRT, renal replacement therapy; CKD, chronic kidney disease; PD, peritoneal dialysis; HD, hemodialysis; Co-het, Compound heterozygous; IS, Immunosuppressant.

In China, the prognosis for CNS was poor before the turn of the 21st century. Significant progress has been made in healthcare, as well as in pediatric nephrology during the past few decades, and the prognosis has improved significantly. In terms of treatment and prognosis for the 30 patients in this study, 12.5% (3/24) of children diagnosed with CNS received kidney transplantation. Up to 30.0% (9/30) of the patients did not receive appropriate treatment after genetic diagnosis because their parents declined treatment due to the high financial burden involved or concerns about poor prognosis. A cross-sectional nationwide survey of CNS and infantile NS in Japan reported that up to 78.8% (26/33) of patients underwent peritoneal dialysis and up to 51.5% (17/33) underwent subsequent renal transplantation (25). On the one hand, due to the very low frequency of renal disease resulting from *NPHS1* variants, individuals and general clinicians are unfamiliar with the disorder as well as its prognosis. On the other hand, most physicians exhibit inadequate recognition and understanding of

this illness and its multidisciplinary requirements. We, therefore, need to develop a greater understanding of CNS, both in medical care and patient care personnel, across the nation in the future.

Some potential limitations should be recognized in the current study. First, it was a retrospective analysis where the interventions could not be well controlled. Such as some patients underwent genetic testing by the clinical panel (targeted gene sequencing) rather than all by WES. Although the clinical panel used in our study included 249 genes which almost covered the main responsible genes in hereditary kidney disease, WES is recommended for these patients, if available. Second, it may be underpowered to perform the statistical analyses in comparison between CNS group and non-CNS group due to the overall sample size of the cohort. Significant differences could be made if a larger cohort size is available. Finally, it was a limited number involving only 30 patients collected from 2014 to 2020, although it represents the largest cohort with *NPHS1* variants in China currently. In the next step, it is necessary to expand the cohort size nationwide and longer follow-up is needed.

In conclusion, variants of *NPHS1* not only cause CNS but also NS in early childhood-onset disease. *NPHS1* genetic testing for CNS with onset within 3 months after birth, and also NS with steroid resistance, is helpful for early diagnosis and prognosis evaluation. *NPHS1* variants in Chinese individuals with NS were mainly compound heterozygous variants, and c.928G>A(p.Asp310Asn) in exon 8 may act as a recurrent variant in the Chinese population, followed by c.616C>A(p.Pro206Thr) in exon 6. Steroids and immunosuppressants may have a beneficial effect on selected patients. Kidney transplantation in children with *NPHS1* variants is effective. Efforts are also needed to raise awareness of CNS among patient family members and to improve treatment coverage in China.

DATA AVAILABILITY STATEMENT

The data that support the findings of this study are available from the corresponding authors upon reasonable request. The datasets presented in this article are not readily available for public repository due to the regulation on the management of human genetic resources from the State Council, CHINA. Requests to access the datasets should be directed to the database for Chinese children renal disease which is publicly available datasets in Chinese language (https://www.ccgkdd.com.cn/).

ETHICS STATEMENT

The studies involving human participants were reviewed and approved by the Institutional Review Board (IRB) of the Children's Hospital of Fudan University (Shanghai, China) (IRB No. 2018286). Written informed consent to participate in this study was provided by the participants' legal guardian/next of kin.

AUTHOR CONTRIBUTIONS

HX and XJ designed the study, reviewed, and revised the manuscript. LR, LC, JR, and QS performed the search, performed the analysis and wrote the manuscript, and they have contributed equally to this work. JM, CF, XW, XK, WH, QM, XL, CL, RF, XG, GD, HY, ZH, MH, QL, QZ, and YL collected the data. GL and JL rechecked the data. All authors contributed to the article and approved the submitted version.

FUNDING

This work was supported by the Science and Technology Planning Project of Guangzhou, China (Grant No. 202103000001).

ACKNOWLEDGMENTS

We thank all participating patients and their families. Additionally, we thank our coordinators from the Chigene (Beijing) Translational Medical Research Center Co. Ltd., WuXiNextCODE in Shanghai, and MyGenostics Co. Ltd. in Beijing, for sequencing technology support. We would also like to thank Editage (www.editage.com) for English language editing.

SUPPLEMENTARY MATERIAL

The Supplementary Material for this article can be found online at: https://www.frontiersin.org/articles/10.3389/fmed.2021.771227/full#supplementary-material

REFERENCES

1. Büscher AK, Kranz B, Büscher R, Hildebrandt F, Dworniczak B, Pennekamp P, et al. Immunosuppression and renal outcome in congenital and pediatric steroid-resistant nephrotic syndrome. *Clin J Am Soc Nephrol.* (2010) 5:2075–84. doi: 10.2215/CJN.01190210
2. Zagury A, Oliveira AL, Montalvao JA, Novaes RH, Sa VM, Moraes C A, et al. Steroid-resistant idiopathic nephrotic syndrome in children: long-term follow-up and risk factors for end-stage renal disease. *J Bras Nefrol.* (2013) 35:191–9. doi: 10.5935/0101-2800.20130031
3. Trautmann A, Bodria M, Ozaltin F, Gheisari A, Melk A, Azocar M, et al. Spectrum of steroid-resistant and congenital nephrotic syndrome in children: the PodoNet registry cohort. *Clin J Am Soc Nephrol.* (2015) 10:592–600. doi: 10.2215/CJN.06260614
4. Li Y, He Q, Wang Y, Dang X, Wu X, Li X, et al. A systematic analysis of major susceptible genes in childhood-onset steroid-resistant nephrotic syndrome. *Ann Clin Lab Sci.* (2019) 49:330–7.
5. Dufek S, Holtta T, Trautmann A, Ylinen E, Alpay H, Ariceta G, et al. Management of children with congenital nephrotic syndrome: challenging treatment paradigms. *Nephrol Dial Transpl.* (2019) 34:1369–77. doi: 10.1093/ndt/gfy165
6. Santín S, García-Maset R, Ruíz P, Giménez I, Zamora I, Pena A, et al. Nephrin mutations cause childhood- and adult-onset focal segmental glomerulosclerosis. *Kidney Int.* (2009) 76:1268–76. doi: 10.1038/ki.2009.381
7. Rao J, Liu X, Mao J, Tang X, Shen Q, Li G, et al. Genetic spectrum of renal disease for 1001 Chinese children based on a multicenter registration system. *Clin Genet.* (2019) 96:402–10. doi: 10.1111/cge.13606

8. Richards S, Aziz N, Bale S, Bick D, Das S, Gastier-Foster J, et al. Standards and guidelines for the interpretation of sequence variants: a joint consensus recommendation of the American College of Medical Genetics and Genomics and the Association for Molecular Pathology. *Genet Med.* (2015) 17:405–24. doi: 10.1038/gim.2015.30
9. Shi Y, Ding J, Liu JC, Wang H, Pu DF. NPHS1 mutation in A Chinese family with congenital nephrotic syndrome. *Chin J Pediatr.* (2005) 43:10—4. doi: 10.3760/j.issn:0578-1310.2005.11.002
10. Kestilä M, Lenkkeri U, Männikkö M, Lamerdin J, McCready P, Putaala H, et al. Positionally cloned gene for a novel glomerular protein–nephrin–is mutated in congenital nephrotic syndrome. *Mol Cell.* (1998) 1:575–82. doi: 10.1016/S1097-2765(00)80057-X
11. Liu L, Doné SC, Khoshnoodi J, Bertorello A, Wartiovaara J, Berggren PO, et al. Defective nephrin trafficking caused by missense mutations in the NPHS1 gene: insight into the mechanisms of congenital nephrotic syndrome. *Hum Mol Genet.* (2001) 10:2637–44. doi: 10.1093/hmg/10.23.2637
12. Heeringa SF, Vlangos CN, Chernin G, Hinkes B, Gbadegesin R, Liu J, et al. Thirteen novel NPHS1 mutations in a large cohort of children with congenital nephrotic syndrome. *Nephrol Dial Transpl.* (2008) 23:3527–33. doi: 10.1093/ndt/gfn271
13. Lenkkeri U, Männikkö M, McCready P, Lamerdin J, Gribouval O, Niaudet P, et al. Structure of the gene for congenital nephrotic syndrome of the finnish type (NPHS1) and characterization of mutations. *Am J Hum Genet.* (1999) 64:51–61. doi: 10.1086/302182
14. Machuca E, Benoit G, Nevo F, Tête M, Gribouval O, Pawtowski A, et al. Genotype–phenotype correlations in non-finnish congenital nephrotic syndrome. *J Am Soc Nephrol.* (2010) 21:1209–17. doi: 10.1681/ASN.2009121309
15. Li G, Cao Q, Shen Q, Sun L, Zhai Y, Liu H, et al. Gene mutation analysis in 12 Chinese children with congenital nephrotic syndrome. *BMC Nephrol.* (2018) 19:382. doi: 10.1186/s12882-018-1184-y
16. Zhuo L, Huang L, Yang Z, Li G, Wang L, et al. A comprehensive analysis of NPHS1 gene mutations in patients with sporadic focal segmental glomerulosclerosis. *BMC Med Genet.* (2019) 20:111. doi: 10.1186/s12881-019-0845-4
17. Yang F, Chen Y, Zhang Y, Qiu L, Chen Y, Zhou J, et al. Novel NPHS1 gene mutations in a Chinese family with congenital nephrotic syndrome. *J Genet.* (2016) 95:161–6. doi: 10.1007/s12041-015-0598-6
18. Feng DN, Yang YH, Wang DJ, Meng DC, Fu R, Wang J, et al. Mutational analysis of podocyte genes in children with sporadic steroid-resistant nephrotic syndrome. *Genet Mol Res.* (2014) 13:9514–22. doi: 10.4238/2014.November.11.16
19. Ulinski T, Aoun B, Toubiana J, Vitkevic R, Bensman A, Donadieu J, et al. Neutropenia in congenital nephrotic syndrome of the Finnish type: role of urinary ceruloplasmin loss. *Blood.* (2009) 113:4820–1. doi: 10.1182/blood-2009-02-204099
20. Fu R, Gou MF, Ma WH, He JJ, Luan Y, Liu J, et al. Novel NPHS1 splice site mutations in a Chinese child with congenital nephrotic syndrome. *Genet Mol Res.* (2015) 14:433–9. doi: 10.4238/2015.January.23.17
21. Zhang R, Zhou WL, Xu LX, Liu Y. The gene mutation in one neonate with Finnish type congenital nephrotic syndrome. *Journal of Clinical Pediatrics.* (2016) 34:185–7.
22. Wu LQ, Hu JJ, Xue JJ, Liang DS. Two novel NPHS1 mutations in a Chinese family with congenital nephrotic syndrome. *Genet Mol Res.* (2011) 10:2517–22. doi: 10.4238/2011.October.18.1
23. Schoeb DS, Chernin G, Heeringa SF, Matejas V, Held S, Vega-Warner V, et al. Nineteen novel NPHS1 mutations in a worldwide cohort of patients with congenital nephrotic syndrome (CNS). *Nephrol Dial Transpl.* (2010) 25:2970–6. doi: 10.1093/ndt/gfq088
24. Bérody S, Heidet L, Gribouval O, Harambat J, Niaudet P, Baudouin V, et al. Treatment and outcome of congenital nephrotic syndrome. *Nephrol Dial Transpl.* (2019) 34:458–67. doi: 10.1093/ndt/gfy015
25. Hamasaki Y, Hamada R, Muramatsu M, Matsumoto S, Aya K, Ishikura K, et al. A cross-sectional nationwide survey of congenital and infantile nephrotic syndrome in Japan. *BMC Nephrol.* (2020) 21:363. doi: 10.1186/s12882-020-02010-5
26. Sharief SN, Hefni NA, Alzahrani WA, Nazer II, Bayazeed MA, Alhasan KA, et al. Genetics of congenital and infantile nephrotic syndrome. *World J Pediatr.* (2019) 15:198–203. doi: 10.1007/s12519-018-00224-0
27. Philippe A, Nevo F, Esquivel EL. Reklaityte D,Gribouval O, Tête, MJ, et al. Nephrin mutations can cause childhood-onset steroid-resistant nephrotic syndrome. *J Am Soc Nephrol.* (2008) 19:1871–8. doi: 10.1681/ASN.2008010059
28. Ovunc B, Ashraf S, Vega-Warner V, Bockenhauer D, Soliman Elshakhs NA, Joseph M, et al. Mutation analysis of NPHS1 in a worldwide cohort of congenital nephrotic syndrome patients. *Nephron Clinical Practice.* (2012) 120:c139–46. doi: 10.1159/000337379
29. Wong W, Morris MC, Kara T. Congenital nephrotic syndrome with prolonged renal survival without renal replacement therapy. *Pediatr Nephrol.* (2013) 28:2313–21. doi: 10.1007/s00467-013-2584-7
30. Jia X, Yamamura T, Gbadegesin R, McNulty MT, Song K, Nagano C, et al. Common risk variants in NPHS1 and TNFSF15 are associated with childhood steroid-sensitive nephrotic syndrome. *Kidney Int.* (2020) 98:1308–22. doi: 10.1016/j.kint.2020.05.029
31. Wang Y, Dang X, He Q, Zhen Y, He X, Yi Z, et al. Mutation spectrum of genes associated with steroid-resistant nephrotic syndrome in Chinese children. *Gene.* (2017) 625:15–20. doi: 10.1016/j.gene.2017.04.050
32. Yu ZH, Wang DJ, Meng DC, Huang J, Nie XJ, et al. Mutations in NPHS1 in a Chinese child with congenital nephrotic syndrome. *Genet Mol Res.* (2012) 11:1460–4. doi: 10.4238/2012.May.18.6
33. Li P. Novel nphs1 gene mutations in two Chinese infants with congenital nephrotic syndrome. *The Indian Journal of Pediatrics.* (2017) 84:489–90. doi: 10.1007/s12098-017-2296-2

Conflict of Interest: The authors declare that the research was conducted in the absence of any commercial or financial relationships that could be construed as a potential conflict of interest.

frontiers in Medicine

CASE REPORT
published: 10 December 2021
doi: 10.3389/fmed.2021.795216

Case Report: Homozygous Pathogenic Variant P209L in the *TTC21B* Gene: A Rare Cause of End Stage Renal Disease and Biliary Cirrhosis Requiring Combined Liver-Kidney Transplantation. A Case Report and Literature Review

Giuseppe Gambino[1†], *Concetta Catalano*[1*†], *Martina Marangoni*[2], *Caroline Geers*[3,4], *Alain Le Moine*[5], *Nathalie Boon*[6], *Guillaume Smits*[7] and *Lidia Ghisdal*[1,8]

[1] Department of Nephrology, Dialysis and Renal Transplantation, Erasmus Erasme Hospital, Free University of Brussels, Brussels, Belgium, [2] Department of Genetics, Erasme Hospital, Free University of Brussels, Brussels, Belgium, [3] Department of Nephropathology, Universitair Ziekenhuis Brussel, Brussels, Belgium, [4] Department of Nephropathology, Brugmann University Hospital, Brussels, Belgium, [5] Department of Nephrology, Dialysis and Renal Transplantation, Erasme Hospital, Free University of Brussels, Brussels, Belgium, [6] Department of Gastroenterology, Erasme Hospital, Free University of Brussels, Brussels, Belgium, [7] Department of Genetics, Erasme Hospital, Free University of Brussels, Brussels, Belgium, [8] Department of Nephrology and Dialysis, Epicura Hospital, Saint-Ghislain, Belgium

OPEN ACCESS

Edited by:
Duan Ma,
Fudan University, China

Reviewed by:
Dorin-Bogdan Borza,
Meharry Medical College, United States
Daw-Yang Hwang,
National Health Research Institutes, Taiwan

***Correspondence:**
Concetta Catalano
concetta.catalano@erasme.ulb.ac.be

[†] *These authors have contributed equally to this work*

Specialty section:
This article was submitted to Nephrology, a section of the journal Frontiers in Medicine

Received: *14 October 2021*
Accepted: *12 November 2021*
Published: *10 December 2021*

Citation:
Gambino G, Catalano C, Marangoni M, Geers C, Moine AL, Boon N, Smits G and Ghisdal L (2021) Case Report: Homozygous Pathogenic Variant P209L in the TTC21B Gene: A Rare Cause of End Stage Renal Disease and Biliary Cirrhosis Requiring Combined Liver-Kidney Transplantation. A Case Report and Literature Review. Front. Med. 8:795216. doi: 10.3389/fmed.2021.795216

Background: Ciliopathies are rare diseases causing renal and extrarenal manifestations. Here, we report the case of a ciliopathy induced by a homozygous pathogenic variant in the *TTC21B* gene.

Case Description: A 47-year-old patient started hemodialysis for chronic kidney disease (CKD) of unknown origin. She presented with early onset of hypertension, pre-eclampsia, myopia and cirrhosis. Renal biopsy showed mild interstitial fibrosis, tubular atrophy, and moderate arteriosclerosis while liver pathology demonstrates grade B biliary cirrhosis. Family history revealed several cases of early-onset severe hypertension and one case of end-stage renal disease (ESRD) needing kidney transplantation at twenty years of age. Clinical exome sequencing showed homozygosis for the pathogenic variant c.626C>T (p.Pro209Leu) in the *TTC21B* gene. The patient underwent combined liver-renal transplantation with an excellent renal and hepatic graft outcome.

Conclusions: *TTC21B* gene mutations can lead heterogeneous to clinical manifestations and represent an underappreciated cause of ESRD. The paradigm in diagnosis of CKD of early onset and/or of unknown origin is changing and genetic counseling should be performed in all patients and families that meet those criteria. Renal or combined liver-renal transplantation represents the best option for patients suffering from those diseases in terms of prognosis and quality of life.

Keywords: ciliopathies, *TTC21B*, clinical exome, end stage renal disease (ESRD), biliary cirrhosis, combined liver and kidney transplant

INTRODUCTION

Ciliopathies are wide and heterogeneous range of human disorders that are caused by cilia dysfunction. Cilia and their components have a key role in multiple human functions including the perception of environmental cues and the development of many vertebrate tissues. Although the term ciliopathy has been used for the first time in 1984, mechanisms related to cilia dysfunctions are not yet completely understood.

Two orders of ciliopathies have been described according to the localization and function of the muted protein. First order ciliopathies are related to dysfunction of a protein localized or functionally connected with the basal body and/or ciliary compartment. Second order ciliopathies are caused by mutations in proteins that are not part of cilium structure and that indirectly interact with cilium formation or function (1).

The *TTC21B* gene is situated in the short arm of chromosome 2 (2q24.3) and codes for an intraflagellar transport-A (IFT-A) ciliary protein called IFT139. The intraflagellar transport (IFT) complex is a group of at least 20 proteins that were discovered in the 1990s, named according to their molecular weight, and which act as adapters between the motor proteins required for movement and ciliary cargo proteins. IFT complexes (IFT-B and IFT-A) are involved in anterograde and retrograde transport respectively (2) and defects in IFT proteins typically disrupt ciliary assembly and attenuate Hedgehog signaling which is a highly conserved intracellular pathway involved in in embryogenesis and organ development (3). IFT complex mutation leads to first order ciliopathies (2).

Here, we report a case of a homozygous pathogenic variant in the *TTC21B* gene, with renal and extrarenal manifestations. The patient's clinical history is summarized in the timeline (**Figure 1**).

CASE DESCRIPTION

A 47-year-old woman was referred to the nephrology department in February 2017, in order to initiate haemodialysis for end-stage renal disease (ESRD).

She was diagnosed with severe hypertension and chronic kidney disease (CKD) at age 20. She was born from an inbred union of a North African family and several cases of hypertension, myopia, and severe kidney disease occurred in the extended family. Her past medical history was unremarkable except for obesity. The genealogical tree (**Figure 2**) showed several loops of consanguinity predisposing to recessive disease. Her brother died at

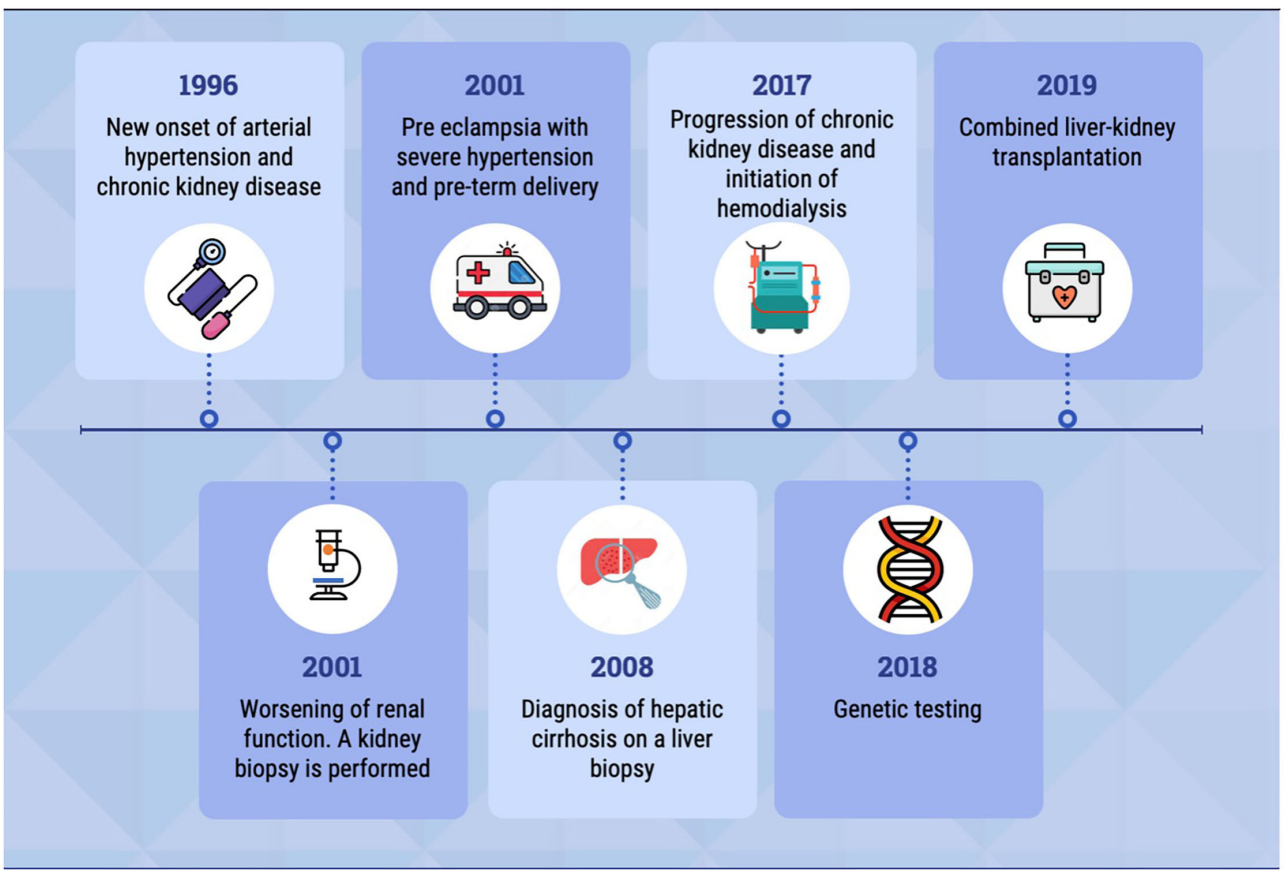

FIGURE 1 | The timeline shows the most relevant events in patient's clinical history.

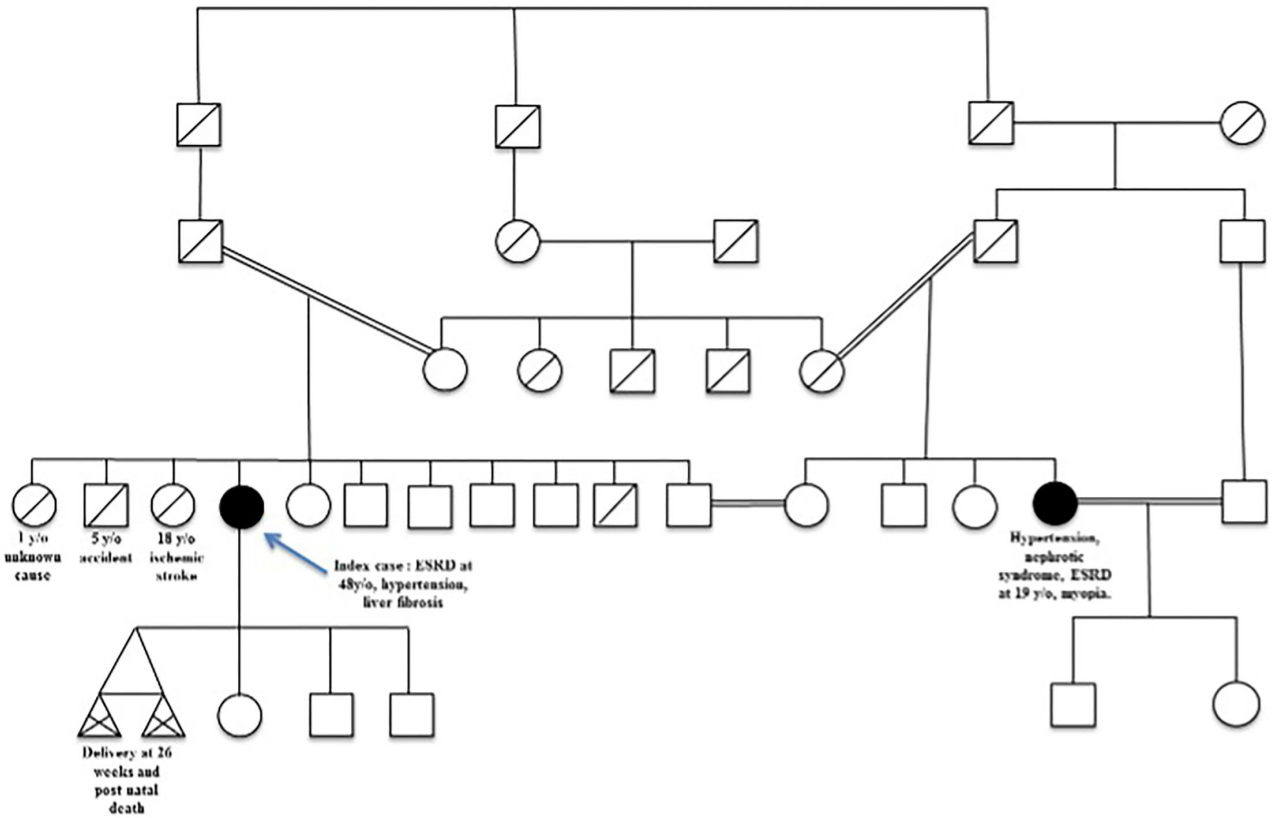

FIGURE 2 | Patient's familial pedigree. The index case is indicated by the blue arrow.

age 5 and one of her sisters died from stroke at age 18 due to severe hypertension. A maternal cousin, also born from an inbred union, presented with myopia, nephrotic syndrome, ESRD, requiring dialysis and renal transplantation at age 20.

At diagnosis, serum creatinine was 1.4 mg/dL. Urinary sediment was within normal limits, while a moderate mixed proteinuria was detected with a protein/creatinine ratio of 1.5 g/g. Auto-immunity screening was negative, but complement was not investigated. Renal ultrasound revealed no abnormalities. Renal magnetic resonance imaging (MRI) ruled out renal arterial stenosis, but no other tests aimed to exclude secondary hypertension were available in the patient's medical record. Angiotensin-converting enzyme inhibitor was started as the only treatment.

Five years after diagnosis, a serum creatinine of 2.79 mg/dL justified a kidney biopsy. Light microscopy (**Figure 3**) showed six glomeruli, five of which were within normal limits while one presented advanced sclerosis. Lesions of mild interstitial fibrosis and tubular atrophy were described. Arteries showed moderate arteriosclerosis (**Figure 4**). Immunofluorescence staining and electron microscopy have not been performed because frozen and glutaraldehyde fixed tissue were not available. An episode of pre-eclampsia occurred during the same year, leading to delivery at 26 weeks and post-natal death of twins.

Concurrently, an isolated cholestasis appeared. Viral serologies and immunological screening were negative. No alpha-1 anti-trypsin (AAT) deficiency was detected. Magnetic resonance imaging (MRI) showed hepatosplenomegaly and hepatic elastography values were consistent with severe fibrosis (64 kPa). Two consecutives liver biopsies showed micro-vacuolar steatosis and periportal fibrosis. Twelve years after diagnosis, because of increasing in liver enzymes and persistent severe itching, a third liver biopsy was performed. It revealed lesions of chronic cholestasis with focal acute cholangitis and peri-portal fibrosis highly suggestive of grade B biliary cirrhosis according to the Child-Pugh score.

Due to irreversible deterioration of renal function and poorly controlled hypertension, the patient started haemodialysis at 48 years of age.

A genetic work-up was performed during pre-transplant screening due to an early-onset of ESRD and liver fibrosis of unknown origin.

Clinical exome sequencing was performed on the patient's DNA using in-house SeqCap EZ choice XL capture (Roche Nimblegen, WI, USA) targeting the coding exons of 3989 genes associated with Mendelian disorders. Libraries were sequenced on an Illumina NovaSeq 6000. Variant filtering and interpretation were carried out through Highlander (https://sites.uclouvain.be/highlander/). In particular, 424 genes

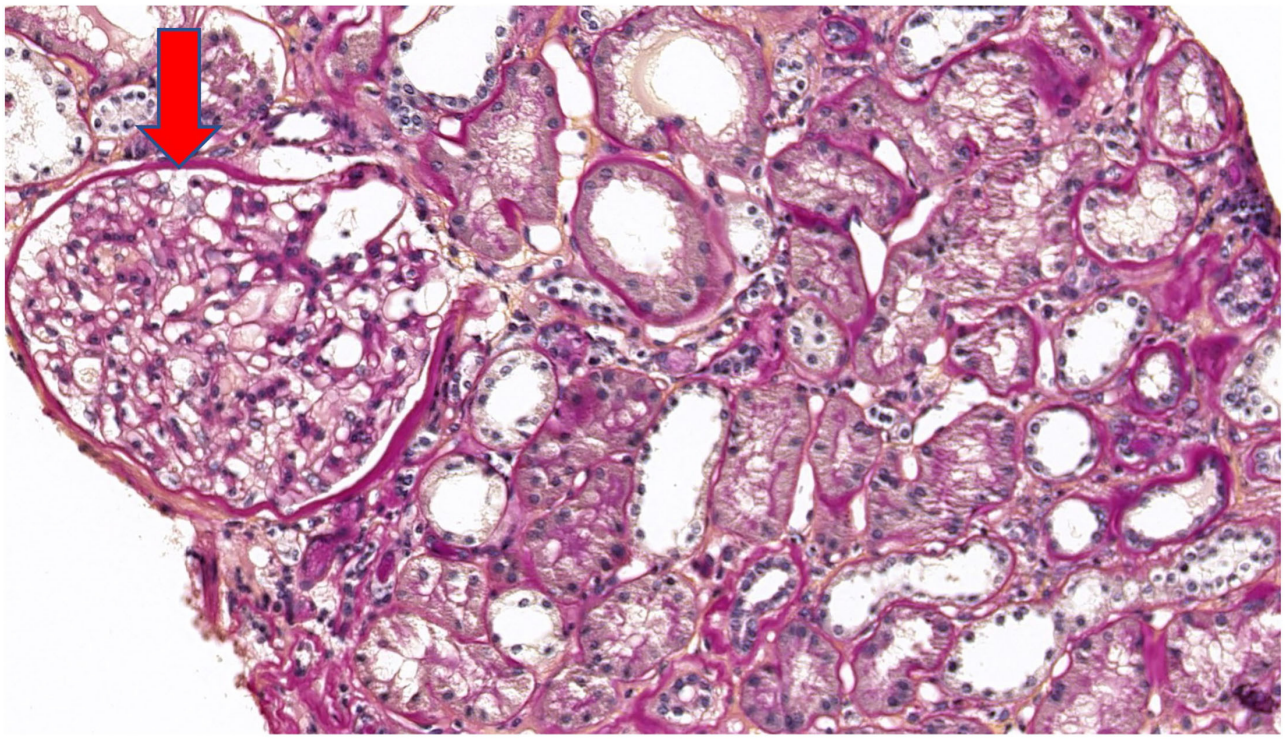

FIGURE 3 | Periodic acid Schiff (PAS) stain at ×20 magnification on light microscopy showing a normal glomerulus (arrow).

involved in kidney disease (i.e., cortico-resistant nephrotic syndrome/focal segmental glomerular sclerosis [FSGS], ciliopathies, etc.) were analysed (gene list available upon request). Variant classification was accomplished according to American College of Medical Genetics (ACMG) guidelines (4). Genetic analysis showed that the patient was homozygous for the c.626C>T (p.Pro209Leu) (P209L) variant in the *TTC21B* gene (NM_024753.5) (**Figure 5A**). The presence of this variant was validated by Sanger sequencing in the patient and her cousin who developed ESRD (**Figure 5B**). This variant is present with a frequency of 0.012% (34/282510 alleles) and has never been seen in the homozygous state in the gnomAD frequency database (https://gnomad.broadinstitute.org/). Several prediction tools (SIFT, MutationTaster, FATHMM, PolyPhen-2, LRT) agree with the prediction that this change is likely to be deleterious. Moreover, it has been previously reported as pathogenic in several studies (5–8). For these reasons, this variant has been classified as pathogenic (class V).

Combined liver-renal transplantation was performed at 50 of age. Basiliximab has been used as induction therapy, while methylprednisolone, tacrolimus and mofetil mycophenolate have been employed for maintenance. The immediate post-operative period was completely unremarkable. However, few months later the patient developed New Onset Diabetes After Transplantation (NODAT) and pulmonary tuberculosis that recovered without complications after treatment with isoniazid, rifampicin and ethambutol. Both liver and renal graft outcomes remained excellent 24 months after transplantation. The patient experienced substantial improvement in quality of life as she reported repeatedly during transplant follow-up.

At last follow-up, the patient's serum creatinine was 1.4 mg/dL, proteinuria was indetectable (<0.05 g/g creatinine), and urinary sediment was unremarkable. Cytolytic enzymes were within the normal limits (Alanine aminotransferase 20 U/L, Aspartate aminotransferase 26 U/L), as well as albumin (43 g/L) and prothrombin time (10.9 sec; INR 1.04).

Blood pressure was on target without any hypotensive treatment.

DISCUSSION AND REVIEW OF THE LITERATURE

In the clinical case depicted above, the patient presented with a homozygous missense mutation modifying the amino sequence of the IFT139 protein that is expressed in distal tubules and podocytes.

Animal models in mice and zebrafish have shown that knockdown or missense mutations of this protein can lead to ciliary impairment in tubular renal cells resulting in primary cilia defects, abnormal cell migration, and cytoskeletal alterations (9).

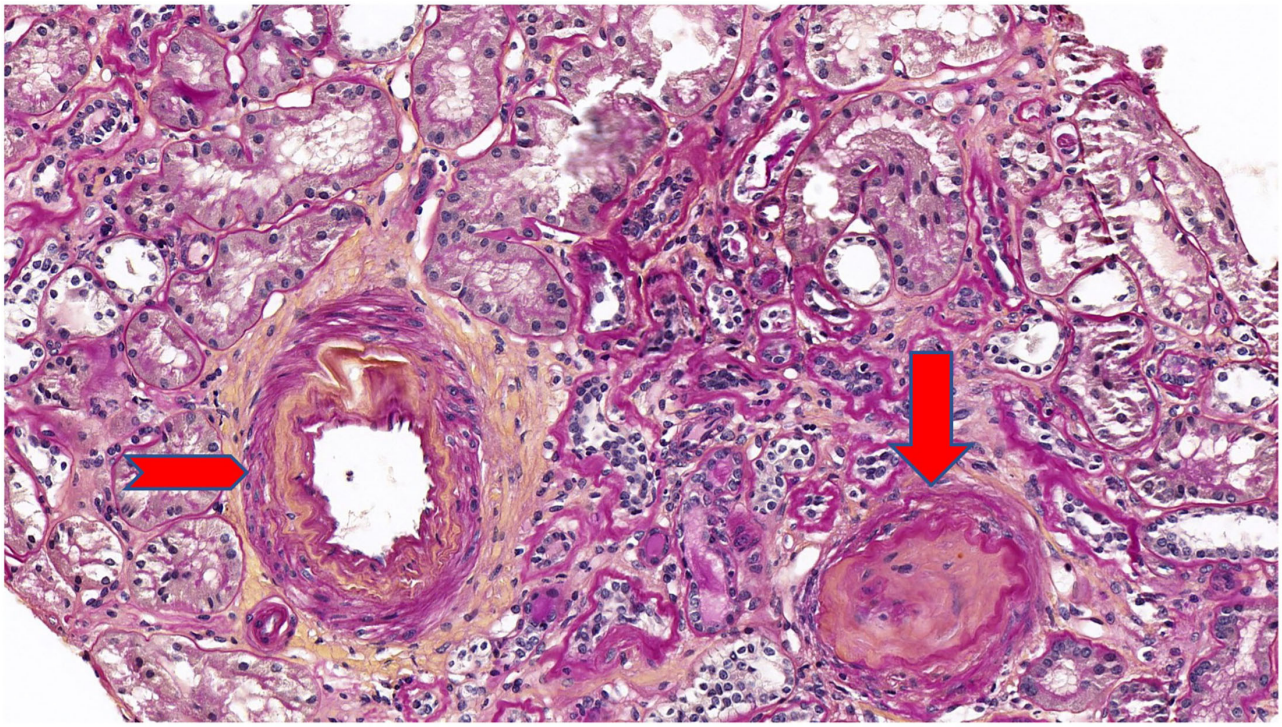

FIGURE 4 | Periodic acid Schiff (PAS) stain at ×20 magnification on light microscopy showing a mild interstitial fibrosis and tubular atrophy. One glomerulus out of 6 showed a complete sclerosis (arrow). Arteries showed a moderate arteriosclerosis (arrowhead).

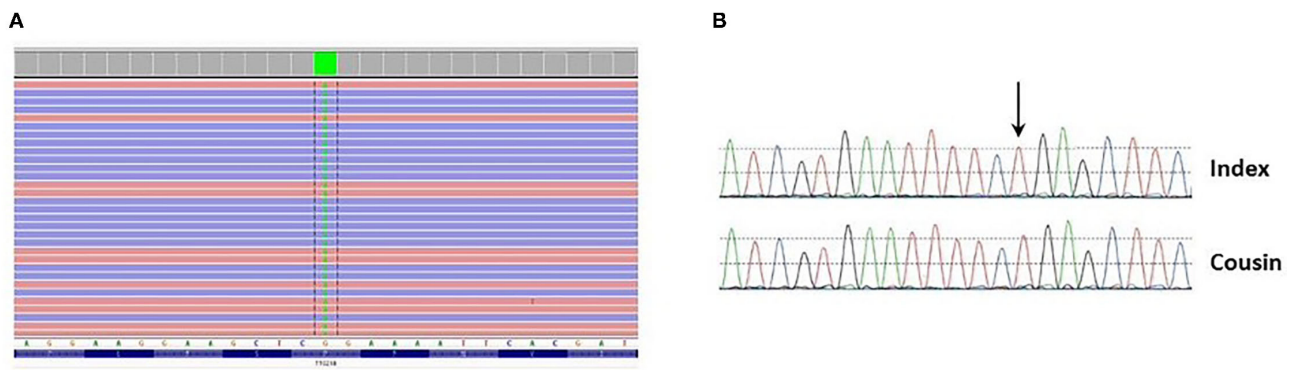

FIGURE 5 | (A) Presence of the c.626C>T p.(Pro209Leu) variant (green block) at homozygous state in exon 6 of the TTC21B gene found through clinical exome sequencing and visualized in Integrative Genomics Viewer (IGV). **(B)** Presence of the variant at homozygous state in the patient and her cousin was confirmed by Sanger sequencing.

Mutations in *TTC21B* gene lead to a wide spectrum of phenotypes such as syndromic Jeune asphyxiating thoracic dystrophy (JATD) and nephronophthisis (NPHP) with or without extrarenal manifestations. The nephronophthisis phenotype is characterized by reduced renal concentrating ability, chronic tubulointerstitial nephritis, cystic renal disease, and progression to ESRD before the age of 30 (10).

p.P209L homozygous mutations have mostly been described in patients of North African or Portuguese descent indicating a founder effect, and several renal and extrarenal manifestations have been associated to this specific mutation in the currently available literature (**Table 1**).

In particular, Cong et al. have described the association between *TTC21B* p.P209L mutation and hereditary FSGS in ten families (18 cases). Clinical features were late-onset proteinuria, steroid-resistant nephrotic syndrome, FSGS associated with tubulointerstitial lesions, high blood pressure and ESRD occurring between the ages of 15 and 35 (5).

TABLE 1 | Publications reporting cases with TTC21B p209L mutation.

References	No. of patients	Phenotype	Renal histology
Doreille et al. (11)	6	CKD ($n = 7$), history of hypertensive emergency ($n = 5$), hepatic involvement ($n = 5$)	Vascular lesions ($n = 6$), TMA ($n = 4$), no tubule-interstitial lesions or FSGS founded.
Cong et al. (5)	18	CKD ($n = 18$), proteinuria ($n = 16$), hypertension ($n = 15$), hepatic involvement ($n = 2$), cerebral aneurism ($n = 2$), myopia ($n = 1$)	FSGS ($n = 10$), tubulointerstitial fibrosis ($n = 10$)
Bullich et al. (6)	3	CKD ($n = 2$), proteinuria ($n = 3$), hypertension ($n = 2$), myopia ($n = 2$)	Global sclerosis ($n = 1$), FSGS ($n = 2$), Tubulointerstitial fibrosis ($n = 3$)

Moreover, Bullich et al. described another three cases with high blood pressure associated to the same homozygous mutation and two other compound heterozygous cases including one p.P209L mutation (3). Out of those 23 cases described in the literature, high blood pressure and myopia were present in 74 and 22% of patients respectively (5, 6).

Doreille et al., have recently reported a series of seven patients with *TTC21B* mutations, six of which presented with a p.P209L homozygous mutation. All those patients presented with severe hypertension (associated with left ventricular hypertrophy and hypertensive retinopathy) and ESRD. Four of them underwent a kidney biopsy showing hypertensive nephrosclerosis with arteriolar thrombotic microangiopathy (TMA), without the usual aspect of nephronophthisis. Two out of seven patients had biologic evidence of TMA.

The authors speculated that hypertension in patients with nephronophthisis could be related to dysfunctional cilia located on endothelium which are key in blood pressure control. They brilliantly coined the term "nephroangionophthisis" to broaden the spectrum of nephronophthisis and to better define the phenotype with vascular injury and hypertension which was nearly unknown before (11).

Therefore, patients affected by *TTC21B* mutations can present with different renal manifestations that may overlap with each other. Phenotypes include not only familial nephrotic syndrome associated with lesions of Focal and Segmental Glomerulosclerosis (FSGS) (10) and tubulo-interstitial abnormalities (2), but also endothelial damage and hypertension with histological and/or biological evidence of TMA (11).

Hepatic impairment is not uncommon in *TTC21B* mutations. Zhang et al., reported one pediatric case with mild cytolysis and one with hepatosplenomegaly, both associated with NPHP. Cong et al., described a case of biliary cirrhosis and one case of chronic chilestasis (5, 12). An association of congenital hepatic fibrosis with NPHP or JATD has also been reported (13). In the series published by Doreille et al. (11), five out of seven patients had liver test abnormalities (mild cholestasis and cytolysis) and MRI showed an aspect of Caroli disease in one patient.

While obesity and diabetes are not typical features of *TTC21B* mutation, a murine model showed that *TTC21B*/*IFT139* knockout mice developed hyperphagic behavior and obesity, resulting in type II diabetes mellitus and fatty liver disease (2).

The renal involvement in our patient was mainly characterized by mild interstitial fibrosis and tubular atrophy. Neither lesions of FSGS nor TMA were seen on kidney biopsy, but the renal sample size was too small to draw conclusions on this point. Extra-renal manifestations included hypertension, obesity, chronic cholestasis and slowly progressive hepatic fibrosis requiring liver transplantation. However, given the degree of inbreeding in the patient's family, the hepatic impairment might be the result of other pathogenic mutations or, less probably, due to non-genetic causes.

The same homozygotic *TTC21B* p.P209L mutation was found after transplantation in the patient's elder cousin who presented with progressive CKD, severe proteinuria and myopia. As one of the patient's sisters died at the age 18 from an ischemic stroke due to severe hypertension, it could be speculated that she was carrying the same mutation, with the nephroangionophthisis phenotype as described by Doreille et al. (11) even if sequencing result for other members of the patient's family, including parents, was not performed. As a result, it cannot be excluded that this pedigree have compound heterozygous mutations containing the c.626C>T and a deletion span of the c.626C>T region that can not be detected by short- read exome and Sanger sequencing.

As treatment is purely supportive, renal or combined liver-renal transplantation represents the best option. It improves survival, especially if liver failure exists, it provides an excellent prognosis because no relapse occurs on the graft, and it ameliorates quality of life due to withdrawal from dialysis. Three cases of combined kidney-liver transplantation (CKLT) have been reported in a French series of pediatric patients suspected of ciliopathy with ESRD and hepatic fibrosis (14). One case of sequential liver-renal transplantation has been described in a juvenile NPHP patient in Japan (15). None of these patients presented with a clear *TTC21B* mutation. To our best knowledge, this is the first case of combined liver-kidney transplantation described in the literature in a genetically proven *TTC21B*-related ciliopathy.

Recent publications underline that the paradigm in diagnosis of CKD of early onset and/or of unknown origin is shifting from precise phenotypic characterization to a focus on genotype. The case described here serves to emphasize the importance of performing genetic analysis in all patients and families that meet testing criteria. Phenotype alone can be misleading for clinicians. In fact, similar disease states with similar pathological findings and can be the expression of unrelated underlying mutations

carrying different prognoses. Reporting such cases should be encouraged in order to strengthen the understanding of rare kidney diseases, thereby improving management and patient outcomes.

CONCLUSIONS

TTC21B gene mutations like p.P209L are rare but underestimated causes of ESRD. Renal involvement includes NPHP, FSGS and TMA, and can be accompanied by life-threatening extrarenal manifestations such as severe hypertension and/or liver cirrhosis and failure. Renal or combined liver-renal transplantation represents the best treatment option, offering excellent graft outcome and improvement in quality of life. In line with the recent literature (10, 16), we strongly encourage the use of genetic testing and counseling in all cases of chronic kidney disease of early onset and/or of unknown origin.

DATA AVAILABILITY STATEMENT

The datasets presented in this study can be found in online repositories. The names of the repository/repositories and accession number(s) can be found below: https://www.lovd.nl/, #0000814750.

AUTHOR CONTRIBUTIONS

CC contributed to the diagnosis of the disease and to write the manuscript. LG contributed to perform clinical exome sequencing lead to the diagnosis, to write the manuscript, and supervised the whole scientific work. NB and AM contributed to write the manuscript. CG performed the pathology lecture and contributed to write the manuscript. MM and GS contributed to perform clinical exome sequencing and to write the manuscript. GG performed all literature review and contributed to write the manuscript. All authors contributed to the article and approved the submitted version.

REFERENCES

1. Reiter JF, Leroux, M. R Genes and molecular pathways underpinning ciliopathies. *Nat Rev Molec Cell Biol.* (2017) 18:533–47. doi: 10.1038/nrm.2017.60
2. Taschner M, Bhogaraju S, Lorentzen, E. Architecture and function of IFT complex proteins in ciliogenesis. *Differentiation.* (2012) 83:S12–22. doi: 10.1016/j.diff.2011.11.001
3. Goetz SC, Anderson KV. The primary cilium: a signalling centre during vertebrate development. *Nat Rev Genet.* (2010) 11:331–44. doi: 10.1038/nrg2774
4. Richards S, Aziz N, Bale S, Bick D, Das S, Gastier-Foster J, et al. Standards and guidelines for the interpretation of sequence variants: a joint consensus recommendation of the American College of Medical Genetics and Genomics and the Association for Molecular Pathology. *Genet Med.* (2015) 17:405–24. doi: 10.1038/gim.2015.30
5. Cong EH, Bizet AA, Boyer O, Woerner S, Gribouval O, Filhol E, et al. A homozygous missense mutation in the ciliary gene TTC21B causes familial FSGS. *J Am Soc Nephrol.* (2014) 25:2435–43. doi: 10.1681/ASN.2013101126
6. Bullich G, Vargas I, Trujillano D, Mendizábal S, Pinero-Fernandez JA, Fraga G, et al. Contribution of the TTC21B gene to glomerular and cystic kidney diseases. *Nephrol Dialysis Transplant.* (2017) 32:151–6. doi: 10.1093/ndt/gfv453
7. Warejko JK, Tan W, Daga A, Schapiro D, Lawson JA, Shril S, et al. Whole exome sequencing of patients with steroid-resistant nephrotic syndrome. *Clin J Am Soc Nephrol.* (2018) 13:53–62. doi: 10.2215/CJN.04120417
8. Abo El Fotoh WMM, Al-fiky AF. A compound heterozygous mutation in the ciliary gene TTC21B causes nephronophthisis type 12. *J Pediat Genet.* (2020) 09:198–202. doi: 10.1055/s-0039-1700804
9. Davis EE, Zhang Q, Liu Q, Diplas BH, Davey LM, Hartley J, et al. TTC21B contributes both causal and modifying alleles across the ciliopathy spectrum. *Nat Genet.* (2011) 43:189–96. doi: 10.1038/ng.756
10. Hildebrandt F, Zhou W. Nephronophthisis-associated ciliopathies. *J Am Soc Nephrol.* (2007) 18:1855–71. doi: 10.1681/ASN.2006121344
11. Doreille A, Raymond L, Lebre AS, Linster C, Lamri RS, Karras A, et al. Nephronophthisis in young adults phenocopying thrombotic microangiopathy and severe nephrosclerosis. *Clin J Am Soc Nephrol.* (2021) 16:615–7. doi: 10.2215/CJN.11890720
12. Zhang H, Su B, Liu X, Xiao H, Ding J, Yao Y. Mutations in TTC21B cause different phenotypes in two childhood cases in China. *Nephrology.* (2018) 23:371–6. doi: 10.1111/nep.13008
13. Gunay-Aygun M, Gahl WA, Heller T. *Congenital Hepatic Fibrosis Overview – retired chapter, for historical reference only.* This publication has been retired this archival version is for historical reference only, and the information may be out of date. (1993).
14. Duclaux-Loras R, Bacchetta J, Berthiller J, Rivet C, Demède D, Javouhey E, et al. Pediatric combined liver–kidney transplantation: a single-center experience of 18 cases. *Pediat Nephrol.* (2016) 31:1517–29. doi: 10.1007/s00467-016-3324-6
15. Udagawa T, Kamei K, Ogura M, Tsutsumi A, Noda S, Kasahara M, et al. Sequential liver-kidney transplantation in a boy with congenital hepatic fibrosis and nephronophthisis from a living donor. *Pediatric Transplant.* (2012) 16:E275–80. doi: 10.1111/j.1399-3046.2011.01611.x
16. Groopman EE, Marasa M, Cameron-Christie S, Petrovski S, Aggarwal VS, Milo-Rasouly H, et al. Diagnostic utility of exome sequencing for kidney disease. *New England J Med.* (2019) 380:142–51. doi: 10.1056/NEJMc1903250

Conflict of Interest: The authors declare that the research was conducted in the absence of any commercial or financial relationships that could be construed as a potential conflict of interest.

frontiers in Medicine

ORIGINAL RESEARCH
published: 05 January 2022
doi: 10.3389/fmed.2021.807898

Robo2 and *Gen1* Coregulate Ureteric Budding by Activating the MAPK/ERK Signaling Pathway in Mice

Yaxin Li[1], *Minghui Yu*[1], *Lihong Tan*[1], *Shanshan Xue*[1], *Xuanjin Du*[1], *Xiaohui Wu*[1,2], *Hong Xu*[1]* *and Qian Shen*[1]*

[1] *Department of Nephrology, Shanghai Kidney Development and Pediatric Kidney Disease Research Center, Children's Hospital of Fudan University, Shanghai, China,* [2] *State Key Laboratory of Genetic Engineering and National Center for International Research of Development and Disease, Collaborative Innovation Center of Genetics and Development, Institute of Developmental Biology and Molecular Medicine, School of Life Sciences, Fudan University, Shanghai, China*

Congenital anomalies of the kidney and urinary tract (CAKUT) are some of the most common developmental defects and have a complicated etiology, indicating an interaction of (epi-) genetic and environmental factors. Single gene mutations and copy number variations (CNVs) do not explain most cases of CAKUT, and simultaneous contributions of more than one gene (di-, oligo-, or polygenic effects; i.e., complex genetics) may lead to the pathogenesis of CAKUT. *Robo2* plays a key role in regulating ureteric bud (UB) formation in the embryo, with mutations leading to supernumerary kidneys. *Gen1* is a candidate gene associated with CAKUT because of its important role in early metanephric development in mice. We established a mouse model with double disruption of *Robo2* and *Gen1* using a *piggyBac* transposon and found that double gene mutation led to significantly increased CAKUT phenotypes in $Robo2^{PB/+}Gen1^{PB/+}$ mouse offspring, especially a duplicated collecting system. Increased ectopic UB formation was observed in the $Robo2^{PB/+}Gen1^{PB/+}$ mice during the embryonic period. *Robo2* and *Gen1* exert synergistic effects on mouse kidney development, promoting cell proliferation by activating the GDNF/RET pathway and downstream MAPK/ERK signaling. Our findings provide a disease model for CAKUT as an oligogenic disorder.

Keywords: *Robo2, GEN1*, congenital anomalies of the kidney and urinary tract, GDNF/RET, oligo-/polygenic disease

OPEN ACCESS

Edited by:
Andrew Mallett, Townsville University Hospital, Australia

Reviewed by:
Jan Halbritter, Leipzig University, Germany
Jennifer Li, The University of Sydney, Australia
Danica Vojisavljevic, James Cook University, Australia

***Correspondence:**
Hong Xu
hxu@shmu.edu.cn
Qian Shen
shenqian@shmu.edu.cn

Specialty section:
This article was submitted to Nephrology, a section of the journal Frontiers in Medicine

Received: *02 November 2021*
Accepted: *13 December 2021*
Published: *05 January 2022*

Citation:
Li Y, Yu M, Tan L, Xue S, Du X, Wu X, Xu H and Shen Q (2022) Robo2 and Gen1 Coregulate Ureteric Budding by Activating the MAPK/ERK Signaling Pathway in Mice. Front. Med. 8:807898. doi: 10.3389/fmed.2021.807898

INTRODUCTION

Congenital anomalies of the kidney and urinary tract (CAKUT) collectively represent a diverse group of structural malformations that occur during embryonic kidney development, including renal hypoplasia/dysplasia, agenesis, multicystic dysplasia, duplex kidney, hydroureters and ureteropelvic junction obstructions (1). CAKUT is caused by defective kidney development. Mouse kidney development begins at E10.5 with formation of the ureteric bud (UB) from the caudal end of the Wolffian duct (WD), which invades the surrounding metanephric mesenchyme (MM) (2). The UB undergoes T-shaped branching at E11.5 and initiates an arborization program of dichotomous branching events, eventually giving rise to the ureteric tree (3). The MM gives rise to both the cap mesenchyme (nephron progenitor cells),

which undergoes a balance of self-renewal and differentiation to sequentially form epithelial nephrons (4, 5), and the stromal elements of the final kidney (6).

The development of the kidney and urinary tract is tightly regulated by multiple genes. However, single gene mutations and copy number variations (CNVs) do not explain the majority of sporadic cases of CAKUT, while complex interactions of multiple genetic and environmental factors may explain a substantial proportion of cases (7). Furthermore, even in mouse models, the phenotypes resulting from genetic deletion vary substantially, suggesting that gene-gene and gene-environment interactions contribute to CAKUT (8). Previous research by our team indicated that a low-protein diet synergizes with *Robo2* mutation to increase the risk of developmental abnormalities in the mouse urinary system (9). Moreover, some mouse polygenic models of CAKUT, such as $Pax2^{+/-}Pax8^{+/-}$ (8), $Hnf1b^{+/-}Pax2^{+/-}$ (9), and $Foxc1^{+/-}Foxc2^{+/-}$ (10) double heterozygous mice, have been established, suggesting that a haploinsufficient genetic combination will result in the CAKUT phenotype. A previous study reported a patient with renal hypodysplasia (RHD) carrying homozygous missense mutations in both *BMP4* (p.N150K) and *DACH1* (p.R684C), which provides a model for RHD as an oligo-/polygenic disorder (11). Therefore, CAKUT is likely associated with multiple gene variants.

Several key regulatory genes involved in normal kidney development in humans and mice, including Roundabout Guidance Receptor 2 (*ROBO2*) and GEN1 Holliday Junction 5′ Flap Endonuclease (*GEN1*), attracted our attention because they play key roles in early urogenital tract development (12–16). ROBO2, as a human CAKUT gene with the OMIM-phenotype number (MIM#610878), a member of the immunoglobulin (Ig) superfamily of cell adhesion molecules (17), binds to its ligand SLIT2 and plays vital roles in maintaining the normal morphogenesis of the kidney. SLIT/ROBO signaling, which is known for its role in axon repulsion, appears to repulse GDNF-expressing cells from the WD, thus causing a physical separation of these two structures in anterior regions (18) and resulting in exposure of the nephrogenic cord to proliferation-inducing signals from which it would normally be shielded by the ureteric mesenchyme. ROBO2 signaling regulates cellular localization by directing the migration of $SIX2^+$ cells; thus, the number of $SIX2^+$ nephron progenitors (NPs) in the nephrogenic cord increases, resulting in an expansion of the GDNF domain (19). In both *Slit2* and *Robo2* mutants, multiple UBs form anterior to where normal UB outgrowth occurs, and hydroureter and multilobular kidneys are observed (20). In addition, SLIT/ROBO signaling is reportedly involved in regulating branching morphogenesis in the mammary gland and is related to breast cancer development and metastasis (21).

GEN1, a Holliday junction resolvase, is involved in the homologous repair of DNA double strand breaks and in maintaining centrosome integrity (22). *GEN1* may play an important role in the development of the mammary gland, as it is likely involved in the DNA damage response of breast cancer cell lines (23). Our team first discovered that *Gen1* may be a potential candidate gene associated with CAKUT in mice (15). *Gen1* mutation results in kidney abnormalities, including hypoplasia, duplex kidney, hydronephrosis, and the vesicoureteral reflux (VUR), in mice (15). During early kidney development, *Gen1* mutation impairs GDNF expression, resulting in defective UB branching during early kidney development. The expression level of the cap mesenchyme marker SIX2 was also decreased in *Gen1* mutant kidney primordia, indicating that the smaller cap mesenchyme impaired metanephros differentiation and led to kidney hypoplasia in *Gen1* mutants (16).

Both *Robo2* and *Gen1* are involved in kidney development by regulating the GDNF/RET pathway, thus affecting ureteric budding and the development of the nephron progenitors. Together, these observations prompted us to assess whether *Robo2* and *Gen1* cooperate in a common signaling pathway during mouse kidney development *in vivo*. Therefore, in the present study, we established a mouse model with *Robo2* and *Gen1* double mutations to observe postnatal urinary malformations and early-stage kidney developmental abnormalities and investigate whether double gene mutations increase the incidence of CAKUT and the underlying mechanism.

MATERIALS AND METHODS

Mice

$Gen1^{PB/+}$ mice were obtained by using PB transposon-based insertional mutagenesis targeted to intron 2 of *Gen1* (Chr: 12.11268138, Ensembl: ENSMUSG00000051235). $Robo2^{PB/+}$ mice were also obtained through PB transposon-based insertional mutagenesis targeted to intron 1 of the *Robo2* gene (Chr: 16.74379623, Ensembl: ENSMUSG00000052516). $Gen1^{PB/+}$ and $Robo2^{PB/+}$ mice were mated with *Hoxb7*/myr-Venus mice to obtain *Gen1* and *Robo2* PB insertion mice specifically expressing fluorescent protein in the UB epithelium ($Gen1^{PB/+}$;*Hoxb7*/myr-Venus abbreviated as $Gen1^{PB/+}$;*Hoxb7* and $Robo2^{PB/+}$; *Hoxb7*/myr-Venus abbreviated as $Robo2^{PB/+}$; *Hoxb7*). $Gen1^{PB/+}$;*Hoxb7* mice were mated with $Robo2^{PB/+}$;*Hoxb7* mice to obtain $Gen1^{PB/+}$ $Robo2^{PB/+}$;*Hoxb7*, $Gen1^{PB/+}$;*Hoxb7*, $Robo2^{PB/+}$;*Hoxb7* and WT mice. We observed the phenotypes of the mice urinary system by selecting the same nest of different genotypes. All mice used in the experiments were specific pathogen-free (SPF) and were maintained at 18–22°C and 50–60% humidity on a 12 h day/night cycle. Animals were maintained and managed according to the animal welfare and usage management regulations of the School of Life Sciences of Fudan University [Protocol Approval No. SYXK (hu) 2020–0011]. All mouse strains were maintained on an FVB/N background.

Histological Analyses

Hematoxylin and eosin (H&E) staining was carried out on 7 μm paraffin sections, and performed according to the standard protocols described in the literature (24).

Quantitative Real-Time PCR

Total RNA was extracted from E12.5 using TRIzol (Life Technologies, United States). Total RNA was extracted from kidney primordia of E10.5 embryos using a RNeasy

mini kit (Qiagen, Germany). The purity of the RNA was confirmed by measuring the ratio of optical densities at 260 nm/280 nm. Aliquots of total RNA (1.0 μg each) from each sample were reverse transcribed into cDNAs according to the instructions of the PrimeScript® RT Reagent Kit (TaKaRa, China). Amplification was performed using AceQ qPCR SYBR Green Master Mix (Vazyme, China) and a real-time qPCR system (Agilent Mx3000P, United States). *Gapdh* was used as the internal control. All primers were obtained from the NCBI GenBank database and were synthesized by Genewiz (Shanghai, China). The primers used for RT-PCR were as follows (5′-3′): *Gen1*-F: 5′-GCCTGGAGTTGGAAAGGAACAAG-3′, *Gen1*-R: 5′-GGAACACACAGAGCAGTGAACCAC-3′; *Robo2*-F: 5′-GCGGATCTTTATTCTTTTTGCG-3′, *Robo2*-R: 5′-TCCTTTTTCCAGTAGATGGTTG-3′; *Gdnf*-F: 5′-GAACCAAGCCAGTGTATCTCCT-3′, *Gdnf*-R: 5′-ATCGTC TCTGCCTTTGTCCTC-3′; *Ret*-F: 5′-TGGCACACCTCT GCTCTATG-3′, *Ret*-R: 5′-GATGCGGATCCAGTCATTCT-3′; *Grem1*-F: 5′-CCTTTCAGTCTTGCTCCTTCTGC-3′, *Grem1*-R: 5′-TTCTTCTTGGTGGGTGGCTGTAGC-3′; *Bmp4*-F: 5′-GCAAGTTTGTTCAAGATTGGCTCC-3′, *Bmp4*-R: 5′-CCATCAGCATTCGGTTACCAGG-3′; *Bmp2*-F: 5′-CACACAGGGACACACCAACC-3′, *Bmp2*-R: 5′-CAAAGA CCTGCTAATCCTCAC-3′; *Six2*-F: 5′- AGTCCGACGTGAT GTGAAC-3′, *Six2*-R:5′-AGAGAAATGAGAATTCAGGTGC-3′; *Foxc1*-F: 5′-GCCAAATGGAATGGAACCCC-3′, *Foxc1*-R: 5′-CGCTGGTGTGAGGAATCTTCTC-3′; *Slit2*-F: 5′-CCTGTGA TGATGGAAATGATGAC-3′, *Slit2*-R: 5′-CCACTGTATCCAA GCAGGT-3′; and *Gapdh*-F: 5′-TGTTCCTACCCCCAAT GTGTCC-3′, *Gapdh*-R: 5′-GGAGTTGCTGTTGAA GTCGCAG-3′. The relative gene expression levels were calculated using the $2^{-\Delta\Delta CT}$ method. Each group contained at least three samples, and each sample was assayed in triplicate.

Phenotype Analysis

After the newborn mice in each group were anesthetized with CO_2, the abdomen was exposed along the midline incision of the anterior abdominal wall. Liver and intestinal tissues were removed to make sure that the urinary systems of the mice were fully exposed. The sex of the mice was determined under a fluorescence stereoscope, and the location, morphology, number of kidneys, ureters and bladders in the newborn pups from each group were observed. Pregnant mice were anesthetized at E11, E11.5 and E12.5 using CO_2. The abdomen of the mice was fully exposed, and the uteri were separated. The placenta and fetal membranes of the mice were removed under a stereoscope. The mouse embryos were flattened, limbs, intestines and liver were removed, and the bean-shaped tissue near the spinal column on the posterior abdominal wall was identified as early embryonic kidney tissue. The location and number of UBs were observed. The images were recorded under a microscope (Leica, Germany).

Whole Mount Immunofluorescence Staining

Embryos were dissected at E11.5 and fixed in 4% paraformaldehyde solution (PFA) (pH 7.4) at 4°C overnight. After the tissues were soaked in PBS/1% Triton X-100 for 20 min and rinsed with PBS several times, they were blocked with PBS (0.3% Triton X-100, 5% normal donkey serum and 1x PBS) overnight at 4°C. The tissues were incubated overnight at 4°C with primary antibodies against phospho-ERK (Cell Signaling Technology, 4,370; 1:100), phospho-AKT (Cell Signaling Technology, 8,272; 1:100), and phospho-PLCγ (Cell Signaling Technology, 8,713; 1:100). The tissues were washed 3 times with PBS for 30 min each, incubated with Cy5-conjugated donkey anti-rabbit secondary antibody (Jackson, 1:500) overnight at 4°C and washed several times with PBS. Images of stained tissue were captured using a Zeiss-LSM880 with Airyscan confocal laser scanning microscope and ZEN ImageJ software (Zeiss, Germany). The details about how the measurements were conducted on the confocal images are described in the literature (25). ImageJ was used to quantify the amount of fluorescence as mean gray value of pERK, pAKT, PLCγ and compare the results among four groups. ImageJ was also used to determine the number of stained cells by phosphorylation of histone H3 (PHH3) to compare the results among these groups.

Statistics

All data were processed using STATA 16.0 statistical software. The data are presented as the means ± SEM. The differences between two groups were determined with an unpaired *t*-test or Fisher's exact test. The significance level was set to $P < 0.05$.

RESULTS

Decreased *Robo2* and *Gen1* Expression in the $Robo2^{PB/+}Gen1^{PB/+}$ Mutant Mice

The insertion of a *piggyBac* (PB) transposon into the second intron of the mouse *Gen1* gene and the first intron of the *Robo2* gene significantly disrupted their expression. We analyzed the expression of *Robo2* and *Gen1* in the control and mutant mice on E12.5 using RT-PCR. In the whole embryos of the $Robo2^{PB/+}Gen1^{PB/+}$ mutant mice, *Robo2* expression significantly decreased by 41% compared with that in the WT mice ($P < 0.0001$), but *Robo2* expression was not different from that in the $Robo2^{PB/+}$ mutant mice. In the whole embryos of the $Robo2^{PB/+}Gen1^{PB/+}$ mutant mice, the expression level of *Gen1* was significantly decreased by 53% compared with that in the WT mice ($P < 0.0001$), but its expression was not different from that in $Gen1^{PB/+}$ mutant mice (**Figure 1A**).

We also analyzed the expression of *Robo2* and *Gen1* in the embryonic kidney tissue on E11.5. *Robo2* was expressed at lower levels in embryonic kidney tissue from the $Robo2^{PB/+}Gen1^{PB/+}$ mutant mice than in the WT mice ($P < 0.0001$) and the $Robo2^{PB/+}$ mutant mice ($P = 0.002$). Lower expression of *Gen1* was detected in the embryonic kidney tissue of the $Robo2^{PB/+}Gen1^{PB/+}$ mutant mice than in the WT mice ($P = 0.004$) and the $Gen1^{PB/+}$ mutant mice ($P = 0.03$) (**Figure 1B**).

Increased Presentation of CAKUT Phenotypes in the Neonatal $Robo2^{PB/+}Gen1^{PB/+}$ Mutants

Ninety-six newborn $Robo2^{PB/+}Gen1^{PB/+}$ mice were grossly dissected for a comprehensive analysis of the urinary system. The number of mice used in each group was listed in a

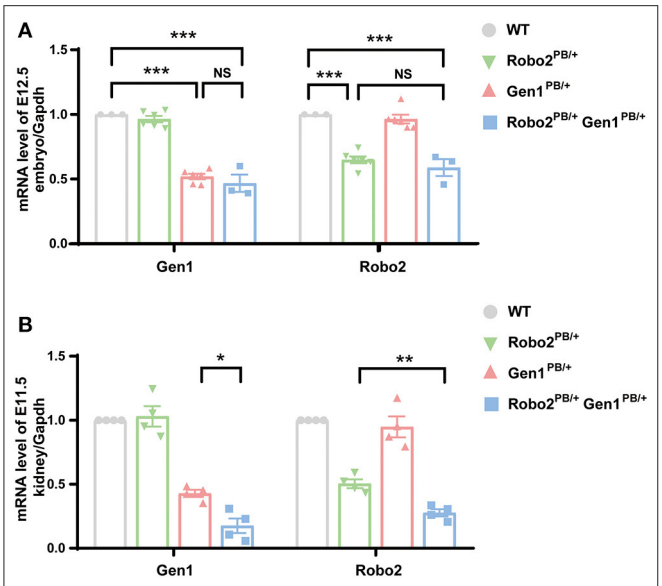

FIGURE 1 | Expression of *Robo2* and *Gen1* in the WT, *Robo2*$^{PB/+}$, *Gen1*$^{PB/+}$ and *Robo2*$^{PB/+}$*Gen1*$^{PB/+}$ mice. **(A)** Expression levels of *Gen1* and *Robo2* in E12.5 whole WT, *Robo2*$^{PB/+}$, *Gen1*$^{PB/+}$, and *Robo2*$^{PB/+}$*Gen1*$^{PB/+}$ mouse embryos. $N = 3$ WT, *Robo2*$^{PB/+}$ and *Robo2*$^{PB/+}$*Gen1*$^{PB/+}$ embryos each; N = 5 *Gen1*$^{PB/+}$ embryos. **(B)** Expression levels of *Gen1* and *Robo2* in kidneys from E11.5 WT, *Robo2*$^{PB/+}$, *Gen1*$^{PB/+}$ and *Robo2*$^{PB/+}$*Gen1*$^{PB/+}$ mice. N = 4 mice each in the four groups. Data are presented as the means ± SEM. NS, nonsignificant; *$P < 0.05$; **$P < 0.001$; ***$P < 0.0001$.

table (**Supplementary Table 1**). The incidence of CAKUT in the neonatal period was 32.3%, which was higher than that in the *Robo2*$^{PB/+}$ group [32.3% (31/96) vs. 13.6% (3/22), $P = 0.01$] and in the *Gen1*$^{PB/+}$ group [32.3% (31/96) vs. 17.3% (9/52), $P = 0.038$] (**Figure 2A**). Among these CAKUT phenotypes, the incidence of duplex kidney was increased in *Robo2*$^{PB/+}$*Gen1*$^{PB/+}$ newborn mice compared with the *Robo2*$^{PB/+}$ group [30.2% (29/96) vs. 4.5% (1/22), $P = 0.017$] and the *Gen1*$^{PB/+}$ group [30.2% (29/96) vs. 13.5% (7/52), $P = 0.045$] (**Figure 2B**). Five percent (1/20) of the WT newborn mice showed duplex kidneys. The incidence of duplex kidney, renal dysplasia (**Supplementary Figure 1A**) and hydronephrosis (**Supplementary Figure 1B**) was 4.5% (1/22) in the *Robo2*$^{PB/+}$ neonatal mice. Thirteen percent (7/52) of the *Gen1*$^{PB/+}$ newborn mice showed duplex kidneys, and 3.8% (2/52) of the mice showed hydronephrosis (**Figure 2B**). The CAKUT phenotype (**Figures 2C–E#**) of the *Robo2*$^{PB/+}$*Gen1*$^{PB/+}$ mice included isolated duplex kidneys (30.2%, 29/96, **Figures 2D,D#**) and hydronephrosis complicated with duplex kidneys [2.1%, (2/96), **Figures 2E,E#**], with isolated duplex kidneys being the most common phenotype. No sex or site preference was observed.

In the duplex kidney, the nephrogenic zone where new nephrons are being generated, which is normally restricted to the periphery of the developing kidney (**Figure 2F**), extended toward the inner cortex of the mutant kidneys (**Figure 2G**).

We also examined urinary tract defects in 36 newborn *Robo2*$^{PB/+}$*Gen1*$^{PB/+}$ mice and confirmed VUR in nine mutant mice. Three refluxes were observed in all 22 *Gen1*$^{PB/+}$ newborn mice, and only one of the 10 *Robo2*$^{PB/+}$ mutant mice had confirmed VUR. In the mutant mice with VUR, we observed methylene blue reflux to the renal pelvis and no significant renal pelvic or ureteral dilatation. However, no significant difference in the proportion of VUR was observed among these three groups (**Supplementary Figure 1**).

Duplex Kidneys Arise From Defective Kidney Induction in the *Robo2*$^{PB/+}$*Gen1*$^{PB/+}$ Mutants

Excessive UB formation was reported to cause duplex kidneys. *Hoxb7*/myr-Venus specifically expresses a fluorescent protein in the UB epithelium. We introduced *Robo2* and *Gen1* mutations in *Hoxb7* transgenic mice by breeding to visualize the morphology of the UB in mutant mice, and the UB and nephric ducts were positive for green fluorescence. From E11–E12.5, when the UB invaded the MM, abnormal ectopic budding from the WD was observed (**Figure 3**, compare **D–F** with **A–C**). The *Robo2*$^{PB/+}$ and *Gen1*$^{PB/+}$ mutant embryos had a single UB at the typical T-stage (E11.5), whereas the *Robo2*$^{PB/+}$*Gen1*$^{PB/+}$ mutants frequently showed ectopic budding that had already branched from the main UB. No ectopic budding was observed in any of the 32 WT mice or in any of the 24 *Robo2*$^{PB/+}$ embryonic control mice. Three percent (1/33) of the *Gen1*$^{PB/+}$ mutant kidneys showed ectopic budding compared with 26.8% (11/41) of the *Robo2*$^{PB/+}$*Gen1*$^{PB/+}$ kidneys (0/32 vs. 11/41, $P = 0.002$; 0/24 vs. 11/41, $P = 0.005$; 1/33 vs. 11/41, $P = 0.005$). The proportion of unilateral ectopic budding in *Gen1*$^{PB/+}$ kidneys was 1/33 (3.0%) compared with 22.0% (9/41) in *Robo2*$^{PB/+}$*Gen1*$^{PB/+}$ kidneys (0/32 vs. 9/41, $P = 0.001$; 0/24 vs. 9/41, $P = 0.003$; 1/33 vs. 9/41, $P = 0.018$) (**Figure 3G**), suggesting that *Robo2* and *Gen1* may synergistically regulate ureteric budding to prevent duplex kidney formation.

GDNF/RET Signaling Is Enhanced in the *Robo2*$^{PB/+}$*Gen1*$^{PB/+}$ Mutants

The *Robo2*$^{PB/+}$*Gen1*$^{PB/+}$ mutants displayed several phenotypes that may be caused by increased GDNF/RET signaling. We examined the expression of *Gdnf* and *Ret* in embryonic kidney tissues at E11.5 using RT-PCR to determine whether RET signaling is increased in the *Robo2*$^{PB/+}$*Gen1*$^{PB/+}$ mutants. Compared with the WT mice, *Gdnf* expression was decreased in the *Gen1*$^{PB/+}$ mutant mice ($P = 0.03$), significantly increased both in the *Robo2*$^{PB/+}$ mutant mice ($P < 0.001$), and in the *Robo2*$^{PB/+}$*Gen1*$^{PB/+}$ mutant mice ($P < 0.001$). *Ret* expression was significantly increased in the *Robo2*$^{PB/+}$, *Gen1*$^{PB/+}$ and *Robo2*$^{PB/+}$*Gen1*$^{PB/+}$ ($P < 0.001$) mutant mice (**Figure 4A**).

Then, we detected the expression of genes involved in regulating the GDNF/RET signaling axis and causing duplex kidney: *Gremlin* (*Grem1*), *Bmp4*, *Bmp2*, *Six2*, *Foxc1*, *Slit2* and *Sox11*. Among them, *Grem1* expression was increased in the *Gen1*$^{PB/+}$ mutant mice ($P = 0.008$) but not in the *Robo2*$^{PB/+}$ mutant mice. *Grem1* expression was increased in the *Robo2*$^{PB/+}$*Gen1*$^{PB/+}$ mutant mice ($P = 0.04$), while both *Bmp2* and *Bmp4* expression levels were markedly decreased in

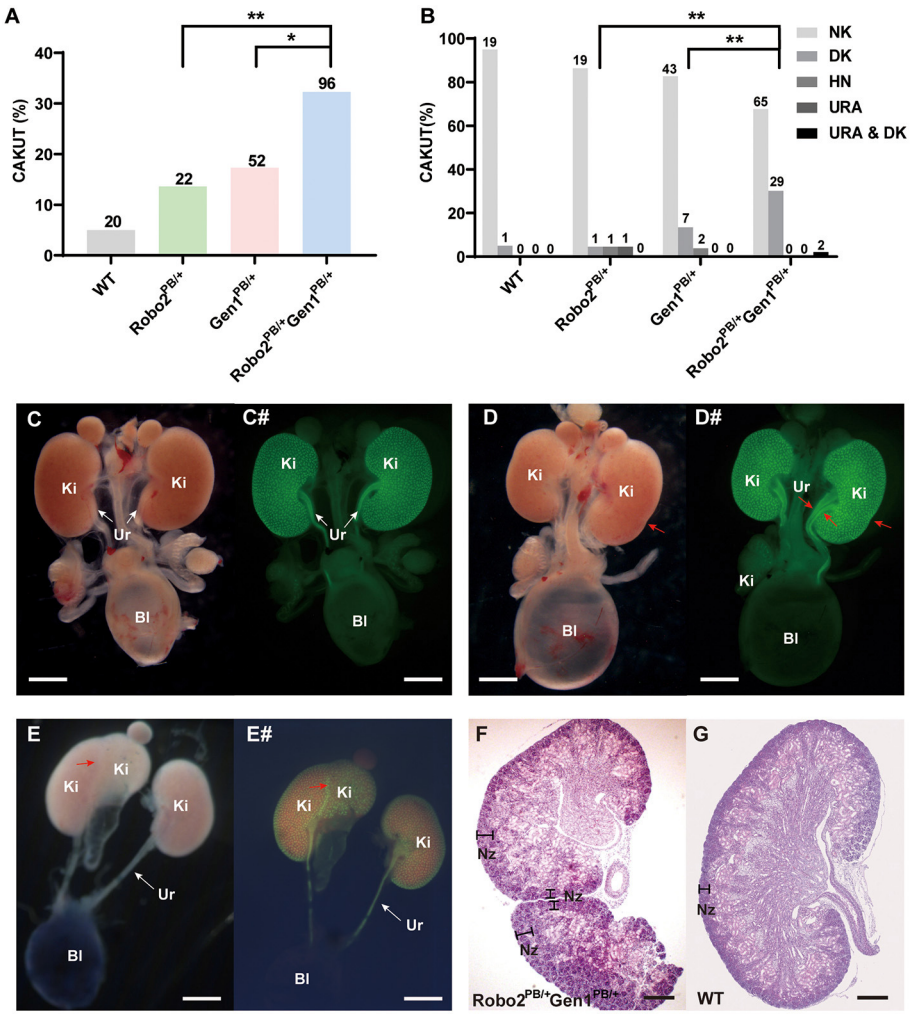

FIGURE 2 | Analysis of newborn mouse phenotypes in the four groups at P0.5. **(A)** Summary of the kidney symptoms in the four groups. **(B)** Percentages of newborn mice with a number of normal kidneys (NK), duplex kidneys (DK), hydronephrosis (HN), unilateral renal agenesis (URA) and hydronephrosis complicated with duplex kidneys (HN & DK). The number n represents the number of cases. **(C–E)** Representative images of the normal kidney **(C)**, duplex kidney **(D)**, and hydronephrosis complicated with duplex kidney **(E)**. **(C#–E#)** Representative images visualized by staining for *Hoxb7* expression in normal kidneys **(C#)**, duplex kidneys **(D#)**, and hydronephrosis complicated with duplex kidneys **(E#)**. Red arrowheads in **(D–E#)** indicate abnormal nephrogenic zones of the duplex kidney and double ureters. White arrows indicate the normal ureter. **(F,G)** Histological sections of P0.5 $Robo2^{PB/+}Gen1^{PB/+}$ **(F)** and WT kidneys **(G)** stained with hematoxylin and eosin. The region where nephrogenesis occurs (nephrogenic zone) indicated by black lines is restricted to the periphery in the WT kidney but extends toward the inner cortex of the $Robo2^{PB/+}Gen1^{PB/+}$ kidney. Scale bars, 2 mm in **(C–E#)**; 200 μm in **(F,G)**. NK, normal kidney; DK, duplex kidney; URA, unilateral renal agenesis; HN, hydronephrosis; Bl, bladder; Ki, kidney; Ur, ureter; Nz, nephrogenic zone; NS, non-significant; $^{*}P < 0.05$; $^{**}P < 0.001$.

the $Robo2^{PB/+}Gen1^{PB/+}$ mutant mice ($P < 0.001$). *Bmp2* was also reduced in the $Gen1^{PB/+}$ mutant mice ($P = 0.04$). *Slit2* expression was significantly increased in the $Robo2^{PB/+}$ mutant mice compared with the WT mice ($P < 0.001$), but not in the $Gen1^{PB/+}$ and $Robo2^{PB/+}Gen1^{PB/+}$ mutant mice. *Six2*, *Foxc1*, *Slit2*, and *Sox11* expression levels were not changed in the four groups (**Figure 4B**).

We examined the phosphorylation of a downstream effector, ERK. pERK has a wide range of both cytosolic and nuclear targets and functions, and its level reflects MAPK signaling downstream of RET. We also examined the phosphorylation of two other downstream effectors, AKT and PLCγ, which are both involved in RET intracellular signaling cascades. The pERK level was significantly increased in the UB and its surrounding nephrogenic cord cells in the E11.5 $Robo2^{PB/+}Gen1^{PB/+}$ kidneys compared with the WT ($P = 0.0014$), $Robo2^{PB/+}$ ($P = 0.0069$), and $Gen1^{PB/+}$ kidneys ($P = 0.0015$) (**Figure 4C**). However, we were unable to detect alterations in pAKT and pPLCγ levels in E11.5 kidneys (**Supplementary Figure 2**). The MAPK pathway, which involves the ERK1/2 cascade, is activated by various stimuli and contributes to the regulation of proliferation, differentiation, and cell survival.

We detected the expression of the RET transcription factor Etv5 to determine whether MAPK/ERK signaling

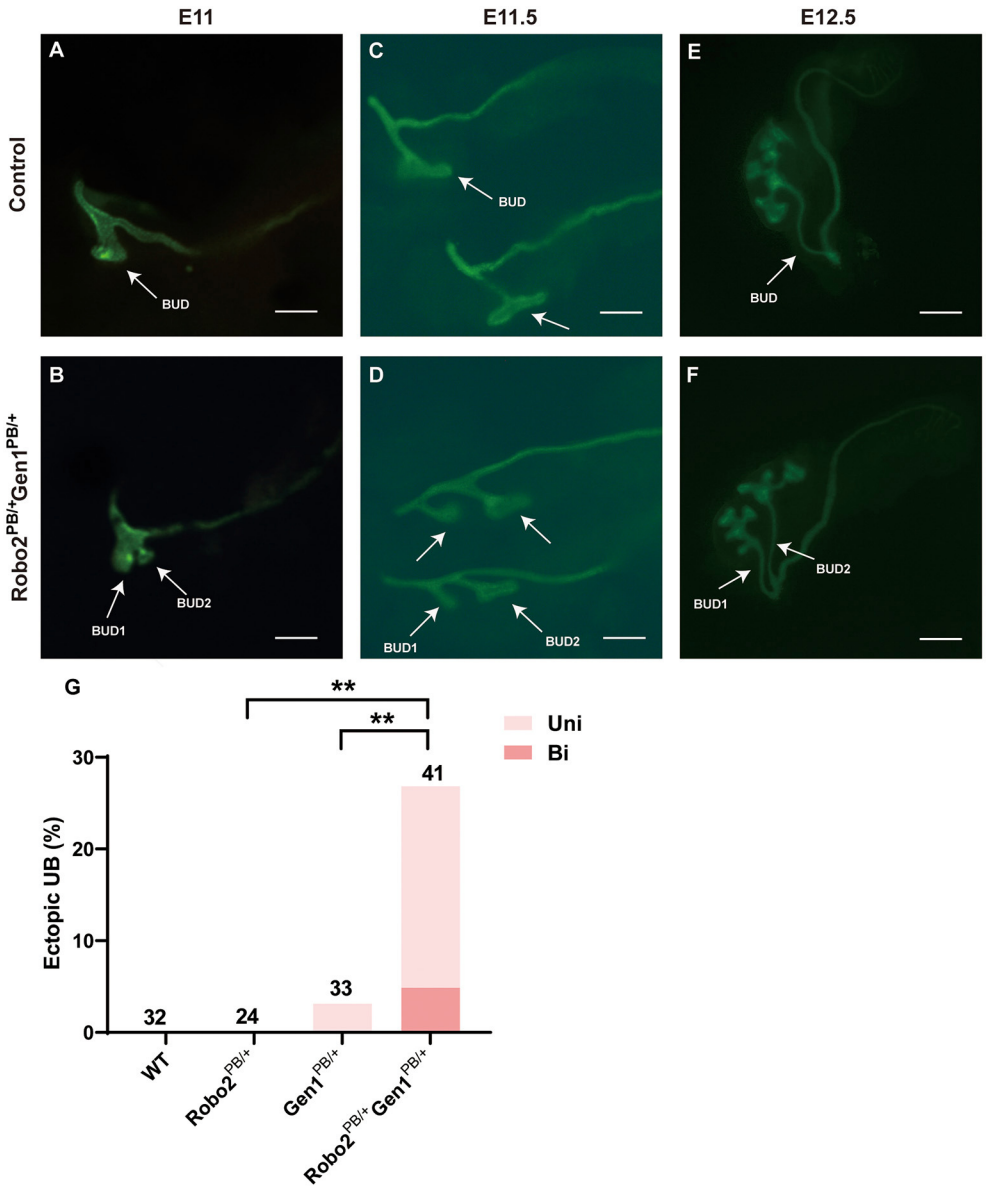

FIGURE 3 | Comparison of ureteric budding in the four groups. **(A–F)** Staining of whole mounts of the *Robo2*$^{PB/+}$*Gen1*$^{PB/+}$ mutants at E11 **(A)**, E11.5 **(C)**, and E12.5 **(E)** visualized using *Hoxb7*/myr-Venus expression shows abnormal ectopic ureteric budding compared with the single normal UB observed in the WT mice **(B,D,F)**. **(G)** Summary of the ectopic budding incidence in the WT, *Robo2*$^{PB/+}$, *Gen1*$^{PB/+}$, and *Robo2*$^{PB/+}$*Gen1*$^{PB/+}$ kidneys. The ectopic budding incidence is shown as the number of kidneys with ectopic budding or branching/total number of kidneys examined. Uni, Unilateral; Bi, Bilateral. Scale bars represent 100 μm in A-D. Scale bars represent 200 μm in E-F. NS, non-significant; $^{**}P < 0.001$.

was upregulated in *Robo2*$^{PB/+}$*Gen1*$^{PB/+}$ mutants. We found increased expression of Etv5 at E12.5, when the ureteric buds were undergoing repeated branching events (**Supplementary Figure 3**). We also determined the level of PHH3, which is an indicator of mitosis. Importantly, in the E11.5 *Robo2*$^{PB/+}$*Gen1*$^{PB/+}$ kidney sections, PHH3 levels were significantly increased compared with the WT ($P < 0.001$), *Robo2*$^{PB/+}$ ($P = 0.0005$), and *Gen1*$^{PB/+}$ groups ($P < 0.001$) (**Figure 4D**).

DISCUSSION

In this study, we showed that double heterozygous mutation for *Robo2* and *Gen1* led to significantly increased CAKUT phenotypes, particularly a duplicated collecting system, indicating a genetic interaction between the two genes. Furthermore, compound heterozygosity results in more ectopic UBs and cell proliferation through the activation of the GDNF/RET pathway and downstream MAPK/ERK cascade.

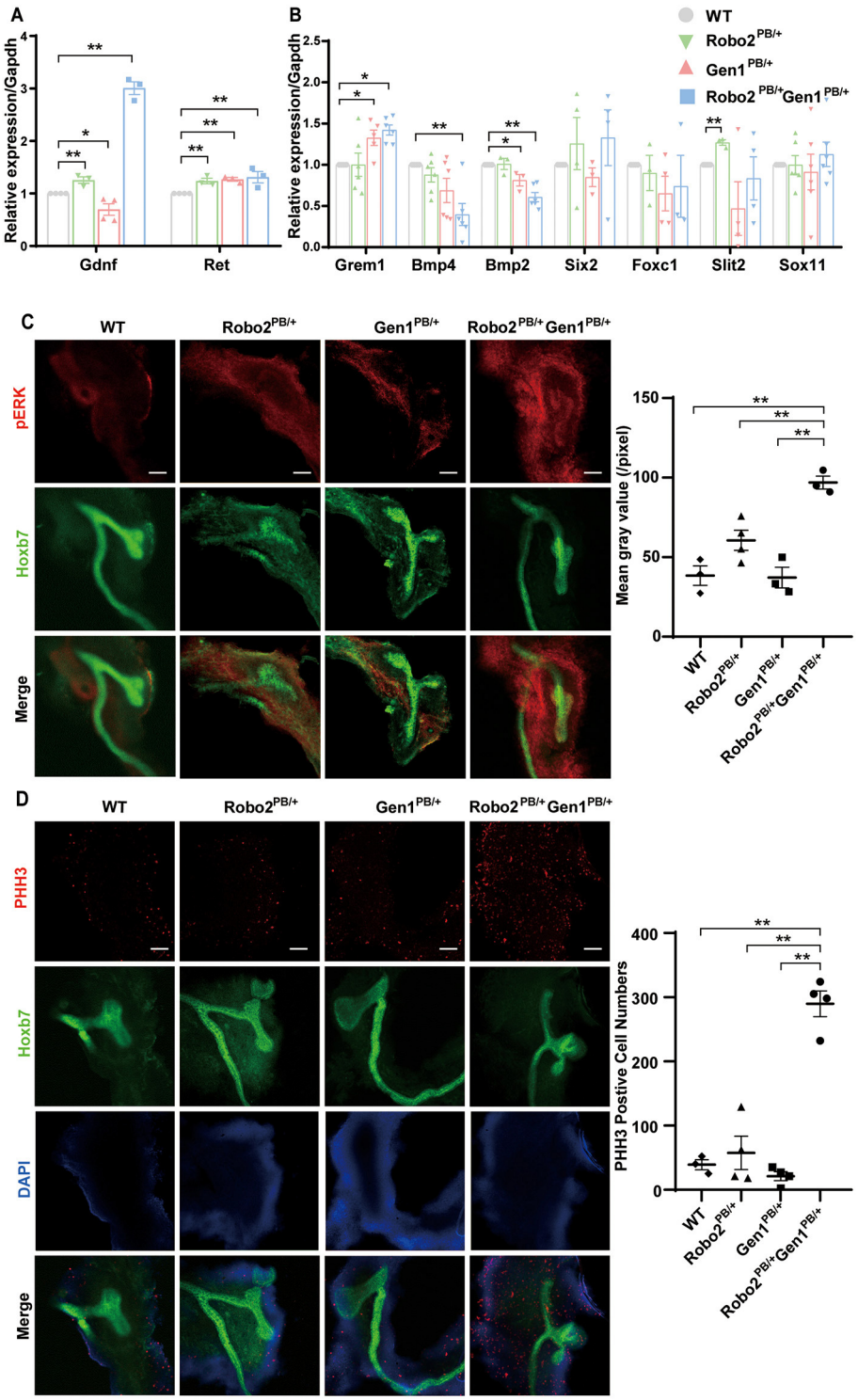

FIGURE 4 | GDNF/RET signaling is increased in the *Robo2*$^{PB/+}$*Gen1*$^{PB/+}$ mutants during metanephric development. **(A)** Changes in *Gdnf* and *Ret* expression in kidneys from the E11.5 WT, *Robo2*$^{PB/+}$, *Gen1*$^{PB/+}$ and *Robo2*$^{PB/+}$*Gen1*$^{PB/+}$ mice, $N = 3$. **(B)** Changes in the expression of key genes involved in metanephric development at E11.5, $N = 3$. **(C)** Immunofluorescence staining with antibodies against pERK in the kidneys of the WT, *Robo2*$^{PB/+}$, *Gen1*$^{PB/+}$, *Robo2*$^{PB/+}$*Gen1*$^{PB/+}$ mice at E11.5. $N = 3$, original magnification × 10. **(D)** Immunofluorescence staining with antibodies against PHH3 in the kidneys of the WT, *Robo2*$^{PB/+}$, *Gen1*$^{PB/+}$, *Robo2*$^{PB/+}$*Gen1*$^{PB/+}$ mice at E11.5. $N = 4$, original magnification × 10. Scale bars represent 100 μm in **(C,D)**. $^{*}P < 0.05$; $^{**}P < 0.001$.

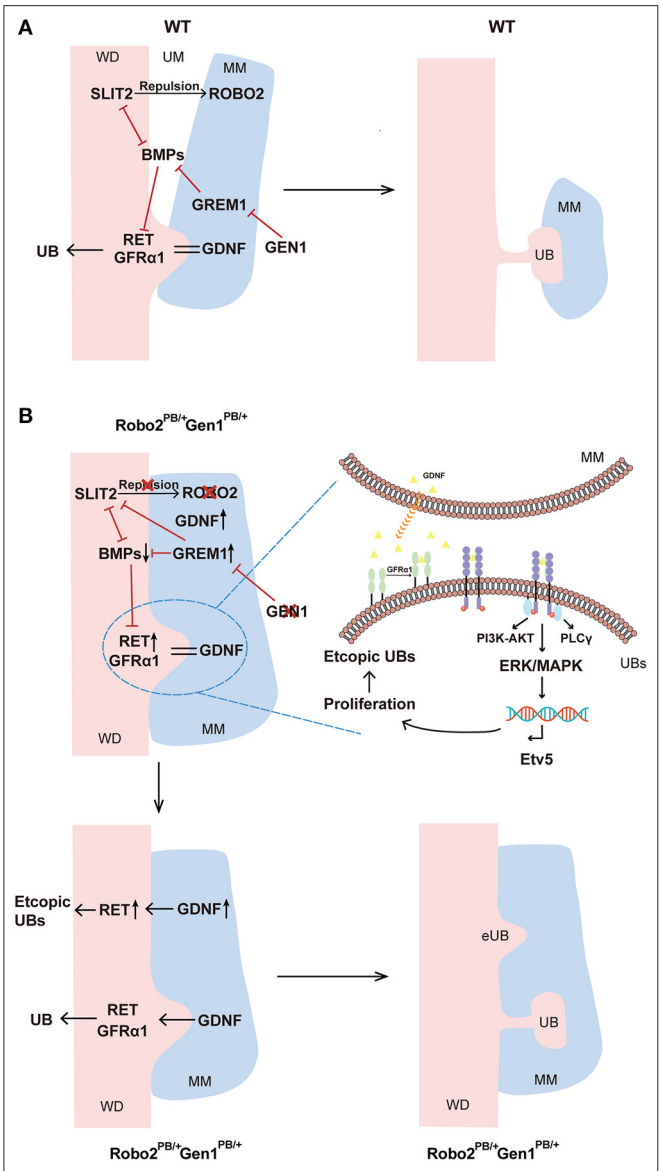

FIGURE 5 | Molecular regulation of ureteric budding and branching morphogenesis. **(A)** In wild-type mice, GEN1 may inhibit GREM1 expression, and GREM1 counteracts BMP signaling. Additionally, direct negative cross-talk is observed between SLIT2 and BMP2-Gremlin signaling. BMP2, BMP4 and ROBO2 inhibit GDNF signal transduction, inhibiting budding and subsequent branching of the ureter via RET and GFRα1, thereby restricting kidney induction to the appropriate site. **(B)** In *Robo2*$^{PB/+}$*Gen1*$^{PB/+}$ mice, decreased GEN1 expression led to increased GREM1 expression, and the high local concentration of GREM1 competitively inhibited ROBO2, reducing the binding between ROBO2 and SLIT2. Prior to UB induction, the nephrogenic cord itself is expanded due to the reduced repulsion between ROBO2 and SLIT2 relative to wild-type. In contrast, the increase in *Grem1* expression exerted an enhanced inhibitory effect on the BMP signaling pathway, which may lead to the decreased inhibitory effect of BMP2 and BMP4 on RET in the WD. At the molecular level, RET is activated and recruited by GFRα1 and GDNF and subsequently activates downstream MAPK/ERK signaling and cell proliferation. As RET transcription factor, Etv5 reflects the activation of MAPK/ERK signaling, driving ectopic UB induction in more anterior metanephric/caudal mesonephric regions. *Gen1* and *Robo2* may exert a synergistic effect on activating the GDNF/RET pathway. WD, Wolffian duct; MM, metanephric mesenchyme; UM, ureteric mesenchyme; UB, ureteric bud; BMPs, BMP2 and BMP4.

In our study, the *Robo2*$^{PB/+}$*Gen1*$^{PB/+}$ mice exhibited an aggravation of the CAKUT phenotype, and the incidence of CAKUT was higher than that in the *Robo2*$^{PB/+}$ and *Gen1*$^{PB/+}$ mice. In addition, the phenotypic distribution of the *Robo2*$^{PB/+}$*Gen1*$^{PB/+}$ mice was relatively concentrated, and duplex kidneys were mainly observed. The proportion of ectopic buds detected in the embryonic stage of mice with double gene mutations was significantly increased. The expression of *Robo2* and *Gen1* in the embryonic kidney of *Robo2*$^{PB/+}$*Gen1*$^{PB/+}$ mutant mice, but not in general in whole embryos, was lower than that in *Robo2*$^{PB/+}$ and *Gen1*$^{PB/+}$ mice, suggesting that *Gen1* and *Robo2* may have interaction and *Gen1* expression seems to depend on *Robo2* expression during kidney development. GDNF expression was decreased at E11.5 in the *Gen1*$^{PB/+}$ mutant mice, increased in the *Robo2*$^{PB/+}$ mutant mice, and significantly increased in the *Robo2*$^{PB/+}$*Gen1*$^{PB/+}$ mutant mice. The expression level of RET was increased in the *Robo2*$^{PB/+}$, *Gen1*$^{PB/+}$ and *Robo2*$^{PB/+}$*Gen1*$^{PB/+}$ mutant mice. According to Grieshammer et al. (18), the primary function of SLIT2/ROBO2 signaling during kidney development is to ensure that GDNF expression becomes localized to the region where the UB normally forms, thereby restricting kidney induction to the appropriate site. Therefore, we speculated that *Robo2* and *Gen1* may work together to regulate the GDNF/RET signaling pathway and play a synergistic role in promoting the expression of RET.

In general, the WD does not respond to the GDNF signal in anterior regions, and two potential explanations have been proposed (26). First, SLIT/ROBO signaling is known for its role in axon repulsion (21) and appears to repulse GDNF-expressing cells from the WD, resulting in a physical separation of these two structures in the anterior regions (19). Second, the anterior intermediate mesoderm (IM) exhibits relatively high levels of BMP signaling, which is thought to be an antagonist that suppresses ureter branching in kidney development (27). Heterozygous *Bmp4* mutations in mice lead to a variety of CAKUT phenotypes, including duplex kidneys (28).

In the *Robo2*$^{PB/+}$*Gen1*$^{PB/+}$ mutant mice, *Gen1* expression was reduced, accompanied by an increase in the expression of *Grem1*, consistent with previous studies (15). Previous studies found that both GREM1 and ROBO2 bind to the same domain of SLIT2 (29, 30). However, the affinity of ROBO2 for the N-terminal fragment of SLIT2 (SLIT2N) is much higher than that of GREM1 (31, 32). A high local concentration of GREM1 is needed to overcome the stronger interaction between SLIT2 and ROBO2. This finding has been verified in neurons, in which only high concentrations of GREM1 block SLIT2-mediated inhibition of neuronal migration. Therefore, GREM1 expression increased, which might result in competitive inhibition with ROBO2, reducing the binding between ROBO2 and SLIT2 (30). This effect may be exacerbated by the presence of a reduction in *Robo2* expression in the *Robo2*$^{PB/+}$*Gen1*$^{PB/+}$ mutant mice. GEN1 may interact with the ROBO2/SLIT2 signaling pathway through GREM1, thereby affecting the expression of GDNF/RET, but its specific mechanism remains to be further confirmed.

MM cells express the BMP inhibitor GREM1, which counteracts BMP function, to permit ureter outgrowth specifically at the proper site of the kidney (33). Both BMP2 and BMP4 are important members of the BMP signaling pathway.

An *in vitro* kidney organogenesis experiment has shown that BMP2 treatment of cells causes a significant decrease in *GDNF* and *GFRα1* mRNA expression during differentiation from the posterior intermediate mesoderm stage to the metanephric mesenchyme (days 7–9) (30). In the $Robo2^{PB/+}Gen1^{PB/+}$ mutant mice, the increase in *Grem1* expression was accompanied by a decrease in BMP expression. Thus, we speculated that the increase in *Grem1* expression exerted an enhanced inhibitory effect on the BMP signaling pathway, which may lead to a decreased inhibitory effect of BMP2 and BMP4 on RET in the WD. Direct negative crosstalk between the SLIT2 and BMP-Gremlin signaling pathways has also been observed. A previous study revealed a negative feedback loop in fibroblasts in which SLIT2 inhibits GREM1 activity and BMP downregulates *Slit2* expression by suppressing *Slit2* promoter activity through canonical BMP signaling pathways (30). Through the negative crosstalk between these molecules, an interaction network was formed between *Robo2* and *Gen1*. We speculated that the combined actions of several molecules increase the expression of GDNF and RET.

As the major inducers of RET signaling in the early developing kidney, GDNF binding to its cognate receptors causes activation of intracellular signaling cascades, including the PI3K/AKT, RAS/MAPK and PLCγ/Ca^{2+} pathways (34). The MAPK/ERK pathway appears to be closely related to ureter branching, and mice lacking the MEK1 and MEK2 kinases do not form an appropriately branched ureteric tree (35). In the present study, we observed increased levels of pERK, which reflects MAPK signaling, in both the UB and its surrounding nephrogenic cord cells, while the levels of pAKT and pPLCγ were not changed in compound heterozygous mice. A previous study reported that Etv5 expression requires activation of the MEK/ERK (MAPK) signaling pathway in neurons (36). Significantly, in E12.5 $Robo2^{PB/+}Gen1^{PB/+}$ kidney sections, *Etv5* expression was increased in the UB tips. A previous study showed that MAPK/ERK activity regulates proliferation in UBs to achieve normal branching and growth (35). As a transcription factor, ETV5 is also dispensable for the cellular self-renewal ability (37). As the PHH3 occurs in late G2 and M phase of the cell cycle, it serves as a specific marker for cells undergoing mitosis (38). In this study, we detected the expression level of PHH3 and observed increased levels in double mutant mice. Therefore, we speculated that cell mitosis may be promoted through the activation of the downstream MAPK/ERK cascade, resulting in increased cell proliferation and finally the formation of ectopic UBs (**Figures 5A,B**).

In our study, pERK levels were increased in the UB and its surrounding nephrogenic cord cells in E11.5 $Robo2^{PB/+}Gen1^{PB/+}$ kidneys. In addition to regulating the UB epithelium, the MAPK/ERK pathway might also participate in the regulation of nephrogenesis, which has multiple functions in the guidance of nephron differentiation (34). NP-specific MAPK inactivation results in an almost complete lack of nephrons in newborn mouse pups (34, 39). Therefore, we speculate that ROBO2 and GEN1 not only coregulate ureteric budding but also exert some common effect on the nephrogenic cord through the activation of the cap mesenchyme marker SIX2 or MAPK/ERK signaling. Further studies are needed to address the combined effects of ROBO2 and GEN1 on nephron progenitor biology and the cap mesenchyme.

The specific interaction between *Gen1* and *Robo2* remains unclear. One interpretation of our results is that *Gen1* may interact with the ROBO2/SLIT2 pathway through *Grem1*. The different affinities of ROBO2 and GREM1 for SLIT2N may play a specific role in metanephric kidney development. The current data do not allow us to discriminate between these possibilities, which would require a detailed analysis of GREM1 and ROBO2. In addition, further studies will be required to search for mutation sites in the two genes in patients with CAKUT and to clarify their role in the development of the human kidney.

This finding is consistent with the recent understanding of CAKUT as an oligomeric/polygenic disorder that may be caused by the accumulation of multiple subtle mutations or polymorphisms (mutational load) that lead to dysfunction of the corresponding developmental program (40). Although some aspects of the roles of *Gen1* and *Robo2* in metanephros development remain to be clarified, our results unambiguously identified a cooperative role for *Gen1* and *Robo2* in metanephric budding.

DATA AVAILABILITY STATEMENT

The datasets presented in this study can be found in online repositories. The names of the repository/repositories and accession number(s) can be found in the article/**Supplementary Material**.

ETHICS STATEMENT

The animal study was reviewed and approved by School of Life Sciences of Fudan University [Protocol Approval No. SYXK (hu) 2020-0011].

AUTHOR CONTRIBUTIONS

XW, HX, and QS conceived and designed research. YL performed experiments, analyzed data, and drafted the manuscript. MY, LT, SX, and XD interpreted results of experiments. YL, MY, and LT prepared figures. QS edited and revised the manuscript and approved final version of the manuscript. All authors contributed to the article and approved the submitted version.

FUNDING

This work was supported by the National Natural Science Foundation of China (81670609 and 81900602) and the Establishment, Performance, and Quality Control of the Standardized Phenotype Analysis Process Grant (No. 2018YFA0801102).

SUPPLEMENTARY MATERIAL

The Supplementary Material for this article can be found online at: https://www.frontiersin.org/articles/10.3389/fmed.2021.807898/full#supplementary-material

REFERENCES

1. Queisser-Luft A, Stolz G, Wiesel A, Schlaefer K, Spranger J. Malformations in newborn: results based on 30,940 infants and fetuses from the Mainz congenital birth defect monitoring system (1990-1998). *Arch Gynecol Obstet.* (2002) 266:163–7. doi: 10.1007/s00404-001-0265-4
2. Short KM, Smyth IM. The contribution of branching morphogenesis to kidney development and disease. *Nat Rev Nephrol.* (2016) 12:754–67. doi: 10.1038/nrneph.2016.157
3. Costantini F, Kopan R. Patterning a complex organ: branching morphogenesis and nephron segmentation in kidney development. *Developmental cell.* (2010) 18:698–712. doi: 10.1016/j.devcel.2010.04.008
4. Kobayashi A, Valerius MT, Mugford JW, Carroll TJ, Self M, Oliver G, et al. Six2 defines and regulates a multipotent self-renewing nephron progenitor population throughout mammalian kidney development. *Cell Stem Cell.* (2008) 3:169–81. doi: 10.1016/j.stem.2008.05.020
5. Short KM, Combes AN, Lefevre J, Ju AL, Georgas KM, Lamberton T, et al. Global quantification of tissue dynamics in the developing mouse kidney. *Dev Cell.* (2014) 29:188–202. doi: 10.1016/j.devcel.2014.02.017
6. Humphreys BD, Lin SL, Kobayashi A, Hudson TE, Nowlin BT, Bonventre JV, et al. Fate tracing reveals the pericyte and not epithelial origin of myofibroblasts in kidney fibrosis. *Am J Pathol.* (2010) 176:85–97. doi: 10.2353/ajpath.2010.090517
7. Nicolaou N, Renkema KY, Bongers EM, Giles RH, Knoers NV. Genetic, environmental, and epigenetic factors involved in CAKUT. *Nat Rev Nephrol.* (2015) 11:720–31. doi: 10.1038/nrneph.2015.140
8. Narlis M, Grote D, Gaitan Y, Boualia SK, Bouchard M. Pax2 and pax8 regulate branching morphogenesis and nephron differentiation in the developing kidney. *J Am Soc Nephrol.* (2007) 18:1121–9. doi: 10.1681/ASN.2006070739
9. Paces-Fessy M, Fabre M, Lesaulnier C, Cereghini S. Hnf1b and Pax2 cooperate to control different pathways in kidney and ureter morphogenesis. *Hum Mol Genet.* (2012) 21:3143–55. doi: 10.1093/hmg/dds141
10. Motojima M, Tanimoto S, Ohtsuka M, Matsusaka T, Kume T, Abe K. Characterization of kidney and skeleton phenotypes of mice double heterozygous for foxc1 and foxc2. *Cells Tissues Organs.* (2016) 201:380–9. doi: 10.1159/000445027
11. Schild R, Knuppel T, Konrad M, Bergmann C, Trautmann A, Kemper MJ, et al. Double homozygous missense mutations in DACH1 and BMP4 in a patient with bilateral cystic renal dysplasia. *Nephrol Dial Transplant.* (2013) 28:227–32. doi: 10.1093/ndt/gfs539
12. Yu M, Tan L, Li Y, Chen J, Zhai Y, Rao J, et al. Intrauterine low-protein diet aggravates developmental abnormalities of the urinary system via the Akt/Creb3 pathway in Robo2 mutant mice. *Am J Physiol Renal Physiol.* (2020) 318:F43–f52. doi: 10.1152/ajprenal.00405.2019
13. Zhang Y, Zhang X, Wang X, Wang H, Wu X, Xu H, et al. Gen1 modulates metanephric morphology through retinoic acid signaling. *DNA Cell Biol.* (2019) 38:263–71. doi: 10.1089/dna.2018.4426
14. Liu J, Sun L, Shen Q, Wu X, Xu H. New congenital anomalies of the kidney and urinary tract and outcomes in Robo2 mutant mice with the inserted piggyBac transposon. *BMC Nephrol.* (2016) 17:98. doi: 10.1186/s12882-016-0308-5
15. Wang H, Zhang C, Wang X, Lian Y, Guo B, Han M, et al. Disruption of Gen1 causes congenital anomalies of the kidney and urinary tract in mice. *Int J Biol Sci.* (2018) 14:10–20. doi: 10.7150/ijbs.22768
16. Wang X, Wang H, Liu J, Gong Y, Zhang C, Fang F, et al. Gen1 mutation caused kidney hypoplasia and defective ureter-bladder connections in mice. *Int J Biol Sci.* (2020) 16:1640–7. doi: 10.7150/ijbs.42855
17. Kidd T, Brose K, Mitchell KJ, Fetter RD, Tessier-Lavigne M, Goodman CS, et al. Roundabout controls axon crossing of the CNS midline and defines a novel subfamily of evolutionarily conserved guidance receptors. *Cell.* (1998) 92:205–15. doi: 10.1016/S0092-8674(00)80915-0
18. Grieshammer U, Le M, Plump AS, Wang F, Tessier-Lavigne M, Martin GR. SLIT2-mediated ROBO2 signaling restricts kidney induction to a single site. *Dev Cell.* (2004) 6:709–17. doi: 10.1016/S1534-5807(04)00108-X
19. Wainwright EN, Wilhelm D, Combes AN, Little MH, Koopman P. ROBO2 restricts the nephrogenic field and regulates Wolffian duct-nephrogenic cord separation. *Dev Biol.* (2015) 404:88–102. doi: 10.1016/j.ydbio.2015.05.023
20. Brose K, Tessier-Lavigne M. Slit proteins: key regulators of axon guidance, axonal branching, and cell migration. *Curr Opin Neurobiol.* (2000) 10:95–102. doi: 10.1016/S0959-4388(99)00066-5
21. Blockus H, Chédotal A. Slit-Robo signaling. *Development.* (2016) 143:3037–44. doi: 10.1242/dev.132829
22. Ip SC, Rass U, Blanco MG, Flynn HR, Skehel JM, West SC. Identification of holliday junction resolvases from humans and yeast. *Nature.* (2008) 456:357–61. doi: 10.1038/nature07470
23. Sun L, Zhang Y, Pan Z, Li B, Sun M, Zhang X. Expression and localization of GEN1 in mouse mammary epithelial cells. *J Biochem Mol Toxicol.* (2014) 28:450–5. doi: 10.1002/jbt.21584
24. Xu PX, Adams J, Peters H, Brown MC, Heaney S, Maas R. Eya1-deficient mice lack ears and kidneys and show abnormal apoptosis of organ primordia. *Nat Genet.* (1999) 23:113–7. doi: 10.1038/12722
25. Zucker RM, Hunter ES, 3rd, Rogers JM. Apoptosis and morphology in mouse embryos by confocal laser scanning microscopy. *Methods.* (1999) 18:473–80. doi: 10.1006/meth.1999.0815
26. Kozlov VM, Schedl A. Duplex kidney formation: developmental mechanisms and genetic predisposition. *F1000Res.* (2020) 9:F1000 Faculty Rev-2. doi: 10.12688/f1000research.19826.1
27. Motamedi FJ, Badro DA, Clarkson M, Lecca MR, Bradford ST, Buske FA, et al. WT1 controls antagonistic FGF and BMP-pSMAD pathways in early renal progenitors. *Nat Commun.* (2014) 5:4444. doi: 10.1038/ncomms5444
28. Miyazaki Y, Oshima K, Fogo A, Hogan BL, Ichikawa I. Bone morphogenetic protein 4 regulates the budding site and elongation of the mouse ureter. *J Clin Invest.* (2000) 105:863–73. doi: 10.1172/JCI8256
29. Howitt JA, Clout NJ, Hohenester E. Binding site for Robo receptors revealed by dissection of the leucine-rich repeat region of Slit. *Embo j.* (2004) 23:4406–12. doi: 10.1038/sj.emboj.7600446
30. Tumelty KE, Higginson-Scott N, Fan X, Bajaj P, Knowlton KM, Shamashkin M, et al. Identification of direct negative cross-talk between the SLIT2 and bone morphogenetic protein-Gremlin signaling pathways. *J Biol Chem.* (2018) 293:3039–55. doi: 10.1074/jbc.M117.804021
31. Brose K, Bland KS, Wang KH, Arnott D, Henzel W, Goodman CS, et al. Slit proteins bind Robo receptors and have an evolutionarily conserved role in repulsive axon guidance. *Cell.* (1999) 96:795–806. doi: 10.1016/S0092-8674(00)80590-5
32. Nguyen Ba-Charvet KT, Brose K, Ma L, Wang KH, Marillat V, Sotelo C, et al. Diversity and specificity of actions of Slit2 proteolytic fragments in axon guidance. *J Neurosci.* (2001) 21:4281–9. doi: 10.1523/JNEUROSCI.21-12-04281.2001
33. Michos O, Gonçalves A, Lopez-Rios J, Tiecke E, Naillat F, Beier K, et al. Reduction of BMP4 activity by gremlin 1 enables ureteric bud outgrowth and GDNF/WNT11 feedback signalling during kidney branching morphogenesis. *Development.* (2007) 134:2397–405. doi: 10.1242/dev.02861
34. Kurtzeborn K, Kwon HN, Kuure S. MAPK/ERK signaling in regulation of renal differentiation. *Int J Mol Sci.* (2019) 20. doi: 10.3390/ijms20071779
35. Ihermann-Hella A, Lume M, Miinalainen IJ, Pirttiniemi A, Gui Y, Peränen J, et al. Mitogen-activated protein kinase (MAPK) pathway regulates branching by remodeling epithelial cell adhesion. *PLoS Genet.* (2014) 10:e1004193. doi: 10.1371/journal.pgen.1004193
36. Fontanet P, Irala D, Alsina FC, Paratcha G, Ledda F. Pea3 transcription factor family members Etv4 and Etv5 mediate retrograde signaling and axonal growth of DRG sensory neurons in response to NGF. *J Neurosci.* (2013) 33:15940–51. doi: 10.1523/JNEUROSCI.0928-13.2013
37. Chen SR, Liu YX. Regulation of spermatogonial stem cell self-renewal and spermatocyte meiosis by Sertoli cell signaling. *Reproduction.* (2015) 149:R159–67. doi: 10.1530/REP-14-0481
38. Fukushima S, Terasaki M, Sakata K, Miyagi N, Kato S, Sugita Y, et al. Sensitivity and usefulness of anti-phosphohistone-H3 antibody

immunostaining for counting mitotic figures in meningioma cases. *Brain Tumor Pathol.* (2009) 26:51–7. doi: 10.1007/s10014-009-0249-9

39. Ihermann-Hella A, Hirashima T, Kupari J, Kurtzeborn K, Li H, Kwon HN, et al. Dynamic MAPK/ERK activity sustains nephron progenitors through niche regulation and primes precursors for differentiation. *Stem Cell Rep.* (2018) 11:912–28. doi: 10.1016/j.stemcr.2018.08.012
40. van der Ven AT, Vivante A, Hildebrandt F. Novel insights into the pathogenesis of monogenic congenital anomalies of the kidney and urinary tract. *J Am Soc Nephrol.* (2018) 29:36–50. doi: 10.1681/ASN.2017050561

Conflict of Interest: The authors declare that the research was conducted in the absence of any commercial or financial relationships that could be construed as a potential conflict of interest.

Publisher's Note: All claims expressed in this article are solely those of the authors and do not necessarily represent those of their affiliated organizations, or those of the publisher, the editors and the reviewers. Any product that may be evaluated in this article, or claim that may be made by its manufacturer, is not guaranteed or endorsed by the publisher.

frontiers in Medicine

CASE REPORT
published: 31 January 2022
doi: 10.3389/fmed.2021.810940

Case Report: A Pathogenic Missense Variant of *WT1* Cosegregates With Proteinuria in a Six-Generation Chinese Family With IgA Nephropathy

Qianqian Li, Li Zhu, Sufang Shi*, Damin Xu, Jicheng Lv and Hong Zhang*

Renal Division, Department of Medicine, Peking University First Hospital; Peking University Institute of Nephrology; Key Laboratory of Renal Disease (Peking University), National Health Commission; Key Laboratory of Chronic Kidney Disease Prevention and Treatment, Ministry of Education, Beijing, China

OPEN ACCESS

Edited by:
Andrew Mallett, Townsville University Hospital, Australia

Reviewed by:
Judy Savige, The University of Melbourne, Australia
Gianluca Caridi, Giannina Gaslini Institute (IRCCS), Italy

***Correspondence:**
Li Zhu
funnyzhuli@bjmu.edu.cn
Sufang Shi
shisufang0510@163.com

Specialty section:
This article was submitted to Nephrology, a section of the journal Frontiers in Medicine

Received: *08 November 2021*
Accepted: *30 December 2021*
Published: *31 January 2022*

Citation:
Li Q, Zhu L, Shi S, Xu D, Lv J and Zhang H (2022) Case Report: A Pathogenic Missense Variant of WT1 Cosegregates With Proteinuria in a Six-Generation Chinese Family With IgA Nephropathy. Front. Med. 8:810940. doi: 10.3389/fmed.2021.810940

Immunoglobulin A (IgA) nephropathy (IgAN) is the most common type of primary glomerulonephritis worldwide. In addition to hematuria, proteinuria is observed in a considerable proportion of patients with IgAN and has proven to be a strong risk factor for disease progression. Although the exact pathogenesis of IgAN is still unclear, genetic factors are widely considered to play a role in its occurrence and development. Here, we investigated a large IgAN-associated pedigree of 47 members belonging to six generations. Two members of the family who presented with proteinuria and hematuria were diagnosed with IgAN through renal biopsy. Four other members also exhibited proteinuria or hematuria but without renal biopsy. Using whole-exome sequencing, we identified a likely pathogenic variant in *WT1* (c.1397C>T; p.Ser466Phe) that cosegregated with proteinuria in the affected family members. In addition, another pathogenic variant in *NPHS1* (c.3478C>T; p.Arg1160Ter) was identified; however, it did not cosegregate with abnormal proteinuria. Compared to individuals in the pedigree with only one heterozygous *WT1* variant (c.1397C>T; p.Ser466Phe), the proband and her younger brother carried an additional *WT1* variant (c.1433-10G>A) and presented with a more severe phenotype and rapid progression to end-stage kidney disease. Our findings suggest the *WT1* missense variant (c.1397C>T; p.Ser466Phe)-induced primary podocyte injury might contribute to the proteinuria phenotype and IgAN progression in this pedigree.

Keywords: IgA nephropathy, proteinuria, *WT1* gene, *NPHS1* gene, pedigree

INTRODUCTION

Immunoglobulin A (IgA) nephropathy (IgAN) is the most common primary glomerulonephritis worldwide and has complex and unclear pathogenesis. IgAN can occur as a sporadic or familial disease depending on the clinical characteristics of the disease. Compared to sporadic IgAN cases, familial IgAN cases have earlier onset and poorer renal outcomes (1). Numerous

familial IgAN reports have shown that genetic factors are involved in its occurrence and development (2, 3). Although hematuria is the most common clinical manifestation of IgAN, proteinuria is a more widely known risk factor for progression to end-stage kidney disease (ESKD) than hematuria in patients with IgAN (4).

The Wilms tumor suppressor 1 (*WT1*) gene, located on chromosome 11p13, contains 10 exons and encodes a transcription factor of the zinc finger protein family. This transcription factor plays a crucial role in the development of the kidney and genitals (5). The *WT1* gene is predominantly expressed in maturing podocytes in adult kidneys, and is related to the glomerular filtration barrier function, especially in proteinuria (6). Previous studies have reported that mutations in the *WT1* gene are related to Frasier syndrome, Denys-Drash syndrome (DDS), focal segmental glomerulosclerosis (FSGS), and nephrotic syndrome, indicating that *WT1* might play an essential role in the differentiation and function of podocytes (6, 7).

Genetic sequencing in familial IgAN cases can help identify causal genes of IgAN and may facilitate the elucidation of the mechanism of IgAN development and progression. In this case study, we report a pathogenic missense variant in the *WT1* gene in a large pedigree. Two members presented with biopsy-proven IgAN, which suggests that the *WT1* gene may be related to the pathogenesis of IgAN.

CASE PRESENTATION

The proband was a 28-year-old Chinese woman (V-6) (**Figure 1**). She presented with proteinuria (++), hematuria, normal blood pressure, and normal renal function based on a pregnancy examination 4 years prior (at the age of 24 years). No renal biopsy or treatment was performed at that time. She was admitted to the hospital because her serum creatinine (Scr) level had increased to 200.5 μmol/l 1 week before admission.

On admission, urine examination showed proteinuria (2.55 g/24 h, normal range: 0–0.15 g), hematuria (720/μl, normal range: 0–10/μl), and elevated Scr levels (230.7 μmol/l, normal range: 53–97 μmol/l). The patient was diagnosed with IgAN through a renal biopsy. Immunofluorescence revealed IgG–, IgA+ + +, C1q+, C3c+ + +, and FRA–, and light microscopy revealed mesangial hypercellularity, segmental sclerosis, and podocyte hypertrophy (**Figure 2A**). Electron microscopy was not performed. Although the proband received antihypertension and corticosteroid therapy, she progressed to ESKD 4 years after renal biopsy and had to undergo hemodialysis.

The 52-year-old uncle (IV-5) of the proband developed proteinuria (1.33 g/d) and hematuria (18/μl) at the age of 32 years. He underwent renal biopsy at the age of 46 years and was diagnosed with IgAN. Immunofluorescence showed IgG–, IgA++, IgM–, C3c–, C1q–, and FRA–, and granular deposits of IgA in the mesangial areas. Light microscopy revealed mesangial hypercellularity, segmental adhesion, and podocyte hypertrophy (**Figure 2B**). Electron microscopy was not performed. He was administered a renin-angiotensin system inhibitor, and his renal function is normal at present.

The 24-year-old younger brother (V-7) of the proband presented with hematuria, proteinuria, normal blood pressure, and normal renal function at the age of 15. No renal biopsy or treatment was performed at that time. At present, his blood pressure has increased to 155/107 mm Hg and urine examination showed red blood cells at 10–20/HP and proteinuria (+++). His serum albumin levels were slightly decreased (36.4 g/l), Scr was within the normal range (902.4 μmol/l), and renal ultrasound showed bilateral renal atrophy. No renal biopsy was performed. He is being provided maintenance hemodialysis.

The father (IV-7), cousin (V-1), and grandmother (III-6) of the proband presented with proteinuria and/or hematuria at the ages of 30, 18, and 50, respectively. Secondary factors inducing renal disease were not found, and no renal biopsy was performed for these patients. The father of the proband progressed to ESKD and received dialysis at the age of 53. The cousin (V-1) and grandmother (III-6) of the proband received renin-angiotensin system blocker therapy and maintained normal blood pressure, stable proteinuria (<0.5 g/d), and normal renal function. In addition, five immediate family members (II-6, III-1, III-3, III-12, and IV-12) presented with proteinuria before death. Of these, III-3 died of a stroke and the others (II-6, III-1, III-12, and IV-12) died of unknown reasons.

GENETIC ANALYSIS

The genetic analysis in this case study complied with the Declaration of Helsinki principles and was approved by the Peking University First Hospital ethics committees (2018-99). Informed consent was obtained from all participants. The genomic DNA of individuals was extracted from peripheral blood cells using the salting-out technique (8). Ten family members (III-5, III-6, IV-5, IV-6, IV-7, IV-8, V-1, V-3, V-6, and V-7), including the proband, were whole-exome sequenced by next-generation sequencing. To identify causal genetic changes, variants in 625 nephropathy-associated genes were selected for further analysis, according to a previous study (9). According to the American College of Medical Genetics and Genomics (ACMG) guidelines, benign variants (MAF > 0.05) and likely benign variants were filtered out (**Supplementary Figure S1**). Of the remaining variants, we explored a likely pathogenic variant in *WT1* and a pathogenic variant in *NPHS1* (**Supplementary Table 2**) for further analysis.

We identified a pathogenic missense variant in the *WT1* gene (NM_024426.6: exon9 c.1397C>T; p.Ser466Phe, dbSNP: rs1421664466) in seven immediate family members (III-6, IV-5, IV-7, V-1, V-6, V-7, and VI-1; **Table 1**), all of which exhibited proteinuria, except a 4-year-old member. This indicated that the variant in *WT1* (exon9: c.1397C>T; p.Ser466Phe) cosegregated with the proteinuria phenotype in this family. This missense variant was determined to be located in exon 9 and within the third zinc finger of the protein, which results in a substitution from serine to phenylalanine at residue 466. Our results suggest that this pathogenic missense variant of *WT1* is related to the development of IgAN in this family.

In addition, we identified a stop-gain pathogenic variant in *NPHS1* (NM_004646.4: exon27: c.3478C>T; p.Arg1160Ter,

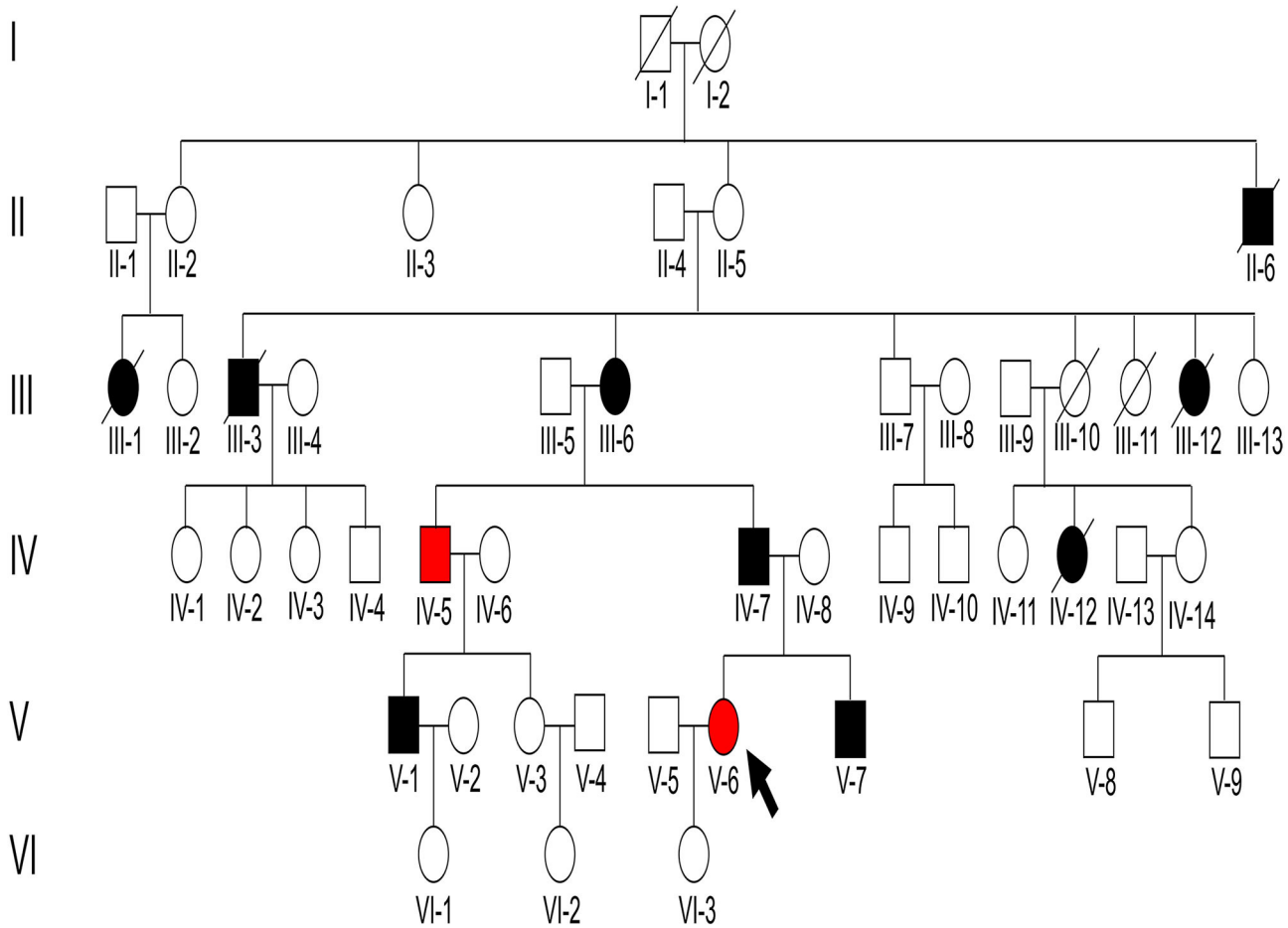

FIGURE 1 | Pedigree structure of the family with immunoglobulin A (IgA) nephropathy (IgAN). There were 47 individuals in the Chinese six-generation IgA pedigree with no close relatives that were married. The arrow indicates the proband, black-filled shapes indicate abnormal proteinuria and/or hematuria results, red-filled shapes indicate patients diagnosed as IgAN, and unfilled shapes indicate unaffected individuals.

dbSNP: rs267606919) in five immediate family members (III-6, III-7, IV-5, V-3, and VI-2). Of them, III-6 and IV-5 showed proteinuria, whereas III-7, V-3, and VI-2 showed normal urinary protein excretion. The *NPHS1* variant did not cosegregate in the affected family members.

Genetic testing also revealed that the proband, her younger brother, and his mother, carried another likely benign variant in the *WT1* gene (NM_024426.6: exon10: c.1433-10G>A), which cosegregated with the disease phenotype. As pathogenic variants of type IV collagen genes (*COL4A3/A4/A5*) have been recently reported to be causal factors for familial IgAN (10, 11), we checked for variants in these genes in the family but detected no pathogenic or likely pathogenic variant. Finally, all above mentioned three variants were verified by Sanger sequencing (**Figure 3**) and the primers used for sequencing were listed (**Table S1**).

DISCUSSION

Owing to the high and variable prevalence of genetic factors in different races and the familial aggregation of IgAN, their role in IgAN is widely accepted. To date, several genome-wide association studies in large sporadic IgAN populations have identified different genetic loci for IgAN susceptibility (10, 12). Whole-exome sequencing has proven to be a powerful tool for the identification of pathogenic mutations in familial diseases, especially Mendelian diseases. Therefore, using whole-exome sequencing, we identified a pathogenic missense variant in *WT1* that cosegregated with an abnormal proteinuria phenotype in a large IgAN pedigree of 47 members belonging to six generations.

In addition to hematuria, a considerable proportion of patients with IgAN exhibit proteinuria and podocyte lesions. An increased number of urinary podocytes and a decreased number of glomerular podocytes have been reported to be associated with IgAN prognosis (13, 14), suggesting the involvement of podocyte injury in IgAN. However, the exact mechanism of podocyte injury in IgAN remains unclear. Lai et al. found that when challenged with IgA deposition, mesangial cells become activated and produce cytokines that induce podocyte injury. The authors named this phenomenon mesangial-podocytic communication and

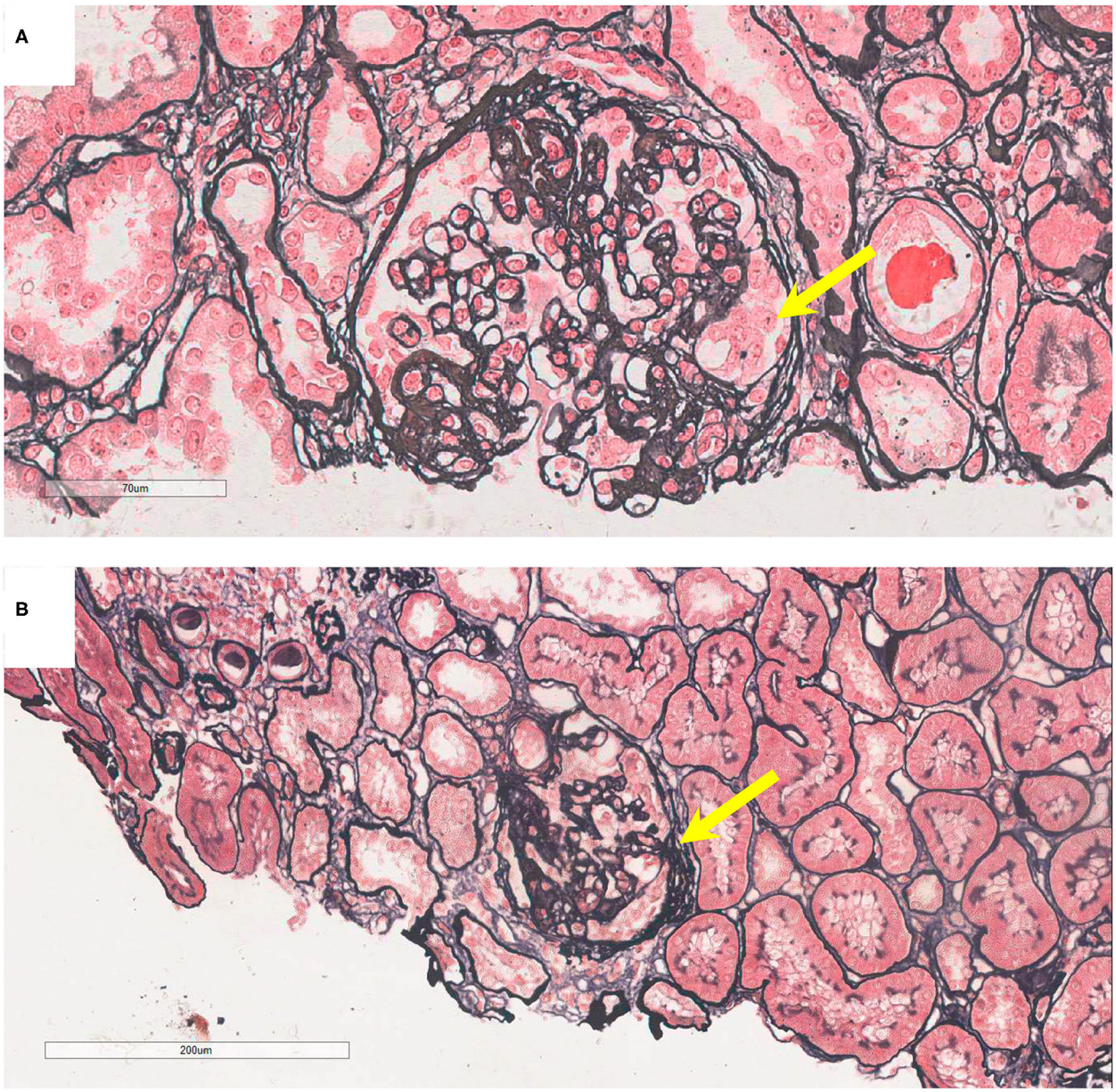

FIGURE 2 | Pathology presentation of patients V-6 and IV-5. **(A)** Patient V-6: light microscopy showed segmental sclerosis and podocyte hypertrophy (yellow arrow), by periodic acid-silver methenamine (PASM) staining; original magnification: 200X. **(B)** Patient IV-5: light microscopy showed segmental adhesion and podocyte hypertrophy (yellow arrow; PASM staining, 100X).

proposed it as a pathogenic factor of podocyte injury in IgAN (15).

In this case study, we reported an IgAN pedigree with a pathogenic missense *WT1* gene variant that cosegregated with proteinuria. *WT1* is an important marker of normal podocytes in mature kidneys (16). The glomerular filtration barrier is composed of endothelial cells, glioblastoma (GBM), and podocytes. Podocyte injury is considered a crucial factor associated with proteinuria, a common phenotype in glomerular diseases (17). According to previous reports, *WT1* heterozygous mutations are associated with several kidney diseases with distinct podocyte lesions, such as FSGS, Frasier syndrome, and DDS, which are consistent with the presence of a missense variant in exon 8 or 9, encoding zinc finger proteins (6, 18, 19).

In our reported pedigree, the occurrence of proteinuria was seen in all members carrying the identified pathogenic missense variant in *WT1* (exon9: c.1397C>T; p.Ser466Phe).

TABLE 1 | Overview of genotypic and phenotypic data of related members in this pedigree.

Individual	Gender	Age	Age at onset*	Renal function	Renal Biopsy#	Gene variants&	WES
III-5	Male	72	NA	Normal	NA	NA	Yes
III-6	Female	73	50/proteinuria/ hematuria	Normal	NA	*WT1*: exon9: c.1397C>T;p.Ser466Phe	Yes
						NPHS1: exon27: c.3478C>T;p.Arg1160Ter	
III-7	Male	71	NA	Normal	NA	*NPHS1*: exon27: c.3478C>T;p.Arg1160Ter	No
III-8	Female	70	NA	Normal	NA	NA	No
IV-4	Male	42	NA	Normal	NA	NA	No
IV-5	Male	52	32/proteinuria	Normal	IgAN	*WT1*: exon9: c.1397C>T;p.Ser466Phe	Yes
						NPHS1: exon27: c.3478C>T;p.Arg1160Ter	
IV-6	Female	54	NA	Normal	NA	NA	Yes
IV-7	Male	50	30/proteinuria/hematuria	ESKD	NA	*WT1*: exon9: c.1397C>T;p.Ser466Phe	Yes
IV-8	Female	49	NA	Normal	NA	*WT1*: exon10: c.1433-10G>A	Yes
IV-9	Male	45	NA	Normal	NA	NA	No
IV-10	Male	42	NA	Normal	NA	NA	No
V-1	Male	31	18/proteinuria	Normal	NA	*WT1*: exon9: c.1397C>T;p.Ser466Phe	Yes
V-2	Female	30	NA	Normal	NA	NA	No
V-3	Male	29	NA	Normal	NA	*NPHS1*: exon27: c.3478C>T;p.Arg1160Ter	Yes
V-4	Female	27	NA	Normal	NA	NA	No
V-6	Female	28	24/proteinuria/hematuria	ESKD	IgAN	*WT1*: exon9: c.1397C>T;p.Ser466Phe	Yes
						WT1: exon10: c.1433-10G>A	
V-7	Male	24	15/proteinuria/hematuria	ESKD	NA	*WT1*: exon9: c.1397C>T;p.Ser466Phe	Yes
						WT1: exon10: c.1433-10G>A	
VI-1	Female	4	NA	Normal	NA	*WT1*: exon9: c.1397C>T;p.Ser466Phe	No
VI-2	Female	5	NA	Normal	NA	*NPHS1*: exon27: c.3478C>T;p.Arg1160Ter	No

WES, whole-exome sequencing; WT1, Wilms tumor suppressor 1; NPHS1, nephrin; IgAN, IgA nephropathy; ESKD, end-stage kidney disease.
**NA means renal function was normal so far.*
#NA means family members did not take renal biopsy.
&NA means no gene variant was detected.

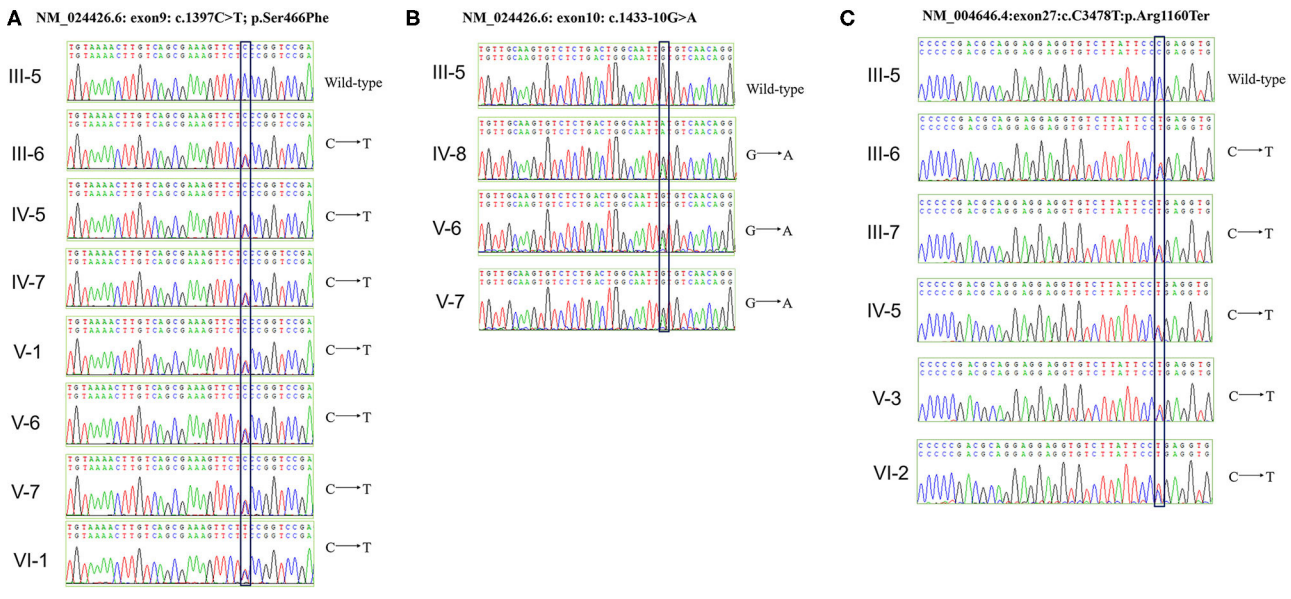

FIGURE 3 | Verification of *WT1 and NPHS1* variants by Sanger sequencing. **(A)** The c.1397C>T; p.Ser466Phe mutation was verified in seven family members (III-6, IV-5, IV-7, IV-8, V-1, V-6, V-7, and VI-1). **(B)** The c.1433-10G>A mutation was verified in three family members (IV-8, V-6, and V-7). **(C)** The c.3478C>T; p.Arg1160Ter mutation was verified in five family members (III-6, III-7, IV-5, V-3, and VI-2).

This variant has previously been identified in a 46-year-old female with isolated nephrotic proteinuria, and in her father who presented with chronic renal failure (20). In the adult kidney, *WT1* expression is limited to the podocytes and plays a crucial role in normal renal podocyte function (21). Mutations in *WT1* can induce dedifferentiation, abnormal proliferation, and morphological alterations in podocytes by affecting its zinc finger domain and disturbing the alternative splicing of ±KTS isoforms (22). The pathogenic variant in exon9, c.1397C>T; p.Ser466Phe, is located in the zinc finger 3 domain of the WT1 protein, and the Ser > Phe change might induce a structural change in the third zinc finger (20). Sakamoto et al. reported that PKA phosphorylation of Ser-393 could decrease the transcriptional activity of *WT1* by repressing its DNA-binding ability (23). Recently, Nagano et al. studied the transcriptional activity of *WT1* through a systematic review and reported that mutations in both the DNA-binding site and C2H2 zinc finger structure may cause severe clinical phenotypes (24). Based on the aforementioned evidence, we postulated that this pathogenic missense variant in *WT1* is the causal factor that induced proteinuria in the IgAN pedigree analyzed in this case study.

Furthermore, we also identified a pathogenic stop-gain variant of *NPHS1* (exon27: c.3478C>T; p.Arg1160Ter), which changes the length of the protein nephrin by causing premature termination, in this family. This stop-gain variant has previously been reported in a patient with congenital nephrotic syndrome of the Finnish type (25). Nephrin plays an important role in the organization of the slit diaphragm (26). Homozygous or compound heterozygous *NPHS1* mutations have been observed in patients with congenital nephrotic syndrome, late-onset steroid-resistant nephrotic syndrome, and FSGS (27–29). In this family, five members (III-6, III-7, IV-5, V-3, and VI-2) were heterozygous for this variant and only two—the grandmother of the proband with proteinuria (III-6) and the uncle of the proband diagnosed with IgAN (IV-5)—had a kidney-associated phenotype. The other three members heterozygous for the *NPHS1* variant (III-7, V-3, and VI-2) showed no kidney-associated phenotype, indicating that this variant did not cosegregate with the disease. Although the grandmother and uncle of the proband carried both *WT1* and *NPHS1* missense variants, until the time this case study was conducted, their renal functions were normal, the clinical phenotypes were mild, and disease progression was slow.

In addition, we also found that two individuals in this pedigree with severe kidney phenotypes—the proband and her younger brother—carried another *WT1* variant (exon10: c.1433-10G>A), which they inherited from their mother, other than the missense variant (exon9: c.1397C>T; p.Ser466Phe), which they inherited from their father. Although the c.1433-10G>A variant was not predicted to be a splicing variant by splicing algorithms (BDGP and ASSP) and was therefore regarded as benign based on the ACMG guidelines, it cosegregated with the disease severity phenotype. The proband and her younger brother progressed to ESKD at ages 28 and 24 years, respectively. In contrast, other individuals in the pedigree exhibiting only the missense *WT1* variant presented with mild kidney injury and slow disease progression. Therefore, we speculate that the c.1433-10G>A variant may also contribute to disease progression and the development of the clinical phenotype in this family and suggest that its influence on *WT1* must be investigated further.

This case study is limited in that not all the family members with kidney disease were biopsied and, therefore, we could not confirm their diagnosis of having developed IgAN. Moreover, renal biopsy samples were not evaluated by electron microscopy, and we failed to accurately evaluate podocyte and GBM lesions. In summary, here, we report an IgAN pedigree with a pathogenic missense heterozygous *WT1* variant (c.1397C>T; p.Ser466Phe) and suggest that *WT1* pathogenic missense variant-induced primary podocyte injury is responsible for the proteinuria phenotype and IgAN progression in this pedigree.

ETHICS STATEMENT

The studies involving human participants were reviewed and approved by The Medical Ethics Committee of Peking University First Hospital. Written informed consent to participate in this study was provided by the participants' legal guardian/next of kin.

AUTHOR CONTRIBUTIONS

Research idea and study design by LZ and SS. Data acquisition and Data analysis/interpretation by QL. Supervision or mentorship by LZ, SS, DX, JL, and HZ. Each author contributed important intellectual content during manuscript drafting or revision and accepts accountability for the overall work by ensuring that questions pertaining to the accuracy or integrity of any portion of the work are appropriately investigated and resolved. All authors contributed to the article and approved the submitted version.

FUNDING

This case study was supported by grants from the National Key Research and Development Program of China (2020YFC2005003), the National Science Foundation of China (81922013, 81970598, and 82070733), the National Science Foundation of Beijing (7192209 and 7202206), the Youth Development Project from Peking University Health Science Center (BMU2021PY004), and the CAMS Innovation Fund for Medical Sciences (2019-I2M-5-046).

SUPPLEMENTARY MATERIAL

The Supplementary Material for this article can be found online at: https://www.frontiersin.org/articles/10.3389/fmed.2021.810940/full#supplementary-material

REFERENCES

1. Shi M, Yu S, Ouyang Y, Jin Y, Chen Z, Wei W, et al. Increased lifetime risk of ESRD in familial IgA nephropathy. *Kidney Int Rep.* (2021) 6:91–100. doi: 10.1016/j.ekir.2020.10.015
2. Scolari F, Amoroso A, Savoldi S, Mazzola G, Prati E, Valzorio B, et al. Familial clustering of IgA nephropathy: further evidence in an Italian population. *Am J Kidney Dis.* (1999) 33:857–65. doi: 10.1016/S0272-6386(99)70417-8
3. Sabatier JC, Genin C, Assenat H, Colon S, Ducret F, Berthoux FC. Mesangial IgA glomerulonephritis in HLA-identical brothers. *Clin Nephrol.* (1979) 11:35–8.
4. Thompson A, Carroll K, A Inker L, Floege J, Perkovic V, Boyer-Suavet S, et al. Proteinuria reduction as a surrogate end point in trials of IgA nephropathy. *Clin J Am Soc Nephrol.* (2019) 14:469–81. doi: 10.2215/CJN.08600718
5. Niaudet P, Gubler MC. WT1 and glomerular diseases. *Pediatr Nephrol.* (2006) 21:1653–60. doi: 10.1007/s00467-006-0208-1
6. Lipska BS, Ranchin B, Iatropoulos P, Gellermann J, Melk A, Ozaltin F, et al. Genotype–phenotype associations in WT1 glomerulopathy. *Kidney Int.* (2014) 85:1169–78. doi: 10.1038/ki.2013.519
7. Hall G, Gbadegesin RA, Lavin P, Wu G, Liu Y, Oh EC, et al. A novel missense mutation of Wilms' Tumor 1 causes autosomal dominant FSGS. *J Am Soc Nephrol.* (2015) 26:831–43. doi: 10.1681/ASN.2013101053
8. Miller SA, Dykes DD, Polesky HF. A simple salting out procedure for extracting DNA from human nucleated cells. *Nucleic Acids Res.* (1988) 16:1215. doi: 10.1093/nar/16.3.1215
9. Groopman EE, Marasa M, Cameron-Christie S, Petrovski S, Aggarwal VS, Milo-Rasouly H, et al. Diagnostic utility of exome sequencing for kidney disease. *N Engl J Med.* (2019) 380:142–51. doi: 10.1056/NEJMoa1806891
10. Stapleton CP, Kennedy C, Fennelly NK, Murray SL, Connaughton DM, Dorman AM, et al. An exome sequencing study of 10 families with IgA nephropathy. *Nephron.* (2020) 144:72–83. doi: 10.1159/000503564
11. Zhu Q, Zhou C, Wang J. A novel frameshift mutation of COL4A5 in a Chinese family with presumed IgA nephropathy and chronic glomerulonephritis. *J Clin Lab Anal.* (2020) 34:e23558. doi: 10.1002/jcla.23558
12. Zhu L, Zhang H. The genetics of IgA nephropathy: an overview from China. *Kidney Dis.* (2015) 1:27–32. doi: 10.1159/000381740
13. Asao R, Asanuma K, Kodama F, Akiba-Takagi M, Nagai-Hosoe Y, Seki T, et al. Relationships between levels of urinary podocalyxin, number of urinary podocytes, and histologic injury in adult patients with IgA nephropathy. *Clin J Am Soc Nephrol.* (2012) 7:1385–93. doi: 10.2215/CJN.08110811
14. Menon MC, Chuang PY, He JC. Role of podocyte injury in IgA nephropathy. *Contrib Nephrol.* (2013) 181:41–51. doi: 10.1159/000348461
15. Lai KN, Leung JC, Chan LY, Saleem MA, Mathieson PW, Lai FM, et al. Activation of podocytes by mesangial-derived TNF-alpha: glomerulo-podocytic communication in IgA nephropathy. *Am J Physiol Renal Physiol.* (2008) 294:F945–55. doi: 10.1152/ajprenal.00423.2007
16. Kreidberg JA, Sariola H, Loring JM, Maeda M, Pelletier J, Housman D, et al. WT-1 is required for early kidney development. *Cell.* (1993) 74:679–91. doi: 10.1016/0092-8674(93)90515-R
17. Jalanko H, Patrakka J, Tryggvason K, Holmberg C. Genetic kidney diseases disclose the pathogenesis of proteinuria. *Ann Med.* (2001) 33:526–33. doi: 10.3109/07853890108995962
18. Chen YM, Liapis H. Focal segmental glomerulosclerosis: molecular genetics and targeted therapies. *BMC Nephrol.* (2015) 16:101. doi: 10.1186/s12882-015-0090-9
19. Coppes MJ, Huff V, Pelletier J. Denys-Drash syndrome: relating a clinical disorder to genetic alterations in the tumor suppressor gene WT1. *J Pediatr.* (1993) 123:673–8. doi: 10.1016/S0022-3476(05)80839-X
20. Guaragna MS, Lutaif ACGB, Piveta CSC, Belangero VMS, Maciel-Guerra AT, Guerra-Junior G, et al. Two distinct WT1 mutations identified in patients and relatives with isolated nephrotic proteinuria. *Biochem Biophys Res Commun.* (2013) 441:371–6. doi: 10.1016/j.bbrc.2013.10.064
21. Cheng C, Chen L, Wen S, Lin Z, Jiang X. Case report: Denys-Drash Syndrome with WT1 causative variant presenting as atypical hemolytic uremic syndrome. *Front Pediatr.* (2020) 8:605889. doi: 10.3389/fped.2020.605889
22. Morrison AA, Viney RL, Saleem MA, Ladomery MR. New insights into the function of the Wilms tumor suppressor gene WT1 in podocytes. *Am J Physiol Renal Physiol.* (2008) 295:F12–7. doi: 10.1152/ajprenal.00597.2007
23. Sakamoto Y, Yoshida M, Semba K, Hunter T. Inhibition of the DNA-binding and transcriptional repression activity of the Wilms' tumor gene product, WT1, by cAMP-dependent protein kinase-mediated phosphorylation of Ser-365 and Ser-393 in the zinc finger domain. *Oncogene.* (1997) 15:2001–12. doi: 10.1038/sj.onc.1201391
24. Nagano C, Takaoka Y, Kamei K, Hamada R, Ichikawa D, Tanaka K, et al. Genotype-phenotype correlation in WT1 exon 8 to 9 missense variants. *Kidney Int Rep.* (2021) 6:2114–21. doi: 10.1016/j.ekir.2021.05.009
25. Lenkkeri U, Männikkö M, McCready P, Lamerdin J, Gribouval O, Niaudet PM, et al. Structure of the gene for congenital nephrotic syndrome of the finnish type (NPHS1) and characterization of mutations. *Am J Hum Genet.* (1999) 64:51–61. doi: 10.1086/302182
26. Büscher AK, Kranz B, Büscher R, Hildebrandt F, Dworniczak B, Pennekamp P, et al. Immunosuppression and renal outcome in congenital and pediatric steroid-resistant nephrotic syndrome. *Clin J Am Soc Nephrol.* (2010) 5:2075–84. doi: 10.2215/CJN.01190210
27. Philippe A, Nevo F, Esquivel EL, Reklaityte D, Gribouval O, Tête MJ, et al. Nephrin mutations can cause childhood-onset steroid-resistant nephrotic syndrome. *J Am Soc Nephrol.* (2008) 19:1871–8. doi: 10.1681/ASN.2008010059
28. Santín S, García-Maset R, Ruíz P, Giménez I, Zamora I, Peña A, et al. Nephrin mutations cause childhood- and adult-onset focal segmental glomerulosclerosis. *Kidney Int.* (2009) 76:1268–76. doi: 10.1038/ki.2009.381
29. Hinkes BG, Mucha B, Vlangos CN, Gbadegesin R, Liu J, Hasselbacher K, et al. Nephrotic syndrome in the first year of life: two thirds of cases are caused by mutations in 4 genes (NPHS1, NPHS2, WT1, and LAMB2). *Pediatrics.* (2007) 119:e907–19. doi: 10.1542/peds.2006-2164

Conflict of Interest: The authors declare that the research was conducted in the absence of any commercial or financial relationships that could be construed as a potential conflict of interest.

frontiers | Frontiers in Medicine

CASE REPORT
published: 07 April 2022
doi: 10.3389/fmed.2022.862514

Late-Onset Bartter Syndrome Type II Due to a Novel Compound Heterozygous Mutation in *KCNJ1* Gene: A Case Report and Literature Review

*Mi Tian[1], Hui Peng[1], Xin Bi[2], Yan-Qiu Wang[1], Yong-Zhe Zhang[1], Yan Wu[1] and Bei-Ru Zhang[1]**

[1] Department of Nephrology, Shengjing Hospital of China Medical University, Shenyang, China, [2] Guangzhou KingMed Center for Clinical Laboratory Co, Ltd., Guangzhou, China

OPEN ACCESS

Edited by:
Ekamol Tantisattamo, University of California, Irvine, United States

Reviewed by:
Junjiang Fu, Southwest Medical University, China
Daw-Yang Hwang, National Institute of Cancer Research, National Health Research Institutes, Taiwan

***Correspondence:**
Bei-Ru Zhang
xiaopei19730704@163.com

Specialty section:
This article was submitted to Nephrology, a section of the journal Frontiers in Medicine

Received: *26 January 2022*
Accepted: *14 March 2022*
Published: *07 April 2022*

Citation:
Tian M, Peng H, Bi X, Wang Y-Q, Zhang Y-Z, Wu Y and Zhang B-R (2022) Late-Onset Bartter Syndrome Type II Due to a Novel Compound Heterozygous Mutation in KCNJ1 Gene: A Case Report and Literature Review. Front. Med. 9:862514. doi: 10.3389/fmed.2022.862514

Background: Bartter syndrome (BS) type II is a rare autosomal recessive renal tubular disorder caused by mutations in the *KCNJ1* gene, which encodes the apical renal outer medullary potassium (ROMK) channel in the thick ascending limb (TAL) of Henle's loop. BS type II is typically considered as a disorder of infancy and seldom seen in adults.

Case Presentation: A 34-year-old woman was admitted with generalized body numbness and hand convulsions, without growth retardation. Laboratory tests revealed hypokalemic metabolic alkalosis, hyperreninemic hyperaldosteronism, and nephrocalcinosis. She was misdiagnosed during the initial diagnosis process and was finally diagnosed with late-onset BS type II *via* genetic testing through next-generation sequencing combined with Sanger sequencing. A novel compound heterozygous p.Leu207Ile/p. Cys308Arg variant in exon 5 of the *KCNJ1* gene from her parents was identified and speculated to be a potential pathogenic gene variation.

Conclusion: We report a case of late-onset BS type II with a novel compound heterozygous mutation in *KCNJ1*. Both variants are novel and have never been reported. Our report will have a significant impact on the diagnosis of BS in other patients without typical clinical presentations and emphasizes the importance of genetic investigation.

Keywords: Bartter syndrome type II, *KCNJ1* gene mutation, nephrocalcinosis, hypokalemia, late onset

INTRODUCTION

Bartter syndrome (BS) is a rare, autosomal recessive or dominant inheritance of salt-losing kidney disorder, with a prevalence of 1 in 1,000,000 (1). It is characterized by hypokalemia, metabolic alkalosis, hyperreninemia, hyperaldosteronism, hypercalciuria, polyuria, and polydipsia, accompanied by normal or low blood pressure (2). BS can be divided into several subtypes according to the mutations in different genes encoding the transporters involved in salt reabsorption in the thick ascending limb (TAL) of Henle's loop (3). BS type I is caused by mutations in *SCL12A1*, which encodes the Na-K-2Cl cotransporter (NKCC2) in the apical membrane of

epithelial cells in the TAL. BS type II is caused by mutations in *KCNJ1*, which encodes the renal outer medullary potassium (ROMK) channel. Potassium recycling through the ROMK channel to maintain the potassium concentrations in the lumina is crucial for proper NKCC2 function; thus, BS type I and type II have similar prenatal presentations (4). BS type III is associated with mutations in *CLCNKB*, which encodes the basolateral chloride channel CLC-Kb. BS type IV comprises two unique defects. BS type IVa is caused by mutations in the *BSND* gene encoding barttin, which is an essential subunit for CIC-Ka and CIC-Kb channels. However, BS type IVb is caused by digenic mutations in both *CLCNKB* and *CLCNKA*, which encode CLC-Kb and CLC-Ka channels, respectively (5). Two other subtypes of BS have been recently identified. (1) Transient neonatal BS is caused by mutations in melanoma-associated antigen D2 (*MAGED2*). In this type of BS, tubulopathy spontaneously improves within the first few months of life in survivors (6). (2) Autosomal dominant hypocalcemia is caused by gain-of-function mutations in the *CASR*, which encodes the calcium ion-sensing receptor (CaSR) in the basolateral cell membrane of the TAL.

Previously, another terminology was proposed to separate BS into "antenatal BS" (type I, II, and IV BS), associated with a more severe presentation, and "classic BS" (type III BS), associated with a later presentation in childhood. Type II BS is an antenatal/neonatal BS in which renal disorder begins in the utero, accounting for the polyhydramnios and premature delivery that is typical in affected infants. It can present life-threatening volume depletion due to severe renal salt wasting and characteristic BS clinical manifestations in the neonatal period, even resulting in stunted growth. This BS type likely represents a disorder in infancy but not in adulthood.

Here, we report an adult case with an unusually mild clinical presentation of BS known as late-onset BS type II, which contributes to a novel potential pathogenic compound heterozygous mutation in the *KCNJ1* gene in an Asian pedigree discovered through genetic testing.

CASE PRESENTATION

A 34-year-old Chinese woman was admitted with the chief complaint of repeated generalized body numbness and hand convulsions experienced for the last 13 years, which have worsened in the 2 months. Thirteen years ago, she presented to the hospital with the same symptoms and had been told that she had hypokalemia and hypocalcemia, but she had not taken potassium chloride supplementation regularly and no follow-up after discharge. During these 13 years, she only took potassium chloride supplements when her symptoms worsened and stopped taking them as long as they were relieved. Occasional tests suggested that hypokalemia persisted. Her symptoms worsened 2 months before the latest hospitalization, and potassium chloride supplements did not significantly alleviate the symptoms. She presented to a local hospital and was informed that she had hypokalemia with a serum potassium level of 2.9 mmol/L, accompanied by hypomagnesemia and hypocalcemia. She was diagnosed with medullary sponge kidney (MSK) based on intravenous pyelography (IVP) examination (**Supplementary Figure 1A**) and renal tubular acidosis (RTA) type I by a local physician and was prescribed potassium citrate granules.

Although information on her antenatal course is not available, she was not a premature baby; she was delivered after a full-term pregnancy. There was no serious dehydration, electrolyte disorders or other symptoms that needed to be treated after birth. She developed normally, without any visible deformity, and had normal intellectual development. However, her parents revealed that she has experienced symptoms of thirst, polydipsia, and polyuria since childhood. Her medical history is unremarkable, and she has denied any medications, including diuretics and laxatives, alcohol, or other drugs. The parental family history is unremarkable, and she has no siblings. She is married and has one healthy child. No one else in the family experienced similar symptoms.

Her weight was 50 kg, height 162 cm, pulse 88/min, and blood pressure 130/80 mmHg. Physical examination results were normal.

Laboratory findings (**Table 1**) revealed hypokalemia with a serum potassium level of 3.43 mmol/L. In a 24-h urine collection, excretion of potassium was 88.36 mmol/d, suggesting renal potassium wasting as the source of hypokalemia. She had hypocalcemia with a calcium level of 2.03 mmol/L, but her 24-h urinary calcium excretion level was normal. She had hypomagnesemia with a serum magnesium concentration of 0.48 mmol/L. Arterial blood gas analysis showed a pH of 7.54, pCO_2 of 31 mmHg, and HCO_3 of 26.5 mmol/L, suggesting metabolic alkalosis. Urinalysis revealed a pH of 7 and specific gravity (SG) of 1.009. After 12 h of water deprivation, she had a reduced urine osmolality of 227 mOsm/kg at a plasma osmolality of 289 mOsm/kg, indicating impaired urine concentration function. There was proteinuria + - and no hematuria. However, her 24-h urinary protein quantification was 1.04 g/d. She also had hyperreninemia and hyperaldosteronism. The sodium and chloride levels were normal. Serum creatinine was 76.1 μmol/L [estimated glomerular filtration rate (eGFR) (CKD-EPI) 88.03 mL/min], indicating normal renal function. Her parathyroid hormone level was normal. Ultrasound examination showed medullary nephrocalcinosis or medullary sponge kidney in both kidneys (**Supplementary Figure 1B**).

GENETIC ANALYSIS

Clinical findings of recurrent hypokalemia with renal potassium wasting, metabolic alkalosis, hyperreninemia, and hyperaldosteronism raised the suspicion of BS or Gitleman syndrome (GS). Differential diagnosis depended on genetic testing.

Following informed consent, genomic deoxyribonucleic acid (DNA) of the patient was extracted from peripheral blood according to the manufacturer's standard procedure using the QIAamp DNA Blood Midi Kit (Qiagen, Hilden, Germany). The extracted DNA was fragmented by DNase, purified using magnetic beads, amplified using polymerase chain reaction (PCR) and connected to the adapter sequence. The target

TABLE 1 | Laboratory investigations performed during the two hospital admissions.

Laboratory findings	First admission	Second admission	Normal values
Serum creatine, umol/L	62.4	76.1	59–104
Serum urea nitrogen, mmol/L	3.83	7.43	3–7.2
Plasma potassium, mmol/L	2.65	3.43	3.5–5.5
Plasma sodium, mmol/L	137.9	140	136–145
Plasma chlorine, mmol/L	94.8	105.5	96–108
Plasma calcium, mmol/L	1.97	2.03	2.1–2.55
Plasma phosphate, mmol/L	1.13	1.15	0.9–1.6
Plasma magnesium, mmol/L	0.59	0.48	0.67–1.15
Plasma parathyroid hormone, pg/mL	16.13	16.13	15–65
Urinary sodium, mmol/day	122	122	130–260
Urinary potassium, mmol/day	97.69	88.36	25–100
Urinary chlorine, mmol/day	301.3	148	170–250
Urinary calcium, mmol/day	10.95	6.84	2.5–7.5
Urinary phosphate, mmol/day	11.23	17.02	23–48
Serum renin, ng/mL	3.4	16.7	0.15–2.33
Serum Aldosterone, pg/mL	325	1038.7	30–160
Urinary pH	7.494	7	4.5–8.0
Urinary SG	1.009	1.009	1.003–1.030
Blood pH	7.494	7.54	7.35–7.45
Plasma bicarbonate, mmol/L	40.5	31	22–26

area of the whole exome was captured and purified using an IDT XGen Exome Research Panel probe (IDT Corporation, United States). All the amplified libraries were subsequently sent to a high-throughput sequencing kit for sequencing on a NovaSeq 6000 sequencer (Illumina, San Diego, CA, United States). For the genetic analysis of *SLC12A1* (NKCC2), *KCNJ1* (ROMK), *CLCNKB* (ClC-Kb), *CLCNKA* (ClC-Ka), *BSND* (Barttin), *CASR* (CaSR), *MAGED2* (MAGE-D2), and *SLC12A3* (NCCT), which are responsible for BS or GS, gene exon coding regions and exon-intron junction regions were sequenced. Because MSK was also suspected in other hospitals, the reported potentially related genes according to the OMIM database, such as *MKS1, TMEM216, TMEM67, CEP290, RPGRIP1 L, CC2D2A, NPHP3, TCTN2, B9D1, B9D2, TMEM231, KIF14,* and *TMEM107*, were also analyzed.

We performed data analysis and bioinformatic processing to detect potential variants. We used the Burrows–Wheeler aligner (BWA) algorithm to compare all data with the reference sequence (UCSC hg19) (7) and the method in the reported literature to annotate the data (8). Data were screened by reference screening process (9). According to variant classification standards proposed by the American College of Medical Genetics and Genomics (ACMG) (10), the clinical significance of these variants was identified (9).

The analysis results showed a compound heterozygous missense mutation in exon 5 of the *KCNJ1* gene. The c.619C > A variant resulted in a change from a leucine codon to an isoleucine codon (p. Leu207Ile), and the c.922C > T variant resulted in a change from a cysteine codon to an arginine codon (p. Cys308Arg). To further prove the inheritance of the variation, we used the Sanger sequencing to examine the mutations in patient's parents with consent, and discovered that c.619C > A was inherited from her father and c.922C > T was inherited from her mother (**Figure 1**). Based on the clinical and genetic findings, the patient was diagnosed with late-onset BS type II.

DISCUSSION

Historically, BS has been categorized by phenotypic characteristics, such as antenatal BS and classic BS, based on age and severity of presentation. However, emerging data show a wide spectrum of severity in all forms of BS; some patients with type I, II, or IV BS present with late-onset form (11), whereas some patients with type III BS may appear with a severe antenatal presentation (12), although relatively rare. Type II BS is classified as antenatal BS. Most patients are born prematurely and present life-threatening volume depletion and electrolyte disorders. If they survive in the neonatal period, they will show growth retardation or even abnormal development. However, a few patients with type II BS can spontaneously manifest transient hyponatremia of prematurity with complete resolution and only demonstrate persistent polyuric and hypercalciuria without the development of nephrocalcinosis (13). To date, six cases of late-onset BS type II have been reported (14–19). All these cases developed normally and were finally diagnosed in adulthood because of various mild clinical symptoms as reported in **Table 2**. These cases strongly suggest that BS is a differential disease that should be considered in adults with similar manifestations, and it requires timely genetic testing. However, it has been reported that a genetic diagnosis cannot be established in approximately two-thirds of patients with adult-onset BS (4).

KCNJ1 is located on chromosome 11q24 and consists of five exons, with exon 5 encoding most of the sequences of the protein channel and being the most influential putative functional domain of *KCNJ1*. More than 70 *KCNJ1* mutations have been described to date (**Figure 2A**), most of which are missense or non-sense mutations substituting conserved amino acid residues, predominantly within coding exon 5 (20). The five reported late-onset BS type II cases discovered through genetic tests had different mutations in *KCNJ1*, but all were in exon 5. Among these, only two cases presented with a compound heterozygous mutation. In this study, we identified a novel compound heterozygous mutation (p.Leu207Ile/p. Cys308Arg), which has not been reported previously. Next generation sequencing-based mutation screening combined with Sanger sequencing has been proven to be a reliable method for molecular diagnosis. These variants were not included in the large public population database gnomAD[1], indicating that they are extremely rare. Although we did not directly verify the effect of heterozygous mutations on protein function, we hypothesized that they are likely to have a significant impact. PolyPhen-2 and Scale Invariant Feature Transform (SIFT) software predicted that both mutations were deleterious. These positions are entirely conserved among species

[1]https://gnomad.broadinstitute.org/

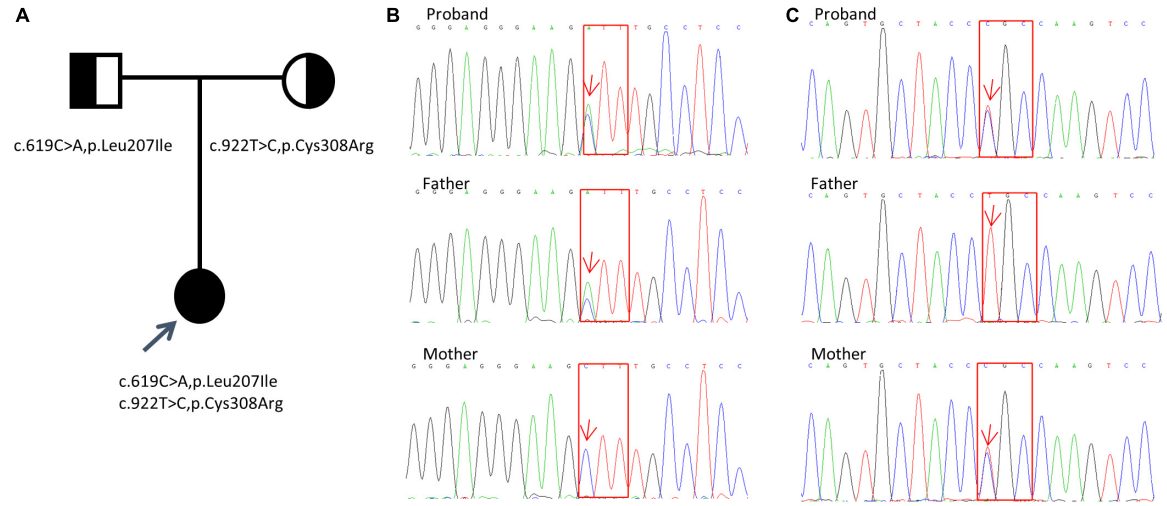

FIGURE 1 | Detection of KCNJ1 variants in a Chinese family. Two novel heterozygous variants (c.619C > A, p.Leu207Ile and c.922T > C, p.Cys308Arg) were identified. **(A)** Pedigree of the family. **(B,C)** Sanger sequencing electropherograms (partial) of the patient and her parents are shown. The results of c.619C > A, p.Leu207Ile variant are shown in **(B)**, and those of the c.922T > C, p.Cys308Arg variant are shown in **(C)**. Red arrows indicate the positions of the variants. Red squares indicate the corresponding altered amino acids.

TABLE 2 | Summary of clinical information and gene mutations of six reported cases of late-onset BS type II and our case.

No	1	2	3	4	5	6	7
Author	Sharma (14)	Huang (15)	Gollasch (16)	Li (17)	Yaqub (18)	Elferl (19)	Present case
Sex	Female	Male	Female	Female	Male	Male	Female
Age of presentation	8.5	35	43	34	38	26	34
Clinical presentation of admission	Polyuria, polydipsia	Lower back pain attribute to nephrocalcinosis	Nephrocalcinosis	Weakness	Fatigue, lethargy, lower limb weakness	Generalized weakness	Generalized body numbness, hands convulsion
Previous clinical manifestations	Polyuria, polydipsia	No	Thirst, polyuria	Polyuria, polydipsia	Bilateral flank pain, polyuria	Thirst, polydipsia, polyuria	Thirst, polydipsia, polyuria
Perinatal period abnormalities	No	Unknown	No	Polyhydramnios	Unknown	Unknown	No
Family history	No	No	No	No	Unknown	No	No
Nephrocalcinosis	(+)	(+)	(+)	(+)	(+)	(+)	(+)
Serum potassium level (mmol/L)	2.5	2.8	3	2.4	1.5	1.7	3.43
Hyperreninemia/ hyperaldosteronemia	(+)	(+)	(+)	(+)	(+)	(+)	(+)
Urine potassium	Increase	Normal	ND	Increase	Increase	Increase	Increase
Serum calcium	Normal	Decrease	Normal	Normal	Decrease	Normal	Decrease
24 h urine calcium	Increase	Increase	Increase	Increase	Increase	Increase	Normal
Serum creatinine (μ mol/L)	44	122	97	105	203	96	76.1
Serum magnesium	Normal	ND	Normal	Normal	Normal	Normal	ND
Mutation	Heterozygous	Homozygous	Heterozygous	Heterozygous	ND	Homozygous	Heterozygous
DNA sequence change	c.268G > T c.632T > G	c.658C > T	c.197T > A c.875G > A	c.701C > T c.212C > T	ND	c.658C > T	c.619C > A c.922C > T
Amino acid change (parent)	p.Gly90Trp(M) p.Ile211Ser(F)	p.Leu220Phe(ND)	p.Ile66Asn(ND) p.Arg292Gln(ND)	p.The234Ile(M) p.Thr71Me(F)	ND	p.Leu220Phe(ND)	p. Leu207Ile(F) p.Cys308Arg(M)

ND, not determined; M, mother; F, father.

(**Figure 2B**), indicating that the mutations severely impair the function of the protein. Furthermore, the combination of mutations in a compound heterozygous state may not be arbitrary but may influence the tertiary or quaternary structure of proteins and further determine the severity of the phenotype (21). Thus, the compound heterozygous state of Leu207Ile and

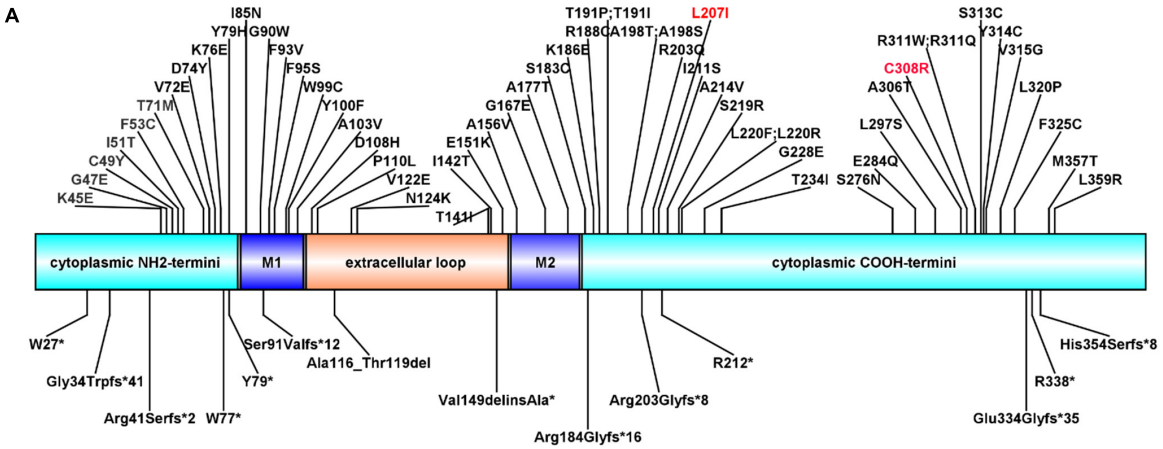

B

Species	Amino Acid Sequence(KCNJ1 L207)	Amino Acid Sequence(KCNJ1 C308)
Homo sapiens	INSFMCGAILAKISRPKKRAKTITFSKNAVISKRGGKLCLLIRVANLRKSLLIGSHIYGKLLKTTVTPEGETIILD	VIDHNSPFFHMAAETLLQQDFELVVFLDGTVESTSATCQVRTSYVPEEVLWGYRFAPIVSKTKEGKYRVDFHNFSK
Canis lupus familiaris	INSFMCGAILAKISRPKKRAKTITFSKNAVISKRGGKLCLLIRVANLRKSLLIGSHIYGKLLKTTVTPEGETIILD	VIDQSSPFFHMAAETLLQQDFELVVFLDGTVESTSATCQVRTSYVPEEVLWGYRFAPIVSKTKEGKYRVDFHNFSK
Myotis lucifugus	INSFMCGAILAKISRPKKRAKTITFSKNAVISKRGGKLCLLIRVANLRKSLLIGSHIYGKLLKTTVTPEGETIILD	IIDHNSPFFDMAAETLLQQDFELVVFLDGTVESTSATCQVRTSYVPEEVLWGYRFAPIVSKTKEGKYRVDFHNFSK
Loxodonta africana	INSFMCGAILAKISRPKKRAKTITFSKNAVISKRGGKLCLLIRVANLRKSLLIGSHIYGKLLKTTVTPEGETIILD	IIDHNSPFFHMAAENLSQQDFELVVFLDGTVESTSATCQVRTSYVPEEVLWGYRFAPIVSKTKEGKYRVDFHNFSK
Rattus norvegicus	INSFMCGAILAKISRPKKRAKTITFSKNAVISKRGGKLCLLIRVANLRKSLLIGSHIYGKLLKTTITPEGETIILD	IIDHNSPFFHMAAETLSQQDFELVVFLDGTVESTSATCQVRTSYVPEEVLWGYRFVPIVSKTKEGKYRVDFHNFGK
Cricetulus griseus	INSFMCGAILAKISRPKKRAKTITFSKNAVISKRGGKLCLLIRVANLRKSLLIGSHIYGKLLKTTIITPEGETIILD	VIDHNSPFFHMAAETLPQQDFELVVFLDGTVESTSATCQVRTSYVPEEVLWGYRFVPIVSKTKEGKYRVDFHNFGK
Monodelphis domestica	INAFMCGAILAKISRPKKRAKTITFSKNAVISKRGGKLCLLIRVANLRKSLLIGSHIYGKLLRTTVTPEGETIILD	VIDHNSPFFHMAAENILQQDFELVVFLDGTVESTSATCQVRTSYVPEEVLWGYRFAPIVSKTKEGKYRVDFHNFSK
Mus musculus	INSFMCGAILAKISRPKKRAKTITFSKNAVISKRGGKLCLLIRVANLRKSLLIGSHIYGKLLKTTITPEGETIILD	IIDHNSPFFHMAAETLSQQDFELVVFLDGTVESTSATCQVRTSYIPEEVLWGYRFVPIVSKTKEGKYRVDFHNFGK
Heterocephalus glaber	INSFMCGAILAKISRPKKRAKTITFSKNAVISKRGGKLCLLIRVANLRKSLLIGGHIYGKLLKTTVTPEGETIILD	IIDHNSPFFHMAAETLSQQEFELVVFLDGTVESTSATCQVRTSYVPEEVLWGYRFVPIVSKTKDGKYRVDFHNFSK
Gallus gallus	INSFMCGAILAKISRSKNRAKTITFSRNAVISKRGGKLCLLIRVANLRKSLLIGSHIYGKLLKTTITPEGETIILD	IIDKNSPFFHMAAETILQQDFELVVFLDGTVEATSATCQVRTSYIPEEVLWGYRFAPIVSKTKEGKYRVDFQNFSK
Xenopus tropicalis	INSFMCGAILAKISRPKKRAKTITFSKNAVISKRGGKLCLLIRVANLRKSLLIGSHIYGKLLKTTVTPEGETIILD	IIDKDSPFFEMSAETLLQHDFELVVFLDGTVESTSATCQVRTSFIPDEVLWGYRFAPLVSKTKEGKYRVDFSNFSK
Xenopus laevis	INSFMCGAILAKISRPKKRAKTITFSKNAVISKRGGKLCLLIRVANLRKSLLIGSHIYGKLLKTTVTPEGETIILD	IIDKDSPFFEMSAETLLQHDFELVVFLDGTVESTSATCQVRTSYIPDEVRWGYRFAPLVSKTKEGKYRVDFSNFSK

FIGURE 2 | ROMK protein structure and conservation of L207 and C308 among homologs. **(A)** Domains of the protein with reported mutations associated with type II Bartter syndrome. M1 and M2 represent two transmembrane domains. Red font indicates the mutations reported in this study. **(B)** Complete preservation of both the leucine amino acid (L207) and cysteine amino acid (C308) among homologs through Xenopus laevis.

Cys308Arg may have partial intrinsic transport, accounting for the late onset.

Gitleman syndrome is also a rare recessive salt-losing tubulopathy that results in impaired salt reabsorption, caused by mutations in the *SLC12A3* gene encoding NaCl cotransporter in distal convoluted tubules (DCT). Although variants of BS and GS are genotypically distinct, there is a considerable overlap in their clinical presentation, such as hypokalemia due to renal potassium loss, normal blood pressure, and metabolic alkalosis, as observed in this case. BS shows an earlier age of onset and heavier clinical symptoms than GS, and patients with BS often have hypercalciuria, whereas GS is often accompanied by hypomagnesemia, low urinary calcium excretion and normal urine volume. In our patient, the late onset, no growth retardation, no hypercalciuria, and hypomagnesemia indicated a diagnosis of GS, but polyuria and impaired urinary concentration function could not be explained by GS. Of course, genetic investigation is fundamental for differential diagnosis between BS and GS. The patient was finally diagnosed with BS, but no GS. In fact, hypomagnesemia is more common in GS and one of important differences between GS and BS. The mechanism of hypomagnesemia is through downregulation of apically located transient receptor potential channel subfamily M, member 6 (TRPM6), a magnesium-permeable channel predominantly expressed in the DCT (22). However, it has been reported that 20-30% of patients with BS also have hypomagnesemia, and the mechanism is unclear. The urinary calcium level is high in BS but low in GS, however, the patient has normal urinary calcium excretion in this administration, which is inconsistent with BS and cannot explain her nephrocalcinosis. However, hypercalciuria in the patient was identified by the test 13 years ago. Nephrocalcinosis is common in patients with BS, which is presumed to be due to their hypercalciuria and can be observed after some weeks of severe hypercalciuria (23). As in a previous reported case of BS, renal ultrasound on day 5 was normal, but on day 27, it showed a thin hyperechoic rim in the pyramids suggestive of nephrocalcinosis (24). The reason for the change in the urinary calcium level in this patient from high to normal is unclear. The fact that nephrocalcinosis is found in all patients with late-onset BS suggests that hypercalciuria will exist in all cases of BS type II in the early stage, although different levels of urinary calcium excretion will occur at the time of diagnosis.

Although the characteristic hypokalemic metabolic alkalosis was not found in MSK, the changes in renal imaging and common clinical manifestations such as urinary concentration dysfunction, thirst, polydipsia, and polyuria led to diagnosis of

MSK, and further hypokalemia was attributed to type I renal tubular acidosis, a common complication of MSK. MSK is a rare congenital malformation defined as the dilatation of the medullary and papillary portions of the collecting ducts due to cystic damage to the distal nephron. The disease is often sporadic and rarely presents with familial inheritance in an autosomal dominant manner (25). The diagnosis of MSK mainly depends on imaging examinations. Currently, IVP is still regarded as the gold standard for diagnosis. Metabolic alkalosis and the clinical finding of hyperreninemic hyperaldosteronism, combined with genetic analysis, ruled out MSK. However, as one of several common causes of medullary nephrocalcinosis, MSK should be a differential diagnosis of BS.

The patient had increased urinary protein levels, with the 24-h urinary protein level of 1.04 g/d. Albumin and immunoglobulin were mainly increased, and urinary a1 microglobulin was normal, suggesting glomerular proteinuria, which could not be explained by tubulopathy. A renal biopsy could not be performed because the patient had nephrocalcinosis. However, there have been reports of patients who develop focal segmental glomerulosclerosis during the course of BS due to chronic stimulation of the renin-angiotensin system with secondary chronic glomerular hyperfiltration (26). At present, prognosis in many cases of BS is good, and the kidney rarely enters the dialysis stage; however, there are few long-term follow-up cases. The interval between the two hospitalizations of this patient was 13 years, and the renal function remained stable, which also suggests that the renal prognosis was good in late-onset BS. However, it is not clear whether an increase in urinary protein levels affects the progression of renal disease.

CONCLUSION

We report a special late-onset BS type II case with a novel compound heterozygous mutation in the *KCNJ1* gene. Our study suggests a high degree of variability in aBS II regarding disease severity and emphasizes the importance of timely genetic testing for individuals with suspected diseases. Although gene monitoring has enhanced the convenience and accuracy of BS diagnosis, the disease remains easily missed or misdiagnosed. Case reports such as this study are expected to improve our understanding and diagnosis of BS. Further studies are required to verify the effects of this novel gene mutation.

ETHICS STATEMENT

The studies involving human participants were reviewed and approved by the China Medical University. The patients/participants provided their written informed consent to participate in this study. Written informed consent was obtained from the individual(s) for the publication of any potentially identifiable images or data included in this article.

AUTHOR CONTRIBUTIONS

MT contributed to data collection and manuscript writing. B-RZ supervised the data collection and finalized the manuscript. HP, Y-QW, Y-ZZ, and YW contributed to data collection. XB participated in the data collection and analysis. All authors contributed to the article and approved the submitted version.

FUNDING

This research was supported by grants from the Guide Project for Natural Science of Liaoning Province (2019-ZD-0771 to B-RZ) and Science and Technology Planning Project of Shenyang (21-173-9-71 to B-RZ).

ACKNOWLEDGMENTS

We would like to thank the patient for providing her case history. We would also like to thank AJE (www.aje.cn) for English language editing.

SUPPLEMENTARY MATERIAL

The Supplementary Material for this article can be found online at: https://www.frontiersin.org/articles/10.3389/fmed.2022.862514/full#supplementary-material

Supplementary Figure 1 | Kidney imaging findings of intravenous pyelography and ultrasound. **(A)** Intravenous pyelography shows "bouquet of flowers" appearance of the dilated tubules within the renal medulla of both kidneys. **(B)** Renal ultrasonography shows multiple irregular hyperechoic stones in the pyramids of both kidneys.

REFERENCES

1. Ji W, Foo JN, O'Roak BJ, Zhao H, Larson MG, Simon DB, et al. Rare independent mutations in renal salt handling genes contribute to blood pressure variation. *Nat Genet.* (2008) 40:592–9. doi: 10.1038/ng.118
2. Seyberth HW, Weber S, Komhoff M. Bartter's and Gitelman's syndrome. *Curr Opin Pediatr.* (2017) 29:179–86. doi: 10.1097/MOP.0000000000000447
3. Cunha TDS, Heilberg IP. Bartter syndrome: causes, diagnosis, and treatment. *Int J Nephrol Renovasc Dis.* (2018) 11:291–301. doi: 10.2147/IJNRD.S155397
4. Mrad FCC, Soares SBM, de Menezes Silva LAW, Dos Anjos Menezes PV, Simoes ESAC. Bartter's syndrome: clinical findings, genetic causes and therapeutic approach. *World J Pediatr.* (2021) 17:31–9. doi: 10.1007/s12519-020-00370-4
5. Komhoff M, Laghmani K. Pathophysiology of antenatal Bartter's syndrome. *Curr Opin Nephrol Hypertens.* (2017) 26:419–25. doi: 10.1097/MNH.0000000000000346
6. Laghmani K, Beck BB, Yang SS, Seaayfan E, Wenzel A, Reusch B, et al. Polyhydramnios, transient antenatal Bartter's syndrome, and MAGED2 mutations. *N Engl J Med.* (2016) 374:1853–63. doi: 10.1056/NEJMoa1507629
7. Li H, Durbin R. Fast and accurate long-read alignment with burrows-wheeler transform. *Bioinformatics.* (2010) 26:589–95. doi: 10.1093/bioinformatics/btp698
8. Zhang L, Zhang J, Yang J, Ying D, Lau YL, Yang W. PriVar: a toolkit for prioritizing SNVs and indels from next-generation sequencing data. *Bioinformatics.* (2013) 29:124–5. doi: 10.1093/bioinformatics/bts627

9. Yang Y, Muzny DM, Reid JG, Bainbridge MN, Willis A, Ward PA, et al. Clinical whole-exome sequencing for the diagnosis of mendelian disorders. *N Engl J Med.* (2013) 369:1502–11. doi: 10.1056/NEJMoa1306555
10. Bahcall OG. Genetic testing. ACMG guides on the interpretation of sequence variants. *Nat Rev Genet.* (2015) 16:256–7. doi: 10.1038/nrg3940
11. Pressler CA, Heinzinger J, Jeck N, Waldegger P, Pechmann U, Reinalter S, et al. Late-onset manifestation of antenatal Bartter syndrome as a result of residual function of the mutated renal Na+-K+-2Cl- co-transporter. *J Am Soc Nephrol.* (2006) 17:2136–42. doi: 10.1681/ASN.2005101071
12. Seys E, Andrini O, Keck M, Mansour-Hendili L, Courand PY, Simian C, et al. Clinical and genetic spectrum of bartter syndrome type 3. *J Am Soc Nephrol.* (2017) 28:2540–52. doi: 10.1681/ASN.2016101057
13. Verma S, Chanchlani R, Siu VM, Filler G. Transient hyponatremia of prematurity caused by mild Bartter syndrome type II: a case report. *BMC Pediatr.* (2020) 20:311. doi: 10.1186/s12887-020-02214-6
14. Sharma A, Linshaw MA. A novel compound heterozygous ROMK mutation presenting as late onset Bartter syndrome associated with nephrocalcinosis and elevated 1,25(OH)(2) vitamin D levels. *Clin Exp Nephrol.* (2011) 15:572–6. doi: 10.1007/s10157-011-0431-3
15. Huang L, Luiken GP, van Riemsdijk IC, Petrij F, Zandbergen AA, Dees A. Nephrocalcinosis as adult presentation of Bartter syndrome type II. *Neth J Med.* (2014) 72:91–3.
16. Gollasch B, Anistan YM, Canaan-Kuhl S, Gollasch M. Late-onset Bartter syndrome type II. *Clin Kidney J.* (2017) 10:594–9. doi: 10.1093/ckj/sfx033
17. Li J, Hu S, Nie Y, Wang R, Tan M, Li H, et al. A novel compound heterozygous KCNJ1 gene mutation presenting as late-onset Bartter syndrome: case report. *Medicine (Baltimore).* (2019) 98:e16738. doi: 10.1097/MD.0000000000016738
18. Yaqub S, Arif MS. A case of Bartter's syndrome presenting in adulthood. *Iran J Kidney Dis.* (2020) 14:65–7.
19. Elfert KA, Geller DS, Nelson-Williams C, Lifton RP, Al-Malki H, Nauman A. Late-onset Bartter syndrome type II due to a homozygous mutation in KCNJ1 gene: a case report and literature review. *Am J Case Rep.* (2020) 21:e924527. doi: 10.12659/AJCR.924527
20. Stenson PD, Mort M, Ball EV, Chapman M, Evans K, Azevedo L, et al. The human gene mutation database (HGMD((R))): optimizing its use in a clinical diagnostic or research setting. *Hum Genet.* (2020) 139:1197–207. doi: 10.1007/s00439-020-02199-3
21. Welling PA, Ho K. A comprehensive guide to the ROMK potassium channel: form and function in health and disease. *Am J Physiol Renal Physiol.* (2009) 297:F849–63. doi: 10.1152/ajprenal.00181.2009
22. Nijenhuis T, Vallon V, van der Kemp AW, Loffing J, Hoenderop JG, Bindels RJ. Enhanced passive Ca2+ reabsorption and reduced Mg2+ channel abundance explains thiazide-induced hypocalciuria and hypomagnesemia. *J Clin Invest.* (2005) 115:1651–8. doi: 10.1172/JCI24134
23. Garnier A, Dreux S, Vargas-Poussou R, Oury JF, Benachi A, Deschenes G, et al. Bartter syndrome prenatal diagnosis based on amniotic fluid biochemical analysis. *Pediatr Res.* (2010) 67:300–3. doi: 10.1203/PDR.0b013e3181ca038d
24. Gomez de la FC, Novoa PJ, Caviedes RN. Bartter syndrome: an infrequent tubulopathy of prenatal onset. *Rev Chil Pediatr.* (2019) 90:437–42. doi: 10.32641/rchped.v90i4.932
25. Fabris A, Anglani F, Lupo A, Gambaro G. Medullary sponge kidney: State of the art. *Nephrol Dial Transplant.* (2013) 28:1111–9. doi: 10.1093/ndt/gfs505
26. Su IH, Frank R, Gauthier BG, Valderrama E, Simon DB, Lifton RP, et al. Bartter syndrome and focal segmental glomerulosclerosis: a possible link between two diseases. *Pediatr Nephrol.* (2000) 14:970–2. doi: 10.1007/s004670050054

Conflict of Interest: XB was employed by Guangzhou KingMed Center for Clinical Laboratory Co, Ltd.

The remaining authors declare that the research was conducted in the absence of any commercial or financial relationships that could be construed as a potential conflict of interest.

frontiers | Frontiers in Medicine

REVIEW
published: 06 May 2022
doi: 10.3389/fmed.2022.905007

An Updated Review and Meta Analysis of Lipoprotein Glomerulopathy

Meng-shi Li[1,2,3,4†], *Yang Li*[1,2,3,4†], *Yang Liu*[1,2,3,4], *Xu-jie Zhou*[1,2,3,4*] *and Hong Zhang*[1,2,3,4]

[1] Renal Division, Peking University First Hospital, Beijing, China, [2] Kidney Genetics Center, Peking University Institute of Nephrology, Beijing, China, [3] Key Laboratory of Renal Disease, Ministry of Health of China, Beijing, China, [4] Key Laboratory of Chronic Kidney Disease Prevention and Treatment (Peking University), Ministry of Education, Beijing, China

More than 200 cases of lipoprotein glomerulopathy (LPG) have been reported since it was first discovered 30 years ago. Although relatively rare, LPG is clinically an important cause of nephrotic syndrome and end-stage renal disease. Mutations in the *APOE* gene are the leading cause of LPG. *APOE* mutations are an important determinant of lipid profiles and cardiovascular health in the population and can precipitate dysbetalipoproteinemia and glomerulopathy. Apolipoprotein E-related glomerular disorders include *APOE*2 homozygote glomerulopathy and LPG with heterozygous *APOE* mutations. In recent years, there has been a rapid increase in the number of LPG case reports and some progress in research into the mechanism and animal models of LPG. We consequently need to update recent epidemiological studies and the molecular mechanisms of LPG. This endeavor may help us not only to diagnose and treat LPG in a more personized manner but also to better understand the potential relationship between lipids and the kidney.

Keywords: lipoprotein glomerulopathy, apolipoprotein E, epidemiology, pathogenesis, meta-analysis, treatment

OPEN ACCESS

Edited by:
Jia Rao,
Fudan University, China

Reviewed by:
Gengru Jiang,
Shanghai Jiao Tong University, China
Jingyuan Xie,
Shanghai Jiao Tong University, China

***Correspondence:**
Xu-jie Zhou
zhouxujie@bjmu.edu.cn

†These authors have contributed equally to this work

Specialty section:
This article was submitted to Nephrology, a section of the journal Frontiers in Medicine

Received: *26 March 2022*
Accepted: *15 April 2022*
Published: *06 May 2022*

Citation:
Li M-s, Li Y, Liu Y, Zhou X-j and Zhang H (2022) An Updated Review and Meta Analysis of Lipoprotein Glomerulopathy. Front. Med. 9:905007. doi: 10.3389/fmed.2022.905007

INTRODUCTION

Since it was first described in 1989 (1), lipoprotein glomerulopathy (LPG) (OMIM: 611771) has been characterized as a rare glomerular disorder leading to nephrotic syndrome and/or kidney failure (2). LPG is characterized clinically by proteinuria and elevated concentrations of triglyceride-rich lipoproteins and their remnants, and histologically characterized by lamellated lipoprotein thrombi in glomerular capillary lumina lacking foam cells. The familial occurrence of LPG has been frequently recognized. LPG is primarily associated with heterozygous *APOE* mutations in the low-density lipoprotein–receptor binding site or around it (3). As a "Mendelian disease" caused by a "single gene" with dominant inherited disease of incomplete penetrance, it also provides a disease model to explore pathogenic roles of *APOE* in some common diseases, such as Alzheimer's disease, type III hyperlipoproteinemia (HLP), and coronary artery disease (2). Trending evidence suggests that *APOE* gene mutations play an important role by potentially increasing the affinity of lipoproteins for the glomerular capillary wall or by enhancing the tendency of mutant apolipoproteins to form aggregates when concentrated. If left untreated, the disease usually progresses to end-stage kidney disease. Lipid-lowering medications, especially fibrates, were found to improve both clinical manifestations and histological alterations. In recent years, there has been a rapid increase in the number of LPG cases reported, and some progress in research into the mechanism and animal models of LPG. We consequently

need to update recent epidemiological studies and the molecular mechanisms of LPG. Using "lipoprotein glomerulopathy" or "lipoprotein nephropathy" as key words, we retrieved data from the PubMed, Wanfang (China National Knowledge Infrastructure) and J-STAGE (online platform for Japanese academic journals) databases for literature review (**Figure 1**). The purpose of this review is to update the epidemiology and clinical features of lipoprotein glomerulopathy, discuss its pathogenesis, summarize current therapeutic options, and present personal perspectives for future research.

HISTORY OF LPG

At the 1988 annual meeting of the Japanese Society of Nephrology, Saito et al. first reported the cases of 2 patients who had similar clinical features of renal impairment and glomerular capillary lipoprotein deposition (4) (**Figure 2**). In 1989, he described the case in the English literature for the first time. The absence of involvement of other organs and the characteristic morphology of the renal lesions could clearly distinguish this disease from other disorders of lipid metabolism. With the presence of lipoproteins in the glomerular deposits and abnormalities in serum lipid levels resembling the pattern observed in type III hyperlipoproteinemia (HLP), this disorder was named "lipoprotein glomerulopathy." Type III HLP is a condition characterized by the elevation of both cholesterol and triglycerides, accumulation of incompletely catabolized triglyceride-rich lipoproteins, plamar xanthoma, and rapidly progressive atherosclerosis (5). Type III HLP has always been found in individuals who are homozygous for apoE mutations (apoE2/2) and rare in heterozygous state. In 1991, Oikawa et al. reported abnormally elevated levels of apoE in patients with LPG (6). In the report, the levels of lipoprotein components, plasma apolipoprotein profiles, and apoE isoforms were checked in 6 patients. Common features included proteinuria (1.6–10 g/d), normal lecithin-cholesterol acyltransferase (LCAT) activity, type III HLP-like lipoprotein profiles, and significantly higher levels of plasma apoE (>10 mg/dL) compared with the control patients with hyperlipidemic nephrotic syndrome without lipoprotein thrombi, or type IIb hyperlipoproteinemia without renal disease. All the patients had rare apoE isoform patterns (E2/3 in five cases and E4/4 in one case). These findings showed the first evidence that apoE hyperlipoproteinemia was associated with the apoE isoform and lipoprotein metabolic derangement. Familial occurrence of LPG was later recognized, as introduced in the below epidemiology section (7, 8). It was suggested that LPG may be an inherited disease in which abnormal lipoproteins composed of *APOE* mutants accumulate within the glomeruli. This finding was supported by observations of mutations named *APOE* Sendai (Arg145Cys) in 1997 and *APOE* Kyoto (Arg25Cys) in 1998. A total of 17 *APOE* variants associated with LPG have been identified to date, highlighting DNA analysis of the *APOE* gene as one of the most important tools for identifying LPG. These 17 mutations were retrieved from published case reports by manually literature searches, among which 13 have been included in the HGMD database (including *APOE* Kyoto, Tokyo-Maebashi, Sendai, Guangzhou, Okayama, Modena, Las Vegas, Osaka or Kurashiki, Hong Kong, Chicago, Tsukuba, E1, and Kanto, **Additional File 1**).

Although it was initially assumed that this disease was restricted to East Asia, several cases have been reported in individuals of European ancestry. With the increased awareness of this disease, several patients with nephrotic syndrome of previously "unrecognized" cause have been grouped into LPG in recent years. The total number of reported LPG cases increased to over 200 hundred (details below).

EPIDEMIOLOGY

The total number of patients was estimated to be <80 in 2011 (9). Due to increased awareness and the advance of genetic testing technology, the number of cases increased to ∼150 by June 2019 (10). By an updated literature review, we estimated that the reported number would be at least 274 up to the beginning of the year 2022.

LPG showed significant regional and familial aggregation. The majority of cases were reported in Japan and China (**Figures 3**, **4**). It is mainly distributed in southwestern and southeastern China and in central and north-central Japan (11). Some hot spots of gene mutations have been described, suggesting a founder effect of the gene mutation. *APOE* Sendai (Arg145Pro) was mainly observed in north-central Japan, particularly in Yamagata and Miyagi (12), whereas it has not been reported in China. *APOE* Kyoto (Arg25Cys) was reported as the most frequent mutation in LPG throughout the world, including in southwestern China, Japan, France and the USA. However, a report in 2014 showed that 35 patients within 31 unrelated Han families with biopsy-proven LPG resided in a small county of Sichuan Basin in southwest China, indicating regional clustering with the same genetic background. It was thus suggested that the descendants of *APOE* Kyoto in this area were derived from a single founder. In contrast, *APOE* Guangzhou and Tokyo-Maebashi were reported to be dominant in cases from the southeast area of China (7, 8, 11, 13). The association of *APOE* Kyoto between the Sichuan Basin and other areas is still difficult to explain. It may be possible that *APOE* Kyoto spread from China across multiple countries worldwide because it is historically known that the international population mobility of Chinese was more frequent than that of Japanese in ancient times (11). This theory may be similar to the idea that LPG cases may have emigrated along with tea culture to expand from China (11). Several other *APOE* variants have recently been reported in Western countries,

Abbreviations: LPG, Lipoprotein glomerulopathy; LCAT, Lecithin-cholesterol acyltransferase; LDLR, Low-density lipoprotein receptor; HSPG, Heparan sulfate proteoglycan; HLP, Hyperlipoproteinemia; LRP, LDL receptor-associated protein; GVHD, Graft-versus-host disease; FcRγ, Fc receptor gamma chain; CML, carboxymethyllysine; HNE, hydroxynonenal; MDA, Malondialdehyde; aHUS, Atypical hemolytic uremic syndrome; PPAR, Peroxisomal proliferator-activated receptor; LPL, Lipoprotein lipase; HMG-CoA, β-hydroxy-β-methylglutaryl-CoA; RAASi, Renin-angiotensin-aldosterone system inhibitor; HELP, Heparin-induced extracorporeal lipoprotein precipitation; MN, membranous nephropathy; IDL, Intermediate density lipoprotein; VLDL, Very low-density lipoprotein; HDL, High-density lipoprotein; TC, Total cholesterol; TG, Total triglyceride.

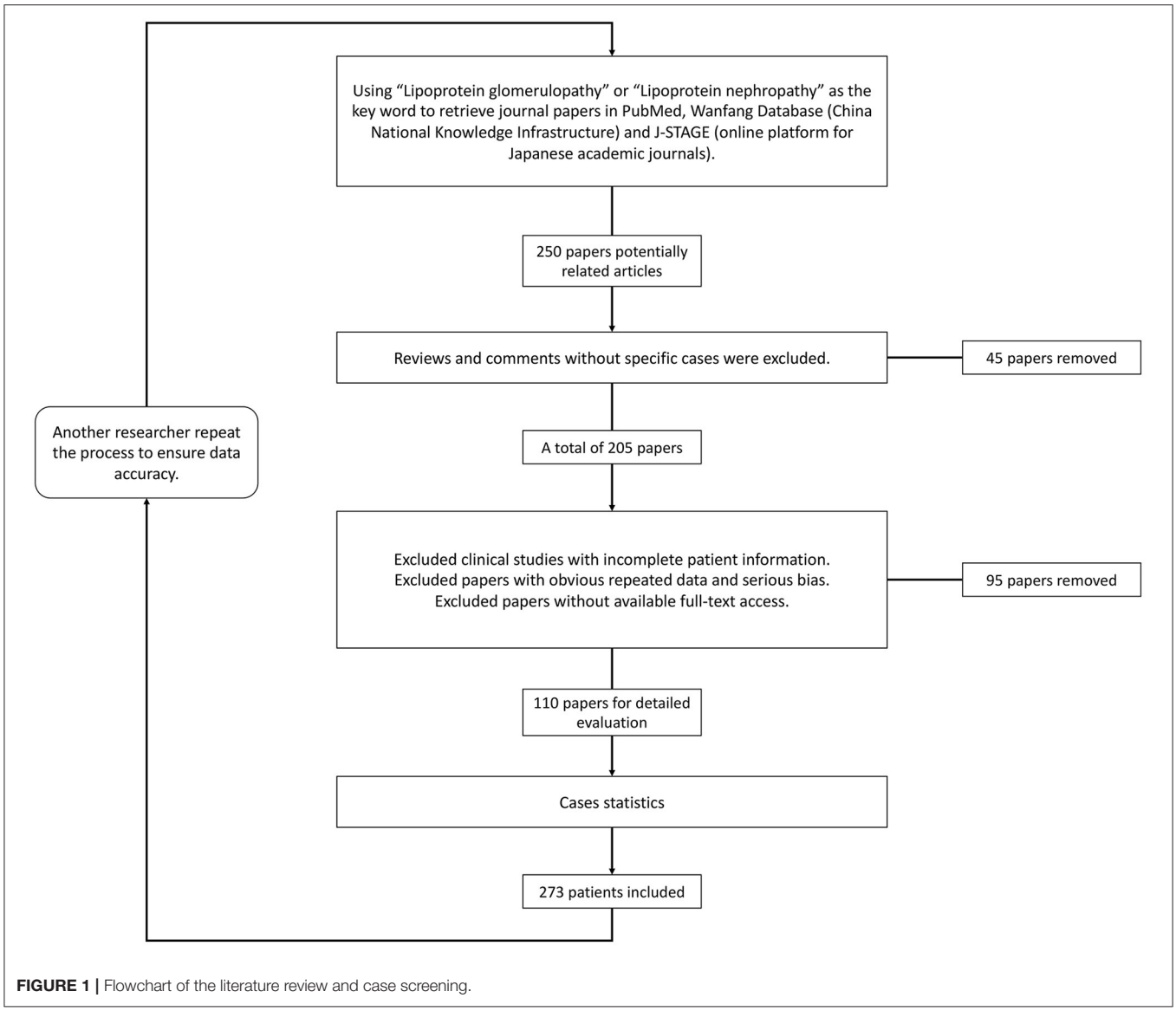

FIGURE 1 | Flowchart of the literature review and case screening.

including the United States, Russia, Italy, Brazil, and France. Other *APOE* variants associated with LPG have been detected across the world (14–20). Although many of the reported cases were reported to be sporadic, some studies reported familial clustering, supporting its genetic component with a single gene inheritance mode (21–23). But perhaps most of the family members lack of symptomatic signs or genetic testing, making them undiagnosed. No heritability studies have been documented to date. One of the largest pedigree was reported in 2008, in which 5 cases in 3 generations were observed (8). Another large pedigree with 3 cases in 2 generations was reported in 2014, together with additional 17 pedigrees with LPG (7).

Apart from humans, interestingly, an observational study in 2016 reported that a captive squirrel (Sciurus vulgaris) spontaneously developed LPG-like disease. This was the first time that LPG-like disease was observed in an organism other than humans. The kidney pathology of squirrels is similar to that of human LPG, but genetic mutations have not been determined (24).

As the majority of the reports on the epidemiology of LPG were based on case reports, to systemically update this information, we conducted a literature review using the search item "lipoprotein glomerulopathy" from various databases (PubMed, China National Knowledge Infrastructure, and J-STAGE) from 1988 to January 2022. A total of 274 LPG cases were identified, and the epidemiological details can be found in **Additional File 1**.

According to updated statistics, China and Japan have a comparatively higher prevalence of LPG, with 207 and 47 patients, respectively. There is still lack of precise epidemiological studies in LPG. Based on the current meta data from literature review, it was estimated that the prevalence of LPG is about 3.74 per 10 million in Japan and 1.43 per 10 million in China. Surely, it may be underestimated. As mentioned above, the areas most

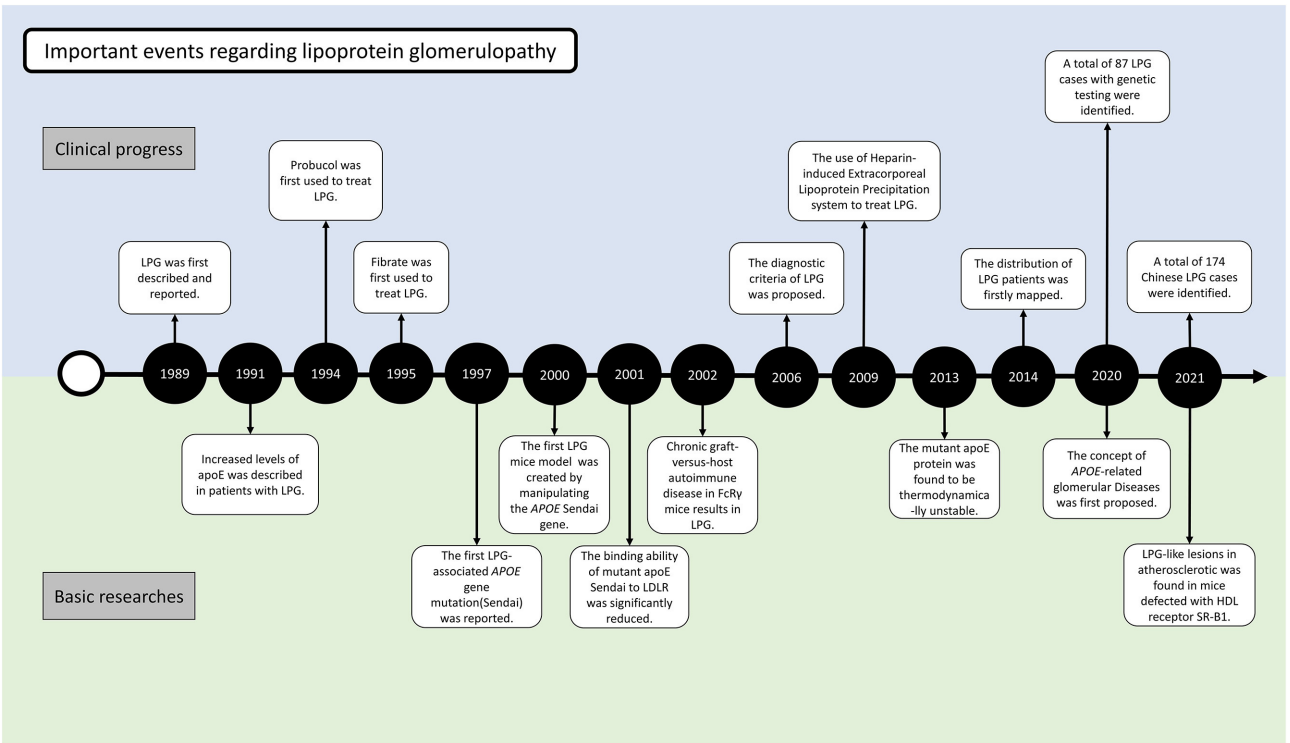

FIGURE 2 | Milestone of LPG research in clinical and basic aspects.

affected by LPG were located in southwestern and southeastern China and central and northeastern Japan. A total of 20 cases have been reported in other countries and territories. Among all the cases, there were 137 males and 137 females, with an average age of diagnosis of 35 years old (from 7 to 72 years). In terms of age of onset, a total of 188 patients had documented information. There were 8, 23, 112, 42 and 3 cases with age of onset $\leq$10, 11–17, 18–45, 46–65, and >65. It suggested that about 60% of the cases were diagnosed in young adults (18–45 years old) (13).

With regard to specific mutation distribution, *APOE* Kyoto, *APOE* Tokyo-Maebashi and *APOE* Sendai are the three major observed forms, with 53, 13, and 14 reported patients, respectively. In China, the Sendai mutant has not yet been reported. The Kyoto mutant is mainly diagnosed in Sichuan Province in southwest China, while the Tokyo-Maebashi variant is mainly diagnosed in Beijing, suggesting that LPG patients in the same region may share a common genetic ancestor; demonstrating the "founder effect."

PATHOGENESIS

The precise pathogenesis of LPG is still not well-understood. Several lines of evidence suggest that alterations in apoE structure and function play a fundamental role in the pathogenesis of LPG. It has long been hypothesized that defective lipoproteins are prone to deposit in the kidney. Indeed, all the patients reported to date were found to have heterozygous mutations in the *APOE* gene, along with elevated serum concentrations of apoE lipoproteins and the presence of apoE in the glomerular deposits. Disturbances in kidney structure or function may also be pivotal in the formation of lipoprotein aggregates, as the disease is kidney specific without other organs obviously affected. However, the recurrence of LPG after renal transplantation suggests that renal abnormalities may not be necessary for the development of the disease.

APOE Gene and apoE Function

The *APOE* gene is located on chromosome 19q13.2 and comprises 4 exons with 3,603 base pairs, which are evolutionarily conserved in a variety of terrestrial and marine vertebrates (25) (**Figure 5**). The apoE protein is a 34 kDa circulating glycoprotein of 299 amino acids, with an additional 18 amino acids as a signal peptide. This protein can be synthesized by several cell types, in which hepatocytes account for the majority. High quantities can also be observed in brain, i.e., by astrocytes and glial cells in the cerebral cortex and by neurons in the frontal cortex and hippocampus (26).

The amino acid sequence of apoE can be simply divided into three parts: the N-terminal (AA 1–199), the hinge region (AA 200–215), and the C-terminal (AA 216–299). There are two important binding regions in the N-terminal sequence that have overlapping gene sequences, the low density lipoprotein receptor (LDLR) binding region (27, 28) (142–150) (29) and the heparin sulfate glycoprotein (144–147) binding region (30). Most *APOE* mutations associated with LPG are observed in these two regions. Other regions with functional significance included four helix

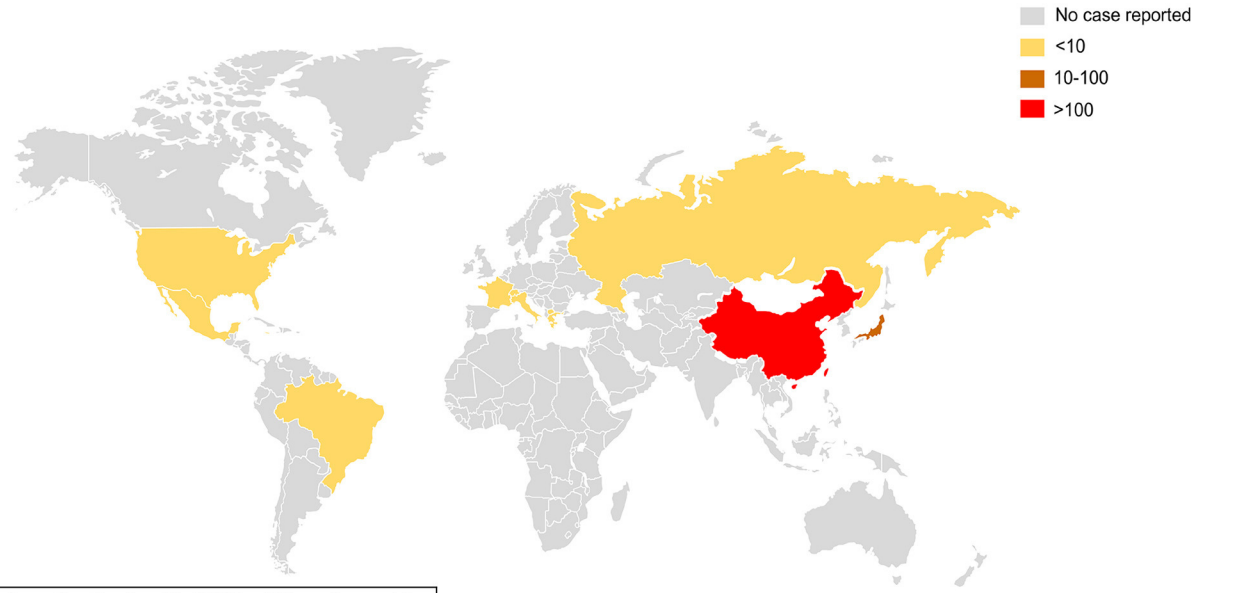

Number of patients with LPG in different countries	
China	207
Japan	47
America	4
Italy	4
Brazil	3
Macedonia	2
France	2
Jamaica	1
Mexico	1
Russia	1
Switzerland	1
Greece	1

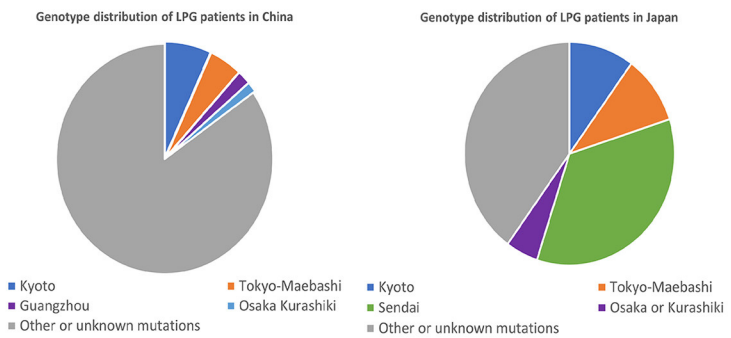

FIGURE 3 | Worldwide distribution of LPG cases. China and Japan are the two countries with the most reported cases of LPG, but the spectra of *APOE* mutation in patients in these two countries are different. In China, *APOE* Kyoto is the major mutant, while in Japan, *APOE* Sendai is the most commonly one. The *APOE* Sendai mutation has not been reported in China thus far.

regions (AA 20–160), a lipid insertion sequence (244–272) and a homo-oligomerization region (248–299) (31–34), which have been investigated less.

As the ligand for the LDL receptor family and heparan sulfate proteoglycans (HSPG), apoE associates with triglyceride-rich lipoproteins in mediating clearance of their remnants (**Figure 6**). When exogenous lipids enter the bloodstream from intestinal villi, new chylomicrons are formed to obtain apoC and apoE from high-density lipoprotein (HDL). Some chylomicrons are utilized by body tissues, while the remaining chylomicrons enter the liver through interactions with apoE and LDL receptor-associated proteins (LRP).

ApoE is also important in endogenous lipid metabolism. Hepatocytes secrete VLDL containing apoE, and these VLDL are converted into IDL. The subsequent metabolism of IDL can be divided into two pathways, through interactions between apoE and LRP or metabolism into LDL (35–37). The degradation of both IDL and VLDL is partially dependent on apoE. This may explain why their concentrations are elevated in the blood of patients with LPG.

APOE Mutations in LPG

Two coding variants in the human *APOE* gene, rs429358 (Cys130Arg) and rs7412 (Arg176Cys), define the apoE protein as three isoforms (E2, E3, and E4) (38), among which E3 is the most common isoform, and they are different in the amino acid residues at residues 112 and 158: both cysteine—apoE2, both arginine—apoE4, and one cysteine—apoE3 (the wild type). It has been confirmed that different subtypes are associated with different predispositions to human diseases (39). The affinity between the E2 subtype and the low-density lipoprotein receptor (LDLR) is only 1% of that of the E3 subtype, resulting in lipid clearance disturbances and type III HLP. The E4 subtype is mainly associated with diseases of the central nervous system, such as Alzheimer's disease (34, 40–42). However, in LPG, the most common subtype was reported to be E3/E3 or E3/E4 (3, 9).

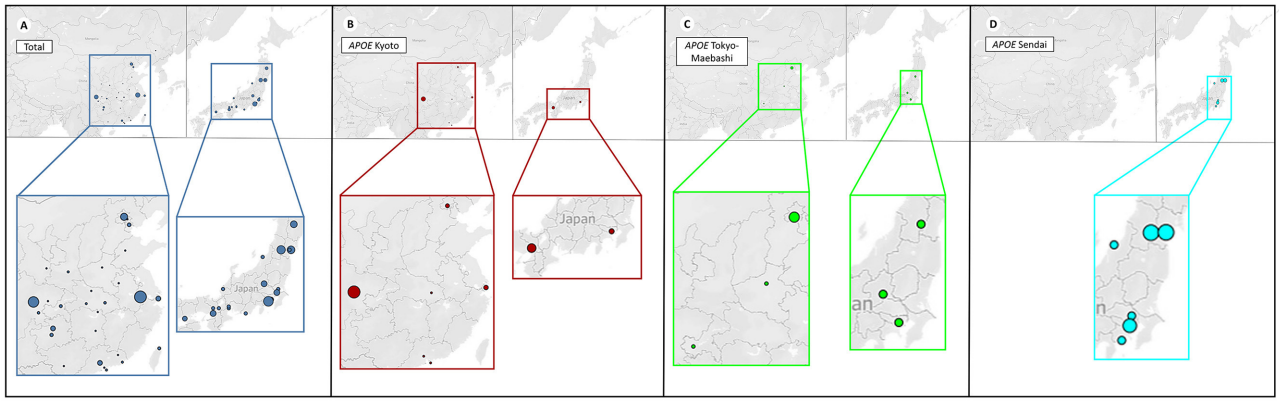

FIGURE 4 | Distribution of patients with different *APOE* mutations. The four plots represent the distribution of patients with different *APOE* mutations in China (left) and Japan (right). For better illustration, each image is shown at the bottom enlarged. The size of each circle represents the number count of people. It can be observed that geographical clustering of LPG cases according to *APOE* mutation types, suggesting a founder effect. **(A)** Patients with LPG were mainly concentrated in the southwestern and southeastern regions in China, and the central and northeastern regions in Japan. **(B)** *APOE* Kyoto was frequently found in southwestern China, and south Japan. **(C)** *APOE* Tokyo-Maebashi was dominant in cases from Beijing in China, and the central Japan. **(D)** *APOE* Sendai was not reported in China, and distributed most in central Japan.

In 1991, abnormally elevated levels of apoE were observed in patients with LPG for the first time (6), followed by the discovery of the mutation *APOE* Sendai in 1997. Further *APOE* mutation has been suggested to be the most important etiologic factor in the pathogenesis of LPG (43, 44). Supporting evidence was obtained from animal models. In 2000, by introducing the *APOE* Sendai mutation into *APOE*-deficient mice, it was observed that both increased lipid levels and LPG-like renal pathology in the mice (45). Several other variants of *APOE* associated with LPG have been identified since then. A similar cause-effect of the *APOE* Kyoto mutation in LPG can also be observed in *APOE*-deficient mice, further supporting that a single gene mutation can cause LPG (46).

To date, a total of 17 *APOE* gene variants associated with LPG have been reported. Eight of these mutations reside in the LDLR binding region (140–150 sites), among which 5 reside in the HSPG binding region (144–147 sites). Another hot spot is located in the region spanning AA 150–180, where 5 mutations have been reported (25, 33), but few functional studies have been conducted. More recently, a case report suggesting a 28-year-old man presenting with severe proteinuria and hyperlipidemia had compound heterogeneous mutations of the *APOE* gene inherited from his mother (p.Arg50His) and father (*APOE* Kyoto). Each his parents with a heterogeneous mutation had normal kidney function without proteinuria (47). This is the first time that the combination of the 2 mutations was identified in the same case as an autosomal recessive genetic disorder. It seemed that the case showed much severe phenotype. But further precise investigation on both genetic and disease mechanisms will be needed. Since the patient carried *APOE* Kyoto mutation, and the new p.Arg50His variant has not been verified functionally pathogenic, therefore, this mutation is not listed in our pathogenic mutations of LPG. We assume that a dominant effect of *APOE* Kyoto cannot be totally rule out. Apart from this, a case was reported to have a combination of *APOE* Kyoto and *APOE* Hong Kong (Asp230Tyr) mutations (48). But as co-segregation analysis was not taken, it was difficult to confirm the significance of the respective mutation. There was also a case report of a 51-year-old Japanese woman who had 2 mutations within the same allele (a combination of *APOE* Chicago (Arg147Pro) and *APOE*5 (Glu3Lys) inherited from her mother. But her mother did not have any phenotypes (49). These data suggested LPG may be far complicated than previously speculated. Additional genetic studies may be needed, i.e., from a hypothesis-free whole genome sequencing in large cohorts.

ApoE Mutation-Related Factors Leading to LPG

Reduced Structural Stability of apoE Protein

Normal apoE protein is highly helical and has the capability to be transformed between different tertiary structures to bind lipids or proteins. In 2013, it was found that different mutated proteins [*APOE* Chicago (Arg147Pro), *APOE* Sendai (Arg145Pro), *APOE* Osaka or Kurashiki (Arg158Pro)] showed different protein structural stabilities (50). Of note, the common resultant characteristic of these three mutations was that arginine was replaced by a proline residue. It is universally suggested that proline residues may breakdown a transmembrane helix. Insertion of a proline residue in the middle of an α-helix is known to destabilize it by over 3 kcal/mol, effectively disrupting the helix (51, 52). These mutated apoE proteins all exhibited reduced helicity, leading to decreased structural stability evidenced as protein denaturation even at the physiological temperature of 37°C. When the hydrophobic surface is exposed, apoE may be more prone to aggregate and form large lipoprotein granules (50). Along with this idea, it was also confirmed that similar structural and functional changes can be observed in three other non-proline-substituted mutants [*APOE* Kyoto (Arg25Cys), *APOE* Tsukuba (Arg114Cys), and *APOE* Las Vegas (Ala152Asp)] (53). *In vitro*, all three mutated proteins showed decreased

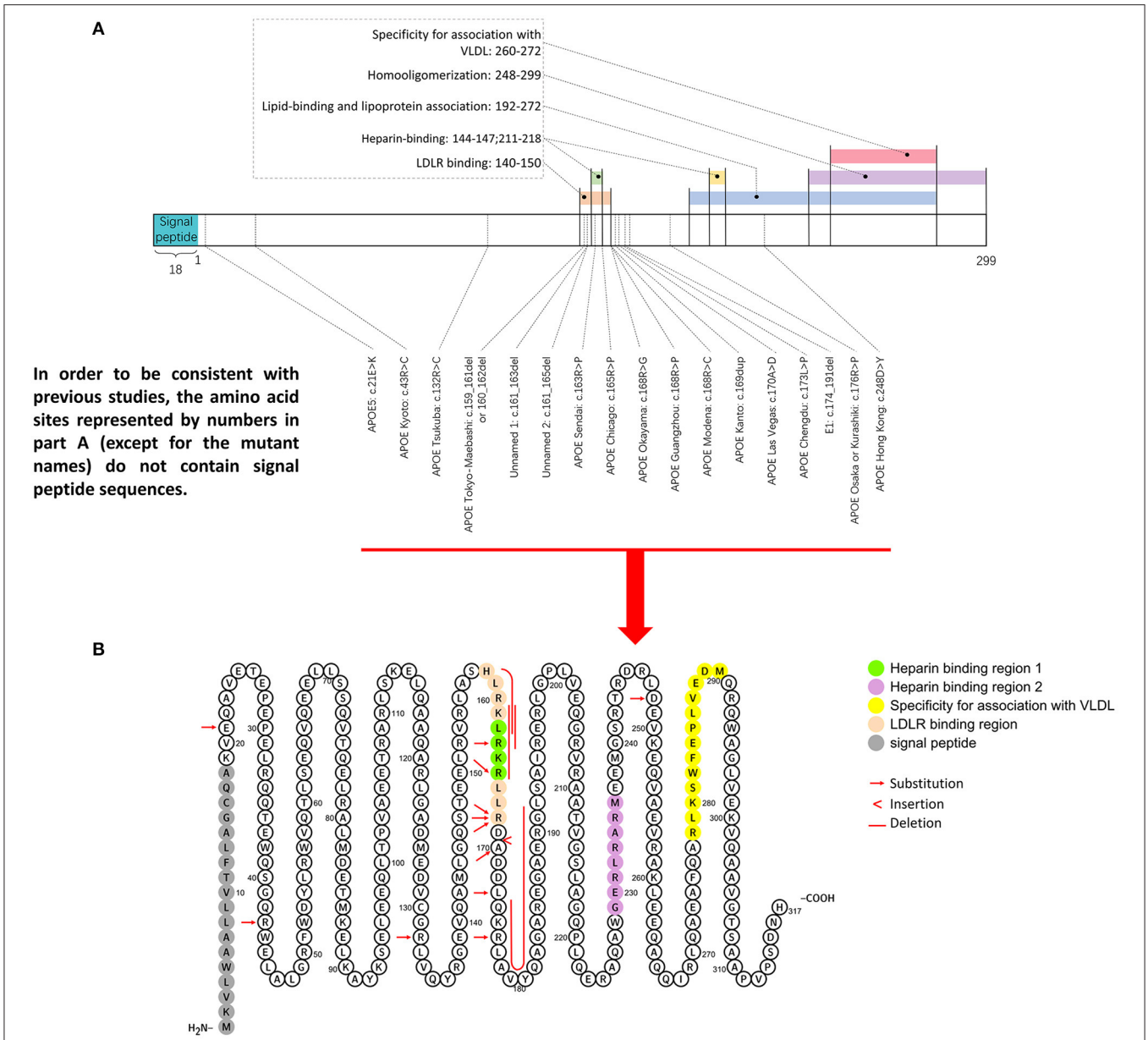

FIGURE 5 | Representative mutation distributions of the apoE protein. **(A)** Seventeen mutations of the *APOE* gene leading to LPG have been located, most of which are concentrated at amino acid sites 140–180. This region contains various important apoE functional domains, including the LDLR binding domain and HSPG binding domain. "Hot spot" mutations suggested that the change in the binding ability of the apoE mutant to LDLR and HSPG is an important factor in LPG pathogenesis. **(B)** *ApoE* mutation sites were labeled in the amino acid sequence diagram of apoE protein. It showed that hot spot of apoE mutation is among AA 140–160.

stability and an increased tendency to aggregate. Likewise, a study in Alzheimer's disease showed that the decreased structural stability of apoE may contribute to the formation of neurotoxic fibrils (54).

Reduced apoE Binding Capacity to Different Receptors

ApoE mutations may also contribute to reduced binding capacities to receptors (55, 56). It was observed that the binding ability of apoE Kyoto and apoE Sendai to LDLR was significantly reduced to just 10 and <5%, respectively, compared to the wild type (57, 58). The decrease in the apoE binding ability contributes to impaired degradation of lipoprotein and accumulation. This is consistent with the observation that hyperlipidemia is common in LPG, especially with increased VLDL and IDL. However, the binding capacity of apoE2 to LDLR was <1% of the normal value (33, 59), while apoE2-induced type III HLP only had dyslipidemia without pathological kidney changes, indicating that impaired LDLR binding abilities may not be the determining factor in kidney damage. Although the *APOE* Sendai mutation

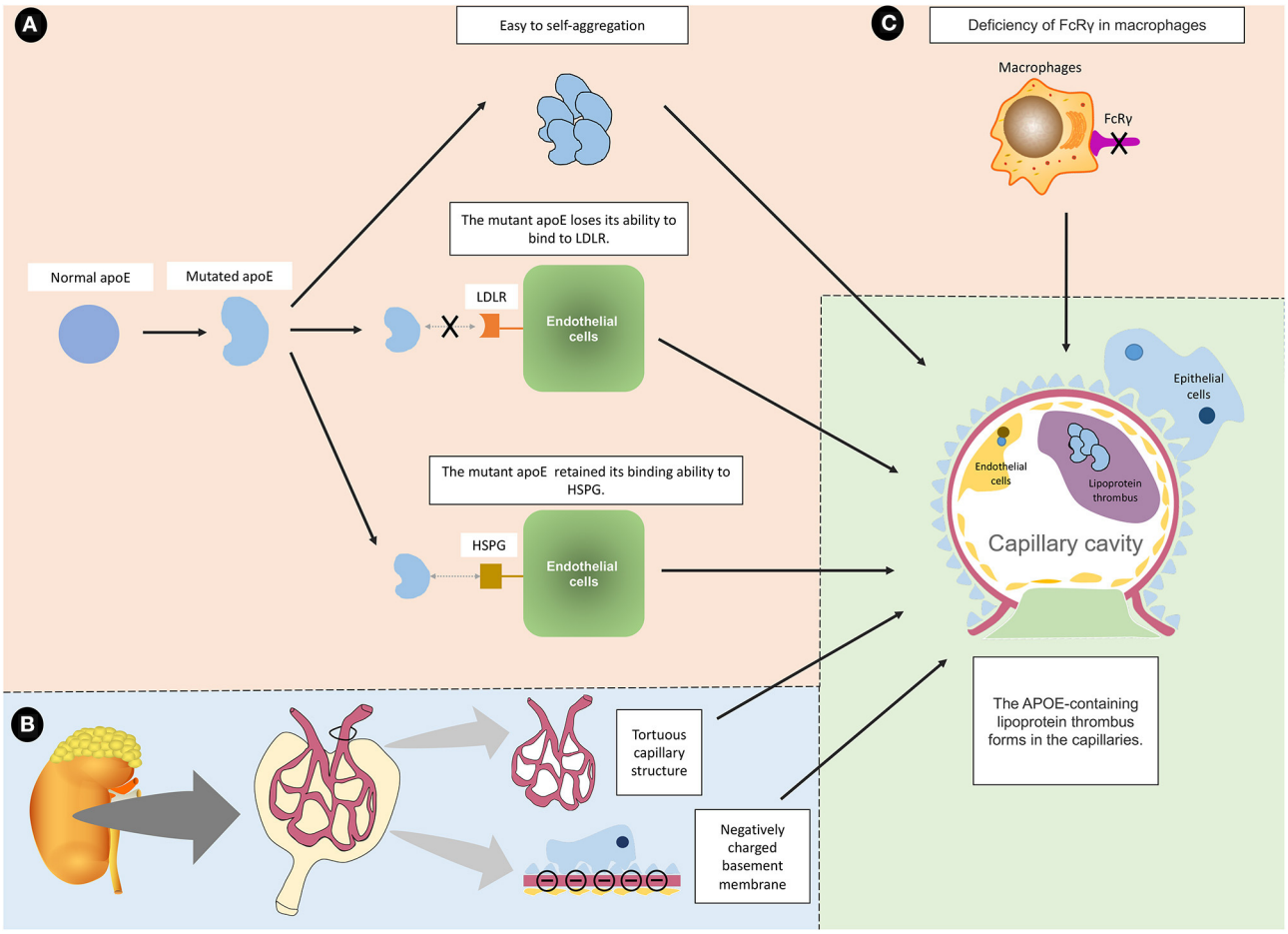

FIGURE 6 | Summary and proposed mechanisms of LPG. **(A)** The mutated apoE protein is known to cause LPG through three main mechanisms. (a) The mutant protein tends to aggregate, and the aggregated macromolecules are more likely to drive the formation of lipoprotein thrombi. (b) The mutant protein loses its ability to bind to LDLR, making it difficult to eliminate. (c) The mutated protein retains the ability to bind to HSPG, which allows it to bind to endothelial cells. For the above reasons, the mutated apoE protein aggregates into macromolecules on the surface of endothelial cells without being cleared. **(B)** In addition to APOE mutation, it is speculated that intrinsic glomerular features may interact with apoE variants and lipoprotein abnormalities, which exacerbate the induction of LPG. For example, tortuous glomerular capillaries are conducive to the formation of thrombi. The negatively charged base membrane and the positively charged mutant protein may attract each other. **(C)** FcRγ deficiency may also lead to LPG because it affects the phagocytic function of macrophages.

decreased the binding ability of apoE with LDLR to <5%, it decreased its binding ability with HSPG to 66% (57). It was suggested that the retained HSPG binding activity could enable apoE-rich lipoproteins to enter and attach to the Disse space (60, 61), which is pivotal in the initial rapid clearance step for lipoproteins. Heparan sulfate proteoglycans (HSPGs), which are also abundant in the space of Disse, may play an important role in mediating this enhanced binding. When apoE arrived and aggregated in the Disse space, they would normally enter the liver through interaction with LDLR, but the mutated apoE lost the LDLR binding ability, so they could not enter the liver to be metabolized (62, 63). Since HSPG is highly expressed in the glomerular basement membrane (64, 65), it may play a role in the renal deposition of lipoprotein. Concordant with this hypothesis, evidence has shown that the binding ability of products is enhanced in apoE Chicago to glomerular capillaries and in apoE Kyoto to human umbilical vein endothelial cells (16, 66).

Other Predisposing or Synergic Factors Leading to LPG

Functional Deficiency of the Fc Gamma Receptor (FcγR) and Macrophages

As some individuals carrying *APOE* mutations are asymptomatic, it is speculated that some other factors may further contribute to LPG (21). Two clinical reports noted the recurrence of LPG in the transplanted kidney. Sustained inflammation induced by chronic graft-vs. host disease (GVHD) might be a predisposing factor (19, 67, 68). By injecting donor spleen cells into recipient mice for 2–4 months, it was observed that GVHD could induce LPG-like changes in Fc receptor gamma chain (FcRγ)-deficient mice,

with hematuria, proteinuria, renal capillary lumen thrombosis and interstitial mononuclear cell infiltration. It was shown that macrophages from FcRγ-deficient mice had a decreased ability to clear LDL (69). Macrophages possess several different pathways in recognition and clearance of modified (oxidized) LDL, including scavenger receptors and FcRs (70, 71). Supporting this, a drastic decline of scavenger receptor CD36 was observed in LPG. It was speculated that partial reduction of modified (oxidized) LDL uptake by macrophages could result in the lipoprotein deposition in the kidney during the long course of chronic GVHD.

More direct evidence was obtained from humanized mice. When the *APOE*3 genotype or *APOE* Sendai mutation was introduced into FcRγ and *APOE* double-knockout mice, both strains of mice developed lipoprotein thrombosis, and the mice with *APOE*3 showed more lipoprotein thrombus in the kidney than those with the *APOE* Sendai genotype. This observation was absent in mice with wild-type *APOE*. Introduction of *APOE*3 in both FcRγ-deficient mice and FcRγ wild-type mice showed lipoprotein thrombosis, whereas the phenotype was much more severe in FcRγ-deficient mice (72). These results indicated macrophage impairments derived from FcRγ deficiency (73–75) were insufficient for the development of LPG, since the FcRγ deficient mice with normal murine apoE showed no lipoprotein thrombosis. However, under conditions with xenogeneic apoE, especially human apoE3, the FcRγ deficient mice may develop severe LPG.

It was also observed that a small amount of apoE can be produced by macrophages, which was considered to play a role in suppressing hyperlipidemia and arteriosclerosis. Because it was showed that expression of macrophages producing apoE Sendai in mice that received a bone marrow transplant protected against atherosclerosis while induced LPG (76–78). It was thus suggested that macrophages may play various roles in apoE related lipoprotein metabolism. Both hyperactivity or suppression can be an important factor in different types of renal lipidosis. LPG depend upon suppression of macrophages. ApoE derived from macrophages is affected by its mutation and may regulate disease activity. Functional studies are still needed in the future.

Renal Intrinsic Factors May Promote Glomerular Lipoprotein Deposition

The above data is insufficient to explain why lipoprotein is specifically deposited in glomerular capillaries in LPG, which is different from other diseases such as atherosclerosis. In particular, because lesions are localized to glomeruli, intrinsic glomerular factors may interact with apoE variants and lipoprotein abnormalities to induce LPG. There might be some special factors in the glomeruli. Mutated apoE protein may present different electric charges compared to normal proteins, and therefore, they exhibit a higher affinity for negatively charged glomerular basement membranes (9). It is suggested that the presence of highly conserved acidic residues within the lipoprotein receptor (LR) modules and the positively charged region of apoE (residues 136–150) may support the hypothesis that ligand–receptor recognition is due to electrostatic interactions, so a change in electron charge might enhance the bonding (79). The tortuous structure of glomerular capillaries might also contribute to lipoprotein deposition.

Oxidative Stress May Dampen Kidney Damage

It has long been believed that hyperlipidemia may play a detrimental role in kidney pathology directly or indirectly through inflammation, ROS production, endogenous electrical stress and other pathways (80, 81). Among these pathways, oxidative stress may be of special importance, as carboxymethyllysine (CML), hydroxynonenal (HNE)-protein, and malondialdehyde (MDA)-lysine were reported to be found in the kidney of a patient with LPG (68). These substances are the products of lipid peroxidation. These aldehydes may cross-link covalently with matrix tissue proteins and further alter structure and function. They may also have direct impact on parenchymal cells by cross-linking cell surface proteins to reduce intracellular responses (82–84). As the antioxidant domain of *APOE* overlaps with the LDLR binding region (85), mutations in the LDLR binding domain may shed unfavorable effects on its antioxidant capacity. Moreover, the roles of oxidative stress and hyperlipidemia in LPG are indirectly supported by clinical evidence that some patients experience remission after treatment with the antioxidant probucol and the lipid-lowering drug fenofibrate (10, 86).

Other Mechanisms

There have been reports that no *APOE* mutations were found in a number of LPG patients (87). Possible explanations include changes in other unknown genes, mutations in introns or regulatory sequences, epigenetics, and environmental influences.

For example, a recent study showed that a defect in HDL receptor named scavenger receptor class B type 1 (SR-B1) was associated with LPG-like lesions in atherosclerotic mice, the severity of which can be alleviated using probucol (88).

Factors affecting CKD progression, such as fibrosis, apoptosis, local tissue injury, and infiltration of immune cells, may also be involved in LPG.

These data support a complex etiology of LPG, and additional pathogenic factors warrant further elucidation.

CLINICAL AND PATHOLOGICAL MANIFESTATIONS

Diagnostic Criteria Proposed by Japanese Nephrologists

In 2006, a single set of diagnostic criteria for LPG was proposed by Japanese nephrologists (2). The criteria were mainly based on four items.

- different levels of proteinuria;
- dilatation of glomerular capillary lumina with pale-stained substances on light microscopy;
- fingerprint-like concentric lamellar structure in electron microscopy;
- Type III HLPs with high apoE concentrations are usually associated with a heterozygous apoE phenotype, E2/3 or E2/4,

by means of isoelectric focusing electrophoresis (IEF), but sometimes with an uncommon type, e.g., E1/3 or others.

It was suggested that although genetic testing was not necessary for definitive diagnosis, it should be performed in patients with suspected LPG whenever possible to confirm the diagnosis.

Clinical Manifestation of Glomerular Disease Is Always Non-specific

Initially, LPG may cause no symptoms. Symptoms and signs are due to the buildup of waste products and fluid retention in the body (49, 89, 90). In general, nephrotic syndrome may be present in ∼70% of patients (91). However, the levels of proteinuria may vary significantly among different patients. The 24 h urinary protein levels reported ranged from 0.5 to 24 g/24 h (92, 93). Without proper treatment, CKD will progress (2, 14, 94–96), and approximately half of patients will develop end-stage kidney disease over 1–27 years.

Elevated Serum ApoE and Hyperlipidemia

One of the most characteristic laboratory indicators of LPG is elevated serum apoE levels. It was reported that patients with LPG had a mean serum apoE concentration of 11.14–17.1 mg/dL (3.9–71.0 mg/dL), approximately twice the upper level of the normal population (2, 7, 23, 97, 98).

Another characteristic is overt dyslipidemia, with a predominance of triglycerides, mostly >6 mmol/L (15, 16, 91). In a few cases, VLDL levels were reported to be elevated (∼4–6 mmol/L) (99, 100). Hyperlipidemia in LPG is similar to that in familial type III HLP. Type III HLP, first recognized in 1967, is caused by homozygous apoE2 mutations. The mutation was reported to weaken the binding force between apoE2 and LDL receptors (101, 102). Although both diseases are associated with the *APOE* gene, LPG and type III HLP show obvious differences. In type III HLP, atherosclerotic cardiovascular disease and xanthomatosis are common (103, 104), but they are rare in LPG.

Great Phenotypic Heterogeneity and Genotype-Phenotype Correlations

We further checked the clinical manifestations of LPG by systematic literature review. An additional file shows this in more detail (see **Additional File 2**). The mean value of plasma albumin for the reported cases was 29.3 g/L (SD = 6.2 g/L, ranging from 12 to 47 g/L), and the mean 24-h urinary protein level was 4.5 g/d (SD = 3.4 g/d, ranging from 0.8 to 24 g/d). Nephrotic range proteinuria and nephrotic syndrome were key features. The mean creatinine was 129.2 μmol/L (SD = 177.5 μmol/L, and ranging from 21.2 to 1859 μmol/L), the mean urea nitrogen was 8.1 mmol/L (SD = 5.52 mmol/L, and ranging from 2.7 to 39.9 mmol/L), and the mean eGFR was 81.6 ml/min/1.73 m^2 (SD = 32.5 ml/min/1.73 m^2). Of these patients, 38.7% had CKD1, 35.5% had CKD2, 18.7% had CKD3, 3.2% had CKD4, and 3.9% had CKD5. In terms of blood lipids, the average triglyceride level of these patients was 3.4 mmol/L (SD = 2.0 mmol/L, ranging from 0.7 to 20.6 mmol/L) (reference range 0.6–1.7 mmol/L), which is approximately twice the normal upper limit. Total cholesterol was 6.8 mmol/L (SD = 2.4 mmol/L, and ranging from 2.8 to 22.9 mmol/L) (reference range 2.8–5.2 mmol/L), LDL was 3.6 mmol/L (SD = 1.4 mmol/L, and ranging from 1.2 to 10.6 mmol/L) (reference range 2.1–3.1 mmol/L), and HDL was 1.4 mmol/L (SD = 0.7 mmol/L, ranging from 0.5 to 8.8 mmol/L) (reference range 0.9–1.6 mmol/L). Most of the patients had significantly elevated serum apoE, with a mean of 12.1 mg/dL (SD = 6.7 mg/dL, and ranging from 3.1 to 42.3 mg/dL). Great fluctuations of standard deviations suggested great clinical heterogeneity of LPG.

We collated the clinical information of the cases with the top four *APOE* genotypes (Kyoto, Tokyo-Maebashi, Sendai and Osaka or Kurashiki) (**Table 1**). The age of onset for patients with *APOE* Tokyo-Maebashi seemed to be younger than that of other mutants. Patients with *APOE* Sendai appeared to have the lowest urinary protein and blood lipid levels. Patients with *APOE* Kyoto had the most severe renal manifestations. There was few clinical prognostic information available for LPG. However, according to literature review and case reports, some of the cases with LPG will progress to ESKD. These reported ESKD caused by LPG can be observed in several *APOE* genotypes including Kyoto, Tokyo-Maebashi, Osaka or Kurashiki, Guangzhou, and Sendai. And the reported *APOE* phenotypes were E2/3 and E3/3 (7, 8, 105–107). Thus, it still difficult to predict prognosis based on mutation types.

Extrarenal Manifestations and Other Complications

Other complications rarely have been reported. Known comorbidities included splenomegaly, thalassemia, psoriasis, abdominal aortic aneurysm, pleural effusion, and neurofibromatosis type I (14, 67, 99, 108, 109). However, there is no evidence of a direct link between LPG and these diseases. The only related extrarenal manifestation of LPG that has been confirmed is intravascular coagulation (110). It was reported that a 50-year-old white man had severe proteinuria with high lipid levels and a kidney pathology of LPG. He also had hypertension and coronary heart disease. The patient's heart failure was speculated to be due to cardiac amyloidosis secondary to multiple myeloma. For this reason, cardiac biopsies were requested and showed that small blood vessels in the endocardia were filled with eosinophilic substances, which were similar to those in the kidney. A more recent case reported that a 21-year-old Malaysian-Swiss male with LPG developed atypical hemolytic uremic syndrome (aHUS). Aggregation of apoE was suggested by the authors as a risk factor in initiating the occurrence of aHUS in his case (107). Regardless, the etiology was unclear and may be difficult to determine.

Pathological Manifestations in the Kidney

The most typical pathological appearance of LPG under light microscopy is the dilatation of the glomerular capillary lumen filled with eosinophilic granular and vacuolar thrombosis (**Figure 7**). The thrombus is positive for oil red O or Sudan red and negative for silver or PAS staining, indicating the presence of a lipid component in the thrombus (14, 22, 110–112). Using immune-electron microscopy, it has been found that lipids are surrounded by apoE and that the thromboid material is composed of lipoproteins (113). Other manifestations under light

TABLE 1 | Genotype and phenotype information based on meta data.

	APOE Kyoto	*APOE* Tokyo-Maebashi	*APOE* Sendai	*APOE* Osaka or Kurashiki	*P*-value
Total number of cases	53	15	13	6	
Age	38.1 (34.5–38.1) ($n = 53$)	20.0 (10–41) ($n = 15$)	31.7 ± 18.9 ($n = 13$)	32.0 ± 8.7 ($n = 6$)	0.142
Albumin (g/L)	26.4 (26.4–26.4) ($n = 48$)	31.5 ± 9.1 ($n = 16$)	NA	27.1 ± 9.4 ($n = 5$)	0.024
Serum creatinine (μmol/L)	98.1 (98.1–98.1) ($n = 46$)	72.0 (43.5–90.5) ($n = 13$)	79.6 (37.1–256.4) ($n = 5$)	NA	0.000
eGFR	79.0 (79.0–79.0) ($n = 46$)	82.0 (59.7–156.5) ($n = 15$)	91.9 ± 27.0 ($n = 12$)	105.7 ± 27.1 ($n = 5$)	0.303
TC (mmol/L)	7.0 (7.0–7.0) ($n = 53$)	6.0 (4.9–7.1) ($n = 14$)	5.8 ± 1.6 ($n = 13$)	5.3 ± 2.8 ($n = 6$)	0.012
TG (mmol/L)	3.5 (3.5–3.5) ($n = 53$)	2.8 ± 1.7 ($n = 14$)	1.7 (1.5–3.8) ($n = 13$)	2.6 ± 1.0 ($n = 6$)	0.031
24 h UPRO (g)	5.1 (3.8–8.8) ($n = 16$)	2.8 ± 1.6 ($n = 10$)	1.6 (1.0–2.2) ($n = 11$)	7.4 ± 4.7 ($n = 5$)	0.006

Data are presented as mean ± SD for normalized data or median (25^{th}-75^{th} percentile) for non-normally distributed data.
Due to missing information for some case reports, n in the bracket represents the amount of data.
NA means data unavailable.

microscopy include swelling of endothelial cells and vacuolar degeneration with a small number of lipid droplets in podocytes. In the advanced stages of the disease, the mesangial cells and stroma are thickened, and there may be uneven insertion, leading to thickening of the basement membrane and the formation of the dual-track sign and eventually glomerular sclerosis. Epithelial vacuoles and granular degeneration may be observed in renal tubules in the early stages. Similar to other glomerulopathies, as the disease progresses, renal tubule atrophy, interstitial edema, monocyte infiltration and fibrosis, and thickening of the arteriole wall will be common (21, 114). A study also reported that CD68+ foam cells were present in patients' kidneys, further suggesting that macrophages may be involved in the pathogenesis of LPG.

The most common deposits are apoE and apoB in immunofluorescence, which might be taken as supporting evidence for the diagnosis of LPG. In the previous literature, however, immunoglobulin and complement, such as IgM, IgA, and C3 depositions, may be observed in mesangial and capillary walls in many cases, and scattered C1q deposits were also reported (16, 23, 48, 114, 115). However, most of these depositions were suggested to be non-specific, and no specific pathology pattern has been described until now.

Under electron microscopy, lipoprotein thrombosis is characterized by a fingerprint-like concentric lamellar structure, sometimes referred to as a sand stone structure (2). Some other pathological descriptions include glomerular telangiectasis, filled with protein material covered with lipid vacuoles, and lamellar vacuoles of varying sizes, with a network of vacuoles separated by high electron density bands. Lysosomes of endothelial cells and podocytes were increased, and lipid vacuoles were also found in the cytoplasm and lysosomes. Podocytes showed diffuse and complete foot process effacement with the accumulation of electron-dense material in the mesangium and glomerular basement membrane. The glomerular basement membrane demonstrated focal subcutaneous electron dense deposition (100, 110–112, 114, 116).

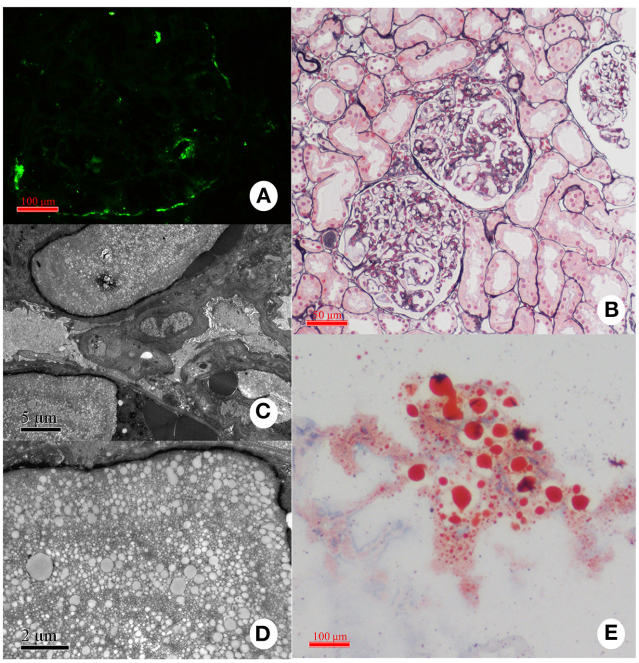

FIGURE 7 | Representative pathological findings in a case with LPG. **(A)** Immunofluorescence study: the deposition of apoE is present mainly in the capillary lumina. **(B)** Light microscopy: Dilated capillary loops exhibiting an eosinophilic lipoprotein thrombus in the capillary lumens. **(C,D)** Electron microscopy: Diffuse foot-process effacement and lamellated fingerprint-like thrombi in capillary lumens, which are composed of granules and vacuoles of various sizes. **(E)** Oil red O staining: Numerous red droplets are seen in the thrombus-like substances in the glomerular capillaries.

Because the main pathological feature of LPG is lipoprotein thrombosis, it should be differentiated from other diseases with thrombotic substances, such as macroglobulinemia nephropathy and cryoglobulinemia nephropathy.

TREATMENT

There is still a lack of specific or targeted therapies for LPG. Most of the regimens available were based on lowering proteinuria and hyperlipidemia. In the absence of clinical trials, current data are mostly from case reports or observational studies.

No Beneficial Effects From Immunosuppressants or Transplantation

Early in the history of LPG, the patient was often treated with glucocorticoids with or without immunosuppressants, similar to other nephrotic syndromes. However, it was soon proven ineffective (43, 95, 108, 117, 118). Additionally, in the twentieth century, it was reported that LPG relapsed in nearly all ESKD patients caused by LPG even with intensive immunosuppressive therapy. Therefore, kidney transplantation and immunosuppressants were not recommended because the culprit was abnormal lipoprotein components in the blood instead of the kidney. However, in some case reports, leflunomide was reported to ameliorate proteinuria in some patients. It was initially used to replace prednisone, which was found to have a complete disappearance of kidney symptoms after leflunomide was added (119). The exact mechanism of leflunomide may not be related to its immunosuppressive effect.

Regimens Targeting Lipoprotein and Hyperlipidemia

Regimens have achieved some success in supporting the pathologically causal role of lipoprotein and hyperlipidemia in LPG. The first drug was probucol, which reduces total TC and LDL levels and is widely used in the treatment of hypercholesterolemia (120). Probucol is also an antioxidant, and it may mitigate glomerular damage caused by oxidative stress of mutated proteins. As early as 1994, it was used in an LPG female case of 54 years old, effectively reducing hyperlipidemia, proteinuria and the complete elimination of her glomerular lipoprotein thrombosis (86). Later, different case reports confirmed the efficacy of probucol therapy (116, 121).

Fenofibrate and benzafibrate can significantly reduce blood VLDL levels by acting on peroxisomal proliferator-activated receptor (PPAR) and activating lipoprotein lipase (LPL) and thus reducing TG and LDL. A small clinical contrast study based on 35 patients supported the efficacy of fibrates in LPG. After 12 months of treatment, their lipid profiles, proteinuria, and serum albumin improved, and their serum apoE decreased significantly with stable renal function (7, 14, 93, 121, 122).

Niceritrol is a nicotinic acid derivative that has been used to lower lipoprotein levels and reduce proteinuria in patients with chronic kidney disease associated with hyperlipidemia (123, 124). It was used to relieve clinical symptoms in two patients with LPG who had failed to respond to statins (125). However, there was still a lack of more widespread attempts.

The other drugs that are still in clinical use today are statins. As a potent inhibitor of 'β-hydroxy β-methylglutaryl-CoA' ('HMG-CoA') reductase, statins can increase the expression of the LDL receptor in the hepatocytes' cell membranes. In addition, statins also have multiple effects, such as reducing TG, improving endothelial function, and anti-oxidation (126). Statins can reduce patients' blood lipid levels but can also effectively lower urinary protein levels and retain renal function. There were very few cases in which statin therapy alone was evaluated (16, 90, 94, 108, 111, 119, 125, 127).

Renin-angiotensin-aldosterone system inhibitor (RAASi) therapy shows reno-protective effects in various forms of proteinuric CKD. Therefore, although there is no evidence that ACEIs and ARBs are effective in LPG, their administration can be considered suitable both for blood pressure control and to reduce proteinuria among LPG patients. Some case reports have suggested that antilipidemic drugs combined with ACEIs and ARBs are an effective treatment for LPG (128). Recently, SGLT2 inhibitors proved to be beneficial for patients who have proteinuric CKD with or without diabetes. With evidence that SGLT2 inhibitors might be safe and useful in hereditary renal diseases such as Alport syndrome (129), whether SGLT2 inhibitors could be a potential treatment for LPG remains to be further investigated.

Plasma Adsorption Therapy

Adsorption therapy also showed a certain effect. LDL apheresis was used when the patient had a poor response to traditional drug therapy. However, allergic reactions to LDL-apheresis are a concern (90). In 2009, a heparin-induced extracorporeal lipoprotein precipitation (HELP) system was first used to treat a 60-year-old white woman with proteinuria, high blood pressure, and renal failure (90). The basic principle of this system is to acidify plasma pH to ∼5 *in vitro* and then use heparin to form a polymer with LDL-cholesterol, LP (a), fibrinogen, and triglyceride to precipitate them out (130, 131). After 25 courses of treatment, the patient achieved significant clinical improvements, including decreased urinary protein, blood creatinine and lipid levels.

Protein A, immunosorbent may also be a treatment option. Since protein A has a strong affinity for the FcγR of IgG, this effect can compensate for the lack of an FcRγ. This technique has previously been shown to reduce proteinuria levels in patients with a variety of nephropathies, including diabetic nephropathy, IgA nephropathy, and amyloidosis (132). In a small pilot study involving 13 cases, immunoadsorption was administered for 10 cycles per session and 10 sessions as a course. A total of 30 L of plasma was regenerated in each course. Apart from proteinuria reduction, a repeated renal biopsy ($n = 12$) showed that intraglomerular lipoprotein thrombi almost disappeared. The proteinuria of six patients returned to baseline levels within 12 months. Four recurrent patients received repeat immunoadsorption treatment and showed repeated efficacy (97). The strategy is advantageous in being rapidly therapeutic and

having relatively stable effects. However, disadvantages include invasive procedure complications, high cost and risk of infection.

Other Possible Treatments

Other lipid-lowering drugs, such as niacin (133) and apoC-III monoclonal antibodies, as well as non-pharmaceutical approaches, such as lipoprotein apheresis, may also be promising (134, 135). Other antioxidants, apart from probucol, including vitamin C, polyphenols, N-acetylcysteine, allopurinol, natural polysaccharides, pentoxifyllin, and bardoxolone methyl, may be candidates to study antioxidant efficacy, since antioxidant therapy apparently reduces CKD progression (136, 137). However, high interindividual variability and off-target effects, such as body weight reduction, need to be further investigated. The anticonvulsant topiramate, which induces weight loss and a moderate reduction in plasma lipids and glucose, has recently been reported to protect *APOE*-deficient mice from kidney damage. Thus, it could be investigated in drug repurposing studies for the treatment of glomerular lipidosis (138).

Gene-based therapeutics, pioneered for the treatment of monogenic inherited retinal disease, are being actively investigated as new treatments for acquired retinal disease. Gene therapy could also be tried in the future, i.e., by CRISPR/Cas9 technology, since it is widely believed that LPG is an inherited disease caused by an abnormality in the *APOE* gene (2, 9).

CONCLUSIONS

Current studies have found that several mutations of the *APOE* gene can lead to LPG, and most of these mutations are concentrated in some hot spots. Future functional research on LPG focusing on hot spot regions for gene mutations may be helpful to explore the specific pathogenesis of the disease and to develop target drugs. It is worth exploring whether different genotypes lead to differences in clinical phenotypes after increasing the number of patients who are enrolled and who can be stratified.

Although the symptoms of LPG are common and fixed, some cases still cannot be explained by the current theory. For example, in 2015, a patient presented with a large number of macrophage infiltrates in the glomerulus. In most cases, macrophage infiltration is not present in the glomerular capillaries of patients with LPG (91). In 2018, a new variant of the *APOE* gene (*APOE* Toyonaka) was discovered. Patients with this gene mutation presented with kidney pathology that resembled membranous nephropathy (MN) rather than LPG (139, 140). For cases such as this, it is still not clear if they belong to a new disease category or a different spectrum of LPG (27, 28, 141). *APOE*-related disorders were recently summarized, mainly including *APOE*2 homozygote glomerulopathy (HLP), MN-like *APOE* disease, and LPG (141). All the cases above indicate that the incidence and manifestations of LPG cannot be fully explained by existing theories. In addition to the new theory of FcRγ pathogenesis, other causes of LPG may be discovered in the future.

The current clinical diagnosis and treatment of LPG still needs to be improved. As the clinical manifestations of LPG are often non-specific, the actual incidence of LPG is underestimated. The diagnosis is beyond the scope of primary care hospitals, and conventional nephropathy treatment has proven ineffective, so the sensitivity of the diagnosis needs to be increased so that more patients can be treated properly. In terms of treatment, effective drugs are not commonly used in practice, and therapy has not been commonly used, so new drug research and development are needed. For those who have been diagnosed, indicators for clinical surveillance are still lacking. As a rare disease, an international registry may be worthwhile, as registries are essential for epidemiological data and collaborative research.

AUTHOR CONTRIBUTIONS

M-sL: collected data, conceived, and wrote the manuscript. YLi: collected data and wrote the manuscript. YLiu: collected data. X-jZ: revised the manuscript critically for important intellectual content and supervised the research group and has given the final approval of the version to be published. HZ: edited the manuscript and has given the final approval of the version to be published. All authors contributed to the article and approved the submitted version.

FUNDING

Support was provided by National Science Foundation of China (82022010, 82131430172, 81970613, 82070733, 82000680, and 82070731); Academy of Medical Sciences—Newton Advanced Fellowship (NAFR13_1033); Beijing Natural Science Foundation (Z190023); Fok Ying Tung Education Foundation (171030); and CAMS Innovation Fund for Medical Sciences (2019-I2M-5-046). The funders had no role in study design, data collection and analysis, decision to publish, or preparation of the manuscript.

ACKNOWLEDGMENTS

We apologize to those whose work or original publication could not be cited because of space limitations.

SUPPLEMENTARY MATERIAL

The Supplementary Material for this article can be found online at: https://www.frontiersin.org/articles/10.3389/fmed.2022.905007/full#supplementary-material

REFERENCES

1. Watanabe Y, Yoshida F, Matsuo S, Mitarai T, Hirose S, Saito T, et al. [Lipoprotein glomerulopathy:–a new kind of glomerular disease with peculiar histological findings]. *Nihon Rinsho.* (1989) 47:1667–74.
2. Saito T, Matsunaga A, Oikawa S. Impact of lipoprotein glomerulopathy on the relationship between lipids and renal diseases. *Am J Kidney Dis.* (2006) 47:199–211. doi: 10.1053/j.ajkd.2005.10.017
3. Saito T, Matsunaga A, Ito K, Nakashima H. Topics in lipoprotein glomerulopathy: an overview. *Clin Exp*

Nephrol. (2014) 18:214–7. doi: 10.1007/s10157-013-0887-4
4. Saito T, Sato H, Kudo K, Oikawa S, Shibata T, Hara Y, et al. Lipoprotein glomerulopathy: glomerular lipoprotein thrombi in a patient with hyperlipoproteinemia. *Am J Kidney Dis.* (1989) 13:148–53. doi: 10.1016/S0272-6386(89)80134-9
5. Eto M, Saito M. [Familial type III hyperlipoproteinemia]. *Nihon Rinsho.* (2013) 71:1590–4.
6. Oikawa S, Suzuki N, Sakuma E, Saito T, Namai K, Kotake H, et al. Abnormal lipoprotein and apolipoprotein pattern in lipoprotein glomerulopathy. *Am J Kidney Dis.* (1991) 18:553–8. doi: 10.1016/S0272-6386(12)80649-4
7. Hu Z, Huang S, Wu Y, Liu Y, Liu X, Su D, et al. Hereditary features, treatment, and prognosis of the lipoprotein glomerulopathy in patients with the APOE Kyoto mutation. *Kidney Int.* (2014) 85:416–24. doi: 10.1038/ki.2013.335
8. Luo B, Huang F, Liu Q, Li X, Chen W, Zhou S-F, et al. Identification of apolipoprotein E Guangzhou (arginine 150 proline), a new variant associated with lipoprotein glomerulopathy. *Am J Nephrol.* (2008) 28:347–53. doi: 10.1159/000111828
9. Tsimihodimos V, Elisaf M. Lipoprotein glomerulopathy. *Curr Opin Lipidol.* (2011) 22:262–9. doi: 10.1097/MOL.0b013e328345ebb0
10. Majeed NK, McLaughlin J, Gonzalez M. Lipoprotein glomerulopathy in a hispanic female: a case report and literature review. *Can J Kidney Health Dis.* (2019) 6:2054358119859576. doi: 10.1177/2054358119859576
11. Saito T, Matsunaga A. Lipoprotein glomerulopathy may provide a key to unlock the puzzles of renal lipidosis. *Kidney Int.* (2014) 85:243–5. doi: 10.1038/ki.2013.404
12. Toyota K, Hashimoto T, Ogino D, Matsunaga A, Ito M, Masakane I, et al. A founder haplotype of APOE-Sendai mutation associated with lipoprotein glomerulopathy. *J Hum Genet.* (2013) 58:254–8. doi: 10.1038/jhg.2013.8
13. Song Y, Yang C, Liu L, Wang H. Case report: a pediatric case of lipoprotein glomerulopathy in china and literature review. *Front Pediatr.* (2021) 9:684814. doi: 10.3389/fped.2021.684814
14. Ku M, Tao C, Zhou A-A, Cheng Y, Wan Q-J. A novel apolipoprotein E mutation (p.Arg150Cys) in a Chinese patient with lipoprotein glomerulopathy. *Chin Med J.* (2019) 132:237–9. doi: 10.1097/CM9.0000000000000050
15. Pêgas KL, Rohde R, Garcia CD, Bittencourt V de B, Keitel E, Poloni JAT, et al. Lipoprotein glomerulopathy: a case report of a rare disease in a Brazilian child. *J Bras Nefrol.* (2014) 36:93–5. doi: 10.5935/0101-2800.20140015
16. Sam R, Wu H, Yue L, Mazzone T, Schwartz MM, Arruda JAL, et al. Lipoprotein glomerulopathy: a new apolipoprotein E mutation with enhanced glomerular binding. *Am J Kidney Dis.* (2006) 47:539–48. doi: 10.1053/j.ajkd.2005.12.031
17. Sipovskii VG, Klemina IK, Zverkov R V, Dobronravov VA, Smirnov A V. [A case of diagnosing lipoprotein glomerulopathy in Russia]. *Arkh Patol.* (2016) 78:52–7. doi: 10.17116/patol201678652-57
18. Pasquariello A, Pasquariello G, Innocenti M, Minnei F, Funel N, Lorusso P, et al. Lipoprotein glomerulopathy: first report of 2 not consanguineous Italian men from the same town. *J Nephrol.* (2011) 24:381–5. doi: 10.5301/JN.2011.7772
19. Meyrier A, Dairou F, Callard P, Mougenot B. Lipoprotein glomerulopathy: first case in a white European. *Nephrol Dial Transplant.* (1995) 10:546–9. doi: 10.1093/ndt/10.4.546
20. Marinaki S, Kalaitzakis E, Kolovou K, Gakiopoulou H, Stylianou K, Papasotiriou M, et al. A case of lipoprotein glomerulopathy in a Greek Caucasian male. *Int Urol Nephrol.* (2022) 54:969–70. doi: 10.1007/s11255-021-02930-7
21. Yang M, Weng Q, Pan X, Hussain HMJ, Yu S, Xu J, et al. Clinical and genetic analysis of lipoprotein glomerulopathy patients caused by APOE mutations. *Mol Genet Genomic Med.* (2020) 8:e1281. doi: 10.1002/mgg3.1281
22. Xie W, Xie Y, Lin Z, Xu X, Zhang Y. A novel apolipoprotein E mutation caused by a five amino acid deletion in a Chinese family with lipoprotein glomerulopathy: a case report. *Diagn Pathol.* (2019) 14:41. doi: 10.1186/s13000-019-0820-6
23. Zhang B, Liu ZH, Zeng CH, Zheng JM, Chen HP, Li LS. Clinicopathological and genetic characteristics in Chinese patients with lipoprotein glomerulopathy. *J Nephrol.* (2008) 21:110–17.
24. Kobayashi R, Chambers JK, Yoshida K, Nakamura T, Yasuno K, Uchida K, et al. Spontaneous lipoprotein glomerulopathy-like nephropathy in a squirrel (*Sciurus vulgaris*). *J zoo Wildl Med.* (2016) 47:663–6. doi: 10.1638/2015-0245.1
25. Huebbe P, Rimbach G. Evolution of human apolipoprotein E (APOE) isoforms: gene structure, protein function and interaction with dietary factors. *Ageing Res Rev.* (2017) 37:146–61. doi: 10.1016/j.arr.2017.06.002
26. Xu PT, Gilbert JR, Qiu HL, Ervin J, Rothrock-Christian TR, Hulette C, et al. Specific regional transcription of apolipoprotein E in human brain neurons. *Am J Pathol.* (1999) 154:601–11. doi: 10.1016/S0002-9440(10)65305-9
27. Fukunaga M, Nagahama K, Aoki M, Shimizu A, Hara S, Matsunaga A, et al. Membranous nephropathy-like apolipoprotein E deposition disease with apolipoprotein E toyonaka (Ser197Cys) and a homozygous apolipoprotein E2/2. *Case Rep Nephrol Dial.* (2018) 8:45–55. doi: 10.1159/000487919
28. Sasaki M, Yasuno T, Ito K, Matsunaga A, Hisano S, Abe Y, et al. Focal segmental glomerulosclerosis with heterozygous apolipoprotein E5 (Glu3Lys). *CEN Case Rep.* (2018) 7:225–8. doi: 10.1007/s13730-018-0331-4
29. Guttman M, Prieto JH, Croy JE, Komives EA. Decoding of lipoprotein-receptor interactions: properties of ligand binding modules governing interactions with apolipoprotein E. *Biochemistry.* (2010) 49:1207–16. doi: 10.1021/bi9017208
30. Cardin AD, Hirose N, Blankenship DT, Jackson RL, Harmony JA, Sparrow DA, et al. Binding of a high reactive heparin to human apolipoprotein E: identification of two heparin-binding domains. *Biochem Biophys Res Commun.* (1986) 134:783–9. doi: 10.1016/S0006-291X(86)80489-2
31. Tudorache IF, Trusca VG, Gafencu AV. Apolipoprotein E - a multifunctional protein with implications in various pathologies as a result of its structural features. *Comput Struct Biotechnol J.* (2017) 15:359–65. doi: 10.1016/j.csbj.2017.05.003
32. Huang Y, Mahley RW. Apolipoprotein E: structure and function in lipid metabolism, neurobiology, and Alzheimer's diseases. *Neurobiol Dis.* (2014) 72 (Pt. A):3–12. doi: 10.1016/j.nbd.2014.08.025
33. Hatters DM, Peters-Libeu CA, Weisgraber KH. Apolipoprotein E structure: insights into function. *Trends Biochem Sci.* (2006) 31:445–54. doi: 10.1016/j.tibs.2006.06.008
34. Phillips MC. Apolipoprotein E isoforms and lipoprotein metabolism. *IUBMB Life.* (2014) 66:616–23. doi: 10.1002/iub.1314
35. Illingworth DR. Lipoprotein metabolism. *Am J Kidney Dis.* (1993) 22:90–7. doi: 10.1016/S0272-6386(12)70173-7
36. Mahley RW, Innerarity TL, Rall SCJ, Weisgraber KH. Plasma lipoproteins: apolipoprotein structure and function. *J Lipid Res.* (1984) 25:1277–94. doi: 10.1016/S0022-2275(20)34443-6
37. Zanoni P, Velagapudi S, Yalcinkaya M, Rohrer L, von Eckardstein A. Endocytosis of lipoproteins. *Atherosclerosis.* (2018) 275:273–95. doi: 10.1016/j.atherosclerosis.2018.06.881
38. Palmer Allred ND, Raffield LM, Hardy JC, Hsu F-C, Divers J, Xu J, et al. APOE genotypes associate with cognitive performance but not cerebral structure: diabetes heart study mind. *Diabetes Care.* (2016) 39:2225–31. doi: 10.2337/dc16-0843
39. Jia L, Xu H, Chen S, Wang X, Yang J, Gong M, et al. The APOE ε4 exerts differential effects on familial and other subtypes of Alzheimer's disease. *Alzheimers Dement.* (2020) 16:1613–23. doi: 10.1002/alz.12153
40. Yin Y, Wang Z. ApoE and neurodegenerative diseases in aging. *Adv Exp Med Biol.* (2018) 1086:77–92. doi: 10.1007/978-981-13-1117-8_5
41. Muñoz SS, Garner B, Ooi L. Understanding the role of ApoE fragments in Alzheimer's disease. *Neurochem Res.* (2019) 44:1297–305. doi: 10.1007/s11064-018-2629-1
42. Marais AD. Apolipoprotein E in lipoprotein metabolism, health and cardiovascular disease. *Pathology.* (2019) 51:165–76. doi: 10.1016/j.pathol.2018.11.002
43. Oikawa S, Matsunaga A, Saito T, Sato H, Seki T, Hoshi K, et al. Apolipoprotein E Sendai (arginine 145–>proline): a new variant associated with lipoprotein glomerulopathy. *J Am Soc Nephrol.* (1997) 8:820–3. doi: 10.1681/ASN.V85820
44. Karet FE, Lifton RP. Lipoprotein glomerulopathy: a new role for apolipoprotein E? *J Am Soc Nephrol.* (1997) 8:840–2. doi: 10.1681/ASN.V85840

45. Ishigaki Y, Oikawa S, Suzuki T, Usui S, Magoori K, Kim DH, et al. Virus-mediated transduction of apolipoprotein E (ApoE)-sendai develops lipoprotein glomerulopathy in ApoE-deficient mice. *J Biol Chem.* (2000) 275:31269–73. doi: 10.1074/jbc.M005906200
46. Wu H, Yang J, Liu Y-Q, Lei S, Yang M, Yang Z, et al. Lipoprotein glomerulopathy induced by ApoE Kyoto mutation in ApoE-deficient mice. *J Transl Med.* (2021) 19:97. doi: 10.1186/s12967-021-02765-x
47. Li Y, Chen J, Zou Y, Wang W, Li G. Lipoprotein glomerulopathy resulting from compound heterogeneous mutations of APOE gene: a case report. *Medicine.* (2022) 101:e28718. doi: 10.1097/MD.0000000000028718
48. Cheung CY, Chan AOK, Chan YH, Lee KC, Chan GPT, Lau GTC, et al. A rare cause of nephrotic syndrome: lipoprotein glomerulopathy. *Hong Kong Med J.* (2009) 15:57–60.
49. Kodera H, Mizutani Y, Sugiyama S, Miyata T, Ehara T, Matsunaga A, et al. A case of lipoprotein glomerulopathy with apoE Chicago and apoE (Glu3Lys) treated with fenofibrate. *Case Rep Nephrol Dial.* (2017) 7:112–20. doi: 10.1159/000478902
50. Georgiadou D, Stamatakis K, Efthimiadou EK, Kordas G, Gantz D, Chroni A, et al. Thermodynamic and structural destabilization of apoE3 by hereditary mutations associated with the development of lipoprotein glomerulopathy. *J Lipid Res.* (2013) 54:164–76. doi: 10.1194/jlr.M030965
51. Nilsson I, Sääf A, Whitley P, Gafvelin G, Waller C, von Heijne G. Proline-induced disruption of a transmembrane alpha-helix in its natural environment. *J Mol Biol.* (1998) 284:1165–75. doi: 10.1006/jmbi.1998.2217
52. Schütz AK, Rennella E, Kay LE. Exploiting conformational plasticity in the AAA+ protein VCP/p97 to modify function. *Proc Natl Acad Sci U.S.A.* (2017) 114:E6822–9. doi: 10.1073/pnas.1707974114
53. Katsarou M, Stratikos E, Chroni A. Thermodynamic destabilization and aggregation propensity as the mechanism behind the association of apoE3 mutants and lipoprotein glomerulopathy. *J Lipid Res.* (2018) 59:2339–48. doi: 10.1194/jlr.M088732
54. Hatters DM, Zhong N, Rutenber E, Weisgraber KH. Amino-terminal domain stability mediates apolipoprotein E aggregation into neurotoxic fibrils. *J Mol Biol.* (2006) 361:932–44. doi: 10.1016/j.jmb.2006.06.080
55. Zhao Y, Yang Y, Xing R, Cui X, Xiao Y, Xie L, et al. Hyperlipidemia induces typical atherosclerosis development in Ldlr and Apoe deficient rats. *Atherosclerosis.* (2018) 271:26–35. doi: 10.1016/j.atherosclerosis.2018.02.015
56. Dybas J, Bulat K, Blat A, Mohaissen T, Wajda A, Mardyla M, et al. Age-related and atherosclerosis-related erythropathy in ApoE/LDLR(-/-) mice. *Biochim Biophys Acta Mol Basis Dis.* (2020) 1866:165972. doi: 10.1016/j.bbadis.2020.165972
57. Hoffmann MM, Scharnagl H, Panagiotou E, Banghard WT, Wieland H, März W. Diminished LDL receptor and high heparin binding of apolipoprotein E2 sendai associated with lipoprotein glomerulopathy. *J Am Soc Nephrol.* (2001) 12:524–530. doi: 10.1681/ASN.V123524
58. Matsunaga A, Sasaki J, Komatsu T, Kanatsu K, Tsuji E, Moriyama K, et al. A novel apolipoprotein E mutation, E2 (Arg25Cys), in lipoprotein glomerulopathy. *Kidney Int.* (1999) 56:421–7. doi: 10.1046/j.1523-1755.1999.00572.x
59. Cambruzzi E, Pêgas KL. Pathogenesis, histopathologic findings and treatment modalities of lipoprotein glomerulopathy: a review. *J Bras Nefrol.* (2019) 41:393–9. doi: 10.1590/2175-8239-jbn-2018-0148
60. Häussinger D, Kordes C. Space of disse: a stem cell niche in the liver. *Biol Chem.* (2019) 401:81–95. doi: 10.1515/hsz-2019-0283
61. Sato Y, Kinami Y, Hashiba K, Harashima H. Different kinetics for the hepatic uptake of lipid nanoparticles between the apolipoprotein E/low density lipoprotein receptor and the N-acetyl-d-galactosamine/asialoglycoprotein receptor pathway. *J Control Release.* (2020) 322:217–226. doi: 10.1016/j.jconrel.2020.03.006
62. Morita S. Metabolism and modification of apolipoprotein B-containing lipoproteins involved in dyslipidemia and atherosclerosis. *Biol Pharm Bull.* (2016) 39:1–24. doi: 10.1248/bpb.b15-00716
63. Mahley RW, Ji ZS. Remnant lipoprotein metabolism: key pathways involving cell-surface heparan sulfate proteoglycans and apolipoprotein E. *J Lipid Res.* (1999) 40:1–16. doi: 10.1016/S0022-2275(20)33334-4
64. Smith RJH, Appel GB, Blom AM, Cook HT, D'Agati VD, Fakhouri F, et al. C3 glomerulopathy - understanding a rare complement-driven renal disease. *Nat Rev Nephrol.* (2019) 15:129–43. doi: 10.1038/s41581-018-0107-2
65. Li J-P, Kusche-Gullberg M. Heparan sulfate: biosynthesis, structure, and function. *Int Rev Cell Mol Biol.* (2016) 325:215–73. doi: 10.1016/bs.ircmb.2016.02.009
66. Murano T, Matsumura R, Misawa Y, Ozaki H, Miyashita Y, Yoshida S, et al. Interaction of endothelial cells and triglyceride-rich lipoproteins with apolipoprotein E (Arg25[rarr]Cys) from a patient with lipoprotein glomerulopathy. *Metabolism.* (2002) 51:201–5. doi: 10.1053/meta.2002.29990
67. Andrews PA, O'Donnell PJ, Dilly SA, Snowden SA, Bewick M. Recurrence of lipoprotein glomerulopathy after renal transplantation. *Nephrol Dial Transplant.* (1997) 12:2442–4. doi: 10.1093/ndt/12.11.2442
68. Miyata T, Sugiyama S, Nangaku M, Suzuki D, Uragami K, Inagi R, et al. Apolipoprotein E2/E5 variants in lipoprotein glomerulopathy recurred in transplanted kidney. *J Am Soc Nephrol.* (1999) 10:1590–5. doi: 10.1681/ASN.V1071590
69. Kanamaru Y, Nakao A, Shirato I, Okumura K, Ogawa H, Tomino Y, et al. Chronic graft-versus-host autoimmune disease in Fc receptor gamma chain-deficient mice results in lipoprotein glomerulopathy. *J Am Soc Nephrol.* (2002) 13:1527–33. doi: 10.1097/01.ASN.0000015615.14428.67
70. Steinbrecher UP. Receptors for oxidized low density lipoprotein. *Biochim Biophys Acta.* (1999) 1436:279–98. doi: 10.1016/S0005-2760(98)00127-1
71. Takai T, Li M, Sylvestre D, Clynes R, Ravetch JV. FcR gamma chain deletion results in pleiotrophic effector cell defects. *Cell.* (1994) 76:519–29. doi: 10.1016/0092-8674(94)90115-5
72. Ito K, Nakashima H, Watanabe M, Ishimura A, Miyahara Y, Abe Y, et al. Macrophage impairment produced by Fc receptor gamma deficiency plays a principal role in the development of lipoprotein glomerulopathy in concert with apoE abnormalities. *Nephrol Dial Transplant.* (2012) 27:3899–907. doi: 10.1093/ndt/gfs329
73. Virella G, Muñoz JF, Galbraith GM, Gissinger C, Chassereau C, Lopes-Virella MF. Activation of human monocyte-derived macrophages by immune complexes containing low-density lipoprotein. *Clin Immunol Immunopathol.* (1995) 75:179–89. doi: 10.1006/clin.1995.1069
74. Stanton LW, White RT, Bryant CM, Protter AA, Endemann G. A macrophage Fc receptor for IgG is also a receptor for oxidized low density lipoprotein. *J Biol Chem.* (1992) 267:22446–51. doi: 10.1016/S0021-9258(18)41692-4
75. Griffith RL, Virella GT, Stevenson HC, Lopes-Virella MF. Low density lipoprotein metabolism by human macrophages activated with low density lipoprotein immune complexes. A possible mechanism of foam cell formation. *J Exp Med.* (1988) 168:1041–59. doi: 10.1084/jem.168.3.1041
76. Fazio S, Babaev VR, Burleigh ME, Major AS, Hasty AH, Linton MF. Physiological expression of macrophage apoE in the artery wall reduces atherosclerosis in severely hyperlipidemic mice. *J Lipid Res.* (2002) 43:1602–9. doi: 10.1194/jlr.M200108-JLR200
77. Dove DE, Linton MF, Fazio S. ApoE-mediated cholesterol efflux from macrophages: separation of autocrine and paracrine effects. *Am J Physiol Cell Physiol.* (2005) 288:C586–92. doi: 10.1152/ajpcell.00210.2004
78. Tavori H, Fan D, Giunzioni I, Zhu L, Linton MF, Fogo AB, et al. Macrophage-derived apoESendai suppresses atherosclerosis while causing lipoprotein glomerulopathy in hyperlipidemic mice. *J Lipid Res.* (2014) 55:2073–81. doi: 10.1194/jlr.M049874
79. Prévost M, Raussens V. Apolipoprotein E-low density lipoprotein receptor binding: study of protein-protein interaction in rationally selected docked complexes. *Proteins.* (2004) 55:874–84. doi: 10.1002/prot.20080
80. de Vries APJ, Ruggenenti P, Ruan XZ, Praga M, Cruzado JM, Bajema IM, et al. Fatty kidney: emerging role of ectopic lipid in obesity-related renal disease. *Lancet Diabetes Endocrinol.* (2014) 2:417–26. doi: 10.1016/S2213-8587(14)70065-8
81. Gai Z, Wang T, Visentin M, Kullak-Ublick GA, Fu X, Wang Z. Lipid accumulation and chronic kidney disease. *Nutrients.* (2019) 11:722. doi: 10.3390/nu11040722
82. Leonarduzzi G, Scavazza A, Biasi F, Chiarpotto E, Camandola S, Vogel S, et al. The lipid peroxidation end product 4-hydroxy-2,3-nonenal up-regulates transforming growth factor beta1 expression in the macrophage lineage: a link between oxidative injury and fibrosclerosis. *FASEB J.* (1997) 11:851–7. doi: 10.1096/fasebj.11.11.9285483

83. Akhand AA, Kato M, Suzuki H, Liu W, Du J, Hamaguchi M, et al. Carbonyl compounds cross-link cellular proteins and activate protein-tyrosine kinase p60c-Src. *J Cell Biochem.* (1999) 72:1–7. doi: 10.1002/(SICI)1097-4644(19990101)72:1<1::AID-JCB1>3.0.CO;2-Y
84. Miyata T, van Ypersele de Strihou C, Kurokawa K, Baynes JW. Alterations in nonenzymatic biochemistry in uremia: origin and significance of "carbonyl stress" in long-term uremic complications. *Kidney Int.* (1999) 55:389–99. doi: 10.1046/j.1523-1755.1999.00302.x
85. Pham T, Kodvawala A, Hui DY. The receptor binding domain of apolipoprotein E is responsible for its antioxidant activity. *Biochemistry.* (2005) 44:7577–82. doi: 10.1021/bi0472696
86. Amenomori M, Haneda M, Morikawa J, Nishigaki I, Maeda S, Hidaka H, et al. A case of lipoprotein glomerulopathy successfully treated with probucol. *Nephron.* (1994) 67:109–13. doi: 10.1159/000187897
87. Chen S, Liu Z-H, Zheng J-M, Zhang X, Li L-S. A complete genomic analysis of the apolipoprotein E gene in Chinese patients with lipoprotein glomerulopathy. *J Nephrol.* (2007) 20:568–75.
88. Liao J, Bai J, An X, Liu Y, Wang Y, Liu G, et al. Lipoprotein glomerulopathy-like lesions in atherosclerotic mice defected with HDL receptor SR-B1. *Front Cardiovasc Med.* (2021) 8:734824. doi: 10.3389/fcvm.2021.734824
89. Li W, Wang Y, Han Z, Luo C, Zhang C, Xiong J. Apolipoprotein e mutation and double filtration plasmapheresis therapy on a new Chinese patient with lipoprotein glomerulopathy. *Kidney Blood Press Res.* (2014) 39:330–339. doi: 10.1159/000355810
90. Russi G, Furci L, Leonelli M, Magistroni R, Romano N, Rivasi P, et al. Lipoprotein glomerulopathy treated with LDL-apheresis (heparin-induced extracorporeal lipoprotein precipitation system): a case report. *J Med Case Rep.* (2009) 3:1–6. doi: 10.1186/1752-1947-3-9311
91. Takasaki S, Maeda K, Joh K, Yamakage S, Fukase S, Takahashi T, et al. Macrophage infiltration into the glomeruli in lipoprotein glomerulopathy. *Case Rep Nephrol Dial.* (2015) 5:204–12. doi: 10.1159/000441715
92. Tokura T, Itano S, Kobayashi S, Kuwabara A, Fujimoto S, Horike H, et al. A novel mutation ApoE2 Kurashiki (R158P) in a patient with lipoprotein glomerulopathy. *J Atheroscler Thromb.* (2011) 18:536–41. doi: 10.5551/jat.8102
93. Arai T, Yamashita S, Yamane M, Manabe N, Matsuzaki T, Kiriyama K, et al. Disappearance of intraglomerular lipoprotein thrombi and marked improvement of nephrotic syndrome by bezafibrate treatment in a patient with lipoprotein glomerulopathy. *Atherosclerosis.* (2003) 169:293–9. doi: 10.1016/S0021-9150(03)00194-1
94. Wu H, Yang Y, Hu Z. The novel apolipoprotein e mutation ApoE chengdu (c.518T>C, p.L173P) in a Chinese patient with lipoprotein glomerulopathy. *J Atheroscler Thromb.* (2018) 25:733–40. doi: 10.5551/jat.41996
95. Wu Y, Chen X, Yang Y, Wang B, Liu X, Tao Y, et al. A case of lipoprotein glomerulopathy with thrombotic microangiopathy due to malignant hypertension. *BMC Nephrol.* (2013) 14:53. doi: 10.1186/1471-2369-14-53
96. Chen H, Liu Z, Gong R, Tang Z, Zeng C, Zhu M, et al. Lipoprotein glomerulopathy: clinical features and pathological characteristics in Chinese. *Chin Med J.* (2004) 117:1513–7. doi: 10.3760/cma.j.issn.0366-6999.2004.10.114
97. Xin Z, Zhihong L, Shijun L, Jinfeng Z, Huiping C, Caihong Z, et al. Successful treatment of patients with lipoprotein glomerulopathy by protein A immunoadsorption: a pilot study. *Nephrol Dial Transplant.* (2009) 24:864–9. doi: 10.1093/ndt/gfn555
98. Zhang B, Liu Z, Zeng C, Zheng J, Chen H, Zhou H, et al. Plasma level and genetic variation of apolipoprotein E in patients with lipoprotein glomerulopathy. *Chin Med J.* (2005) 118:555–60. doi: 10.5555/cmj.0366-6999.118.07.p555.01
99. Takasaki S, Matsunaga A, Joh K, Saito T. A case of lipoprotein glomerulopathy with a rare apolipoprotein E isoform combined with neurofibromatosis type I. *CEN Case Rep.* (2018) 7:127–31. doi: 10.1007/s13730-018-0309-2
100. Zou GM, Zhuo L, Tan M, Li WG. [Clinicopathologic features of lipoprotein glomerulopathy: observation of 6 cases]. *Chin Med J.* (2018) 98:2910–3. doi: 10.3760/cma.j.issn.0376-2491.2018.36.007
101. Blum CB. Type III hyperlipoproteinemia: still worth considering? *Prog Cardiovasc Dis.* (2016) 59:119–24. doi: 10.1016/j.pcad.2016.07.007
102. Sniderman AD, de Graaf J, Thanassoulis G, Tremblay AJ, Martin SS, Couture P. The spectrum of type III hyperlipoproteinemia. *J Clin Lipidol.* (2018) 12:1383–9. doi: 10.1016/j.jacl.2018.09.006
103. Nordestgaard BG. Triglyceride-Rich lipoproteins and atherosclerotic cardiovascular disease: new insights from epidemiology, genetics, and biology. *Circ Res.* (2016) 118:547–63. doi: 10.1161/CIRCRESAHA.115.306249
104. Boot CS, Luvai A, Neely RDG. The clinical and laboratory investigation of dysbetalipoproteinemia. *Crit Rev Clin Lab Sci.* (2020) 57:458–69. doi: 10.1080/10408363.2020.1745142
105. Koitabashi Y, Ikoma M, Miyahira T, Fujita R, Mio H, Ishida M, et al. Long-term follow-up of a paediatric case of lipoprotein glomerulopathy. *Pediatr Nephrol.* (1990) 4:122–8. doi: 10.1007/BF00858822
106. da Silveira-Neto JN, de Oliveira Ahn GJ, de Menezes Neves PDM, Baptista VAF, de Almeida Araújo S, Wanderley DC, et al. Lipoprotein glomerulopathy associated with the Osaka/Kurashiki APOE variant: two cases identified in Latin America. *Diagn Pathol.* (2021) 16:65. doi: 10.1186/s13000-021-01119-x
107. Kollbrunner L, Hirt-Minkowski P, Sanz J, Bresin E, Neuhaus TJ, Hopfer H, et al. Case report: lipoprotein glomerulopathy complicated by atypical hemolytic uremic syndrome. *Front Med.* (2021) 8:679048. doi: 10.3389/fmed.2021.679048
108. Chang C-F, Lin C-C, Chen J-Y, Yang A-H, Shiao M-S, Kao J-T, et al. Lipoprotein glomerulopathy associated with psoriasis vulgaris: report of 2 cases with apolipoprotein E3/3. *Am J kidney Dis.* (2003) 42:E18–23. doi: 10.1016/S0272-6386(03)00798-4
109. Ando M, Sasaki J, Hua H, Matsunaga A, Uchida K, Jou K, et al. A novel 18-amino acid deletion in apolipoprotein E associated with lipoprotein glomerulopathy. *Kidney Int.* (1999) 56:1317–23. doi: 10.1046/j.1523-1755.1999.00677.x
110. Morris CS, Bois MC, Aust CH, Thomas R, Sethi S, Maleszewski JJ. Intravascular cardiac lipoproteinosis: extrarenal manifestation of lipoprotein glomerulopathy. *Cardiovasc Pathol.* (2019) 42:6–9. doi: 10.1016/j.carpath.2019.04.006
111. Lui DTW, Lee ACH, Yap DYH, Chan GSW, Tan KCB. A young Chinese man with nephrotic syndrome due to lipoprotein glomerulopathy. *J Clin Lipidol.* (2019) 13:251–3. doi: 10.1016/j.jacl.2018.12.004
112. Bomback AS, Song H, D'Agati VD, Cohen SD, Neal A, Appel GB, et al. A new apolipoprotein E mutation, apoE Las Vegas, in a European-American with lipoprotein glomerulopathy. *Nephrol Dial Transplant.* (2010) 25:3442–6. doi: 10.1093/ndt/gfq389
113. Zhang P, Matalon R, Kaplan L, Kumar A, Gallo G. Lipoprotein glomerulopathy: first report in a Chinese male. *Am J Kidney Dis.* (1994) 24:942–50. doi: 10.1016/S0272-6386(12)81066-3
114. Boumendjel R, Papari M, Gonzalez M. A rare case of lipoprotein glomerulopathy in a white man: an emerging entity in Asia, rare in the white population. *Arch Pathol Lab Med.* (2010) 134:279–82. doi: 10.5858/134.2.279
115. Kinomura M, Sugiyama H, Saito T, Matsunaga A, Sada K, Kanzaki M, et al. A novel variant apolipoprotein E Okayama in a patient with lipoprotein glomerulopathy. *Nephrol Dial Transplant.* (2008) 23:751–6. doi: 10.1093/ndt/gfm675
116. Usui R, Takahashi M, Nitta K, Koike M. Five-year follow-up of a case of lipoprotein glomerulopathy with APOE Kyoto mutation. *CEN Case Rep.* (2016) 5:148–53. doi: 10.1007/s13730-016-0214-5
117. Shimizu M, Ohno T, Kimoto H, Hosono S, Nozawa M. A newborn infant with lipoprotein glomerulopathy associated with congenital nephrotic syndrome. *Pediatr Int.* (2001) 43:78–80. doi: 10.1046/j.1442-200x.2001.01344.x
118. Konishi K, Saruta T, Kuramochi S, Oikawa S, Saito T, Han H, et al. Association of a novel 3-amino acid deletion mutation of apolipoprotein E (Apo E Tokyo) with lipoprotein glomerulopathy. *Nephron.* (1999) 83:214–8. doi: 10.1159/000045513
119. Han J, Pan Y, Chen Y, Li X, Xing G, Shi J, et al. Common apolipoprotein e gene mutations contribute to lipoprotein glomerulopathy in China. *Nephron Clin Pract.* (2010) 114:260–7. doi: 10.1159/000276578
120. Yamashita S, Masuda D, Matsuzawa Y. Did we abandon probucol too soon? *Curr Opin Lipidol.* (2015) 26:304–16. doi: 10.1097/MOL.0000000000000199

121. Ieiri N, Hotta O, Taguma Y. Resolution of typical lipoprotein glomerulopathy by intensive lipid-lowering therapy. *Am J Kidney Dis.* (2003) 41:244–9. doi: 10.1053/ajkd.2003.50016
122. Karube M, Nakabayashi K, Fujioka Y, Yoshihara K, Yamada A, Matsunaga A, et al. Lipoprotein glomerulopathy-like disease in a patient with type III hyperlipoproteinemia due to apolipoprotein E2 (Arg158 Cys)/3 heterozygosity. *Clin Exp Nephrol.* (2007) 11:174–9. doi: 10.1007/s10157-007-0469-4
123. Owada A, Suda S, Hata T. Antiproteinuric effect of niceritrol, a nicotinic acid derivative, in chronic renal disease with hyperlipidemia: a randomized trial. *Am J Med.* (2003) 114:347–53. doi: 10.1016/S0002-9343(02)01567-X
124. Yamauchi K, Tanahashi Y, Okada M, Tsuzuki J, Sato A, Abe K, et al. Long-term effects of niceritrol on serum lipoprotein(a) and lipids in patients with high levels of lipoprotein(a). *Clin Ther.* (1995) 17:52–9. doi: 10.1016/0149-2918(95)80006-9
125. Hamatani H, Hiromura K, Kobatake K, Yoshida H, Kobayashi S, Yoneda N, et al. Successful treatment of lipoprotein glomerulopathy in a daughter and a mother using niceritrol. *Clin Exp Nephrol.* (2010) 14:619–24. doi: 10.1007/s10157-010-0333-9
126. Sirtori CR. The pharmacology of statins. *Pharmacol Res.* (2014) 88:3–11. doi: 10.1016/j.phrs.2014.03.002
127. Liao M-T, Tsai I-J, Cheng H-T, Lin W-C, Chang Y-W, Lin Y-H, et al. A rare cause of childhood-onset nephrotic syndrome: lipoprotein glomerulopathy. *Clin Nephrol.* (2012) 78:237–40. doi: 10.5414/CN106876
128. Matsunaga A, Furuyama M, Hashimoto T, Toyoda K, Ogino D, Hayasaka K. Improvement of nephrotic syndrome by intensive lipid-lowering therapy in a patient with lipoprotein glomerulopathy. *Clin Exp Nephrol.* (2009) 13:659–62. doi: 10.1007/s10157-009-0207-1
129. Boeckhaus J, Gross O. Sodium-Glucose cotransporter-2 inhibitors in patients with hereditary podocytopathies, alport syndrome, and FSGS: a case series to better plan a large-scale study. *Cells.* (2021) 10:1815. doi: 10.3390/cells10071815
130. Susca M. Heparin-Induced extracorporeal low-density lipoprotein precipitation futura, a new modification of HELP apheresis: technique and first clinical results. *Ther Apher.* (2001) 5:387–93. doi: 10.1046/j.1526-0968.2001.00371.x
131. Waldmann E, Parhofer KG. Apheresis for severe hypercholesterolaemia and elevated lipoprotein(a). *Pathology.* (2019) 51:227–32. doi: 10.1016/j.pathol.2018.10.016
132. Esnault VL, Besnier D, Testa A, Coville P, Simon P, Subra JF, et al. Effect of protein A immunoadsorption in nephrotic syndrome of various etiologies. *J Am Soc Nephrol.* (1999) 10:2014–7. doi: 10.1681/ASN.V1092014
133. Tuteja S. Activation of HCAR2 by niacin: benefits beyond lipid lowering. *Pharmacogenomics.* (2019) 20:1143–50. doi: 10.2217/pgs-2019-0092
134. Thompson G, Parhofer KG. Current role of lipoprotein apheresis. *Curr Atheroscler Rep.* (2019) 21:26. doi: 10.1007/s11883-019-0787-5
135. Khetarpal SA, Zeng X, Millar JS, Vitali C, Somasundara AVH, Zanoni P, et al. A human APOC3 missense variant and monoclonal antibody accelerate apoC-III clearance and lower triglyceride-rich lipoprotein levels. *Nat Med.* (2017) 23:1086–94. doi: 10.1038/nm.4390
136. Ahmad KA, Yuan Yuan D, Nawaz W, Ze H, Zhuo CX, Talal B, et al. Antioxidant therapy for management of oxidative stress induced hypertension. *Free Radic Res.* (2017) 51:428–38. doi: 10.1080/10715762.2017.1322205
137. Huang G, Mei X, Hu J. The antioxidant activities of natural polysaccharides. *Curr Drug Targets.* (2017) 18:1296–300. doi: 10.2174/1389450118666170123145357
138. Manzini S, Busnelli M, Parolini C, Minoli L, Ossoli A, Brambilla E, et al. Topiramate protects apoE-deficient mice from kidney damage without affecting plasma lipids. *Pharmacol Res.* (2019) 141:189–200. doi: 10.1016/j.phrs.2018.12.022
139. Hirashima H, Komiya T, Toriu N, Hara S, Matsunaga A, Saito T, et al. A case of nephrotic syndrome showing contemporary presence of apolipoprotein E2 homozygote glomerulopathy and membranous nephropathy-like findings modified by apolipoprotein E Toyonaka. *Clin Nephrol Case Stud.* (2018) 6:45–51. doi: 10.5414/CNCS109509
140. Kato T, Ushiogi Y, Yokoyama H, Hara S, Matsunaga A, Muso E, et al. A case of apolipoprotein E toyonaka and homozygous apolipoprotein E2/2 showing non-immune membranous nephropathy-like glomerular lesions with foamy changes. *CEN Case Rep.* (2019) 8:106–11. doi: 10.1007/s13730-019-00380-w
141. Saito T, Matsunaga A, Fukunaga M, Nagahama K, Hara S, Muso E. Apolipoprotein E–related glomerular disorders. *Kidney Int.* (2020) 97:279–88. doi: 10.1016/j.kint.2019.10.031

Conflict of Interest: The authors declare that the research was conducted in the absence of any commercial or financial relationships that could be construed as a potential conflict of interest.

Publisher's Note: All claims expressed in this article are solely those of the authors and do not necessarily represent those of their affiliated organizations, or those of the publisher, the editors and the reviewers. Any product that may be evaluated in this article, or claim that may be made by its manufacturer, is not guaranteed or endorsed by the publisher.

frontiers | Frontiers in Medicine

STUDY PROTOCOL
published: 26 May 2022
doi: 10.3389/fmed.2022.891223

The HIDDEN Protocol: An Australian Prospective Cohort Study to Determine the Utility of Whole Genome Sequencing in Kidney Failure of Unknown Aetiology

Jacqueline Soraru[1], Sadia Jahan[2,3], Catherine Quinlan[4,5,6,7], Cas Simons[4,6], Louise Wardrop[4,6], Rosie O'Shea[4,6], Alasdair Wood[4,6], Amali Mallawaarachchi[4,8,9], Chirag Patel[4,10], Zornitza Stark[4,6,7] and Andrew John Mallett[3,4,10,11,12] on behalf of the KidGen Collaborative*

[1] Department of Nephrology and Hypertension, Perth Children's Hospital, Perth, WA, Australia, [2] Kidney Health Service, Royal Brisbane and Women's Hospital, Brisbane, QLD, Australia, [3] Faculty of Medicine, Institute for Molecular Bioscience, The University of Queensland, Brisbane, QLD, Australia, [4] Australian Genomics, Murdoch Children's Research Institute, Melbourne, VIC, Australia, [5] Royal Children's Hospital, Melbourne, VIC, Australia, [6] Murdoch Children's Research Institute, Melbourne, VIC, Australia, [7] Department of Paediatrics, University of Melbourne, Melbourne, VIC, Australia, [8] Department of Medical Genomics, Royal Prince Alfred Hospital, Camperdown, NSW, Australia, [9] Garvan Institute of Medical Research, Sydney, NSW, Australia, [10] Genetic Health Queensland, Royal Brisbane and Women's Hospital, Brisbane, QLD, Australia, [11] Townsville University Hospital, Townsville, QLD, Australia, [12] College of Medicine and Dentistry, James Cook University, Townsville, QLD, Australia

OPEN ACCESS

Edited by:
Hoon Young Choi,
Yonsei University, South Korea

Reviewed by:
Hee Gyung Kang,
Seoul National University, South Korea
Gianluca Caridi,
Giannina Gaslini Institute (IRCCS), Italy

***Correspondence:**
Andrew John Mallett
andrew.mallett@health.qld.gov.au

Specialty section:
This article was submitted to Nephrology, a section of the journal Frontiers in Medicine

Received: 07 March 2022
Accepted: 10 May 2022
Published: 26 May 2022

Citation:
Soraru J, Jahan S, Quinlan C, Simons C, Wardrop L, O'Shea R, Wood A, Mallawaarachchi A, Patel C, Stark Z and Mallett AJ (2022) The HIDDEN Protocol: An Australian Prospective Cohort Study to Determine the Utility of Whole Genome Sequencing in Kidney Failure of Unknown Aetiology. Front. Med. 9:891223. doi: 10.3389/fmed.2022.891223

Early identification of genetic kidney disease allows personalised management, clarification of risk for relatives, and guidance for family planning. Genetic disease is underdiagnosed, and recognition of genetic disease is particularly challenging in patients with kidney failure without distinguishing diagnostic features. To address this challenge, the primary aim of this study is to determine the proportion of genetic diagnoses amongst patients with kidney failure of unknown aetiology, using whole genome sequencing (WGS). A cohort of up to 100 Australian patients with kidney failure of unknown aetiology, with onset <50 years old and approved by a panel of study investigators will be recruited *via* 18 centres nationally. Clinically accredited WGS will be undertaken with analysis targeted to a priority list of ∼388 genes associated with genetic kidney disease. The primary outcome will be the proportion of patients who receive a molecular diagnosis (diagnostic rate) *via* WGS compared with usual -care (no further diagnostic investigation). Participant surveys will be undertaken at consent, after test result return and 1 year subsequently. Where there is no or an uncertain diagnosis, future research genomics will be considered to identify candidate genes and new pathogenic variants in known genes. All results will be relayed to participants *via* the recruiting clinician and/or kidney genetics clinic. The study is ethically approved (HREC/16/MH/251) with local site governance approvals in place. The future results of this study will be disseminated and inform practical understanding of the potential

monogenic contribution to kidney failure of unknown aetiology. These findings are anticipated to impact clinical practice and healthcare policy.

Study Registration: [https://dora.health.qld.gov.au], identifier [HREC/16/MH/251].

Keywords: kidney failure, genomics, genetic condition, unknown aetiology, genetic kidney disease

BACKGROUND

An estimated 10% of chronic kidney disease (CKD), including kidney failure (KF), is attributed to an underlying genetic condition (1, 2). Identifying a genetic cause can aid medical management (3), with potential benefits in slowing the rate of kidney function decline, prognosticating risk of disease recurrence in the event of kidney transplantation, improving monitoring or management of extra-renal manifestations, impacting informed reproductive decisions, and facilitating cascade testing (3). Many causes of CKD lead to KF with the prevalence of KF in 2020 being almost 32,000 individuals in Australia and New Zealand combined (4). Kidney replacement therapies for KF are resource-intensive [>$80,000/year/patient (5), >1,000,000 admissions/year in Australia (6)] and place a significant burden on individuals, families, and healthcare systems (6).

Up to 5% of Australian and 4% of New Zealand KF populations do not have a diagnosis for their kidney disease (6). Many diseases that cause KF have genetic origins; however, if there are no clear clinical features to indicate genetic disease, or patients present in later-stage disease, diagnosis can be delayed or missed. Missed or delayed diagnosis potentially affects disease progression and time to KF (3). Genetic diagnosis also significantly impacts kidney transplantation, with between 20 and 51% of transplant recipients under the age of 50 having a monogenic cause for their kidney disease (7, 8). Early molecular diagnosis can clarify the risk of primary disease recurrence in kidney transplant recipients, limiting the use of therapies with significant side effect profiles and helping to identify potential unaffected living-related kidney donors (3).

The benefits of detection of genetic kidney disease are not limited to the individual. Genetic diagnosis also facilitates the early identification of affected relatives which could vastly improve their medical management outcomes, including their trajectory to KF (9). For this reason, there is an increasing emphasis on integrating genomics into mainstream healthcare (10), including kidney medicine. The KidGen Collaborative is an Australian consortium of nephrology and genetics clinicians, diagnostic laboratory scientists and researchers committed to improving diagnosis and treatment of genetic kidney disease (11). It utilises a network of multidisciplinary clinics across Australia, along with a research pipeline to identify and functionally characterise novel disease-causing genes in families with no diagnosis. A previous multisite Australian prospective cohort study of 204 kidney disease patients with a suspected monogenic cause revealed a diagnostic yield from exome sequencing of 39% (12).

The aim of the HIDDEN (wHole genome Investigation to iDentify unDEtected Nephropathies) study is to investigate the utility and diagnostic yield of clinically accredited whole genome sequencing (WGS) in patients with early-onset unexplained KF, in order to inform how genomic testing should be translated into the clinical care of this patient group. The results will provide "real world" applicability of WGS in the kidney clinic. In addition, the study is anticipated to improve our understanding of genotype-phenotype correlations and potentially lead to the discovery of new genes and pathogenic variants in kidney disease.

METHODS AND DESIGN

Aims

The primary aim of the study is to compare standard-of-care (no further diagnostic investigation) against WGS for younger patients with kidney failure of unknown cause. The primary outcome is to:

1. Determine if WGS can identify a genetic aetiology for a prospectively recruited cohort of Australian patients with KF of unknown cause.

Recruitment of Patients

A cohort of up to 100 Australian patients with KF with no definitive diagnosis and matching the inclusion criteria of the following (**Supplementary Material: S5 File**); an absence of identified cause or aetiology for kidney disease, CKD Stage 5 (eGFR $\leq$ 15 ml/min/1.73 m2; CKD-EPI equation) at $\leq$50 years of age and negative genetic test if a specific genetic kidney diagnosis has been suspected will be recruited into the study. The exclusion criteria include those with an existing kidney clinical or phenotypic diagnosis, specifically; a likely or proven diabetic nephropathy, renovascular disease, renal sarcoidosis, primary nephrotic-range proteinuric disorder, or tuberculosis, paraproteinemia (except when excluded on kidney biopsy), exposure to nephrotoxin causing kidney dysfunction, or obstructive uropathy, nephromegaly (>14 cms for adults; normagram for paediatric patients) and a family history of cystic kidneys, identified glomerular disorder on kidney biopsy that clarifies a diagnosis, identified and proven primary renal diagnosis (as per ANZDATA coding), and isolated Congenital Anomaly of Kidney and Urinary Tract (CAKUT). The criteria for CAKUT exclusion will be based upon clinical consensus of the National Panel, with classification of CAKUT approximating that of **Figure 1** from Khan et al.

(13). Cases with a lower yield of defects in urinary system morphogenesis ranging from the number, structure, and/or position of the kidneys; obstructive or non-obstructive dilatation of the urinary tract; to dysplastic kidney lesions, including cystic disorders will be evaluated to allow for appropriate exclusion. Those excluded from the study will continue with standard clinically indicated care. The recruitment pathway will involve the 18 local sites nationally identifying potential participants (**Figure 1**). The recruitment pathway will involve the local sites identifying candidate participants believed to meet the inclusion/exclusion criteria *via* local service databases and local site ANZDATA registry reports/searches. Sites may reach out to other services that are within their local, regional, or state-wide referral networks through standard or telehealth means to identify additional individuals for participation. Each potential participant will then be nominated by their local site clinician for assessment of potential suitability by a Panel of the study's lead clinical investigators (AJM, CP, ZS, CQ, and ACM) through a nomination form (**Supplementary Material: S1 File**). The Consensus Panel will apply the inclusion/exclusion criteria and decision on suitability to recruit will be reached within 1 week of nomination and on the basis of a majority vote with the outcome communicated to the nominating clinician by the Panel Chair (AJM). This iterative case identification, nomination and review process will ensure consistency and adherence to the inclusion criteria. For more detailed information on the recruitment pathway refer to **Supplementary Figure 1**.

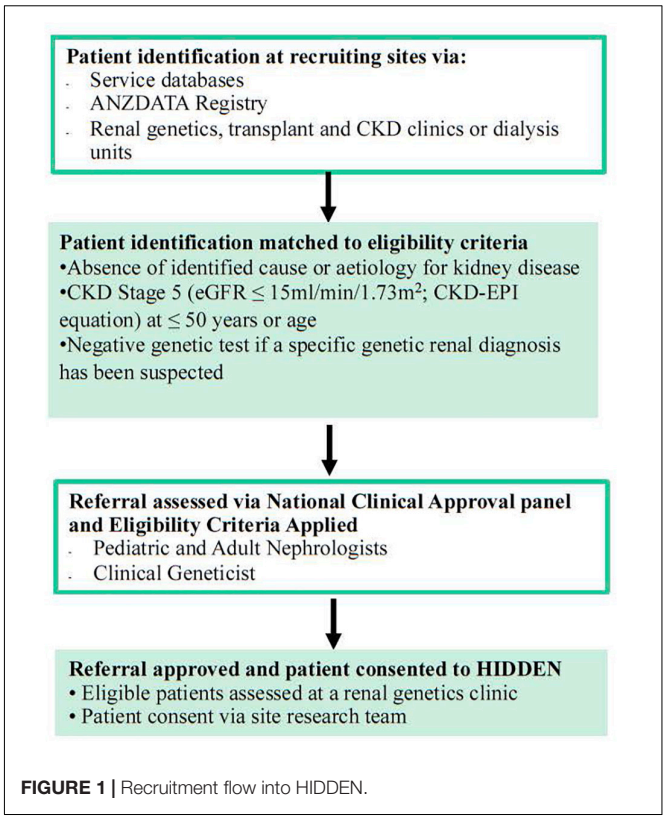

FIGURE 1 | Recruitment flow into HIDDEN.

Prospective Cohort Data Collection and Analysis

Australia wide there are 1,150 eligible patients and a timeframe of 1–2 years for identifying, consenting, enrolling, and sequencing of 100 cases is anticipated nationally. A consecutively identified series of eligible KF patients will be recruited through their standard of care (SOC) where regular blood testing occurs and sampling for DNA extraction/storage can occur during SOC pathways. The turnaround time from consent to sample receipt to results will be 3 months to inform patient care. In addition, parental and familial samples will be collected if required for variant assessment such as for phasing or segregation. Consent for recruitment and participation will be obtained from individual recruitment sites (**Supplementary Figure 1** and **Supplementary Material: S2 File**). The prospective cohort will be compared with a retrospective cohort of matched controls from the ANZDATA registry (the national dialysis and kidney transplantation data), in whom WGS has not been applied and an unresolved diagnostic odyssey exists. The registry-coded Primary Renal Diagnosis is "Unknown" and outcomes are reported by ANZDATA in their public annual reporting. A pilot sample of ten initial HIDDEN recruits from one recruiting state (Queensland) will have pharmacogenomic testing as a proof of principle.

Detailed data collection on phenotype will be entered for each consented participant into a secure REDCap database (**Supplementary Material: S3 File**). WGS analysis will be undertaken in facilities with NATA (The National Association of Testing Authorities) accreditation for clinical reporting. This includes specific NATA accreditation to perform WGS in accordance with the requirements of the National Pathology Accreditation Advisory Council of Australia and AS ISO 15189-2013. A gene panel comprising ∼388 genes associated with kidney disease (KidneyOme) will be applied in the analysis. Previous work (12) informed the curated list of genes for inclusion in the KidneyOme and a final gene list is available in **Supplementary Material: S4 File** and was informed by a virtual gene panel that is clinically available.[1] WGS is optimal at identifying a range of variants, including copy number variants (CNVs; not uncommon in inherited kidney disease), splicing, and intronic variants. The diagnostic laboratory WGS method is being provided by three NATA accredited laboratories providing a mean coverage of >30X, with >98% of canonical protein coding transcripts and splice sites covered at >15X. Sensitivity is >99% for single nucleotide variants and >95% for small indels <20 bp. Sensitivity is >81% for copy number losses <500 bpin size and 96% for >500 bp.

Genome analysis in those clinically accredited diagnostic laboratories is being undertaken with the Illumina sequencing genome platform with reads being aligned to the human genome reference sequence (GRCh37/GRCh38) and variant calls made using the Genome Analysis Tool Kit and ClinSV. Single nucleotide and small indel variants will be classified according to the joint consensus recommendations of the American

[1]https://panelapp.agha.umccr.org/panels/275/

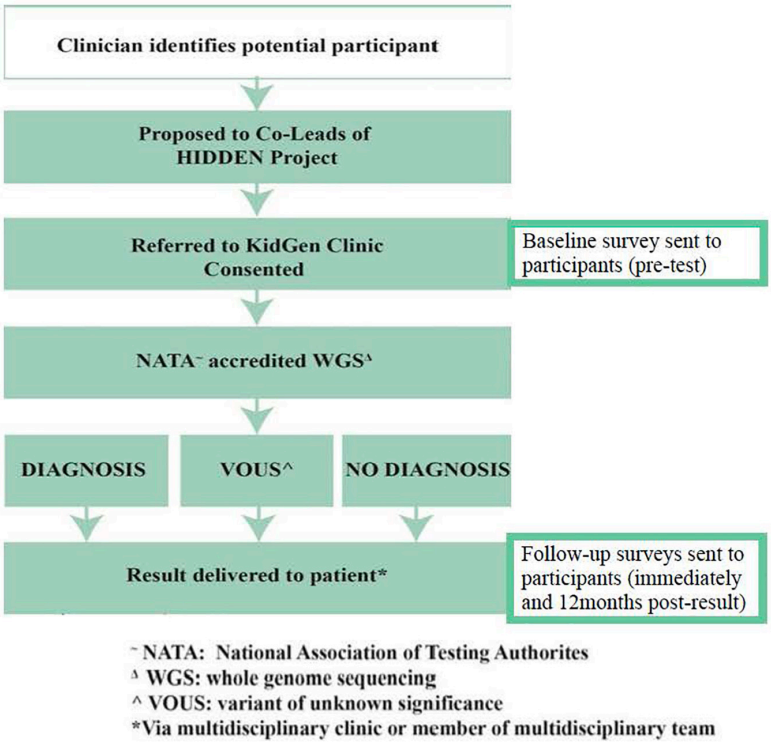

FIGURE 2 | Data collection and WGS workflow for HIDDEN.

College of Medical Genetics and Genomics and the Association for Molecular Pathology. These will be reported using HGVS nomenclature. Copy number variants will be classified similarly according to recommendations of the American College of Medical Genetics and Genomics.

Where there is no diagnosis, or the diagnosis is uncertain, further research analysis will be considered through the KidGen research and functional genomics pipeline to identify candidate genes and new pathogenic variants in known genes (**Figure 2**). The timeframe for recruitment and sequencing is over a 1–2-year period. An electronically communicated REDCap participant survey will be distributed at consent, at or shortly after test return, and 1 year subsequent to that.

Delivery of Results

All results, where a WGS diagnosis is made or there is an uncertain or uninformative result, will be returned to patients *via* their clinicians at the recruitment sites (**Figure 2**). Additional input and support from the relevant local KidGen multidisciplinary kidney genetics clinic will be provided if/as required in addition to discussion of any results at the discretion of the recruiting clinician/s at a KidGen National Multidisciplinary Team meeting to ensure closure of the clinic-research-clinic translational loop.

Ethics Approval

This study has been approved by the Melbourne Health Human Research Ethics Committee (HREC/16/MH/251) *via* approved amendment on 26 February, 2018 (Australian Genomics Health Alliance: Preparing Australia for Genomic Medicine, Protocol V7). All sites across all Australian states and territories achieved subsequent local research governance site specific approval under the National Ethics Statement and associated frameworks of the National Health and Medical Research Council.

DISCUSSION

The HIDDEN protocol presents the first prospective application of WGS-clinic-based testing in KF patients from all states and territories in Australia. The prospective, multi-site study design along with consistent application of inclusion criteria through a national clinical referral approval panel enables strong consistency and applicability. Previous studies in KF cohorts applied genomic testing in single centre cross-sectional analyses to understand the diagnostic utility of whole exome sequencing (WES) (7, 8). HIDDEN will extend knowledge regarding the diagnostic utility and benefit of genomic testing by prospectively applying WGS in a cohort of KF in a real-world clinical setting. Understanding diagnostic yield when the strict variant analysis protocols utilised by hospital diagnostic laboratories are applied will allow seamless translation of the study results into the clinic.

Although individual inherited kidney diseases are rare, together they account for approximately 10% of KF and 70% of paediatric kidney disease (14, 15). To date, more than 500 genes have been implicated in causing various forms of kidney disease

(16), with a monogenic cause being identified in around 20% of those with early-onset CKD (14) and 39% amongst those with a suspected monogenic kidney condition (12). Previous cohort studies retrospectively applied WES to early-onset (<50-year-old) and paediatric cohorts of KF patients with a diagnostic yield of between 20 and 50% (8, 17). In addition, WES and specific kidney gene panel retrospective application to adult and paediatric KF patients on transplant waiting lists similarly revealed a 10–50% diagnostic yield (7, 18, 19). The application of WES to KF cohorts of unknown genetic disease aetiology harbours some limitations, including difficulty in diagnosis due to broad phenotypic and genetic heterogeneity, and higher rate of detecting variants of uncertain significance (9). Recent cohort studies in the adult setting applying WES to 114 (20) and 92 patients (21) achieved a 56 and 59% diagnostic yield, respectively (**Supplementary Material: S6 File**). However, limitations of WES due to inability to detect complex deletion-insertion, copy-number variants, or variants that reside within a promotor or other intronic region cannot be detected, which may explain cases without a molecular diagnosis in these CKD cohorts. The application of WGS in the HIDDEN study has the capacity to overcome some of the limitations of WES, thus increasing diagnostic power (3).

The key novel features of this study are the prospective recruitment and application of WGS to KF patients <50 years with unknown disease aetiology in a national Australian cohort. We are hopeful that WGS application will yield a definitive diagnosis for a proportion of our cohort. It was previously estimated that the diagnostic rate may be somewhere in the realm of 5–40%, with more recent evidence demonstrating diagnostic rates of 11–51% (7, 8). The potential diagnostic value can be exemplified in the case of patients with an established histological diagnosis of Focal Segmental Glomerulosclerosis (FSGS) due to various aetiologies. FSGS accounts for 4–5% of incident KF (6), and a study by Gast et al. (22) demonstrated that an unappreciated monogenic cause for FSGS was present in 22 and 10% of cases with and without a family history of kidney disease.

It has been reported that 10–29% of patients with KF have a family history of kidney disease, with these relatives being 2–3 times more likely to have incident KF (23). These family members may be unaware of their increased risk for CKD and KF, which can arise from a combination of genetic and environmental factors. For HIDDEN patients where a molecular genetic diagnosis is made, cascade testing can be offered to family members, and may result in; early intervention or close monitoring for those already showing signs of disease or prior to symptoms/disease onset, and may have an impact on family planning (3). Whilst not clearly of direct benefit to a patient cohort already experiencing established KF, such as the cohort in this study, these potential benefits may be realised by at-risk relatives or by their treating clinicians for other patients at earlier stages of CKD including avoidance of unnecessary and burdensome investigations, in particular kidney biopsies, which carry morbidity and mortality risk (3). Testing family members allows identification of suitable live-related kidney donors for the proband. HIDDEN patients who do not receive a molecular genetic diagnosis, but have a strong family history of kidney disease, may be considered for subsequent collaborative research and/or functional genomic analysis.

A specific genetic diagnosis may lead to direct surveillance for extra-renal disease manifestations such as sensorineural hearing loss and visual impairment in Alport Syndrome, establishing social and educational supports in those conditions that significantly impact sight, vision, learning, and behaviour (3). Affected individuals of child-bearing age can also use this information to access accurate genetic counselling and reproductive genetic services prior to starting a family (3). The above benefits and utility of clinical genomic testing were demonstrated in an Australian prospective cohort study (12). Thirty-nine percent of kidney disease patients had a change in their clinical diagnosis, with 56% having a change to their clinical management, such as: 13% avoiding the need for diagnostic kidney biopsy, 44% changing surveillance, and 20% changing the treatment plan. Cascade testing was offered to 50% of families and 79% had an impact on the management of family members (12).

The potential pitfalls or unintended effects may include the following: (1) participant decisional regret to pursue genetic testing, which will be assessed by the baseline and follow up survey, (2) identifying a diagnosis that ends the diagnostic odyssey but does not have specific management strategy, (3) a genetic diagnosis may be of relevance to at-risk family members. Pre- and post-test genetic counselling is part of the enrolling clinics where support and information is provided to assist with family communication strategies, and (4) the study may not identify an answer. However, that is the current clinical *status quo* without other investigative courses of action. Pre-test genetic counselling provides information on this outcome pre-test.

Identifying an underlying genetic cause for kidney disease is the first step in identifying the group of patients and families who may benefit from interventions to reduce the burden of disease. The HIDDEN study hopes to identify a number of patients with a monogenic cause for their kidney disease that are currently undiagnosed by standard care pathways. Diagnosis positively benefits the management of their kidney disease and the management of their family. In addition, we hope to establish the diagnostic utility for this investigation pathway and demonstrate how it can be integrated into standard clinical practice.

AUTHOR CONTRIBUTIONS

AnM, AmM, CQ, CS, CP, and ZS conceived the study and lead it. JS, SJ, LW, RO'S, and AW assisted with coordination and operation of the study. JS, SJ, RO'S, and AnM drafted the manuscript. All coauthors reviewed and edited the manuscript. All authors contributed to the article and approved the submitted version.

FUNDING

This study has been funded by an investigator-initiated Rare Disease Flagship Grant of the Australian Genomics Health Alliance. Additional research funding has been granted by the

Royal Brisbane and Women's Hospital Foundation in addition to in-kind support from the 18 participating Australian kidney genetics clinics.

ACKNOWLEDGMENTS

We wish to acknowledge all of the clinicians and investigators taking part in this study across Australia within the KidGen Collaborative. We also wish to acknowledge direct and in-kind support from the health services operating the participating kidney genetics clinics, The University of Queensland, RBWH Foundation, Murdoch Children's Research Institute, Royal Prince Alfred Hospital Department of Renal Medicine, Royal Children's Hospital Foundation, Melbourne Genomics, and Australian Genomics.

SUPPLEMENTARY MATERIAL

The Supplementary Material for this article can be found online at: https://www.frontiersin.org/articles/10.3389/fmed.2022.891223/full#supplementary-material

REFERENCES

1. Mallett A, Patel C, Salisbury A, Wang Z, Healy H, Hoy W. The prevalence and epidemiology of genetic renal disease amongst adults with chronic kidney disease in Australia. *Orphanet J Rare Dis.* (2014) 9:98. doi: 10.1186/1750-1172-9-98
2. Groopman EE, Marasa M, Cameron-Christie S, Petrovski S, Aggarwal VS, Milo-Rasouly H, et al. diagnostic utility of exome sequencing for kidney disease. *N Engl J Med.* (2019) 380:142–51.
3. de Haan A, Eijgelsheim M, Vogt L, Knoers NVAM, de Borst MH. Diagnostic yield of next-generation sequencing in patients with chronic kidney disease of unknown etiology. *Front Genet.* (2019) 10:1264. doi: 10.3389/fgene.2019.01264
4. ANZDATA Registry. *43rd Report, Chapter 1: Incidence of Renal Replacement Therapy for End Stage Kidney Disease*. Adelaide, SA: Australia and New Zealand Dialysis and Transplant Registry (2020).
5. Wyld ML, Lee CMY, Zhuo X, White S, Shaw JE, Morton RL, et al. Cost to government and society of chronic kidney disease stage 1-5: a national cohort study. *IMJ.* (2015) 45:741–7. doi: 10.1111/imj.12797
6. Australian Institute of Health and Welfare (AIHW). *My Hospitals Data Reports on Admitted Patients Table 4.8*. Canberra, ACT: AIHW (2020).
7. Schrezenmeier E, Kremerskothen E, Halleck F, Staeck O, Liefeldt L, Choi M, et al. The underestimated burden of monogenic kidney disease in adults waitlisted for kidney transplantation. *Genet Med.* (2021) 23:1219–24. doi: 10.1038/s41436-021-01127-8
8. Snoek R, van Jaarsveld RH, Nguyen TQ, Peters EDJ, Elferink MG, Ernst RF, et al. Genetics-first approach improves diagnostics of ESKD patients younger than 50 years. *Nephrol Dial Transplant.* (2020) 37:349–57. doi: 10.1093/ndt/gfaa363
9. Hays T, Groopman EE, Gharavi AG. Genetic testing for kidney disease of unknown etiology. *Kidney Int.* (2020) 98:590–600. doi: 10.1016/j.kint.2020.03.031
10. Stark Z, Dolman L, Manolio TA, Ozenberger B, Hill SL, Caulfied MJ, et al. Integrating genomics into healthcare: a global responsibility. *Am J Hum Genet.* (2019) 104:13–20. doi: 10.1016/j.ajhg.2018.11.014
11. Jayasinghe K, Stark Z, Patel C, Mallawaarachchi A, McCarthy H, Faull R, et al. Comprehensive evaluation of a prospective Australian patient cohort with suspected genetic kidney disease undergoing clinical genomic testing: a study protocol. *BMJ Open.* (2019) 9:e029541. doi: 10.1136/bmjopen-2019-029541
12. Jayasinghe K, Stark Z, Kerr PG, Gaff C, Martyn M, Whitlam J, et al. Clinical impact of genomic testing in patients with suspected monogenic kidney disease. *Genet Med.* (2021) 1:183–91. doi: 10.1038/s41436-020-00963-4
13. Khan K, Ahram DF, Liu YP, Westland R, Sampogna RV, Katsanis N, et al. Multidisciplinary approaches for elucidating genetics and molecular pathogenesis of urinary tract malformations. *Kidney Int.* (2022) 3:473–84. doi: 10.1016/j.kint.2021.09.034
14. Vivante A, Hildebrandt F. Exploring the genetic basis of early-onset chronic kidney disease. *Nat Rev Nephrol.* (2016) 12:133–46. doi: 10.1038/nrneph.2015.205
15. Ingelfinger JR, Kalantar-Zadeh K, Schaefer F. World Kidney Day Steering Committee. World Kidney Day 2016: averting the legacy of kidney disease — focus on childhood. *Pediatr Nephrol.* (2016) 31:343–8. doi: 10.1016/j.kint.2016.04.001
16. Groopman EE, Rasouly HM, Gharavi AG. Genomic medicine for kidney disease. *Nat Rev Nephrol.* (2018) 14:83–104.
17. Mann N, Braun DA, Amann K, Tan W, Shril S, Connaughton DM, et al. Whole-exome sequencing enables a precision medicine approach for kidney transplant recipients. *J Am Soc Nephrol.* (2019) 30:201–15. doi: 10.1681/ASN.2018060575
18. Ottlewski I, Münch J, Wagner T, Schönauer R, Bachmann A, Weimann A, et al. Value of renal gene panel diagnostics in adults waiting for kidney transplantation due to undetermined end-stage renal disease. *Kidney Int.* (2019) 96:222–30. doi: 10.1016/j.kint.2019.01.038
19. Wang Z, Xu H, Xiang T, Liu D, Xu F, Zhao L, et al. An accessible insight into genetic findings for transplantation recipients with suspected genetic kidney disease. *NPJ Genom Med.* (2021) 6:57. doi: 10.1038/s41525-021-00219-3
20. Connaughton DM, Kennedy C, Shril S, Mann N, Murray SL, Williams PA, et al. Monogenic causes of chronic kidney disease in adults. *Kidney Int.* (2019) 4:914–28. doi: 10.1016/j.kint.2018.10.031
21. Lata S, Marasa M, Li Y, Fasel DA, Groopman E, Jobanputra V, et al. Whole-exome sequencing in adults with chronic kidney disease: a pilot study. *Ann Intern Med.* (2018) 16:100–9. doi: 10.7326/M17-1319
22. Gast C, Pengelly RJ, Lyon M, Bunyan DJ, Seaby EG, Graham N, et al. Collagen (COL4A) mutations are the most frequent mutations underlying adult focal segmental glomerulosclerosis. *Nephrol Dial Transplant.* (2016) 31:961–70. doi: 10.1093/ndt/gfv325
23. McClellan WM, Satko SG, Gladstone E, Krisher JO, Narva AS, Freedman BI. Individuals with a family history of ESRD are a high-risk population for CKD: implications for targeted surveillance and intervention activities. *Am J Kidney Dis.* (2009) 53:S100–6. doi: 10.1053/j.ajkd.2008.07.059

Conflict of Interest: The authors declare that the research was conducted in the absence of any commercial or financial relationships that could be construed as a potential conflict of interest.

frontiers | Frontiers in Medicine

ORIGINAL RESEARCH
published: 09 June 2022
doi: 10.3389/fmed.2022.885178

The Clinical and Genetic Features in Chinese Children With Steroid-Resistant or Early-Onset Nephrotic Syndrome: A Multicenter Cohort Study

Xiujuan Zhu[1†], Yanqin Zhang[2†], Zihua Yu[3†], Li Yu[4†], Wenyan Huang[5†], Shuzhen Sun[6†], Yingjie Li[7†], Mo Wang[8†], Yongzhen Li[9†], Liangzhong Sun[10†], Qing Yang[11†], Fang Deng[12†], Xiaoshan Shao[13†], Ling Liu[14†], Cuihua Liu[15,16†], Yuanhan Qin[17†], Shipin Feng[18†], Hongtao Zhu[19†], Fang Yang[20†], Weimin Zheng[21†], Wanqi Zheng[22†], Rirong Zhong[23†], Ling Hou[24†], Jianhua Mao[1], Fang Wang[2*] and Jie Ding[2*]*

[1] Department of Nephrology, The Children Hospital of Zhejiang University School of Medicine, Hangzhou, China, [2] Department of Pediatrics, Peking University First Hospital, Beijing, China, [3] Department of Pediatrics, Fuzong Clinical Medical College, Fujian Medical University, Fuzhou, China, [4] Department of Pediatrics, Guangzhou First People's Hospital, Guangzhou, China, [5] Department of Nephrology and Rheumatology, Shanghai Children's Hospital, Shanghai Jiaotong University, Shanghai, China, [6] Department of Pediatric Nephrology and Rheumatism and Immunology, Shandong Provincial Hospital Affiliated to Shandong University, Jinan, China, [7] Guangzhou Women and Children's Medical Center, Guangzhou, China, [8] Department of Nephrology, Ministry of Education Key Laboratory of Child Development and Disorders, Chongqing Key Laboratory of Pediatrics, National Clinical Research Center for Child Health and Disorders, China International Science and Technology Cooperation Base of Child Development and Critical Disorders, Children's Hospital of Chongqing Medical University, Chongqing, China, [9] Department of Pediatrics, The Second Xiangya Hospital, Central South University, Changsha, China, [10] Department of Pediatrics, Nanfang Hospital, Southern Medical University, Guangzhou, China, [11] Department of Nephrology, The Second Affiliated Hospital and Yuying Children's Hospital of Wenzhou Medical University, Wenzhou, China, [12] Department of Nephrology, Anhui Provincial Children's Hospital, Hefei, China, [13] Department of Nephrology and Immunization, Guiyang Maternal and Child Health Care Hospital, Guiyang, China, [14] Department of Nephrology and Rheumatology, Children's Hospital of Hebei Province, Shijiazhuang, China, [15] Department of Nephrology and Rheumatology, Children's Hospital Affiliated to Zhengzhou University, Henan Children's Hospital, Zhengzhou Children's Hospital, Zhengzhou, China, [16] Zhengzhou Key Laboratory of Pediatric Kidney Disease Research, Zhengzhou, China, [17] Department of Pediatrics, The First Hospital of Guangxi Medical University, Nanning, China, [18] Chengdu Women's and Children's Central Hospital, School of Medicine, University of Electronic Science and Technology of China, Chengdu, China, [19] Department of Pediatrics, The First Affiliated Hospital of Xinjiang Medical University, Urumqi, China, [20] Department of Pediatrics, The First Affiliated Hospital of Jinan University, Guangzhou, China, [21] Department of Nephrology, Jiangxi Provincial Children's Hospital, The Affiliated Children's Hospital Nanchang University, Nanchang, China, [22] Department of Pediatrics, The Second Hospital of Dalian Medical University, Dalian, China, [23] Department of Pediatrics, Fujian Provincial Hospital, Fuzhou, China, [24] Department of Pediatrics, Shengjing Hospital of China Medical University, Shenyang, China*

OPEN ACCESS

Edited by:
Aihua Zhang,
Nanjing Children's Hospital, China

Reviewed by:
Qian Shen,
Fudan University, China
Changli Wei,
Rush University, United States

***Correspondence:**
Jianhua Mao
maojh88@zju.edu.cn
Fang Wang
wangfangped@163.com
Jie Ding
djnc_5855@126.com

[†]These authors have contributed equally to this work

Specialty section:
This article was submitted to Nephrology, a section of the journal Frontiers in Medicine

Received: *27 February 2022*
Accepted: *25 April 2022*
Published: *09 June 2022*

Citation:
Zhu X, Zhang Y, Yu Z, Yu L, Huang W, Sun S, Li Y, Wang M, Li Y, Sun L, Yang Q, Deng F, Shao X, Liu L, Liu C, Qin Y, Feng S, Zhu H, Yang F, Zheng W, Zheng W, Zhong R, Hou L, Mao J, Wang F and Ding J (2022) The Clinical and Genetic Features in Chinese Children With Steroid-Resistant or Early-Onset Nephrotic Syndrome: A Multicenter Cohort Study. Front. Med. 9:885178. doi: 10.3389/fmed.2022.885178

Steroid-resistant nephrotic syndrome (SRNS) is one of the major causes of end-stage kidney disease (ESKD) in children and young adults. For approximately 30% of children with SRNS results from a genetic cause. In this study, genotype-phenotype correlations in a cohort of 283 pediatric patients with SRNS or early-onset NS (nephrotic syndrome presenting within the first year of life) from 23 major pediatric nephrology centers in China were analyzed. All patients were performed with next-generation sequencing and Sanger sequencing. The overall mutation detection rate was 37.5% (106 of 283 patients). WT1 was the most frequently detected mutation, followed by NPHS1, NPHS2, and ADCK4, and these four major causative genes (WT1, NPHS1, NPHS2, and ADCK4) account for 73.6% of patients with monogenic SRNS. Thirteen of 106 individuals (12.3%) carried

mutations in ADCK4 that function within the coenzyme Q10 biosynthesis pathway. In the higher frequently ADCK4-related SRNS, two mutations, c.737G>A (p.S246N) and c.748G>C (p.D250H), were the most prevalent. Our study provides not only definitive diagnosis but also facilitate available targeted treatment for SRNS, and prediction of prognosis and renal outcome. Our indications for genetic testing are patients with FSGS, initial SRNS, cases of positive family history or those with extra-renal manifestations.

Keywords: steroid-resistant nephrotic syndrome, genetic testing, phenotype, prognosis, children

INTRODUCTION

Idiopathic nephrotic syndrome (INS) is characterized by a group of symptoms: massive proteinuria, hypoalbuminemia, edema, and hyperlipidemia (1, 2). Most pediatric cases respond well to steroids, and the long-term prognosis is favorable (3). However, about 10–20% of children who do not show complete remission of proteinuria following 4–8 weeks treatment with corticosteroids are considered to have steroid-resistant nephrotic syndrome (SRNS), with high risk of end-stage kidney disease (3, 4). Kidney biopsy of SRNS shows minimal change disease (MCD) or focal segmental glomerulosclerosis (FSGS) in majority of cases (3, 5). For ∼30% of children with SRNS, the condition results from a genetic cause, and who will not achieve remission after treatment with steroids and/or immunosuppression (6); and identification of these causative genes has provided fundamental insights into the pathogenesis of SRNS (3, 7–10).

Recently, increasing number of monogenic SRNS has been reported worldwide. To date, more than 60 monogenic causes of SRNS/FSGS have been identified, and novel causative genes are continually being discovered (3, 8, 11–13). Genetic testing for the children with initial SRNS, cases of positive family history with proteinuria and those with extra-renal manifestations is recommended, according to IPNA (International Pediatric Nephrology Association) clinical practice recommendations for the diagnosis and management of children with SRNS (14). In addition, most patients with early onset nephrotic syndrome presenting within the first year of life are caused by monogenic defects and resistant to immunosuppressive therapy, thus this condition is also an indication of genetic screening. The genetic testing about SRNS has been reported in America, Europe, and Asia such as in China, Korea, Japan and India (12, 13, 15–17). However, the high heterogeneity of genetic SRNS highlights the value of thoroughly delineating the correlations between genotype and phenotype based on large cohorts of patients with different ethnicities, molecular diagnosis and longitudinal follow-up. In this study we aimed to expand the genotypes of SRNS or early-onset NS in China and investigate potential correlations between genotype and phenotypes.

MATERIALS AND METHODS

Patients

Pediatric patients with SRNS or early-onset NS, undergoing next-generation sequencing analysis, from 23 major pediatric nephrology centers in China, recorded in an on-line registry of pediatric hereditary kidney diseases in China (http://chkd.tiamal.com/, set up in 2012) from January 1, 2018 to December 31, 2020 were recruited. All patients had fully developed nephrotic syndrome (NS) (24 h urinary protein excretion ≥50 mg/kg or urinary protein creatinine ratio ≥ 2 g/g plus serum albumin <30 g/L). SRNS is consist of resistance to conventional daily oral 2 mg/kg prednisone (maximum dose 60 mg/day) therapy either at the initial presentation (initial steroid non-responders) or during follow-up (late steroid non-responders). An initial non-responder is defined as "failure to achieve complete remission after 4–8 weeks of corticosteroid therapy", and a late non-responder is defined as "persistent proteinuria during 4 or more weeks of corticosteroids following one or more remissions" (18). Early-onset nephrotic syndrome is an uncommon disorder with onset of the nephrotic syndrome presenting within the first year of life. Demographics, clinical presentations at first visit to the participating centers, response to immunosuppressive agent, kidney biopsy information if performed, the last follow-up data, family history, parental consanguinity and genetic data were collected. The age-adjustment of serum creatinine concentrations based Chronic Kidney Disease Epidemiology Collaboration equation was used to estimate the glomerular filtration rate (19). When the patients were younger than 2 years, kidney dysfunction was defined as serum creatinine increasing >30% from the upper reference limits related to age and gender (20). For evaluation of renal outcomes, the primary end point included a set of major morbidity events such as reaching ESKD, renal replacement therapy (RRT, hemodialysis, peritoneal dialysis, kidney transplantation), and mortality from renal cause.

Genomic DNA was isolated from blood lymphocyte in all participants and subjected to exome capture using Agilent's SureSelect human all exon kit V5 and NimbleGen technology followed by next generation sequencing on the Illumina HiSeq 2500 platform. The genetic test results which were detected by next-generation sequencing and Sanger sequencing in the DNA diagnostic laboratories were collected and classified according to the American College of Medical Genetics and Genomics (**ACMG**) guidelines (21). The patients harbored pathogenic or likely pathogenic sequence variants plus consistent with the reported inheritance were considered establishing a genetic diagnosis.

The procedures were approved by the ethics committees of the 23 centers. The informed consent was obtained from the patients or their family members.

Statistical Analysis

To determine significant differences between groups with or without pathogenic variants, categorical variables were analyzed using the chi-square test or Fisher's exact test, and continuous variables were compared using the *t*-test or Mann–Whitney *U*-test. All values are reported as the median (interquartile range, IQR).

RESULTS

Cohort Description

Totally 283 pediatric patients (male: female = 151:132) from 280 families were recruited from the 23 major pediatric nephrology centers in China. All patients had fully developed early-onset NS or SRNS. Among the patients with available respective information, parental consanguinity was not reported, and 30 (10.6%) patients had a family history of proteinuria and/or renal failure (**Table 1** and **Figure 1**).

Phenotypes

The clinical features of 283 patients [including 92 cases reported from our previous study (13)] are summarized in **Table 1**. Among them, 35 (12.4%) patients showed congenital onset, 29 (10.2%) patients manifested as infantile onset, 91 (32.2%) at age of 1–2 years. The number decreased to 46 cases (16.3%) at age 3–5 years, 72 (25.4%) at age 6–12 years and 10 (3.5%) patients at age 12–18 years.

Among 283 patients recruited in the present study, 29 patients were not given steroid therapy because they presented with congenital onset ($n = 24$), 4–12 months ($n = 2$), CKD ($n = 1$) and 2 patients deny steroid therapy. Then as described in **Figure 2**, conventional steroid therapy was administered to 254 patients and all showed steroid resistance, consist of initial SRNS (189 patients) and late SRNS (23 patients) and 42 patients of SRNS not known initial or secondary. Among the 254 patients, 74 patients were not given immune therapy, 64 patients showed response to immune therapy, and 116 patients showed no response to immune therapy. Of the patients who responded to immunotherapy whereas presented with initial/secondary SRNS or without steroid therapy, the genetic diagnosis was established in 3 children (**Supplemental Table 1**). Patient 9th had the compound heterozygous pathogenic NPHS1 mutation (c.2515delC, p.Q839 Rfs*8 and c.928G>A, p.D310 N), developed NS at age of 2 month, Kidney biopsy was not performed and was then only given tacrolimus treatment from age of onset, proteinuria decreased and complete remission of proteinuria was observed after one year, this patient had a normal renal function after a 2-year follow up. Patient 232th displayed with initial SRNS and was given tacrolimus treatment**,** complete remission of proteinuria was observed, compound heterozygous pathogenic NPHS2 mutation (c.370T>C, p.C124R and c.535-1G>T) was detected in this boy, with the renal biopsy revealing mild mesangial proliferative glomerulonephritis and renal function was normal after one-year follow up. Patient 57th, a 7-year-old boy, was admitted to hospital for proteinuria due to nephrotic syndrome, then displayed with late-SRNS. Renal biopsy revealed Lipoprotein glomerulopathy. DNA sequence studies revealed a heterozygous pathogenic missense mutation of ApoE (c.127C>T, p.R43C).

Renal biopsy was performed in 187 (66.1%) patients, which included 97 cases of FSGS, 42 cases of MCD, and 23 patients with mesangial proliferative glomerulonephritis (MsPGN). Renal biopsy was done in 85% cases aged older than 3 years, 66.3% aged 1–2 years, and 22.2% in infant, respectively. Genetic abnormalities were found in 37.4% of patients with FSGS, 30% of patients with MsPGN, and 9.3% of patients with MCD. FSGS counts for 71.5% in the patients with an identified genetic mutation, whereas only 44.4% in the patients without genetic mutation. MCD was seen in 3.7% of the patients with a genetic diagnosis (4/107), all manifested at age of 6–12 years old. **Table 2** summarized the data on the genetic disease detection rate from the previous large cohort studies and compared to the present study (12, 15, 22).

The median duration of follow-up from the onset was 2.1 years (IQR 1.2–3.4 years) in present study. 96 patients had maintained a normal estimated glomerular filtration rate (eGFR), 28 patients progressed to CKD stages 2–4, 48 patients progressed to ESKD and RRT, 27 patients end with mortality. Among the children who underwent mutation screening, the patients with an identified gene mutation are more likely to step into renal dysfunction: 9 patients (8.5%) with CKD, 28 patients (26.4%) with ESKD or RRT, and 16 (15.1%) patient end with mortality. Conversely in the patients not identified: 19 (10.7%) in patients with CKD stages 2–4, 20 (11.3%) in patients with ESKD or RRT and 11 patients (6.2%) end with mortality. SRNS children with identified causative genes showed worse long-term outcome than the patients without causative genetic mutation.

Genotypes

The distribution of the detected causative genes was evaluated in **Table 3**. The overall detection rate of disease-causing mutations was 37.5% (106 of 283 patients). Among 106 patients with disease-causing mutations, 44 (41.5%) patients had AD mutations, 56 (52.8%) patients had AR mutations, and 6 (5.6%) patients had X-linked or mitochondrial mutations. WT1 was the most common causative gene (11.3%, 32 patients), followed by NPHS1 (6.4%, 18 patients), NPHS2 (5.3%, 15 patients), ADCK4 (4.6%, 13 patients), TRPC6 (2.1%, 6 patients) and others. Among these, mutations from 25 patients had been reported in our previous study (13).

Genotype-Phenotype Correlations

To examine genotype-phenotype correlations, the 7 most frequently mutated genes (WT1, NPHS2, NPHS1, TRPC6, ACTN4, ADCK4 and LAMB2) were evaluated in **Table 3**. In the patient with AD mutations, 6.8% patients showed congenital onset, and 15.9% showed infantile onset. This fraction changed to 43.2% at age 1–5 years, 29.5% at age 6–12 years, and 4.5% at age 12–18 years. For the AR mutations, 39.3% patients showed congenital onset, and 10.7% showed infantile onset. This fraction decreased to 26.8% at age 1–5 years, 19.6% at age 6–12 years, and 3.6% at age 12–18 years. The distribution of causative genes within the first 3 months of life was as follows: NPHS1 ($n = 17$), WT1 ($n = 3$), NPHS2 ($n = 2$), LAMB2 ($n = 2$), ADCK4 ($n =$

TABLE 1 | Genotype-phenotype correlations in pediatric patients with steroid-resistant nephrotic syndrome.

		CNS *n* = 35(12.4%)		Infantile *n* = 29 (10.2%)		1–2 years *n* = 91 (32.2%)		3–5 years *n* = 46 (16.3%)		6–12 years *n* = 72 (25.4%)		≥12 years *n* = 10 (3.5%)		Total patient *n* = 283		*P*-value
		Mutation (–) *n* = 10	Mutation (+) *n* = 25	Mutation (–) *n* = 16	Mutation (+) *n* = 13	Mutation (–) *n* = 70	Mutation (+) *n* = 21	Mutation (–) *n* = 31	Mutation (+) *n* = 15	Mutation (–) *n* = 43	Mutation (+) *n* = 29	Mutation (–) *n* = 7	Mutation (+) *n* = 3	Mutation (–) *n* = 177	Mutation (+) *n* = 106	
Sex	Male:female	7:3	15:10	5.11	7:6	42:28	8.13	16.15	8:7	29:14	11.18	2:5	1:2	101:76	50:56	
Response to steroid	No treatment	6	18	0	2	0	0	2	0	0	1	0	0	8 (4.5%)	21 (19.8%)	
	Initial non-respond	3	5	14	9	50	16	16	14	36	19	4	3	123 (69.5%)	66 (62.3%)	
	Late non-responder	0	0	2	0	7	0	7	0	4	1	2	0	22 (12.4%)	1 (0.9%)	
	Data unavailable	1	2	0	2	13	5	6	1	3	8	1	0	24 (13.6%)	18 (17.0%)	
Response to immune therapy	No treatment	7	22	9	8	11	9	7	4	9	12	1	1	44 (24.9%)	56 (51.9%)	
	Responder	0	1	1	0	28	1	12	0	19	0	3	0	63 (35.6%)	2 (1.9%)	
	Non-responder	3	2	6	5	31	11	12	11	15	17	3	2	70 (39.5%)	48 (46.2%)	<0.001[a]
Kidney biopsy	FSGS	1	1	5	3	18	6	16	9	19	15	1	3	60 (33.9%)	37 (34.9%)	<0.01[f]
	MCD	0	0	1	0	17	0	8	0	10	4	2	0	38 (21.5%)	4 (3.8%)	<0.01[f]
	MsPGN	0	1	0	2	9	3	4	0	2	1	1	0	16 (9%)	7 (6.6%)	
	Others	1	0	0	0	6	1	0	2	10	1	3	0	20 (11.3%)	4 (3.8%)	
	Not done	8	23	10	8	20	11	3	4	1	8	0	0	42 (23.7%)	54 (51.0%)	
Family history	Yes	1	1	3	2	6	4	3	1	3	6	0	1	16 (8.8%)	14 (13.2%)	
	No	8	24	12	10	60	17	27	14	39	22	7	2	153 (86.2%)	90 (84.9%)	<0.01[d]
	Data unavailable	1	0	1	1	4	0	1	0	1	1	0	0	8 (4.5%)	2 (1.8%)	
Extrarenal manifestations	Yes	4	8	2	5	5	4	5	6	7	3	0	0	23 (11.5%)	26 (24.5%)	
	No	6	17	14	8	65	17	26	9	36	26	7	4	154 (87%)	80 (75.5%)	<0.001[e]
Renal outcome at follow-up	Normal eGFR	1	5	7	3	31	5	11	8	16	7	2	0	68 (38.4%)	28 (26.4%)	
	CKD stages 2–4	0	0	1	1	3	0	6	1	7	5	2	2	19 (10.8%)	9 (8.5%)	<0.01[b]
	ESKD/RRT	0	0	1	3	7	10	6	4	6	11	0	0	20 (11.3%)	28 (26.4%)	<0.01[c]
	Mortality	4	8	2	3	5	3	0	1	0	1	0	0	11 (6.2%)	16 (15.1%)	
	Data unavailable	5	12	5	3	24	3	8	1	14	5	3	1	59 (33.3%)	25 (23.6%)	
Renal transplantation	Yes	0	0	0	1	3	7	0	0	1	6	0	0	4 (2.2%)	14 (13.2%)	
	No	6	20	11	10	34	12	18	11	37	19	4	2	110 (62.1%)	74 (70%)	
	Data unavailable	4	5	5	2	33	2	13	4	5	4	3	1	63 (35.6%)	18 (17.0%)	

[a] *respond to immune thearpy group vs. non-responders.*
[b] *normal eGFR vs. CKD stage 2–4.*
[c] *CKD stage 2–4 vs. groups(ESKD+Mortality).*
[d] *groups with family history vs. groups without family history.*
[e] *groups with extrarenal manifestations vs. groups without extrarenal manifestations.*
[f] *FSGS vs. MCD.*

CNS, congenital nephrotic syndrome; FSGS, focal segmental glomerulosclerosis; MCD, Minimal change disease; MsPGN, Mesangial proliferative glomerulonephritis; eGFR, estimated glomerular filtration rate; CKD, chronic kidney disease; ESKD, end-stage renal disease; RRT, Renal replacement therapy (hemodialysis, peritoneal dialysis, kidney transplantation).

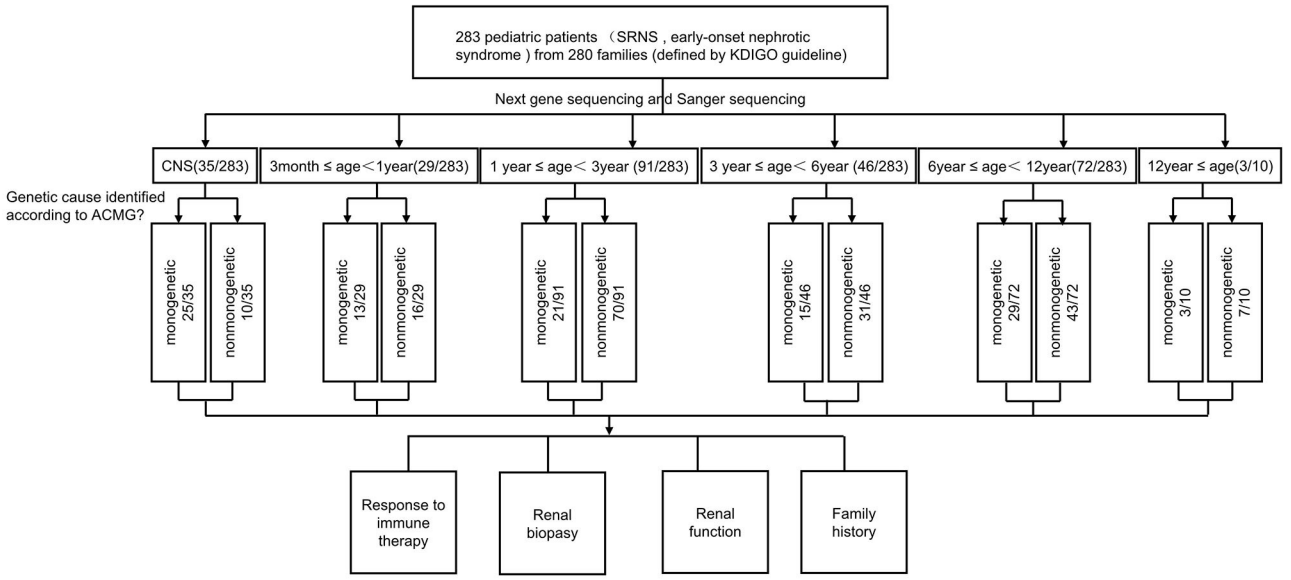

FIGURE 1 | Flow chart of patients by phenotype at presentation, age, and genetic diagnosis.

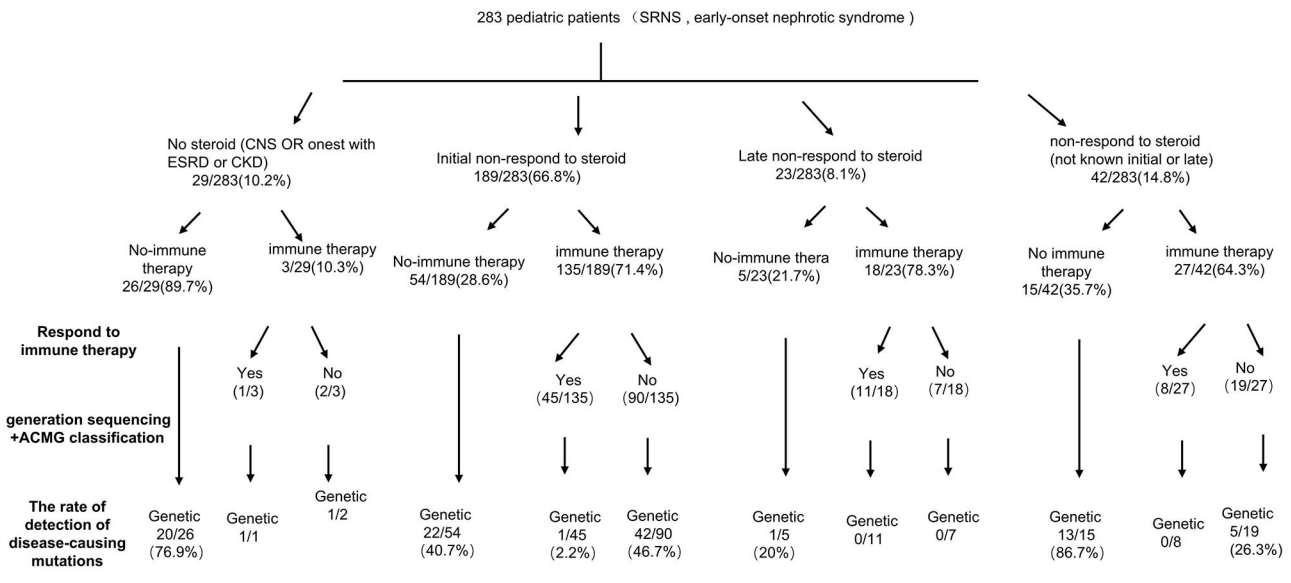

FIGURE 2 | A precision medicine-based guide to investigation of SRNS.

1). Patients with AR mutations are more likely to display with congenital-onset SRNS, especially NPHS1, 17 (94.4%) onset at <3 months old.

FSGS was the most common pathological finding on renal biopsy in this cohort study, 34% for AD mutation and 32.1% for AR mutation. But in AR mutation, 32 (57.1%) biopsy was not performed most likely because of the high risk of percutaneous renal biopsy in patients with congenital-onset SRNS.

For WT1 mutations, 12 participants revealed non-truncating transcriptional variants and 20 participants revealed truncating mutation, 10 patients with non-truncating mutation show almost onset <3 years old (**Table 4**), 20 patients with truncating mutation show a wide distribution from 3 months to 12 years onset. 9 patients with truncating mutation end with ESKD/RRT or death. For the 18 NPHS1-related SRNS comprised of 17 CNS, all displayed with compound heterozygous mutation, 2 patients were lost to follow-up.

For the NPHS2 mutations, patients carried truncating mutation showed onset at earlier age, 4 cases carried compound

TABLE 2 | Age at onset, comparison with previous large studies.

	The age of onset	Present study	Eujin Park (Korea)	China Nagano (Japan)	Carolin E
Percent with causative mutation detectation	1–3 m	25/35 (71.4%)	27/35 (77.1%)	11/13 (84%)	163/235 (69.5%)
	3 m−1 y	13/29 (44.8%)	11/25 (44%)	8/15 (53%)	81/163 (49.6%)
	1–3 y	21/91 (23.1%)	40/114 (35%)*	23/89 (26%)	177/700 (25%)
	3–6 y	15/46 (32.6%)		6/36 (17%)	56/315 (17.7%)
	6–12 y	29/72 (40.3%)	15/36 (27.7%)	16/52 (31%)	19/176 (11%)
	12–18 y	3/10 (33.3%)	2/3 (66.7%)	3/15 (20%)	6/28 (21.4%)
CNS	NPHS1 (17/25)	WT1 (15/31)	NPHS1 (4/11)	NPHS1 (94/163)	
	WT1 (3/25)	NPHS1 (11/31)	LAMB2 (4/11)	NPHS2 (25/163)	
	NPHS2 (2/25)	COQ3 (3/31)	WT1 (2/11)	WT1 (20/163)	
	LAMB2 (2 /25)	LAMB2 (2/31)	LAMA5 (1/11)	LAMB2 (13/163)	
	ADCK4 (1/25)				

CNS, congenital nephrotic syndrome.
**The percent of causative mutation detectation rate at age of oneset of 3–6 years.*

heterozygous mutation step into ESKD or was given renal replacement therapy.

As for ADCK4 mutations, it can be detected in 13 (4.6%) in the SRNS. 6 patients present with homozygous and 7 patients displayed with compound heterozygous mutations. In present study, all 13 cases carried c.737G>A (p.S246N) and/or c.748G>C (p.D250H), 6 (42%) cases progressed to ESKD <1 years after diagnosis and 6 patients has family history of proteinuria (**Figure 3**).

Twenty-six patients (24.3%) with genetic-SRNS have extrarenal manifestations, mainly in WT1, SMARCAL1 and LAMB2. Thirty-seven percent of WT1-related SRNS showed genital abnormalities or a predisposition to Wilms tumor, 2 cases of SMARCAL1-related SRNS showed growth failure and poor cellular immunity. As to the three LAMB2-related SRNS, the age of onset was all younger than 1 years old, 2 of them with bilateral microcoria, presented with Pierson syndrome.

In our cohort study, five families of SRNS with disease-causing collagen COL4A5 mutations were identified. Extrarenal manifestations and family history of kidney disease were denied in these 5 patients. Light microscopy showed FSGS in 4 patients and MCD in 1 patient, while 1 patient revealed GBM lamellation, another showed segmental thickening in GBM.

A mutation in the CLCN5 gene was detected by exome sequencing in a family that had been defined as SRNS on clinical grounds. Patient 85th carried c.1942 C>T from his mother, and the light microscopy in this 10-year-old male with a CLCN5 mutation was MCD.

In family 48th, we detected a PAX2 splice mutation (c.70dupG). The patient presented with SRNS at the age of 4 year. Renal biopsy showed FSGS. The patient's father was diagnosed as ESKD.

DISCUSSION

In this cohort study, 283 children with SRNS or early-onset nephrotic syndrome were recruited from 23 pediatric nephrology centers in China, and 106 cases (37.5%) were identified with monogenic mutation. Specifically, the genetic finding of CNS was 71.4% in our study, the fraction of causative gene is only 23.1% at patients aged 1–3 years, and 35.8% at patients aged 3–18 years. Four major causative genes (WT1, NPHS1, NPHS2, and ADCK4) account for 73.6% of patients with monogenic SRNS. Among the 13 cases (12.3%) with ADCK4 mutation, 6 families with homozygous mutations and 7 families with compound heterozygous mutations, further, they all carried either **c.737G>A** (S246N) or **c.748G>C** (D250H) mutation.

Our previously cohort study enrolled 110 children with SRNS and 10 children with isolated proteinuria from 5 centers in China, and genetic etiology was identified in 28.3% patients and the most common mutated genes were ADCK4 (6.67%), NPHS1 (5.83%), WT1 (5.83%), and NPHS2 (3.33%), which was quite different from this study. In 2019, national cohort of children with renal disease from 13 different regions of China were recruited from 2014 to 2018, ADCK4, WT1 and NPHS1 were the top three commonly mutated genes in the SRNS group with mutation rates of 5.7, 5.4, and 2.8%, respectively (17). One possible explanation for this discrepancy is the geographical differences in our two series: two-thirds of the participants (80 of 120 cases) in our previous series came from Northern China, whereas more than 50% of the participants (157 of 283 cases) in this study came from Southern China. While in the study reported by Jia Rao, 89.9% of the participants come from Eastern China. In addition, more individuals of SRNS in the present study were recruited than before, which might be the second cause for discrepancy. Age at first disease manifestation present almost half between 1 and 6 years of age in our previous study and this study, 10.2% were at early infantile and 25% at age 6–12 years in this study, 15% at early infantile and 28.3% at age 6–12 years in our previous cohort, which might be the third cause.

The genetic detection rate of CNS was 71.4% in our study. The distribution of causative genes of CNS was NPHS1, WT1, NPHS2, LAMB2 and ADCK4, respectively. According the study reported by Eujin Park (15) in 2020, WT1 was the most commonly mutated gene in CNS, followed by NPHS1, COQ3 and LAMB2. While in the study by Nagano C from Japan

TABLE 3 | Genotype-phenotype correlations in pediatric patients with steroid-resistant nephrotic syndrome of AD mutation and AR mutation.

		AD					AR					
		WT1 (*n* = 32)	**TRPC6 (*n* = 6)**	**ACTN4 (*n* = 3)**	**Others (*n* = 3)**	**Total (*n* = 44)**	**NPHS1 (*n* = 18)**	**NPHS2 (*n* = 15)**	**ADCK4 (*n* = 13)**	**LAMB2 (*n* = 3)**	**Others (*n* = 7)**	**Total (*n* = 56)**
Sex	Male:Female	8:24	4:2	1:2	2:1	15:29	14:4	9:6	4:9	0:3	5:2	32:24
Age of onset	1–3 m	3	0	0	0	3 (6.8%)	17	2	1	2	0	22 (39.3%)
	3 m–1 y	6	1	0	0	7 (15.9%)	0	3	1	1	1	6 (10.7%)
	1–2 y	9	2	0	0	11 (25%)	0	5	3	0	2	10 (17.9%)
	3–5 y	5	1	1	1	8 (18.2%)	1	0	2	0	2	5 (8.9%)
	6–12 y	7	2	2	2	13 (29.5%)	0	3	6	0	2	11 (19.6%)
	≥12 y	2	0	0	0	2 (4.5%)	0	2	0	0	0	2 (3.6%)
Kidney biopsy	FSGS	8	4	2	1	15 (34%)	1	6	5	1	5	18 (32.1%)
	MCD	1	0	0	0	1 (2.2%)	0	1	0	0	0	1 (1.8%)
	MsPGN	1	0	0	0	1 (2.2%)	1	3	1	0	0	5 (8.9%)
	Others	3	1	0	1	5 (11.3%)	0	0	0	0	0	0
	Not done	19	1	1	1	22 (50%)	16	5	7	2	2	32 (57.1%)
Renal outcome at follow-up	Normal eGFR	6	1	0	2	9 (20.5%)	4	8	3	0	3	18 (32.1%)
	CKD stages 2–4	4	0	0	0	4 (9.1%)	2	0	0	1	1	4 (7.1%)
	ESKD/RRT	9	5	2	1	17 (38.7%)	0	5	6	0	2	13 (23.2%)
	Mortality	8	0	1	0	9 (20.5%)	6	0	0	0	1	7 (12.5%)
	Data unavailable	5	0	0	0	5 (11.4%)	6	2	4	2	0	14 (25%)
Family history	Yes	2	0	0	1	3 (6.7%)	0	5	6	0	1	12 (21.4%)
	No	29	6	3	2	40 (91%)	17	10	7	2	5	31 (55.4%)
	Data unavailable	1	0	0	0	1 (2.2%)	1	0	0	1	1	3 (5.3%)
Extrarenal manifestations	Yes	12	0	0	0	12 (27.2%)	4	4	0	2	3	13 (23.2%)
	No	20	6	3	3	32 (72.7%)	14	11	15	1	4	43 (76.8%)
Renal transplantation	Yes	2	3	0	0	5 (11.4%)	0	3	2	0	2	9 (16.1%)
	No	24	2	3	3	32 (72.7%)	12	8	8	0	2	30 (53.6%)
	Data unavailable	6	1	0	0	7 (15.9%)	5	4	3	3	3	17 (30.3%)

AD, autosomal dominant; AR, autosomal recessive.FSGS, focal segmental glomerulosclerosis; MCD, Minimal change disease; MsPGN, Mesangial proliferative glomerulonephritis; eGFR, estimated glomerular filtration rate; CKD, chronic kidney disease; ESKD, end-stage renal disease;RRT, Renal replacement therapy (hemodialysis, peritoneal dialysis, kidney transplantation).

(23), NPHS1, LAMB2 and WT1 was the most commonly gene detected in CNS. So, the genetic detection rate and the leading genes in CNS vary among different countries and district worldwide. In present study, 11 CNS patients were treated with steroid but no response happened, therefore, identification of the causative mutation may avoid unnecessary initiation or extension of steroid treatment.

The fraction of causative gene is 59.3% in in the first year of life, and 26.3% at patients aged 2–6 years, 39.1% at age 7–18 years. In 2020, in the study reported by Eujin Park (15), 291 Korean pediatric patients with SRNS/FSGS were analyzed, the mutation detection rate onset at age 6–18 years is 43.5%. however, In the Caroline E's study (12), an international cohort of 1783 families were included, disease-causing mutation in 61.3% of children in the first year of life. This fraction decreased to approximately 25% at age 2–5 years, to 12.3% at age 6 and older groups, these participants did not include patients from Russia, China, sub-Saharan Africa, or Pacific Rim countries. The difference between the studies may be due, at least in part, to differences in geographical distribution.

The mortality rate is 33% in the patients with NPHS1 mutation, whereas 11.1% (10/90) in the groups with other gene mutation in our present study and 16% (6/37) of the children with NPHS1 mutations in a nationwide retrospective study conducted by Bérody S (24). Children who had *NPHS2* heterozygous mutations had significantly lower renal survival than those of children with homozygous mutations, well in line with previous cohort studies (25). Of cases with ADCK4 mutation, 46.1% presented with ESRD/RRT, compared with 40% of WT1 and 33.3% of NPHS2 cases, whereas 38.5% of ADCK4 disease progressed to ESRD, compared with 15.6% of WT1 and 2.9% of NPHS2 cases in a study of 534 consecutive SRNS cases (26).

In our study, 2 monogenic SRNS cases (1 for NPHS1 and 1 for NPHS2 mutation) responded fully to tacrolimus. It was reported that SRNS with WT1 mutation were more likely to respond to Calcineurin inhibitors (CNIs), followed by PLCE1, NPHS1, NPHS2 (27). It seems that CNIs can ameliorate proteinuria by affecting podocyte proteins, instead of immune mechanism in monogenetic SRNS. Several studies

TABLE 4 | Mutation screening results.

		WT1		NPHS1		NPHS2				ADCK4	
		Heterozygous		Compound heterozygous		Hom mutation		Compound heterozygous		Hom mutation	Compound heterozygous
		Non-truncating (*n* = 12)	Truncating (*n* = 20)	Truncating +truncating (*n* = 9)	Truncating +missense (*n* = 9)	Missense (*n* = 2)	Truncating (*n* = 4)	Truncating + truncating (*n* = 5)	Truncating + missense (*n* = 4)	Missense (*n* = 6)	Missense + missense (*n* = 4)	Truncating + missense (*n* = 3)
Age of onset	1–3 m	2	1	9	8	0	0	1	1	1	0	0
	3 m–1 y	3	3	0	0	0	3	0	0	0	0	1
	1–2 y	5	4	0	0	0	1	2	2	2	1	0
	3–5 y	0	3	0	1	0	0	1	0	1	0	1
	6–12 y	1	6	0	0	1	0	1	1	2	3	1
	≥12 y	1	1	0	0	1	0	0	0	0	0	0
Renal Outcome at follow-up	Normal eGFR	1	5	2	2	1	2	3	2	2	1	0
	CKD stages 2–4	1	3	0	1	0	0	0	0	0	0	0
	ESKD/RRT	2	6	1	0	0	1	2	2	2	2	2
	Mortality	5	3	3	3	0	0	0	0	0	0	0
	Data unavailable	3	3	3	3	1	1	0	0	2	1	1

CKD, chronic kidney disease; ESKD, end-stage kidney disease; RRT, Renal replacement therapy (hemodialysis, peritoneal dialysis, kidney transplantation).

reported non-immunomodulatory mechanisms of CNIs on renal protection. Faul et al. have reported that CsA blocks the calcineurin-mediated dephosphorylation of synaptopodin, which is easy to be degraded and participated in the podocyte injury and proteinuria (28). Treatment with tacrolimus can suppress the redistribution of Nephrin, Podocin and other slit diaphragm components and then ameliorate proteinuria (29). However, there is still a far way to look for effective therapy for genetic kidney disease.

Compared with studies from other countries, one of the most striking findings in this study was the high prevalence of ADCK4 mutations, as identified in 12.3% of patients with monogenic SRNS, and in 4.6% of all SRNS in children. Similar with our study, 20 patients (5.8%) with biallelic mutations of ADCK4 was screened for in the Chinese children with SRNS, non-nephrotic proteinuria, or CKD of unknown origin by Raojia et al. in 2020 (30), two mutations, namely c.737G>A (p.S246N) and c.748G>C (p.D250H), were the most prevalent in these two studies. In the study by Eujin Park (15) in 2020, 291 Korean children with SRNS or FSGS was recruited, ADCK4 accounts 6.3% of the patients with mutations and 6 patients carried S246N mutation. In 2020, A total of 230 patients (22) (CNS, INS, SRNS, FSGS, or asymptomatic proteinuria with likely genetic disease) in Japan were included. ADCK4 accounts 2.4% of the patients with mutations, and these four cases showed compound heterozygous mutations and all carried S246N mutation. On the contrary, mutations in ADCK4 accounted for only 0.3% of patients in the PodoNet Registry study (31), while 1655 patients were registered and underwent comprehensive screening for a panel of 31 podocyte genes in 2015. ADCK4 mutations were found in 26 patients from 12 families (1.9%) from France, Turkey and Germany, c.1339dupG (p.E447Gfs*10) and c.532C>T (p.R178W) were the most prevalent mutation (26).

According to literature, ADCK4-related nephropathy usually presents in adolescence (median age, 14.1 years) (26). In our study, most ADCK4-related SRNS presented from 1 to 12 years old (IQR 2.3–7 years), and one case showed CNS, significantly younger at time of diagnosis. Furthermore, 6 cases progressed to ESKD <1 year after diagnosis. The fact that all 13 cases of our study carried S246N and D250H mutation, may prompt us to find more precise diagnosis and therapy to ADCK4-related SRNS.

In our overall cohort, 7 of 106 (6.6%) cases could be explained as phenocopies. 5 cases were genetically proven Alport syndrome (AS) that presented as SRNS clinically at onset without family history of hematuria and proteinuria. Among them, 4 cases proved to be FSGS and 1 case with MCD on renal biopsy. It is reported that, rare variants in COL4A3 and COL4A4 may be disease-causing in the patients with familial FSGS (32). In our study, variants in COL4A4 may be disease-causing, the symptoms of AS are atypical at early stage to be neglected and SRNS occurred due to primary GBM defect. It is known that mutations in LAMB2 can cause FSGS, (33) the GBM provide a mechanical foothold for its adjacent cells such as podocyte, LAMB2 and COL4A4 are the components of the GBM, the mutation of COL4A4 may cause glomerular disease through the same or different functional pathway, some mechanism study need to be further studied. One patient in present study was

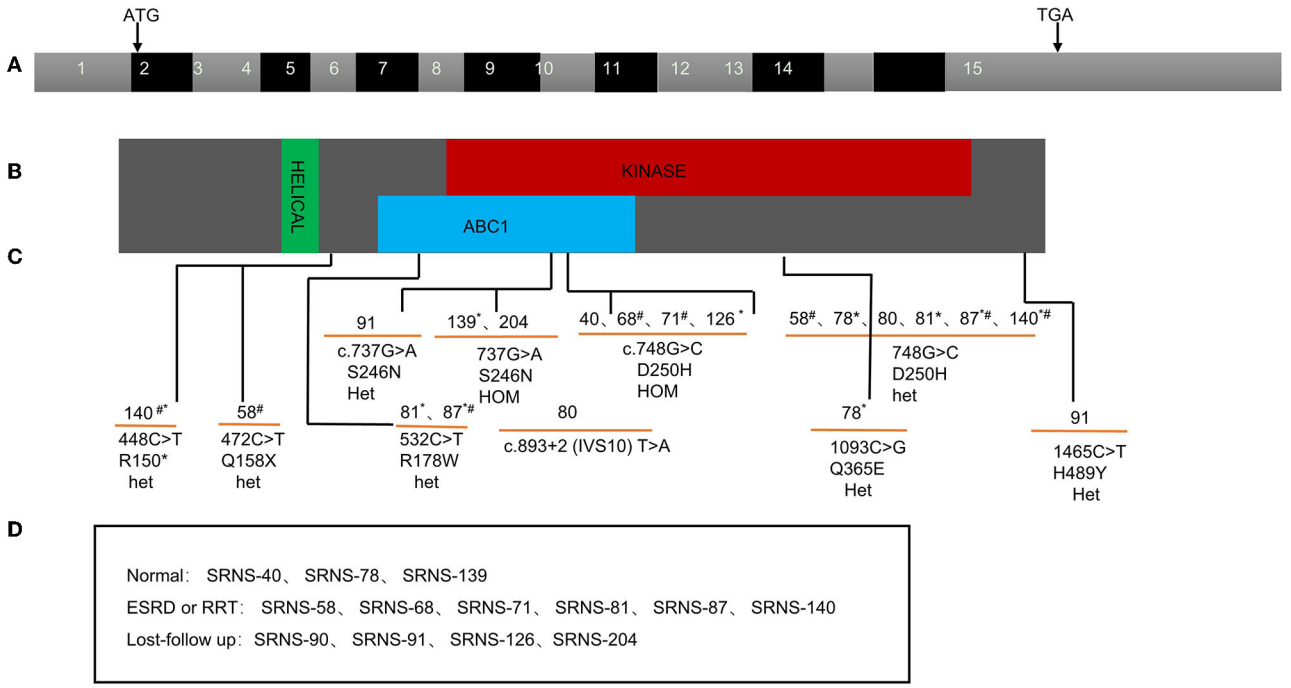

FIGURE 3 | ADCK4 mutation found in pediatric SRNS in China. Exon capture revealed ADCK4 mutations as causing SRNS and CNS. **(A)** Exon structure of human ADCK4 cDNA which contains 15 exons. Positions of start codon (ATG) and of stop codon (TGA) are noted. **(B)** Domain structure of the ADCK4 protein. Extent of predicted domains, helical, ABC1, and kinase is depicted by colored bars, in relation to encoding exon position. **(C)** 13 different ADCK4 mutations with SRNS or or early-onset nephrotic syndrome. **(D)** The renal outcome of the patients during the follow-up. *Family history of proteinuria; #Ending into ESKD or RRT during follow-up.

genetically proved Dent disease displaying clinical feature as SRNS. Mutations in CLCN5, which was encodes a voltage-gated chloride ion channel in the renal tubule, are the major cause of Dent disease. More than 50% patients with Dent disease will present with nephrotic-range proteinuria, which is the important reason for misdiagnosis as SRNS. One mutation in the CLCN5 gene (c.2000delC) was reported in a family of SRNS by the PodoNet cohort (34), and our case illustrated similar phenotypic traits at all (35). To our knowledge, 3 different mechanisms might explain patients with phenocopies: one for misdiagnosis: clinical or genetic misdiagnosis; the second for concomitant of two different diseases; the third one is the real phenocopy as causality was not established between certain phenotypes and genotypes. After all, phenocopy is common, and it should be careful to define the relation between phenotype and genotype in children with monogenic SRNS.

In 2020, IPNA clinical practice recommendations for the diagnosis and management of children with steroid-resistant nephrotic syndrome was published (14), and genetic testing is recommended for patients with initial SRNS, cases of positive family history and those with extra-renal manifestations, but not for patients with secondary steroid resistance. In the present study, 23 patients showed secondary steroid resistance. Among them, only 1 patient was identified carrying pathogenic mutation of ApoE. In our study, the mutation detection rate was higher in patients with FSGS than in patients with MCD (38.1 vs. 9.5%, $p < 0.01$). So, the patients with FSGS, initial SRNS, cases of positive family history or those with extra-renal manifestations are more likely to due to the genetic cause. In clinical practice, these patients are suggested to do genetic testing.

This study also had some limitations. First, 84 study participants in the present study were lost to follow-up, Thus, there was no chance to observe the effect of treatment and the renal outcome. Second, because our study is retrospective, it is inevitable that data may be missing and there is possibility for information bias. In addition, it is not feasible to complete multivariate analysis in order to find the factors those relate with the gene variants in SRNS.

In conclusion, the overall mutation detection rate in this cohort of Chinese children with SRNS was 37.5%. WT1 was the most frequently detected mutation, followed by NPHS1, NPHS2, and ADCK4. In the higher frequently ADCK4-related SRNS (12.3% in monogenic SRNS), two mutations, c.737G>A (p.S246N) and c.748G>C (p.D250H), were the most prevalent. The detection rate of ADCK4 was quite higher than the rate from Western country. Our indications for genetic testing are patients with FSGS, initial SRNS, cases of positive family history or those with extra-renal manifestations.

DATA AVAILABILITY STATEMENT

The raw data supporting the conclusions of this article will be made available by the corresponding authors on reasonable request.

ETHICS STATEMENT

The studies involving human participants were reviewed and approved by Ethics Committees of the 23 centers in this study. Written informed consent to participate in this study was provided by the participants' legal guardian/next of kin.

AUTHOR CONTRIBUTIONS

All authors listed have made a substantial, direct, and intellectual contribution to the work and approved it for publication.

FUNDING

This study was supported by the National Natural Foundation of China (U20A20351), Key Research and Development Plan of Zhejiang Province (2021C03079), the Major projects jointly constructed by the Zhejiang Province and National Health Commission (WKJ-ZJ-1908), National Twelfth Five-Year Science and Technology Support Project (No. 2012BAI03B02), National Key Research and Development Program of China (2016YFC0901505), and Beijing key laboratory of molecular diagnosis and study on pediatric genetic diseases (BZ0317). These funding sustained the design of the study, and the collection and analysis of data.

SUPPLEMENTARY MATERIAL

The Supplementary Material for this article can be found online at: https://www.frontiersin.org/articles/10.3389/fmed.2022.885178/full#supplementary-material

REFERENCES

1. Noone DG, Iijima K, Parekh R. Idiopathic nephrotic syndrome in children. *Lancet.* (2018) 392:61–74. doi: 10.1016/S0140-6736(18)30536-1
2. Lee JM, Kronbichler A, Shin JI, Oh J. Current understandings in treating children with steroid-resistant nephrotic syndrome. *Pediatr Nephrol.* (2021) 36:747–61. doi: 10.1007/s00467-020-04476-9
3. Trautmann A, Schnaidt S, Lipska-Zietkiewicz BS, Bodria M, Ozaltin F, Emma F, et al. Long-term outcome of steroid-resistant nephrotic syndrome in children. *J Am Soc Nephrol.* (2017) 28:3055–65. doi: 10.1681/ASN.2016101121
4. Lombel RM, Gipson DS, Hodson EM. Treatment of steroid-sensitive nephrotic syndrome: new guidelines from KDIGO. *Pediatr Nephrol.* (2013) 28:415–26. doi: 10.1007/s00467-012-2310-x
5. Tullus K, Webb H, Bagga A. Management of steroid-resistant nephrotic syndrome in children and adolescents. *Lancet Child Adolesc Health.* (2018) 2:880–90. doi: 10.1016/S2352-4642(18)30283-9
6. Kemper MJ, Lemke A. Treatment of genetic forms of nephrotic syndrome. *Front Pediatr.* (2018) 6:72. doi: 10.3389/fped.2018.00072
7. McCarthy HJ, Saleem MA. Genetics in clinical practice: nephrotic and proteinuric syndromes. *Nephron Exp Nephrol.* (2011) 118:e1–8. doi: 10.1159/000320878
8. Preston R, Stuart HM, Lennon R. Genetic testing in steroid-resistant nephrotic syndrome: why, who, when and how? *Pediatr Nephrol.* (2019) 34:195–210. doi: 10.1007/s00467-017-3838-6
9. Atmaca M, Gülhan B, Atayar E, Bayazit AK, Candan C, Arici M. Long-term follow-up results of patients with ADCK4 mutations who have been diagnosed in the asymptomatic period: effects of early initiation of CoQ10 supplementation. *Turk J Pediatr.* (2019) 61:657–63. doi: 10.24953/turkjped.2019.05.003
10. Atmaca M, Gulhan B, Korkmaz E, Inozu M, Soylemezoglu O, Candan C, et al. Follow-up results of patients with ADCK4 mutations and the efficacy of CoQ10 treatment. *Pediatr Nephrol.* (2017) 32:1369–75. doi: 10.1007/s00467-017-3634-3
11. Lovric S, Ashraf S, Tan W, Hildebrandt F. Genetic testing in steroid-resistant nephrotic syndrome: when and how? *Nephrol Dial Transplant.* (2016) 31:1802–13. doi: 10.1093/ndt/gfv355
12. Sadowski CE, Lovric S, Ashraf S, Pabst WL, Gee HY, Kohl S. et al. A single-gene cause in 295% of cases of steroid-resistant nephrotic syndrome. *J Am Soc Nephrol.* (2015) 26:1279–89. doi: 10.1681/ASN.2014050489
13. Wang F, Zhang Y, Mao J, Yu Z, Yi Z, Yu L, et al. Spectrum of mutations in Chinese children with steroid-resistant nephrotic syndrome. *Pediatr Nephrol.* (2017) 32:1181–92. doi: 10.1007/s00467-017-3590-y
14. Trautmann A, Vivarelli M, Samuel S, Gipson D, Sinha A, Schaefer F, et al. IPNA clinical practice recommendations for the diagnosis and management of children with steroid-resistant nephrotic syndrome. *Pediatr Nephrol.* (2020) 35:1529–61. doi: 10.1007/s00467-020-04519-1
15. Park E, Lee C, Kim NKD, Ahn YH, Park YS, Lee JH, et al. Genetic study in Korean pediatric patients with steroid-resistant nephrotic syndrome or focal segmental glomerulosclerosis. *J Clinic Med.* (2020) 9:2013. doi: 10.3390/jcm9062013
16. Ogino D, Hashimoto T, Hattori M, Sugawara N, Akioka Y, Tamiya G, et al. Analysis of the genes responsible for steroid-resistant nephrotic syndrome and/or focal segmental glomerulosclerosis in Japanese patients by whole-exome sequencing analysis. *J Hum Genet.* (2016) 61:137–41. doi: 10.1038/jhg.2015.122
17. Rao J, Liu X, Mao J, Tang X, Shen Q, Li G, et al. Genetic spectrum of renal disease for 1001 Chinese children based on a multicenter registration system. *Clin Genet.* (2019) 96:402–10.
18. Mekahli D, Liutkus A, Ranchin B, Yu A, Bessenay L, Girardin E, et al. Long-term outcome of idiopathic steroid-resistant nephrotic syndrome: a multicenter study. *Pediatr Nephrol.* (2009) 24:1525–32. doi: 10.1007/s00467-009-1138-5
19. Björk J, Nyman U, Larsson A, Delanaye P, Pottel H. Estimation of the glomerular filtration rate in children and young adults by means of the CKD-EPI equation with age-adjusted creatinine values. *Kidney Int.* (2021) 99:940–7. doi: 10.1016/j.kint.2020.10.017
20. Zhong XH, Ding J, Zhou JH, Yu ZH, Sun SZ, Bao Y, et al. [A multicenter study of reference intervals for 15 laboratory parameters in Chinese children]. *Zhonghua er ke za zhi = Chin Journal Pediatr.* (2018) 56:835–45. doi: 10.3760/cma.j.issn.0578-1310.2018.11.009
21. Bean L, Bayrak-Toydemir P. American college of medical genetics and genomics standards and guidelines for clinical genetics laboratories, 2014 edition: technical standards and guidelines for Huntington disease. *Genet Med.* (2014) 16:e2. doi: 10.1038/gim.2014.146
22. Nagano C, Yamamura T, Horinouchi T, Aoto Y, Ishiko S, Sakakibara N, et al. Comprehensive genetic diagnosis of Japanese patients with severe proteinuria. *Sci Rep.* (2020) 10:270. doi: 10.1038/s41598-019-57149-5
23. Nagano C, Takaoka Y, Kamei K, Hamada R, Ichikawa D, Tanaka K, et al. Genotype-phenotype correlation in WT1 Exon 8 to 9 missense variants. *Kidney Int Rep.* (2021) 6:2114–21. doi: 10.1016/j.ekir.2021.05.009
24. Bérody S, Heidet L, Gribouval O, Harambat J, Niaudet P, Baudouin V, et al. Treatment and outcome of congenital nephrotic syndrome. *Nephrol Dial Transplant.* (2019) 34:458–67. doi: 10.1093/ndt/gfy015
25. Caridi G, Gigante M, Ravani P, Trivelli A, Barbano G, Scolari F, et al. Clinical features and long-term outcome of nephrotic syndrome associated with heterozygous NPHS1 and NPHS2 mutations. *Clin J Am Soc Nephrol.* (2009) 4:1065–72. doi: 10.2215/CJN.03910808
26. Korkmaz E, Lipska-Zietkiewicz BS, Boyer O, Gribouval O, Fourrage C, Tabatabaei M, et al. ADCK4-Associated glomerulopathy causes adolescence-onset FSGS. *J Am Soc Nephrol.* (2016) 27:63–8. doi: 10.1681/ASN.2014121240
27. Malakasioti G, Iancu D, Tullus K. Calcineurin inhibitors in nephrotic syndrome secondary to podocyte gene mutations: a systematic

review. *Pediatr Nephrol.* (2021) 36:1353–64. doi: 10.1007/s00467-020-04695-0
28. Faul C, Donnelly M, Merscher-Gomez S, Chang YH, Franz S, Delfgaauw J, et al. The actin cytoskeleton of kidney podocytes is a direct target of the antiproteinuric effect of cyclosporine A. *Nat Med.* (2008) 14:931–8. doi: 10.1038/nm.1857
29. Wakamatsu A, Fukusumi Y, Hasegawa E, Tomita M, Watanabe T, Narita I, et al. Role of calcineurin (CN) in kidney glomerular podocyte: CN inhibitor ameliorated proteinuria by inhibiting the redistribution of CN at the slit diaphragm. *Physiol Rep.* (2016) 4:e12679. doi: 10.14814/phy2.12679
30. Song X, Fang X, Tang X, Cao Q, Zhai Y, Chen J, et al. COQ8B nephropathy: Early detection and optimal treatment. *Mol Genomic Med.* (2020) 8:e1360. doi: 10.1002/mgg3.1360
31. Trautmann A, Bodria M, Ozaltin F, Gheisari A, Melk A, Azocar M, et al. Spectrum of steroid-resistant and congenital nephrotic syndrome in children: the PodoNet registry cohort. *Clinic J Am Soc Nephrol.* (2015) 10:592–600. doi: 10.2215/CJN.06260614
32. Malone AF, Phelan PJ, Hall G, Cetincelik U, Homstad A, Alonso AS, et al. Rare hereditary COL4A3/COL4A4 variants may be mistaken for familial focal segmental glomerulosclerosis. *Kidney Int.* (2014) 86:1253–9. doi: 10.1038/ki.2014.305
33. Maselli RA, Arredondo J, Ferns MJ, Wollmann RL. Synaptic basal lamina-associated congenital myasthenic syndromes. *Ann N Y Acad Sci.* (2012) 1275:36–48. doi: 10.1111/j.1749-6632.2012.06807.x
34. Mufson EJ, He B, Ginsberg SD, Carper BA, Bieler GS, Crawford F, et al. Gene profiling of nucleus basalis tau containing neurons in chronic traumatic encephalopathy: a chronic effects of neurotrauma consortium study. *J Neurotrauma.* (2018) 35:1260–71. doi: 10.1089/neu.2017.5368
35. Becherucci F, Landini S, Cirillo L, Mazzinghi B, Romagnani P. Look Alike, Sound Alike: Phenocopies in Steroid-Resistant Nephrotic Syndrome. *Int J Environ Res Public Health*. (2020) 17:8363. doi: 10.3390/ijerph17228363

Conflict of Interest: The authors declare that the research was conducted in the absence of any commercial or financial relationships that could be construed as a potential conflict of interest.

Publisher's Note: All claims expressed in this article are solely those of the authors and do not necessarily represent those of their affiliated organizations, or those of the publisher, the editors and the reviewers. Any product that may be evaluated in this article, or claim that may be made by its manufacturer, is not guaranteed or endorsed by the publisher.

frontiers | Frontiers in Medicine

ORIGINAL RESEARCH
published: 17 June 2022
doi: 10.3389/fmed.2022.936578

Combined Preimplantation Genetic Testing for Genetic Kidney Disease: Genetic Risk Identification, Assisted Reproductive Cycle, and Pregnancy Outcome Analysis

Min Xiao[1†], Hua Shi[2†], Jia Rao[2†], Yanping Xi[1], Shuo Zhang[1], Junping Wu[1], Saijuan Zhu[1], Jing Zhou[1], Hong Xu[2], Caixia Lei[1*] and Xiaoxi Sun[1,3*]*

[1] Shanghai Ji Ai Genetics and IVF Institute, The Obstetrics and Gynecology Hospital of Fudan University, Shanghai, China, [2] Department of Nephrology, Children's Hospital of Fudan University, National Pediatric Medical Center of China, Shanghai, China, [3] Shanghai Key Laboratory of Female Reproductive Endocrine-Related Diseases, The Obstetrics and Gynecology Hospital of Fudan University, Shanghai, China

Background: Genetic kidney disease is a major cause of morbidity and mortality in neonates and end-stage renal disease (ESRD) in children and adolescents. Genetic diagnosis provides key information for early identification of congenital kidney disease and reproductive risk counseling. Preimplantation genetic testing for monogenic disease (PGT-M) as a reproductive technology helps prospective parents to prevent passing on disease-causing mutations to their offspring.

Materials and Methods: A retrospective cohort of couples counseled on PGT who had a risk to given birth to a child with genetic kidney disease or had a history of prenatal fetal kidney and urinary system development abnormalities from 2011 to 2021. Through a combination of simultaneously screening for aneuploidy and monogenic kidney disease, we achieved reproductive genetic intervention.

Results: A total of 64 couples counseled on PGT for monogenic kidney disease in a single reproductive center during the past 10 years, of whom 38 different genetic kidney diseases were identified. The most frequent indications for referral were autosomal recessive disease (54.7%), then autosomal dominant disease (29.7%), and X-linked disease (15.6%). Polycystic kidney disease was the most common diseases counted for 34.4%. After oocyte-retrieval in all of 64 females, a total of 339 embryos were diagnosed and 63 embryos were transferred in succession. Among 61 cycles of frozen-embryo transfer (FET), ongoing pregnancy/live birth rate (OP/LBR) reached 57.38%. The cumulative OP/LBR in our cohort for the 64 couples was 54.69%. In addition, we have carried out expanded carrier screening (ECS) in all the *in vitro* fertilization (IVF) couples

OPEN ACCESS

Edited by:
Aihua Zhang,
Nanjing Children's Hospital, China

Reviewed by:
Harvey J. Stern,
Genetics and IVF Institute, United States
Giuseppe Gullo,
Azienda Ospedaliera Ospedali Riuniti Villa Sofia Cervello, Italy
Jianhua Mao,
Zhejiang University School of Medicine, China

***Correspondence:**
Hong Xu
hxu@shmu.edu.cn
Caixia Lei
caixialei@hotmail.com
Xiaoxi Sun
xiaoxi_sun@aliyun.com

[†] These authors have contributed equally to this work

Specialty section:
This article was submitted to Nephrology, a section of the journal Frontiers in Medicine

Received: *05 May 2022*
Accepted: *30 May 2022*
Published: *17 June 2022*

Citation:
Xiao M, Shi H, Rao J, Xi Y, Zhang S, Wu J, Zhu S, Zhou J, Xu H, Lei C and Sun X (2022) Combined Preimplantation Genetic Testing for Genetic Kidney Disease: Genetic Risk Identification, Assisted Reproductive Cycle, and Pregnancy Outcome Analysis. Front. Med. 9:936578. doi: 10.3389/fmed.2022.936578

performed PGT covering 7,311 individuals. The carrier frequency of the candidate genes for monogenic kidney diseases accounted for 12.19%.

Conclusion: Overall, the customization PGT-M plan in our IVF center is pivotal to decreasing the morbidity and implementing reproductive genetic intervention of genetic kidney disease.

Keywords: preimplantation genetic testing, monogenic kidney disease, haplotype analysis, pregnancy outcomes, expanded carrier screening

INTRODUCTION

Genetic kidney disease is a major cause of chronic kidney disease (CKD) in children, resulting in substantial morbidity and mortality as well as the high healthcare costs (1). Genetic kidney disease includes congenital anomalies of the kidney and urinary tract (CAKUT), congenital nephrotic syndrome, renal tubular diseases and cystic kidney disease. Renal phenotypes are also associated with many syndromic disorders and rare diseases. A number of individuals with genetic kidney disease failed to get a precise diagnosis until developing into renal failure. Genetic diagnosis for kidney disease enables counseling for all the affected pedigree members on prognosis and therapeutic options, as well as family risk counseling and planning (2, 3).

Preimplantation genetic testing (PGT) is one assisted reproductive technology (ART) available to individuals who carry a disease-causing genetic variant. PGT collects the embryo's genetic material for genetic analysis to identify healthy embryo prior to frozen- embryo transfer (FET). PGT is conducted as part of an *in vitro* fertilization (IVF) cycle and requires embryo biopsy, which may undertake at the cleavage stage (day 3 of development) with the removal of 1–2 cells or now more commonly carried out at the blastocyst stage (day 5–7 of development) with the removal of up to 10 cells (4). This approach thereby greatly reduces the chance of having a pregnancy affected with the genetic disease. Since the initial practice of PGT in the monogenetic disorders in 1990s (5), it has been extensively employed in the diagnosis of monogenic disease, X-linked disorders, aneuploidy, and chromosomal rearrangements (3, 6–10). Carrier screening is becoming standard practice for egg and sperm donors and couples seeking assisted reproduction, due to the introduction of target panels that screen for multiple variants in low risk populations to detect carriers of single-gene disorders (11). There have been over 500 disorders in which PGT-M has been successfully applied across the world (12). Several studies have reported the patient series with PGT for genetic kidney disease (4, 5, 11). Advances in molecular genetics have made a great impact on PGT application in China, whereas few studies reported the clinical outcome of PGT and the gene frequency of genetic kidney disease through carrier screening.

This study focused on combined PGT (PGT-M/A/SR) for monogenetic kidney disease at a single medical center from 2011 to 2021. The retrospect analysis on the clinical features, genotypes of PGT, pregnancy rate and outcomes were performed to provide clinical suggestions and decision making for PGT with monogenetic kidney disease.

Abbreviations: AD, autosomal dominant; AR, autosomal recessive; ART, assisted reproductive technology; ACMG, the American College of Medical Genetics and Genomics; BPR, biochemical pregnancy rate; CAKUT, congenital anomalies of the kidney and the urinary tract; CKD, chronic kidney disease; CNV, copy number variations; COH, controlled ovarian hyperstimulation; CSA, clinical sequence analyser; E2, estradiol; ECS, expanded carrier screening; ESRD, end-stage renal disease; FHB, fetal heartbeat; FETs, frozenembryo transfers; GnRH, gonadotrophic releasing hormone; HGVS, human genome variation society; hCG, human chorionic gonadotropin; ICSI, intracytoplasmic sperm injection; IR, implantation rate; IVF, *in vitro* fertilization; MII, metaphase II stage; NGS, next-generation sequencing; NS, nephrotic syndrome; NPHP, nephronophthisis; OP/LBR, ongoing pregnancy/live birth rate; PGT, preimplantation genetic testing; PGT-A, PGT for aneuploidies; PGT-SR, PGT for structural rearrangements; PGT-M, preimplantation genetic testing for monogenic disease; PHCG, positive-human chorionic gonadotropin; PKD, polycystic kidney disease; PND, invasive prenatal diagnosis; TE, trophectoderm; SAB, spontaneous abortion; SNP, single nucleotide polymorphism; WES, whole exome sequencing; WGS, whole genome sequencing.

MATERIALS AND METHODS

Study Design and Participants

The local ethics committee of Shanghai JIAI Genetics and IVF Institute approved and supervised this retrospective cohort study, adhering to the Declaration of Helsinki. Prior to enrolling individuals in the PGT cycles, written informed permissions from all the participants were obtained. All the participants were retrospectively recruited between January 2011 and December 2021 at Shanghai JIAI Genetics and IVF Institute. The eligibility enrollment included couples at risk for reproductive genetic kidney disease with comprehensive phenotype, genotype, karyotype, gestation history, family history, pedigree information, and/or the outcome of pregnancy. ECS genotype information including variants of known monogenetic disease causative genes (**Supplementary Table 1**) were collected to evaluated of risk for monogenic conditions. And we also collected all of records of the pregnancies that the couples who had counseled on PGT. Exclusion criteria were oocytes or sperm from a donor source which led to changes in the genetic probability of the genetic kidney disease and incomplete records of the above information or the couples who transmitted to other medical centers after consulting.

Clinical Process of Preimplantation Genetic Testing and *in vitro* Fertilization Cycle

The PGT process at our center is shown in the flowchart (**Figure 1**). Consultants transferred from the specialties should fetch their genetic test results or go through the WES/WGS

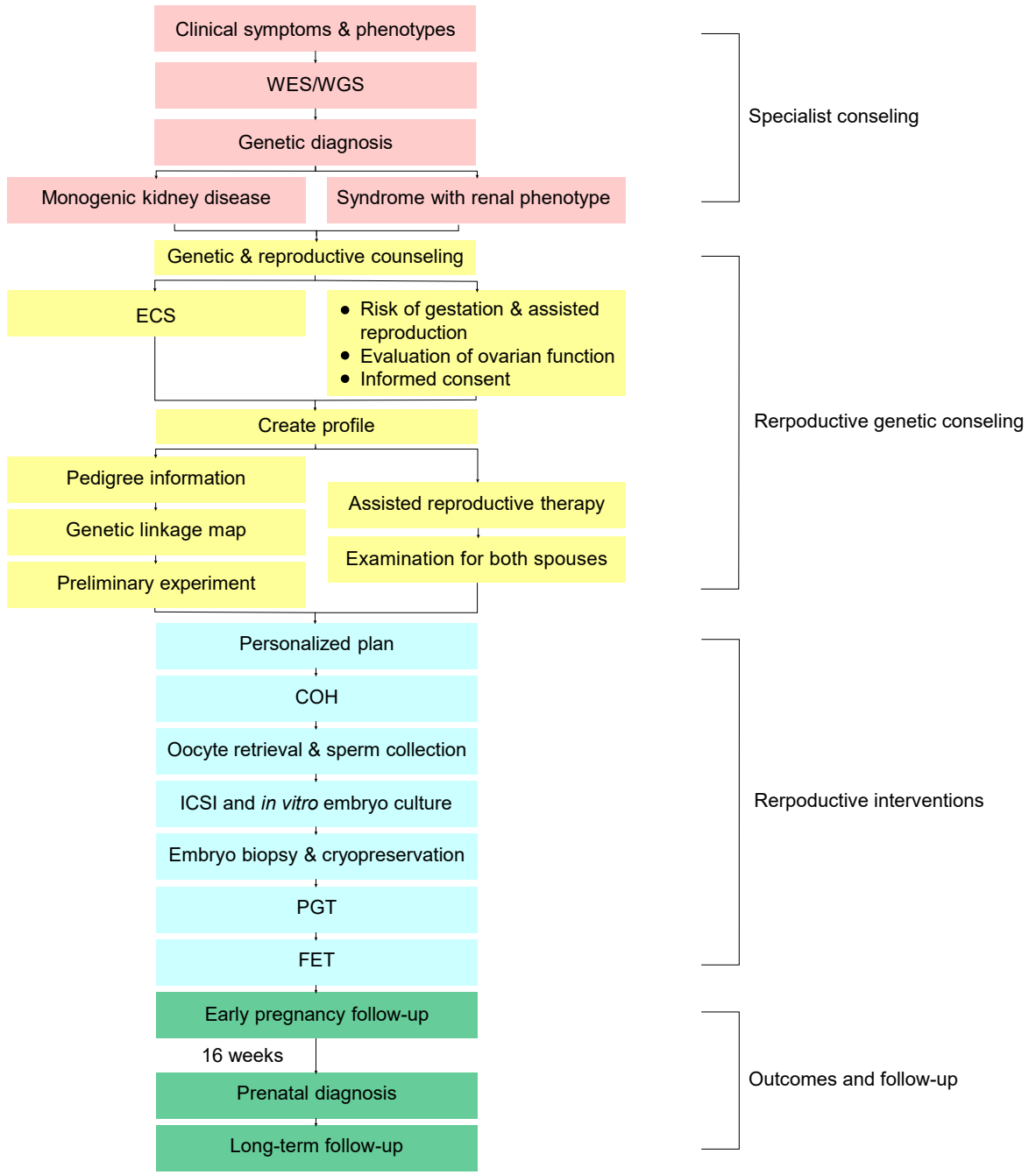

FIGURE 1 | Flowchart showing the preimplantation genetic testing for monogenic disease (PGT-M) procedures and follow-up of couples with genetic kidney disease. WES/WGS, whole exome sequencing/whole genome sequencing; ECS, expanded carrier screening; ICSI, intracytoplasmic sperm injection; COH, controlled ovarian hyperstimulation; PGT, preimplantation genetic testing; FET, frozen-embryo transfer.

depending on the clinical assessments of the clinical geneticists and the nephrologists. Variant interpretation was performed manually by a panel of nephrologists and clinical molecular geneticists. The final diagnosis was confirmed according to the combination of clinical manifestations, pedigree verification and the genetic test results. The variants were classified according to the American College of Medical Genetics and Genomics (ACMG) guidelines (13). Besides the causative genes, other locus with possibility of pathogenesis was checked in expanded carrier screening (ECS) (11). After final diagnosis and ECS, a PGT-M scheme was designed by the doctors with consent of consultants, and the genetic linkage map was built.

Examination was needed for both males and females before making a personalized plan of oocyte retrieval. The ovarian

stimulation for IVF included long gonadotrophic releasing hormone (GnRH) agonist, short GnRH agonist, antagonist, and mild stimulation protocols. About one and a half days after triggering with human chorionic gonadotropin (hCG) or an agonist, the oocyte was retrieved under transvaginal ultrasound guidance. Intracytoplasmic sperm injection (ICSI) was applied to all PGT-IVF schemes along with the FET. The embryos were washed and cultured to develop to the blastocyst stage interspersed with making an 18-μm hole in the zona pellucida on day 4 (D4) after fertilization. Blastocysts with trophectoderm (TE) cells were chosen for biopsy on D5 or D6. In general, 3–8 biopsied TE cells were used directly for whole genome amplification (WGA) followed by karyomapping. All experiments and data analysis were performed in the JIAI local laboratory. The prenatal diagnosis was performed at about the 16th week after FET. All the above procedures adopt the standard IVF techniques of Shanghai JIAI Genetics and IVF Institute (14).

Expanded Carrier Screening

Expanded carrier screening was routinely offered as an option to all patients seeking PGT in JIAI center between 1 May 2017 and 31 December 2021. The panel covers 213 genes implicated in 147 recessive (autosomal or X-linked) diseases in order to help couples to further reduce the risk of childbearing children with other recessive genetic diseases. The ECS assay used Agilent custom capture probe kit, Illumina Cluster and SBS kit. Based on Illumina platform (Illumina, San Diego, CA, United States[1]), high-throughput sequencing was performed on exons and introns within ± 10 bp of 213 genes in the genomic DNA of the subjects. The sequencing results were compared with human reference gene sequences, and all sequenced fragments were identified by bases. In this test, the target region capture high-throughput sequencing technology was adopted, and only the target gene coding region was sequenced, with an average coverage of 110–160×.

Sentieon software suite was used to analyze sequencing data. The sequencing fragments were compared with the Sentieon BWA and UCSC Hg19 reference genome. Variations are annotated by VEP software (Variant Effect Predictor) (15). Three major databases of known or suspected pathogenic variants, including ClinVar, OMIM, and HGMD, will be used to screen known pathogenic variants, as well as multiple tools for predicting missense variants and annotation of non-coding regulatory sequences. Population-based large-scale sequencing databases (gnomAD V2.1.1) were used to exclude mutations with a high frequency in the normal population (16).

Each variation in this assay will be evaluated using Clinical Sequence Analyzer (CSA) software (Mingma Technologies, Shanghai, China). After optimization according to the Sequence Variation Interpretation Standards and Guidelines published by ACMG and the latest guidelines developed by ClinGen, each variation was curated (17–19). This test reports only those mutations curated as pathogenic or likely pathogenic (P/LP) in the exon and intron segments within ±10 bp of the genes contained in the schedule. Standard Human Genome Variation Society recommendations (HGVS Nomenclature v15.11) nomenclature was used for sequence variation (20).

The copy number variation (CNV) analysis tool based on high-throughput sequencing was used to detect CNV, including specific CNV in *DMD*, *SMN1*, *HBA1*, and *HBA2* genes of the subjects, and the suspected positive samples were verified by multi-junction probe amplification technology and capillary electrophoresis technology. Coffalyser.Net software (MRC-Holland, Amsterdam, Netherlands[2]) was used for quality control and data analysis.

Genetic Testing of Blastocyst

Whole genome amplification was performed using a REPLI-g Single Cell Kit (QIAGEN, Hilden, Germany) according to the manufacturer's protocol as described earlier (14). For tissue and peripheral blood samples from the family, the DNA was isolated using DNeasy Blood & Tissue Kit as described in the manufacturers' protocol (QIAGEN, Germany). The single nucleotide polymorphism (SNP) genotype and intensity of the WGA products and DNA samples from peripheral blood or tissue were determined with an Illumina HumanKaryomap-12 v1.0 microarray for PGT-M (Illumina, Inc., San Diego, CA, United States). Each bead chip can simultaneously analyze approximately 300,000 SNP loci (Illumina, Inc. San Diego, CA, United States). The SNP array experiments followed the reported standardized procedures in accordance with the infinium chip protocol. Then the BeadChips were imaged on an iScan System (Illumina, Inc., San Diego, CA, United States). The microarray scanning results were processed using the B allele frequency and Log R Ratio. The software used for subsequent analysis and the analysis process are as previously reported (14). The Karyomapping data for each sample was imported into BlueFuse-Multi V4.0 software (Illumina, San Diego, CA, United States) according to the analysis guidelines (21) recommended by the manufacturer for genome wide analysis of genetic disease based on SNP haplotyping mapping crossovers between parental haplotypes to distinguish the chromosomes that carried the mutation.

As in **Supplementary Table 2**, embryos can be classified as euploid, aneuploid and low-level mosaicism according to chromosomal abnormalities. Mosaicism referred to the occurrence of two or more genomes in an individual/embryo derived from a single zygote, including whole-chromosome and CNV-level mosaicism (22, 23). The low-level mosaicism (≤50%) referred to the simple mosaicism of a single chromosome or a segmental chromosome. The proportion of abnormal mosaicism was less than 50% and the simple low-level mosaicism could be the secondary candidates of FET (14). Euploid embryos were sub-classified into three categories: the unaffected embryos refer to the embryos without paternal or maternal variants; the affected embryos refer to those with variants from both paternal and maternal in AR diseases, at least one variants of dominant diseases associated gene, or the hemizygous variants of X-linked recessive diseases associated gene; the embryos of carrier embryos refer to the one which carried only one paternal/maternal

[1] www.illumina.com

[2] www.mlpa.com

variants in AR diseases or the heterozygote variants of X-linked recessive diseases.

Primary Outcomes, Embryo Transfer, Antenatal Examination, and Antenatal Genetic Diagnosis

Pregnancy outcomes were primarily observed as positive-human chorionic gonadotropin (PHCG), implantation rate (IR), fetal heartbeat (FHB), ongoing pregnancy/live birth rate (OP/LBR), biochemical pregnancy rate (BPR), and spontaneous abortion (SAB) rate (14). Cumulative OP/LBR were also calculated, which were the percentage of all couples who underwent IVF cycles that ultimately had at least one OP/LBR.

Under ultrasound guidance, embryos free of disease-causing genes and chromosome abnormalities were transferred. After that, 5 early pregnancy follow-up visits will be conducted in our IVF center, and the birth follow-up will be conducted by telephone and relevant indicators will be registered as previously published (14). The prenatal examination was performed with ultrasonography throughout the gestations of our consultants. In the second trimester pregnancy, the invasive prenatal genetic diagnosis was performed using chorionic villus sampling (starting at about the 12th week of pregnancy) or amniocentesis (starting at about the 16th week of pregnancy).

Statistical Analysis

All the statistical analysis was performed with MS Excel and SPSS (version 25.0, IBM, Armonk, NY, United States). Graph was created using GraphPad prism 8.3.0. Statistical significance was defined as a *P*-value of less than 0.05.

TABLE 1 | Baseline characteristics of preimplantation genetic testing for monogenic disease (PGT-M) couples in the genetic kidney diseases/syndromes with renal phenotypes cohort.

Characteristic	Total couples, *n* = 64
Clinical information	**Year, mean ± SD (range)**
Maternal age at first counseling	30.3 ± 4.1 (23–42)
Paternal age at first counseling	33.5 ± 4.8 (26–44)
Diseases of the proband	***n* (%)**
Renal disease	44 (68.8)
Syndrome with renal phenotypes	20 (31.3)
Complains	***n* (%)**
Abnormal gestation	29 (45.3)
Birth defect	27 (42.2)
Family history of genetic kidney disease	17 (26.6)
Infertility	10 (15.6)
PGT-M	
Number of females undergo oocyte-retrieval (*n*, %)	64 (100)
Number of females undergo IVF-FET (*n*, %)	43 (67.2)
Age at oocyte-retrieval (years ± SD, range)	31.3 ± 4.1 (24–42)
Maternal age at oocyte-retrieval ≥ 35 years	15.6% (10/64)
Maternal age at IVF-FET (years ± SD, range)	30.6 ± 3.0 (25–37)
Paternal age at IVF-FET (years ± SD, range)	34.4 ± 5.1 (26–47)
Maternal age at IVF-FET ≥ 35 years	9.3% (4/43)

FET, frozen-embryo transfer; IVF, in vitro fertilization; PGT-M, preimplantation genetic testing for monogenic disease.

RESULTS

Clinical Characteristics

Between 2011 and 2021, we analyzed a total of 463 cases (8.0%) for PGT-M from the 5,770 couples who received fertility and reproductive counseling at a signal medical center in Shanghai, China. There were 64 couples who were diagnosed with pathogenic/likely pathogenic (P/LP) variants of known disease causative genes for kidney disease or the syndromes with renal phenotypes, which accounted for 13.8% (64/463) of all PGT-M (**Table 1**).

Between 2011 and 2016, our center counseled less than five couples with kidney disease every year. It has grown since 2018, reaching 17 occurrences in 2021 (**Figure 2**). Cumulatively, 35 couples have been conceived through IVF-FET from 2016 to end 2021. Maternal age was 2 years younger than paternal age at the time of first counseling, with a mean age of 30.3 years.

Among the 64 couples who had identified the P/LP variants of known kidney disease, the main reasons for their ART requests included abnormal pregnancy (29, 45.3%), birth defect (27, 42.2%) with some overlaps of abnormal pregnancy (8). Only 17 (26.6%) couples had a positive family history of kidney disease (**Table 1** and **Supplementary Figure 1**).

Genetic Diagnosis for Monogenetic Kidney Disease

Genetic findings for the 64 couples identified the P/LP variants in 38 known disease-causing genes for kidney disease and clinical outcomes were also listed (**Figure 3A**, **Table 2**, and **Supplementary Table 3**). The P/LP variations founded in 20 monogenetic diseases were carried by 44 couples (68.8%), whereas P/LP variations in 18 syndromic diseases with both renal and extrarenal phenotypes were carried by 20 couples (31.3%). There were 35 couples (54.7%) with diagnosis of autosomal recessive (AR) disease (**Supplementary Table 4**), 19 couples (29.7%) with a high risk for autosomal dominant (AD) disease and 10 (15.6%) with diagnosis of X-linked disease. Polycystic kidney disease (PKD) was the most common disease in

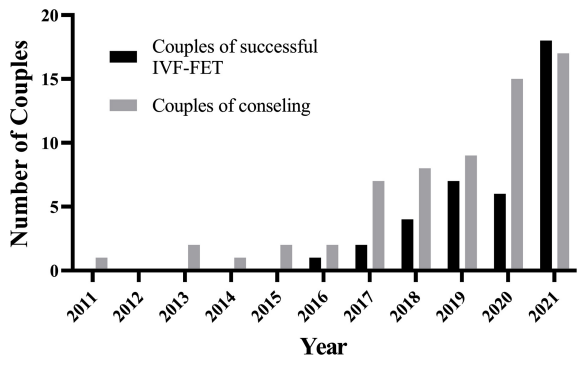

FIGURE 2 | The number of couples of consulting/successful IVF-FET has grown since 2018 in one medical center. IVF-FET, *in vitro* fertilization and frozen-embryo transfer.

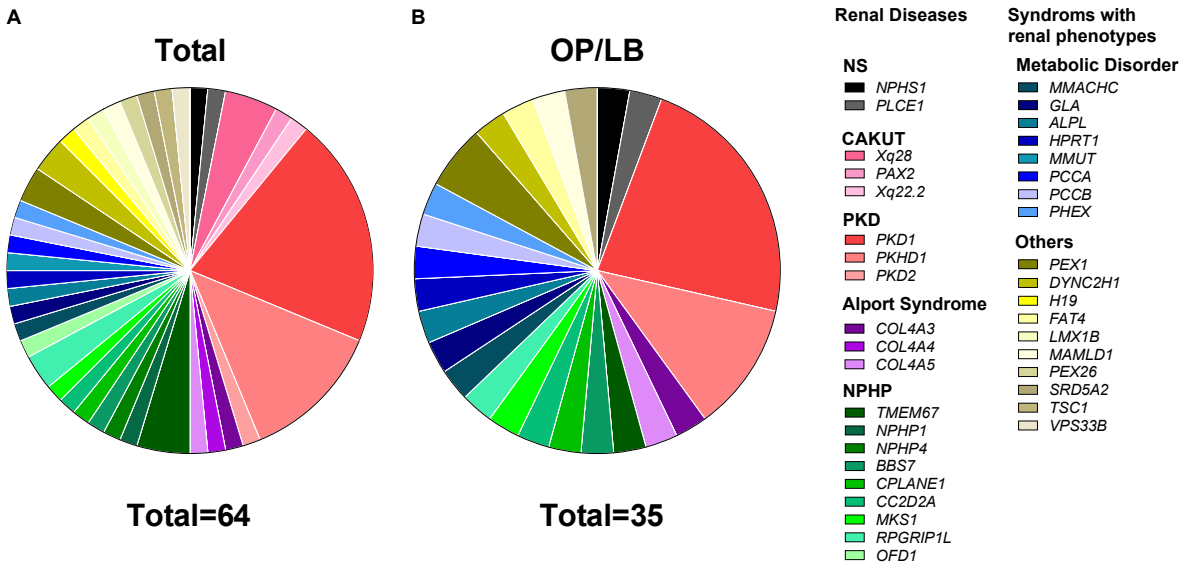

FIGURE 3 | Proportion of cases with diagnosis of pathogenic/likely pathogenic variants in genetic kidney disease. **(A)** Genetic spectrum of kidney disease in 64 couples who were diagnosed with pathogenic/likely pathogenic variants of known disease causative genes for kidney disease or the syndromes with distinct renal phenotypes. **(B)** The gene distribution of 35 couples with ongoing pregnancy/live birth (OP/LB) by the end of 2021. CAKUT, congenital anomalies of the kidney and the urinary tract; NPHP, nephronophthisis; NS, nephrotic syndrome; PKD, polycystic kidney disease.

our cohort accounted for 34.4%, followed by nephronophthisis (NPHP, 18.8%), metabolic disease (12.5%) and congenital anomalies of the kidney and urinary tract (CAKUT, 7.8%).

Disease Carrier Frequencies in Expanded Carrier Screening

Our reproductive department would propose that all couples who referred to PGT undertook ECS screening to minimize the risk of having children with additional recessive genetic illnesses. During the study period, we performed a total of 7,311 expanded carrier tests in individuals request PGT. Considering the P/LP variants for known monogenetic diseases, there were 12.19% (891/7,311) carriers of known genetic kidney diseases and syndromic disorders with renal phenotypes. The most frequently P/LP variants were reported in *SLC26A4* gene with a carrier rate of 2.38% (174/7,311), followed by *USH2A* accounted for 2.37% (173/7,311), *PKHD1* (1.29%, 94/7,311), *MMACHC* (1.00%, 73/7,311), *ETFDH* (0.85%, 62/7,311), and *CEP290* (0.53%, 39/7,311) (detailed in **Supplementary Table 1**).

Clinical Cycles of Assisted Reproductive

The critical procedure, oocyte-retrieval was performed in all of 64 females who came for counseling after a planned process including genetic diagnosis, examination, assisted reproductive therapy if necessary and personalized decision making. As a result, each participant retrieved 13.4 ± 8.2 oocytes after 10.0 ± 2.0 days COH with 31.2 ± 11.7 mIU/mL gonadotrophin (Gn), undergoing 1-4 oocyte-retrieval cycle on average. With an average of 4, 220.2 pg/ml, the estradiol (E2)-peak varied from 211 to 12, 235 pg/ml. The metaphase II stage (MII) rate of oocytes was 82.0 ± 17.0% for each participant in terms of oocyte quality and the blastocyst formation rate was 56.8 ± 29.3% (**Supplementary Table 5**). In our cohort, the mean maternal age at oocyte-retrieval were 31.3 ± 4.1 years (range 24–42 years), including 15.6% (10/64) over 35 years old (**Table 1**).

Analysis of Preimplantation Genetic Testing for Monogenic Disease Diagnostic

In the 64 cases with P/LP variants of known disease-causing genes for kidney disease, 344 embryos biopsy samples were analyzed, among which five failed to sequencing due to insufficient embryo DNA. There were 65.4% of blastocyst being a euploid, whereas 29.9% of blastocyst being an aneuploid. In total, 31.6% (71/225) of the euploid embryos were unaffected, 33.3% (75/225) of the embryos were affected, 35.1% (79/225) of the embryos were carrier. There were 3.2% (11/344) low-level mosaicism ($\leq$ 50%) were identified which could be the secondary candidates of FET if they also did not carry the disease-causing gene (**Supplementary Table 2**). The frequency of euploid embryos was calculated as 66.3% (193/291) and 60.4% (32/53) in maternal age group of $<$35 years and $\geq$35 years, respectively. As for the aneuploid embryos, the frequency accordingly was 28.2% (103/291) and 39.6% (21/53) in each age group, respectively ($P > 0.05$, **Supplementary Table 2**). Between 2011 and 2021, each couple who underwent the PGT-M experienced 1.30 ± 0.53 cycles of PGT-M test with at least one cell biopsy. A total of 339 (98.5%) embryos were successfully analyzed, 150 (43.6%) of them were transferable and to date 63 (18.6%) was transferred. The average transferable embryos were 0.9 ± 0.4 per oocyte-retrieval cycles and 2.2 ± 1.6 per PGT-M test cycles, respectively. In 64 cases

TABLE 2 | Genes and variants list in the preimplantation genetic testing for monogenic disease (PGT-M) cohort of genetic kidney diseases/syndromes with renal phenotypes cohort.

ID	Affected gene	Mutation type	Transcript	Map location	DNA change	Amino acid change	Paternal (P)/ Maternal (M)	Clinical outcomes
1	*ALPL*	Missense	NM_000478.6	*1p36.12*	c.212G>A	p.Arg71His	M	LB
2	*BBS7*	Missense	NM_176824.3	*4q27*	c.634T>C	p.Ser212Pro	P	OP
	BBS7	Missense	NM_176824.3	*4q27*	c.849 + 1G>C	–	M	
3	*CC2D2A*	Missense	NM_001080522.2	*4p15.32*	c.2728C>T	p.Arg910Ter	M	LB
	CC2D2A	Missense	NM_001080522.2	*4p15.32*	c.4598T>C	p.Leu1533Pro	P	
4	*COL4A3*	Missense	NM_000091.5	*2q36.3*	c.1918G>A	p.Gly640Arg	M	LB
5	*COL4A5*	Missense	NM_000495.5	*Xq22.3*	c.619G>C	p.Gly207Arg	P & M	OP
6	*CPLANE1*	Missense	NM_023073.3	*5p13.2*	c.7978C>T	p.Arg2660Ter	P	LB
	CPLANE1	Missense	NM_023073.3	*5p13.2*	c.3830G>A	p.Cys1277Tyr	M	
7	*DYNC2H1*	Missense	NM_001080463.2	*11q22.3*	c.7594C>T	p.Arg2532Trp	P	Implantation failure
	DYNC2H1	Missense	NM_001080463.2	*11q22.3*	c.5176C>T	p.Arg1726Ter	M	
8	*DYNC2H1*	Missense	NM_001080463.2	*11q22.3*	c.10163C>T	p.Pro3388Leu	P	Frozen
	DYNC2H1	Missense	NM_001080463.2	*11q22.3*	c.7574A>C	p.Glu2525Ala	P	
9	*DYNC2H1*	Missense	NM_001080463.2	*11q22.3*	c.10163C>T	p.Pro3388Leu	P	OP
	DYNC2H1	Missense	NM_001080463.2	*11q22.4*	c.703T>C	p.Trp235Arg	M	
10	*FAT4*	Missense	NM_024582.5	*4q28.1*	c.10261A>C	p.Thr3421Pro	P	OP
	FAT4	Missense	NM_024582.5	*4q28.1*	c.5191C>T	p.Gln1731*	M	
11	*GLA*	Missense	NM_000169.2	*Xq22.1*	c.888G>A	p.Met296Ile	M	LB
12	*H19*	Gross deletion	NR_002196.2	*11p15.4*	H19-up-214nt, H19-up-454nt	–	M	Frozen
13	*HPRT1*	Missense	NM_000194.3	*Xq26.2-q26.3*	c.533-9T>G	–	M	OP
14	*LMX1B*	Small deletion	NM_001174146.2	*9q33.3*	c.712_714del	p.Phe238del	M	Implantation failure
15	*MAMLD1*	Missense	NM_001177465.3	*Xq28*	c.2398C>T	p.Gln800Ter	M	LB
16	*MKS1*	Repeat variants	NM_017777.4	*17q22*	c.1411dup	p.Glu471GlyfsTer120	P & M	LB
17	*MMACHC*	Missense	NM_015506.3	*1p34.1*	c.609G>A	p.Trp203Ter	M	LB
	MMACHC	Small deletion	NM_015506.3	*1p34.1*	c.656_658del	p.Lys220del	P	
18	*MMUT*	Missense	NM_000255.4	*6p12.3*	c.1106G>A	p.Arg369His	P	Frozen
	MMUT	Missense	NM_000255.4	*6p12.3*	c.914T>C	p.Leu305Ser	M	
19	*NPHP1*	Gross deletion	NM_000272.5	*2q13*	exon1-20del	–	P & M	Frozen
20	*NPHP4*	Small deletion	NM_015102.5	*1p36.31*	c.3122del	p.Phe1041SerfsTer42	P	Frozen
	NPHP4	Small deletion	NM_015102.5	*1p36.31*	c.169_176del	p.His57SerfsTer5	M	
21	*NPHS1*	Missense	NM_004646.4	*19q13.12*	c.3478C>T	p.Arg1160Ter	M	LB
	NPHS1	Missense	NM_004646.4	*19q13.12*	c.2663G>A	p.Arg888Lys	P	
22	*OFD1*	Small deletion	NM_003611.3	*Xp22.2*	c.2del	p.Met1ArgfsTer14	M	Frozen
23	*PAX2*	Missense	NM_003987.5	*10q24.31*	c.254G>A	p.Gly85Asp	M	Frozen
24	*PCCA*	Small deletion	NM_000282.4	*13q32.3*	c.376del	p.Ala126Profs*58	M	LB
	PCCA	Missense	NM_000282.4	*13q32.3*	c.809T>C	p.Ile270Thr	P	
25	*PCCB*	Non-sense	NM_001178014.1	*3q22.3*	c.184-2A>G	–	P	LB
	PCCB	Missense	NM_001178014.1	*3q22.4*	c.331C>T	p.Arg111Ter	M	
26	*PEX1*	Missense	NM_000466.3	*7q21.2*	c.1483 + 1G>A	–	P	LB
	PEX1	Repeat variants	NM_000466.3	*7q21.2*	c.1725dup	p.Arg577ThrfsTer15	M	
27	*PEX1*	Repeat variants	NM_000466.3	*7q21.2*	c.892_895dup	p.Asn299IlefsTer2	M	LB
	PEX1	Small deletion	NM_000466.3	*7q21.2*	c.2927-2del	–	P	
28	*PEX26*	Small deletion	NM_017929.6	*22q11.21*	c.34del	p.Leu12SerfsTer70	P	Frozen
	PEX26	Small deletion	NM_017929.6	*22q11.21*	c.34del	p.Leu12SerfsTer70	M	
29	*PHEX*	Small deletion	NM_000444.4	*Xp22.11*	c.917del	p.Ser306Metfs*3	M	OP
30	*PKD1*	Missense	NM_001009944.3	*16p13.3*	c.2534T>C	p.Leu845Ser	P	LB
31	*PKD1*	Missense	NM_001009944.3	*16p13.3*	c.8311G>A	p.Glu2771Lys	P	LB
32	*PKD1*	Missense	NM_001009944.3	*16p13.3*	c.1938G>A	p.Trp646Ter	P	LB
33	*PKD1*	Small deletion	NM_001009944.3	*16p13.3*	c.12494_12501del	p.Ser4165TrpfsX42	P	LB
34	*PKD1*	Missense	NM_001009944.3	*16p13.3*	c.6424C>T	p.Gln2142Ter	M	LB
35	*PKD1*	Small deletion	NM_001009944.3	*16p13.3*	c.9388_9393 del	p.Arg3130_Gly3131 del	M	LB
36	*PKD1*	Missense	NM_001009944.3	*16p13.3*	c.12031C>T	p.Gln4011*	M	LB
37	*PKD1*	Missense	NM_001009944.3	*16p13.3*	c.9547C>T	p.Arg3183*	P	OP
38	*PKD1*	Repeat variants	NM_001009944.3	*16p13.3*	c.786dup	p.Thr263HisfsTer108	M	Implantation failure

(Continued)

TABLE 2 | (Continued)

ID	Affected gene	Mutation type	Transcript	Map location	DNA change	Amino acid change	Paternal (P)/Maternal (M)	Clinical outcomes
39	*PKD1*	Small deletion	NM_001009944.3	*16p13.3*	c.11241_11255del	p.Arg3750_Leu3754 del	P	Implantation failure
40	*PKD1*	Repeat variants	NM_001009944.3	*16p13.3*	c.7415dup	p.Ser2475LeufsTer26	M	Frozen
41	*PKD1*	Missense	NM_001009944.3	*16p13.3*	c.6132C>G	p.Asn2044Lys	M	Frozen
42	*PKD1*	Missense	NM_001009944.3	*16p13.3*	c.10821 + 1G>A	p.Leu3608Met	P	Frozen
43	*PKD2*	Missense	NM_000297.4	*4q22.1*	c.1081C>T	p.Arg361*/p.Arg361 Ter	M	Implantation failure
44	*PKHD1*	Missense	NM_138694.4	*6p12.3-p12.2*	c.11314C>T	p.Arg3772Ter	M	LB
	PKHD1	Small indels	NM_138694.4	*6p12.3-p12.2*	c.9235_9236 delinsAA	p.Ala3079Lys	P	
45	*PKHD1*	Missense	NM_138694.4	*6p12.3-p12.2*	c.11074C>T	p.Arg3692*	M	LB
	PKHD1	Missense	NM_138694.4	*6p12.3-p12.2*	c.5993T>C	p.Ile1998Thr	P	
46	*PKHD1*	Missense	NM_138694.4	*6p12.3-p12.2*	c.2914A>T	p.Lys972Ter	M	LB
	PKHD1	Missense	NM_138694.4	*6p12.3-p12.3*	c.9662C>T	p.Pro3221Leu	P	
47	*PKHD1*	Missense	NM_138694.4	*6p12.3-p12.2*	c.1139T>C	p.Phe380Ser	P	BPR
	PKHD1	Missense	NM_138694.4	*6p12.3-p12.2*	c.1639T>C	p.Cys547Arg	M	
48	*PKHD1*	Small insertion	NM_138694.4	*6p12.3-p12.2*	c.1023_1024 insACTG	P.Glu342ThrfsTer5	P	OP
	PKHD1	Missense	NM_138694.4	*6p12.3-p12.2*	c.2947T>C	p.Cys983Arg	M	
49	*PKHD1*	Missense	NM_138694.4	*6p12.3-p12.2*	c.8518C>T	p.Arg2840Cys	P	Frozen
	PKHD1	Gross deletion	NM_138694.4	*6p12.3-p12.2*	Exon19del	–	M	
50	*PKHD1*	Missense	NM_138694.4	*6p12.3-p12.2*	c.11074C>T	p.Arg3692*	P	Frozen
	PKHD1	Missense	NM_138694.4	*6p12.3-p12.2*	c.5935G>A	p.Gly1979Arg	M	
51	*PKHD1*	Missense	NM_138694.4	*6p12.3-p12.2*	c.103G>T	p.G35* /p.Gly35Ter	M	Frozen
	PKHD1	Missense	NM_138694.4	*6p12.3-p12.2*	c.5935G>A	p.Gly1979Arg	P	
52	*PLCE1*	Missense	NM_016341.4	*10q23.33*	c.5426T>C	p.Ile1809Thr	P & M	LB
53	*PLP1*	Repeat variants	NM_199478.3	*Xq22.2*	g.103010788-103232003dup	–	M	Frozen
54	*RPGRIP1L*	Missense	NM_015272.5	*16q12.2*	c.427C>T	p.Gln143Ter	M	LB
	RPGRIP1L	Missense	NM_015272.5	*16q12.2*	c.1351-11A>G	–	P	
55	*RPGRIP1L*	Missense	NM_015272.5	*16q12.2*	c.2122G>A	p.Gly708Ser	M	Implantation failure
	RPGRIP1L	Small deletion	NM_015272.5	*16q12.2*	c.1419-1421del	–	P	
56	*SRD5A2*	Missense	NM_000348.4	*2p23.1*	c.680G>A	p.Arg227Gln	P & M	LB
57	*TMEM67*	Missense	NM_153704.6	*8q22.1*	c.1645C>T	p.R549C	M	LB
	TMEM67	Missense	NM_153704.6	*8q22.2*	c.2434G>T	p.Glu812Ter	P	
58	*TMEM67*	Small deletion	NM_153704.6	*8q22.1*	c.296del	p.Lys99fs	M	Frozen
	TMEM67	Missense	NM_153704.6	*8q22.1*	c.1243G>A	p.Val415Met	P	
59	*TMEM67*	Missense	NM_153704.6	*8q22.1*	c.166G>T	p.Asp56Tyr	M	Frozen
	TMEM67	Missense	NM_153704.6	*8q22.1*	c.1388G>A	p.Arg463Gln	P	
60	*TSC1*	Repeat variants	NM_001362177.2	*9q34*	c.989dup	p.Gly331ArgfsTer7	M	Frozen
61	*VPS33B*	Missense	NM_018668.5	*15q26.1*	c.1594C>T	p.Arg532Ter	P & M	BPR
62	*Xq28*	Repeat variants	–	*Xq28*	g.152932475-153683298dup	–	M	Frozen
63	*Xq28*	Repeat variants	–	*Xq28*	g.152925133-153530814dup	–	M	Frozen
64	*Xq28*	Gross deletion	–	*Xq28*	g.154120000-154580000del	–	M	Frozen

*GRCh37 (hg19); BP, biochemical pregnancy; LB, live birth; M, maternal; OP, ongoing pregnancy; P, paternal. paternal; According to HGVS Nomenclature, * denotes termination code (nonsense mutation).*

with oocyte-retrieval, the cumulative rate of obtained transferable embryos for each couple was 85.9% (**Supplementary Table 6**).

Pregnancy Outcome

There were 61 FET cycles underwent in the 43 couples with high risk of genetic kidney disease in our cohort. Single blastocyst was most frequently transferred (59/61) and a total of two double blastocyst transfers were performed. There were no monozygotic or dizygotic twins in any of the successful pregnancies. The chemical pregnancy rate, as defined by a positive beta hCG level, was 67.21% (41/61). The implantation rate, as defined by the presence of a gestational sac was 59.02% (36/61) and presence of fetal heartbeat was 57.38% (35/62). It should be noted that one of the couples with double blastocyst transferred had experienced SAB. Therein one blastocyst with no HB and the other blastocyst had a live birth. The biochemical pregnancy and spontaneous abortion rates were 9.84% (6/61) and 1.64% (1/61), respectively (**Table 3**).

TABLE 3 | Pregnancy outcomes in 43 couples with high risk of genetic kidney disease.

Characteristics	Total = 61 FET cycles	Female age at IVF-FET < 35 years (*n* = 55)	Female age at IVF-FET ≥ 35 years (*n* = 6)	*P*-value
PHCG	67.21% (41/61)	67.27% (37/55)	66.67% (4/6)	1.000
IR	59.02% (36/61)	58.18% (32/55)	66.67% (4/6)	1.000
HB	57.38% (35/61)	56.36% (31/55)	66.67% (4/6)	1.000
BPR	9.84% (6/61)	10.91% (6/55)	0.00% (0/6)	0.394
SAB	1.64% (1/61)	0.00% (0/55)	16.67% (1/6)	0.098
OP/LBR	57.38% (35/61)	56.36% (31/55)	66.67% (4/6)	1.000

BPR, biochemical pregnancy; FET, frozen-embryo transfer; HB, fetal heartbeat; IR, implantation rate; IVF, in vitro fertilization; OP/LBR, ongoing pregnancy/live birth rate; PHCG, positive-HCG; rate; SAB, spontaneous abortion.

In the 61 cycles of FET for genetic kidney disease, ongoing pregnancy (OP)/live birth rate (LBR) reached 57.38% (35/61). And the cumulative OP/LBR in our cohort was 54.69% (35/64) by the end of 2021 (**Figure 3B**). The follow-up rate of amniotic fluid was 100%, which was consist with PGT-M (data not shown). The mean gestation week was 38.9 weeks. And the mean birth weight was 3530.6 ± 423.1 g. There is no significant difference in the gender (boys vs. girls: 5:4) of the babies. During the follow-up in our medical centers with pediatrics and consultants of nephrology, no neonate malformations or any condition associated with renal disease were reported.

DISCUSSION

In the current study, we presented the clinical outcome of kidney-related PGT-M performed in a single medical center over the past 10 years. A cumulative ongoing pregnancy/live birth rate 54.69% by the end of 2021 were achieved in our cohort with risk of genetic kidney disease. It highlighted the necessity of molecular genetic diagnosis for kidney disease and the importance of reproductive counseling for the couples with potential risk of kidney disease.

Preimplantation genetic testing entails genetic testing of embryos obtained through IVF to screening out the genetic disorders. Only embryos that are free of the disorders are then suitable for implantation. According to a report from the Netherlands based on a 25-year history of using PGT to prevent the offspring with kidney disorders, two-thirds achieved at least one live birth rate, which was comparable to IVF outcomes in general (3). The majority of couples in this retrospective cohort had AD or X-linked disease, with the mother more being the affected parent than the father. Among the 537 embryos for biopsy from the 52 couples, 35% were free of the genetic kidney disease and suitable for transfer (3). Here, our PGT cohort from 2011 to 2021 provided the number of kidney-related PGT-M involved in analyzing of the 64 couples and 344 embryos with 20.6% unaffected euploid embryos and 150 (43.6%) were free of the genetic kidney disease and suitable for transfer. The cumulative ongoing pregnancy/live birth of 54.69% was acceptable and better compared to the previous report of Dutch cohort (3). The average maternal age of 30.6 years at FET, which was younger than the Dutch cohort (32 years old) might have contributed to the higher ongoing pregnancy/live birth. It has been demonstrated that women <35 years old had significantly higher euploid blastocyst rates when compared women >35 years old (24). More blastocysts to biopsy and vitrify means more euploid blastocysts to choose from in the corresponding FET cycle for the young participants. In addition, the MII rate (82.0%) and blastocyst formation rate (56.8%) in our center were at the leading level, which made enough blastocysts available for analysis and implantation. Unfortunately, there was no detail information on the blastocyst euploidy and implantation rates from the Dutch cohort (3). Furthermore, the trend of higher incidence of aneuploidy in the group over 35 years old compared with that under 35 years old was in line with expectations, but not statistically significant. It may be due to that the aged female in this cohort accounted for a small proportion and the average age was relatively young. It was worth exploring with a larger sample size as the growing consciousness of the advantages of PGT-M in the future.

Underlying the genetic findings of kidney-related PGT is crucial for the parents at risk for passing a genetic condition to their children, especially when faced with the difficult decision of pregnancy termination if the fetus has been diagnosed with congenital abnormalities generally in the second trimester. During the study period, P/LP variants of known disease-causing genes for kidney disease were identified in 13.8% of the total cases of PGT-M referred to our medical center. In our cohort, 54.7% of the couples had AR genes, 29.7% had AD genes and 15.6% had XL genes. Among the 38 genetic kidney diseases, PKD was the most common one, followed by NPHP, metabolic disease and CAKUT. A report from a commercial laboratory detailed the experience with kidney-related PGT-M in 389 cases referred from 98 different IVF clinics across America between 2010 and 2019 (24). In the American cohort, 52% of couples referred for AR genes, 32% were screened for AD genes and 14% for XL inheritance (24). Comparing with the gene spectrum presented from Dutch cohort (3), American cohort (6), and our Chinese cohort, PKD and Alport syndrome were the most common diseases referred for PGT. Furthermore, we presented more cases with genetic kidney disease which have not been published in the literature of the experience on PGT such as congenital nephrotic syndrome caused by *PLCE1* or *NHPS1*, and NPHP caused by *NPHP1, TMEM67,* or *MKS1* et al.

A growing variety of preconception carrier tests for genetic disease are now available for couples planning to conceive.

Initially, carrier testing for AR disease was conducted for genes that were frequent in high risk population for certain inherited disease groups (25). The chance of being a carrier for a genetic disease is dependent on ethnicity and family history, with certain populations having a higher baseline incidence of certain condition (26). However, *de novo* variants can also occur, and genetic condition is not isolated within a certain community. As is well-known the majority of genetic kidney disease is AR disease, ECS for assisted conception couples combined with PGT is necessary for reproductive counseling. Our results showed the effectiveness of the ECS prior to PGT cycle with a carrier rate of 12.2% in known genes for monogenetic kidney diseases and syndromic disorders with renal phenotypes. Offering ECS to couples with family history of kidney disease would seem preferable, whereas couples who are unaware of the risk of genetic kidney disease carriers will confront a difficult decision-making process. Genetic kidney diseases are the fourth most common cause of renal failure in the world. Many kidney diseases such as ARPKD, Alport syndrome, or NPHP may be diagnosed until the development of renal failure during adolescence or adult stage. In general, the implementation of PGT-M relies heavily on prior specialist molecular diagnosis. For CAKUT, as we knew, less to 50% of the patients can be identified carrying genetic background (27). For the parents with this child, it is much difficult for PGT-M than other genetic kidney disease such as polycystic kidney disease. Prioritizing the embryo transfer order based on the information of PGT and ECS data (ranking), is expected to minimized the risk of an adverse pregnancy outcome (biochemical pregnancy, clinical miscarriage, and artificial abortion).

There were some limitations to current study. First, our cohort was from a single center, which was not population-based. However, the center is one of the largest IVF and PGT center in China, involving couples from various regions, thus diminishing the regional bias. Secondly, further work on the long-term follow-up is to carried out to analyze the periconceptional effect on clinical outcomes of PGT-M. However, there were no records of spontaneous pregnancy or PGT-M misdiagnoses among our cohort. In addition, cases of sperm and egg donation in various forms to reduce the risk of having children with genetic kidney disease were not included in this retrospective study (28). Fertility preservation for women with genetic kidney disease wishing to conceive is also not involved in our case (29, 30). The applied range of PGT-M at the present stage still has limitations in some specific situation in our center. For example, PGT-M refers to testing for nuclear DNA pathogenic variant(s) exclusion testing and disorders caused by pathogenic variants in the mitochondrial DNA (mtDNA). Nuclear transfer has been applied to minimize transmission risk of mtDNA diseases. However, it is not allowed in China for ethical reasons and some patients who came to our IVF center for consultation would choose to reduce the risk through egg donation. Furthermore, for special cases, including *de novo* (31) and germline mosaicism (32) pathogenic variants in husband or wife, PGT-M currently adopts the strategy of constructing haploid for linkage analysis by SNPs through next-generation sequencing (NGS) or Karyomapping array combined with direct sequencing methods such as Sanger sequencing. Our center has carried out relevant cases and achieved successful healthy live births. For *de novo* variants, direct detection methods such as Sanger sequencing are used to find variant carriers in sperm, polar bodies or blastocysts as probands. For germline mosaicism (32) pathogenic variants, embryos that the linkage analysis showed carrying allele different from the diseased proband and the Sanger sequencing did not detect the pathogenic variant were recommended as priority embryos for transfer; embryos that the linkage analysis showed carrying allele same as the diseased proband but the sanger sequencing did not detect the pathogenic variant were recommended as secondary transfer embryos.

In conclusion, we provided the overview of PGT referrals for genetic kidney disease over the ten-year study from one medical center in China. Due to the advance in genetic kidney disease, there has been an increase of kidney-related PGT referral since 2018. In our cohort, the high rate of unaffected live born children following PGT in monogenic kidney disease can support the counseling for families at risk of kidney disease. As the need for decision-making assistance for prospective parents and appropriate referrals to reproductive specialists grows, awareness of PGT as a reproductive option for couples among the nephrology community is crucial.

DATA AVAILABILITY STATEMENT

The datasets presented in this article are not readily available due to patient privacy and confidentiality. Requests to access the datasets should be directed to to XS, xiaoxi_sun@aliyun.com.

ETHICS STATEMENT

The studies involving human participants were reviewed and approved by the Medicine Ethics Committee of Children's hospital, Fudan University (NO. 2018_286). The patients/participants provided their written informed consent to participate in this study.

AUTHOR CONTRIBUTIONS

MX, HS, and JR completed the main data analysis and manuscript writing. YX was mainly responsible for the analysis of ECS data. CL and JW performed genetic counseling of patients. XS was responsible for the IVF process of our center. JR and HX were responsible for nephropathy diagnosis in this cohort. MX and ShZ analyzed bioinformatics data of PGT. SaZ and JZ performed preimplantation genetic testing (PGT) experiments. All authors contributed to the article and approved the submitted version.

FUNDING

This work was supported by the National Natural Science Foundation of China (82101753), the Special Project for Clinical Research in the Health Industry of the Shanghai

Municipal Health Commission (20204Y0071), Key Development Program of Children's Hospital of Fudan University (EK2022ZX01), and Shanghai Shen Kang Hospital Development Center Municipal Hospital New Frontier Technology Joint Project (SHDC12017105).

ACKNOWLEDGMENTS

We thank the entire team at the embryo laboratory and the clinicians of Shanghai JIAI Genetics and IVF Institute for invaluable contributions to this work and to all patients for participating and sharing clinical information for this study. At the same time, we would like to thank the multidisciplinary consultation team (MDT) jointly established by Shanghai JIAI Genetics and IVF Institute and Children's Hospital of Fudan University for their support for the inclusion of this cohort of patients. Thanks to the MDT team members for their continuous efforts.

SUPPLEMENTARY MATERIAL

The Supplementary Material for this article can be found online at: https://www.frontiersin.org/articles/10.3389/fmed.2022.936578/full#supplementary-material

REFERENCES

1. Fang Y, Shi H, Xiang T, Liu J, Liu J, Tang X, et al. Genetic architecture of childhood kidney and urological diseases in China. *Phenomics.* (2021) 1:91–104. doi: 10.1007/s43657-021-00014-1
2. Liu Y, Shi H, Yu X, Xiang T, Fang Y, Xie X, et al. Risk factors associated with renal and urinary tract anomalies delineated by an ultrasound screening program in infants. *Front Pediatr.* (2022) 9:728548. doi: 10.3389/fped.2021.728548
3. Snoek R, Stokman MF, Lichtenbelt KD, van Tilborg TC, Simcox CE, Paulussen ADC, et al. Preimplantation genetic testing for monogenic kidney disease. *Clin J Am Soc Nephrol.* (2020) 15:1279–86. doi: 10.2215/CJN.03550320
4. Kokkali G, Coticchio G, Bronet F, Celebi C, Cimadomo D, Goossens V, et al. ESHRE PGT consortium and SIG embryology good practice recommendations for polar body and embryo biopsy for PGT. *Hum Reprod Open.* (2020) 2020:hoaa020. doi: 10.1093/hropen/hoaa020
5. Liu J, Lissens W, van Broeckhoven C, Löfgren A, Camus M, Liebaers I, et al. Normal pregnancy after preimplantation DNA diagnosis of a dystrophin gene deletion. *Prenat Diagn.* (1995) 15:351–8. doi: 10.1002/pd.1970150409
6. Chaperon JL, Wemmer NM, McKanna TA, Clark DM, Westemeyer MA, Gauthier P, et al. Preimplantation genetic testing for kidney disease-related genes: a laboratory's experience. *Am J Nephrol.* (2021) 52:684–90. doi: 10.1159/000518253
7. Berckmoes V, Verdyck P, De Becker P, De Vos A, Verheyen G, Van der Niepen P, et al. Factors influencing the clinical outcome of preimplantation genetic testing for polycystic kidney disease. *Hum Reprod.* (2019) 34:949–58. doi: 10.1093/humrep/dez027
8. Shi W-H, Ye M-J, Chen S-C, Zhang J-Y, Chen Y-Y, Zhou Z-Y, et al. Case report: preimplantation genetic testing and pregnancy outcomes in women with alport syndrome. *Front Genet.* (2021) 12:633003. doi: 10.3389/fgene.2021.633003
9. Tšuiko O, Fernandez Gallardo E, Voet T, Vermeesch JR. Single-cell technologies at the forefront of PGT and embryo research. *Reproduction.* (2020) 160:A19–31. doi: 10.1530/REP
10. Huang S, Niu Y, Li J, Gao M, Zhang Y, Yan J, et al. Complex preimplantation genetic tests for Robertsonian translocation, HLA, and X-linked hyper IgM syndrome caused by a novel mutation of CD40LG gene. *J Assist Reprod Genet.* (2020) 37:2025–31. doi: 10.1007/s10815-020-01846-y
11. Xi Y, Chen G, Lei C, Wu J, Zhang S, Xiao M, et al. Expanded carrier screening in Chinese patients seeking the help of assisted reproductive technology. *Mol Genet Genomic Med.* (2020) 8:e1340. doi: 10.1002/mgg3.1340
12. Harton GL, de Rycke M, Fiorentino F, Moutou C, SenGupta S, Traeger-Synodinos J, et al. ESHRE PGD consortium best practice guidelines for amplification-based PGD. *Hum Reprod.* (2011) 26:33–40. doi: 10.1093/humrep/deq231
13. Richards S, Aziz N, Bale S, Bick D, Das S, Gastier-Foster J, et al. Standards and guidelines for the interpretation of sequence variants: a joint consensus recommendation of the American college of medical genetics and genomics and the association for molecular pathology. *Genet Med.* (2015) 17:405–24. doi: 10.1038/gim.2015.30
14. Xiao M, Lei C-X, Xi Y-P, Lu Y-L, Wu J-P, Li X-Y, et al. Next-generation sequencing is more efficient at detecting mosaic embryos and improving pregnancy outcomes than single-nucleotide polymorphism array analysis. *J Mol Diagn.* (2021) 23:710–8. doi: 10.1016/j.jmoldx.2021.02.011
15. McLaren W, Pritchard B, Rios D, Chen Y, Flicek P, Cunningham F. Deriving the consequences of genomic variants with the Ensembl API and SNP Effect Predictor. *Bioinformatics.* (2010) 26:2069–70. doi: 10.1093/bioinformatics/btq330
16. Karczewski KJ, Francioli LC, Tiao G, Cummings BB, Alföldi J, Wang Q, et al. The mutational constraint spectrum quantified from variation in 141,456 humans. *Nature.* (2020) 581:434–43. doi: 10.1038/s41586-020-2308-7
17. Li MM, Datto M, Duncavage EJ, Kulkarni S, Lindeman NI, Roy S, et al. Standards and guidelines for the interpretation and reporting of sequence variants in cancer: a joint consensus recommendation of the association for molecular pathology, American society of clinical oncology, and college of American pathologists. *J Mol Diagn.* (2017) 19:4–23. doi: 10.1016/j.jmoldx.2016.10.002
18. Richards CS, Bale S, Bellissimo DB, Das S, Grody WW, Hegde MR, et al. ACMG recommendations for standards for interpretation and reporting of sequence variations: revisions 2007. *Genet Med.* (2008) 10:294–300. doi: 10.1097/GIM.0b013e31816b5cae
19. MacArthur DG, Manolio TA, Dimmock DP, Rehm HL, Shendure J, Abecasis GR, et al. Guidelines for investigating causality of sequence variants in human disease. *Nature.* (2014) 508:469–76. doi: 10.1038/nature13127
20. den Dunnen JT, Dalgleish R, Maglott DR, Hart RK, Greenblatt MS, McGowan-Jordan J, et al. HGVS Recommendations for the description of sequence variants: 2016 update. *Hum Mutat.* (2016) 37:564–9. doi: 10.1002/humu.22981
21. Natesan SA, Bladon AJ, Coskun S, Qubbaj W, Prates R, Munne S, et al. Genome-wide karyomapping accurately identifies the inheritance of single-gene defects in human preimplantation embryos in vitro. *Genet Med.* (2014) 16:838–45. doi: 10.1038/gim.2014.45
22. Taylor TH, Gitlin SA, Patrick JL, Crain JL, Wilson JM, Griffin DK. The origin, mechanisms, incidence and clinical consequences of chromosomal mosaicism in humans. *Hum Reprod Update.* (2014) 20:571–81. doi: 10.1093/humupd/dmu016
23. Thorpe J, Osei-Owusu IA, Avigdor BE, Tupler R, Pevsner J. Mosaicism in human health and disease. *Annu Rev Genet.* (2020) 54:487–510. doi: 10.1146/annurev-genet-041720-093403
24. Taylor TH, Patrick JL, Gitlin SA, Crain JL, Wilson JM, Griffin DK. Blastocyst euploidy and implantation rates in a young (<35 years) and old (≥35 years) presumed fertile and infertile patient population. *Fertil Steril.* (2014) 102:1318–23. doi: 10.1016/j.fertnstert.2014.07.1207
25. Committee on Genetics. Committee opinion no. 690: carrier screening in the age of genomic medicine. Obstet Gynecol. (2017) 129:e35–40. doi: 10.1097/AOG.0000000000001951
26. Scriven PN. Carrier screening and PGT for an autosomal recessive monogenic disorder: insights from virtual trials. *J Assist Reprod Genet.* (2022) 39:331–40. doi: 10.1007/s10815-022-02398-z
27. Ahn YH, Lee C, Kim NKD, Park E, Kang HG, Ha I-S, et al. Targeted exome sequencing provided comprehensive genetic diagnosis of congenital anomalies

of the kidney and urinary tract. *J Clin Med.* (2020) 9:751. doi: 10.3390/jcm9030751
28. Gullo G, Petousis S, Papatheodorou A, Panagiotidis Y, Margioula-Siarkou C, Prapas N, et al. Closed vs. Open oocyte vitrification methods are equally effective for blastocyst embryo transfers: prospective study from a sibling oocyte donation program. *Gynecol Obstet Invest.* (2020) 85:206–12. doi: 10.1159/000506803
29. Cavaliere AF, Perelli F, Zaami S, D'Indinosante M, Turrini I, Giusti M, et al. Fertility sparing treatments in endometrial cancer patients: the potential role of the new molecular classification. *Int J Mol Sci.* (2021) 22:12248. doi: 10.3390/ijms222212248
30. Gullo G, Etrusco A, Cucinella G, Perino A, Chiantera V, Laganà AS, et al. Fertility-sparing approach in women affected by stage I and low-grade endometrial carcinoma: an updated overview. *Int J Mol Sci.* (2021) 22:11825. doi: 10.3390/ijms222111825
31. Shi H, Niu W, Liu Y, Jin H, Song W, Shi S, et al. A novel monogenic preimplantation genetic testing strategy for sporadic polycystic kidney caused by de novo PKD1 mutation. *Clin Genet.* (2021) 99:250–8. doi: 10.1111/cge.13871
32. Xu C, Yang C, Ye Q, Xu J, Tong L, Zhang Y, et al. Mosaic PKHD1 in polycystic kidneys caused aberrant protein expression in the mitochondria and lysosomes. *Front Med (Lausanne).* (2021) 8:743150.

Conflict of Interest: XS was the guarantor of this work, and as such, had full access to all the data in the study and took responsibility for the integrity of the data and accuracy of the data analysis.

The remaining authors declare that the research was conducted in the absence of any commercial or financial relationships that could be construed as a potential conflict of interest.

Publisher's Note: All claims expressed in this article are solely those of the authors and do not necessarily represent those of their affiliated organizations, or those of the publisher, the editors and the reviewers. Any product that may be evaluated in this article, or claim that may be made by its manufacturer, is not guaranteed or endorsed by the publisher.

frontiers | Frontiers in Medicine

ORIGINAL RESEARCH
published: 20 June 2022
doi: 10.3389/fmed.2022.924579

N^6-Methyladenosine Methylomic Landscape of Ureteral Deficiency in Reflux Uropathy and Obstructive Uropathy

Hua Shi[1,2,3†], *Tianchao Xiang*[1,2,3†], *Jiayan Feng*[4†], *Xue Yang*[1,2,3], *Yaqi Li*[1,2,3], *Ye Fang*[1,2,3], *Linan Xu*[1,2,3], *Qi Qi*[1,2,3], *Jian Shen*[5], *Liangfeng Tang*[5], *Qian Shen*[1,2,3], *Xiang Wang*[5*], *Hong Xu*[1,2,3*] *and Jia Rao*[1,3,6*]

[1] Department of Nephrology, Children's Hospital of Fudan University, Shanghai, China, [2] Shanghai Kidney Development and Pediatric Kidney Disease Research Center, Shanghai, China, [3] Shanghai Key Lab of Birth Defect, Children's Hospital of Fudan University, Shanghai, China, [4] Department of Pathology, Children's Hospital of Fudan University, Shanghai, China, [5] Department of Urology, Children's Hospital of Fudan University, Shanghai, China, [6] State Key Laboratory of Medical Neurobiology, Institutes of Brain Science and School of Basic Medical Science, Fudan University, Shanghai, China

Background: Congenital anomalies of the kidneys and urinary tracts (CAKUT) represent the most prevalent cause for renal failure in children. The RNA epigenetic modification N^6-methyladenosine (m^6A) methylation modulates gene expression and function post-transcriptionally, which has recently been revealed to be critical in organ development. However, it is uncertain whether m^6A methylation plays a role in the pathogenesis of CAKUT. Thus, we aimed to explore the pattern of m^6A methylation in CAKUT.

Methods: Using m^6A-mRNA epitranscriptomic microarray, we investigated the m^6A methylomic landscape in the ureter tissue of children with obstructive megaureter (M group) and primary vesicoureteral reflux (V group).

Results: A total of 228 mRNAs engaged in multiple function-relevant signaling pathways were substantially differential methylated between the "V" and "M" groups. Additionally, 215 RNA-binding proteins that recognize differentially methylated regions were predicted based on public databases. The M group showed significantly higher mRNA levels of m^6A readers/writers (YTHDF1, YTHDF2, YTHDC1, YTHDC2 and WTAP) and significantly lower mRNA levels of m^6A eraser (FTO) according to real-time PCR. To further investigate the differentially methylated genes, m^6A methylome and transcriptome data were integrated to identified 298 hypermethylated mRNAs with differential expressions (265 upregulation and 33 downregulation) and 489 hypomethylated mRNAs with differential expressions (431 upregulation and 58 downregulation) in the M/V comparison.

Conclusion: The current results highlight the pathogenesis of m^6A methylation in obstructive and reflux uropathy.

Keywords: uropathy, megaureter, vesicoureteral reflux, m^6A, N^6-methyladenosine, microarray

OPEN ACCESS

Edited by:
Xu-jie Zhou,
First Hospital, Peking University, China

Reviewed by:
Yanqin Zhang,
First Hospital, Peking University, China
Yafeng Li,
The Fifth Hospital of Shanxi Medical University, China

***Correspondence:**
Xiang Wang
wangxiang3333@hotmail.com
Hong Xu
hxu@shmu.edu.cn
Jia Rao
jiarao@fudan.edu.cn

[†]These authors have contributed equally to this work

Specialty section:
This article was submitted to Nephrology, a section of the journal Frontiers in Medicine

Received: *20 April 2022*
Accepted: *23 May 2022*
Published: *20 June 2022*

Citation:
Shi H, Xiang T, Feng J, Yang X, Li Y, Fang Y, Xu L, Qi Q, Shen J, Tang L, Shen Q, Wang X, Xu H and Rao J (2022) N^6-Methyladenosine Methylomic Landscape of Ureteral Deficiency in Reflux Uropathy and Obstructive Uropathy. Front. Med. 9:924579. doi: 10.3389/fmed.2022.924579

INTRODUCTION

N^6-methyladenosine (m^{6}A) methylation is the most abundant and conserved internal modification in messenger RNA (mRNA) and long non-coding RNAs (1). m^{6}A can be produced by the "writer" complex methyltransferase-like 3 (METTL3), methyltransferase-like 14 (METTL14) (2), and Wilms tumor 1-associated protein (WTAP) (3), removed by the demethylases ("erasers") fat mass and obesity associated protein (FTO) (4) and alkB homolog 5 (ALKBH5) (5), and recognized by "readers" such as the YTH family of proteins (6). m^{6}A is involved in mRNA splicing, polyadenylation, export, translation, and stability (7). Throughout life, m^{6}A-modified mRNAs play a role in variety of physiological activities, developmental processes and disease pathologies (7, 8). Multiple diseases, such as heart failure (9), type 2 diabetes (10), kidney injury (11) and asthma (12) and various malignancies are associated with changes in m^{6}A methylation.

Thousands of m^{6}A peaks in mammalian mRNA have been identified in techniques of the high-throughput sequencing. According to the Nephroseq database (www.nephroseq.org, University of Michigan, Ann Arbor, MI) (13), hypoexpression of METTL3, METTL14 and WTAP has been reported in diabetic mice, in patients with chronic kidney disease (CKD) and patients with focal segmental glomerulosclerosis, indicating the feedback disruption of m^{6}A. It has been demonstrated that METTL14-induced m^{6}A methylation could posttranscriptionally modulate Sirt1 mRNA, contributing to podocyte injury(14). Other studies discovered the METTL14-YAP1 pathway participated in the renal ischemia-reperfusion injury (15) and METTL14-regulated PI3K/Akt signaling pathway is involved in renal tubular cell epithelial-mesenchymal transition in diabetic nephropathy (16). Despite recent advances in m^{6}A and numerous physiological and pathological processes associated with kidney disease (10), little is known about m^{6}A-mediated regulatory effect in kidney development.

Congenital anomalies of the kidneys and urinary tracts (CAKUT) are embryonic disorder that causes a spectrum of defects in the kidneys, the ureters, the bladder and the urethra during development. CAKUT affects ∼5 per 1,000 live newborns and accounts for 30% to 50% of all children end-stage renal disease (ESRD) (17). CAKUT induces renal deficiency that is constantly associated with urinary tract infection (UTI) and urine outflow abnormalities. Outflow abnormalities include obstructive nephropathies caused by obstruction of ureteropelvic junction/ureterovesical junction, megaureter, posterior urethral valves, and reflux uropathy induced by vesicoureteral reflux (VUR). During nephrogenesis, genetic and epigenetic changes have been demonstrated to be important (17, 18). Even though there have been significant advances in kidney diseases, the etiology and morphogenesis of uropathy are still unknown. Megaureter might lead to functional obstruction with an adynamic ureteral ending segment. In neonates, primary obstructive megaureter is involved in the fetal ureteric folds that remain or delay in the process of peristalsis. Primary VUR is distinct from megaureter, which is caused by a short or missing intravesical ureter or other vesico-ureteric junction disruption, accompanied by normal structural and functional ureters. Early diagnosis of reflux or obstructive uropathy is critical to prevent renal damage from reflux, obstruction and infection. Due to the lack of adequate knowledge of the mechanism, it is difficult to predict the renal prognosis of children with reflux or obstructive nephropathy.

To gain a better understanding of the role of m^{6}A in uropathy, we enrolled the ureter samples from patients with VUR or megaureter to investigate of the distribution schema and readout of the differentially methylated mRNA. The differential methylation site was employed to make a prediction on the RNA-binding protein (RBP) candidates. A final integrated analysis of the m^{6}A microarray data was performed to determine the association between the mRNAs methylation and the gene expression levels. In this paper, we illustrated the critical role of m^{6}A methylation in ureteral defects of CAKUT.

MATERIALS AND METHODS

Patients and Human Materials

After receiving approval from the Research Ethics Board of Children's Hospital of Fudan university (2020-363), our local ethics board, patients with obstructive uropathy or reflux uropathy were enrolled into the study from January 2020 to October 2020. Prior to enrolling patients in this study, we received written informed permission from all parents or legal guardians. The diagnosis of different types of CAKUT was established through a series of radiological examinations. Primary obstructive megaureter was diagnosed by combining the clinical features and radiological findings of diuretic renography. The surgery criteria for primary obstructive megaureter were the differential renal function $<$40% and/or anterior–posterior diameter of the renal pelvis on ultrasonographic scan $>$100 mm and half-time of the elimination phase (T1/2) of 99mTc –DTPA diuretic renogram $>$20 min. VUR diagnosis criteria were based on the parameters that was established by the International Reflux Study Committee in 1981 (19). Exclusion criteria were associated anomalies including pelviureteric junction obstruction, ectopic ureter, duplicated collecting systems, ureterocele, posterior urethral valves, neurogenic bladder or prune belly. The children were categorized into two study groups. Patients with primary non-refluxing megaureter were distributed into the patient group of "M" (M group). Patients with primary VUR who had no other urinary tract defects were distributed into the patient group of "V" (V group). The reflux degree of these patients was greater than grade three.

Specimens were obtained from children who underwent ureteral reimplantation surgeries at our hospital. Due to the nature of subject, it was impossible to obtain tissue samples from completely normal distal ureteric ends. Therefore, there were no normal controls. We compared the pathological features among the ureter tissue samples from patients with megaureter or VUR. The surgical cut in the ureter tissue was 3–5 mm long, and roughly 1 mm tissue was removed from the distal ureter, and sent to the department of pathology. The surgeon and the pathologist made sure the complete of samples and prevented contamination. The pathologist dehydrated the tissue before

embedding it in paraffin. The remaining tissues were cut into 1 mm blocks and deposited in RNA preservation solution, which was preserved at 4°C overnight before being transferred to an −80°C freezer for long-term storage.

m^{6}A mRNA Epitranscriptomic Microarray

Total RNA was isolated from each sample using TRIzol reagent (Invitrogen, Carlsbad, CA, USA) as directed by the manufacturer. The NanoDrop ND-1000 was used to determine purity and amount of total RNA samples (Thermo Fisher, Shanghai, China). To detect and verify the integrity of total RNA (RIN values >7.0), we employed a Bioanalyzer 2100 (Agilent, Santa Clara, CA, USA) for agarose electrophoresis.

Due to the RNA sample requirements for microarray and limited tissue samples from children's ureters, we utilized the m^{6}A microarray (total RNA <1 ug) rather than MeRIP Seq (total RNA >120 ug). The Arraystar Human m^{6}A-mRNA&lncRNA Epitranscriptomic microarray analysis was conducted in the three samples from patients with primary non-refluxing megaureter compared with the three samples from patients with primary VUR. In brief, m^{6}A antibody was used to immunoprecipitate total RNAs isolated from specimens. As the "IP", the modified RNAs were eluted from the immunoprecipitated magnetic beads. The unmodified RNAs were recovered as "Sup" from the supernatant. The Arraystar Super RNA Labeling Kit was used to label the "IP" and "Sup" RNAs with Cy5 and Cy3 respectively as cRNAs in separate procedures. Arraystar Human mRNA&lncRNA Epitranscriptomic Microarray (8x60K, Arraystar) with 44,122 mRNA degenerate probes degenerate probes was used to hybridize the cRNAs. After washing the slides, an Agilent Scanner G2505C were used to scan the arrays in two-color channels.

Microarray Data Analysis

To analyze acquired array images, Agilent Feature Extraction software (version 11.0.1.1) was unutilized. The average value of log2-scaled Spike-in RNA intensities was presented to standardize the raw intensities of IP (immunoprecipitated, Cy5-labeled) and Sup (supernatant, Cy3-labeled). Following Spike-in normalization, the probe signals with Present (P) or Marginal (M) QC flags in the Excel sheet were kept as "All Targets Value" for further evaluation of "m^{6}A methylation level," "m^{6}A amount," and "expression level". Based on the IP (Cy5-labeled) and Sup (Cy3-labeled) normalized intensities, the "m^{6}A methylation level" was assessed for the percentage of alteration. The calculating formula was provided in the **Supplementary Tables S2, S3**). Based on the IP (Cy5-labeled) normalized intensities, the "m^{6}A quantity" was derived for the m^{6}A methylation amount. The sum of IP (Cy5-labeled) and Sup (Cy3-labeled) normalized intensities of RNA was used to calculate "expression level." Filtering with the fold change and statistical significance (p-value) thresholds were performed to identify the differently m^{6}A-methylated RNAs or differentially expressed RNAs between the two comparisons. To illustrate the distinct m^{6}A-methylation or expression pattern among samples, hierarchical clustering was conducted.

Methylated RNA Immunoprecipitation (MeRIP)-qPCR Validation

MeRIP assay was conducted for the same six RNA samples using the Magna MeRIP^{TM} m^{6}A Kit (Millipore, Billerica, MA, USA). Magnetic IP with a monoclonal antibody against m^{6}A and IgG antibody was used following total RNA fragmentation into 100 nucleotides. qRT-PCR normalized the input RNA to analyze the immunoprecipitated RNA. Each experiment was performed in triplicate independently. The primers sequences with reference to the m^{6}A motif regions of the mRNAs were displayed in **Supplementary Table S1**.

Real-Time PCR

The m^{6}A writers (METTL3, METTL14, and WTAP), readers (YTHDC1, YTHDC2, YTHDF1, YTHDF1, YTHDF2 and YTHDF3) and erasers (FTO and ALKBH5) were selected and analyzed by real-time PCR in ureteral samples. Due to the quantity restriction of tissue samples, the independent set of ureteral samples was performed the qRT-PCR. With the High Capacity RNA to cDNA Kit, cDNA was reverse transcribed from 1 μg of total RNA (Applied Biosystems). The mRNA levels were assessed by real-time PCR analysis with SYBR-green protocol by gene-specific primers (**Supplementary Table S1**). 18S rRNA was selected as house-keeping control. For MeRIP-qPCR analysis of differentially methylated RNAs, equal volume of immunoprecipitated RNA or 10% of input RNA was converted to cDNA and amplified using gene-specific primers for mRNAs (**Supplementary Table S1**). Triplicates of real-time PCR experiments were performed.

Data Processing and Statistical Analysis

Differentially m^{6}A-methylated RNAs and differentially expressed RNAs in the M/V group comparison were presented by filtering with the fold change (FC $\geq$ 1.5 or $\leq$ 0.7) and were identified at a false discovery rate (FDR) of $<$ 0.05. We retrieved a gene list from the Enrichr platform by searching for "uropathy" in the metadata including libraries created from TRRUST, BioPlanet, GWAS Catalog, the UK Biobank, ClinVar, PheWeb, and DepMap (20). The matching genes were highlighted into the m^{6}A quantity and m^{6}A expressing level profiling data (**Supplementary Table S2**). For differentially m^{6}A-methylated or expressed RNAs, a hierarchical clustering heatmap was displayed. Differentially m^{6}A-methylated or expressed mRNAs were analyzed for Gene Ontology (GO) analysis using the top GO package (R environment) and Kyoto Encyclopedia of Genes and Genomes (KEGG) pathway enrichment. Fisher's exact test were used to determine the differences between the two groups with a $P < 0.05$ defined as statistically significance.

RESULTS

Patient Sample Characteristics

A total of 24 ureteral samples were collected. The "V" group had 18 patients (male: female 11:7) with a median age of 42 months. There were seven cases of grade IV reflux, and 11 cases with grade V reflux. The "M" group had six patients (male: female 4:2) of megaureter with the median age of 47 months. Among the 24

cases, no pathogenic variants or copy number variants (CNVs) were identified through trio-whole exome sequencing. No marked differences were found in the morphology of the ureter tissue. The "M" group presented disruption in the muscular layers of specimens with an extracellular matrix accumulation. In the "V" group, there were no aberrant changes in the muscular layers and no rearrangement of collagen fibers, fibrocytes or fibroblasts in the adventitia (**Figures 1A,B**). Hence, we decided to explore the m^{6}A patterns in the ureter tissue samples from patients with primary obstructive uropathy compared with those from the patients with VUR as controls.

Distribution Patterns of m^{6}A Methylation in Reflux or Obstructive Uropathy

We investigated immunoprecipitated m^{6}A methylation RNAs extracted from the ureters of patients with VUR and patients with obstructive megaureter disease to elucidate the regulation of transcript-specific m^{6}A on ureteral phenotype. Microarray profiling revealed a difference in m^{6}A methylation of 228 transcripts (228 mRNAs) between "V" (VUR) and "M" (Megaureter) groups (FC $\geq$ 1.5 or, $\leq$ 0.7) (**Supplementary Tables S2, S3**). The majority of the differentially methylated mRNAs (81.2%) were substantially hyper-methylated in the M/V comparison. The association between the samples were identified by hierarchical clustering, which were categorized based on m^{6}A methylation level (**Figures 1C,D**). The peaks of the transcriptome-wide m^{6}A in ureteral tissues were distributed across the 23 chromosomes shown in the **Figure 2**, indicating the broadly distributed peaks on the chromosomes. Additionally, the distribution pattern matched the density of gene content (**Figures 2A,B**). When the density of these differentially methylated peaks was calculated, it was found that they were not distributed homogeneously (chi square test, $P < 0.05$). Chromosomes 1, 2, 16, 19, 17, 7, and X were the top six chromosomes having the most methylated peaks. In detail, chromosome 1 (hypermethylated peaks, 22; hypomethylated peaks, 4) was followed by chromosome 2 (hypermethylated peaks, 18; hypomethylated peaks, 3), chromosome 16 (hypermethylated peaks, 19), chromosome 19 (hypermethylated peaks, 16; hypomethylated peaks, 2), chromosome 17 (hypermethylated peaks, 13; hypomethylated peaks, 2), chromosome 7 (hypermethylated peaks, 14; hypomethylated peaks, 1) and chromosome X (hypermethylated peaks, 10; hypomethylated peaks, 3). In the M/V comparison, most hypermethylated regions were enriched in chromosomes 1 (22 peaks), 2 (18 peaks), 16 (19 peaks), 19 (16 peaks) and 7 (14 peaks), whereas most hypomethylated peaks were enriched in chromosomes 1 (4 peaks), 4 (3 peaks), 2 (3 peaks), and X (3 peaks) (**Figure 2A**). Besides, the hypermethylated peaks with the maximal widths were located on chromosomes 14, 13, 7 and 5, whereas hypomethylated peaks with the maximal widths were observed on chromosomes 4, 6, 2 and 1. The peak site positions across the human chromosomes were displayed by mapping differentially methylated areas (inside mRNA transcripts) to the human chromosomes (**Figure 2B**). Ten hypermethylated peaks located in the *16p11.2* (6 hypermethylated peaks), *17q12* (2 hypermethylated peaks), *22q11.2* (1 hypermethylated peaks) and *4p16.3* (1 hypermethylated peaks), which are the known pathogenic CNVs for CAKUT. The top 20 differentially methylated mRNAs in M-group were listed in **Table 1** based on log2 Fold change. The differently methylated genes located in the *17q12, 16p11.2, 22q11.2 and 4p16.3* were presented in the **Supplementary Table S2**, none of which matched the gene list associated with uropathy reported in the Enrichr metadata (20).

Differentially Methylated mRNAs in Reflux or Obstructive Uropathy

To explore the mRNA expression patterns between Megaureter and VUR, the total mRNAs tagged with Cy3 fluorescent dye were profiled using microarray. Most of the differentially methylated mRNAs were hypermethylated in the ureteral samples from M-group compared with that from V-group (196/228) (**Figure 2C**). The top 20 differentially methylated mRNAs with differential expressions were listed in **Table 2**.

Additionally, GO and KEGG enrichment analyses were conducted to investigate the biological impact of the differentially methylated mRNAs on the uropathy pathogenic processes. A summary of the distributions of the differentially methylated mRNAs enriched in several GO categories was displayed in **Figure 3A**. In the biological process (BP) category, differentially methylated mRNAs were notably enriched in "actin filament-based transport" (fold enrichment 17.0, $P = 0.7\times10^{-3}$), "response to mitochondrial depolarization" (fold enrichment 17.0, $P = 0.5\times10^{-3}$), and "glycogen biosynthetic process" (fold enrichment 10.3, $P = 0.7\times10^{-3}$). In the cellular component (CC) category, the top three enriched functions were "mRNA cleavage and polyadenylation specificity factor complex" (fold enrichment 13.4, $P = 0.010$), "collagen trimer" (fold enrichment 5.5, $P = 0.006$), and "nuclear speck" (fold enrichment 2.7, $P = 0.006$). In the molecular function (MF) category, "UDP-glucosyltransferase activity" (fold enrichment 20.0, $P = 0.004$), "semaphorin receptor binding" and (fold enrichment 12.2, $P = 0.011$) were the most enriched terms. Likewise, the clustering analysis of the differentially methylated mRNAs were analyzed in the 10 KEGG categories (**Figure 3B**). The enrichment of KEGG pathways by the differentially methylated mRNAs included "Endometrial cancer", "VEGF signaling pathway", "GnRH secretion" and "Aldosterone-regulated sodium reabsorption" ($P = 0.05$, **Figures 3B,C**). Among these pathways, the *HRAS* and *PIK3R3* genes participated in most of the signaling pathways. And the *TCF7L2* gene as a key transcription factor in Wnt/β-catenins pathway participated in four of the signaling pathways shown by KEGG analysis. Further information on the enriched GO items, KEGG pathways and the corresponding genes were listed in **Supplementary Tables S4, S5**.

Differentially Expressed Genes in Reflux or Obstructive Uropathy

Comparison of the expressed level of genes between the M group and the V group indicated 1530 differentially expressed genes in total (**Supplementary Table S3**), among which 1469 were upregulated and 61 were downregulated (**Figure 2D**). Among

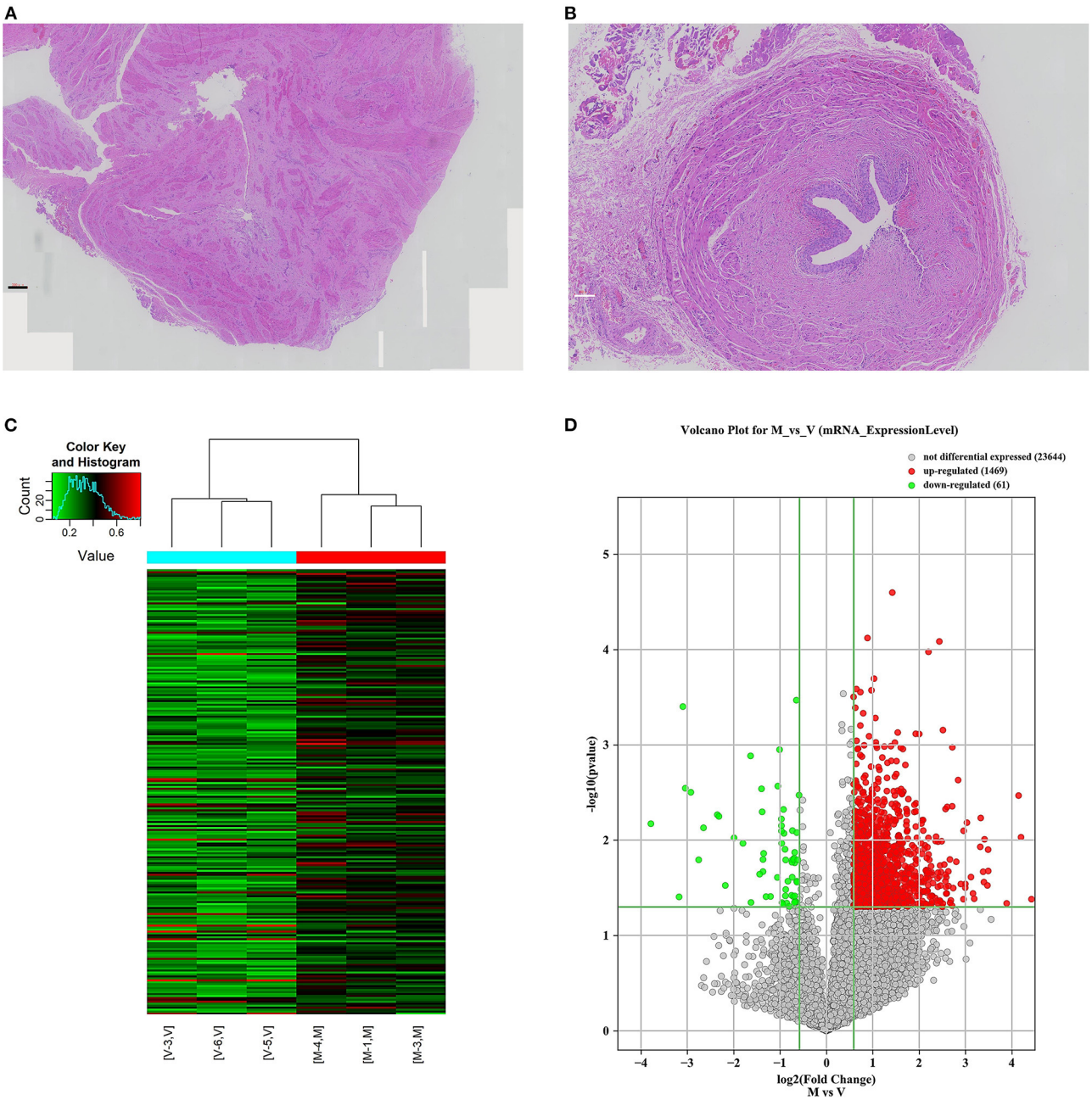

FIGURE 1 | mRNA m^{6}A modification profile changes and mRNA expression analysis in different ureteral phenotypes. **(A)** The ureter tissue from a patient with megaureter showed the atrophy and derangement in the muscular layers of specimen with increased extracellular matrix. **(B)** The ureter tissue from a patient with vesicoureteral reflux (VUR) showed no normal mucosal and muscular architecture. **(C)** Hierarchical clustering of all samples addressing the non-random partitioning of samples into two major groups: V-group (VUR), M-group (Megaureter). Each column represents one sample and each row represents one mRNA. **(D)** Volcano plot analysis of 1,469 upregulated and 61 downregulated mRNAs (M-group vs. V-group, $P < 0.05$). Red boxes represent $\geq$ 0.5-fold change difference, $P < 0.05$. Green boxes represent $\leq$ 0.7-fold change difference, $P < 0.05$.

the differentially expressed genes, 116 genes matched the gene list associated with uropathy reported in the Enrichr platform (20) including *ACE, PAX2, RUNX2* (**Supplementary Table S3**). These differentially expressed genes were subsequently analyzed through GO and KEGG enrichment (**Figures 3D–F**). The findings of GO enrichment included "regulation of nitrogen compound metabolic process", "regulation of macromolecule metabolic process", "nucleoplasm", "organelle lumen", and "transcription factor binding" and "transcription regulator activity" (**Figure 3D**, **Supplementary Table S6**). KEGG analysis

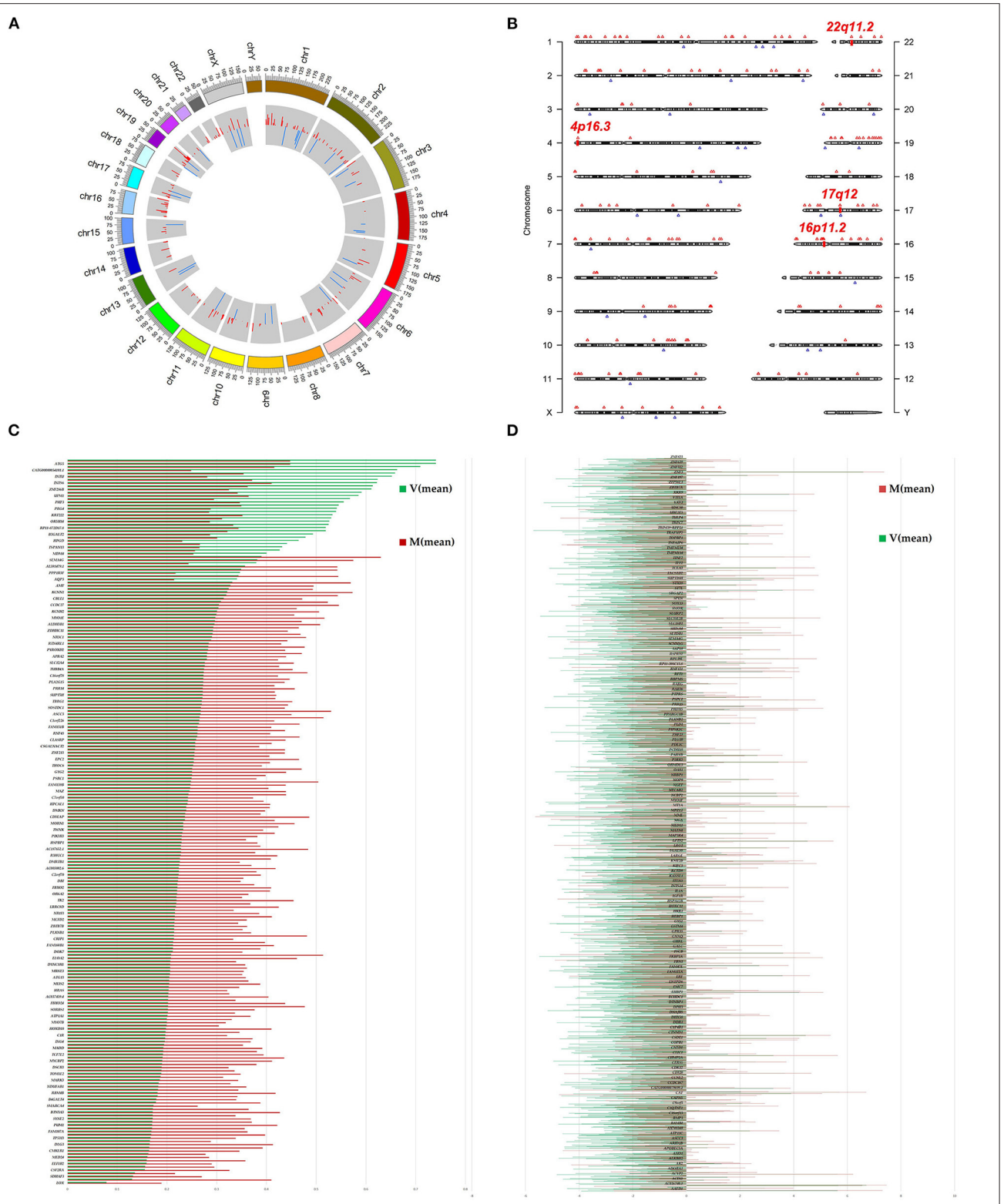

FIGURE 2 | Landscape of *N6*-methyladenosine (m^{6}A)-modified transcript in ureter tissue samples from patients with megaureter (M) or vesicoureteral reflux (VUR, V). **(A)** The m^{6}A peaks' density distribution along the chromosomes. The first (red circle) and second (blue circle) tracks indicate the frequency distribution of the hyper- and hypomethylated peaks, respectively. chr, chromosome. **(B)** Chromosomal distribution patterns of the hypermethylated (red) and hypomethylated (blue) m6A peaks within mRNAs. **(C)** Differentially methylated mRNAs based on log2(FC). **(D)** Differentially expressed mRNAs based on log2(FC).

TABLE 1 | The top 20 differentially methylated mRNAs based on log2(FC).

Gene name	Chromosome	Peak start	Peak end	*p*-value	Log_2(FC)	Regulation	Methylated region
GYS1	chr19	49471387	49496567	2.55E-03	3.16	Hyper	Exon
DLG3	chrX	69672155	69725337	3.47E-02	2.50	Hyper	Exon, Intron
BTN3A3	chr6	26440784	26452145	6.90E-03	2.49	Hyper	Intron
PUM1	chr1	31404353	31538551	5.38E-03	2.47	Hyper	Exon, Intron
RPL13	chr16	89627119	89630950	3.32E-02	2.47	Hyper	Exon
LOX	chr5	121398890	121413980	1.24E-02	2.41	Hyper	Exon
HIRIP3	chr16	30004311	30006964	2.72E-02	2.38	Hyper	Exon, Intron
PEX14	chr1	10534944	10690815	1.99E-02	2.36	Hyper	Exon, Intron
IL5RA	chr3	3133488	3151664	3.84E-02	2.36	Hyper	Exon, Intron
RBM4B	chr11	66432766	66445295	1.27E-03	2.31	Hyper	Exon, Intron
RP11-872D17.8	chr11	57154260	57158130	8.04E-03	0.66	hypo	Exon, Intron
KRT222	chr17	38811872	38821393	2.16E-02	0.66	hypo	Exon, Intron
INTS6	chr13	51939364	51995510	2.93E-02	0.66	hypo	Exon, Intron
UGT1A6	chr2	234601512	234681946	3.18E-02	0.64	hypo	Exon, Intron
TMIGD3	chr1	112026191	112106556	2.28E-02	0.64	hypo	Exon, Intron
HDX	chrX	83572886	83757461	2.58E-02	0.64	hypo	Exon, Intron
MDM4	chr1	204485507	204527247	4.76E-04	0.63	hypo	Exon, Intron
MORF4L2	chrX	102930428	102941746	5.72E-03	0.63	hypo	Exon
AQP3	chr9	33441806	33447551	3.44E-02	0.63	hypo	Exon
PPP1R3F	chrX	49126333	49143632	4.39E-02	0.63	hypo	Exon, Intron

revealed several significantly enriched pathways involved in metabolism and development, such as "glyoxylate and dicarboxylate metabolism", "Carbon metabolism", "ubiquitin mediated proteolysis", "MAPK signaling pathway", "VEGF signaling pathway" and "adherens junction" (**Figures 3E,F**, **Supplementary Table S7**).

Prediction of RNA-Binding Proteins

The RMBase (v2.0) database was utilized to predict the RNA-Binding Proteins (RBPs) that might interact with the differentially methylated mRNAs (21). The hypermethylated regions yielded 113 candidate RBPs, whereas the hypomethylated regions yielded 102 candidate RBPs (**Supplementary Table S8**). We analyzed the RBPs binding abundance in the differentially methylated m^{6}A regions. The RBPs that bound the most of regions were *EIF4A3, AGO, WDR33, ELAVL, IGF2BP1* and *FBL*. The RBPs in the hypermethylated group were mostly distributed in regions with log2(Fold change) 1.5-2.0, while RBPs in the hypomethylated group were mostly distributed in regions with log2 (Fold change) 0.5–1.0 (**Figure 4A**). RBP binding was more abundant in hypermethylated regions than in hypomethylated regions (**Figure 4A**), indicating that the RBPs might prefer to target hypermethylated gene sets. We found the known "Readers", "Writers" and "Eraser" for m^{6}A mostly distributed in the hyper-methylated regions included YTHDF1, YTHDF2, YTHDC1, METTL3, METTL14, WTAP and ALKBH5 (**Figures 4B,C**). Additionally, we also predated the enrichment of the RBPs associated with kidney disease including IGF2BP2 and MSI1 in the hypermethylated group.

According to GO and KEGG enrichment, these 215 RBPs were significantly enriched in GO items and KEGG pathways linked to the biogenesis and metabolism of RNA. For example, RBPs were significantly enriched in the GO items "Pre-miRNA processing", "regulation of mRNA binding", "RISC complex" and "RNAi effector complex" (**Figure 4D**, **Supplementary Table S8**). And the KEGG enrichment indicated the pathway in "spliceosome", "mRNA surveillance pathway" and "Ribosome biogenesis" (**Figure 4E**, **Supplementary Table S8**).

Additionally, the mRNA levels of the m^{6}A readers, writers and erasers were measured via qRT-PC. When the mRNA levels in the ureteral tissue samples from the M group were compared to that from the V group, the levels of YTHDF1, YTHDF2, YTHDC1, YTHDC2 and WTAP were significantly higher, whereas the level of FTO was significantly lower ($P < 0.05$; $n = 6$/group) (**Figure 4F**).

Joint Profiling of m^{6}A Methylation and Gene Expression in Reflux or Obstructive Uropathy

In the M/V comparison, joint analysis of the differentially methylated m^{6}A mRNAs and differentially expressed mRNA revealed the four modes of m^{6}A modification-associated mRNAs: (i) m^{6}A hyper-methylated and upregulated mRNAs; (ii) m^{6}A hyper-methylated and downregulated mRNAs; (iii) m^{6}A hypo-methylated and upregulated mRNAs, (iv) m^{6}A hypo-methylated and downregulated mRNAs. We teased out the significant differential expressions in 787 differentially methylated mRNA transcripts. Among the 298 hypermethylated mRNAs, we found 265 upregulated and 33 downregulated expressed mRNAs. Among the 489 hypomethylated mRNAs, we found 431 upregulated and 58 downregulated expressed mRNAs

TABLE 2 | The top 20 differently methylated mRNAs with differential expressions.

Gene name	Chromosome	Methylation regulation			Expression regulation		
		Log2(FC)	*p*-value	Regulation	Log2(FC)	*p*-value	Regulation
MAPK8IP3	chr16	0.75	1.76E-02	Hyper	2.11	2.10E-03	Up
MADD	chr11	1.02	8.43E-03	Hyper	2.09	9.59E-03	Up
RBM4B	chr11	1.21	1.27E-03	Hyper	1.76	4.47E-02	Up
OCEL1	chr19	0.92	3.16E-03	Hyper	1.68	8.86E-03	Up
DSP	chr6	0.77	4.14E-02	Hyper	1.61	4.39E-02	Up
MYCBP2	chr13	1.11	8.65E-03	Hyper	1.56	2.53E-02	Up
MORN1	chr1	0.97	4.62E-02	Hyper	1.54	4.56E-02	Up
SNRNP200	chr2	0.76	2.03E-02	Hyper	1.49	4.63E-02	Up
EWSR1	chr22	0.76	4.65E-02	Hyper	1.47	1.83E-02	Up
ZDHHC11	chr5	0.60	2.64E-03	Hyper	1.45	3.21E-02	Up
BTN3A3	chr6	1.32	6.90E-03	Hyper	1.44	2.37E-02	Up
TCF7L2	chr10	1.04	4.93E-02	Hyper	1.37	2.80E-02	Down
FAM131B	chr7	0.65	9.98E-03	Hyper	1.30	4.28E-02	Up
FAM160B1	chr10	0.97	3.48E-02	Hyper	1.26	4.57E-02	Up
TOM1L2	chr17	1.15	4.12E-02	Hyper	1.26	1.71E-03	Up
FXYD3	chr19	−0.79	1.53E-02	Hypo	1.72	4.65E-02	Up
SPOCK3	chr4	−0.90	4.50E-02	Hypo	0.90	1.69E-02	Up
TBX18	chr6	−0.33	3.77E-02	Hypo	2.04	2.88E-02	Up
BMP4	chr14	−0.91	4.76E-02	Hypo	−0.88	3.84E-02	Down
SOX2	chr3	−0.99	3.40E-02	Hypo	−0.75	4.01E-02	Down

(**Figure 5A**, **Supplementary Table S9**). The methylation levels of these 787 mRNAs were positively correlated with their expression levels according to Pearson's correlation analysis ($R^2 = 0.20$, $P < 0.05$) (**Figure 5B**). It indicated the crucial role of m^{6}A methylation in the gene expression regulation in uropathy.

Likewise, we performed GO and KEGG enrichment analyses (**Figures 5C,D**, **Supplementary Table S10**). GO analysis showed that "cell-substrate junction", "focal adhesion" and "cell leading edge" are major cellular component; "protein localization to cell periphery", "proteasome-mediated ubiquitin-dependent protein catabolic process" and "positive regulation of catabolic process" are major biological processes; "DNA-binding transcription factor binding", "RNA polymerase II-specific DNA-binding transcription factor binding" and "transcription coregulator activity" are major molecular functions of differentially m^{6}A methylated transcripts. KEGG analysis also showed that "MAPK signaling", "AGE–RAGE signaling pathway", "EGFR tyrosine kinase inhibitor resistance", and "regulation of actin cytoskeleton" are the major pathways associated with the differentially m^{6}A methylated transcripts in megaureter obstructive uropathy.

Validation of the Microarray Data by MeRIP and qRT-PCR Analyses

To confirm the m^{6}A mRNA microarray findings in ureteral tissues, we employed MeRIP to detect the m^{6}A levels of four mRNAs involved in the pathway regulatory network, which matched the gene list associated with uropathy reported in the Enrichr metadata (20). As shown in **Figure 5**, the m^{6}A levels of BMP4, TBX18 and SOX2 mRNAs were lower in the ureter samples from patients with megaureter (M group) than those from patients with VUR (V group). While the m^{6}A levels of TCF7L2 mRNAs in the M group were higher than those in the V group (**Figure 5E**). Next, we detected the expression levels via qRT-PCR to demonstrate whether mRNA expression was correlated with m^{6}A modification. It revealed that the mRNAs of BMP4, SOX2 and TCF7L2 were downregulated in the M group, but the mRNAs of TBX18 were upregulated in the M group (**Figure 5F**). The results indicated that hypo-methylated TBX18 may induce the stability of mRNA expression, while hyper-methylated TCF7L2 may display a low level of mRNA expression. The m^{6}A modification was also associated with the BMP4 and SOX2 mRNAs levels (**Figures 5E,F**).

DISCUSSION

Despite the growing knowledge of the impact of the m^{6}A modifications on mRNA degradation and translation, it is still unclear how the modifications affect organ development. We provided revealing insights into the m^{6}A modification patterns in ureter tissue samples from patients with obstructive megaureter and patients with VUR. The analysis of the uropathy-related methylated genes and their potential functions enlighten us the unique pathogenesis of obstructive and reflux uropathy.

Advances in clinical diagnostics and molecular techniques have helped us better understand several causes of CAKUT. Increasing evidence suggests that kidney and urinary tract development is controlled by classical signaling pathways, as

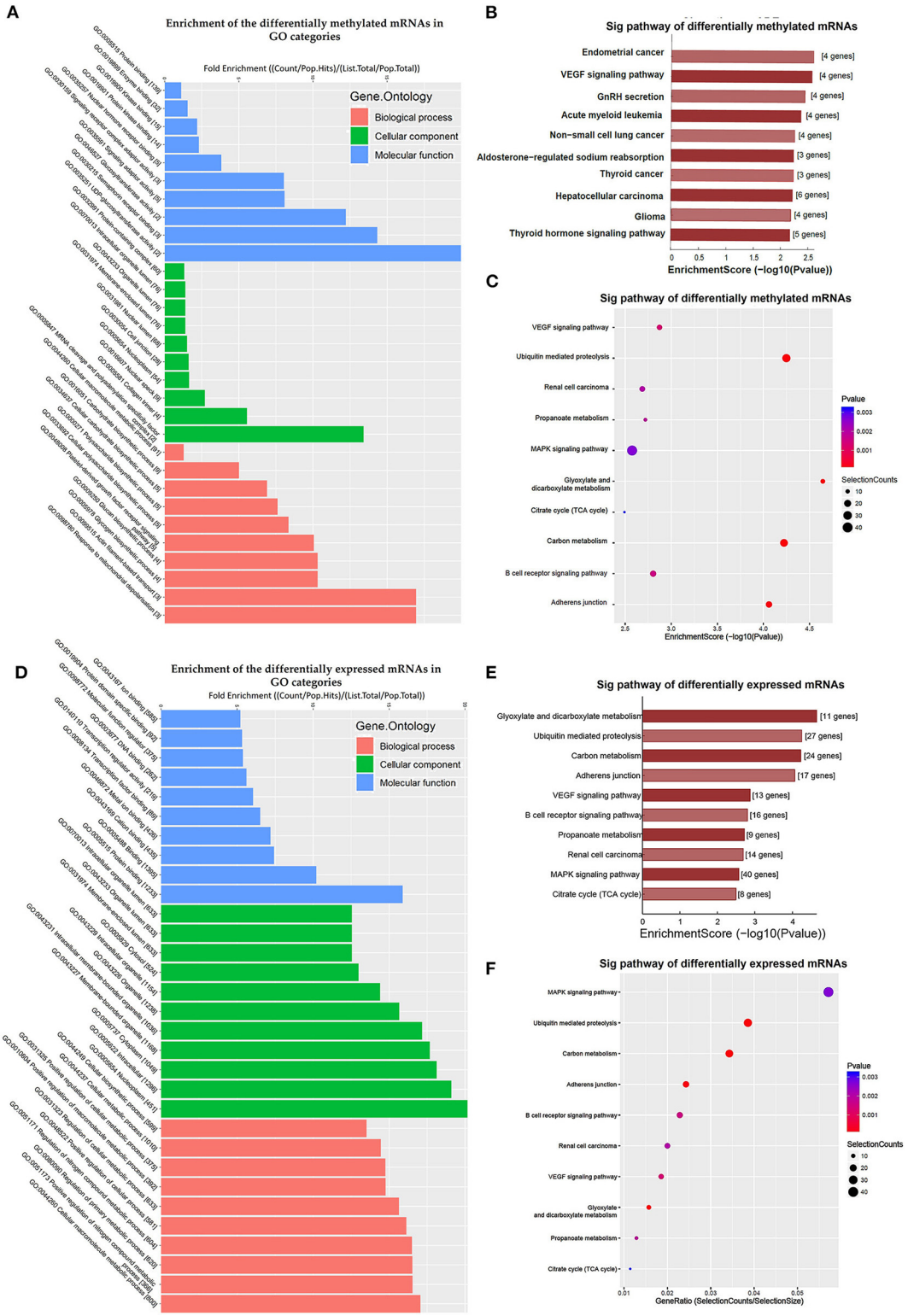

FIGURE 3 | Clustering analyses of the differentially methylated mRNAs through Gene Ontology (GO) function and Kyoto Encyclopedia of Genes and Genomes (KEGG) pathway. **(A)** Enrichment of the differentially methylated mRNAs in GO categories such as biological process (BP), cellular component (CC), and molecular function (MF). **(B,C)** KEGG pathway involvement of differentially m^{6}A mRNAs in patients with megaureter (M group) compared with vesicoureteral reflux (VUR, V group). **(D)** Enrichment of the differentially expressed mRNAs in GO categories such as BP, CC and MF. **(E,F)** KEGG pathway involvement of differentially expressed mRNAs in patients with the M group compared with the V group.

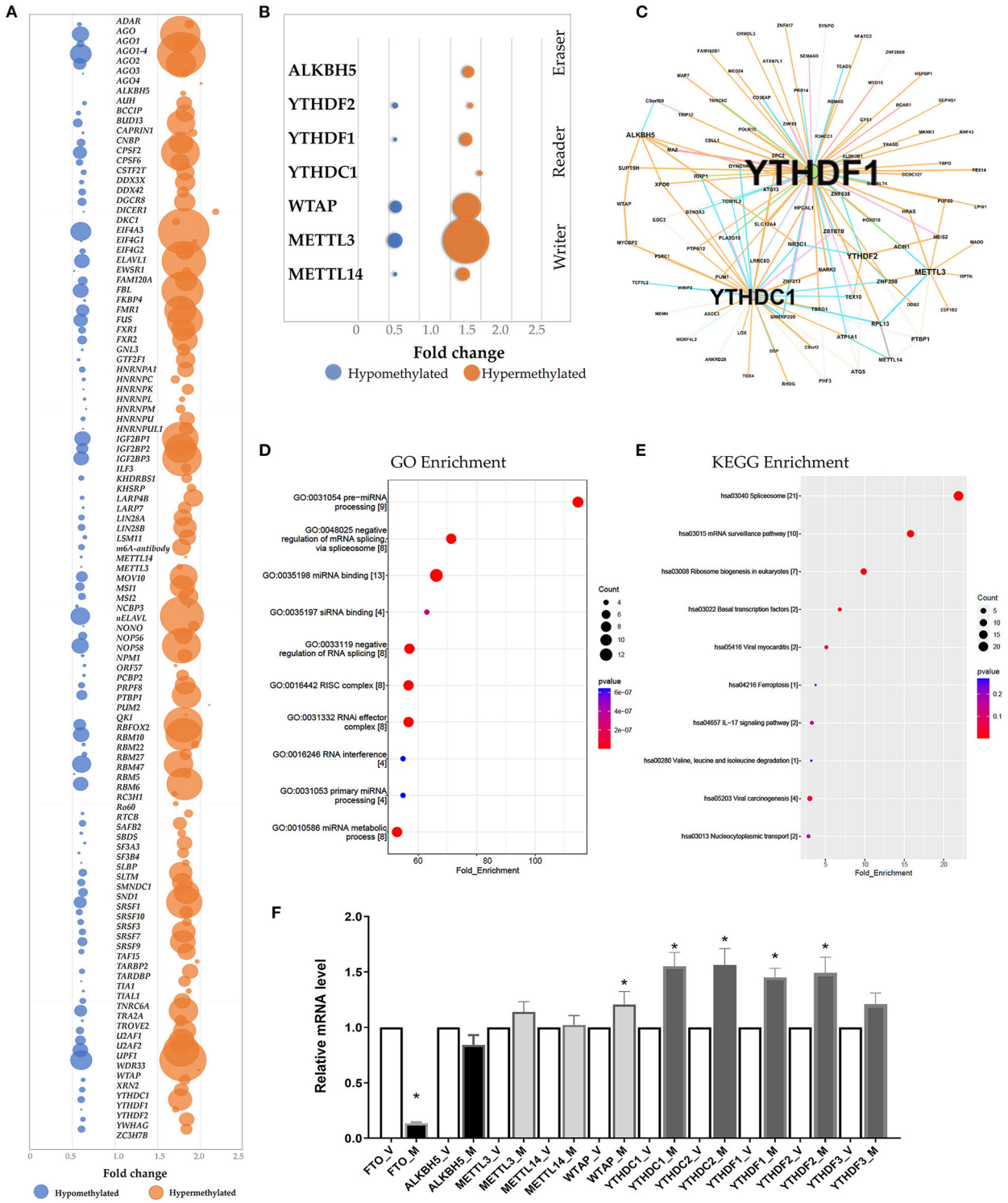

FIGURE 4 | Prediction and function of RNA-binding proteins (RBPs) for N^6-methyladenosine (m^{6}A) methylation. **(A)** Bubble chart represented as the binding rates of the 140 RBPs. Values were displayed as the differentially methylated mRNAs based on log2(FC). The number of genes binding to the RBPs by prediction was presented by bubble size. **(B)** Bubble chart showing the binding rates of the known m^{6}A readers (YTHDF1, YTHDF2, YTHDC1), m^{6}A writers (WTAP, METTL3, METTL14) and eraser ALKBH5 by prediction. **(C)** Network mapping showing the genes binding to the m^{6}A readers, writers and erasers by prediction. **(D,E)** Enrichment analyses of Gene Ontology (GO) and Kyoto Encyclopedia of Genes and Genomes (KEGG) of the 215 candidate RBP genes. **(F)** Real-time PCR confirmed the mRNA levels of m6A readers (YTHDC1, YTHDC2, YTHDF1, YTHDF2, YTHDF3), erasers (FTO and ALKBH5) and writers (WTAP, METTL3, METTL14).

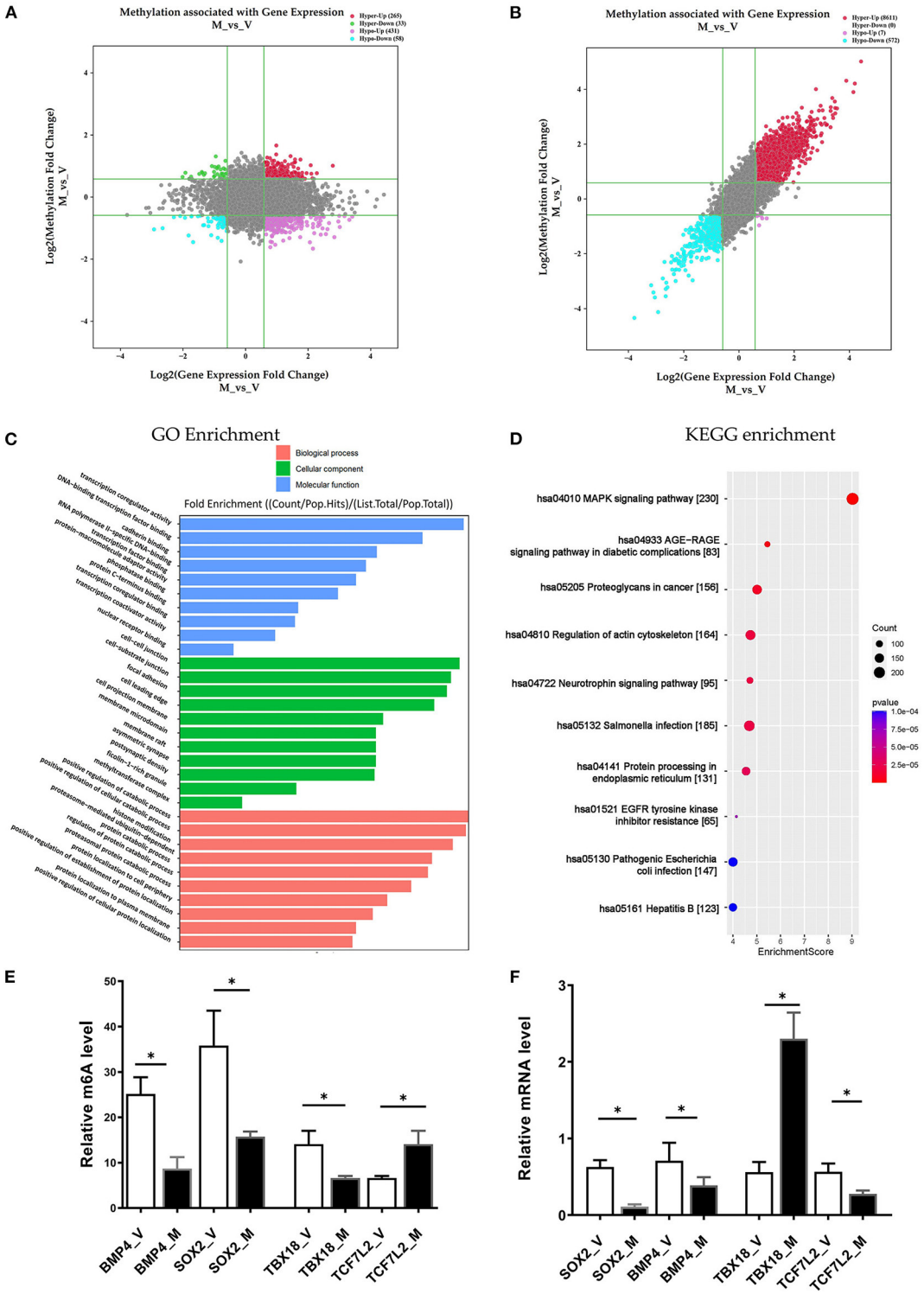

FIGURE 5 | Conjoint analysis of m^{6}A methylation and mRNA expression in different ureteral phenotypes. **(A)** Four-quadrant plot indicating the differentially methylated peaks within differentially expressed mRNAs (log2 FC> 0.5, $P < 0.05$). **(B)** Dot plot of Log2 fold change (FC) (mRNA expression) vs. Log2 FC (differential m^{6}A methylation) revealing a positive association between total m^{6}A methylation and level of mRNA expression (Pearson $R^2 = 0.20$, $P < 0.05$). **(C,D)** Enrichment analyses of mRNAs with both differential methylation and expression via Gene Ontology (GO) and Kyoto Encyclopedia of Genes and Genomes (KEGG). **(E)** MeRIP-qPCR validation of m^{6}A level changes in four hyper-methylated or hypo-methylated genes in megaureter group (M) and vesicoureteral reflux (VUR) group (V) samples. **(F)** Relative mRNA levels of four genes were assessed by real-time PCR in megaureter group (M) and vesicoureteral reflux (VUR) group (V) samples. Data are expressed as mean ± SD; data were analyzed using the nonparametric *t*-test. *$P < 0.05$; M group vs. V group ($n = 6$ per group). Hypo, hypomethylation; Hyper, hypermethylation; Up, upregulated expression; Down, downregulated expression.

well as by epigenetic mechanisms involving chromatin histone modifications, DNA methylation and RNA modification (18). m^{6}A has a broad range of functions in organ development and disease processing (22, 23). Several studies have delineated the regulation mechanism of m^{6}A modification in glomerulopathy and renal fibrosis (16, 24). Thus far, few studies have investigated the involvement of m^{6}A in kidney and ureter development. Hydronephrosis is the most common features in CAKUT which can be caused by obstructive uropathy or reflux uropathy. A cause of obstructive uropathy in children is primary megaureter, which represents a ureter with a larger diameter than usual, resulting in vesicoureteral junction obstruction. The morpho-pathogenesis of megaureter is characterized by apoptotic epitheliums and smooth muscle cells, as well as tissue deterioration in the ureter epithelium and connective tissue (25). Primary VUR represents the retrograde flow of urine from the bladder into the ureter, resulting in reflux nephropathy. Refluxing ureters are distinguished by lesions at the vesico-ureteric junction, which includes disordered smooth muscle fibers and the destruction of smooth muscle cell structure, resulting in valve incompetence. (26). The mechanism of primary megaureter and VUR is poorly understood and remains controversial. Here, the m^{6}A methylomic landscape of ureters was studied to get insight into the megaureter and VUR.

In this study, MeRIP combined with microarray analysis revealed the different m^{6}A methylation patterns in ureters between the megaureter and VUR. The majority of the differentially methylated mRNAs in the megaureter (M) group were substantially hyper-methylated compared to the VUR (V) group. Mapping the differentially methylated regions with visualized the peak site locations in the chromosomes showed the enrichment of methylation in chromosomes 1, 2, 16, 19, 17, 7, and X. There were 10 methylated peaks located in the *17q12*, *16p11.2*, *22q11.2* and *4p16.3* which are the known pathogenic CNVs for CAKUT. Pathogenic CNVs have been identified in 22.5% of patients with syndromic deformities and in 14.5% of patients with isolated CAKUT (27). It has been documented that large deletions were mostly detected in upper urinary tract disorders (e.g., kidney agenesis or dysplasia), whereas duplications were more common in lower urinary tract phenotypes (e.g., duplex kidney, VUR, or posterior urethral valves) (18). Although the known pathogenic CNVs were not detected in the participants in our study, the enrichment of m^{6}A modifications in these regions may participate in the development of the ureteric bud (UB) as the origin of lower urinary tract. Further exploration on the genes and long noncoding RNA (lncRNA) located the CNVs regions with multiple methylated peaks may provide more information of pathogenesis of uropathy.

A total of 228 mRNAs were revealed to be substantially differential methylated in the M/V comparison. Understanding the specific m^{6}A-modified transcripts provided the clues to delineate the pathogenesis between obstructive uropathy and reflux uropathy. GO and KEGG pathway analysis indicated several pathways. Among them, the *HRAS, PIK3R3* and *TCF7L2* genes participated in most of the signaling pathways. A case with PUV has identified the pathogenic CNVs (deletion at *1p34.1*), which covers both *PIK3R3* and *TSPAN1* genes' exonic regions (28). PIK3R3 represents a regulatory subunit of PI3K which coordinates multiple cell functions such as cell migration, cell proliferation, and cell survival. Members of the Ras superfamily can also modulate cell growth, differentiation, proliferation, and migration. It was demonstrated that UB cells with R-Ras–expressing participated in cell growth and branching morphology. H-Ras–expressing UB cells had a high ability to migrate forming long unbranched tubules, whereas TC21-expressing UB cells were characterized with branching excessively with a reduced capacity to migrate (29). Additionally, the diabetes gene and Wnt pathway effector *TCF7L2* may increase susceptibility to both diabetes and kidney disease (30). Hence, the differentially methylated mRNAs provide the clues for understanding the distinct pathogenesis of uropathy.

Joint analysis of the methylated mRNAs with expression level revealed a large proportion of hypermethylated mRNAs with high expression in the ureters of patients with uropathy. It indicated the role of m^{6}A methylation on the of mRNAs stability. However, some differential mRNAs in the M/V comparison, such as hypermethylated mRNAs with downregulated expression may contribute to uropathy as well, despite accounting for a minor proportion of the total. Notably, we confirmed the downregulated expression of *TCF7L2* as hypermethylated mRNAs, the upregulated expression of *TBX18* as hypomethylated mRNAs, the downregulated expression of *BMP4* and *SOX2* as hypomethylated mRNAs in the M group compared with the V group. We selected these four representative mRNAs (*TCF7L2*, *TBX18, BMP4* and *SOX2*) from the key pathways associated with the differentially m^{6}A-methylated mRNAs in uropathy. *TCF7L1/TCF7L2* complexes were confirmed as a β-catenin-driven switcher to enhance the differentiation-promoting target genes during the initiation of nephron progenitor cells (31). *Tbx18* is expressed in the mesenchymal compartment of the ureter of the fetal mouse (32), and mutations of *TBX18* have been identified as the pathogenic variants of CAKUT (33). *BMP4*, a member of the TGF-β superfamily, plays a key role in the early phase of the kidney and urinary tract morphogenesis. It can restrain ectopic budding from the UB or the ureter stalk by blocking inductive signals from the metanephric mesenchyme. It may also contribute to the branching process of metanephros' ureter (34). *SOX2* is a key transcription factor during the organ development that can control the pluripotency of early embryonic cells. SOX2 anophthalmia syndrome is an autosomal dominant disorder characterized by severe developmental eye deformities as well as abnormalities in esophageal, brain, genital, and kidney abnormalities (35).

Cellular m^{6}A homeostasis is maintained through coordinating the activity of m^{6}A methylase complex (i.e., writers), demethylases (i.e., erasers) and the m^{6}A binding proteins (i.e., readers) to regulate RNA fate. Currently, the differential m^{6}A methylation in uropathy was associated with the decline of the subunits of the m^{6}A erasers (FTO) and the increase of the readers (YTHDF1, YTHDF2, YTHDC1 and YTHDC2). Interestingly, FTO showed the highest change of mRNA level between the M group and V group of all the m^{6}A regulators tested. It has been reported loss of FTO antagonized

Wnt signaling resulting in development defeats in mice (36). FTO can also modulated fibrogenic response in mouse models of obstructive nephropathy (37). We cannot fully explain the enhancement of all the m^{6}A regulators. Further detecting the m^{6}A modification of space-time could gain more information on epigenetic modulation during different phase of UB development and disease processing.

RNA-binding proteins (RBPs) are of crucial role in post-transcriptional gene regulation and protein synthesis. RBPs contribute to a wide spectrum of kidney disease, including glomerular disease, diabetic kidney disease and cystic kidney disease. RNA interactome capture (RIC) can identify RBPs bound to polyA-tailed transcripts (38). RBPs recognize m^{6}A sites with a high degree of specificity (39). We predicted the candidate RBPs binding to the methylated peak sites using the RMBase database (21). Subsequent results showed that the binding abundance of RBPs in the hypermethylated regions. This hinted that the RBPs prefer to target hypermethylated peaks. Concordantly, the m^{6}A regulators (YTHDF1, YTHDF2, YTHDC1, METTL3, METTL14, WTAP and ALKBH5) were mostly distributed in the hyper-methylated regions. The prediction of the enrichment of the RBPs associated with kidney disorders (40) was laid out with *IGF2BP2* and *MSI1* in the hypermethylated group. Downregulation o*f MSI1* can induce tubulointerstitial fibrosis (41). *IGF2BP2* was involved in the damage of glomerular basement membrane (42). We speculated that RBPs may regulate RNA processes and consequently play a role in the pathogenesis of uropathy by controlling the differentially methylated transcripts.

This study had potential limitations. First, we could not examine the expression level of all the m^{6}A-related genes and RBPs in the ureter tissue because of the limitation of specimens from pediatric patients. We should start more work on the possible crosstalk between the differentially methylated genes and RBPs, as well as the mechanism of RBPs regulating the gene expression. Functional studies of the candidate genes in various animal models of uropathy need to be conducted to examine the different expression levels during the development course. Second, although the target genes modified by m^{6}A were outlined, the process of methylation readers, erasers or writers regulating the target genes was not delineated. Further studies should be conducted to investigate whether readers, erasers or writers regulate the stability, translation efficiency, or degradation of target genes. In addition, the involvement of the differentially methylated mRNAs and the m^{6}A-related enzymes and RBPs in the other types of CAKUT such as renal dysplasia and cystic renal disease deserve further investigation. The common changes in methylated mRNAs in both obstructive nephropathy and reflux nephropathy are to be detected in the renal parenchymal compared with normal control, which may provide novel findings on the epigenetic mechanisms on renal development.

In conclusion, we presented a summary of differentially methylated mRNAs and their potential binding proteins, which might be key regulators in the development of obstructive and reflux uropathy. To our knowledge, we provided the initial m^{6}A methylomic landscape in the ureter tissue of children, which highlighted a new direction for unraveling the distinct mechanism of m^{6}A methylation in uropathy.

DATA AVAILABILITY STATEMENT

The data discussed in this publication have been deposited in NCBI's Gene Expression Omnibus and are accessible through GEO Series accession number GSE195849 (https://www.ncbi.nlm.nih.gov/geo/query/acc.cgi?acc=GSE195849).

ETHICS STATEMENT

The studies involving human participants were reviewed and approved by No. 2020_363. Written informed consent to participate in this study was provided by the participants' legal guardian/next of kin.

AUTHOR CONTRIBUTIONS

JR and HX led and supervised the project and were involved in all aspects of the study. JR, XW, and HS conceived and designed the experiments. HS, TX, JF, XY, YL, YF, LX, QQ, JS, QS, and LT performed the experiments. JR and TX analyzed the data, interpreted the results, and prepared the figures. HS and JR wrote the paper with input from QQ. All authors commented and made edits to the manuscript and contributed to the article and approved the final version.

FUNDING

JR is supported by a grant from the National Key Research and Development Program of China (2021YFC2701100), a grant from Clinical Research Plan of SHDC(SHDC2020CR2064B), and a grant from National Natural Science Foundation of China (NSFC-8182207). HX is supported by a grant from National Natural Science Foundation of China (NSFC-81873593).

SUPPLEMENTARY MATERIAL

The Supplementary Material for this article can be found online at: https://www.frontiersin.org/articles/10.3389/fmed.2022.924579/full#supplementary-material

REFERENCES

1. Wang X, Zhao BS, Roundtree IA, Lu Z, Han D, Ma H, et al. N(6)-methyladenosine modulates messenger RNA translation efficiency. *Cell.* (2015) 161:1388–99. doi: 10.1016/j.cell.2015.05.014
2. Liu J, Yue Y, Han D, Wang X, Fu Y, Zhang L, et al. A METTL3-METTL14 complex mediates mammalian nuclear RNA N6-adenosine methylation. *Nat Chem Biol.* (2014) 10:93–5. doi: 10.1038/nchembio.1432
3. Ping X-L, Sun B-F, Wang L, Xiao W, Yang X, Wang W-J, et al. Mammalian WTAP is a regulatory subunit of the RNA N6-methyladenosine

methyltransferase. *Cell Res.* (2014) 24:177–89. doi: 10.1038/cr.2014.3
4. Jia G, Fu Y, Zhao X, Dai Q, Zheng G, Yang Y, et al. N6-methyladenosine in nuclear RNA is a major substrate of the obesity-associated FTO. *Nat Chem Biol.* (2011) 7:885–7. doi: 10.1038/nchembio.687
5. Zheng G, Dahl JA, Niu Y, Fedorcsak P, Huang C-M, Li CJ, et al. ALKBH5 is a mammalian RNA demethylase that impacts RNA metabolism and mouse fertility. *Mol Cell.* (2013) 49:18–29. doi: 10.1016/j.molcel.2012.10.015
6. Wang X, Lu Z, Gomez A, Hon GC, Yue Y, Han D, et al. N6-methyladenosine-dependent regulation of messenger RNA stability. *Nature.* (2014) 505:117–20. doi: 10.1038/nature12730
7. Frye M, Harada BT, Behm M, He C. RNA Modifications modulate gene expression during development. *Science.* (2018) 361:1346–9. doi: 10.1126/science.aau1646
8. Zhao L-Y, Song J, Liu Y, Song C-X, Yi C. Mapping the epigenetic modifications of DNA and RNA. *Protein Cell.* (2020) 11:792–808. doi: 10.1007/s13238-020-00733-7
9. Mathiyalagan P, Adamiak M, Mayourian J, Sassi Y, Liang Y, Agarwal N, et al. FTO-Dependent N6-methyladenosine regulates cardiac function during remodeling and repair. *Circulation.* (2019) 139:518–32. doi: 10.1161/CIRCULATIONAHA.118.033794
10. Gu HF. Genetic and epigenetic studies in diabetic kidney disease. *Front Genet.* (2019) 10:507. doi: 10.3389/fgene.2019.00507
11. Wang J-N, Wang F, Ke J, Li Z, Xu C-H, Yang Q, et al. Inhibition of METTL3 attenuates renal injury and inflammation by alleviating TAB3 m6A modifications via IGF2BP2-dependent mechanisms. *Sci Transl Med.* (2022) 14:eabk2709. doi: 10.1126/scitranslmed.abk2709
12. Teng F, Tang W, Wuniqiemu T, Qin J, Zhou Y, Huang X, et al. N6-Methyladenosine methylomic landscape of lung tissues in murine acute allergic asthma. *Front Immunol.* (2021) 12:740571. doi: 10.3389/fimmu.2021.740571
13. Martini S, Eichinger F, Nair V, Kretzler M. Defining human diabetic nephropathy on the molecular level: integration of transcriptomic profiles with biological knowledge. *Rev Endocr Metab Disord.* (2008) 9:267–74. doi: 10.1007/s11154-008-9103-3
14. Lu Z, Liu H, Song N, Liang Y, Zhu J, Chen J, et al. METTL14 aggravates podocyte injury and glomerulopathy progression through N6-methyladenosine-dependent downregulating of Sirt1. *Cell Death Dis.* (2021) 12:881. doi: 10.1038/s41419-021-04156-y
15. Xu Y, Yuan XD, Wu JJ, Chen RY, Xia L, Zhang M, et al. The N6-methyladenosine mRNA methylase METTL14 promotes renal ischemic reperfusion injury via suppressing YAP1. *J Cell Biochem.* (2020) 121:524–33. doi: 10.1002/jcb.29258
16. Xu Z, Jia K, Wang H, Gao F, Zhao S, Li F, et al. METTL14-regulated PI3K/Akt signaling pathway via PTEN affects HDAC5-mediated epithelial-mesenchymal transition of renal tubular cells in diabetic kidney disease. *Cell Death Dis.* (2021) 12:32. doi: 10.1038/s41419-020-03312-0
17. Murugapoopathy V, Gupta IR. A primer on congenital anomalies of the kidneys and urinary tracts (CAKUT). *Clin J Am Soc Nephrol.* (2020) 15:723–31. doi: 10.2215/CJN.12581019
18. Khan K, Ahram DF, Liu YP, Westland R, Sampogna RV, Katsanis N, et al. Multidisciplinary approaches for elucidating genetics and molecular pathogenesis of urinary tract malformations. *Kidney Int.* (2021). doi: 10.1016/j.kint.2021.09.034
19. International Reflux Study Committee. Medical versus surgical treatment of primary vesicoureteral reflux. *Pediatrics.* (1981) 67:392–400. doi: 10.1542/peds.67.3.392
20. Chen EY, Tan CM, Kou Y, Duan Q, Wang Z, Vaz Meirelles G, et al. Enrichr: interactive and collaborative HTML5 gene list enrichment analysis tool: BMC Bioinformatics. *BMC Bioinformatics.* (2013) 14:128. doi: 10.1186/1471-2105-14-128
21. Sun W-J, Li J-H, Liu S, Wu J, Zhou H, Qu L-H, et al. RMBase: a resource for decoding the landscape of RNA modifications from high-throughput sequencing data. *Nucleic Acids Res.* (2016) 44:D259–65. doi: 10.1093/nar/gkv1036
22. Xiao S, Cao S, Huang Q, Xia L, Deng M, Yang M, et al. The RNA N6-methyladenosine modification landscape of human fetal tissues. *Nat Cell Biol.* (2019) 21:651–61. doi: 10.1038/s41556-019-0315-4
23. Tang Y, Chen K, Song B, Ma J, Wu X, Xu Q, et al. m6A-Atlas: a comprehensive knowledgebase for unraveling the N6-methyladenosine (m6A) epitranscriptome. *Nucleic Acids Res.* (2021) 49:D134–43. doi: 10.1093/nar/gkaa692
24. Zhao H, Pan S, Duan J, Liu F, Li G, Liu D, et al. Integrative analysis of m6A regulator-mediated RNA methylation modification patterns and immune characteristics in lupus nephritis. *Front Cell Dev Biol.* (2021) 9:724837. doi: 10.3389/fcell.2021.724837
25. Walker KA, Sims-Lucas S, Bates CM. Fibroblast growth factor receptor signaling in kidney and lower urinary tract development. *Pediatr Nephrol.* (2016) 31:885–95. doi: 10.1007/s00467-015-3151-1
26. Sofikerim M, Sargon M, Oruc O, Dogan HS, Tekgul S. An electron microscopic examination of the intravesical ureter in children with primary vesico-ureteric reflux. *BJU Int.* (2007) 99:1127–31. doi: 10.1111/j.1464-410X.2007.06751.x
27. Verbitsky M, Westland R, Perez A, Kiryluk K, Liu Q, Krithivasan P, et al. The copy number variation landscape of congenital anomalies of the kidney and urinary tract. *Nat Genet.* (2019) 51:117–27. doi: 10.1038/s41588-018-0281-y
28. Boghossian NS, Sicko RJ, Kay DM, Rigler SL, Caggana M, Tsai MY, et al. Rare copy number variants implicated in posterior urethral valves. *Am J Med Genet A.* (2016) 170:622–33. doi: 10.1002/ajmg.a.37493
29. Pozzi A, Coffa S, Bulus N, Zhu W, Chen D, Chen X, et al. R-Ras, and TC21 differentially regulate ureteric bud cell branching morphogenesis. *Mol Biol Cell.* (2006) 17:2046–56. doi: 10.1091/mbc.e05-08-0800
30. Del Bosque-Plata L, Martínez-Martínez E, Espinoza-Camacho MÁ, Gragnoli C. The role of TCF7L2 in type 2 diabetes. *Diabetes.* (2021) 70:1220–8. doi: 10.2337/db20-0573
31. Guo Q, Kim A, Li B, Ransick A, Bugacov H, Chen X, et al. A β-catenin-driven switch in TCF/LEF transcription factor binding to DNA target sites promotes commitment of mammalian nephron progenitor cells. *Elife.* (2021) 10. doi: 10.7554/eLife.64444.sa2
32. Airik R, Bussen M, Singh MK, Petry M, Kispert A. Tbx18 regulates the development of the ureteral mesenchyme. *J Clin Invest.* (2006) 116:663–74. doi: 10.1172/JCI26027
33. Vivante A, Kleppa M-J, Schulz J, Kohl S, Sharma A, Chen J, et al. Mutations in TBX18 cause dominant urinary tract malformations via transcriptional dysregulation of ureter development. *Am J Hum Genet.* (2015) 97:291–301. doi: 10.1016/j.ajhg.2015.07.001
34. Y Miyazaki K Oshima, A Fogo, B L Hogan, I Ichikawa. Bone morphogenetic protein 4 regulates the budding site and elongation of the mouse ureter. *J Clin Invest.* 105:863–73. doi: 10.1172/JCI8256
35. Bakrania P, Robinson DO, Bunyan DJ, Salt A, Martin A, Crolla JA, et al. SOX2 anophthalmia syndrome: 12 new cases demonstrating broader phenotype and high frequency of large gene deletions. *Br J Ophthalmol.* (2007) 91:1471–6. doi: 10.1136/bjo.2007.117929
36. Osborn DP, Roccasecca RM, McMurray F, Hernandez-Hernandez V, Mukherjee S, Barroso I, et al. Loss of FTO antagonises Wnt signaling and leads to developmental defects associated with ciliopathies. *PLoS ONE.* (2014) 9:e87662. doi: 10.1371/journal.pone.0087662
37. Wang C-Y, Shie S-S, Tsai M-L, Yang C-H, Hung K-C, Wang C-C, et al. FTO modulates fibrogenic responses in obstructive nephropathy. *Sci Rep.* (2016) 6:18874. doi: 10.1038/srep18874
38. Castello A, Fischer B, Eichelbaum K, Horos R, Beckmann BM, Strein C, et al. Insights into RNA biology from an atlas of mammalian mRNA-binding proteins. *Cell.* (2012) 149:1393–406. doi: 10.1016/j.cell.2012.04.031
39. Zhang Z, Luo K, Zou Z, Qiu M, Tian J, Sieh L, et al. Genetic analyses support the contribution of mRNA N6-methyladenosine (m6A) modification to human disease heritability. *Nat Genet.* (2020) 52:939–49. doi: 10.1038/s41588-020-0644-z
40. Seufert L, Benzing T, Ignarski M, Müller R-U. RNA-binding proteins and their role in kidney disease. *Nat Rev Nephrol.* (2021). doi: 10.1038/s41581-021-00497-1
41. Jadhav S, Ajay AK, Trivedi P, Seematti J, Pellegrini K, Craciun F, et al. RNA-binding protein Musashi homologue 1 regulates kidney fibrosis by translational inhibition of p21 and Numb mRNA. *J Biol Chem.* (2016) 291:14085–94. doi: 10.1074/jbc.M115.713289
42. Schaeffer V, Hansen KM, Morris DR, LeBoeuf RC, Abrass CK. RNA-binding protein IGF2BP2/IMP2 is required for laminin-β2 mRNA translation and

is modulated by glucose concentration. *Am J Physiol Renal Physiol.* (2012) 303:F75–82. doi: 10.1152/ajprenal.00185.2012

Conflict of Interest: The authors declare that the research was conducted in the absence of any commercial or financial relationships that could be construed as a potential conflict of interest.

Publisher's Note: All claims expressed in this article are solely those of the authors and do not necessarily represent those of their affiliated organizations, or those of the publisher, the editors and the reviewers. Any product that may be evaluated in this article, or claim that may be made by its manufacturer, is not guaranteed or endorsed by the publisher.

frontiers | Frontiers in Medicine

REVIEW
published: 05 July 2022
doi: 10.3389/fmed.2022.921631

Chromatin Methylation Abnormalities in Autosomal Dominant Polycystic Kidney Disease

Jing Xu[1,2†], *Cheng Xue*[1†], *Xiaodong Wang*[2,3†], *Lei Zhang*[2,3,4*], *Changlin Mei*[1*] and *Zhiguo Mao*[1*]

[1] Kidney Institute, Department of Nephrology, Shanghai Changzheng Hospital, Second Military Medical University, Shanghai, China, [2] State Key Laboratory of Cell Biology, Center for Excellence in Molecular Cell Science, Shanghai Institute of Biochemistry and Cell Biology, Chinese Academy of Sciences, University of Chinese Academy of Sciences, Shanghai, China, [3] School of Life Science and Technology, Shanghai Tech University, Shanghai, China, [4] School of Life Science, Hangzhou Institute for Advanced Study, University of Chinese Academy of Sciences, Hangzhou, China

OPEN ACCESS

Edited by:
Andrew Mallett,
Townsville University Hospital, Australia

Reviewed by:
John Andrew Sayer,
Newcastle University, United Kingdom
Sayanthooran Saravanabavan,
Westmead Institute for Medical Research, Australia

***Correspondence:**
Zhiguo Mao
maozhiguo93@126.com
Changlin Mei
Changlinmei@smmu.edu.cn
Lei Zhang
rayzhang@sibcb.ac.cn

[†]These authors have contributed equally to this work

Specialty section:
This article was submitted to Nephrology, a section of the journal Frontiers in Medicine

Received: 16 April 2022
Accepted: 02 June 2022
Published: 05 July 2022

Citation:
Xu J, Xue C, Wang X, Zhang L, Mei C and Mao Z (2022) Chromatin Methylation Abnormalities in Autosomal Dominant Polycystic Kidney Disease. Front. Med. 9:921631. doi: 10.3389/fmed.2022.921631

Autosomal dominant polycystic kidney disease (ADPKD) is the most common inherited kidney disease worldwide and is one of the major causes of end-stage renal disease. *PKD1* and *PKD2* are two genes that mainly contribute to the development and progression of ADPKD. The precise mechanism is not fully understood. In recent years, epigenetic modification has drawn increasing attention. Chromatin methylation is a very important category of PKD epigenetic changes and mostly involves DNA, histone, and RNA methylation. Genome hypomethylation and regional gene hypermethylation coexist in ADPKD. We found that the genomic DNA of ADPKD kidney tissues showed extensive demethylation by whole-genome bisulphite sequencing, while some regional DNA methylation from body fluids, such as blood and urine, can be used as diagnostic or prognostic biomarkers to predict PKD progression. Histone modifications construct the histone code mediated by histone methyltransferases and contribute to aberrant methylation changes in PKD. Considering the complexity of methylation abnormalities occurring in different regions and genes on the PKD epigenome, more specific therapy aiming to restore to the normal genome should lead to the development of epigenetic treatment.

Keywords: DNA methylation, histone methylation, RNA methylation, autosomal dominant polycystic kidney disease, epigenetics

INTRODUCTION

Autosomal dominant polycystic kidney disease (ADPKD) is the most common form of inherited kidney disease and is one of the major causes of end-stage kidney disease (ESKD), affecting 1 in 2,500 to 1,000 individuals worldwide (1, 2). The mutation in either of two genes mainly contributed to the development and progression of ADPKD (3): *PKD1* and *PKD2*. *PKD1* encodes a large, multidomain integral membrane protein, polycystin-1 (PC1) (4), and *PKD2* encodes a calcium ion channel of the transient receptor potential family, polycystin-2 (PC2) (5, 6). The *PKD1* gene mutation accounts for approximately 80% of ADPKD cases in clinically identified populations, while *PKD2* gene mutation is responsible for approximately 10% of cases, and GANAB, DNAJB11, ALG9, IFT140, etc. account for the rest (7).

Defects in the expression or function of PC1 or PC2 result in cystogenesis; however, the precise mechanism has not been fully understood, although numerous studies have been carried out on the functional roles of PC1 and PC2 and their downstream effector pathways.

The phenotype and progression of ADPKD are highly variable, irrespective of mutations in the same *PKD* genes (8). Even in the same family or with an identical gene mutation background, the disease course and rate of progression to renal failure are diverse, suggesting that there are factors in addition to gene mutations that influence patient prognosis (9). The molecular mechanism for the variability still remains unsolved, but epigenetic modification might be responsible and has drawn increasing attention in recent years (10).

Epigenetics focuses on genome-wide changes in gene expression or phenotype caused by DNA methylation, non-coding RNA modifications, histone modifications, including acetylation, methylation, and ubiquitination (10–12). Similar to the arrangement of DNA sequences, epigenetic information can also be inherited, and its activation and silencing are the switches that turn genes on and off (13, 14). It also provides clues to the interpatient variabilities of disease progression and response to treatment (12). Chromatin methylation is a very important category of PKD epigenetic changes and mostly involves DNA methylation and histone methylation; moreover, RNA methylation has aroused great interest recently (15). Recent evidence suggests that alterations of DNA and histone methylation, as well as RNA methylation on specific genes and the whole genome, contribute to the pathogenesis of PKD.

DNA METHYLATION AND ADPKD

DNA methylation is a key epigenomic feature that controls the suppression and expression of genes by the addition of a chemical methyl group mediated by DNA methyltransferases (DNMTs) (16). DNMT1, as the maintenance methyltransferase, binds mainly to hemimethylated DNA during DNA replication and is responsible for accurately replicating DNA methylation patterns during the S phase of the cell cycle, while *de novo* methylation is preferentially mediated by DNMT3a and DNMT3b (16). DNA methylation in the whole genome and at specific loci can be quantified across the entire genome in a sequence-specific manner to generate a methylome map and can be quantified in either circulating free DNA or single cells.

DNA methylation commonly emerges at cytosine-guanosine dinucleotides (CpGs), where the methyl group is added to the fifth carbon of the cytosine, forming 5-methylcytosine (17). Approximately 10% of human genomes contain CpG sites. DNA is methylated at approximately 75% of all CpG sites in mammalian genomes, primarily in heterochromatic regions (18). Clusters of grouped CpGs called CpG islands are often located near the promoter or enhancer regions of human genes. Methylation within a gene promoter has usually been considered a repressor of the gene by reducing the binding ability of transcription factors. One mechanism for transcription factor inhibition by methylation is chromatin remodeling, as there is epigenetic crosstalk between methylation and histone modification (18). However, methylation of CpGs within the gene body is sometimes controversial compared with promoter methylation, which typically results in increased or sustained gene expression. Only ∼2% of regions of DNA are rigorously protected from methylation and are associated with transcription start sites in almost half of human genes. Possible mechanisms have been proposed: methylated regions contain genomic elements responsible for alternative splicing, containing transcription factors interfering with host gene expression when hypomethylated, or residual genomic imprinting developed from embryonic stages (18). Moreover, several studies have shown that the hypermethylation of gene bodies can silence gene expression, especially in highly expressed genes (18).

Genome-Wide Platforms to Detect DNA Methylation in ADPKD

The first technology used in ADPKD research was the methylated CpG island recovery assay (MIRA) (**Figure 1A**) (19). The principle of this method is that the methylation-CpG-binding protein MBD2 specifically recognizes and binds to the methylation sequence (20). The MBD3L1 protein can enhance the binding ability of MBD2 to methylated CpG. Based on this principle, different DNA fragments with different methylation levels are separated by the chromatographic column method according to the different retention times of DNA bound to MBD2 in the chromatographic column (21). After connecting these DNA fragments to oligonucleotide junctions, the whole genome was amplified by PCR, purified, hybridized with an Agilent chip, and sequenced by the Agilent platform. This technique can find highly methylated regions in the genome, but it cannot analyse methylation at a single base level (resolution is approximately 150 bp). It can only judge whether methylation exists in a certain region by the enrichment peak. It also cannot quantify the level of methylation. Moreover, the detection of this technique has an obvious tendency. It can only detect areas with high CpG density and methylation (22).

Four years later, Bowden et al. (23) used reduced representation bisulphite sequencing (RRBS) to detect the genomic DNA methylation of ADPKD. However, RRBS only sequenced a reduced, representative sample of the whole genome (approximately 1% of the genome region) (24). For epigenetic therapy to be applied to ADPKD, we need to obtain the specific distribution of methylated CpG across the genome, not just globally or selectively (25).

Whole-genome bisulphite sequencing (WGBS) is currently considered the gold standard in DNA methylation profiling (24), potentially allowing the investigation of every CpG site in the genome. WGBS can provide single-base resolution with full genome coverage without the biases associated with selecting agents (26). As next-generation sequencing costs decrease, WGBS has become increasingly accessible for clinical research. These methods could profile different areas of the genome based on a design to identify important regions and reveal DNA methylation changes in *PKD1*.

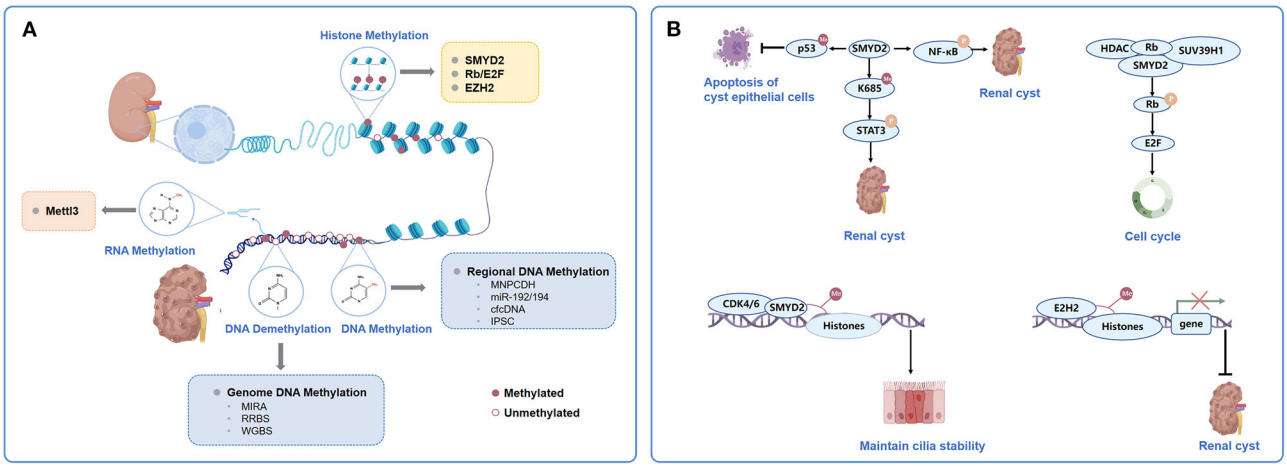

FIGURE 1 | Major types and mechanism of chromatin methylation in ADPKD. **(A)**. Categorization of chromatin methylation in ADPKD. The chromatin methylation in ADPKD mostly involves DNA methylation, histone methylation and RNA methylation. Genome-wide platforms to detect DNA methylation in ADPKD including MIRA, RRBS and WGBS. Genome hypomethylation and gene hypermethylation coexist in ADPKD. Regional DNA methylations could predict application as biomarkers in ADPKD, such as methylation of MUPCDH, miR-192/194, cfcDNA and iPSC. Histone methylations were mediated by HMTs. Some of the mediators and modulators to be closely related to the pathogenesis and acceleration of cystic phenotypes together with or acting as the HMTs, mainly represented by SMYD2, Rb/E2F and EZH2. The adenosine methylation at the 6th nitrogen position known as m6A, mediated by the multi-protein m6A writer complex composed of Mettl3, was involved in pathogenesis of mouse and human ADPKD. **(B)** Participation of SMYD2, Rb/E2F and EZH2 in histone methylation in ADPKD. ADPKD, autosomal dominant polycystic kidney disease; MIRA, methylated- CpG Islandisland recovery assay; RRBS, reduced representation bisulfitebisulphite sequencing; WGBS, whole-genome bisulfitebisulphite sequencing; MUPCDH, mucin-like protocadherin; cfcDNA, cell-free circulating DNA; iPSC, induced pluripotent stem cells; HMT, histone methyltransferases; Rb,Retinoblastoma tumourtumor suppressor protein.

TABLE 1 | Summary of DNA methylation analysis in ADPKD.

Study	Year	Platform	Number	Sample Type	ADPKD overall	*PKD1* gene	PKD1 expression
Woo	2014	MIRA-Seq	6	Kidney	Hypermethylation	Hypermethylation in gene-body	Decreased
Bowden	2018	RRBS	3& non-ADPKD	Kidney	Hypomethylation	Hypermethylation in gene-body	Increased
Bowden	2020	RRBS	8 cysts from 1 ADPKD	Kidney	Hypomethylation in cysts	NA	NA
Hajirezaei	2021	MS-HRM	80	Kidney	NA	PKD1 promoter hypomethylation	Increased
Our study	2022	WGBS	10	Kidney	Hypomethylation	Hypomethylation in gene body and promoter	NA

NA, not available.

Genome DNA Methylation in Human ADPKD

DNA methylation is a key epigenetic modification that plays a critical role in the modulation of gene expression in diseases, especially cancers (27, 28). Global hypomethylation is one of the major characteristics of cancer; however, focally hypermethylated DNA methylomes also coexist in cancers, which are usually located at CpG islands and are closely associated with promoter activity and gene expression (29). This also explains the theory of using methyltransferase inhibitors to treat cancers (13).

As a tumor-like disease, ADPKD might theoretically share similar DNA methylation properties with cancers (30). To date, the characteristics of DNA methylation in ADPKD remain inconclusive (**Table 1**). In 2014, Woo et al. (31) reported global DNA methylation levels in human ADPKD for the first time. This study was conducted on kidneys from 3 ADPKD patients compared with 3 non-ADPKD samples by pyrosequencing. This study found that 91% of over 13,000 unique fragments of the genome in ADPKD exhibited hypermethylation, mainly at exonic regions. Woo et al. also found hypermethylation of exon 43 in *PKD1* gene-body regions, along with silencing of *PKD1* expression, which is involved in cystogenesis (31). Moreover, demethylation of an ADPKD cell line (WT 9–12) resulted in increased *PKD1* expression, and treatment with a DNMT inhibitor repressed the cyst growth of the MDCK cyst-forming cell line. In 2018, Bowden et al. (23) observed approximately 2% global hypomethylation of the genome in ADPKD compared with non-ADPKD kidneys using RRBS for genome-wide methylation analysis. The *PKD1* gene body was hypermethylated in ADPKD by the RRBS method, but Bowden et al. (23) found that hypermethylation was associated with an increase in *PKD1* expression rather than a decrease. However, Hajirezaei et al. (32) found that the *PKD1* promoter was hypomethylated and was inversely correlated with *PKD1*

expression in patient blood, further indicating the controversial role of DNA methylation in *PKD1* expression. To further investigate the epigenetic mechanism of discrepant developments of renal cysts in the same ADPKD context, a genome-wide DNA methylation analysis by Bowden et al. (33) included eight renal cysts from one ADPKD patient. The results showed that 14.6% of the analyzed fragments exhibited a large amount of intercyst DNA methylation variants. Fragments in CpG islands and gene bodies harbored most of the methylation variations across each cyst, while intergenic fragments were comparatively stable. The epigenetic variation overlapped with the transcriptional activity in ADPKD. This study showed the global methylation patterns of individual cysts.

We used WGBS to examine the ADPKD DNA methylome in humans (34). DNA was extracted from the renal cortex tissues of five ADPKD patients and five non-ADPKD patients with renal cell carcinoma (cortex tissue far away carcinoma). We generated $\sim 33 \times 10^7$ 150 bp paired-end reads corresponding to the global coverage of $\sim 30\times$ sequencing depth in WGBS and successfully mapped ∼80% of the genome for each sample. The full set of WGBS data from ADPKD and non-ADPKD samples is illustrated in **Figure 2A** using Circos. CpG methylation profiling is shown in **Figure 2B**. The mean methyl CpG levels of the two groups are shown in **Figure 2C** (rank-sum *test,* $p < 0.0001$). ADPKD showed global hypomethylation compared with non-ADPKD. For functional genomics, we observed methylated CpGs on various genomic compartments, such as the transcriptional start site (TSS, ± 2 kb around the transcription start site) and intronic, exonic, and intergenic regions (for each region: rank-sum *test,* $p < 0.0001$, **Figure 2D**). The short (approximately 1 kb) CpG-rich regions, known as CpG islands, are often located within and close to sites of approximately 40% of promoters. After subclassifying the promoters according to their CpG density, we found that ADPKD DNA exhibited more unmethylated CpGs, especially at CpG-poor promoters, than non-ADPKD samples (**Figure 2E**). We confirmed that hypermethylation was not enriched in CpG islands in ADPKD, which was different from cancer (35). Overall, we found that the genomic DNA of human ADPKD kidney tissues showed extensive demethylation; however, the overall hypomethylation of the ADPKD genome could not exclude the possibility that a few areas may be hypermethylated, some of which could even predict disease progression and prognosis (36). More studies are needed to investigate the influence and functional changes of methylation diversity, mainly focusing on genome hypomethylation, in ADPKD pathogenesis.

Regional DNA Methylations as Biomarkers in ADPKD

Genome hypomethylation and gene hypermethylation coexist in ADPKD. DNA methylation from body fluids, such as blood and urine, can be detected and quantified as diagnostic or prognostic biomarkers in ADPKD (**Figure 1A**) (12, 37). We could predict their application as potential markers in ADPKD for renal cyst development, altered renal function, and ultimately disease progression. Mucin-like protocadherin (MUPCDH) is a novel member of the cadherin superfamily, which is especially expressed at the apical surface of differentiated proximal tubule epithelial cells of the kidney (36, 38). Methylated CpG island recovery assay-DNA sequencing (MIRA-seq) analysis detected the DNA methylation pattern of the MUPCDH gene promoter region (36). Further study showed that in random urine samples from ADPKD, patients with a fully methylated MUPCDH promoter had a higher percent annual change in total kidney volume (TKV), reflecting the faster progression of cyst growth. Urine methylated-modified MUPCDH might be a prognostic biomarker for ADPKD. Whether the methylation status of urinary genomic DNA can predict cyst development and loss of renal function in ADPKD requires further investigation.

As epigenetic regulators, microRNAs (miRs) are endogenous, small, non-coding RNAs that are ∼22 nt in length and could be used to predict disease progression and patient prognosis (39). Genome-wide analyses of miR expression and DNA methylation status in ADPKD showed that two members of the miR-192 family, miR-192 and miR-194, displayed greater enrichment of the methylated DNA fraction and diminished expression in ADPKD (38). They can affect cyst enlargement by targeting endothelial-mesenchymal transition (EMT)-related genes, such as zinc finger E-box-binding homeobox-2 (ZEB2) and cadherin-2 (CDH2).

Cell-free circulating DNA (cfcDNA) in blood has been reported to carry distinctive DNA methylation markers in certain GC-rich fragments, which comprise CpG islands (40). Differential DNA methylation analysis of cfcDNA has been used successfully for prenatal diagnosis with applications for cancer diagnosis and monitoring of treatment efficacy (41), which might provide specific and sensitive potential epigenetic signatures for diagnosis, prognosis and prediction of response to therapy in ADPKD.

Finally, Gribnau et al. (14) generated induced pluripotent stem cells (iPSCs) from ADPKD patients. The cell whole-genome DNA methylation analysis (MeD-seq) showed that cystic epithelium-derived iPSCs maintained kidney-specific DNA methylation memory. Gene ontology (GO) analysis with PKD-specific hypermethylated gene body differentially methylated regions (DMRs) retrieved gene ontology (GO) terms, such as cell–cell adhesion and cell–cell signaling, which were retained as epigenetic signatures.

HISTONE METHYLATIONS IN ADPKD

Aberrant methylation changes in PKD also correlate with histone modifications, which are the second epigenetic mechanism that regulates gene expression and protein function (**Figure 1A**) (12). They can lead to either gene activation or repression depending on which histone residue is modified (11). Park et al. (31) performed histone ChIP–qPCR in ADPKD patients and found that active histone methylation marks, viz. H3K36me3 and H3KAc increased significantly in the *Pkd1* gene-body region, whereas a repressive histone modification mark (H3K27me3) decreased. Modifications of these residues were associated with the elimination of DNA methylation in *Pkd1*.

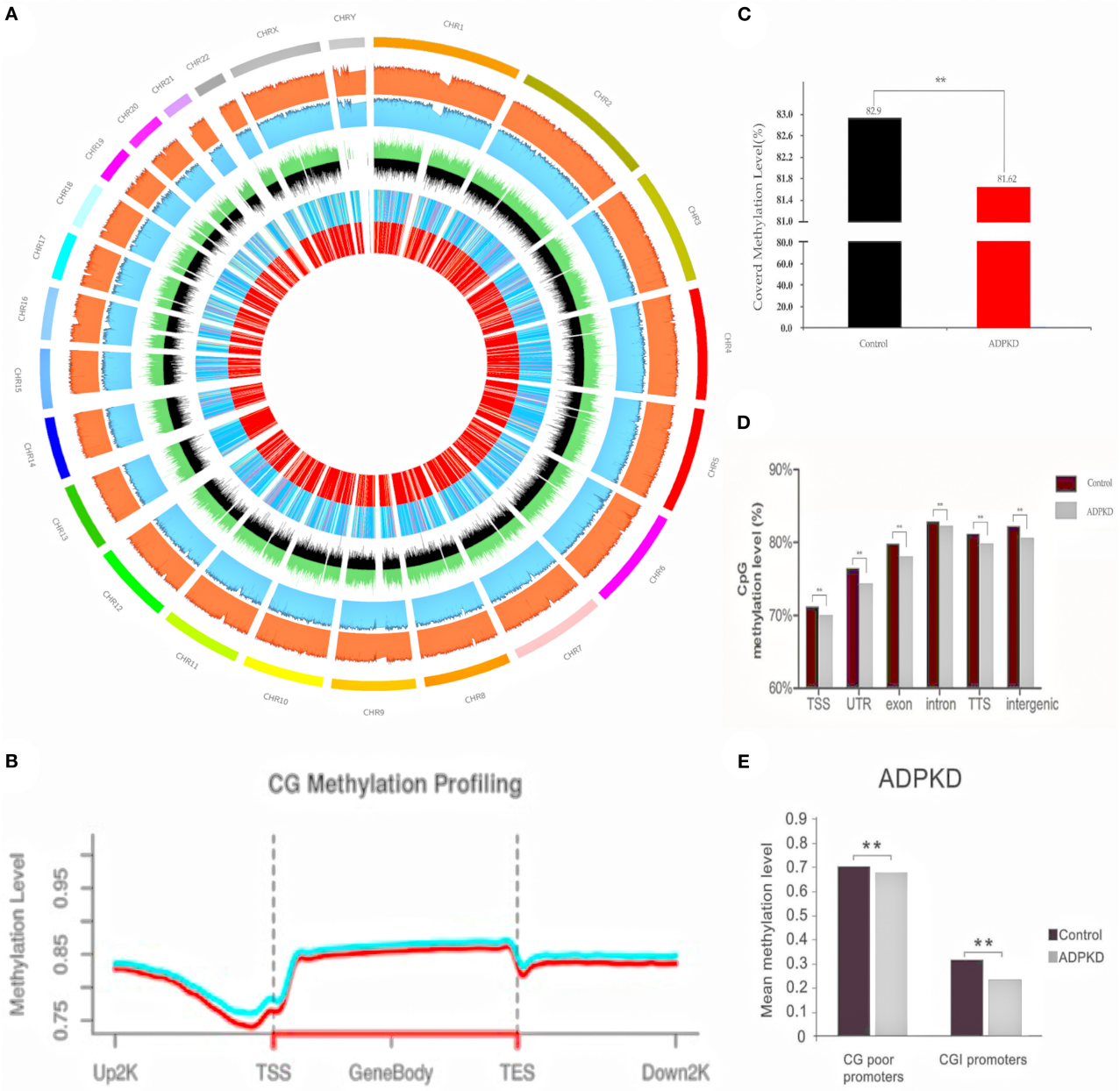

FIGURE 2 | WGBS of five non-ADPKD and five ADPKD kidneys. **(A)** Circos representation of genome-wide DNA methylation levels in the non-ADPKD and ADPKD groups. Average levels for all of the CGs in 29710-Mbp windows. The inner track indicates the magnitude of the difference between the non-ADPKD and ADPKD groups for each window (color scale and red line). Average methylation levels in all of the regions are expressed as β-values (0–1) and are colored blue. **(B)** CG methylation profiling graph for the non-ADPKD group (green line) and the ADPKD group (red line). **(C)** Methylation level of covered CpG in the non-ADPKD group and the ADPKD group (rank-sum test, ** $p < 0.01$). **(D)** Mean CpG methylation levels among different genomic sequences in the non-ADPKD group and the ADPKD group (rank-sum test, ** $p < 0.01$). **(E)** Mean CpG methylation levels among promoters in the non-ADPKD and ADPKD groups in the presence or absence of a CpG island (rank-sum test, ** $p < 0.01$). The mean methylation level was calculated by the number of total methylated reads divided by the number of total reads covering CpG sites located in the sum of the features analyzed.

Histone methylation is mediated by histone methyltransferases (HMTs), which are epigenetic modifiers that directly modify the epigenome (12). There are two families of HMTs, which have specificities for arginine and lysine residues (42). In PKD, they are located upstream of epigenetic mediators, which are the direct targets of them or their downstream targets of epigenetic modification; meanwhile, they are downstream of epigenetic modulators, which influence the activity or

localization of the epigenetic modifiers and the epigenetic states mediated by them (43). Some of the mediators and modulators have been reported to be closely related to the pathogenesis and acceleration of cystic phenotypes together with or acting as the HMTs (44). They form covalent modifications on the N-terminal tails of PKD genes, which are rich in histone residues, and construct the histone code together through their interacting arrangements.

Smyd2

SMYD2 is a SET and MYND (myeloid-Nervy-DEAF1) domain protein (45). It acts as a lysine methyltransferase to regulate cyst growth in ADPKD through multiple signaling pathways (**Figure 1B**) (46–48). First, SMYD2 acts as a downstream mediator of Pkd1 mutation and activates phosphorylated STAT3 in JAK/STAT signaling, which serves as a positive regulator of cyst growth, via lysine methylation at K685 (48). It can also promote cystic renal epithelial cell proliferation and survival by methylating the subunit of NF-κB, p65 at lysine 310 and partially at lysine 221, leading to its phosphorylation and activation (48). Moreover, SMYD2 could integrate epigenetic regulation and renal inflammation in cyst development through the formation of two positive feedback loops: SMYD2/IL-6/STAT3/SMYD2 and SMYD2/TNF-α/NF-κB/SMYD2 (48). Furthermore, it could increase the methylation of p53 and prevent p53-dependent cystic renal epithelial cell apoptosis (45, 48). Double conditional knockout of the Pkd1 and Smyd2 genes in a PKD mouse model delayed renal cyst growth and preserved renal function (48). Specifically, inhibiting Smyd2 could slow disease progression, indicating that it is a novel therapeutic target for ADPKD treatment.

Further study showed that epigenetic histone modifications by SMYD2 were also involved in the regulation of the cell cycle and ciliagenesis in ADPKD (47). SMYD2 was found to be colocalized at the basal body of the primary cilia together with cyclin-dependent kinase 4 (CDK4) and its closely related CDK6 (49). CDK4/6 can form complexes with D-type cyclins and drive G1 phase quiescent cells into DNA synthesis S phase (50). CDK4/6 interacts with SMYD2 and regulates the methylation of histone H3 lysine 4 (H3K4) and lysine 36 (H3K36), which promote the phosphorylation and enzymatic activity of SMYD2; on the other hand, methylation of histone H3K4 at the promoters of CDK4 and CDK6 by SMYD2 positively regulates their transcription (47). CDK4/6-SMYD2 signaling maintained the balance of microtubule dynamics through methylation of the key components affecting cilia assembly: (i) it methylated α-tubulin at lysine-394 (TubK394me) and retarded the stability of microtubules, which facilitated the trafficking of cilia proteins from the Golgi to the ciliary base; (ii) it also methylated histone H3K36 at the promoter of intraflagellar transport protein IFT20, which encodes a key IFT protein that regulates the trafficking of ciliary proteins from the Golgi to cilia, to repress its transcription. Depletion or inhibition of CDK4/6-SMYD2 signaling selectively decreased the methylation of α-tubulin and increased the expression of IFT20, resulting in an improved fidelity in the number of ciliated cells and cilia length, which might contribute to the slowing down of cystic renal epithelial cell proliferation and cyst growth (47).

Rb/E2F

Retinoblastoma tumor suppressor protein (Rb)/E2F could be both epigenetic mediators and modulators in cyst development in ADPKD (**Figure 1B**) (10). The hypophosphorylated state Rb acted as a repressor of E2F-mediated transcriptional activity, which could form a complex with histone deacetylases (HDACs), DNMT1 and SUV39H1, an HMT that recruits them to E2F-site-containing promoters, including cyclin A/E and Cdk2 (51). SMYD2 has been reported to methylate Rb at lysine 810, which enhances Ser807/811 phosphorylation of the Rb protein. This accelerates E2F transcriptional activity and promotes cell cycle progression (46). HDAC inhibition targeting Rb/E2F has been reported to decrease cystic epithelial cell proliferation and reduce cyst development by acting as an inhibitor of differentiation 2 (Id2) (52) and sirtuin 1 (53), respectively; however, its influence on histone methylation in ADPKD cystogenesis requires further investigation.

EZH2

The polycomb group (PcG) gene EZH2, also known as the homolog of Enhancer of zeste in mammals, is a histone modifier that plays a crucial role in differentiation gene silencing in a cell cycle-dependent manner (54). It is the major methyltransferase for H3 lysine 27 and plays a crucial role in differential gene silencing, such as for HOX genes and SOX family members (55). It is also the direct target of the core cell cycle transcriptional regulator E2F (56). EZH2 is upregulated in cystic renal epithelial cells, the targeting of which delayed cyst growth in Pkd1 knockout mouse models (**Figure 1B**) (12). Further investigations will be required to fully understand how elevated EZH2 coordinates with the cell cycle machinery, such as Rb/E2F, to promote cystic cell proliferation.

RNA METHYLATION

Modifications of RNA can change its processing, stability, or translational efficiency, similar to DNA (57). The methylation of RNA has been a recently discovered aspect of epigenetic modification in ADPKD (15). Adenosine methylation at the 6th nitrogen position known as N^6-methyladenosine (m^6A), recognized as the most common eukaryotic RNA modification and mediated by the multiprotein m^6A writer complex composed of Mettl3, etc., was increased in mouse and human ADPKD samples (**Figure 1A**) (15, 58). Kidney-tubule-specific Mettl3 overexpression induced the occurrence and enlargement of tubular cysts, and conversely, Mettl3 deletion attenuated cyst growth in three different orthologous ADPKD transgenic mouse models, irrespective of the type of *PKD1* mutation or dynamics of cyst growth (15). Further immunoprecipitation of m^6A-modified mRNAs and high-throughput sequencing (MeRIP-seq) showed that c-Myc and Avpr2 mRNA had significantly higher m^6A modification and translation, which enhanced c-Myc and Avpr2 protein expression and resulted in cyst proliferation and fluid protein synthesis through the c-Myc and cAMP signaling pathways. Moreover, dietary methionine and S-adenosylme thionine, which could induce Mettl3 expression, aggravated cyst growth *ex vivo* (59); in contrast, dietary methionine restriction

attenuated mouse ADPKD, indicating a potential dietary therapy to slow down disease progression (15, 60).

EPIGENETIC THERAPY IN ADPKD AND FUTURE PERSPECTIVES

Unlike genetic mutation, epigenetic silencing is a potentially reversible alteration, which means that through optimal epigenetic therapy, it can be restored to the normal status and used as a treatment for ADPKD (61). For example, restoring the diminished expression of miR-192 and miR-194 by injection of their precursors to replace the hypermethylated non-functional ones could reduce the size of cysts in a Pkd1 knockout mouse model (38). Restoration of MUPCDH expression by using 5-azacytidine to inhibit DNMT and reduce DNA methylation can regulate the anti-proliferative property of MUPCDH in HRCE and WT9-7 PKD cell lines, making it a potential therapeutic target (36). Apart from DNMT, specific inhibitors targeting HMTs, such as Smyd2 and EZH2, with their inhibitors delayed cyst growth in Pkd1 mutant mouse kidneys (12, 48). Since epigenetic modifying enzymes function in a wide range of organs in the body, more specific epigenetic treatment aiming to reverse the alterations occurring in PKD should lead to the development of treatment to reduce unwanted side effects, considering the complexity of methylation abnormalities occurring in different regions and genes on the PKD epigenome.

AUTHOR CONTRIBUTIONS

The research idea and study design were devised by ZM and CM. LZ revised the manuscript. JX and CX were the primary authors of this manuscript. XW finished data collection and statistical analysis. All authors read and approved the final manuscript.

FUNDING

This work was supported by the National Natural Science Foundation of China (82070705, 81770670, 81873595, and 32030025), the National Key Research and Development Program of China (2019YFA0802001), Shanghai Municipal Key Clinical Specialty (shslczdzk02503), Shanghai Science and Technology Talent Program (19YF1450300), and Research Projects of Shanghai Science and Technology Committee (17411972100).

REFERENCES

1. Iglesias CG, Torres VE, Offord KP, Holley KE, Beard CM, Kurland LT. Epidemiology of adult polycystic kidney disease, Olmsted County, Minnesota:1935-1980. Am J Kidney Dis. (1983) 2:630–9. doi: 10.1016/S0272-6386(83)80044-4
2. Collins AJ, Foley RN, Herzog C, Chavers BM, Gilbertson D, Ishani A, et al. Excerpts from the US renal data system 2009 annual data report. *Am J Kidney Dis*. (2010) 55(Suppl. 1): A426-7. doi: 10.1053/j.ajkd.2009.10.009
3. Cornec-Le Gall E, Audrezet MP, Le Meur Y, Chen JM, Ferec C. Genetics and pathogenesis of autosomal dominant polycystic kidney disease: 20 years on. *Hum Mutat*. (2014) 35:1393–406. doi: 10.1002/humu.22708
4. Consortium TIPKD. Polycystic kidney disease:the complete structure of the PKD1 gene and its protein. *Cell*. (1995) 81:289–98. doi: 10.1016/0092-8674(95)90339-9
5. Mochizuki T, Wu G, Hayashi T, Xenophontos SL, Veldhuisen B, Saris JJ, et al. PKD2, a Gene for Polycystic Kidney Disease That Encodes an Integral Membrane Protein. *Science*. (1996) 272:1339-42. doi: 10.1126/science.272.5266.1339
6. Leonidas Tsiokas TA, Chenwen ZHU, Gerdwalz, Vikas P. Sukhatme Specific association of the gene product of PKD2 with the TRPC1 channel. *Proc Natl Acad Sci USA*. (1999) 96:3934–9. doi: 10.1073/pnas.96.7.3934
7. Harris PC, Rossetti S. Molecular diagnostics for autosomal dominant polycystic kidney disease. *Nat Rev Nephrol*. (2010) 6:197–206. doi: 10.1038/nrneph.2010.18
8. Y P. Nature and nurture on phenotypic variability of autosomal dominant polycystic kidney disease. *Kid Int*. (2005) 67:1630–31. doi: 10.1111/j.1523-1755.2005.00252.x
9. Milutinovic J, Rust PF, Fialkow PJ, Agodoa LY, Phillips LA, Rudd TG, et al. Intrafamilial phenotypic expression of autosomal dominant polycystic kidney disease. *Am J Kidney Dis*. (1992) 19:465–72. doi: 10.1016/S0272-6386(12)80956-5
10. Li X. Epigenetics and autosomal dominant polycystic kidney disease. *Biochim Biophys Acta*. (2011) 1812:1213–8. doi: 10.1016/j.bbadis.2010.10.008
11. Li X. Epigenetics in ADPKD: understanding mechanisms and discovering treatment. In: Li X, editor. *Polycystic Kidney Disease*. Brisbane, QLD: Codon Publications (2015).
12. Li X. Epigenetics and cell cycle regulation in cystogenesis. *Cell Signal*. (2020) 68:109509. doi: 10.1016/j.cellsig.2019.109509
13. Egger G, Liang G, Aparicio A, Jones PA. Epigenetics in human disease and prospects for epigenetic therapy. *Nature*. (2004) 429:457–63. doi: 10.1038/nature02625
14. Kenter AT, Rentmeester E, van Riet J, Boers R, Boers J, Ghazvini M, et al. Cystic renal-epithelial derived induced pluripotent stem cells from polycystic kidney disease patients. *Stem Cells Transl Med*. (2020) 9:478–90. doi: 10.1002/sctm.18-0283
15. Ramalingam H, Kashyap S, Cobo-Stark P, Flaten A, Chang CM, Hajarnis S, et al. A methionine-Mettl3-N(6)-methyladenosine axis promotes polycystic kidney disease. *Cell Metab*. (2021) 33:1234–1247. doi: 10.1016/j.cmet.2021.03.024
16. McCabe MT, Davis JN, Day ML. Regulation of DNA methyltransferase 1 by the pRb/E2F1 pathway. *Cancer Res*. (2005) 65:3624–32. doi: 10.1158/0008-5472.CAN-04-2158
17. Deaton AM, Bird A. CpG islands and the regulation of transcription. *Genes Dev*. (2011) 25:1010–22. doi: 10.1101/gad.2037511
18. Bowden SA, Rodger EJ, Chatterjee A, Eccles MR, Stayner C. Recent discoveries in epigenetic modifications of polycystic kidney disease. *Int J Mol Sci*. (2021) 22:13327. doi: 10.3390/ijms222413327
19. Marc Jung WX. Swati Kadam,Tibor A. MIRA-seq for DNA methylation analysis of CpG islands. *Epigenomics*. (2015) 7:695–706. doi: 10.2217/epi.15.33
20. Jiang CL, Jin SG, Pfeifer GP. MBD3L1 is a transcriptional repressor that interacts with methyl-CpG-binding protein 2 (MBD2) and components of the NuRD complex. *J Biol Chem*. (2004) 279:52456–64. doi: 10.1074/jbc.M409149200
21. Rauch T, Li H, Wu X, Pfeifer GP. MIRA-assisted microarray analysis, a new technology for the determination of DNA methylation patterns, identifies frequent methylation of homeodomain-containing genes in lung cancer cells. *Cancer Res*. (2006) 66:7939–47. doi: 10.1158/0008-5472.CAN-06-1888
22. Rauch TA, Pfeifer GP. The MIRA method for DNA methylation analysis. *Methods Mol Biol*. (2009) 507:65–75. doi: 10.1007/978-1-59745-522-0_6
23. Bowden SA, Rodger EJ, Bates M, Chatterjee A, Eccles MR, Stayner C. Genome-Scale single nucleotide resolution analysis of DNA methylation in human autosomal dominant polycystic kidney disease. *Am J Nephrol*. (2018) 48:415–24. doi: 10.1159/000494739

24. Chatterjee A RE, Morison IM, Eccles MR, Stockwell PA. Tools and strategies for analysis of genome-wide and gene-specific DNA methylation patterns. *Methods Mol Biol.* (2017) 1537:249–77. doi: 10.1007/978-1-4939-6685-1_15
25. M G-G, M F. CpG islands in vertebrate genomes. *J Mol Biol*. (1987) 196:261–82. doi: 10.1016/0022-2836(87)90689-9
26. Adusumalli S, Mohd Omar MF, Soong R, Benoukraf T. Methodological aspects of whole-genome bisulfite sequencing analysis. *Brief Bioinform.* (2015) 16:369–79. doi: 10.1093/bib/bbu016
27. Nicoglou A, Merlin F. Epigenetics: A way to bridge the gap between biological fields. *Stud Hist Philos Biol Biomed Sci.* (2017) 66:73–82. doi: 10.1016/j.shpsc.2017.10.002
28. Jin Z, Liu Y, DNA. methylation in human diseases. *Genes Dis.* (2018) 5:1–8. doi: 10.1016/j.gendis.2018.01.002
29. Reddington JP, Sproul D, Meehan RR. DNA methylation reprogramming in cancer: does it act by re-configuring the binding landscape of Polycomb repressive complexes? *BioEssays.* (2014) 36:134–40. doi: 10.1002/bies.201300130
30. Ke Sun DX. Changlin Mei. The association between autosomal dominant polycystic kidney disease and cancer. *Int Urol Nephrol.* (2019) 51:93–100. doi: 10.1007/s11255-018-1951-5
31. Woo YM, Bae J-B, Oh Y-H, Lee Y-G, Lee MJ, Park EY. Genome-wide methylation profiling of ADPKD identified epigenetically regulated genes associated with renal cyst development. *Hum Genet*. (2013) 133:281–97. doi: 10.1007/s00439-013-1378-0
32. Hajirezaei F, Ghaderian SMH, Hasanzad M, Nafar M, Ghadiani MH, Biglari S, et al. Methylation of the PKD1 promoter inversely correlates with its expression in autosomal dominant polycystic kidney disease. *Rep Biochem Mol Biol.* (2020) 9:193–8. doi: 10.29252/rbmb.9.2.193
33. Bowden SA, Stockwell PA, Rodger EJ, Parry MF, Eccles MR, Stayner C, et al. Extensive inter-cyst DNA methylation variation in autosomal dominant polycystic kidney disease revealed by genome scale sequencing. *Front Genet*. (2020) 11:348. doi: 10.3389/fgene.2020.00348
34. Bu L. The role of abnormal DNA methylation inautosomal dominant polycystic kidney disease and its mechanism [D] Wangfang Database. (2019).
35. Hansen KD, Timp W, Bravo HC, Sabunciyan S, Langmead B, McDonald OG, et al. Increased methylation variation in epigenetic domains across cancer types. *Nat Genet.* (2011) 43:768–75. doi: 10.1038/ng.865
36. Woo YM, Shin Y, Hwang JA, Hwang YH, Lee S, Park EY, et al. Epigenetic silencing of the MUPCDH gene as a possible prognostic biomarker for cyst growth in ADPKD. *Sci Rep*. (2015) 5:15238. doi: 10.1038/srep15238
37. Bronkhorst AJ, Ungerer V, Holdenrieder S. The emerging role of cell-free DNA as a molecular marker for cancer management. *Biomol Detect Quantif.* (2019) 17:100087. doi: 10.1016/j.bdq.2019.100087
38. Kim DY, Woo YM, Lee S, Oh S, Shin Y, Shin JO, et al. Impact of miR-192 and miR-194 on cyst enlargement through EMT in autosomal dominant polycystic kidney disease. *FASEB J.* (2019) 33:2870–84. doi: 10.1096/fj.201800563RR
39. Bartel DP. MicroRNAs: genomics, biogenesis, mechanism, and function. *Cell.* (2004) 116:281–97. doi: 10.1016/S0092-8674(04)00045-5
40. Levenson VV, DNA. methylation as a universal biomarker. *Expert Rev Mol Diagn.* (2010) 10:481–8. doi: 10.1586/erm.10.17
41. Swarup V, Rajeswari MR. Circulating (cell-free) nucleic acids–a promising, non-invasive tool for early detection of several human diseases. *FEBS Lett*. (2007) 581:795–9. doi: 10.1016/j.febslet.2007.01.051
42. Sawan C, Herceg Z. Histone modifications and cancer. *Adv Genet.* (2010) 70:57–85. doi: 10.1016/B978-0-12-380866-0.60003-4
43. Zhang Y, Reinberg D. Transcription regulation by histone methylation: interplay between different covalent modifications of the core histone tails. *Genes Dev*. (2001) 15:2343–60. doi: 10.1101/gad.927301
44. KDIGO Clinical Practice Guidelines for Glomerulonephritis. Chapter 3: Steroid-sensitive nephrotic syndrome in children. *Kidney Int Suppl.* (2012) 2:163-171. doi: 10.1038/kisup.2012.16
45. Huang J, Perez-Burgos L, Placek BJ, Sengupta R, Richter M, Dorsey JA, et al. Repression of p53 activity by Smyd2-mediated methylation. *Nature.* (2006) 444:629–32. doi: 10.1038/nature05287
46. Cho HS, Hayami S, Toyokawa G, Maejima K, Yamane Y, Suzuki T, et al. RB1 methylation by SMYD2 enhances cell cycle progression through an increase of RB1 phosphorylation. *Neoplasia.* (2012) 14:476–86. doi: 10.1593/neo.12656
47. Li LX, Zhou JX, Wang X, Zhang H, Harris PC, Calvet JP et al. Cross-talk between CDK4/6 and SMYD2 regulates gene transcription, tubulin methylation, and ciliogenesis. *Sci Adv*. (2020) 6:eabb3154. doi: 10.1126/sciadv.abb3154
48. Li LX, Fan LX, Zhou JX, Grantham JJ, Calvet JP, Sage J, et al. Lysine methyltransferase SMYD2 promotes cyst growth in autosomal dominant polycystic kidney disease. *J Clin Invest.* (2017) 127:2751–64. doi: 10.1172/JCI90921
49. Plotnikova OV, Pugacheva EN, Golemis EA. Primary cilia and the cell cycle. *Methods Cell Biol.* (2009) 94:137–60. doi: 10.1016/S0091-679X(08)94007-3
50. Sherr CJ, Beach D, Shapiro GI. Targeting CDK4 and CDK6: from discovery to therapy. *Cancer Discov.* (2016) 6:353–67. doi: 10.1158/2159-8290.CD-15-0894
51. Vandel L, Nicolas E, Vaute O, Ferreira R, Ait-Si-Ali S, Trouche D. Transcriptional repression by the retinoblastoma protein through the recruitment of a histone methyltransferase. *Mol Cell Biol.* (2001) 21:6484–94. doi: 10.1128/MCB.21.19.6484-6494.2001
52. Fan LX Li X, Magenheimer B, Calvet JP Li X. Inhibition of histone deacetylases targets the transcription regulator Id2 to attenuate cystic epithelial cell proliferation. *Kidney Int.* (2012) 81:76–85. doi: 10.1038/ki.2011.296
53. Zhou X, Fan LX, Sweeney WE. Jr., Denu JM, Avner ED, Li X. Sirtuin 1 inhibition delays cyst formation in autosomal-dominant polycystic kidney disease *J Clin Invest.* (2013) 123:3084–98. doi: 10.1172/JCI64401
54. Kuzmichev A, Nishioka K, Erdjument-Bromage H, Tempst P, Reinberg D. Histone methyltransferase activity associated with a human multiprotein complex containing the Enhancer of Zeste protein. *Genes Dev.* (2002) 16:2893–905. doi: 10.1101/gad.1035902
55. Cao R, Wang L, Wang H, Xia L, Erdjument-Bromage H, Tempst P, et al. Role of histone H3 lysine 27 methylation in Polycomb-group silencing. *Science.* (2002) 298:1039–43. doi: 10.1126/science.1076997
56. Bracken AP, Pasini D, Capra M, Prosperini E, Colli E, Helin K. EZH2 is downstream of the pRB-E2F pathway, essential for proliferation and amplified in cancer. *EMBO J.* (2003) 22:5323–35. doi: 10.1093/emboj/cdg542
57. Nachtergaele S, He C. Chemical Modifications in the Life of an mRNA Transcript. *Annu Rev Genet.* (2018) 52:349–72. doi: 10.1146/annurev-genet-120417-031522
58. Bokar JA, Shambaugh ME, Polayes D, Matera AG, Rottman FM. Purification and cDNA cloning of the AdoMet-binding subunit of the human mRNA (N6-adenosine)-methyltransferase. *RNA*. (1997) 3:1233–47.
59. Jia G, Fu Y, He C. Reversible RNA adenosine methylation in biological regulation. *Trends Genet.* (2013) 29:108–15. doi: 10.1016/j.tig.2012.11.003
60. Padovano V, Podrini C, Boletta A, Caplan MJ. Metabolism and mitochondria in polycystic kidney disease research and therapy. *Nat Rev Nephrol.* (2018) 14:678–87. doi: 10.1038/s41581-018-0051-1
61. Jones PA, Baylin SB. The epigenomics of cancer. *Cell.* (2007) 128:683–92. doi: 10.1016/j.cell.2007.01.029

Conflict of Interest: The authors declare that the research was conducted in the absence of any commercial or financial relationships that could be construed as a potential conflict of interest.

frontiers | Frontiers in Medicine

ORIGINAL RESEARCH
published: 07 July 2022
doi: 10.3389/fmed.2022.873923

Spatially Resolved Transcriptomes of Mammalian Kidneys Illustrate the Molecular Complexity and Interactions of Functional Nephron Segments

Arti M. Raghubar[1,2,3,4,5], Duy T. Pham[5†], Xiao Tan[5†], Laura F. Grice[5,6†], Joanna Crawford[5], Pui Yeng Lam[5], Stacey B. Andersen[7,8], Sohye Yoon[7], Siok Min Teoh[9], Nicholas A. Matigian[10], Anne Stewart[4], Leo Francis[4], Monica S. Y. Ng[1,2,3,5,11], Helen G. Healy[1,2,3], Alexander N. Combes[12], Andrew J. Kassianos[1,2,3], Quan Nguyen[5‡] and Andrew J. Mallett[3,5,13,14*‡]*

[1] Kidney Health Service, Royal Brisbane and Women's Hospital, Herston, QLD, Australia, [2] Conjoint Internal Medicine Laboratory, Chemical Pathology, Pathology Queensland, Health Support Queensland, Herston, QLD, Australia, [3] Faculty of Medicine, University of Queensland, Brisbane, QLD, Australia, [4] Anatomical Pathology, Pathology Queensland, Health Support Queensland, Herston, QLD, Australia, [5] Institute for Molecular Bioscience, University of Queensland, Brisbane, QLD, Australia, [6] School of Biomedical Sciences, The University of Queensland, Brisbane, QLD, Australia, [7] Genome Innovation Hub, University of Queensland, Brisbane, QLD, Australia, [8] UQ Sequencing Facility, Institute for Molecular Bioscience, University of Queensland, Brisbane, QLD, Australia, [9] UQ Diamantina Institute, Faculty of Medicine, The University of Queensland, Woolloongabba, QLD, Australia, [10] QCIF Facility for Advanced Bioinformatics, Institute for Molecular Bioscience, The University of Queensland, Brisbane, QLD, Australia, [11] Nephrology Department, Princess Alexandra Hospital, Woolloongabba, QLD, Australia, [12] Department of Anatomy and Developmental Biology, Stem Cells and Development Program, Monash Biomedicine Discovery Institute, Monash University, Melbourne, VIC, Australia, [13] College of Medicine & Dentistry, James Cook University, Townsville, Queensland, QLD, Australia, [14] Department of Renal Medicine, Townsville University Hospital, Townsville, Queensland, QLD, Australia

Available transcriptomes of the mammalian kidney provide limited information on the spatial interplay between different functional nephron structures due to the required dissociation of tissue with traditional transcriptome-based methodologies. A deeper understanding of the complexity of functional nephron structures requires a non-dissociative transcriptomics approach, such as spatial transcriptomics sequencing (ST-seq). We hypothesize that the application of ST-seq in normal mammalian kidneys will give transcriptomic insights within and across species of physiology at the functional structure level and cellular communication at the cell level. Here, we applied ST-seq in six mice and four human kidneys that were histologically absent of any overt pathology. We defined the location of specific nephron structures in the captured ST-seq datasets using three lines of evidence: pathologist's annotation, marker gene expression, and integration with public single-cell and/or single-nucleus RNA-sequencing datasets. We compared the mouse and human cortical kidney regions. In the human ST-seq datasets, we further investigated the cellular communication within glomeruli and regions of proximal tubules–peritubular capillaries by screening for co-expression of ligand–receptor gene pairs. Gene expression signatures of distinct nephron structures and microvascular regions were spatially resolved within the mouse and human ST-seq datasets. We identified

OPEN ACCESS

Edited by:
Tara Sigdel,
University of California, San Francisco, United States

Reviewed by:
Vijayakumar Kakade,
Yale University, United States
Markus Bitzer,
University of Michigan, United States

***Correspondence:**
Andrew J. Mallett
Andrew.Mallett@health.qld.gov.au
Quan Nguyen
quan.nguyen@imb.uq.edu.au

†These authors have contributed equally to this work and share the second authorship
‡These authors share senior authorship

Specialty section:
This article was submitted to Nephrology, a section of the journal Frontiers in Medicine

Received: 11 February 2022
Accepted: 23 May 2022
Published: 07 July 2022

Citation:
Raghubar AM, Pham DT, Tan X, Grice LF, Crawford J, Lam PY, Andersen SB, Yoon S, Teoh SM, Matigian NA, Stewart A, Francis L, Ng MSY, Healy HG, Combes AN, Kassianos AJ, Nguyen Q and Mallett AJ (2022) Spatially Resolved Transcriptomes of Mammalian Kidneys Illustrate the Molecular Complexity and Interactions of Functional Nephron Segments. Front. Med. 9:873923. doi: 10.3389/fmed.2022.873923

7,370 differentially expressed genes ($p_{adj} < 0.05$) distinguishing species, suggesting changes in energy production and metabolism in mouse cortical regions relative to human kidneys. Hundreds of potential ligand–receptor interactions were identified within glomeruli and regions of proximal tubules–peritubular capillaries, including known and novel interactions relevant to kidney physiology. Our application of ST-seq to normal human and murine kidneys confirms current knowledge and localization of transcripts within the kidney. Furthermore, the generated ST-seq datasets provide a valuable resource for the kidney community that can be used to inform future research into this complex organ.

Keywords: spatial transcriptomics, kidney, human, mouse, cell-cell interactions

INTRODUCTION

The mammalian kidney contains millions of nephrons, each composed of functional structures including the distal tubule, the loop of Henle, the proximal tubule, and the glomerulus. Nephrons are connected to a collecting duct network and surrounded by stroma and microvasculature (1, 2). The nephrons maintain homeostasis of body fluids, electrolyte and acid–base balance, and the excretion of metabolic waste products (3–5). The spatial organization of nephrons facilitates the homeostatic function of the mammalian kidney. However, to date, transcriptome studies of normal human and murine nephrons have utilized bulk RNA-sequencing, single-cell and/or single-nucleus RNA-sequencing (scRNA-seq/snRNA-seq), which require manipulation of tissue, including tissue homogenization or cell dissociation and resulting in the loss of crucial spatial information (6–13).

Unlike bulk RNA-seq, scRNA-seq, and snRNA-seq, ST-seq provides crucial spatial information with transcriptome profiling by integrating histology with RNA-seq within intact tissue (14–32). Both histological assessment and RNA-seq are completed sequentially on the same tissue section placed on a glass slide with printed oligo-dT spots, termed ST-spots (14, 17, 33, 34). Transcriptomes within the tissue section are captured by the underlying ST-spots and receive a spatial barcode in the process. The sequenced ST-spot transcriptomes are subsequently aligned with the Hematoxylin and Eosin (H&E) image to visualize gene expression within the intact tissue. Current applications of ST-seq in mammalian kidneys have been limited to inflammatory or developmental murine models, with no to minimal studies in normal/control mouse and human kidneys (6–9).

In this study, we used a commercially available 10x Genomics ST platform to investigate spatially resolved gene expression in normal mouse and human kidney tissues. We generated transcriptional profiles of the mammalian kidney to identify functional nephron structures and major cell types. Next, we used the generated ST-seq data to investigate differences in gene expression and biological processes between cortical regions of mouse and human kidneys. Last, we predicted cell-cell interactions within glomeruli and regions of proximal tubules–peritubular capillaries (PT–PC). We found that the generated spatial transcriptomic data from normal human and murine kidneys matched current knowledge and localization of transcripts. The generated ST-seq datasets are a valuable data resource for the kidney community to inform future research into this complex organ.

MATERIALS AND METHODS

Kidney Tissue Samples

Whole mouse kidneys utilized in this ST study were from three male (8 weeks old) and three female (6 weeks old) C57BL/6J wild-type mice (Animal Ethics Committee approval UQDI/452/16 and IMB123/18). The mouse kidneys were collected during tissue harvesting and snap frozen in standard biopsy cryomolds (Tissue-Tek, Sakura Finetek, United States) with optimum cutting temperature (OCT) compound (Tissue-Tek). These freshly frozen adult mouse kidneys were then stored at −80°C on site. Cryosections of 10 μm were cut from the mouse samples, stained with H&E, and confirmed as normal by a Consultant Pathologist. These samples were subsequently used for ST-seq with the ST platform (100 μm ST-spots; **Figures 1**, **2A**).

We utilized human cortical kidney tissues taken a minimum of 3 cm away from the tumor margins of four patients that were matched for comorbidities (2 women, 51–53 years old and 2 men, 54 and 56 years old; **Table 1**). The use of human kidney tissues was approved by the Royal Brisbane and Women's Hospital Human Research Ethics Committee (2002/011). Human kidney tissue was snap frozen in standard biopsy cryomolds (Tissue-Tek) with OCT compound (Tissue-Tek). Cryosections of 10 μm were cut from the human kidney samples, stained with H&E, and confirmed as normal by a Consultant Pathologist. These samples were subsequently used for ST-seq with the Visium ST platform (55 μm ST-spots; **Figures 1**, **3A** and **Supplementary Figure 1A**).

RNA Quality

Two 10 μm scrolls of tissue were collected in pre-chilled 1.5 ml Eppendorf tubes from each frozen OCT block of mouse whole kidneys ($n = 6$) and human cortical kidneys ($n = 4$). RNA from each sample was extracted from the cryosectioned scrolls according to the QIAGEN RNeasy micro kit (Hilden, Germany). RNA content was quantified according to the Qubit RNA HS assay kit (Invitrogen, Thermo Fisher Scientific, Singapore) and the RNA integrity number (RIN) was assessed according to

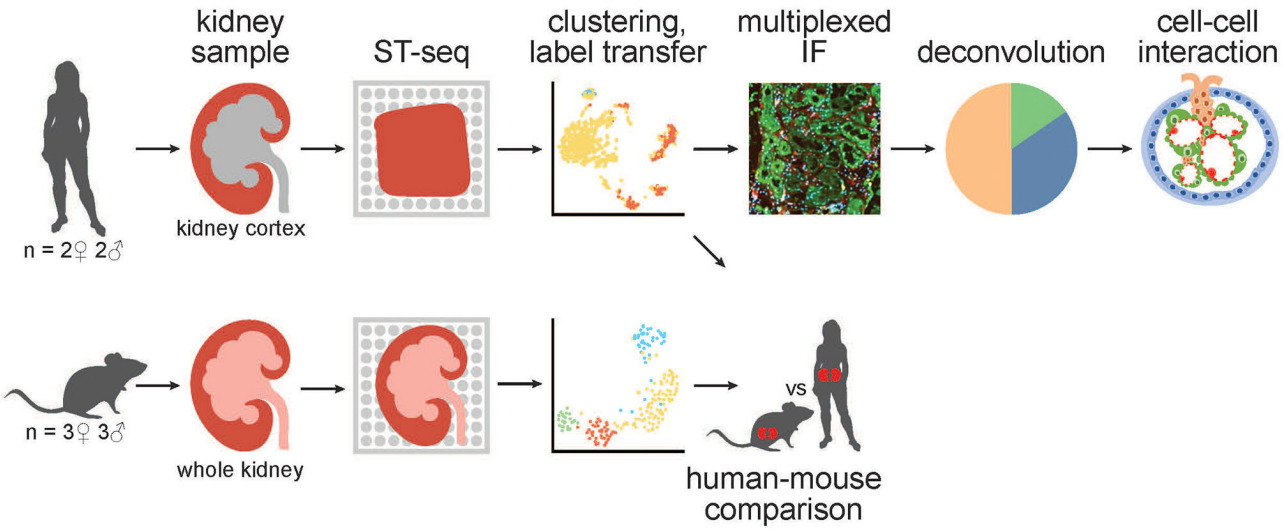

FIGURE 1 | A schematic of the workflow for generation and analysis of mammalian kidney ST-seq datasets. (From left to right) We performed ST-seq on four human kidney cortical tissues (2 women, 51–53 years old and 2 men, 54 and 56 years old) and six mice whole kidneys (3 males, 8 weeks old and 3 females, 6 weeks old). With the generated ST-seq datasets, we performed clustering and label transfer to define the location of specific nephron segments or regions in human and mouse kidneys, respectively. We selected the cortical kidney regions in the mouse ST-seq datasets and performed functional analysis on genes that were differentially expressed between species in the cortex. In the human cortical kidney tissues, we performed multiplexed IF on consecutive deeper sections to correlate the label transfer annotation of the functional nephron segments with histomorphology. Last, we investigated the CCI by screening for L–R gene pair co-expression in glomerular and PT–PC ST-spots identified by deconvolution.

the Agilent 2100 Bioanalyzer RNA 6000 Pico assay (Agilent Technologies, Inc., United States). The measured RINs for all kidney tissues were >7.

Tissue Optimization

Tissue optimization was performed according to the 10x Genomics ST Tissue Optimization Manual (version 190219, 10x Genomics, United States) to determine the ideal permeabilization time. Frozen 10 μm cryosectioned tissue from mouse and human kidney tissues were utilized for this optimization. The kidney tissue sections were dried at 37°C for 1 min, fixed in pre-chilled 100% methanol at −20°C for 30 min, and stained in Mayer's Hematoxylin (Dako, Agilent Technologies, Inc., United States) for 5 min and Eosin (Sigma–Aldrich Pty. Ltd., Australia) for 2 min. Imaging was performed on an Aperio XT brightfield slide scanner (Leica).

After H&E imaging, the kidney tissue sections were placed in a permeabilization mix over a range of time points to allow the mRNA to drop down from the tissue sections and bind to the oligo-dTs printed on the slide. The captured mRNAs on the slide surface were then reverse transcribed to fluorescently labeled cDNA. This fluorescent cDNA signal was imaged on a Leica confocal microscope (SP8 STED 3X). The ideal permeabilization time of 12 min was determined by comparing both the H&E and fluorescent images from the tissue optimization slide. This optimized permeabilization time was utilized for generating ST libraries for sequencing from mouse and human kidney tissue sections.

Library Preparation

ST library preparation of the mouse kidney tissues ($n = 6$) was performed according to the ST Library Preparation Manual (version 190219, 10x Genomics, United States). ST library preparation of the human cortical kidney tissues ($n = 4$) was performed according to the Visium Spatial Gene Expression Reagent Kits User Guide (CG000239 Rev C, 10x Genomics, United States). In brief, 10 μm cryosectioned mouse and human kidney tissues were placed onto pre-chilled library preparation slides. The mouse kidneys were multiplexed into two arrays based on gender (three mouse kidneys per array). Sections of the human kidney were placed in four separate arrays such that each patient received an individual array. We placed two consecutive sections in arrays A and D. Tissue sections were dried on the slides at 37°C for 1 min, then fixed in pre-chilled 100% methanol at −20°C for 30 min, and stained in Mayer's Hematoxylin for 5 min and Eosin for 2 min. Brightfield imaging was performed on an Axio Z1 slide scanner (Zeiss). Based on the shorter (539–683 bp) cDNA libraries generated from the human cortical kidney tissue sections, we reduced the fragmentation reaction and the SPRI bead ratio from the manufacturer's recommendation. To further remove smaller library insert sizes, we gel extracted the library preparations for patients A, B, and C, followed by DNA clean-up according to the Monarch PCR and DNA clean-up kit (New England BioLabs). All libraries were loaded at 1.8 pM. Libraries from patients A, B, and C, and mice kidneys were sequenced using a High output reagent kit (Illumina). Library from patient D was sequenced using a Mid output reagent kit (Illumina) on a NextSeq500 (Illumina) instrument. Sequencing was performed using the following

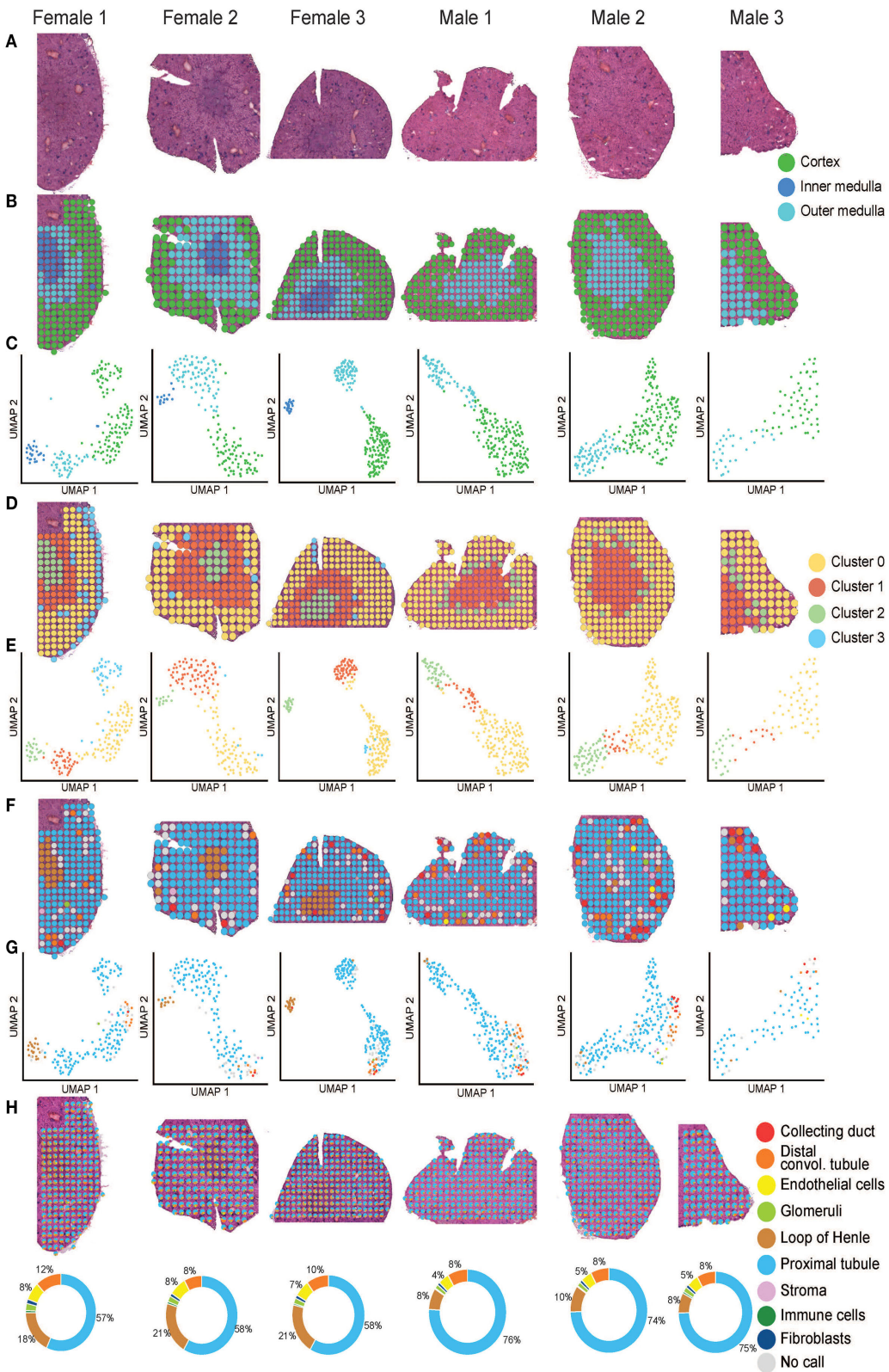

FIGURE 2 | Mouse ST-seq consensus labels. **(A)** H&E images of the mouse kidney tissues from three females and three males. **(B, C)** The functional cortical and medullary regions, which were annotated within the mouse ST-seq datasets by a Consultant Pathologist were mapped to the H&E tissue sections and presented in the UMAP. **(D, E)** The spatial organization of the KNN clusters was mapped to the H&E tissue images and presented in a UMAP. **(F,G)** The spatial organization of the consensus-based label transfer results was mapped to the H&E tissue images and presented in a UMAP, respectively. **(H)** The spatial organization of the deconvoluted functional structures was mapped to the H&E tissue images and presented as simple pie charts to demonstrate the proportions.

TABLE 1 | Patient cohort characteristics.

Patient ID	A	B	C	D
Age (years)/ gender (M/F)	51/F	54/M	53/F	56/M
eGFR (mL/min/1.73m^2)	>90	88	89	86
Serum creatinine (mmol/L)	50	86	68	86
Pathology	ccRCC	ccRCC	ccRCC	ccRCC
Metastasis	neg	neg	neg	neg
Co-morbidities				
Hypertension	neg	neg	neg	neg
Smoker	neg	neg	neg	yes
Coronary artery disease	neg	neg	neg	neg
Peripheral vascular disease	neg	neg	neg	neg
Diabetes mellitus	neg	neg	neg	neg
Hepatitis B and C	neg	neg	neg	neg

Key, ccRCC is clear cell renal cell carcinoma.

protocol: Read1–28bp, Index1–10bp, Index2–10bp, Read2–120bp.

ST-Seq Data Processing and Mapping

Illumina generated ST-seq libraries were first converted from raw base call (BCL) files to FASTQ files using bcl2fastq/2.17. Complex ST-seq libraries were retained and the FASTQ reads were trimmed of poly-A sequences on the 3' end and TSO sequences on the 5' end using cutadapt/1.8.3 (35). The cleaned FASTQ files were then mapped by Space Ranger V1.0 (10x Genomics) to the mouse reference genome and gene annotations (GRCm38–mm10) or human reference genome and gene annotations (GRCh38–3.0.0). The captured genes were mapped to the spatial coordinates across the H&E image obtained during the library preparation based on the detection of the tissue area and the alignment to fiducial markings. The multiplexed mouse ST-seq datasets were extracted to individual tissue sections using Loupe Browser (v4.0, 10x Genomics, United States).

We collectively detected more than 22,000 genes (GRCm38 – mm 10) across 1,160 ST-spots within the mouse ST-seq datasets. The median number of genes per spot ranged from 3,310 to 5,994 while median UMIs captured per spot spanned 10,491–31,145 (**Supplementary Figure 2A**). Within the human ST-seq datasets, we collectively detected over 23,000 genes (GRCh38-3.0.0) across 4,918 ST-spots. The median number of genes per spot ranged from 674 to 1,519, while the median unique molecular identifiers (UMIs) captured per spot spanned from 1,139 to 3,037 (**Supplementary Figure 3A**).

Spatial Analysis Using a Seurat Analytical Pipeline

Both mouse and human ST-seq datasets were analyzed using Seurat v4 (36–39). Preliminary quality control steps involved the filtration of ST-spots containing more than 50% mitochondrial genes (mtRNA) or 50% ribosomal genes (rbRNA). No ST-spots reached this rbRNA threshold. In the mouse ST-seq datasets, the level of mtRNA expression was consistently below 20% (**Supplementary Figure 2B**). However, high levels (median ∼ 12–28% total reads) of mtRNA expression were observed in the human ST-seq datasets (**Supplementary Figure 3B**). Thus, we used a threshold to filter only those ST-spots where mtRNA represented less than 50% of total reads for the human ST-seq datasets. Visual inspection of the mtRNA distribution in human kidney tissue sections with filtering (**Supplementary Figures 3C,D**) and the mouse kidney tissue sections with no filtering (**Supplementary Figure 2C**) showed a similar mtRNA expression pattern.

The top 2,000 most variable genes across ST-spots were detected by Seurat and were normalized using Scran before running principal component analysis (40, 41). Uniform manifold approximation and projection (UMAP) dimensionality reduction and clustering were performed using the top 50 principal components (42). Clustering was tested using a range of resolution values from 0.1 to 1.6, and the highest average stable resolution value was selected for each sample using the SC3 stability measure from Clustree (43). The generated clustering results were visualized in both two-dimensional UMAP space and spatial context mapped over the H&E images.

We performed label transfer in two sequential steps using a collection of publicly available snRNA-seq and/or scRNA-seq kidney datasets to predict cell types (**Supplementary Tables 1, 2**). This label transfer method projects existing reference datasets and new datasets with unknown cell types (query) into a shared low-dimensional space. The equivalent cell types (or anchor cell types) are arranged in the same neighborhood thus, allowing for inference of cell types in the new query datasets from the reference datasets. For each query cell type, a confidence score (scaled 0 to 1) was calculated based on the shared neighbor information with the reference cell type. First, label transfer annotation from mouse scRNA-seq and human snRNA-seq reference datasets was used to determine high-confidence ST-spot annotations. In the second round, mouse and human scRNA-seq reference datasets were used to label the remaining unlabeled ST-spots (**Supplementary Figures 4**, **5**). In both rounds, the transfer of cell-type annotations from the reference to a query ST-spot was made if the confidence score for the top match was >0.6.

Differential Gene Expression Analysis Within the Cortical Regions Between Species

We focused the differential gene expression analysis on the 708 cortical kidney ST-spots in the mouse ST-seq datasets. Raw gene expression counts were first aggregated by tissue samples to remove potential technical variation between intra-sample ST-spots and to account for species as two conditions and samples as biological replicates (44). The aggregation was performed using aggregateAcrossCells() function in Scater package and then normalized by library size, using sample-specific normalization factors calculated by the function calcNormFactors() in edgeR package (45, 46). Each tissue sample was treated as pseudo-bulk data to fit in a gene-wise linear model glmQLFit(), which estimates quasi-likelihood dispersions across species (conditions)

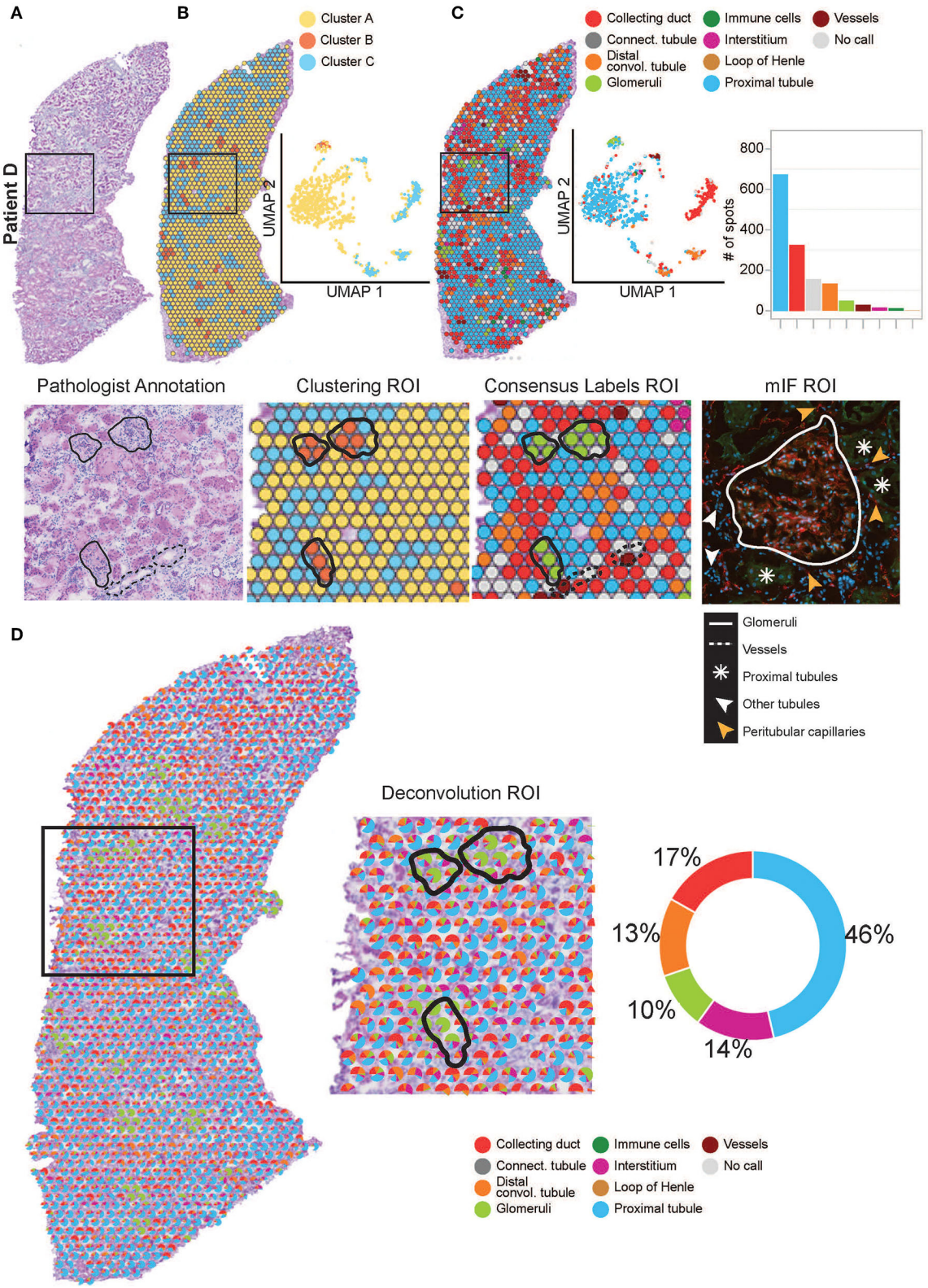

FIGURE 3 | Annotation of functional structures within patient D. **(A)** H&E image and a zoomed-in region of interest (ROI) of the pathologist's annotation of glomeruli and large vasculature. **(B)** The spatial organization of the KNN clusters was mapped to the H&E tissue images, presented in a UMAP and a zoomed-in ROI of clustering. **(C)** The spatial organization of the consensus-based label transfer results was mapped to the H&E tissue images, in a UMAP, a simple bar chart, and a

(Continued)

FIGURE 3 | zoomed-in ROI of consensus-based label transfer. A zoomed-in ROI stained with mIF (red = anti-CD31 for endothelial cells, green = anti-AQP1 for proximal tubule cells, and blue = DAPI for nuclei) demonstrates the abutting nature of functional structures within the cortical kidney tissue. **(D)** Further deconvolution demonstrates the distribution and proportions of functional structures within the cortical kidney tissue which are mapped to the H&E image, presented as a simple pie chart and a zoomed-in ROI. For the annotation of functional structures within patients A, B, and C cortical kidney tissue, ***see*** **Supplementary Figure 1**.

and samples (biological replicates). We then implemented empirical Bayes quasi-likelihood F-tests in the glmQLFTest() function to identify differentially expressed genes (all genes with an FDR < 0.05 and no log-fold change cut-off).

Deconvolution at the Functional Structure and Cell-Type Level

Deconvolution compares the expression profile from thousands of genes detected in each ST-spot to the expression patterns of cell type–specific marker genes within the reference datasets, to predict the proportion of different functional structures present in each ST-spot. We identified the proportion of specific cell types within each ST-spot using robust cell-type decomposition (RCTD)—a method that accounts for technical variation between different technologies, (47). In both mouse and human ST-seq datasets, we completed deconvolution to the functional structure level. In the human ST-seq datasets, we selected the ST-spots that were deconvoluted at the functional level as glomerular, proximal tubular, and peritubular capillaries for further deconvolution to cell-type level to perform cell-cell interaction (CCI) analysis.

StLearn Cell-Cell Interaction Analysis Within the Human ST-Seq Datasets

Cell-cell interaction analysis was performed using stLea "rn to predict interactions between spots or within each spot (48). "Between-spot" mode tests for significantly enriched CCI scores between any given ST-spot and its adjacent neighbors within the tissue, while "within-spot" mode tests for significantly enriched CCI scores within each ST-spot itself as multiple cells could be present within the each ST-spot. Briefly, there are four main steps in the CCI analysis. Step 1: CCI identifies cell-type diversity across the tissue. Step 2: CCI identifies L–R co-expression (CCI–LR) between or within spots for every ST-spot underlying the tissue. We used connectomeDB for the human ST-seq datasets (49). Step 3: The cell-type diversity score CCI–HET spot and CCI–LR spot score are standardized to unit variance and multiplied to form composite CCI scores that account for both cell-type diversity and the level of local co-expression values for each L–R pair. A high CCI score for an L–R pair indicates tissue areas that are most likely to harbor active CCI of the pair. Step 4: A negative binomial model is fitted to a null distribution of CCI scores calculated for thousands of random pairings of non-interacting protein–protein pairs. The best fit model is then used to statistically test for significance of discovering highly interacting spots, by calculating the probability of observing a CCI score for a given L–R pair given the null distribution.

Multiplex Immunofluorescence Staining

Consecutive deeper 10 μm cryosections from the human cortical kidney tissues ($n = 4$) used for ST-seq were placed onto room temperature SuperFrost Ultra Plus slides (Thermo Scientific, United States). The tissue sections were then adhered to the slides by drying for 1 min at 37°C and fixed with pre-chilled 100% methanol at−20°C for 30 min. Non-Specific binding was blocked with 10% donkey serum (Merck–Millipore, Burlington, MA, United States) for 15 min. Sections were incubated in a primary antibody mix comprising anti-endothelial cells (monoclonal mouse anti-human CD31; Clone JC70A; Dako Omnis) and anti-Aquaporin-1 (polyclonal rabbit anti-human AQP1 (H-55); SC-20810; Santa Cruz Biotechnology) for 20 min. Fluorescent labeling was obtained with AlexaFluor-conjugated secondary antibodies [donkey anti-mouse AlexaFluor PLUS 555 and donkey anti-rabbit AlexaFluor PLUS 488 (Invitrogen)] and DAPI (Sigma) incubation for 15 mi. Slides were coverslipped with a fluorescence mounting medium (Agilent Technologies, Santa Clara, CA, United States). Imaging was performed on an Axio Z1 slide scanner (Zeiss) at 20x objective with Cyanine 3 (567 nm), FITC (475 nm), and DAPI (385 nm) fluorescent channels. Image acquisition and analysis were performed within ZEN software (ZEN 2.6 lite; Carl Zeiss). Annotation of specific functional structures seen in the H&E image from the library preparation slide was compared against the deeper consecutive multiplexed immunofluorescence image of the human cortical kidney tissue sections.

RESULTS

Annotation of Cortical and Medullary Regions in Mouse ST-Seq Datasets

We used the pathologist's annotation of the functional mouse kidney regions (**Figures 2B,C**) to explore and predict functional nephron regions within the generated ST-seq dataset (38). Louvain clustering based on the K-nearest neighbor (KNN) of the ST-spots identified two to three distinct clusters in each sample (50). ST-spot clusters were then mapped to the H&E tissue images to examine the spatial distribution of the resulting clusters.

In female mice, three distinct clusters were mapped to the cortex and outer medulla, composed of the outer and inner stripe layers (**Figures 2D,E**). Within the cortex cluster, an additional small sub-cluster (Cluster 3 blue) was mapped to the edges of the tissue sections. This sub-cluster contained hemoglobin genes in the top 10 significant marker genes, implicating the presence of accumulated blood (**Supplementary Table 3**). Both spatial mapping and UMAP demonstrated colocalization of this sub-cluster with the cortex cluster (Cluster 0 yellow). Thus, we have classified them together as a cortex for further analysis.

In male mice, we noted two distinct clusters that mapped to the cortical and the outer stripe of the outer medulla (**Figures 2D,E**). Within the cortex cluster, an additional small sub-cluster (Cluster 2 green) was mapped to the edges of the

outer stripe of the outer medulla. We observed that the top 10 significant genes within this sub-cluster contained genes that mapped to the female mice's outer stripe of the outer medulla (**Supplementary Table 3**). Both spatial mapping and UMAP demonstrated colocalization of this sub-cluster with the outer stripe of the outer medulla cluster (Cluster 1 orange). Therefore, we have classified them together as outer medulla for further analysis.

We observed that clusters mapped to the cortex contained marker genes for glomeruli (*Nphs2* and *Gpx3*; p_{adj} <0.05). Clusters mapped to the outer stripe of the outer medulla contained marker genes for proximal tubules (*Acy3* and *Aqp1*; p_{adj} <0.05). Clusters mapped to the inner stripe of the outer medulla contained marker genes for the loop of Henle (*Egf* and *Umod*; p_{adj} <0.05) (51–53). Subsequent visualization of the clusters mapped to the H&E tissue images confirmed the presence of these dominant functional nephron structures in the mouse kidneys.

After implementing an unbiased clustering approach, we performed label transfer at the functional structure level to determine the cellular identities of all ST-spots (54, 55). The consensus annotations were then mapped to the H&E tissue images (**Figures 2F,G**). This consensus-based label transfer annotated the majority of the ST-spots in the cortex and the outer stripe of the outer medulla as proximal tubules (*Lrp2* and *Slc22a7*; p_{adj} <0.05) and those in the inner stripe of the outer medulla as the loop of Henle (*Slc12a1* and *Umod*; p_{adj} <0.05; **Supplementary Table 4**).

We performed deconvolution at the functional structure level in the mouse ST-seq datasets. This demonstrated that all the mouse ST-spots contained multiple functional structures (**Figure 2H**). Deconvolution within the ST-spots overlying the cortical regions detected a higher proportion of proximal tubule signatures and a lower proportion of glomerular signatures. Re-examination of the clusters mapped to the cortical region confirmed the expression of proximal tubule marker genes (51, 52).

Annotation of Functional Structures Within the Human ST-Seq Datasets

We performed similar identification of functional structures, their transcriptional signatures, and spatial locations within the human cortical ST-seq datasets using Seurat clustering and label transfer (38). We initially defined the spatial organization of the human cortical kidney by performing Louvain clustering based on KNN to identify ST-spots with distinct transcriptome profiles. We mapped these cluster identities to the H&E tissue images (**Figure 3B**; **Supplementary Figure 1B**). For patient A, two clusters were mapped to the glomerular and mixed cortical renal parenchyma ST-spots. For patients B–D, three clusters were mapped to the glomerular, tubules, and mixed cortical renal parenchyma ST-spots. We observed that clusters mapping to the glomerular ST-spots contained marker genes for podocytes (*PODXL* and *NPHS2*; p_{adj} <0.05; **Supplementary Table 5**) (51, 52). Clusters mapping to the tubules contained marker genes for proximal tubules (*LRP2* and *GPX3*; p_{adj} <0.05) (51, 52). Concurrent assessment of the mapped clusters to the H&E tissue images revealed that glomeruli were the dominant functional nephron structures overlying the ST-spots.

We performed label transfer at functional structure level to determine the cellular identities of all ST-spots (**Figure 3C**; **Supplementary Figure 1C**) (6, 12). We found that the consensus-based label transfer resulted in the identification of collecting ducts (*AQP2* and *ATP6V0D2*; p_{adj} <0.05), distal convoluted tubules (*SLC12A3* and *DEFB1*; p_{adj} <0.05), glomeruli (*PODXL* and *NPHS2*; p_{adj} <0.05), immune cells (*IL7R* and *CD86*; p_{adj} <0.05), interstitium (*COL1A2* and *COL3A1*; p_{adj} <0.05), loop of Henle (*UMOD* and *SLC12A1*; p_{adj} <0.05), proximal tubules (*SLC22A8* and *ALDOB*; p_{adj} <0.05) and vessels (*TAGLN, MYH11,* and *ELN*; p_{adj} <0.05; **Supplementary Table 6**).

The consensus-based label transfer identified the primary functional structure within the cortical human kidney tissue as proximal tubules. We independently validated this result by comparing the cortical functional structures annotated by label transfer to the pathologist's annotation of the H&E images and multiplexed immunofluorescence (mIF) staining (**Figure 3**, **Supplementary Figure 1**). The label transfer, pathologist's H&E annotation, and mIF staining collectively identified glomeruli, vessels, and proximal tubules in the normal human cortical kidney tissues.

Differential Expression Within Cortical Kidney Regions Between Species

We compared gene signatures between human and mouse cortical kidney regions by identifying differentially expressed (DE) genes between the ST-seq datasets in humans and mice. Considering that the human ST-seq datasets comprised only cortical kidney, we used the pathologist's annotation to select the cortical kidney regions within the mouse ST-seq datasets. We identified 11,997 orthologous genes among the cortical kidney genes in the mouse ST-seq datasets (**Supplementary Figure 6**). After integration and removal of lowly expressed genes, 10,830 genes shared across the cortical kidney regions were used to test for DE genes and to assess functional and biological processes that vary between the species (**Supplementary Table 7**). In brief, we found 7,370 DE genes (FDR <0.05; no log-fold change cut-off) between human and mouse cortical kidney regions (**Figure 4A**). Examination of the top 20 DE genes showed high consistency across biological replicates and their distinct expression profiles between humans and mice (**Figure 4B**). The cortical location of the top 20 DE genes was further validated by their expression within cortical kidney cells in the Kidney Cell Explorer scRNA-seq database (https://cello.shinyapps.io/kidneycellexplorer/) and the Kidney Interactive Transcriptomics sn/scRNA-seq database (http://humphreyslab.com/SingleCell/, **Supplementary Table 8**) (56–58). We tested functional enrichment among all the significant DE genes, within Biological Processes Gene Ontology (GO:BP) terms (**Figure 4C**). We examined the top 20 GO:BP terms with the most significant *p*-values. In human cortical tissues, the most statistically significant GO:BP terms were associated with structural maintenance (**Supplementary Table 9**). In contrast,

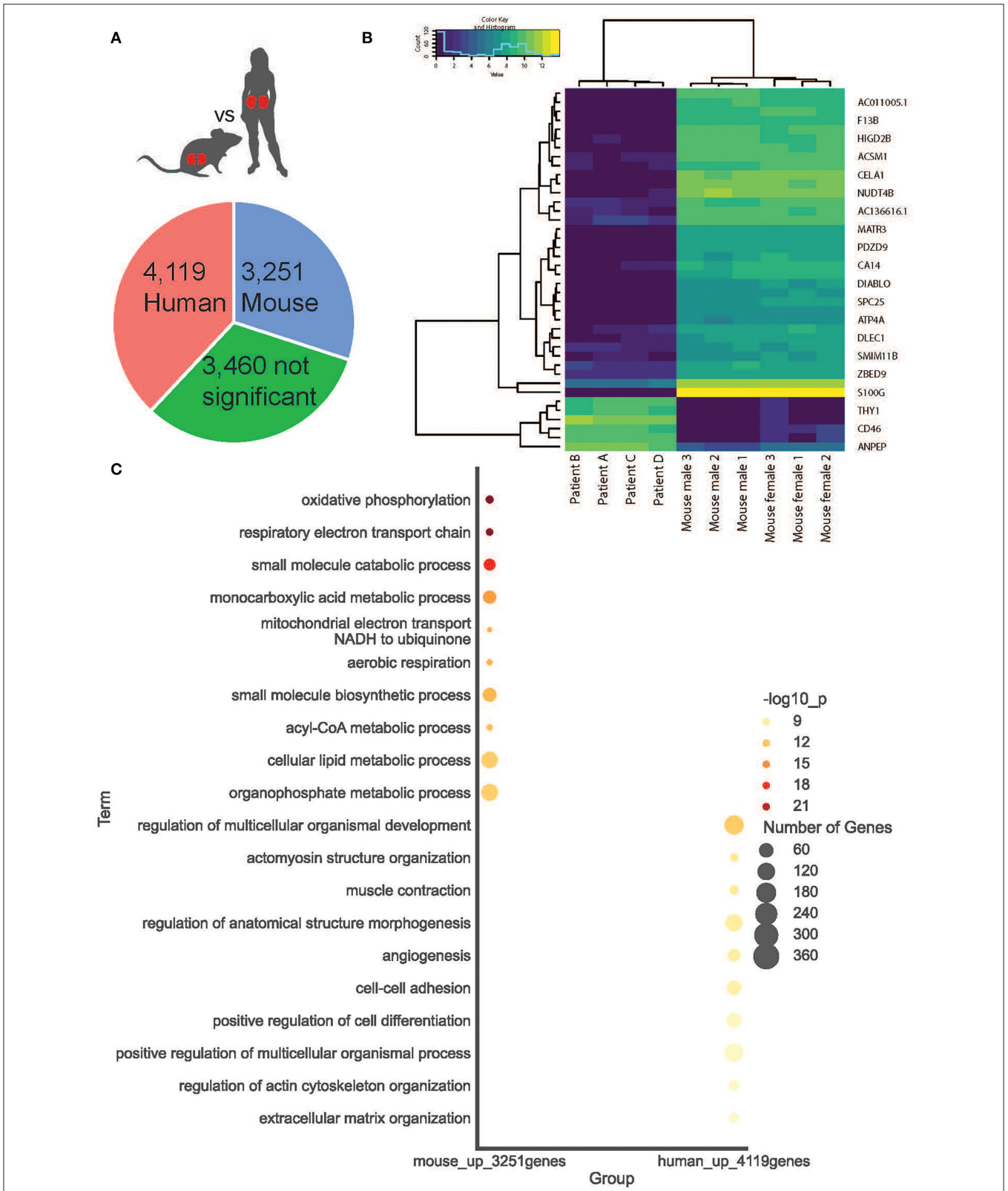

FIGURE 4 | Cortical kidney genes differentially expressed between species. **(A)** A simple pie chart demonstrates the proportion of statistically significant DE genes identified within each species. **(B)** The top 20 DE genes between species are presented as a heat map. **(C)** Within mice and humans, the top 10 statistically significant Gene Ontology Biological Processes.

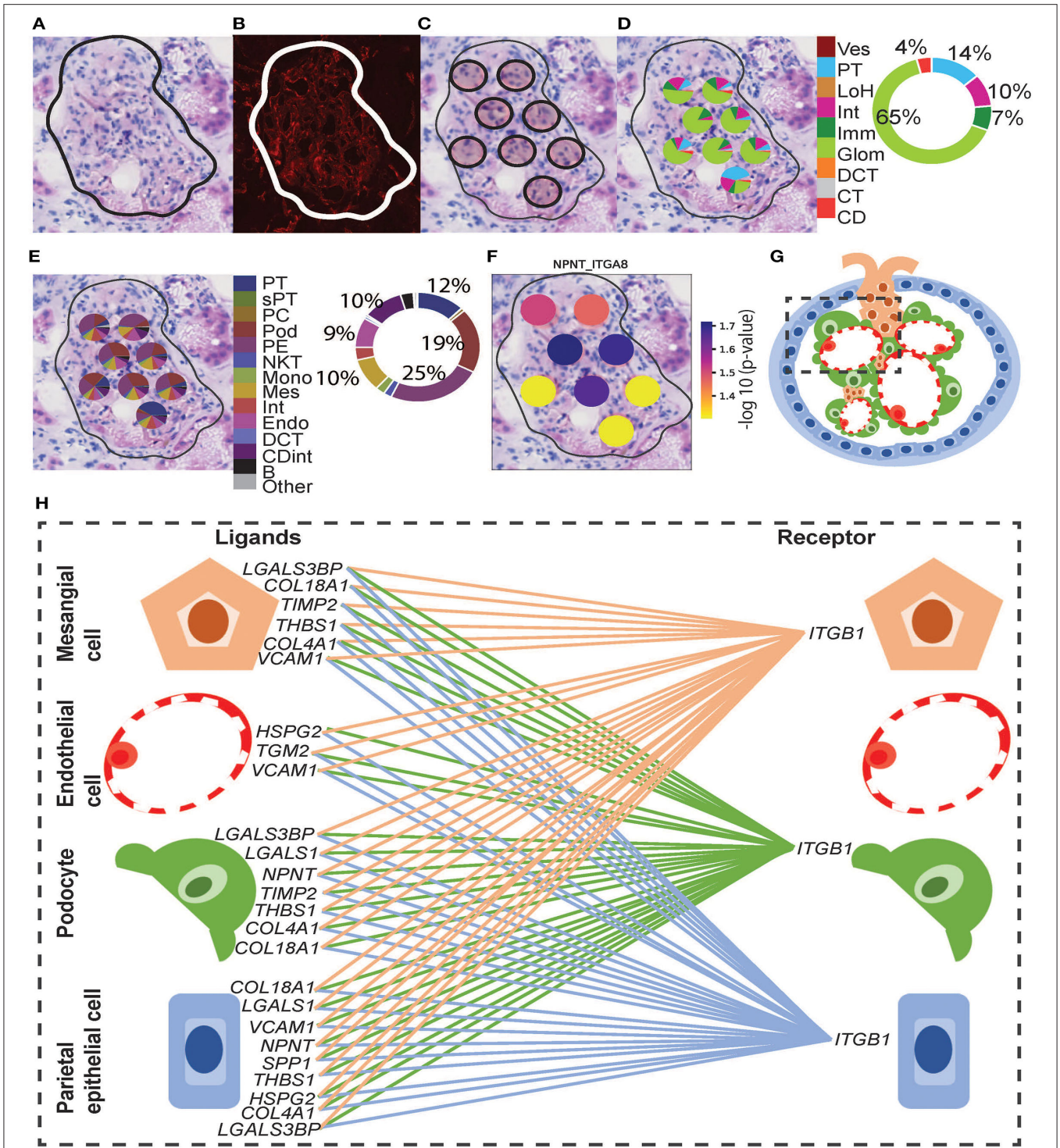

FIGURE 5 | Integrative analysis of glomerular morphology, deconvolution, and cellular interactions in patient D. To confirm the morphology of glomerular functional structures, we investigated H&E and mIF images within a selected glomerulus. **(A)** Zoomed-in H&E image of the selected glomerulus annotated by the pathologist. **(B)** Anti-CD31 (red) immunofluorescence staining confirms the presence of endothelial cells and validates the pathologist's glomerular annotation. Next, we visualized the ST-spots underlying the glomerulus. **(C)** The positions of the eight underlying ST-spots were mapped within the selected glomerulus. To perform deconvolution, we selected the ST-spots identified by label transfer as glomeruli. **(D)** Deconvolution at the functional structure level for the selected glomerulus was mapped to the H&E image. The pie chart provides a summary of functional structures underlying all glomerular ST-spots in the entire tissue section for patient D. (**E)** Deconvolution at a cell-type level for the selected glomerulus was mapped to the H&E image. The pie chart provides a summary of the cell types underlying all glomerular ST-spots in the entire tissue section for patient D. Finally, we investigated our ST-seq datasets for cellular interactions in glomerular ST-spots. **(F)** The spatial expression of the

(Continued)

FIGURE 5 | *NPNT-ITGA8* L–R gene pair for the selected glomerulus was mapped to the H&E image. **(G)** A diagrammatic presentation of parietal epithelial, podocytes, endothelial, and mesangial cells that form the functional glomerular structures in mammalian cortical kidney regions. **(H)** The cellular interaction involved in extracellular matrix maintenance within the glomerulus for integrin receptor *ITGB1* was mapped between the glomerular cell types.

the most statistically significant GO:BP terms were associated with energy production and metabolic processes in mouse cortical regions (**Supplementary Table 10**).

Cell-Cell Interaction Within and Between ST-Spots Containing Glomeruli in Human ST-Seq Datasets

Functional structure level deconvolution results were used to select the ST-spots that contained glomerular structures (**Figure 5**). In these selected glomerular ST-spots, we further deconvoluted to cell-type level and found that podocytes, mesangial, endothelial, and parietal epithelial cells were the major cell types. We identified co-expression of 330 L–R gene pairs within and between glomerular ST-spots (**Supplementary Table 11**). We selected the top 40 L–R gene pairs identified as the most statistically significant (p_{adj} <0.05) within and between glomerular ST-spots (**Table 2**) (57–61). We identified 23 L–R gene pairs involving integrin receptors *ITGA3, ITGAV, ITGA8, ITGB1, ITGB5,* and laminin receptor *RPSA* within the extracellular matrix maintenance group. We identified five L–R gene pairs with co-expression of vascular endothelial growth factor *VEGF-A, KDR,* and *FLT1* within the angiogenic regulation group. Additional novel L–R gene pairs *FGF-NRP1*, *THBS1-SDC4,* and *ANXA2-ROBO4* are non-*VEGF* L–R pairs, identified within the angiogenic regulation group and previously shown to regulate and maintain the microvasculature within glomeruli (62–65). We identified six L–R gene pairs with co-expression of Human Leukocyte Antigens (*HLA-A, HLA-B, and HLA-F*) ligands, Amyloid beta Precursor Protein (*APP*), Macrophage migration Inhibitory Factor (*MIF*), and Megalin (*LRP2*) within the immune and endocytic activity group. Additional novel L–R gene pairs *GRN-SORT1* and *TIMP1-CD63* identified within the immune and endocytic activity group are known L–R pairs within the nervous system but novel within the glomerular structure (66–68).

CCI Within and Between ST-Spots Containing Proximal Tubules–Peritubular Capillaries in Human ST-Seq Datasets

We extended the CCI investigation to ST-spots containing PT–PC to investigate potential cross-talk within and between these cell types. To perform this analysis, we selected human ST-spots that after deconvolution was annotated to contain proximal tubule cells plus endothelial cells, but not annotated as glomerular endothelial cell types (**Figure 6**). Again, we tested the >2,000 L–R pairs curated in the connectomeDB2020 database, using stLearn CCI analysis with both within and between spots (48). We identified significant co-expression of 170 L–R gene pairs in PT–PC ST-spots (**Supplementary Table 11**). We selected the top 20 L–R gene pairs identified as statistically significant (p_{adj} <0.05) within and between PT–PC ST-spots (**Table 3**) (57–61). We identified six L–R gene pairs with co-expression of *LRP2, APP*, Low-Density Lipoprotein Receptor (*LDLR*), and TIMP Metallopeptidase Inhibitor 1 (*TIMP1*) within the transportation and signaling group. We identified eight L—R gene pairs with co-expression of Integrin (*ITGB1, ITGB5,* and *ITGAV*), CD44 molecule, and Epithelial Cell Adhesion Molecule (*EPCAM*) within the adhesion group. We identified four L–R gene pairs with the co-expression of *HLA* and *MIF* within the immune modulation group. Finally, within the angiogenic regulation group, we identified two L–R gene pairs with the co-expression of Thrombospondin 1 (*THBS1*) and Syndecan (*SDC1* and *SDC4*).

DISCUSSION

Available transcriptome profiles of normal nephrons have utilized bulk and/or scRNA-seq/snRNA-seq methods requiring the manipulation of tissue, including tissue homogenization or cell dissociation, resulting in the loss of crucial spatial information. In this study, we performed ST-seq to resolve gene expression within intact normal tissues of six mice and four human kidneys. We captured more genes and reads in the mouse kidneys (median genes 3,310–5,994 and median reads 10,491–31,145) compared to human kidneys (median genes 674–1,519 and median reads 1,139–3,037). Within the captured ST-seq datasets, we defined the spatial location of specific nephron segments, compared DE genes between species, and spatially mapped the putative cellular communication occurring in glomerular and PT–PC regions in the human ST-seq datasets.

In the mouse ST-seq datasets, we defined the functional regions with KNN clustering to the cortex and the outer and inner stripes of the outer medulla regions. We confirmed the cluster identities by marker gene expression and found a direct correlation with the pathologist's annotation. However, label transfer–based annotation of the functional nephron regions using publicly available mouse scRNA-seq datasets identified only two distinct clusters (54, 55). The outer stripe of the outer medulla was indistinguishable from the cortical layer in female and male mice kidneys. We attributed this curious result to the large ST-spot size and the small size and dense assembly of cortical functional structures, such as the proximal tubules, in mouse kidneys. To address the latter, we performed deconvolution with the mouse ST-seq datasets and found multiple functional structures within all 100 μm ST-spots. Furthermore, deconvolution within both the cortex and the outer stripe of the outer medulla identified a higher proportion of proximal tubule signatures—a stochastic variation noted by other transcriptome studies (51, 178, 179). Therefore, we conclude that the discrepancy between cluster and pathologist annotation against the label transfer annotations occurred due to

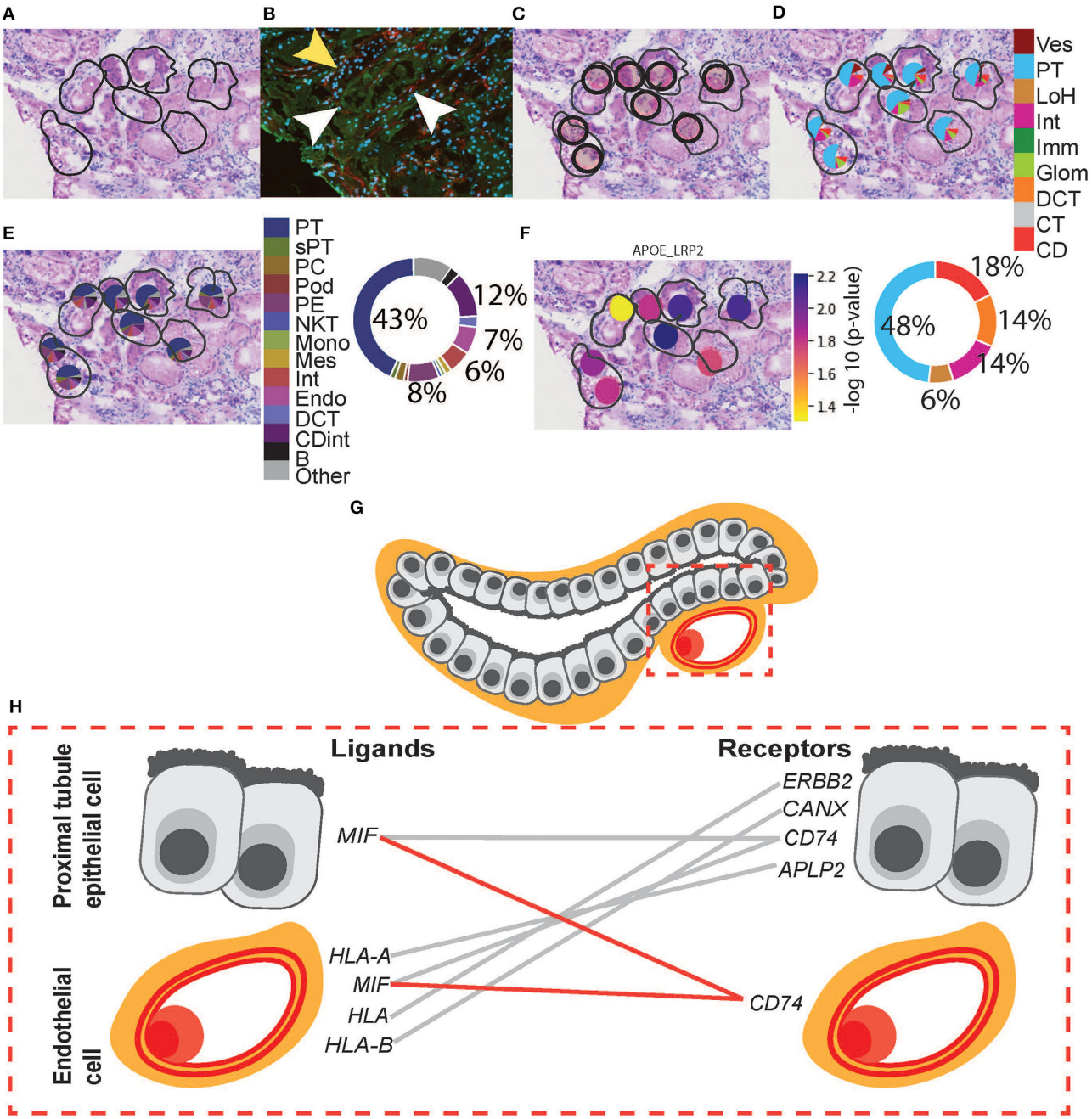

FIGURE 6 | Integrative analysis of PT–PC morphology, deconvolution, and cellular interactions in patient D. To confirm the morphology of PT, we investigated H&E and mIF images within an ROI. **(A)** Zoomed-in H&E image of PT was annotated by the pathologist. **(B)** mIF staining with anti-AQP1 (green) demonstrates proximal tubules, anti-CD31 (red; white arrowheads) demonstrates peritubular capillaries, and DAPI (blue) demonstrates nuclei. The mIF staining confirms the presence of PT and PC structures and validates the pathologist's annotation. (Note: yellow arrowhead denotes tubular patterned DAPI staining with an absence of anti-AQP1 indicating the presence of non-PT structures). **(C)** The positions of eight underlying ST-spots were mapped within the selected ROI. To perform deconvolution, we selected the ST-spots identified by label transfer as PT. **(D)** Deconvolution at the functional structure level for the selected eight PT ST-spots was mapped to the H&E image. The pie chart provides a summary of functional structures underlying all PT ST-spots in the entire tissue section for patient D. **(E)** Deconvolution at the cell-type level for the selected eight PT ST-spots was mapped to the H&E image. The pie chart provides a summary of the cell types underlying all PT ST-spots in the entire tissue section for patient D. Finally, we investigated our ST-seq datasets for cellular interactions in PT–PC ST-spots. **(F)** The spatial expression of the *APOE-LRP2* L–R gene pair for the selected PT was mapped to the H&E image. **(G)** A diagrammatic presentation of PT epithelial cells and PC endothelial cells within mammalian cortical kidney regions. **(H)** The cellular interactions involved in immune modulation within PT–PC cells were mapped. Functional structure level key: Ves—vessels, PT—proximal tubules, LoH—loop of Henle, Int—interstitium, Imm—immune cells, Glom—glomeruli, DCT—distal convoluted tubule, CT—connecting tubule, and CD—collecting duct. Cell-type level key: PT—proximal tubule cell, sPT—proximal straight tubule cell, PC—principal cell, Pod—podocytes, PE—parietal epithelial cell, NKT—natural killer T-cell, Mono—monocytes, Mes—mesangial cell, Int—interstitium, Endo—endothelial cell, DCT —distal convoluted tubule cell, CDint - collecting duct intercalated cell and B—B cell.

TABLE 2 | CCI identified within and between glomerular ST-spots.

	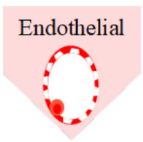		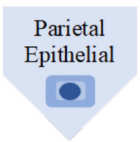	
Mesangial	Endothelial	Podocyte	Parietal Epithelial	
Extracellular matrix maintenance				
CALR- ITGA3	*CALR- ITGA3*	*CALR- ITGA3*	*CALR- ITGA3*	(69–71)
TIMP2-ITGA3	*TIMP2-ITGA3*	*TIMP2-ITGA3*	*TIMP2-ITGA3*	(72–74)
THBS1-ITGA3	*THBS1-ITGA3*	*THBS1-ITGA3*	*THBS1-ITGA3*	(75–77)
SPP1-ITGAV	*SPP1-ITGAV*	*SPP1-ITGAV*	*SPP1-ITGAV*	(78)
CALR- ITGAV	*CALR- ITGAV*	*CALR- ITGAV*	*CALR- ITGAV*	(71, 79)
CX3CL1- ITGAV	*CX3CL1ITGAV*	*CX3CL1- ITGAV*	*CX3CL1- ITGAV*	(80–82)
COL4A1-ITGAV	*COL4A1-ITGAV*	*COL4A1- ITGAV*	*COL4A1- ITGAV*	(83, 84)
COL4A3- ITGAV	*COL4A3- ITGAV*	*COL4A3- ITGAV*	*COL4A3- ITGAV*	(85, 86)
NPNT- ITGA8	*NPNT- ITGA8*	*NPNT- ITGA8*	*NPNT- ITGA8*	(79, 87–90)
SPP1-ITGB1	*SPP1-ITGB1*	*SPP1-ITGB1*	*SPP1-ITGB1*	(79, 91–95)
TIMP2- ITGB1	*TIMP2- ITGB1*	*TIMP2- ITGB1*	*TIMP2- ITGB1*	(73, 74)
NPNT- ITGB1	*NPNT- ITGB1*	*NPNT- ITGB1*	*NPNT- ITGB1*	(79, 90, 96, 97)
COL18A1- ITGB1	*COL18A1- ITGB1*	*COL18A1- ITGB1*	*COL18A1- ITGB1*	(98–100)
LGALS1- ITGB1	*LGALS1- ITGB1*	*LGALS1- ITGB1*	*LGALS1- ITGB1*	(101, 102)
THBS1- ITGB1	*THBS1- ITGB1*	*THBS1- ITGB1*	*THBS1- ITGB1*	(103, 104)
LGALS3BP- ITGB1	*LGALS3BP- ITGB1*	*LGALS3BP-ITGB1*	*LGALS3BP- ITGB1*	(102, 105)
COL4A1-ITGB1	*COL4A1-ITGB1*	*COL4A1-ITGB1*	*COL4A1-ITGB1*	(86, 106)
HSPG2-ITGB1	*HSPG2-ITGB1*	*HSPG2-ITGB1*	*HSPG2-ITGB1*	(107–109)
TGM2- ITGB1	*TGM2- ITGB1*	*TGM2- ITGB1*	*TGM2- ITGB1*	(110, 111)
VCAM1- ITGB1	*VCAM1- ITGB1*	*VCAM1- ITGB1*	*VCAM1- ITGB1*	(112–114)
SPP1- ITGB5	*SPP1- ITGB5*	*SPP1- ITGB5*	*SPP1- ITGB5*	(115, 116)
THY1- ITGAV	*THY1- ITGAV*	*THY1- ITGAV*	*THY1- ITGAV*	(117, 118)
LAMB2- RPSA	*LAMB2- RPSA*	*LAMB2- RPSA*	*LAMB2- RPSA*	(119, 120)
Angiogenic regulation				
TIMP3-KDR	*TIMP3-KDR*	*TIMP3-KDR*	*TIMP3-KDR*	(121–123)
VEGF-A-FLT1	*VEGF-A-FLT1*	*VEGF-A-FLT1*	*VEGF-A-FLT1*	(121, 124–126)
VEGF-A-NRP1	*VEGF-A-NRP1*	*VEGF-A-NRP1*	*VEGF-A-NRP1*	(121, 125, 127, 128)
VEGF-A-KDR	*VEGF-A-KDR*	*VEGF-A-KDR*	*VEGF-A-KDR*	(121, 125, 126, 129)
COL18A1-KDR	*COL18A1-KDR*	*COL18A1-KDR*	*COL18A1-KDR*	(121, 130)
FGF1-NRP1	*FGF1-NRP1*	*FGF1-NRP1*	*FGF1-NRP1*	(128)
THBS1-SDC4	*THBS1-SDC4*	*THBS1-SDC4*	*THBS1-SDC4*	(63, 64, 131)
ANXA2-ROBO4	*ANXA2-ROBO4*	*ANXA2-ROBO4*	*ANXA2-ROBO4*	(65, 132)
Immune and endocytic activity				
APP-CD74	*APP-CD74*	*APP-CD74*	*APP-CD74*	(133–137)
APP-NCSTN	*APP-NCSTN*	*APP-NCSTN*	*APP-NCSTN*	(136, 138, 139)
MIF-CD74	*MIF-CD74*	*MIF-CD74*	*MIF-CD74*	(140, 141)
HLA-A-APLP2	*HLA-A-APLP2*	*HLA-A-APLP2*	*HLA-A-APLP2*	(136, 142–144)
HLA-B-CANX	*HLA-B-CANX*	*HLA-B-CANX*	*HLA-B-CANX*	(144–146)
HLA-F-B2M	*HLA-F-B2M*	*HLA-F-B2M*	*HLA-F-B2M*	(144, 147)
GRN-SORT1	*GRN-SORT1*	*GRN-SORT1*	*GRN-SORT1*	(68, 148, 149)
TIMP1-CD63	*TIMP1-CD63*	*TIMP1-CD63*	*TIMP1-CD63*	(150–152)
APOE-LRP2	*APOE-LRP2*	*APOE-LRP2*	*APOE-LRP2*	(153–155)

Key, L-R presence indicated by back text and absence indicated by the gray text.
The literature-based locations of the top 40 glomerular L–R gene pairs were confirmed in sc/snRNA-seq datasets, as an expression within glomerular cell types. In particular the sc/snRNA-seq datasets within the Kidney Interactive Transcriptomics [Healthy Adult Kidney - Epithilia (57), Healthy Mouse Dataset (58), Human Diabetic Kidney (59), and Human Kidney snRNA/ATAC-seq (60), and The Human Nephrogenesis Atlas (Human week 14 scRNA-seq) (61) were utilized.

TABLE 3 | CCI identified within and between proximal tubule and endothelial ST-spots.

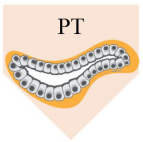	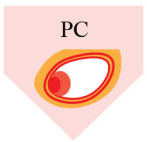	
Transportation and signaling		
APOE-LRP2	*APOE-LRP2*	(156)
APP-CD74	*APP-CD74*	(133)
ALB-LRP2	*ALB-LRP2*	(157)
APOE-LDLR	*APOE-LDLR*	(158)
SERPINE1-LRP2	*SERPINE1-LRP2*	(159)
TIMP1-CD63	*TIMP1-CD63*	(160, 161)
Adhesion		
THBS1-ITGB1	*THBS1-ITGB1*	(162, 163)
COL18A1-ITGB1	*COL18A1-ITGB1*	(130, 164, 165)
PLG-ITGB1	*PLG-ITGB1*	(166)
SPP1-ITGB5	*SPP1-ITGB5*	(167)
SPP1-ITGB1	*SPP1-ITGB1*	(94, 168)
SPP1-ITGAV	*SPP1-ITGAV*	(92, 169)
SPP1-CD44	*SPP1-CD44*	(170)
EPCAM- EPCAM	*EPCAM- EPCAM*	(171)
Immune modulation		
HLA-B-CANX	*HLA-B-CANX*	(146, 172)
HLA-A-APLP2	*HLA-A-APLP2*	(143, 173, 174)
MIF-CD74	*MIF-CD74*	(175)
HLA-ERBB2	*HLA-ERBB2*	(163)
Angiogenic regulation		
THBS1-SDC1	*THBS1-SDC1*	(64)
THBS1-SDC4	*THBS1-SDC4*	(64, 176, 177)

The literature based location of the top 20 PT-PC L–R gene pairs were confirmed in sc/snRNA-seq datasets, as an expression within proximal tubule (segments 1, 2, and 3), peritubular capillary, and endothelial cell types. In particular, the sc/snRNA-seq datasets within the Kidney Interactive Transcriptomics (Healthy Adult Kidney—Epithilia (57), Healthy Mouse Dataset (58), Human Diabetic Kidney (59) and Human Kidney snRNA/ATAC-seq (60), and The Human Nephrogenesis Atlas [Human week 14 scRNA-seq (61)] were utilized.

the dense assembly of functional structures in mouse kidneys, resulting in the capture of multiple structures in individual ST-spots.

In the human ST-seq datasets, we defined glomerular, collecting duct, and mixed cortical renal parenchyma ST-spots with KNN clustering. However, distinct functional nephron tubular segments were not apparent by clustering. We, therefore, performed further label transfer–based annotation of functional structures using published human kidney snRNA-seq and scRNA-seq datasets as references (6, 12). This resulted in the annotation of collecting ducts, distal convoluted tubules, glomeruli, immune cells, interstitium, the loop of Henle, proximal tubules, and vessels. The low immune infiltrate within the normal human cortical kidney tissue has been attributed to normal immune-surveillance/immune-regulatory functions (12, 51, 60, 179–189). We checked the cluster identities and label transfer annotations against marker gene expression, the pathologist's annotation, and mIF staining, demonstrating consistent agreement of the major functional nephron structures in normal human cortical kidney tissue.

We subsequently performed DE gene analysis between mouse and human cortical kidney regions. In this study, 7,370 DE genes ($p < 0.05$) were identified between mouse and human cortical kidney regions and were tested for functions associated with the GO:BP terms. The top 10 statistically significant GO:BP terms up-regulated within the mouse cortical regions compared to humans associated with energy production and metabolic processes. This higher metabolic rate is a known phenomenon in mouse tissue, however, the actual cause remains unknown (190, 191). We hypothesize that some of the interspecies variations between our normal mice and human kidneys may be due to differences in age and environment (192–198). The mice in our study were 8 weeks old corresponding to humans <20 years of age and the human samples were from patients in their fifth decade of life. Therefore, the changes to mitochondrial energy production and metabolic processes detected between species may be secondary to the large differences in relative age and environment.

In the human ST-seq datasets, we investigated CCI in glomerular and PT–PC ST-spots, using L–R gene co-expression. In the glomerular ST-spots, we identified co-expression of 300 L–R gene pairs but focused on the top 40 L–R gene pairs ($p_{adj} < 0.05$). Consistent with published sc/snRNA-seq datasets (57–60), these top 40 L–R pairs were associated with structural, vascular, and/or immune interactions within and between mesangial, endothelial, podocytes, and parietal epithelial cells. The glomeruli are unique functional filtration structures composed of tufts of vascular endothelial capillaries surrounded by mesangial, podocyte, and parietal epithelial cells (3, 199). The mesangial cells, podocytes, and endothelial cells secrete extracellular matrix (ECM) components to establish a glomerular basement membrane (GBM) and form the glomerular filtration barrier, which allows fluid and solutes to pass into the nephron (200). ECM components such as integrins facilitate important signaling interactions between the mesangial cells, podocytes, and endothelial cells that surround and maintain the GBM (121, 201). Integrins are a large family of transmembrane receptors which, upon ligand activation, control signal transduction, cell adhesion, proliferation, and ECM maintenance (91, 200, 202–204). Consistent with expectations, 22 out of the top 40 L–R gene pairs identified were involved with integrin receptors *ITGA3*, *ITGAV*, *ITGA8*, *ITGB1,* and *ITGB5*. Moreover, five L–R gene pairs were involved in the regulation of angiogenesis and glomerular filtration barrier maintenance *via* VEGF-mediated signaling.

In the PT–PC ST-spots, we identified co-expression of 170 L–R gene pairs but focused on the top 20 L–R gene pairs ($p_{adj} < 0.05$). Consistent with published sc/snRNA-seq datasets (57–60), these top 20 L–R pairs were associated with lipid and protein transportation and signaling, adhesion, and/or immune interactions within and between proximal tubule epithelial cells and peri-tubular capillary endothelial cells. Proximal tubules are primarily responsible for the reabsorption of amino acids,

glucose, solutes, and low–molecular weight proteins from the glomerular filtrate (205). Components reabsorbed from the filtrate are then taken up into the bloodstream *via* peritubular capillaries surrounding the proximal tubules. Consistent with expectations, six L–R gene pairs identified were involved in transportation and signaling facilitated by proximal tubule-specific endocytic receptors *LRP2* and *APP*. Eight L–R gene pairs identified were involved in cell adhesion primarily involving integrin-based interactions between proximal tubule cells aside from a predicted tubulo-vascular interaction involving *COL18A1-ITGB1*. Four L–R gene pairs identified were linked to immune modulation *via* the formation of the MHC class I loading complex *HLA* and *MIF*. Furthermore, two L–R gene pairs identified were linked to vascular maintenance *via SDC1* and *SDC4*. The identified top L–R gene pairs within and between glomerular and PT–PC ST-spots were validated by both localization and co-expression within the required cell types in published sc/snRNA-seq datasets (57–60). Additional identification of pathways established as fundamental to normal kidney function in published literature act as further validation of the specificity of the ST-seq approach for examining CCI within the glomerular and tubular compartments.

Our generated ST-seq datasets and analysis provide demonstration and confirmation of normal kidney tissue and physiological pathways. This is anticipated to assist with the future description and understanding of molecular signals and pathways in states of kidney disease, and thus support the development of therapeutics and diagnostic interventions for clinical translation.

DATA AVAILABILITY STATEMENT

The datasets presented in this study can be found in online repositories. The names of the repository/repositories and accession number(s) can be found below:
— The human and mouse kidney ST-seq datasets and codes are publicly available here: GitHub, https://github.com/BiomedicalMachineLearning/SpatialKidney.
— The raw data are publicly available here: ArrayExpress, https://www.ebi.ac.uk/arrayexpress, E-MTAB-11721.

ETHICS STATEMENT

The studies involving human participants were reviewed and approved by Royal Brisbane and Women's Hospital Human Research Ethics Committee (Reference Number 2002/011). The patients/participants provided their written informed consent to participate in this study. The animal study was reviewed and approved by University of Queensland Animal Ethics Committee (UQDI/452/16 and IMB123/18).

AUTHOR CONTRIBUTIONS

AR, AC, AK, HH, QN, and AM conceived and designed the study. AR, PL, SY, ST, JC, and SA carried out the experiments. AR, MN, AK, HH, and AM reviewed the patient data. DP, XT, LG, and QN performed the bioinformatics analyses. AR, AK, AS, and LF performed the histological examination of the kidney. AR, DP, XT, NM, LG, AK, HH, AC, QN, and AM drafted the article. All authors revised and approved the final version of the manuscript. All authors contributed to the article and approved the submitted version.

FUNDING

This study was supported by funding from Pathology Queensland-Study, Education and Research Committee, Royal Brisbane and Women's Hospital Foundation Project Grant 2019, Robert and Janelle Bird Postdoctoral Research Fellowship 2020, and the University of Queensland (UQ)-Genome Innovation Hub. AR is supported by an Australian Government Research Training Program (RTP) Scholarship. AM is supported by a Queensland Health Advancing Clinical Research Fellowship.

ACKNOWLEDGMENTS

The authors would like to thank the tissue donors, Queensland Health clinicians, pathologists, scientists, and Conjoint Internal Medicine Laboratory for their support and discussions. The authors would like to thank the Australian Cancer Research Foundation (ACRF)/Institute for Molecular Bioscience (IMB) Cancer Biology Imaging Facility (established with the support of the ACRF), the UQ School of Biomedical Sciences Imaging Facility, and the UQ IMB Sequencing Facility for helpful discussions and guidance. The authors would like to thank Ronan Kapetanovic (IMB) and Ian Frazer (University of Queensland Diamantina Institute) for providing the mouse kidney tissues.

SUPPLEMENTARY MATERIAL

The Supplementary Material for this article can be found online at: https://www.frontiersin.org/articles/10.3389/fmed.2022.873923/full#supplementary-material

REFERENCES

1. Little MH. *Kidney Development, Disease, Repair and Regeneration*. Academic Press (2015). p. 614.
2. Chevalier RL, Charlton JR. Kidney development in renal pathology. In: Faa G, Fanos V, editors. *Current Clinical Pathology*. 1st ed. New York, NY: Humana Press (2014). doi: 10.1007/978-1-4939-0947-6
3. Kitchin AR, Hutton HL. The players: cells involved in glomerular disease. *Clin J Am Soc Nephrol*. (2016) 11:1664–74. doi: 10.2215/CJN.13791215
4. Boron W, Boron WF, Boulpaep EL. *Medical Physiology: A Cellular and Molecular Approach*. Philadelphia, PA: W.B. Saunders (2003). p. 1319.
5. Hoenig MP, Zeidel ML. Homeostasis, the milieu interieur, and the wisdom of the nephron. *Clin J Am Soc Nephrol*. (2014) 9:1272–81. doi: 10.2215/CJN.08860813

6. Lake BB, Chen S, Hoshi M, Plongthongkum N, Salamon D, Knoten A. A single-nucleus RNA-sequencing pipeline to decipher the molecular anatomy and pathophysiology of human kidneys. *Nat Commun.* (2019) 10:2832. doi: 10.1038/s41467-019-10861-2
7. Lacar B, Linker SB, Jaeger BN, Krishnaswami SR, Barron JJ, Kelder MJE. Nuclear RNA-seq of single neurons reveals molecular signatures of activation. *Nat Commun.* (2016) 7:11022. doi: 10.1038/ncomms11022
8. Lake BB, Codeluppi S, Yung YC, Gao D, Chun J, Kharchenko PV. A comparative strategy for single-nucleus and single-cell transcriptomes confirms accuracy in predicted cell-type expression from nuclear RNA. *Sci Rep.* (2017) 7:6031. doi: 10.1038/s41598-017-04426-w
9. Wu H, Humphreys BD. The promise of single-cell RNA sequencing for kidney disease investigation. *Kidney Int.* (2017) 92:1334–42 doi: 10.1016/jkint06(2017)033
10. Zhou Q, Xiong Y, Huang XR, Tang P, Lan Y. Identification of Genes Associated with Smad3-dependent Renal Injury by RNA-seq-based Transcriptome Analysis. *Sci Rep*. (2015) 5:17901. doi: 10.1038/srep17901
11. Nakagawa S, Nishihara K, Miyata H, Shinke H, Tomita E, Kajiwara M. Molecular markers of tubulointerstitial fibrosis and tubular cell damage in patients with chronic kidney disease. *PLoS ONE.* (2015) 10:e0136994. doi: 10.1371/journal.pone.0136994
12. Liao J, Chen YuZ, Bao Y, Zou M, Zhang CH, et al. Single-cell RNA sequencing of human kidney. *Sci Data*. (2020) 7:4. doi: 10.1038/s41597-019-0351-8
13. Lee JW, Chou CL, Knepper MA. Deep sequencing in microdissected renal tubules identifies nephron segment–specific transcriptomes. J Am Soc Nephro. (2015). 26:2669–77. doi: 10.1681/ASN.2014111067
14. Ståhl PL, Salmén F, Vickovic S, Lundmark A, Navarro JF, Magnusson J, et al. Visualization and analysis of gene expression in tissue sections by spatial transcriptomics. *Science*. (2016) 353:78–82. doi: 10.1126/science.aaf2403
15. Vickovic S, Ståhl PL, Salmén F, Giatrellis S, Westholm JO, Mollbrink A. Massive and parallel expression profiling using microarrayed single-cell sequencing. *Nat Commun.* (2016) 7:13182. doi: 10.1038/ncomms13182
16. Asp M, Salmén F, Ståhl PL, Vickovic S, Felldin U, Löfling M. Spatial detection of fetal marker genes expressed at low level in adult human heart tissue. *Sci Rep.* (2017) 7:12941. doi: 10.1038/s41598-017-13462-5
17. Wong K, Fernández Navarro J, Bergenstråhle LSTS. A web-based application for automatic spot and tissue detection for Spatial Transcriptomics image data sets. (2018). Available online at: https://academic.oup.com/bioinformatics/advance-article-pdf/doi/10
18. Thrane K, Eriksson H, Maaskola J, Hansson J, Lundeberg J. spatially resolved transcriptomics enables dissection of genetic heterogeneity in stage iii cutaneous malignant melanoma. *Cancer Res*. (2018) 78:5970–9. doi: 10.1200/JCO.36, 15._suppl.e21587
19. Lundmark A, Gerasimcik N, Båge T, Jemt A, Mollbrink A, Salmén F. Gene expression profiling of periodontitis-affected gingival tissue by spatial transcriptomics. *Sci Rep*. (2018) 8:9370. doi: 10.1038/s41598-018-27627-3
20. Berglund E, Maaskola J, Schultz N, Friedrich S, Marklund M, Bergenstråhle J. Spatial maps of prostate cancer transcriptomes reveal an unexplored landscape of heterogeneity. *Nat Commun.* (2018) 9:2419. doi: 10.1038/s41467-018-04724-5
21. Maniatis S, Äijö T, Vickovic S, Braine C, Kang K, Mollbrink A, et al. Spatiotemporal dynamics of molecular pathology in amyotrophic lateral sclerosis. *Science*. (2019) 364:89–93. doi: 10.1126/science.aav9776
22. Carlberg K, Korotkova M, Larsson L, Catrina AI, Ståhl PL, Malmström V. Exploring inflammatory signatures in arthritic joint biopsies with spatial transcriptomics. *Sci Rep*. (2019) 9:18975. doi: 10.1038/s41598-019-55441-y
23. Asp M, Giacomello S, Larsson L, Wu C, Fürth D, Qian X. A Spatiotemporal organ-wide gene expression and cell atlas of the developing human heart. *Cell 2019 Dec 12;179(7):1647-1660e19* doi: 10.1016/jcell11.(2019)025.
24. Ortiz C, Navarro JF, Jurek A, Märtin A, Lundeberg J, Meletis K. Molecular atlas of the adult mouse brain. *Sci Adv*. (2020) 6:eabb3446. doi: 10.1126./sciadv.abb3446
25. Moncada R, Barkley D, Wagner F, Chiodin M, Devlin JC, Baron M. Integrating microarray-based spatial transcriptomics and single-cell RNA-seq reveals tissue architecture in pancreatic ductal adenocarcinomas. *Nat Biotechnol.* (2020) 38:333–42. doi: 10.1038/s41587-019-0392-8
26. Chen WT, Lu A, Craessaerts K, Pavie B, Frigerio CS, Corthout N. Spatial Transcriptomics and In Situ Sequencing to Study Alzheimer's Disease. *Sci Rep*. (2020) 182:976–991.e19. doi: 10.1016/j.cell.2020.06.038
27. Rubin JiAL, Thrane AJ, Jiang K, Reynolds S, Meyers DL. RM, et al. Multimodal analysis of composition and spatial architecture in human squamous cell. *Carcinoma Cell*. (2020) 182:497–514e22 doi: 10.1016/jcell05.(2020)039
28. Melo Ferreira R, Sabo AR, Winfree S, Collins KS, Janosevic D, Gulbronson CJ. Integration of spatial and single-cell transcriptomics localizes epithelial cell-immune cross-talk in kidney injury. *JCI Insight*. (2021) 6:147703. doi: 10.1172/jci.insight.147703
29. Lake BB, Menon R, Winfree S, Hu Q, Ferreira RM. An atlas of healthy and injured cell states and niches in the human kidney. bioRxiv. (2021). doi: 10.1101/2021.07.28.454201
30. Sanchez-Ferras O, Pacis A, Sotiropoulou M, Zhang Y, Wang YC, Bourgey M. A coordinated progression of progenitor cell states initiates urinary tract development. *Nat Commun.* (2021) 12:2627. doi: 10.1038/s41467-021-22931-5
31. Janosevic D, Myslinski J, McCarthy TW, Zollman A, Syed F, Xuei X, et al. The orchestrated cellular and molecular responses of the kidney to endotoxin define a precise sepsis timeline. *Elife*. (2021) 10:6227. doi: 10.7554/eLife.62270
32. Dixon EE, Wu H, Muto Y, Wilson PC, Humphreys BD. Spatially resolved transcriptomic analysis of acute kidney injury in a female Murine model. *J Am Soc Nephrol.* (2022) 33:279–89. doi: 10.1681/ASN.2021081150
33. Rusk, N. Spatial transcriptomics. *Nat Methods*. (2016) 13:710. doi: 10.1038/nmeth.3985
34. Salmén F, Ståhl PL, Mollbrink A, Navarro JF, Vickovic S, Frisén J. Barcoded solid-phase RNA capture for Spatial Transcriptomics profiling in mammalian tissue sections. *Nat Protoc.* (2018) 13:2501–34. doi: 10.1038/s41596-018-0045-2
35. Martin, M. Cutadapt removes adapter sequences from high-throughput sequencing reads. *EMBnet.J*. (2011) 17:10–2. doi: 10.14806/ej.17.1.200
36. Satija R, Farrell JA, Gennert D, Schier AF, Regev A. Spatial reconstruction of single-cell gene expression data. *Nat Biotechnol.* (2015) 33:495–502. doi: 10.1038/nbt.3192
37. Butler A, Hoffman P, Smibert P, Papalexi E, Satija R. Integrating single-cell transcriptomic data across different conditions, technologies, and species. *Nat Biotechnol.* (2018) 36:411–20. doi: 10.1038/nbt.4096
38. Stuart T, Butler A, Hoffman P, Hafemeister C, Papalexi E, Mauck WM. 3rd, et al. Comprehensive integration of single-cell. *Data Cell*. (2019) 177:1888–1902e21 doi: 10.1016/jcell05.(2019)031
39. Hao Y, Hao S, Andersen-Nissen E, Mauck WM. 3rd, Zheng S, Butler A, et al. Integrated analysis of multimodal single-cell data. *Cell.* (2021) 184:3573–87e29 doi: 10.1016/jcell04.(2021)048
40. Lun ATL, Bach K, Marioni JC. Pooling across cells to normalize single-cell RNA sequencing data with many zero counts. *Genome Biol.* (2016) 17:75. doi: 10.1186/s13059-016-0947-7
41. Haghverdi L, Lun ATL, Morgan MD, Marioni JC. Batch effects in single-cell RNA-sequencing data are corrected by matching mutual nearest neighbors. *Nat Biotechnol.* (2018) 36:421–7. doi: 10.1038/nbt.4091
42. Becht E, McInnes L, Healy J, Dutertre C-A, Kwok IWH, Ng LG, et al. Dimensionality reduction for visualizing single-cell data using UMAP. *Nat Biotechnol*. (2018) 3:4314. doi: 10.1038/nbt.4314
43. Zappia, L., and Oshlack, A. Clustering trees: a visualization for evaluating clusterings at multiple resolutions. *GigaScience*. (2018) 7:giy083. doi: 10.1093/gigascience/giy083
44. Crowell HL, Soneson C, Germain PL, Calini D, Collin L, Raposo C. Muscat detects subpopulation-specific state transitions from multi-sample multi-condition single-cell transcriptomics data. *Nat Commun*. (2020) 11:6077. doi: 10.1038/s41467-020-19894-4
45. McCarthy DJ, Campbell KR, Lun AT, Wills QF. Scater: pre-processing, quality control, normalization and visualization of single-cell RNA-seq data in R. *Bioinformatics*. (2017) 33:1179–86. doi: 10.1093/bioinformatics/btw777
46. Robinson MD, McCarthy DJ, Smyth GK. EdgeR: a Bioconductor package for differential expression analysis of digital gene expression data. *Bioinformatics*. (2010) 26:139–40. doi: 10.1093/bioinformatics/btp616

47. Cable DM, Murray E, Zou LS, Goeva A, Macosko EZ, Chen F. Robust decomposition of cell type mixtures in spatial transcriptomics. *Nat Biotechnol*. (2021) 18. doi: 10.1038/s41587-021-00830-w
48. Pham DT, Tan X, Xu J, Grice LF, Lam PY, Raghubar A. Stlearn: integrating spatial location, tissue morphology and gene expression to find cell types, cell-cell interactions and spatial trajectories within undissociated tissues. bioRxiv. 2020. doi: 10.1101/2020.05.31.125658
49. Hou R, Denisenko E, Ong HT, Ramilowski JA, Forrest ARR. Predicting cell-to-cell communication networks using NATMI. *Nat Commun*. (2020) 11:5011. doi: 10.1038/s41467-020-18873-z
50. Waltman L, van Eck NJA. smart local moving algorithm for large-scale modularity-based community detection. *Eur Phys J B*. (2013) 86:471. doi: 10.1140/epjb/e2013-40829-0
51. Stewart BJ, Ferdinand JR, Young MD, Mitchell TJ, Loudon KW, Riding AM. Spatiotemporal immune zonation of the human kidney. *Science*. (2019) 365:1461–6. doi: 10.1126/science.aat5031
52. He B, Chen P, Zambrano S, Dabaghie D, Hu Y, Möller-Hackbarth K, et al. Single-cell RNA sequencing reveals the mesangial identity and species diversity of glomerular cell transcriptomes. *Nat Commun*. (2021) 12:2141. doi: 10.1038/s41467-021-22331-9
53. Nielsen, S., Kwon, T-. H., Dimke, H., and Frøkiær, J. Aquaporin water channels in mammalian kidney [Internet]. *Seldin Giebisch's the Kidney*. (2008) 1095–121. doi: 10.1016/B978-012088488-9.50041-3
54. Park J, Shrestha R, Qiu C, Kondo A, Huang S, Werth M. Single-cell transcriptomics of the mouse kidney reveals potential cellular targets of kidney disease. *Science*. (2018) 360:758–63. doi: 10.1126/science.aar2131
55. Miao Z, Balzer MS, Ma Z, Liu H, Wu J, Shrestha R. Single cell regulatory landscape of the mouse kidney highlights cellular differentiation programs and disease targets. *Nat Commun*. (2021) 12:2277. doi: 10.1038/s41467-021-22266-1
56. Ransick A, Lindström NO, Liu J, Zhu Q, Guo JJ, Alvarado GF, et al. Single-Cell profiling reveals sex, lineage, and regional diversity in the mouse kidney. *Dev Cell*. (2019) 51:399–413.e7. doi: 10.1016/j.devcel.10, 005.
57. Wu H, Malone AF, Donnelly EL, Kirita Y, Uchimura K, Ramakrishnan SM. Single-Cell Transcriptomics of a Human Kidney Allograft Biopsy Specimen Defines a Diverse Inflammatory Response. *J Am Soc Nephrol*. (2018) 29:2069–80. doi: 10.1681/ASN.2018020125
58. Wu H, Kirita Y, Donnelly EL, Humphreys BD. Advantages of single-nucleus over single-cell RNA sequencing of adult kidney: rare cell types and novel cell states revealed in fibrosis. *J Am Soc Nephrol*. (2019) 30:23–32. doi: 10.1681/ASN.2018090912
59. Wilson PC, Wu H, Kirita Y, Uchimura K, Ledru N, Rennke HG. The single-cell transcriptomic landscape of early human diabetic nephropathy. *Proc Natl Acad Sci U S A*. (2019) 116:19619–25. doi: 10.1073/pnas.1908706116
60. Muto Y, Wilson PC, Ledru N, Wu H, Dimke H, Waikar SS. Single cell transcriptional and chromatin accessibility profiling redefine cellular heterogeneity in the adult human kidney. *Nat Commun*. (2021) 12:2190. doi: 10.1038/s41467-021-22368-w
61. Lindström NO, Sealfon R, Chen X, Parvez RK, Ransick A, De Sena Brandine G, et al. Spatial transcriptional mapping of the human nephrogenic program. *Dev Cell*. (2021) 56:2381–98.e6. doi: 10.1016/j.devcel.07, 017.
62. West DC, Rees CG, Duchesne L, Patey SJ, Terry CJ, Turnbull J, et al. Interactions of multiple heparin binding growth factors with neuropilin-1 and potentiation of the activity of fibroblast growth factor-2. *J Biol Chem*. (2005) 280:13457–64. doi: 10.1074/jbc.M410924200
63. Bender HR, Campbell GE, Aytoda P, Mathiesen AH, Duffy D. Thrombospondin 1 (THBS1) promotes follicular angiogenesis, luteinization, and ovulation in primates. *Front Endocrinol*. (2019) 10:727. doi: 10.3389/fendo.2019.00727
64. Hu X, Chen J, Huang H, Yin S, Zheng S, Zhou L. Syndecan-4 promotes vascular beds formation in tissue engineered liver via thrombospondin 1. *Bioengineered*. (2020) 11:1313–24. doi: 10.1080/21655979.2020.1846897
65. Li W, Chen Z, Yuan J, Yu Z, Cheng C, Zhao Q, et al. Annexin A2 is a Robo4 ligand that modulates ARF6 activation-associated cerebral trans-endothelial permeability. *J Cereb Blood Flow Metab*. (2019) 39:2048–60. doi: 10.1177/0271678X18777916
66. Philtjens S, Van Mossevelde S, van der Zee J, Wauters E, Dillen L, Vandenbulcke M. Rare nonsynonymous variants in SORT1 are associated with increased risk for frontotemporal dementia. *Neurobiol Aging*. (2018) 66:181e3–181. doi: 10.1016/j.neurobiolaging.2018.02.011
67. Aaberg-Jessen C, Sørensen MD, Matos ALSA, Moreira JM, Brünner N, Knudsen A, et al. Co-expression of TIMP-1 and its cell surface binding partner CD63 in glioblastomas. *BMC Cancer*. (2018) 18:270. doi: 10.1186/s12885-018-4179-y
68. Hardt S, Valek L, Zeng-Brouwers J, Wilken-Schmitz A, Schaefer L, Tegeder I. Progranulin deficient mice develop nephrogenic diabetes insipidus. *Aging Dis*. (2018) 9:817–30. doi: 10.14336/AD.2017.1127
69. Biwer LA, Askew-Page HR, Hong K, Milstein J, Johnstone SR, Macal E, et al. Endothelial calreticulin deletion impairs endothelial function in aged mice. *Am J Physiol Heart Circ Physiol*. (2020) 318:H1041–8. doi: 10.1152/ajpheart.00586.2019
70. Leung-Hagesteijn CY, Milankov K, Michalak M, Wilkins J, Dedhar S. Cell attachment to extracellular matrix substrates is inhibited upon downregulation of expression of calreticulin, an intracellular integrin alpha-subunit-binding protein. *J Cell Sci*. (1994) 107 (Pt 3):589–600. doi: 10.1242/jcs.107.3.589
71. Coppolino MG, Woodside MJ, Demaurex N, Grinstein S, St-Arnaud R, Dedhar S. Calreticulin is essential for integrin-mediated calcium signalling and cell adhesion. *Nature*. (1997) 386:843–7. doi: 10.1038/386843a0
72. Han SY, Jee YH, Han KH, Kang YS, Kim HK, Han JY. An imbalance between matrix metalloproteinase-2 and tissue inhibitor of matrix metalloproteinase-2 contributes to the development of early diabetic nephropathy. *Nephrol Dial Transplant*. (2006) 21:2406–16. doi: 10.1093/ndt/gfl238
73. Cosgrove D, Meehan DT, Delimont D, Pozzi A, Chen X, Rodgers KD. Integrin alpha1beta1 regulates matrix metalloproteinases via P38 mitogen-activated protein kinase in mesangial cells: implications for Alport syndrome. *Am J Pathol*. (2008) 172:761–73. doi: 10.2353/ajpath.2008.070473
74. Kitsiou PV, Tzinia AK, Stetler-Stevenson WG, Michael AF, Fan WW, Zhou B, et al. Glucose-induced changes in integrins and matrix-related functions in cultured human glomerular epithelial cells. *Am J Physiol Renal Physiol*. (2003) 284:F671–9. doi: 10.1152/ajprenal.00266.2002
75. Rodrigues RG, Guo N, Zhou L, Sipes JM, Williams SB, Templeton NS. Conformational regulation of the fibronectin binding and alpha 3beta 1 integrin-mediated adhesive activities of thrombospondin-1. *J Biol Chem*. (2001) 276:27913–22. doi: 10.1074/jbc.M009518200
76. Julovi SM, Sanganeria B, Minhas N, Ghimire K, Nankivell B, Rogers NM. Blocking thrombospondin-1 signaling via CD47 mitigates renal interstitial fibrosis. *Lab Invest*. (2020) 100:1184–96. doi: 10.1038/s41374-020-0434-3
77. Poczatek MH, Hugo C, Darley-Usmar V, Murphy-Ullrich JE. Glucose stimulation of transforming growth factor-beta bioactivity in mesangial cells is mediated by thrombospondin-1. *Am J Pathol*. (2000) 157:1353–63. doi: 10.1016/S0002-9440(10)64649-4
78. Hafdi Z, Lesavre P, Nejjari M, Halbwachs-Mecarelli L, Droz D, Noël LH. Distribution of αvβT3, αvβTB5 Integrins and the Integrin Associated Protein — IAP (CD47) in Human Glomerular Diseases. *Cell Adhes Commun*. (2000) 7 441–51. doi: 10.3109/15419060009040302
79. Marek I, Hilgers KF, Rascher W, Woelfle J, Hartner A. A role for the alpha-8 integrin chain (itga8) in glomerular homeostasis of the kidney. *Mol Cell Pediatr*. (2020) 7:13. doi: 10.1186/s40348-020-00105-5
80. Hirono K, Imaizumi T, Aizawa T, Watanabe S, Tsugawa, K, Shiratori, T. Endothelial expression of fractalkine (CX3CL1) is induced by Toll-like receptor 3 signaling in cultured human glomerular endothelial cells. *Mod Rheumatol*. (2020) 30:1074–81. doi: 10.1080/14397595.2019.1682768
81. Aizawa-Yashiro T, Imaizumi T, Tsuruga K, Watanabe S, Matsumiya T, Hayakari R. Glomerular expression of fractalkine is induced by polyinosinic-polycytidylic acid in human mesangial cells: possible involvement of fractalkine after viral infection. *Pediatr Res*. (2013) 73:180–6. doi: 10.1038/pr.2012.165
82. Fujita M, Takada YK, Takada Y. Integrins αvβ3 and α4β1 act as coreceptors for fractalkine, and the integrin-binding defective mutant of fractalkine is an antagonist of CX3CR1. *J Immunol*. (2012) 189:5809–19. doi: 10.4049/jimmunol.1200889
83. Colorado PC, Torre A, Kamphaus G, Maeshima Y, Hopfer H, Takahashi K, et al. Anti-angiogenic cues from vascular basement membrane collagen. *Cancer Res*. (2000) 60:2520–6.

84. Nyberg P, Xie L, Sugimoto H, Colorado P, Sund M, Holthaus K. Characterization of the anti-angiogenic properties of arresten, an alpha1beta1 integrin-dependent collagen-derived tumor suppressor. *Exp Cell Res*. 2008 14:3292–305 doi: 10.1016/jyexcr08(2008)011
85. Slattery ML, Mullany LE, Sakoda LC, Wolff RK, Stevens JR, Samowitz WS. The PI3K/AKT signaling pathway: Associations of miRNAs with dysregulated gene expression in colorectal cancer. *Mol Carcinog.* (2018) 57:243–61. doi: 10.1002/mc.22752
86. Gudmundsdottir V, Pedersen HK, Allebrandt KV, Brorsson C, van Leeuwen N, Banasik K. Integrative network analysis highlights biological processes underlying GLP-1 stimulated insulin secretion: a DIRECT study. *PLoS ONE*. (2018) 13:e0189886. doi: 10.1371/journal.pone.0189886
87. Ekwa-Ekoka C, Diaz GA, Carlson C, Hasegawa T, Samudrala R, Lim KC, et al.. Genomic organization and sequence variation of the human integrin subunit alpha8 gene (ITGA8). Matrix Biol. (2004) 237:487–96. doi: 10.1016/j.matbio.08, 005.
88. Lu Y, Ye Y, Yang Q, Shi S. Single-cell RNA-sequence analysis of mouse glomerular mesangial cells uncovers mesangial cell essential genes. *Kidney Int*. (2017) 92:504–13 doi: 10.1016/j.kint.2017.01.016
89. Brandenberger R, Schmidt A, Linton J, Wang D, Backus C, Denda S. Identification and characterization of a novel extracellular matrix protein nephronectin that is associated with integrin alpha8beta1 in the embryonic kidney. *J Cell Biol.* (2001) 154:447–58. doi: 10.1083/jcb.200103069
90. Zimmerman SE, Hiremath C, Tsunezumi J, Yang Z, Finney B, Marciano DK. Nephronectin Regulates mesangial cell adhesion and behavior in glomeruli. *J Am Soc Nephrol.* (2018) 29:1128–40. doi: 10.1681/ASN.2017070752
91. Iervolino A, De La Motte LR, Petrillo F, Prosperi F, Alvino FM, Schiano G, et al. Integrin Beta 1 Is Crucial for urinary concentrating ability and renal medulla architecture in adult mice. Front Physiol. (2018) 9:01273. doi: 10.3389/fphys.2018.01273
92. Hu DD, Lin EC, Kovach NL, Hoyer JR, Smith JW. A biochemical characterization of the binding of osteopontin to integrins alpha v beta 1 and alpha v beta 5. *J Biol Chem*. (1995) 270:26232–8. doi: 10.1074/jbc.270.44.26232
93. Yokosaki Y, Matsuura N, Sasaki T, Murakami I, Schneider H, Higashiyama S. The integrin alpha(9)beta(1) binds to a novel recognition sequence (SVVYGLR) in the thrombin-cleaved amino-terminal fragment of osteopontin. *J Biol Chem.* (1999) 274:36328–34. doi: 10.1074/jbc.274.51.36328
94. Xie Y, Sakatsume M, Nishi S, Narita I, Arakawa M, Gejyo F. Expression, roles, receptors, and regulation of osteopontin in the kidney. *Kidney Int*. (2001) 60:1645–57. doi: 10.1046/j.1523-2001, 00032.x
95. Bieritz B, Spessotto P, Colombatti A, Jahn A, Prols F, Hartner A. Role of alpha8 integrin in mesangial cell adhesion, migration, and proliferation. *Kidney Int*. (2003) 64:119–27. doi: 10.1046/j.1523-2003, 00057.x
96. Teo AED, Garg S, Johnson TI, Zhao W, Zhou J, Gomez-Sanchez CE. Physiological and pathological roles in human adrenal of the glomeruli-defining matrix protein NPNT (Nephronectin). *Hypertension*. (2017) 69:1207–16. doi: 10.1161/HYPERTENSIONAHA.117.09156
97. Müller-Deile J, Dannenberg J, Schroder P, Lin MH, Miner JH, Chen R, et al. Podocytes regulate the glomerular basement membrane protein nephronectin by means of miR-378a-3p in glomerular diseases. *Kidney Int*. (2017) 92:836–49. doi: 10.1016/j.kint.03, 005.
98. Faye C, Chautard E, Olsen BR, Ricard-Blum S. The first draft of the endostatin interaction network. *J Biol Chem.* (2009) 284:22041–7. doi: 10.1074/jbc.M109.002964
99. Hamano Y, Okude T, Shirai R, Sato I, Kimura R, Ogawa M, et al. Lack of Collagen XVIII/endostatin exacerbates immune-mediated glomerulonephritis. *J Am Soc Nephrol*. (2010) 9:1445–55. doi: 10.1681/ASN.2009050492
100. Kuo CJ. LaMontagne KR Jr, Garcia-Cardeña G, Ackley BD, Kalman D, Park S, et al. Oligomerization-dependent regulation of motility and morphogenesis by the collagen XVIII NC1/endostatin domain. *J Cell Biol.* (2001) 152:1233–46. doi: 10.1083/jcb.152.6.1233
101. He J, Baum LG. Presentation of galectin-1 by extracellular matrix triggers T cell death. *J Biol Chem*. (2004) 279:4705–12. doi: 10.1074/jbc.M311183200
102. Moiseeva EP, Williams B, Goodall AH, Samani NJ. Galectin-1 interacts with beta-1 subunit of integrin. *Biochem Biophys Res Commun*. 2003 310:1010–6. doi: 10.1016/j.bbrc.2003.09.112
103. Chandrasekaran L, He CZ, Al-Barazi H, Krutzsch HC, Iruela-Arispe ML, Roberts DD. Cell contact-dependent activation of alpha3beta1 integrin modulates endothelial cell responses to thrombospondin-1. *Mol Biol Cell.* (2000) 11:2885–900. doi: 10.1091/mbc.11.9.2885
104. Maimaitiyiming H, Zhou Q, Wang S. Thrombospondin 1 Deficiency Ameliorates the Development of Adriamycin-Induced Proteinuric Kidney Disease. *PLoS ONE.* (2016) 11:e0156144. doi: 10.1371/journal.pone.0156144
105. Sasaki T, Brakebusch C, Engel J, Timpl R. Mac-2 binding protein is a cell-adhesive protein of the extracellular matrix which self-assembles into ring-like structures and binds beta1 integrins, collagens and fibronectin. *EMBO J.* (1998) 17:1606–13. doi: 10.1093/emboj/17.6.1606
106. Gonzalez Porras MA, Stojkova K, Vaicik MK, Pelowe A, Goddi A, Carmona A. Integrins and extracellular matrix proteins modulate adipocyte thermogenic capacity. *Sci Rep*. (2021) 11:1–14. doi: 10.1038/s41598-021-84828-z
107. Lennon R, Randles MJ, Humphries MJ. The importance of podocyte adhesion for a healthy glomerulus. *Front Endocrinol.* (2014) 5:160. doi: 10.3389/fendo.2014.00160
108. Brown JC, Sasaki T, Göhring W, Yamada Y, Timpl R. The C-terminal domain V of perlecan promotes beta1 integrin-mediated cell adhesion, binds heparin, nidogen and fibulin-2 and can be modified by glycosaminoglycans. *Eur J Biochem*. (1997) 250:39–46. doi: 10.1111/j.1432-1997, t01–1.-00039.x
109. Raats CJ, Van Den Born J, Berden JH. Glomerular heparan sulfate alterations: mechanisms and relevance for proteinuria. *Kidney Int*. (2000) 57:385–400. doi: 10.1046/j.1523-2000, 00858.x
110. Bagatur Y, Ilter Akulke AZ, Bihorac A, Erdem M, Telci D. Tissue transglutaminase expression is necessary for adhesion, metastatic potential and cancer stemness of renal cell carcinoma. *Cell Adh Migr*. (2018) 12:138–51. doi: 10.1080/19336918.2017.1322255
111. Schelling JR. Tissue transglutaminase inhibition as treatment for diabetic glomerular scarring: it's good to be glueless. *Kidney Int.* (2009) 76:363–5. doi: 10.1038/ki.2009.179
112. He L, Sun Y, Takemoto M, Norlin J, Tryggvason K, Samuelsson T. The glomerular transcriptome and a predicted protein-protein interaction network. *J Am Soc Nephrol.* (2008) 19:260–8. doi: 10.1681/ASN.2007050588
113. Pall AA, Howie AJ, Adu D, Richards GM, Inward CD, Milford DV. Glomerular vascular cell adhesion molecule-1 expression in renal vasculitis. *J Clin Pathol.* (1996) 49:238–42. doi: 10.1136/jcp.49.3.238
114. Chakravorty SJ, Howie AJ, Cockwell P, Adu D, Savage COT. lymphocyte adhesion mechanisms within inflamed human kidney: studies with a Stamper-Woodruff assay. *Am J Pathol.* (1999) 154:503–14. doi: 10.1016/S0002-9440(10)65296-0
115. Yokosaki Y, Tanaka K, Higashikawa F, Yamashita K, Eboshida A. Distinct structural requirements for binding of the integrins alphavbeta6, alphavbeta3, alphavbeta5, alpha5beta1 and alpha9beta1 to osteopontin. *Matrix Biol.* (2005) 24:418–27. doi: 10.1016/j.matbio.2005.05.005
116. Barry ST, Ludbrook SB, Murrison E, Horgan CMA. regulated interaction between alpha5beta1 integrin and osteopontin. *Biochem Biophys Res Commun.* (2000) 267:764–9. doi: 10.1006/bbrc.1999.2032
117. Sauzay C, Voutetakis K, Chatziioannou A, Chevet E, Avril T. CD90/Thy-1, a Cancer-Associated Cell Surface Signaling Molecule. *Front Cell Dev Biol.* (2019) 7:66. doi: 10.3389/fcell.2019.00066
118. Yamamoto T, Wilson CB. Quantitative and qualitative studies of antibody-induced mesangial cell damage in the rat. *Kidney Int.* (1987) 32:514–25. doi: 10.1038/ki.1987.240
119. Noakes PG, Miner JH, Gautam M, Cunningham JM, Sanes JR, Merlie JP. The renal glomerulus of mice lacking s–laminin/laminin β2: nephrosis despite molecular compensation by laminin β1. *Nat Genet.* (1995) 10:400–6. doi: 10.1038/ng0895-400
120. Borza CM, Chen X, Zent R, Pozzi A. Cell Receptor-Basement Membrane Interactions in Health and Disease: A Kidney-Centric View. *Curr Top Membr.* (2015) 76:231–53. doi: 10.1016/bs.ctm.2015.07.003
121. Scott RP, Quaggin SE. The cell biology of renal filtration. *J Cell Biol.* (2015) 209:199–210. doi: 10.1083/jcb.201410017

122. Schrimpf C, Xin C, Campanholle G, Gill SE, Stallcup W, Lin SL, et al. Pericyte TIMP3 and ADAMTS1 modulate vascular stability after kidney injury. *J Am Soc Nephrol*. (2021) 23:868–83. doi: 10.1681/ASN.2011080851
123. Masson D, Rioux-Leclercq N, Fergelot P, Jouan F, Mottier S, Théoleyre S. Loss of expression of TIMP3 in clear cell renal cell carcinoma. *Eur J Cancer*. (2010) 46:1430–7. doi: 10.1016/j.ejca.2010.01.009
124. Liu LiLM, Wang X, Wang L, Liu Y, Tian X. X, et al. A novel dual eigen-analysis of mouse multi-tissues' expression profiles unveils new perspectives into type 2 diabetes. *Sci Rep*. (2017) 7:5044. doi: 10.1038/s41598-017-05405-x
125. Roskoski R. Jr. Vascular endothelial growth factor (VEGF) and VEGF receptor inhibitors in the treatment of renal cell carcinomas. *Pharmacol Res*. (2017) 120:116–32 doi: 10.1016/jphrs03(2017)010
126. Tanabe K, Wada J, Sato Y. Targeting angiogenesis and lymphangiogenesis in kidney disease. *Nat Rev Nephrol*. (2020) 16:289–303. doi: 10.1038/s41581-020-0260-2
127. Guo, H-. F., and Vander Kooi, C. W. Neuropilin functions as an essential cell surface receptor. *J Biol Chem*. (2015) 290:29120–6. doi: 10.1074/jbc.R115.687327
128. Wild JR, Staton CA, Chapple K, Corfe BM. Neuropilins: expression and roles in the epithelium. *Int J Exp Pathol*. (2012) 93:81–103. doi: 10.1111/j.1365-2012, 00810.x
129. Sato W, Tanabe K, Kosugi T, Hudkins K, Lanaspa MA, Zhang L. Selective stimulation of VEGFR2 accelerates progressive renal disease. *Am J Pathol*. (2011) 179:155–66 doi: 10.1016/jajpath03.(2011)024
130. Goyanes AM, Moldobaeva A, Marimoutou M, Varela LC, Wang L, Johnston LF, et al. F. Functional impact of human genetic variants of COL18A1/endostatin on pulmonary endothelium. Am *J Respir Cell Mol Biol*. (2020) 62:524–34. doi: 10.1165/rcmb.2019-0056OC
131. Lambert J, Makin K, Akbareian S, Johnson R, Alghamdi AAA, Robinson SD, et al. ADAMTS-1 and syndecan-4 intersect in the regulation of cell migration and angiogenesis. *J Cell Sci*. (2020) 133:235762. doi: 10.1242/jcs.235762
132. Dai C, Gong Q, Cheng Y, Su G. Regulatory mechanisms of Robo4 and their effects on angiogenesis. *Biosci Rep*. (2019) 39:BSR20190513. doi: 10.1042/BSR20190513
133. Valiño-Rivas L, Baeza-Bermejillo C, Gonzalez-Lafuente L, Sanz AB, Ortiz A, Sanchez-Niño MD. CD74 in Kidney Disease. *Front Immunol*. (2015) 6:483. doi: 10.3389/fimmu.2015.00483
134. Brunskill EW, Potter SS. Changes in the gene expression programs of renal mesangial cells during diabetic nephropathy. *BMC Nephrol*. (2012) 13:70. doi: 10.1186/1471-2369-13-70
135. Matsuda S, Matsuda Y, D'Adamio L. CD74 interacts with APP and suppresses the production of Aβ. *Mol Neurodegener*. (2009) 4:1–10. doi: 10.1186/1750-1326-4-41
136. d'Uscio LV, He T, Katusic ZS. Expression and processing of amyloid precursor protein in vascular endothelium. *Physiology*. (2017) 32:20–32. doi: 10.1152/physiol.00021.2016
137. Yamazaki T, Sasaki S, Okamoto T, Sato Y, Hayashi A, Ariga T. Up-Regulation of CD74 expression in parietal epithelial cells in a mouse model of focal segmental glomerulosclerosis. *Nephron*. (2016) 134:238–52. doi: 10.1159/000448221
138. Yu G, Nishimura M, Arawaka S, Levitan D, Zhang L, Tandon A, et al. Nicastrin modulates presenilin-mediated notch/glp-1 signal transduction and betaAPP processing. *Nature*. (2000) 407:48–54. doi: 10.1038/35024009
139. Dawkins E, Small DH. Insights into the physiological function of the β-amyloid precursor protein: beyond Alzheimer's disease. *J Neurochem*. (2014) 129:756–69. doi: 10.1111/jnc.12675
140. Djudjaj S, Lue H, Rong S, Papasotiriou M, Klinkhammer BM, Zok S. Macrophage Migration Inhibitory Factor Mediates Proliferative GN via CD74. *J Am Soc Nephrol*. (2016) 27:1650–64. doi: 10.1681/ASN.2015020149
141. Sanchez-Niño MD, Sanz AB, Ihalmo P, Lassila M, Holthofer H, Mezzano S. The MIF receptor CD74 in diabetic podocyte injury. *J Am Soc Nephrol*. (2009) 20:353–62. doi: 10.1681/ASN.2008020194
142. Sharmin S, Taguchi A, Kaku Y, Yoshimura Y, Ohmori T, Sakuma T, et al. Human induced pluripotent stem cell–derived podocytes mature into vascularized glomeruli upon experimental transplantation. *J Am Soc Nephrol*. (2016) 27:1778–91. doi: 10.1681/ASN.2015010096
143. Tuli A, Sharma M, Wang X, Simone LC, Capek HL, Cate S. Amyloid precursor-like protein 2 association with HLA class I molecules. *Cancer Immunol Immunother*. (2009) 58:1419–31. doi: 10.1007/s00262-009-0657-z
144. Goldwich A, Burkard M, Olke M, Daniel C, Amann K, Hugo C, et al. Podocytes are nonhematopoietic professional antigen-presenting cells. *J Am Soc Nephrol*. (2013) 24:906–16. doi: 10.1681/ASN.2012020133
145. Wu VY, Shearman CW, Cohen MP. Identification of calnexin as a binding protein for amadori-modified glycated albumin. *Biochem Biophys Res Commun*. (2001) 284:602–6. doi: 10.1006/bbrc.2001.4982
146. Diedrich G, Bangia N, Pan M, Cresswell P. A role for calnexin in the assembly of the MHC class I loading complex in the endoplasmic reticulum. *J Immunol*. (2001) 166:1703–9. doi: 10.4049/jimmunol.166.3.1703
147. Lin A, Yan WH. The emerging roles of human leukocyte antigen-F in immune modulation and viral infection. *Front Immunol*. (2019) 10:964. doi: 10.3389/fimmu.2019.00964
148. Hu F, Padukkavidana T, Vægter CB, Brady OA, Zheng Y, Mackenzie IR. Sortilin-mediated endocytosis determines levels of the frontotemporal dementia protein, progranulin. *Neuron*. (2010) 68:654–67. doi: 10.1016/j.neuron.2010.09.034
149. Boggild S, Molgaard S, Glerup S, Nyengaard JR. Spatiotemporal patterns of sortilin and SorCS2 localization during organ development. *BMC Cell Biol*. (2016) 17:8. doi: 10.1186/s12860-016-0085-9
150. Jung KK, Liu XW, Chirco R, Fridman R, Kim HR. Identification of CD63 as a tissue inhibitor of metalloproteinase-1 interacting cell surface protein. *EMBO J*. (2006) 25:3934–42. doi: 10.1038/sj.emboj.7601281
151. Masciantonio MG, Gill SE. Tissue inhibitor of metalloproteinase. In: Choi S, editor. *Encyclopedia of Signaling Molecules*. New York, NY: Springer New York. (2017). p. 1–9. doi: 10.1007/978-1-4614-6438-9_101950-1
152. Garcia-Fernandez N, Jacobs-Cachá C, Mora-Gutiérrez JM, Vergara A, Orbe J, Soler MJ. Matrix metalloproteinases in diabetic kidney disease. *J Clin Med Res*. (2020) 9: 9020472. doi: 10.3390/jcm9020472
153. Prabakaran T, Christensen EI, Nielsen R, Verroust PJ. Cubilin is expressed in rat and human glomerular podocytes. *Nephrol Dial Transplant*. (2012) 27:3156–9. doi: 10.1093/ndt/gfr794
154. Saito T, Matsunaga A, Fukunaga M, Nagahama K, Hara S, Muso E. Apolipoprotein E–related glomerular disorders. *Kidney Int 2020 Feb 1;97(2):279–88* doi: 10.1016/jkint10.(2019)031
155. Marzolo MP, Farfán P. New insights into the roles of megalin/LRP2 and the regulation of its functional expression. *Biol Res*. (2011) 44:89–105. doi: 10.4067/S0716-97602011000100012
156. Dumas SJ, Meta E, Borri M, Luo Y, Rabelink LiX. Phenotypic diversity and metabolic specialization of renal endothelial cells. *Nat Rev Nephrol*. (2021) 17:441–64. doi: 10.1038/s41581-021-00411-9
157. Sun J, Hultenby K, Axelsson J, Nordström J, He B, Wernerson A. Proximal tubular expression patterns of megalin and cubilin in proteinuric nephropathies. *Kidney Int Rep*. (2017) 4:721–32 doi: 10.1016/jekir02.(2017)012
158. Merscher S, Pedigo CE, Mendez AJ. Metabolism, energetics, and lipid biology in the podocyte - cellular cholesterol-mediated glomerular injury. *Front Endocrinol*. (2014) 5:169. doi: 10.3389/fendo.2014.00169
159. Christensen EI, Willnow TE. Essential role of megalin in renal proximal tubule for vitamin homeostasis. *J Am Soc Nephrol*. (1999) 10:2224–36. doi: 10.1681/ASN.V10102224
160. Yan Q, Sui W, Wang B, Zou H, Zou G, Luo H. Expression of MMP-2 and TIMP-1 in renal tissue of patients with chronic active antibody-mediated renal graft rejection. *Diagn Pathol*. (2012) 7:141. doi: 10.1186/1746-1596-7-141
161. Schulze U, Brast S, Grabner A, Albiker C, Snieder B, Holle S. Tetraspanin CD63 controls basolateral sorting of organic cation transporter 2 in renal proximal tubules. *FASEB J*. (2017) 31:1421–33. doi: 10.1096/fj.201600901R
162. Jain R, Rawat A, Verma B, Markiewski MM, Weidanz JA. Antitumor Activity of a Monoclonal Antibody Targeting Major Histocompatibility Complex Class I–Her2 Peptide Complexes. *J Natl Cancer Inst*. (2013) 105:202–18. doi: 10.1093/jnci/djs521
163. Kersh AE, Sasaki M, Cooper LA, Kissick HT, Pollack BP. Understanding the impact of ErbB activating events and signal transduction on antigen processing and presentation: mhc expression as a model. *Front Pharmacol*. (2016) 7:327. doi: 10.3389/fphar.2016.00327

164. Miosge N, Simniok T, Sprysch P, Herken R. The collagen type XVIII endostatin domain is co-localized with perlecan in basement membranes in vivo. *J Histochem Cytochem.* (2003) 51:285–96. doi: 10.1177/002215540305100303
165. Duncan MB, Yang C, Tanjore H, Boyle PM, Keskin D, Sugimoto H. Type XVIII collagen is essential for survival during acute liver injury in mice. *Dis Model Mech.* (2013) 6:942–51. doi: 10.1242/dmm.011577
166. Tarui T, Mazar AP, Cines DB, Takada Y. Urokinase-type plasminogen activator receptor (CD87) is a ligand for integrins and mediates cell-cell interaction. *J Biol Chem*. (2001) 276:3983–90. doi: 10.1074/jbc.M008220200
167. Pasqualini R, Bodorova J, Ye S, Hemler ME. A study of the structure, function and distribution of beta 5 integrins using novel anti-beta 5 monoclonal antibodies. *J Cell Sci*. (1993) 105:101–11. doi: 10.1242./jcs.105.1.101
168. Elias BC, Mathew S, Srichai MB, Palamuttam R, Bulus N, Mernaugh G. The integrin β1 subunit regulates paracellular permeability of kidney proximal tubule cells. *J Biol Chem.* (2014) 289:8532–44. doi: 10.1074/jbc.M113.526509
169. Erikson DW, Burghardt RC, Bayless KJ, Johnson GA. Secreted Phosphoprotein 1 (SPP1, Osteopontin) Binds to Integrin Alphavbeta6 on Porcine Trophectoderm Cells and Integrin Alphavbeta3 on Uterine Luminal Epithelial Cells, and Promotes Trophectoderm Cell Adhesion and Migration1 [Internet]. *Biol Reprod*. (2009):814–25. doi: 10.1095/biolreprod.109.078600
170. Rouschop KM, Claessen N, Pals ST, Weening JJ, Florquin S. CD44 Disruption Prevents Degeneration of the capillary network in obstructive nephropathy via reduction of TGF-β1–Induced Apoptosis. *J Am Soc Nephrol*. (2006) 17:746–53. doi: 10.1681/ASN.2005080808
171. Trzpis M. McLaughlin PM, van Goor H, Brinker MGL, van Dam GM, de Leij LM, et al. Expression of EpCAM is up-regulated during regeneration of renal epithelia. *J Pathol.* (2008) 216:201–8. doi: 10.1002/path.2396
172. Evans PR, Trickett LP, Smith JL. MacIver AG, Tate D, Slapak M. Varying expression of major histocompatibility complex antigens on human renal endothelium and epithelium. *Br J Exp Pathol.* (1985) 66:79–87.
173. Rui-Mei L, Kara AU, Sinniah R. Upregulation of major histocompatibility complex (MHC) antigen in nephritis associated with murine malaria infection. *J Pathol*. (1998) 185:212. doi: 10.1002/(SICI)1096-9896(199806)185:2<212::AID-PATH61>3.0.CO;2-T
174. Cong R, Li Y, Biemesderfer D. ADAM 10 activity sheds the ectodomain of the amyloid precursor like protein-2 and regulates protein expression in proximal tubule cells. *Am J Physiol Cell Physiol*. (2011). 300:C1366–74 doi: 10.1152./ajpcell.00451.2010
175. Djudjaj S, Martin IV, Buhl EM, Nothofer NJ, Leng L, Piecychna M. Macrophage migration inhibitory factor limits renal inflammation and fibrosis by counteracting tubular cell cycle arrest. *J Am Soc Nephrol.* (2017) 28:3590–604. doi: 10.1681/ASN.2017020190
176. Do HS, Park SW, Im I, Seo D, Yoo HW, Go H. Enhanced thrombospondin-1 causes dysfunction of vascular endothelial cells derived from Fabry disease-induced pluripotent stem cells. *EBioMedicine*. (2020) 52:102633. doi: 10.1016/j.ebiom.2020.102633
177. Ishiguro K, Kadomatsu K, Kojima T, Muramatsu H, Matsuo S, Kusugami, K. Syndecan-4 Deficiency Increases Susceptibility to κ-Carrageenan–Induced Renal Damage. *Lab Invest*. (2001) 81:509–16. doi: 10.1038/labinvest.3780259
178. Lindgren D, Eriksson P, Krawczyk K, Nilsson H, Hansson J, Veerla S. Cell-type-specific gene programs of the normal human nephron define kidney cancer subtypes. *Cell Rep*. (2017) 20:1476–89 doi: 10.1016/jcelrep07.(2017)043
179. Zhang Y, Narayanan SP, Mannan R, Raskind G, Wang X, Vats P. Single-cell analyses of renal cell cancers reveal insights into tumor microenvironment, cell of origin, and therapy response. *Proc Natl Acad Sci U S A*. (2021) 118:e2103240118. doi: 10.1073/pnas.2103240118
180. Carrega P, Bonaccorsi I, Carlo Di, Morandi E, Paul B, Rizzello P. V, et al. CD56(bright)perforin(low) noncytotoxic human NK cells are abundant in both healthy and neoplastic solid tissues and recirculate to secondary lymphoid organs via afferent lymph. *J Immunol.* (2014) 192:3805–15. doi: 10.4049/jimmunol.1301889
181. Kassianos AJ, Wang X, Sampangi S, Afrin S, Wilkinson R, Healy H. Fractalkine-CX3CR1-dependent recruitment and retention of human CD1c+ myeloid dendritic cells by *in vitro*-activated proximal tubular epithelial cells. *Kidney Int*. (2015) 87:1153–63. doi: 10.1038/ki.2014.407
182. Law BMP, Wilkinson R, Wang X, Kildey K, Lindner M, Rist MJ. Interferon-γ production by tubulointerstitial human CD56bright natural killer cells contributes to renal fibrosis and chronic kidney disease progression. *Kidney Int.* (2017) 92:79–88. doi: 10.1016/j.kint.2017.02.006
183. Wang X, Wilkinson R, Kildey K, Potriquet J, Mulvenna J, Lobb RJ. Unique molecular profile of exosomes derived from primary human proximal tubular epithelial cells under diseased conditions. *J Extracell Vesicles*. (2017) 6:1314073 doi: 10.1080/2002017.(13078)1314073
184. Riedel JH, Becker M, Kopp K, Düster M, Brix SR, Meyer-Schwesinger C. IL-33–mediated expansion of type 2 innate lymphoid cells protects from progressive glomerulosclerosis. *J Am Soc Nephrol*. (2017) 28:2068–80. doi: 10.1681/ASN.2016080877
185. Chevrier S, Levine JH, Zanotelli VRT, Silina K, Schulz D, Bacac M. An immune atlas of clear cell renal cell carcinoma. *Cell*. (2017) 169:736–749e18. doi: 10.1016/j.cell.2017.04.016
186. Young MD, Mitchell TJ, Vieira Braga FA, Tran MGB, Stewart BJ, Ferdinand JR. Single-cell transcriptomes from human kidneys reveal the cellular identity of renal tumors. *Science.* (2018) 361:594–9. doi: 10.1126/science.aat1699
187. Law BMP, Wilkinson R, Wang X, Kildey K, Giuliani K, Beagley KW. Human tissue-resident mucosal-associated invariant T (MAIT) cells in renal fibrosis and CKD. *J Am Soc Nephrol.* (2019) 30:1322–35. doi: 10.1681/ASN.2018101064
188. So WKW, Chan DNS, Law BMH, Choi KC, Krishnasamy M, Chan CWH. Effector γδ T cells in human renal fibrosis and chronic kidney disease. *Nephrol Dial Transplant*. (2019) 34:40–8. doi: 10.1093/ndt/gfy098
189. Park JG, Na M, Kim MG, Park SH, Lee HJ, Kim DK, et al. Author Correction: Immune cell composition in normal human kidneys. *Sci Rep*. (2021) 11:4313. doi: 10.1038/s41598-021-83841-6
190. Cheval L, Pierrat F, Rajerison R, Piquemal D, Doucet A. Of mice and men: divergence of gene expression patterns in kidney. *PLoS ONE*. (2012) 7:e46876. doi: 10.1371/journal.pone.0046876
191. Terpstra AH. Differences between humans and mice in efficacy of the body fat lowering effect of conjugated linoleic acid: role of metabolic rate. *J Nutr*. (2001) 131:2067–8. doi: 10.1093/jn/131.7.2067
192. Nzerue CM, Demissochew H, Tucker JK. Race and kidney disease: role of social and environmental factors. *J Natl Med Assoc*. (2002) 94(Suppl. 8):28S—8S.
193. Tschöp MH, Speakman JR, Arch JRS, Auwerx J, Brüning JC, Chan L. A guide to analysis of mouse energy metabolism. *Nat Methods.* (2011) 9:57–63. doi: 10.1038/nmeth.1806
194. Kazancioglu R. Risk factors for chronic kidney disease: an update. *Kidney Int Suppl.* (2013) 3:368–71. doi: 10.1038/kisup.2013.79
195. Obrador GT, Schultheiss UT, Kretzler M, Langham RG, Nangaku M, Pecoits-Filho R. Genetic and environmental risk factors for chronic kidney disease. *Kidney Int Suppl.* (2017) 7:88–106. doi: 10.1016/j.kisu.2017.07.004
196. Toyama T, Kitagawa K, Oshima M, Kitajima S, Hara A, Iwata Y. Age differences in the relationships between risk factors and loss of kidney function: a general population cohort study. *BMC Nephrol.* (2020) 21:477. doi: 10.1186/s12882-020-02121-z
197. Norris KC, Beech BM. Social determinants of kidney health: focus on poverty. *Clin J Am Soc Nephrol.* (2021) 16:809–11. doi: 10.2215/CJN.12710820
198. Luyckx VA, Al-Aly Z, Bello AK, Bellorin-Font E, Carlini RG, Fabian J. Publisher correction: sustainable development goals relevant to kidney health: an update on progress. *Nat Rev Nephrol.* (2021) 17:704. doi: 10.1038/s41581-021-00473-9
199. Vernier RL. Ultrastructure of the glomerulus and changes in fine structure associated with increased permeability of the glomerulus to protein. In: *Ciba Foundation Symposium-Renal Biopsy: Clincal and Pathological Significance*. Wiley Online Library. (1961). p. 4–31.
200. Pozzi A, Zent R. Integrins in kidney disease. *J Am Soc Nephrol.* (2013) 24:1034–9. doi: 10.1681/ASN.2013010012
201. Lazareth H, Lenoir O, Tharaux PL. Parietal epithelial cells role in repair versus scarring after glomerular injury. *Curr Opin Nephrol Hypertens*. (2020) 29:293–301. doi: 10.1097/MNH.0000000000000600

202. Jones SD, van der Flier A, Sonnenberg A. Genomic organization of the human alpha 3 integrin subunit gene. *Biochem Biophys Res Commun.* (1998) 248:896–8. doi: 10.1006/bbrc.1998.9071
203. Tarone G, Hirsch E, Brancaccio M, De Acetis M, Barberis L, Balzac F, et al. Integrin function and regulation in development. *Int J Dev Biol.* (2004) 44:725–31.
204. Anderson LR, Owens TW, Naylor MJ. Integrins in development and cancer. *Biophys Rev.* (2014) 6:191–202. doi: 10.1007/s12551-013-0123-1
205. Zhuo JL, Proximal LiXC. nephron. *Compr Physiol.* (2013) 3:1079–123. doi: 10.1002/cphy.c110061

Conflict of Interest: The authors declare that the research was conducted in the absence of any commercial or financial relationships that could be construed as a potential conflict of interest.

Publisher's Note: All claims expressed in this article are solely those of the authors and do not necessarily represent those of their affiliated organizations, or those of the publisher, the editors and the reviewers. Any product that may be evaluated in this article, or claim that may be made by its manufacturer, is not guaranteed or endorsed by the publisher.

frontiers | Frontiers in Medicine

TYPE Original Research
PUBLISHED 28 September 2022
DOI 10.3389/fmed.2022.971297

OPEN ACCESS

EDITED BY
Andrew Mallett,
Townsville University Hospital, Australia

REVIEWED BY
Pravin C. Singhal,
North Shore Long Island Jewish Health System, United States
Karl Skorecki,
Bar-Ilan University, Israel

*CORRESPONDENCE
Marguerite R. Irvin
irvinr@uab.edu

SPECIALTY SECTION
This article was submitted to Nephrology, a section of the journal Frontiers in Medicine

RECEIVED 16 June 2022
ACCEPTED 29 August 2022
PUBLISHED 28 September 2022

CITATION
Chaudhary NS, Armstrong ND, Hidalgo BA, Gutiérrez OM, Hellwege JN, Limdi NA, Reynolds RJ, Judd SE, Nadkarni GN, Lange L, Winkler CA, Kopp JB, Arnett DK, Tiwari HK and Irvin MR (2022) *SMOC2* gene interacts with *APOL1* in the development of end-stage kidney disease: A genome-wide association study. *Front. Med.* 9:971297. doi: 10.3389/fmed.2022.971297

SMOC2 gene interacts with *APOL1* in the development of end-stage kidney disease: A genome-wide association study

Ninad S. Chaudhary[1,2], Nicole D. Armstrong[1], Bertha A. Hidalgo[1], Orlando M. Gutiérrez[3], Jacklyn N. Hellwege[4], Nita A. Limdi[5], Richard J. Reynolds[6], Suzanne E. Judd[7], Girish N. Nadkarni[8], Leslie Lange[9], Cheryl A. Winkler[10], Jeffrey B. Kopp[11], Donna K. Arnett[12], Hemant K. Tiwari[7] and Marguerite R. Irvin[1]*

[1]Department of Epidemiology, University of Alabama at Birmingham, Birmingham, AL, United States, [2]Department of Epidemiology, Human Genetics, and Environmental Sciences, School of Public Health, Human Genetics Center, University of Texas Health Science Center at Houston, Houston, TX, United States, [3]Department of Medicine, University of Alabama at Birmingham, Birmingham, AL, United States, [4]Division of Genetic Medicine, Department of Medicine, Vanderbilt Genetics Institute, Vanderbilt Epidemiology Center, Vanderbilt University Medical Center, Nashville, TN, United States, [5]Department of Neurology, University of Alabama at Birmingham, Birmingham, AL, United States, [6]Division of Clinical Immunology and Rheumatology, Department of Medicine, University of Alabama at Birmingham, Birmingham, AL, United States, [7]Department of Biostatistics, University of Alabama at Birmingham, Birmingham, AL, United States, [8]Division of Data-Driven and Digital Medicine (D3M), Icahn School of Medicine at Mount Sinai, New York, NY, United States, [9]Department of Medicine, University of Colorado Denver - Anschutz Medical Campus, Denver, CO, United States, [10]Basic Research Program, National Cancer Institute, National Institutes of Health, Frederick National Laboratory for Cancer Research, Frederick, MD, United States, [11]National Institute of Diabetes and Digestive and Kidney Diseases, National Institutes of Health, Bethesda, MD, United States, [12]Deans Office, College of Public Health, University of Kentucky, Lexington, KY, United States

Background: Some but not all African-Americans (AA) who carry *APOL1* nephropathy risk variants (*APOL1*) develop kidney failure (end-stage kidney disease, ESKD). To identify genetic modifiers, we assessed gene–gene interactions in a large prospective cohort of the REasons for Geographic and Racial Differences in Stroke (REGARDS) study.

Methods: Genotypes from 8,074 AA participants were obtained from Illumina Infinium Multi-Ethnic AMR/AFR Extended BeadChip. We compared 388 incident ESKD cases with 7,686 non-ESKD controls, using a two-locus interaction approach. Logistic regression was used to examine the effect of *APOL1* risk status (using recessive and additive models), single nucleotide polymorphism (SNP), and *APOL1**SNP interaction on incident ESKD, adjusting for age, sex, and ancestry. *APOL1**SNP interactions that met the threshold of 1.0×10^{-5} were replicated in the Genetics of Hypertension Associated Treatment (GenHAT) study (626 ESKD cases and 6,165 controls). In a sensitivity analysis, models were additionally adjusted for diabetes status. We conducted additional replication in the BioVU study.

Results: Two *APOL1* risk alleles prevalence (recessive model) was similar in the REGARDS and GenHAT studies. Only one *APOL1*–SNP interaction,

for **rs7067944** on chromosome 10, ~10 KB from the *PCAT5* gene met the genome-wide statistical threshold ($P_{interaction} = 3.4 \times 10^{-8}$), but this interaction was not replicated in the GenHAT study. Among other relevant top findings (with $P_{interaction} < 1.0 \times 10^{-5}$), a variant (**rs2181251**) near *SMOC2* on chromosome six interacted with *APOL1* risk status (additive) on ESKD outcomes (REGARDS study, $P_{interaction} = 5.3 \times 10^{-6}$) but the association was not replicated (GenHAT study, $P_{interaction} = 0.07$, BioVU study, $P_{interaction} = 0.53$). The association with the locus near *SMOC2* persisted further in stratified analyses. Among those who inherited ≥1 alternate allele of rs2181251, *APOL1* was associated with an increased risk of incident ESKD (OR [95%CI] = 2.27[1.53, 3.37]) but *APOL1* was not associated with ESKD in the absence of the alternate allele (OR [95%CI] = 1.34[0.96, 1.85]) in the REGARDS study. The associations were consistent after adjusting for diabetes.

Conclusion: In a large genome-wide association study of AAs, a locus *SMOC2* exhibited a significant interaction with the *APOL1* locus. *SMOC2* contributes to the progression of fibrosis after kidney injury and the interaction with *APOL1* variants may contribute to an explanation for why only some *APOLI* high-risk individuals develop ESKD.

KEYWORDS

***APOL1*, gene–gene interaction, SMOC2, kidney disease, end-stage kidney disease, genome-wide analysis, African-Americans**

Introduction

Two risk variants in the *APOL1* gene on chromosome 22, collectively referred to as *APOL1* nephropathy risk alleles are associated with an increased risk of chronic kidney disease, and kidney failure (end-stage kidney disease, ESKD) among self-reported African-American (AA) individuals (1, 2). However, these variants are not completely penetrant for kidney disease incidence or progression, and a better understanding of the role of modifying environmental and/or genetic factors are needed (3, 4). The extent of molecular interactions in gene regulation and metabolic systems suggests that the interactive relationship between DNA variants can better explain the biological underpinnings of clinical endpoints than analysis based only on the variants.

Previous studies have investigated the role of various single nucleotide polymorphisms (SNPs) and the *APOL1* risk variants in kidney diseases (5–7). Bostrom et al. (5) performed a case-control association study of 1,420 SNPs in 962 AA non-diabetic nephropathy cases and 932 AA non-nephropathy controls. They found six SNPs that met an interactive *p*-value threshold of 0.001 with *APOL1* variants, under recessive, additive, or dominant models (5). Divers et al. (6) expanded these findings in a larger sample size of 1,367 AA non-diabetic ESKD patients and 1,504 related controls using a similar pooled set of SNPs specific to kidney diseases. The study examined interactions among the top 42 genes identified in the main effects association analysis, and found a variant, rs16854341, in the podocin gene to be of particular importance (6). Although the variant did not meet the genome-wide significant threshold, the presence of this variant reduced the odds of developing ESKD due to *APOL1* risk variants. These studies focused on populations without diabetes and identified only genes relevant to non-diabetic nephropathy.

In the present study, using genotype data from 8,074 AA participants from a community sample of the REasons for Geographic and Racial Differences in Stroke study (REGARDS), we tested whether SNPs from GWAS modify the association of *APOL1* risk variants with ESKD in a different AA cohort. Genotypic data was obtained from a contemporary 1.4 million SNPs multi-ethnic genotype array, which was further enriched for extensive new African variant coverage. The findings were replicated in 6,791 AA from the Genetics of Hypertension Associated Treatment (GenHAT) study using the same array.

Methods

Discovery population

The REGARDS study is one of the largest ongoing prospective population-based studies in the U.S. and was designed to measure stroke incidence and associated risk factors in AA and European-Americans adults ≥45 years of age (8). From January 2003 to October 2007, 30,239 participants (42% AA, 55% women) were recruited from the 48 contiguous U.S.

states and the District of Columbia. At baseline, demographics, medical history, and clinical data were obtained via telephone and an in-home visit. Blood and urine samples were also obtained at the baseline in-home visit. Participants were subsequently contacted every 6 months by telephone to assess data on new-onset stroke, coronary heart disease, and death which was further adjudicated by retrieving the pertinent medical records. Additionally, a linkage with United States Renal Dialysis System (USRDS) was established to identify participants who may have developed ESKD during the follow-up (9). After limiting the participants to those with known ESKD status and *APOL1* status as well as meeting the quality control standards of genotyping (see below), the data on 8,074 AA participants were available for analysis.

Replication populations

Genetics of Hypertension Associated Treatment is a pharmaco-genetic ancillary study to the Anti-hypertensive and Lipid-Lowering Treatment to Prevent Heart Attack Trial (ALLHAT), designed to identify the genes associated with anti-hypertensive treatment response that can potentially modify the risk of cardiovascular outcomes (10). Anti-hypertensive and Lipid-Lowering Treatment to Prevent Heart Attack Trial was the largest randomized, double-blind multi-center anti-hypertensive clinical trial, and included persons ≥55 years with hypertension and at least one cardiovascular risk factor (11). Participants were evaluated at 3, 6, 9, and 12 months during the first year, and every 4 months thereafter to monitor adherence to the treatment plan and to collect clinical data and blood and urine samples. Data on estimated glomerular filtration rate and ESKD were obtained as secondary outcomes. The present analytical sample consisted of 6,791 AA participants who met the inclusion criteria described above for the REGARDS study. Additional replication at one locus (*SMOC2*) was conducted in the Vanderbilt Biobank of DNA (BioVU DNA) repository. The BioVU DNA Repository is a deidentified database of electronic health records (EHR) that are linked to patient DNA samples at Vanderbilt University Medical Center. A detailed description of the database and how it is maintained has been published elsewhere (12).

Genotyping

Genome-wide genotyping was performed within each study independently using Illumina Infinium Multi-Ethnic AMR/AFR BeadChip Arrays (MEGA chip; Illumina, San Diego, CA). Similar imputation and quality control procedures were implemented for REGARDS and GenHAT study groups. Briefly, data were imputed using the NHLBI TOPMed release 2 reference panel (Freeze 8) using the TOPMED Imputation server developed at the University of Michigan (13, 14). Around one million variants in the REGARDS study and 970k variants in the GenHAT study were imputed. Samples with call rates <95%, internal duplicates, or sex mismatches were removed. Ancestry information was obtained using principal component analysis in the EIGENSTRAT program (15, 16). Individuals who were outliers for ancestry (more than six standard deviations) were removed. Approximately 21 million variants were available for association analysis with imputation quality scores (MACH r^2) ≥0.3 and minor allele count ≥20 in both the REGARDS and GenHAT populations. Quality control for the BioVU cohort included excluding samples or variants with missingness rates above 2%. Samples were also excluded if consent had been revoked, a sample was duplicated, or failed sex concordance checks. The data for BioVU was also imputed using the NHLBI TOPMed release 2 reference panel (Freeze 8).

APOL1 genotyping

APOL1 risk variants consist of two missense mutations (rs73885319 and rs60910145) (together labeled as G1), and one 6-bp deletion (rs71785313; labeled as G2). The G1 risk alleles are 128 bp apart and are in perfect or almost perfect disequilibrium representing the G1 haplotype (1, 17, 18). These variants were directly identified in the REGARDS study using TaqMan SNP Genotyping Assays in prior projects (19, 20). The number of *APOL1* risk alleles was recorded as two copies if participants had either G1/G1, G1/G2, or G2/G2 and one copy if participants had G1/G0 or G2/G0. The state of G0/G0 indicates absence of both G1 and G2 variants. The primary genetic inheritance model was additive, such that each risk allele conferred additional risk while the secondary genetic inheritance model was recessive so that those with zero or one copy were compared to those with two copies. Data for *APOL1* variants in the GenHAT study were obtained using the genotypic array data. The genotyped data on the rs143830837 variant (hg38 base pair, 36265995) was available in GenHAT instead of rs71785313 (hg38 base pair 36265996). Single nucleotide polymorphism (SNP) rs14383087 is merged with rs71785313 in subsequent assembly as reported in the NCBI dbSNP database (https://www.ncbi.nlm.nih.gov/snp/?term=rs143830837) and are the same variants. BioVU *APOL1* was assessed using variants directly genotyped on the MEGA array (only G2 and one of the G1 SNPs). The imputation of both G1 SNPs was evaluated and had 99.9% concordance with the directly genotyped G1 variant.

Outcomes

The main study outcome was incident ESKD, identified using an existing linkage of the REGARDS study with USRDS data accessed through December 2019 (9). The USRDS is

a comprehensive national registry that collects, analyzes, and distributes information on the ESKD population in the U.S., including treatment failure and mortality (21). For the REGARDS study with available *APOL1* data, there were 388 incident ESKD events retrieved via the USRDS link. In the GenHAT study, incident ESKD ($n = 128$) was recorded if the participant started on dialysis or had a kidney transplant. In the BioVU study, ESKD was identified using diagnostic (ICD 9 and 10) codes for dialysis (2 or more instances of codes V45.11 or Z99.2), kidney transplant (2 or more instances of codes V42.0 or Z94.0), and ESKD (5 or more instances of codes 585.6 or N18.6) across the entire available deidentified electronic medical record.

Covariates

Information on age, sex, and diabetes status was obtained from baseline visits in both studies. Diabetes mellitus in the REGARDS study was defined as fasting serum glucose ≥126 mg/dl, non-fasting serum glucose ≥200 mg/dl, or use of glucose-lowering medication. Diabetes mellitus in the GenHAT study was defined as fasting serum glucose >140 mg/dl, or non-fasting serum glucose >200 mg/dl in the past 2 years, and/or use of injected or oral insulin or oral hypoglycemic agents. In BioVU EHR data, age was assigned as the earliest outcome code age for cases, and the age at the end of their medical record for controls (i.e., the latest age at which they were determined to be ESKD-free). Diabetes status for the BioVU study was assigned based on ICD codes, and hypertension status was defined as taking anti-hypertension medications, having two or more ICD codes for hypertension, or having two or more outpatient blood pressures >140/90.

Statistical analysis

Baseline characteristics of both the REGARDS and GenHAT population were tabulated. PLINK2 software was used to perform logistic regression for incident ESKD outcomes, including a term for two-locus interaction (22). For this approach, *APOL1* risk status was analyzed under the additive model and the recessive genetic model (binary variable). Each GWAS SNP was analyzed under an additive genetic model such that each analytical model consisted of *APOL1* risk status, SNP, *APOL1**SNP, age, sex, and principal components of ancestry. The genome-wide threshold for significant interaction was $P_{\text{interaction}} < 5.0 \times 10^{-8}$. As the interaction studies of *SNP–SNP* or *SNP*–environment suffer greater power limitations compared to main effect SNP studies, there is a greater chance that variants of potential biological significance may be missed (type II error). We accordingly applied a liberal threshold of $P_{\text{interaction}} < 1.0 \times 10^{-5}$ to identify any SNPs of potential biological significance (referred below as "potentially relevant SNPs"). For the replication, we highlighted SNPs with marginal significance ($P_{\text{interaction}} < 0.05$). A $P_{\text{interaction}} < 0.006$ was required to meet the statistically significant threshold for testing of eight variants in the replication data using Bonferroni correction. Odds ratios (ORs) for the *APOL1* association with ESKD are presented for those with and without at least one alternate allele of the GWAS SNP of interest. Gene annotation was completed using ANNOVAR (23). Manhattan and QQ plots for $P_{\text{interaction}}$ terms were generated using the R package qqman (24).

Because previously published studies were conducted among cases with non-diabetic nephropathy, we examined significant SNPs from discovery, by adjusting for diabetes in a sensitivity analysis. We further tested the associations in a sub-group of REGARDS participants who did not have diabetes at baseline. Finally, we report the estimates from both the discovery and replication cohorts for 14 SNPs that were statistically significant in earlier *APOL1*–SNP interaction studies for comparison (5, 6).

Results

Among 8,074 participants in the REGARDS study, 3,357 had zero *APOL1* risk alleles, 3,697 had one risk allele, and 1,020 (13%) had two risk alleles. Similarly, the GenHAT study had 871 participants with two *APOL1* risk alleles, accounting for 13% of the cohort. The mean age of participants was 63.6 years (SD = 9.2) in REGARDS and 66.1 years (SD = 7.7) in GenHAT. Participants in the REGARDS study were less likely to be male compared to GenHAT (Table 1). While all the participants in GenHAT had a diagnosis of hypertension, 71% of REGARDS participants had a diagnosis of hypertension. The GenHAT inclusion criteria required participants to have hypertension and at least one other cardiovascular risk factor, and so the prevalence of diabetes was higher in GenHAT compared to REGARDS. Participants in the BioVU study were younger [mean (SD) = 47.0 (17.0)] compared to other studies. Characteristics of the BioVU study population can be found in Supplementary Table 1.

Manhattan and QQ Plots discovery analysis in REGARDS are presented in Figure 1 (Left and Right panels) and Supplementary Figure 1. Only one variant (rs7067944) on chromosome 10 (∼10 kB from the *PCAT5* gene) interacted with *APOL1* under additive inheritance with statistical significance after correcting for multiple testing ($P_{\text{interaction}} = 3.4 \times 10^{-8}$). Two SNPs in the same region almost met the statistical significance threshold (Table 2). None of these top SNPs were replicated in the GenHAT study. A total of 183 SNPs interacted with *APOL1* risk status under the additive genetic model with $P_{\text{interaction}} < 1.0 \times 10^{-5}$ for incident ESKD. Two loci of interest in REGARDS included *RNLS* (rs536243, $P_{\text{interaction}} = 3.6 \times 10^{-7}$) and *SYMD3* (rs75431828, $P_{\text{interaction}} = 1.3 \times 10^{-7}$) but these loci did not replicate in GenHAT ($P_{\text{interaction}}$

TABLE 1 Baseline characteristics of discovery and replication cohort.

	REGARDS (discovery)	GenHAT (replication)
Mean (SD) or *N* (%)	8,074	6,791
Age	63.6 (9.2)	66.1 (7.7)
Male	3,177 (39.4)	3,028 (44.6)
Diabetes at baseline	2,330 (29.2)	4,063 (59.8)
Hypertension at baseline	5,738 (71.2)	6,791 (100)
Incident ESKD	388 (4.8)	128 (1.9)
APOL1 risk alleles		
0	3,357 (41.6)	3,032 (44.6)
1	3,697 (45.7)	2,888 (42.5)
2	1,020 (12.6)	871 (12.8)

ESKD, end-stage kidney disease; REGARDS, REasons for Geographic and Racial Difference in Stroke; GenHAT, Genetics of Hypertension Associated Treatment.

> 0.05). See Supplementary File 1 Dataset S1 for the 183 top results in REGARDS along with the corresponding replication in GenHAT. When considering *APOL1* under a recessive genetic inheritance model, none of the variants met the genome-wide statistical significance threshold. However, 147 SNPs interacted with *APOL1* risk status with $P_{\text{interaction}} < 1.0 \times 10^{-5}$ for incident ESKD. Among these, the top hit for the recessive model was an intronic variant on the *SMOC2* gene located at chromosome 6 (rs62423404, *p*-interaction $= 1.88 \times 10^{-7}$); this was a region of interest identified in the *APOL1* additive inheritance model.

Among 183 SNPs identified in the discovery analysis for an additive inheritance, only five had a consistent direction of the interaction term in the GenHAT study (Table 2, Supplementary Table 2). Of those five SNPs (one intronic on SMOC2 gene, and four intergenic between *SMOC2* and *LOC105378146* on chromosome 6), rs62423403 was the most statistically significant (REGARDS $P_{\text{interaction}} = 8.0 \times 10^{-6}$) and rs2181251 had the most consistent magnitude of association in both studies. Carriers of the alternate allele at rs2181251 variant had increased risk for ESKD associated with *APOL1* (OR [95%CI]: REGARDS: 2.27 [1.53, 3.37]; GenHAT: 1.83 [1.19, 2.81]), while non-carriers did not have elevated risk associated with *APOL1* (OR [95%CI] = 1.34 [0.96, 1.85]). The relationship was also similar for the other SNPs (Table 2). The associations for potentially-relevant variants of biological significance were similar for the *APOL1* recessive model in both REGARDS and GenHAT studies (Table 3).

In the sensitivity analysis adjusting for diabetes status, the *APOL1*–SNP interactions for the four SNPs near *SMOC2* were consistent with the primary analysis in REGARDS as well as in the GenHAT replication cohort (Supplementary Tables 3, 4). Results were also consistent when the analysis was restricted to participants without diabetes in each study (Supplementary Tables 3, 4). Although the direction and strength of the associations between *APOL1* risk variants and ESKD were consistent among those with at least one minor allele of SNP of interest, the *p*-interaction value for SNPs did not replicate in the BioVU study (Supplementary Tables 5, 6). None of the SNPs from prior studies were replicated in our cohort (Supplementary Tables 7, 8).

Discussion

In this study of *APOL1* by gene interaction in community-dwelling AA with incident ESKD, we found a potential modifier locus that increased the risk of ESKD. *APOL1* risk status was significantly associated with incident ESKD among carriers but not among non-carriers of a minor allele at five SNPs near *SMOC2*. The findings were consistent with those in GenHAT (another large population of AA from a clinical trial of anti-hypertensive agents), but in GenHAT the interaction term did not meet the criteria for statistical significance. These variants are of interest due to the role of *SMOC2* in kidney injury. Further, findings from previous studies of *APOL1*-by-SNP interaction were not significant among participants without diabetes in the present study.

The primary SNPs identified in REGARDS (*rs2181251, rs62423451, rs11751195, rs4286744*) were in an intergenic region 2–5 kb downstream from the *SMOC2* gene. Additionally, another variant of interest (*rs62423403*) was intronic in the protein-coding transcript of the *SMOC2* gene. The relationship of *APOL1* with ESKD was heightened in the minor allele carriers of these SNPs. The relationship between *APOL1* and ESKD was OR [95% CI] = 4.38 (2.70, 7.12) for rs62323403 minor allele carriers vs. 1.00 (0.70, 1.42) for the common variant under the recessive model in REGARDS. Though potentially artifactual due to the restricted sample, these carrier differences were strongest among REGARDS participants without diabetes at baseline. For example, in our sensitivity analysis the *APOL1* OR [95% CI] for rs62423451 carriers was 8.2 [4.1, 16.5] and for non-carriers was 1.35[0.78, 2.35].

SMOC2 (SPARC-related modular calcium binding 2) is a protein-coding gene influencing growth factor signaling, migration, proliferation, and angiogenesis (25, 26). SMOC2 protein is upregulated in renal tubular epithelial cells of kidney biopsies showing pathological fibrosis and SMOC2 plays a role in the progression of fibrosis (27). *SMOC2* is overexpressed in cell culture in response to angiotensin II-related progression of podocyte injury (28). APOL1 protein may not be expressed in tubular cells and filtered APOL1 could potentially interact with SMOC2 protein in podocytes inducing injury and subsequent proteinuria. In our analyses, the interaction effect between *SMOC2* and *APOL1* was present in absence of a main effect of the SNPs near *SMOC2*; this could explain the lack of data on this gene in a single-locus analysis. Still detecting a physical

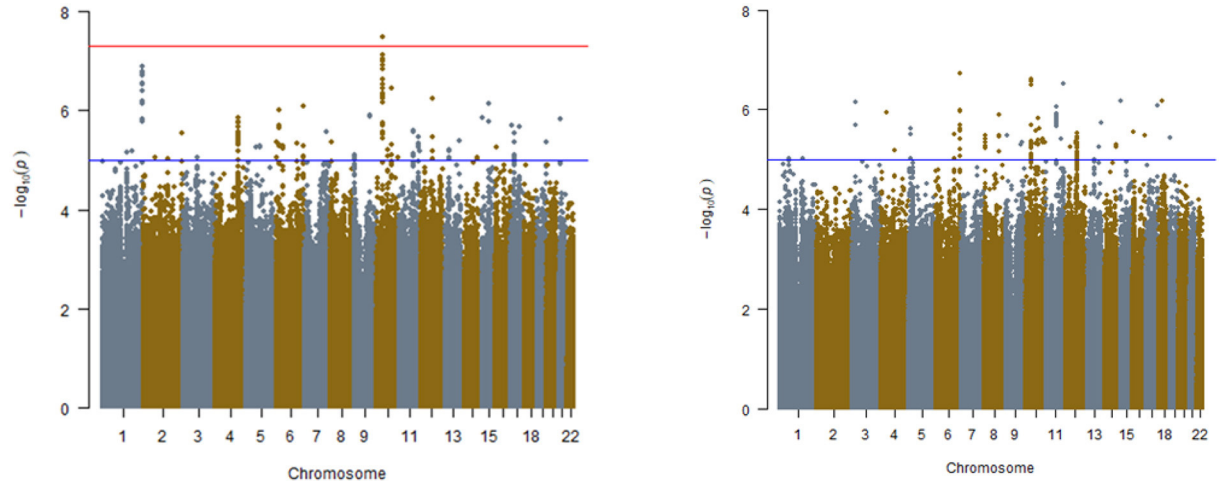

FIGURE 1
Manhattan plots for interaction analyses in REGARDS study. **(Left)** *APOL1* risk status determined by additive model, **(Right)** *APOL1* risk status determined by recessive model. Models include *APOL1*, SNP, *APOL1**SNP, age, sex, and ancestry. The red line is indicative of genome-wide significance $p \leq 5.00 \times 10^{-08}$. Blue line is indicative of suggestive significance, $p \leq 1.00 \times 10^{-05}$.

interaction is beyond the scope of population genetic studies such as ours. Additional population studies of ESKD among AA with and without diabetes are warranted.

We identified two loci, *RNLS* (encoding renalase) and *SMYD3* (SET and MYND domain containing 3), that are associated with kidney disorders in the REGARDS study but did not replicate in the GenHAT study. The *RNLS* renalase gene has been associated with ESKD and chronic kidney disease in prior studies (7, 29, 30). The gene codes for a protein secreted by the kidney which decreases systemic blood pressure in response to an increase in blood pressure or release of catecholamines, and regulates cardiovascular function (31). As renalase expression is associated with chronic kidney disease, the interesting possibility that *APOL1* interacts with this pathway requires further investigation. Additionally, *SMYD3* may contribute to autosomal dominant polycystic kidney disease and renal carcinoma via its lysine methyltransferase activity (32, 33). The variants that met the genome-wide statistical significance threshold for the *APOL1**SNP interaction were in the intergenic region of *PCAT5* and *ANKRD30A* genes which have not previously been linked to kidney function and further characterization are warranted.

Differences between our study and prior gene modifier studies of *APOL1*-renal risk are that other studies focused on SNPs with main effects on ESKD as well as data from participants with non-diabetic ESKD. Bostrom et al. and Divers et al. examined a similar set of ESKD-related SNPs highlighting potential *APOL1* modifier variants in *NPHS2*, *SDCCAG8*, and *BMP4* (all known nephropathy loci) (5–7, 34, 35). In another study that used a case-only design, *APOL1* risk genotypes were associated with a variant, rs79741405 (base pair: 160673237), on chromosome 6 but this locus was far from the SNPs we identified on chromosome 6 in our study (7). Unfortunately, none of these variants were replicated in our study. One possible explanation could be the broader ESKD definition used in our study. However, our results did not change after adjusting our analyses for diabetes and/or restricting to those without diabetes at baseline.

A strength of our study was the use of more contemporary genotype data enriched for additional African variant coverage in three large cohorts of AA which allowed us to better define population substructure and test for additional variants. The identification of incident events from prospective cohort studies may have reduced selection bias as non-ESKD controls are representative of the population that produced the cases. Being a population-based study, there are always chances of measurement bias. Specifically, we could not discern the specific type of nephropathy or underlying cause associated with ESKD diagnosis in our cohorts. Better characterizing of phenotypes in our study as well as harmonizing of the phenotypes with prior studies could have improved our consistency with other published studies. BioVU study is an EHR-based study, and the population was younger compared to REGARDS and GenHAT. We did not test whether the interaction effects are age-dependent but there is a chance that biological mechanisms driven by these variants could be age-related. We cannot rule out the possibility that a higher rate of incident ESKD could also be a proxy for improved survival of CKD. APOL1 high-risk genotypes are associated with better survival after accounting for kidney-related comorbidities and genetic ancestry (36). However, high-risk APOL1 status has been associated with the progression of kidney function to ESKD among those

TABLE 2 Top APOL1–SNP interaction effects on ESKD in the REGARDS and GenHAT studies under *APOL1* additive model.

Gene	Region	rsID	Chr	BP (hg38)	R	A	EAF	REGARDS			GenHAT		
***APOL1* additive**								***APOL1* OR (95%CI)**		$P_{interaction}$	***APOL1* OR (95%CI)**		$P_{interaction}$
								≥1 GWAS SNP minor alleles	**0 GWAS SNP MINOR Alleles**		**≥1 GWAS SNP minor alleles**	**0 GWAS SNP MINOR Alleles**	
Statistically significant SNPs													
PCAT5;ANKRD30A	Intergenic	*rs7067944*	chr10	35810852	A	G	0.54	1.23 (0.90, 1.67)	3.19 (1.99, 5.11)	3.4E-08	1.48 (1.10, 1.99)	0.93 (0.60, 1.55)	0.45
PCAT5;ANKRD30A	Intergenic	*rs744372*	chr10	35809696	C	G	0.50	1.29 (0.96, 1.74)	3.11 (1.89, 5.15)	7.5E-08	1.44 (1.08, 1.93)	0.94 (0.54, 1.62)	0.68
PCAT5;ANKRD30A	Intergenic	*rs7086402*	chr10	35811113	T	C	0.54	1.28 (0.95, 1.75)	3.11 (1.91, 5.17)	8.9E-08	1.45 (1.08, 1.93)	0.85 (0.48, 1.50)	0.56
Potentially relevant SNPs													
SMOC2	Intronic	*rs62323403*	chr6	168647687	G	A	0.05	2.38 (1.78, 3.45)	1.03 (0.86, 1.22)	8.0E-07	1.66 (0.97, 2.83)	1.22 (0.91, 1.64)	0.27
SMOC2;LOC105378146	Intergenic	*rs2181251*	chr6	168669997	T	C	0.19	2.27 (1.53, 3.37)	1.34 (0.96, 1.85)	5.3E-06	1.83 (1.19, 2.81)	1.09 (0.80, 1.56)	0.07
SMOC2;LOC105378146	Intergenic	*rs62423451*	chr6	168672559	A	T	0.11	2.96 (1.78, 4.90)	1.34 (1.00, 1.80)	8.8E-06	2.10 (1.19, 3.71)	1.16 (0.87, 1.54)	0.20
SMOC2;LOC105378146	Intergenic	*rs11751195*	chr6	168672766	T	C	0.11	2.96 (1.78, 4.90)	1.34 (1.00, 1.80)	8.9E-06	2.10 (1.19, 3.71)	1.16 (0.87, 1.54)	0.20
SMOC2;LOC105378146	Intergenic	*rs4286744*	chr6	168672106	A	G	0.11	2.96 (1.78, 4.88)	1.34 (1.00, 1.80)	8.6E-06	2.10 (1.19, 3.71)	1.16 (0.87, 1.54)	0.28

Adjusted for age, sex, and principal components of ancestry; R, reference allele; A, alternate allele; EAF, effect allele frequency; chr, chromosome.

10.3389/fmed.2022.971297

TABLE 3 Top APOL1–SNP interaction effects on ESKD in the REGARDS and GenHAT studies under *APOL1* recessive model.

Gene	Region	rsID	Chr	BP (hg38)	R	A	EAF	REGARDS			GenHAT		
***APOL1* recessive**								***APOL1* OR (95%CI)**		$P_{interaction}$	***APOL1* OR (95%CI)**		$P_{interaction}$
								≥1 GWAS SNP minor alleles	**0 GWAS SNP minor alleles**		**≥1 GWAS SNP minor alleles**	**0 GWAS SNP minor alleles**	
Potentially relevant SNPs													
SMOC2	Intronic	*rs62323403*	chr6	168647687	G	A	0.05	4.38 (2.70, 7.12)	1.00 (0.70, 1.42)	1.8E-07	2.10 (0.86, 5.11)	1.38 (0.81, 2.35)	0.37
SMOC2;LOC105378146	Intergenic	*rs2181251*	chr6	168669997	T	C	0.19	2.27 (1.53, 3.37)	0.93 (0.62, 1.39)	8.5E-06	1.93 (0.93, 4.01)	1.28 (0.71, 2.30)	0.25
SMOC2;LOC105378146	Intergenic	*rs62423451*	chr6	168672559	A	T	0.11	2.96 (1.78, 4.90)	1.05 (0.73, 1.49)	1.1E-06	2.77 (1.10, 6.96)	1.26 (0.74, 2.15)	0.30
SMOC2;LOC105378146	Intergenic	*rs11751195*	chr6	168672766	T	C	0.11	2.96 (1.78, 4.90)	1.05 (0.73, 1.49)	1.1E-06	2.77 (1.10, 6.96)	1.26 (0.74, 2.15)	0.30
SMOC2;LOC105378146	Intergenic	*rs4286744*	chr6	168672106	A	G	0.11	2.96 (1.78, 4.90)	1.01 (0.7, 1.43)	1.1E-06	2.84 (1.13, 7.14)	1.25 (0.74, 2.13)	0.35

Adjusted for age, sex, and principal components of ancestry; R, reference allele; A, alternate allele; EAF, effect allele frequency; Chr, chromosome.

10.3389/fmed.2022.971297

with chronic kidney disease (37). Due to lack of multiple time-point measurements in our cohorts, we cannot discern these differences between improved survival and progression of CKD. While we found biologically relevant associations, we cannot rule out the possibility of type II error due to the underestimation of interaction effects in the standard regression-based interaction tests or lack of replication (38). However, the direction of the associations was consistent in the replication study which asserts the significance of these findings to a certain extent. Further translational work and well-powered studies can help determine if these associations are valid. *APOL1* is located at the Chromosome 22 locus which is enriched for intrachromosomal duplications and duplicated *APOL1* genotype segments with apparent risk genotypes have been observed in a few samples of 1,000 Genome population (39). Identifying such duplicated segments in our study population was beyond the scope of our study.

In conclusion, using a large GWAS effort in an AA population, we found that SNPs near the *SMOC2* gene had a significant interaction with *APOL1* in determining the risk of ESKD. In particular, *APOL1* was associated with a higher risk of ESKD in the presence of alternate alleles at those SNPs. The findings could help improve our understanding of the potential modifiers of *APOL1* risk status that contribute to the observed incomplete penetrance of that locus.

Data availability statement

Publicly available datasets were analyzed in this study. This data can be found here: The raw REGARDS genotype and phenotype data used in this study can be found in dbGaP accession number phs002719.v1.p1. The raw GenHAT genotypic and phenotypic data used in this study are deposited in the National Center for Biotechnology Information (NCBI) Database for Genotypes and Phenotypes (dbGaP), accession number phs002716.v1.p1. The genotypes and phenotypes from BioVU are available to researchers who meet the criteria for access to confidential data, upon request and clearance from Vanderbilt University Medical Center Institutional Review Board and BioVU. Interested and eligible researchers may contact the BioVU data access team at biovu@vanderbilt.edu for more detailed information regarding access to phenotype data from BioVU.

Ethics statement

The studies involving human participants were reviewed and approved by University of Alabama at Birmingham Institutional Review Board. The patients/participants provided their written informed consent to participate in this study.

Author contributions

NC, MI, OG, HT, BH, NL, and RR: contributed to the study design. MI, OG, CW, and JK: oversaw the genotyping performed for the parent study. NC, NA, JH, HT, and MI: data analysis and interpretation. SJ, MI, and LL: parent study participant recruitment and data collection. MI, JH, and DA: replication study, participant, data collection, and access. NC, HT, and MI: first draft preparation. NC, NA, MI, OG, HT, BH, NL, RR, CW, JK, SJ, GN, LL, DA, and JH: critical inputs on the manuscript. All authors contributed important intellectual content during manuscript drafting or revision and agrees to be personally accountable for the individual's contributions and to ensure that questions pertaining to the accuracy or integrity of any portion of the work, even one in which the author was not directly involved, are appropriately investigated and resolved.

Funding

This study was supported by the National Institutes of Health (NIH) National Heart, Lung, and Blood Institute (NHLBI) grants R01HL123782 (MI) and R01HL136666 (MI and LL). The research project is supported by cooperative agreement U01 NS041588 co-funded by the National Institute of Neurological Disorders and Stroke (NINDS) and the National Institute on Aging (NIA), National Institutes of Health, Department of Health and Human Service. JK was supported by the Intramural Research Program of National Institute of Diabetes and Digestive and Kidney Diseases (NIDDK). CW was supported in part by the National Institutes of Health and the National Cancer Institute Intramural Research Program and under contract HHSN26120080001E. NC was supported by American Heart Association Predoctoral Fellowship (AHA Award #18PRE34000021). GN was supported by R01DK127139. JH was supported by K12 HD04348. The dataset(s) used for the analyses described were obtained from Vanderbilt University Medical Center's BioVU which is supported by numerous sources: institutional funding, private agencies, and federal grants. These include the NIH-funded Shared Instrumentation Grant S10RR025141; and CTSA grants UL1TR002243, UL1TR000445, and UL1RR024975. Genomic data are also supported by investigator-led projects that include U01HG004798, R01NS032830, RC2GM092618, P50GM115305, U01HG006378, U19HL065962, R01HD074711, and additional funding sources listed at https://victr.vumc.org/biovu-funding/. Representatives from American Heart Association did not have any role in the design and conduct of the study, the collection, management, analysis, interpretation of the data, and the preparation or approval of the manuscript.

Acknowledgments

The authors thank the other investigators, the staff, and the participants of the REGARDS study for their valuable contributions. A full list of participating REGARDS investigators and institutions can be found at: https://www.uab.edu/soph/regardsstudy/.

Conflict of interest

The authors declare that the research was conducted in the absence of any commercial or financial relationships that could be construed as a potential conflict of interest.

Publisher's note

All claims expressed in this article are solely those of the authors and do not necessarily represent those of their affiliated organizations, or those of the publisher, the editors and the reviewers. Any product that may be evaluated in this article, or claim that may be made by its manufacturer, is not guaranteed or endorsed by the publisher.

Author disclaimer

The content is solely the responsibility of the authors and does not necessarily represent the official views of the NINDS or the NIA.

Supplementary material

The Supplementary Material for this article can be found online at: https://www.frontiersin.org/articles/10.3389/fmed.2022.971297/full#supplementary-material

SUPPLEMENTARY FIGURE 1
QQ plots for interaction analyses in the REGARDS study (corresponding to Figure 1 Manhattan plots). **(Left)** *APOL1* risk status determined by additive model; **(Right)** *APOL1* risk status determined by the recessive model. Models include *APOL1*, SNP, *APOL1**SNP, age, sex, and ancestry.

References

1. Tzur S, Rosset S, Shemer R, Yudkovsky G, Selig S, Tarekegn A, et al. Missense mutations in the APOL1 gene are highly associated with end stage kidney disease risk previously attributed to the MYH9 gene. *Hum Genet.* (2010) 128:345–50. doi: 10.1007/s00439-010-0861-0

2. Genovese G, Friedman DJ, Pollak MR. APOL1 variants and kidney disease in people of recent African ancestry. *Nat Rev Nephrol.* (2013) 9:240–4. doi: 10.1038/nrneph.2013.34

3. Freedman BI. APOL1 and nephropathy progression in populations of African ancestry. *Semin Nephrol.* (2013) 33:425–32. doi: 10.1016/j.semnephrol.2013.07.004

4. Kopp JB. Rethinking hypertensive kidney disease: arterionephrosclerosis as a genetic, metabolic, and inflammatory disorder. *Curr Opin Nephrol Hypertens.* (2013) 22:266–72. doi: 10.1097/MNH.0b013e3283600f8c

5. Bostrom MA, Kao WH, Li M, Abboud HE, Adler SG, Iyengar SK, et al. Genetic association and gene-gene interaction analyses in African American dialysis patients with nondiabetic nephropathy. *Am J Kidney Dis.* (2012) 59:210–21. doi: 10.1053/j.ajkd.2011.09.020

6. Divers J, Palmer ND, Lu L, Langefeld CD, Rocco MV, Hicks PJ, et al. Gene-gene interactions in APOL1-associated nephropathy. *Nephrol Dial Transplant.* (2014) 29:587–94. doi: 10.1093/ndt/gft423

7. Langefeld CD, Comeau ME, Ng MCY, Guan M, Dimitrov L, Mudgal P, et al. Genome-wide association studies suggest that APOL1-environment interactions more likely trigger kidney disease in African Americans with nondiabetic nephropathy than strong APOL1-second gene interactions. *Kidney Int.* (2018) 94:599–607. doi: 10.1016/j.kint.2018.03.017

8. Howard VJ, Cushman M, Pulley L, Gomez CR, Go RC, Prineas RJ, et al. The REasons for Geographic and Racial Differences in Stroke Study: objectives and design. *Neuroepidemiology.* (2005) 25:135–43. doi: 10.1159/000086678

9. Tanner RM, Calhoun DA, Bell EK, Bowling CB, Gutierrez OM, Irvin MR, et al. Incident ESRD and treatment-resistant hypertension: the REasons for Geographic and Racial Differences in Stroke (REGARDS) Study. *Am J Kidney Dis.* (2014) 63:781–8. doi: 10.1053/j.ajkd.2013.11.016

10. Arnett DK, Boerwinkle E, Davis BR, Eckfeldt J, Ford CE, Black H. Pharmacogenetic approaches to hypertension therapy: design and rationale for the Genetics of Hypertension Associated Treatment (GenHAT) study. *Pharmacogenomics J.* (2002) 2:309–17. doi: 10.1038/sj.tpj.6500113

11. Davis BR, Cutler JA, Gordon DJ, Furberg CD, Wright, J. T. Jr., et al. Rationale and design for the Antihypertensive and Lipid Lowering Treatment to Prevent Heart Attack Trial (ALLHAT). ALLHAT Research Group. *Am J Hypertens.* (1996) 9:342–60. doi: 10.1016/0895-7061(96)00037-4

12. Roden DM, Pulley JM, Basford MA, Bernard GR, Clayton EW, Balser JR, et al. Development of a large-scale de-identified DNA biobank to enable personalized medicine. *Clin Pharmacol Ther.* (2008) 84:362–9. doi: 10.1038/clpt.2008.89

13. Fuchsberger C, Abecasis GR, Hinds DA. minimac2: faster genotype imputation. *Bioinformatics.* (2015) 31:782–4. doi: 10.1093/bioinformatics/btu704

14. Das S, Forer L, Schönherr S, Sidore C, Locke AE, Kwong A, et al. Next-generation genotype imputation service and methods. *Nat Genet.* (2016) 48:1284–7. doi: 10.1038/ng.3656

15. Patterson N, Price AL, Reich D. Population structure and eigenanalysis. *PLoS Genet.* (2006) 2:e190. doi: 10.1371/journal.pgen.0020190

16. Price AL, Patterson NJ, Plenge RM, Weinblatt ME, Shadick NA, Reich D. Principal components analysis corrects for stratification in genome-wide association studies. *Nat Genet.* (2006) 38:904–9. doi: 10.1038/ng1847

17. Genovese G, Friedman DJ, Ross MD, Lecordier L, Uzureau P, Freedman BI, et al. Association of trypanolytic ApoL1 variants with kidney disease in African Americans. *Science.* (2010) 329:841–5. doi: 10.1126/science.1193032

18. Kopp JB, Nelson GW, Sampath K, Johnson RC, Genovese G, An P, et al. APOL1 genetic variants in focal segmental glomerulosclerosis and HIV-associated nephropathy. *J Am Soc Nephrol.* (2011) 22:2129–37. doi: 10.1681/ASN.2011040388

19. Gutierrez OM, Irvin MR, Chaudhary NS, Cushman M, Zakai NA, David VA, et al. APOL1 nephropathy risk variants and incident cardiovascular disease events in community-dwelling black adults. *Circ Genom Precis Med.* (2018) 11:e002098. doi: 10.1161/CIRCGEN.117.002098

20. Chaudhary NS, Moore JX, Zakai NA, Judd SE, Naik RP, Limou S, et al. APOL1 nephropathy risk alleles and risk of sepsis in blacks. *Clin J Am Soc Nephrol.* (2019) 14:1733–40. doi: 10.2215/CJN.04490419

21. Collins AJ, Foley RN, Gilbertson DT, Chen SC. United States Renal Data System public health surveillance of chronic kidney disease and end-stage renal disease. *Kidney Int Suppl (2011).* (2015) 5:2–7. doi: 10.1038/kisup.2015.2

22. Chang CC, Chow CC, Tellier LC, Vattikuti S, Purcell SM, Lee JJ. Second-generation PLINK: rising to the challenge of larger and richer datasets. *Gigascience.* (2015) 4:s13742-015-0047-8. doi: 10.1186/s13742-015-0047-8

23. Wang K, Li M, Hakonarson H. ANNOVAR: functional annotation of genetic variants from high-throughput sequencing data. *Nucleic Acids Res.* (2010) 38:e164. doi: 10.1093/nar/gkq603

24. Turner SD. qqman: an R package for visualizing GWAS results using QQ and manhattan plots. *BioRXiv.* (2014). doi: 10.1101/005165

25. Vannahme C, Gosling S, Paulsson M, Maurer P, Hartmann U. Characterization of SMOC-2, a modular extracellular calcium-binding protein. *Biochem J.* (2003) 373:805–14. doi: 10.1042/bj20030532

26. Rocnik EF, Liu P, Sato K, Walsh K, Vaziri C. The novel SPARC family member SMOC-2 potentiates angiogenic growth factor activity. *J Biol Chem.* (2006) 281:22855–64. doi: 10.1074/jbc.M513463200

27. Gerarduzzi C, Kumar RK, Trivedi P, Ajay AK, Iyer A, Boswell S, et al. Silencing SMOC2 ameliorates kidney fibrosis by inhibiting fibroblast to myofibroblast transformation. *JCI Insight.* (2017) 2:e90299. doi: 10.1172/jci.insight.90299

28. Xu M, Yi M, Li N. MicroRNA-17-5p restrains the dysfunction of Ang-II induced podocytes by suppressing secreted modular calcium-binding protein 2 via NF-kappaB and TGFbeta signaling. *Environ Toxicol.* (2021) 36:1402–11. doi: 10.1002/tox.23136

29. Desir GV, Peixoto AJ. Renalase in hypertension and kidney disease. *Nephrol Dial Transplant.* (2014) 29:22–8. doi: 10.1093/ndt/gft083

30. Stec A. Rs10887800 renalase gene polymorphism influences the level of circulating renalase in patients undergoing hemodialysis but not in healthy controls. *BMC Nephrol.* (2017) 18:118. doi: 10.1186/s12882-017-0543-4

31. Desir GV. Regulation of blood pressure and cardiovascular function by renalase. *Kidney Int.* (2009) 76:366–70. doi: 10.1038/ki.2009.169

32. Li LX, Fan LX, Zhou JX, Grantham JJ, Calvet JP, Sage J, et al. Lysine methyltransferase SMYD2 promotes cyst growth in autosomal dominant polycystic kidney disease. *J Clin Invest.* (2017) 127:2751–64. doi: 10.1172/JCI90921

33. Liu C, Liu L, Wang K, Li, X.-F., Ge, et al.-Y., Ma, R.-Z., et al. VHL-HIF-2α axis-induced SMYD3 upregulation drives renal cell carcinoma progression via direct trans-activation of EGFR. *Oncogene.* (2020) 39:4286–98. doi: 10.1038/s41388-020-1291-7

34. Karle SM, Uetz B, Ronner V, Glaeser L, Hildebrandt F, Fuchshuber A. Novel mutations in NPHS2 detected in both familial and sporadic steroid-resistant nephrotic syndrome. *J Am Soc Nephrol.* (2002) 13:388–93. doi: 10.1681/ASN.V132388

35. Otto EA, Hurd TW, Airik R, Chaki M, Zhou W, Stoetzel C, et al. Candidate exome capture identifies mutation of SDCCAG8 as the cause of a retinal-renal ciliopathy. *Nat Genet.* (2010) 42:840–50. doi: 10.1038/ng.662

36. Gutierrez OM, Irvin MR, Zakai NA, Naik RP, Chaudhary NS, Estrella MM, et al. APOL1 nephropathy risk alleles and mortality in African American adults: a cohort study. *Am J Kidney Dis.* (2020) 75:54–60. doi: 10.1053/j.ajkd.2019.05.027

37. Parsa A, Kao WH, Xie D, Astor BC, Li M, Hsu CY, et al. APOL1 risk variants, race, and progression of chronic kidney disease. *N Engl J Med.* (2013) 369:2183–96. doi: 10.1056/NEJMoa1310345

38. Gilbert-Diamond D, Moore JH. Analysis of gene-gene interactions. *Curr Protoc Hum Genet.* (2011) Chapter 1:Unit 1.14. doi: 10.1002/0471142905.hg0114s70

39. Ruchi R, Genovese G, Lee J, Charoonratana VT, Bernhardy AJ, Alper SL, et al. Copy number variation at the APOL1 locus. *PLoS ONE.* (2015) 10:e0125410. doi: 10.1371/journal.pone.0125410

frontiers | Frontiers in Medicine

TYPE Original Research
PUBLISHED 20 October 2022
DOI 10.3389/fmed.2022.953643

OPEN ACCESS

EDITED BY
Chunlin Gao,
Nanjing General Hospital of Nanjing Military Command, China

REVIEWED BY
Moshe Levi,
Georgetown University, United States
Jacklyn Hellwege,
Vanderbilt University Medical Center, United States
Yue Du,
ShengJing Hospital of China Medical University, China

*CORRESPONDENCE
Julia Hoefele
julia.hoefele@tum.de

†These authors have contributed equally to this work

SPECIALTY SECTION
This article was submitted to Nephrology, a section of the journal Frontiers in Medicine

RECEIVED 26 May 2022
ACCEPTED 21 September 2022
PUBLISHED 20 October 2022

CITATION
Günthner R, Knipping L, Jeruschke S, Satanoskij R, Lorenz-Depiereux B, Hemmer C, Braunisch MC, Riedhammer KM, Comić J, Tönshoff B, Tasic V, Abazi-Emini N, Nushi-Stavileci V, Buiting K, Gjorgjievski N, Momirovska A, Patzer L, Kirschstein M, Gross O, Lungu A, Weber S, Renders L, Heemann U, Meitinger T, Büscher AK and Hoefele J (2022) Renal X-inactivation in female individuals with X-linked Alport syndrome primarily determined by age.
Front. Med. 9:953643.
doi: 10.3389/fmed.2022.953643

Renal X-inactivation in female individuals with X-linked Alport syndrome primarily determined by age

Roman Günthner[1,2], Lea Knipping[3], Stefanie Jeruschke[3], Robin Satanoskij[1], Bettina Lorenz-Depiereux[4], Clara Hemmer[2], Matthias C. Braunisch[1,2], Korbinian M. Riedhammer[1,2], Jasmina Comić[1,2], Burkhard Tönshoff[5], Velibor Tasic[6], Nora Abazi-Emini[6], Valbona Nushi-Stavileci[7], Karin Buiting[8], Nikola Gjorgjievski[9], Ana Momirovska[10], Ludwig Patzer[11], Martin Kirschstein[12], Oliver Gross[13], Adrian Lungu[14], Stefanie Weber[15], Lutz Renders[1], Uwe Heemann[1], Thomas Meitinger[2], Anja K. Büscher[3†] and Julia Hoefele[2*†] on behalf of the German Pediatric Nephrology (GPN) Study Group

[1]Department of Nephrology, Klinikum rechts der Isar, Technical University of Munich, School of Medicine, Munich, Germany, [2]Institute of Human Genetics, Klinikum rechts der Isar, Technical University of Munich, School of Medicine, Munich, Germany, [3]Pediatric Nephrology, University Hospital Essen, Essen, Germany, [4]Molecular Epidemiology, Helmholtz Zentrum München, Munich, Germany, [5]Department of Pediatrics I, University Children's Hospital Heidelberg, Heidelberg, Germany, [6]University Children's Hospital, Medical Faculty of Skopje, Skopje, North Macedonia, [7]Pediatric Clinic, University Clinical Center of Kosovo, Pristina, Kosovo, [8]Institute for Human Genetics, University Hospital Essen, Essen, Germany, [9]University Hospital of Nephrology, Faculty of Medicine, University "Ss Cyril and Methodius," Skopje, North Macedonia, [10]PHI SYNLAB Skopje Laboratories, Skopje, North Macedonia, [11]Department of Pediatrics, Children's Hospital St. Elisabeth and St. Barbara, Halle (Saale), Germany, [12]Department of Pediatrics, General Hospital, Celle, Germany, [13]Clinic for Nephrology and Rheumatology, University Medical Center Göttingen, Göttingen, Germany, [14]Fundeni Clinical Institute, Pediatric Nephrology Department, Bucharest, Romania, [15]Department of Pediatrics II, University Children's Hospital, Philipps-University Marburg, Marburg, Germany

X-linked Alport syndrome (AS) caused by hemizygous disease-causing variants in *COL4A5* primarily affects males. Females with a heterozygous state show a diverse phenotypic spectrum ranging from microscopic hematuria to end-stage kidney disease (ESKD) and extrarenal manifestations. In other X-linked diseases, skewed X-inactivation leads to preferential silencing of one X-chromosome and thus can determine the phenotype in females. We aimed to show a correlation between X-inactivation in blood and urine-derived renal cells and clinical phenotype of females with a heterozygous disease-causing variant in *COL4A5* compared to healthy controls. A total of 56 females with a heterozygous disease-causing *COL4A5* variant and a mean age of 31.6 ± 18.3 SD years were included in this study. A total of 94% had hematuria, 62% proteinuria >200 mg/day, yet only 7% had decreased eGFR. Using human androgen receptor assay X-inactivation was examined in blood cells of all 56

individuals, in urine-derived cells of 27 of these individuals and in all healthy controls. X-inactivation did not correlate with age of first manifestation, proteinuria or eGFR neither in blood, nor in urine. The degree of X-inactivation showed a moderate association with age, especially in urine-derived cells of the patient cohort (*rho* = 0.403, p = 0.037). Determination of X-inactivation allelity revealed a shift of X-inactivation toward the *COL4A5* variant bearing allele. This is the first study examining X-inactivation of urine-derived cells from female individuals with AS. A correlation between phenotype and X-inactivation could not be observed suspecting other genetic modifiers shaping the phenotype in female individuals with AS. The association of X-inactivation with age in urine-derived cells suggests an escape-mechanism inactivating the *COL4A5* variant carrying allele in female individuals with AS.

KEYWORDS

Alport syndrome, X-inactivation, *COL4A5*, urine-derived cells, microscopic hematuria, proteinuria, end-stage kidney disease

Introduction

Alport syndrome (AS) is a hereditary nephropathy characterized by (microscopic) hematuria, proteinuria, chronic kidney disease potentially progressing to end-stage kidney disease (ESKD), hearing loss, and typical ocular changes (1, 2). The syndrome is caused by disease-causing [(likely) pathogenic] variants in genes encoding collagen type IV leading to an altered glomerular basement membrane (GBM). AS can be inherited in an X-linked form due to disease-causing variants in *COL4A5* or by disease-causing variants in *COL4A3* or *COL4A4* comparable with an autosomal inheritance (3–9).

Males with X-linked AS show a distinct genotype-phenotype correlation, illustrated by more severe symptoms in individuals with loss-of-function variants and less severe symptoms in individuals with missense variants or in-frame deletions. Additionally, variants located at the 5′ end have been described to present with earlier onset of ESKD and higher risk of extrarenal manifestations (10, 11).

Female individuals with heterozygous disease-causing variants in *COL4A5* have traditionally been described as healthy carriers even though the penetrance is variable both intrafamilial and interfamilial, showing a broad spectrum of clinical symptoms, varying from mild isolated microscopic hematuria to severe AS (12–15). By age 60 years, 15–30% of these female individuals develop ESKD. Furthermore, extrarenal manifestation like eye abnormalities and hearing impairment have been described and can affect up to 30% of female individuals (13). Until now, the cause for the phenotypic variability in female individuals with a heterozygous disease-causing variant in *COL4A5* is unclear. In contrast to male individuals, genotype-phenotype correlation is less-well described in females so far but severe variants (e.g., loss-of-function variants) appear to result in a more severe phenotype–similarly to affected males (13, 16).

Interindividual variability in females with a heterozygous disease-causing *COL4A5* variant might be explained by skewed, i.e., preferential X-inactivation of one X chromosome, as already discussed in the literature (12, 17, 18). X-inactivation results in transcriptional silencing of one X chromosome in females to attain gene dosage parity between XX female and XY male mammals (19). Either the maternal or the paternal X chromosome is randomly silenced through a complex cellular process resulting in a female being a mosaic of cells with either an active maternal or paternal X chromosome (17). X-inactivation has long been thought to be an irreversible occurrence. In recent years, there is increasing evidence, that in cells with rapid turnover, such as peripheral blood cells and buccal cells, skewing of X-inactivation increases with older age (20–23). However, an age-dependent mechanism in other tissues and their possible implications have not been shown yet.

So far, only insufficient molecular genetic investigations can be found focusing on X-inactivation in AS. Vetrie et al. tried to detect a correlation between the X-inactivation allelity of female carriers and the severity of their disease, but in DNA derived from peripheral blood lymphocytes no correlation was found (17). In contrast, Rheault et al. could show that X-inactivation is a major modifier of the female carrier phenotype in murine X-linked AS (24).

In this study, the relationship of X-inactivation of female individuals with a heterozygous disease-causing *COL4A5* variant with phenotypic characteristics in blood as well as urine-derived cells consisting of podocytes and tubular cells was investigated. Furthermore, these X-inactivation data were compared with those from healthy controls.

Materials and methods

Study population and design

Inclusion criteria of the study were proof of a heterozygous disease-causing *COL4A5* variant and biologically female gender. Individuals of all ages were allowed to be included in the study (age range of included individuals: 5–79 years). There were no comorbidities observed in the included individuals. Exclusion criteria were missing written informed consent and absence of above-mentioned inclusion criteria. Recruitment was primarily achieved by acquiring relatives of known male AS individuals with disease-causing *COL4A5* variants. Altogether 60 female individuals were recruited fulfilling the inclusion criteria. Four individuals had to be excluded due to indistinguishable X-inactivation analysis (see subsection X-inactivation analysis), leading to 56 available individuals from 43 unrelated families. In 49 of those individuals, a blood sample from an AS-affected relative was available needed for determining the potential skewing.

A total of 43/56 patients were recruited as part of the NephroGen cohort of the Institute of Human Genetics at the Klinikum rechts der Isar of the Technical University of Munich, and 2/56 at the Department of Pediatrics I of the University Children's Hospital in Heidelberg. The remaining 11 patients were recruited at the Department of Pediatric Nephrology of the University Hospital in Essen, Germany. The study was approved by the respective local ethics committee of each contributing center and performed in accordance to the standards of the 2013 Helsinki Declaration. All individuals or their legal guardians gave written and informed consent.

Phenotypic characteristics

Phenotypic information was gathered by studying medical records and interviews. Age of first manifestation was considered as time point of first proof of an abnormal renal phenotype (either microscopic hematuria, macroscopic hematuria or proteinuria >200 mg/day) or diagnosis of an extrarenal manifestation. When 24-h urine collection was not available, urinary protein/creatinine ratio of more than 200 mg/g creatinine was considered as proteinuria. Semi-quantitative urine dipstick measurements with the result "negative" were considered as proteinuria less than 200 mg/day. Serum creatinine values were determined by the treating physician. eGFR was calculated for individuals >14 years with CKD-EPI formula (25), for individuals ≤14 years with the "Bedside Schwartz formula" (26) considering the height and serum creatinine of the individual.

Healthy female control individuals without history of AS in their families were recruited and blood was drawn as well as spontaneous urine collected. Out of 40 healthy control individuals, five were homozygous for the AR locus and therefore not useable for the control cohort of this study. X-inactivation data of the remaining 35 female healthy controls were available for the study.

Genotype characteristics

Supplementary Table 1 displays *COL4A5* variants and the clinical phenotype of the affected individuals. Variants were adjusted to the RefSeq Sequence NM_033380.3. Frameshift, non-sense and canonical splice site variants as well as a large deletion (70 kb, exons 38–51) were considered loss-of-function variants. For statistical calculation, two variants with small in-frame deletions were grouped with missense variants (c.2048_2050delCTG, p.Pro683_Gly684delinsArg, and c.1751_1756delCAGGGC, p.Pro584_Gly585del). Additionally, they were counted as glycine-affecting variants.

The severity of variants was calculated based on a classification of variants according to their position in the transcript. Variants were not located in the signal peptide and NC2 domain. Variants were classified according to their domain and the proximity to the 5′-end. Variants in the 5′-end near collagenous domain (c.124-c.2246) were considered "severe," variants in the 3′-end near collagenous domain (c.2247-c.4386) were considered "moderate" and variants in the NC1 domain (c.4399-c.5073; 3′-end part of the protein) were considered "mild" (**Supplementary Table 2**) (10).

Blood and urine cell DNA isolation

DNA was automatically extracted from EDTA blood samples with "Chemagic DNA Blood 5 k Kit" using a Chemagen 360 (PerkinElmer, Waltham, MA, USA) according to the manufacturer's instructions.

Kidney tissue from biopsy samples is the gold standard to obtain renal-derived cells but was seldom available for analysis. Therefore, we compared X-inactivation in tissue-derived and urine-derived cells from individuals without renal disease and achieved comparable (less than 20% difference) results in 75% of individuals.

In addition, urine-derived cells were analyzed in five individuals with AS of the study cohort regarding the presence of podocytes and tubular cells. Therefore, podocytes and tubular cells were isolated from urine samples with magnetic cell separation using the "CD10 Microbead Kit human" (Miltenyi Biotec B.V. & Co.KG, Bergisch Gladbach, Germany). Subsequent FACS analysis confirmed the enrichment of CD10 positive cells. DNA was then extracted from these cells with Qiagen's "DNeasy Blood and Tissue Kit 250" (Qiagen GmbH, Hilden, Germany).

The expression of CD10 in podocytes and tubular cells has been demonstrated in immunohistochemical stainings (**Supplementary Figure 1**). In 80% of analyses both cell types were detected within the urinary sediment. For these analyses

first morning urine was collected and urine samples were immediately centrifuged for 10 min at 14,000 rpm at 4°C. Afterward the supernatant was discarded and urine cells were isolated right away or immediately frozen and stored at −80°C (for DNA isolation).

X-inactivation analysis

The X-inactivation status was measured by assessing the DNA methylation based on the difference between the number of trinucleotide repeats at the human androgen receptor locus (*AR*, Xq11-12; HUMARA-Assay) (21).

Due to the correlation of X-inactivation with hypermethylation, digestion with methylation sensitive restriction enzymes (*Hpall*) can differentiate between active and inactive alleles. A male sample was enclosed in each assay in order to control sufficient *Hpall* digestion. Subsequent to digestion and amplification of the samples with fluorescence-tagged PCR primers, fragment length analysis of the PCR products was run on an ABI 3130XL genetic analyzer and the GeneMarker software (Softgenetics, PA, USA). If amplified DNA fragments exhibited the same size on both alleles, X-inactivation could not be determined.

X-inactivation data was generated and is displayed in two different ways depending on the availability of an affected male relative. In a first step, skewness of X-inactivation was measured with the ratio of inactivation between the two alleles without knowledge which of the alleles carried the *COL4A5* variant (e.g., 80:20 or 72:28). These data are referred to as "X-inactivation without allelity" and are displayed in a range from theoretically 50% (not skewed, both alleles with same X-inactivation percentage) to 100% (completely skewed).

In families with an available affected male, segregation analysis of the male individual (0% X-inactivation, *COL4A5* variant bearing allele not inactivated at all) allowed determining which of the two alleles in a female individual with a heterozygous disease-causing variant was the one bearing the *COL4A5* variant (27). Thus X-inactivation data could be displayed in a range from theoretically 0% (*COL4A5* variant bearing allele not inactivated at all) to 100% (*COL4A5* variant bearing allele completely inactivated). This dataset is referred to as "X-inactivation with allelity."

Statistical analysis

Parametric data are presented as mean ± standard deviation and non-parametric data as median [Interquartile range, IQR]. For correlation analyses Spearman's rho was calculated (**Figures 2**, **3** and **Table 1**). When comparing two groups (**Table 2** and **Supplementary Table 3**) we used Mann–Whitney *U*-test for non-parametric variables, Student's *t*-test for parametric variables and Chi square test for categorical variables. For comparison of more than 2 groups Kruskal–Wallis test was applied due to the non-normal distribution of the dependent parameters (**Supplementary Table 2**). SPSS® Statistics, version 26 (IBM, Armonk, NY, USA), was used for all statistical tests.

Results

Demographics and phenotype/genotype of individuals

In total, 56 resp. 27 female individuals with a disease-causing variant in *COL4A5* with X-inactivation data in peripheral blood cells resp. in urine-derived cells were available for analysis (**Figure 1**). In 49 of the 56 blood X-inactivation datasets, the *COL4A5*-dependent allelity of X-inactivation was revealed by analyzing affected male relatives. For the urine-derived samples, *COL4A5*-dependent X-inactivation allelity could be determined in 26 out of 27 samples (**Figure 1**).

The mean age of the included individuals was 31.6 ± 18.3 years (mean ± SD; **Table 3**). Almost every female individual with a heterozygous disease-causing *COL4A5* variant had a renal manifestation (94.6%) with first symptoms/abnormal urine analysis detected at a median age of 9.5 [IQR 5.3; 19.7] years. Most common manifestation was hematuria (93.7%; microscopic or macroscopic) followed by proteinuria >200 mg/day (62.3%), whereas mean eGFR was normal. Four of the 56 individuals progressed to ESKD with a mean age of onset at 32.8 ± 5.3 years (mean ± SD). Extrarenal manifestation defined as hearing impairment (5.4%) or ocular manifestation (7.1%) were detected only in a few individuals.

Loss-of-function variants were present in 42.9% of cases, mostly represented by frameshift and canonical splice site variants (**Table 3**). Individuals with missense variants had primarily glycine-variants except for 3 out of 32 individuals. Most variants were located in the collagenous domain of the *COL4A5* gene (87.5%).

Comparing the total cohort of 56 individuals with the 27 individuals with additional urine samples, the subcohort of individuals with X-inactivation data from urine-derived cells were slightly older, had less proteinuria, slightly decreased eGFR and did not include individuals with ESKD due to loss of remaining urine excretion or history of kidney transplantation (**Table 3**).

Healthy controls (n = 35) had no history of AS in the family, were all female and had a mean age of 37.1 ± 19.1 years (mean ± SD).

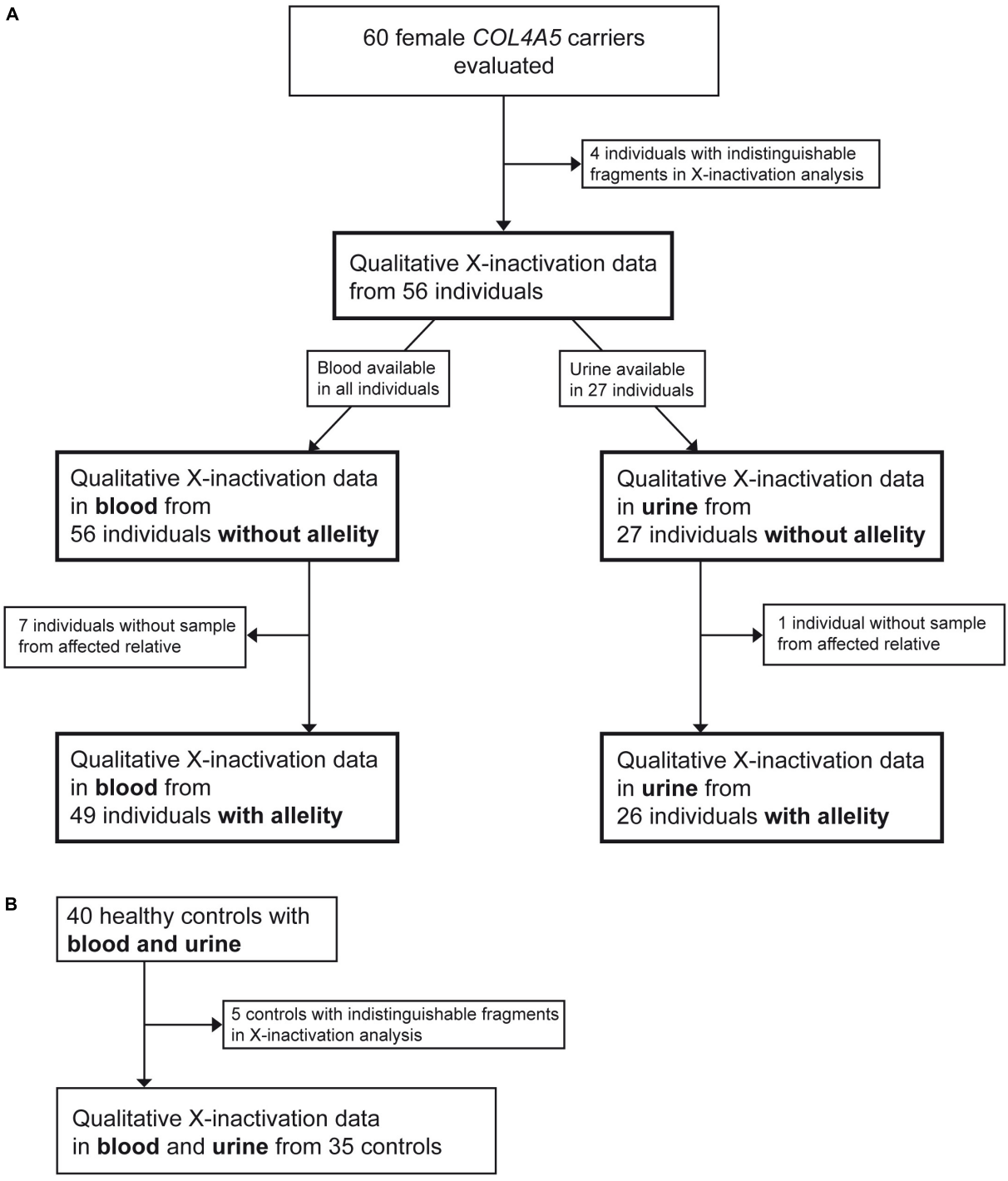

FIGURE 1
Flowchart illustrating the recruitment process of participants. Figure shows recruitment procedure for individuals with a heterozygous disease-causing *COL4A5* variant **(A)** and healthy controls **(B)**.

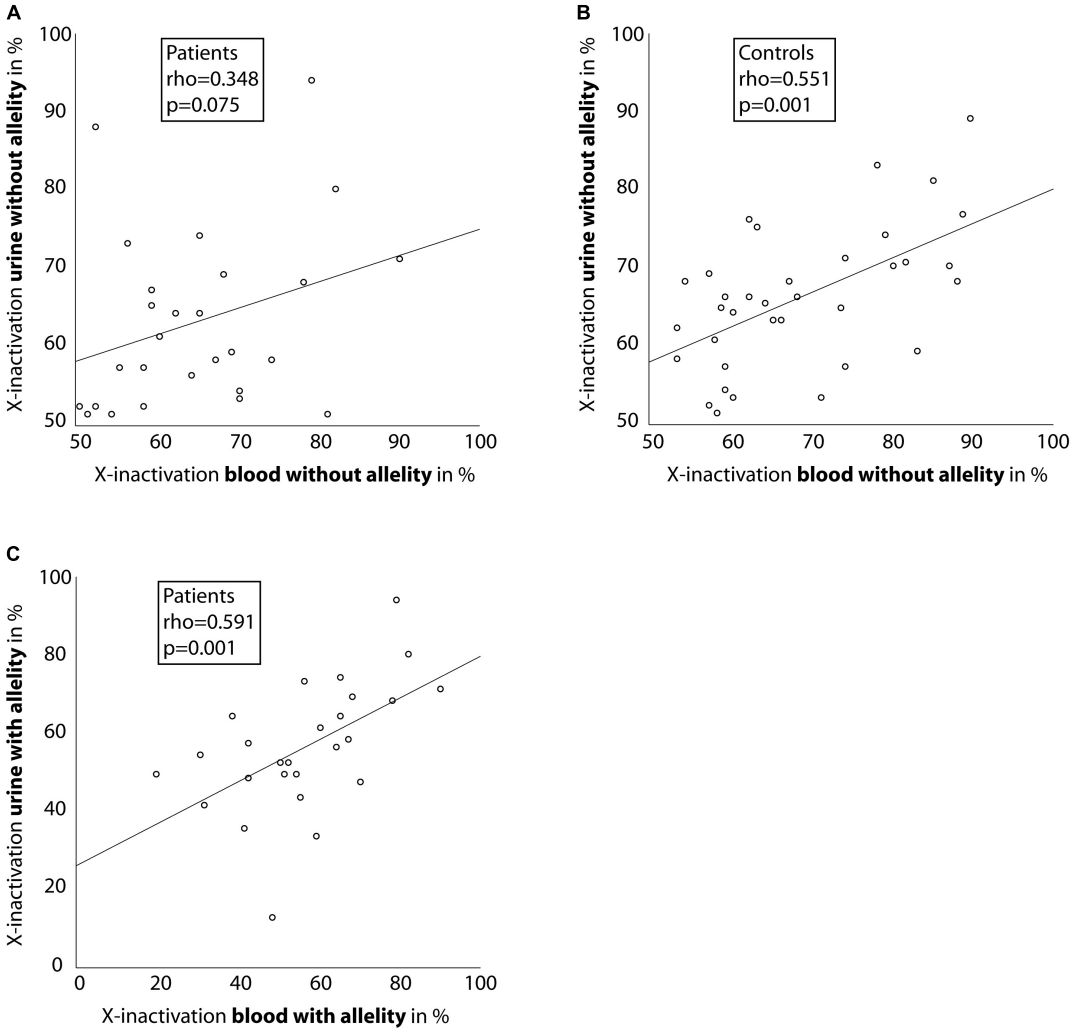

FIGURE 2
Correlation between X-inactivation in blood and urine cells. Scatter-dot plots of the relationship of X-inactivation between blood and urine cells for individuals with a heterozygous disease-causing *COL4A5* variant **(A,C)** and healthy controls **(B)**. Spearman's rho was calculated and is displayed in the boxes. Linear regression lines were plotted for illustration purposes.

Age of first manifestation in females with a disease-causing *COL4A5* variant depends on variant type

Median age of first manifestation was significantly lower in individuals with loss-of-function variants compared to individuals with missense variants (Table 2) (6.6 vs. 12.4 years, p = 0.011). Individuals with ocular manifestations or hearing impairment predominately carried loss-of-function variants.

After classification of variants according to their expected severity (10), most variants were located in the collagenous domain, which can be divided in the more severe 5′-end near part and the less severe 3′-end near part (**Supplementary Table 2**). Individuals with variants near the 5′-end showed earlier first manifestation, higher percentage of proteinuria >200 mg/day, ocular manifestation and ESKD, yet without significance. The variants of the four individuals who progressed to ESKD were three missense and one splice site variant.

X-inactivation shows strong association between blood and urine-derived cells

Median X-inactivation of cases without considering allelity was 65% [IQR 58; 72] in blood cells and 59% [IQR 53; 69] in urine-derived cells (data not shown). Analysis of *COL4A5*-dependent X-inactivation of blood and urine samples showed a tendency toward inactivation of the variant bearing allele (55% and 56%). For the controls, the degree of X-inactivation

amounted to median 65% [IQR 59; 79] for blood cells and 66% [IQR 59; 70] for urine-derived cells.

X-inactivation measured without allelity showed a medium to strong association between blood and urine-derived cells in affected female individuals and healthy controls (*rho* = 0.348, $p = 0.075$ and *rho* = 0.551, $p = 0.001$; **Figures 2A,B**), however the association was not significant in affected individuals. Regarding the *COL4A5*-dependent X-inactivation allelity, the association between blood and urine-derived cells was even higher (*rho* = 0.591, $p = 0.001$; **Figure 2C**).

Age determines X-inactivation of female individuals with disease-causing *COL4A5* variants especially in urinary cells

Correlating age with X-inactivation (without allelity) in urine-derived cells of the affected individuals, a significant association with a Spearman's rho of 0.403 ($p = 0.037$, **Figure 3A**) was seen. Considering X-inactivation with *COL4A5*-dependent allelity, the association with age was similar (*rho* = 0.348, **Supplementary Figure 2A**), however not significant. In comparison, X-inactivation in blood cells of affected individuals showed weak, non-significant correlations with age, with or without considering the *COL4A5*-dependent allelity (**Figure 3B** and **Supplementary Figure 2B**).

Comparing the individuals to healthy controls, the latter showed only a weak association of X-inactivation with age for both, blood and urinary cells (**Figures 3C,D**; *rho* = 0.237; $p = 0.171$, and *rho* = 0.281; $p = 0.101$; **Supplementary Figure 3**).

Phenotype and X-inactivation in female individuals with heterozygous variants causing X-linked Alport syndrome

Correlation analyses of phenotypic characteristics and X-inactivation could not demonstrate a significant association for age of first manifestation, eGFR or proteinuria (**Table 1**). There was a trend toward decreased eGFR with enhanced X-inactivation, however eGFR and age naturally showed a strong dependency in our cohort (*rho* = −0.547, $p < 0.001$; data not shown).

Further analysis of blood of individuals with ESKD ($n = 4$) revealed increased X-inactivation without allelity (77% in ESKD vs. 64% in non-ESKD) as well as increased X-inactivation with *COL4A5*-dependent allelity (72% in ESKD vs. 55% in non-ESKD, **Supplementary Table 3**).

Individuals with ocular manifestation or hearing impairment showed increased X-inactivation in urine-derived cells. X-inactivation with and without allelity was 71% in individuals with ocular manifestations vs. 53–58% in individuals without ocular manifestations. Regarding hearing impairment, the results were similar (69–73% in individuals affected by hearing impairment vs. 54–58% without hearing impairment; **Supplementary Table 3**). However, blood cells did not show differences in X-inactivation when comparing individuals with and without extrarenal manifestations. Of the 5 individuals presenting with extrarenal manifestations, everyone had normal eGFR, but four individuals exhibited proteinuria >200 mg/day with one individual presenting with proteinuria of 1.42 g/day. However, statistical analysis was not possible due to the small number of individuals with ESKD or extrarenal manifestations.

Discussion

This is the first study investigating X-inactivation in urine-derived cells of female individuals with X-linked AS. Additionally, the *COL4A5*-dependent allelity of X-inactivation depending on the *COL4A5* variant bearing allele was included in the analysis as a novelty in a human AS cohort.

Unlike the hypothesis, X-inactivation was not relevantly associated with phenotypic characteristics like age of first manifestation, proteinuria or decreased eGFR. However, we were able to demonstrate a statistically significant correlation of age with skewed X-inactivation in urine-derived cells of female individuals with AS. This correlation was also found in peripheral blood cells of the individuals as well as in urine-derived and blood cells of the healthy controls, yet only in a weak, not statistically significant fashion.

The variability of X-inactivation and its association with age has been proven in cross-sectional and recently in longitudinal studies enrolling healthy controls (22, 28, 29). The mechanisms for this association are unclear, but intrinsic as well as environmental influences have been suggested (28). So far, correlation of X-inactivation with age has only been demonstrated for rapidly proliferating tissues like blood granulocytes or buccal epithelium (21, 23). A recent study including over 300 healthy females could not show an age-dependent effect in slowly proliferating cells like fat or skin tissue, but it did show an effect in lymphocyte-derived cells (22). The only study investigating cells isolated from urine of approximately 40 healthy controls was not able to show an age-dependent effect of X-inactivation (21). Our results in healthy controls show only a weak, non-significant correlation of age with X-inactivation in urine-derived cells, which underlines the observation for slowly proliferating cells in the existing literature.

In contrast, urine-derived cells from our individuals with AS exhibited a moderate and statistically significant correlation of age with X-inactivation. Older individuals with AS were also more likely to present with increased X-inactivation of the variant allele (*rho* = 0.348, $p = 0.076$) and the

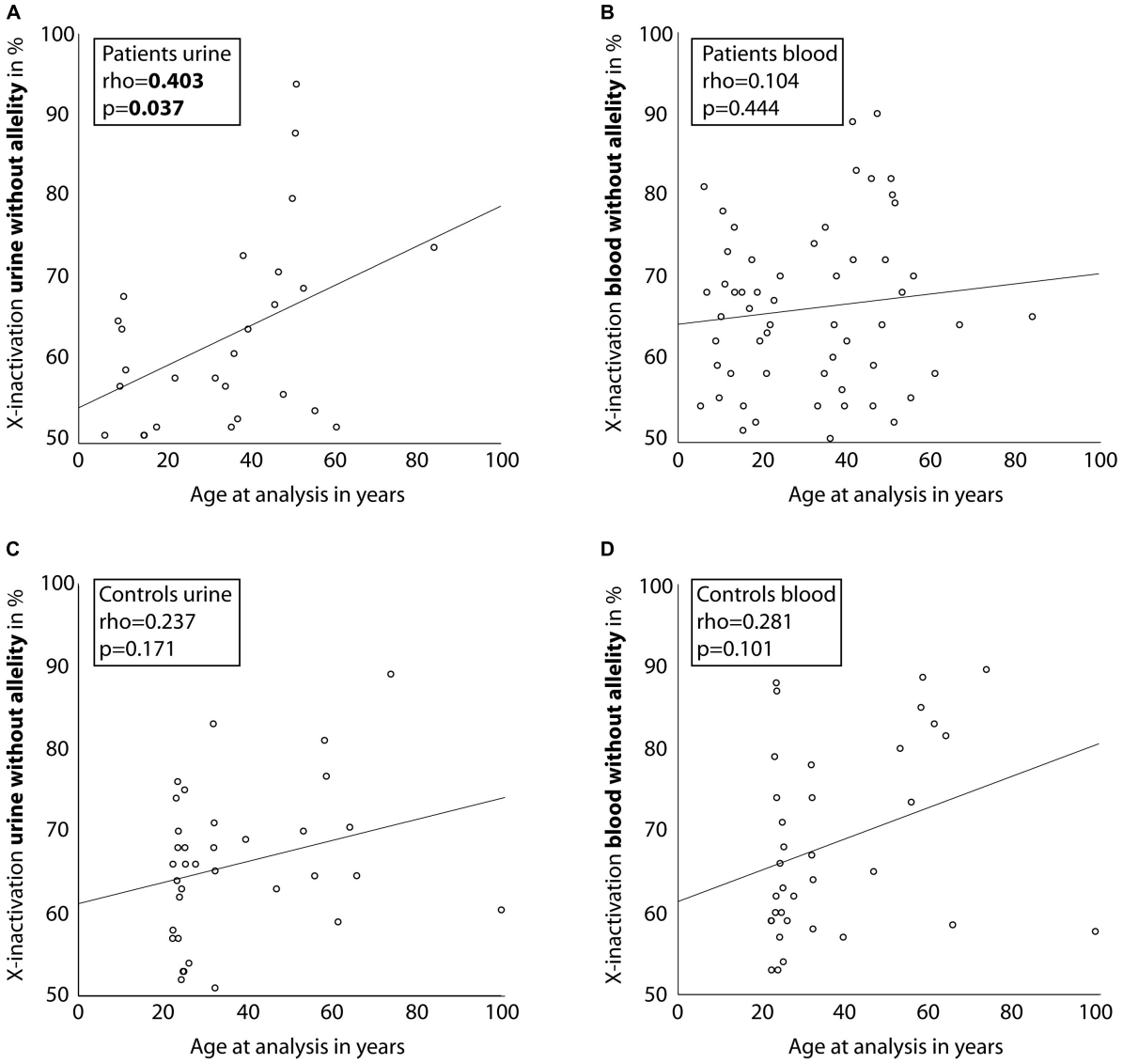

FIGURE 3
Correlation between age of individuals and X-inactivation in blood and urine cells. Scatter-dot plots of the association of participant age and X-inactivation in blood and urine cells for individuals with a heterozygous disease-causing *COL4A5* variant **(A,B)** and healthy controls **(C,D)**. Spearman's rho was calculated and is displayed in the boxes. Linear regression lines were plotted for illustration purposes.

degree of X-inactivation of the disease-causing allele amounted to 55% in blood cells and 56% in urine-derived cells. This suggests that X-inactivation could serve as an escape-mechanism protecting individuals from the development of severe complications of AS as they get older. Involvement of X-inactivation has been described for heterozygous carriers in X-linked diseases like severe combined immunodeficiency (30) and X-linked intellectual disability (31). In these individuals the allelity of X-inactivation also led to a more inactive disease variant bearing allele in heterozygous carriers. Thus, the gene dosage is adjusted in favor of the wild-type allele by silencing the mutant allele. The proposed mechanism for this phenomenon is a survival selection of cells which have inactive disease-causing alleles. Even though the data might suggest that this is also the case in individuals with a heterozygous disease-causing variant in *COL4A5*, the size of the present study cohort is not sufficient to definitely draw this conclusion. Further studies including more individuals with a severe phenotype would be needed to elucidate these mechanisms.

Regarding the relationship between the tissues, the data showed a moderate to high and significant correlation between X-inactivation in blood and urine-derived cells (*rho* = 0.551, p = 0.001 for controls; and *rho* = 0.591, p = 0.001 for cases

TABLE 1 Correlation coefficients of X-inactivation in blood and urine with phenotypic markers in female individuals with a heterozygous variant in *COL4A5*.

		X-inactivation urine without allelity	X-inactivation urine with allelity	X-inactivation blood without allelity	X-inactivation blood with allelity
Age at analysis	*rho*	**0.403**	0.348	0.104	0.202
	p-value	**0.037**	0.076	0.444	0.165
	n	27	27	56	56
Age of first manifestation	*rho*	0.139	0.137	−0.084	0.051
	p-value	0.507	0.513	0.548	0.737
	n	25	25	53	46
eGFR	*rho*	−0.032	−0.110	−0.298	−0.043
	p-value	0.895	0.655	0.056	0.797
	n	19	19	42	38
Proteinuria >200 mg/day	*rho*	−0.213	−0.017	0.103	0.192
	p-value	0.307	0.937	0.462	0.19
	n	25	25	53	48

X-inactivation without allelity: The ratio of inactivation was measured between the two alleles without knowledge which of the alleles carried the *COL4A5* variant. X-inactivation with allelity: The ratio of inactivation was measured between the two alleles with knowledge which of the alleles carried the *COL4A5* variant. Bold values indicate p-value < 0.05.

TABLE 2 Phenotypic characteristics and type of variant.

***COL4A5* variants**	**Loss-of-function (*n* = 24)**	**Missense (*n* = 32)**	***P*-value**
Any manifestation, in %	95.8% (23/24)	93.8% (30/32)	0.732
Age of first manifestation, years, median [IQR]	6.6 [3.9; 10.8]	12.4 [6.5; 27.8]	**0.011**
Proteinuria >200 mg/day[§], in %	65.2% (15/23)	60.0% (18/30)	0.698
eGFR, ml/min/1.73 m^2, mean ± SD[§]	103 ± 24	101 ± 29	0.775
End-stage kidney disease, in %	4.2% (1/24)	9.4% (3/32)	0.454
Ocular manifestation[§§], in %	12.5% (3/24)	3.1% (1/32)	0.178
Hearing impairment[§§], in %	8.3% (2/24)	3.1% (1/32)	0.392

[§]Differing patient numbers: eGFR (n = 42), proteinuria (n = 53). [§§]Affected individuals were examined by a specialized ophthalmologist and otologist. Bold values indicate p-value < 0.05.

considering *COL4A5*-dependent X-inactivation allelity). These associations were stronger than described in the literature for cells from other slowly proliferating tissues (like fat and skin) (22). As blood cells are known to have the highest degrees of X-inactivation skewness in healthy subjects compared to other tissues (22, 23), urine cells should be considered when analyzing X-inactivation in certain cases.

Nonetheless, the hypothesized X-inactivation-phenotype relationship could not be shown in blood or urine-derived cells. This is in line with the previous observation in 30 female individuals with a heterozygous disease-causing variant in *COL4A5* in blood cells only (17). Murine data, however, point to a role for X-inactivation in phenotype development in an AS mouse model (24). X-inactivation of the mutant allele was correlated with less proteinuria and plasma urea nitrogen, demonstrated in cells from whole murine kidneys. Yet one has to keep in mind that X-inactivation is measured differently in mice, and the effect of age, which evidently plays an important role in human X-inactivation, is not accounted for. Additionally, a standardized inbred murine model cannot be compared with humans, especially as more evidence emerges demonstrating a role for other genetic modifiers influencing the phenotype like *FMN1*, which has been described to be associated with albuminuria in *COL4A5*-deficient mice (32). In general, the genotype-phenotype correlation in female individuals with a heterozygous disease-causing *COL4A5* variant is weak compared to descriptions in male individuals with AS (16). A slight, but significant difference in age of first manifestation between loss-of-function and missense variants could be seen, however, no difference regarding renal parameters relevant for prognosis were found (proteinuria, eGFR). As X-inactivation does not seem to play a big role in female individuals with AS apart from age, other genetic modifiers like disease-causing variants or single nucleotide polymorphisms in other genes like autosomal *COL4A3*, *COL4A4* or recently described *FMN1*

TABLE 3 Phenotype and genotype of individuals for total and urine-analysis containing cohort.

Demographics and phenotype	Total cohort (n = 56)	Urine analysis available (n = 27)
Age at analysis, years, mean ± SD	31.6 ± 18.3	34.7 ± 19.9
Any manifestation, in %	94.6% (53/56)	926% (25/27)
First manifestation, age in years, median [IQR]	9.5 [5.3; 19.7]	10.0 [5.5; 18.1]
Hematuria, in %	93.7% (52/56)	92.6% (25/27)
Microscopic hematuria, in %	82.1% (46/56)	85.2% (23/27)
Macroscopic hematuria, in %	10.7% (6/56)	7.4% (2/27)
Proteinuria >200 mg/day, in %	62.3 (33/53)	56.0% (14/25)
Proteinuria quantified per day, median [IQR][§]	0.34 [0.17; 0.80]	0.29 [0.13; 0.49]
eGFR, ml/min/1.73 m^2, mean ± SD[§]	101.7 ± 26.9	89 ± 27
End-stage kidney disease, in %	7.1% (4/56)	0%
Age of onset ESKD, years, mean ± SD	32.8 ± 5.3	–
Renal transplant, in %	1.8% (1/56)	–
Hearing impairment, in %	5.4% (3/56)	11.1% (3/27)
Ocular manifestation, in %	7.1% (4/56)	7.4% (2/27)
Genotype		
LoF variant, in %	42.9% (24/56)	51.9% (14/27)
Frameshift, in %	21.4% (12/56)	29.6% (8/27)
Nonsense, in %	3.6% (2/56)	7.4% (2/27)
Exon-spanning deletion, in %	3.6% (2/56)	–
Splice, in %	14.3% (8/56)	14.8% (4/27)
Missense variant[§§], in %	57.1% (32/56)	48.1% (13/27)
Glycine, in %	51.8% (29/56)	40.7% (11/27)
Non-glycine, in %	5.4% (3/56)	7.4% (2/27)
Severity of variant (Bekheirnia et al.)		
5′-end, in %	3.6% (2/56)	3.7% (1/27)
Collagenous, in %	87.5% (49/56)	77.8% (21/27)
3′-end, in %	8.9% (5/56)	18.5% (5/27)

[§]Differing individual numbers. Urine cohort: eGFR (n = 19), proteinuria quantified (n = 11); blood cohort: eGFR (n = 42), proteinuria quantified (n = 38). [§§]Includes two in-frame indel mutations. LoF; loss-of-function; ESKD; end-stage kidney disease.

become increasingly important and future studies should be dedicated to these (32).

One limitation of the present study is the relatively young age of included individuals (31.6 years), which also led to decreased numbers of individuals with ESKD and extrarenal manifestations. This bias is based on the recruitment process, which mostly included sisters or mothers of pediatric patients. The degree of skewness in blood cells evidently accelerates above the age of 60 years (22). Thus, associations of X-inactivation with phenotypic characteristics could have been detected with an older study population. Additionally, our study population primarily included individuals of Caucasian descent and therefore the results might not be applicable for all ethnicities. Another limitation of the study applies to the method of X-inactivation measurement. Indistinguishable PCR fragments due to same-sized trinucleotide repeats can make an analysis impossible as it was the case in nine participants of this study. Moreover, collection of urine-derived cells in individuals with ESKD is difficult due to loss of urine production or kidney transplantation, which often excludes severely affected individuals from X-inactivation analysis of urine-derived cells. Renal cell isolation and transportation (dry ice) is also more complex than drawing EDTA-blood resulting in a markedly reduced number of urine X-inactivation data.

In conclusion, our data show an association of X-inactivation and age in urine-derived cells of female individuals with AS, which could present an escape-mechanism to avoid expression of the *COL4A5* variant as individuals get older. A relationship between X-inactivation and phenotypic characteristics was not present in blood as well as urine cells. Future studies about X-inactivation in female individuals should focus on older cohorts.

Data availability statement

The datasets presented in this study can be found in online repositories. The names of the repository/repositories

and accession number(s) can be found in the article/**Supplementary material**.

Ethics statement

This study was approved by the respective local ethics committee of each contributing center. Written informed consent to participate in this study was provided by the participants' legal guardian/next of kin. Written informed consent was obtained from the individual(s), and minor(s)' legal guardian/next of kin, for the publication of any potentially identifiable images or data included in this article.

Author contributions

RG, LK, SJ, BL-D, CH, KR, JC, and KB performed the analysis. RS, MB, BT, VT, NA-E, VN-S, NG, AM, LP, MK, OG, AL, SW, LR, UH, TM, and AB cared for the patients and acquired and provided the clinical data. RG, AB, and JH were responsible for writing and revision of the manuscript. All authors contributed to the article and approved the submitted version.

Funding

This study was supported by the German Pediatric Nephrology Association and the Technical University of Munich (TUM) in the framework of the Open Access Publishing Program.

Acknowledgments

We thank the individuals and their families for participation in this study. Especially, we also thank "Alport Selbsthilfegruppe e.V.," a non-profit organization consisting of many Alport syndrome patients.

Conflict of interest

The authors declare that the research was conducted in the absence of any commercial or financial relationships that could be construed as a potential conflict of interest.

Publisher's note

Supplementary material

The Supplementary Material for this article can be found online at: https://www.frontiersin.org/articles/10.3389/fmed.2022.953643/full#supplementary-material

References

1. Gross O, Netzer KO, Lambrecht R, Seibold S, Weber M. Meta-analysis of genotype-phenotype correlation in X-linked Alport syndrome: impact on clinical counselling. *Nephrol Dial Transplant.* (2002) 17:1218–27. doi: 10.1093/ndt/17.7.1218

2. Williamson DA. Alport's syndrome of hereditary nephritis with deafness. *Lancet.* (1961) 2:1321–3. doi: 10.1016/S0140-6736(61)90899-6

3. Weber S, Strasser K, Rath S, Kittke A, Beicht S, Alberer M, et al. Identification of 47 novel mutations in patients with Alport syndrome and thin basement membrane nephropathy. *Pediatr Nephrol.* (2016) 31:941–55. doi: 10.1007/s00467-015-3302-4

4. Funk SD, Lin MH, Miner JH. Alport syndrome and Pierson syndrome: diseases of the glomerular basement membrane. *Matrix Biol.* (2018) 7:250–61. doi: 10.1016/j.matbio.2018.04.008

5. Abou Tayoun AN, Pesaran T, DiStefano MT, Oza A, Rehm HL, Biesecker LG, et al. Recommendations for interpreting the loss of function PVS1 ACMG/AMP variant criterion. *Hum Mutat.* (2018) 39:1517–24. doi: 10.1002/humu.23626

6. Kearney HM, Thorland EC, Brown KK, Quintero-Rivera F, South ST, Working Group of the American College of Medical Genetics Laboratory Quality Assurance Committee. American college of medical genetics standards and guidelines for interpretation and reporting of postnatal constitutional copy number variants. *Genet Med.* (2011) 13:680–5. doi: 10.1097/GIM.0b013e3182217a3a

7. Richards S, Aziz N, Bale S, Bick D, Das S, Gastier-Foster J, et al. Standards and guidelines for the interpretation of sequence variants: a joint consensus recommendation of the American college of medical genetics and genomics and the association for molecular pathology. *Genet Med.* (2015) 17:405–24. doi: 10.1038/gim.2015.30

8. Ellard, S, Baple EL, Berry I, Forrester N, Turnbull C, Owens M, et al. *ACGS Best Practice Guidelines for Variant Classification 2019.* (2019). Available online at: https://www.acgs.uk.com/media/11631/uk-practice-guidelines-for-variant-classification-v4-01-2020.pdf (accessed May 25, 2022).

9. Gibson J, Fieldhouse R, Chan MMY, Sadeghi-Alavijeh O, Burnett L, Izzi V, et al. Prevalence estimates of predicted pathogenic COL4A3-COL4A5 variants in a population sequencing database and their implications for Alport syndrome. *J Am Soc Nephrol.* (2021) 32:2273–90. doi: 10.1681/ASN.2020071065

10. Bekheirnia MR, Reed B, Gregory MC, McFann K, Shamshirsaz AA, Masoumi A, et al. Genotype-phenotype correlation in X-linked Alport syndrome. *J Am Soc Nephrol.* (2010) 21:876–83. doi: 10.1681/ASN.2009070784

11. Jais JP, Knebelmann B, Giatras I, Marchi M, Rizzoni G, Renieri A, et al. X-linked Alport syndrome: natural history in 195 families and genotype- phenotype correlations in males. *J Am Soc Nephrol.* (2000) 11:649–57. doi: 10.1681/ASN.V114649

12. Rheault MN. Women and Alport syndrome. *Pediatr Nephrol.* (2012) 27:41–6. doi: 10.1007/s00467-011-1836-7

13. Savige J, Colville D, Rheault M, Gear S, Lennon R, Lagas S, et al. Alport syndrome in women and girls. *Clin J Am Soc Nephrol.* (2016) 11:1713–20. doi: 10.2215/CJN.00580116

14. Yamamura T, Nozu K, Fu XJ, Nozu Y, Ye MJ, Shono A, et al. Natural history and genotype-phenotype correlation in female X-linked Alport syndrome. *Kidney Int Rep.* (2017) 2:850–5. doi: 10.1016/j.ekir.2017.04.011

15. Kashtan CE, Ding J, Garosi G, Heidet L, Massella L, Nakanishi K, et al. Alport syndrome: a unified classification of genetic disorders of collagen IV alpha345: a position paper of the Alport syndrome classification working group. *Kidney Int.* (2018) 93:1045–51. doi: 10.1016/j.kint.2017.12.018

16. Jais JP, Knebelmann B, Giatras I, De Marchi M, Rizzoni G, Renieri A, et al. X-linked Alport syndrome: natural history and genotype-phenotype correlations in girls and women belonging to 195 families: a "European community Alport syndrome concerted action" study. *J Am Soc Nephrol.* (2003) 14:2603–10. doi: 10.1097/01.ASN.0000090034.71205.74

17. Vetrie D, Flinter F, Bobrow M, Harris A. X inactivation patterns in females with Alport's syndrome: a means of selecting against a deleterious gene? *J Med Genet.* (1992) 29:663–6. doi: 10.1136/jmg.29.9.663

18. Shimizu Y, Nagata M, Usui J, Hirayama K, Yoh K, Yamagata K, et al. Tissue-specific distribution of an alternatively spliced COL4A5 isoform and non-random X chromosome inactivation reflect phenotypic variation in heterozygous X-linked Alport syndrome. *Nephrol Dial Transplant.* (2006) 21:1582–7. doi: 10.1093/ndt/gfl051

19. Deakin JE, Chaumeil J, Hore TA, Marshall Graves JA. Unravelling the evolutionary origins of X chromosome inactivation in mammals: insights from marsupials and monotremes. *Chromosome.* (2009) 17:671–85. doi: 10.1007/s10577-009-9058-6

20. Bolduc V, Chagnon P, Provost S, Dubé MP, Belisle C, Gingras M, et al. No evidence that skewing of X chromosome inactivation patterns is transmitted to offspring in humans. *J Clin Invest.* (2008) 118:333–41. doi: 10.1172/JCI33166

21. Sharp A, Robinson D, Jacobs P. Age- and tissue-specific variation of X chromosome inactivation ratios in normal women. *Hum Genet.* (2000) 107:343–9. doi: 10.1007/s004390000382

22. Zito A, Davies MN, Tsai PC, Roberts S, Andres-Ejarque R, Nardone S, et al. Heritability of skewed X-inactivation in female twins is tissue-specific and associated with age. *Nat Commun.* (2019) 10:5339. doi: 10.1038/s41467-019-13340-w

23. Knudsen GP, Pedersen J, Klingenberg O, Lygren I, Orstavik KH. Increased skewing of X chromosome inactivation with age in both blood and buccal cells. *Cytogenet Genome Res.* (2007) 116:24–8. doi: 10.1159/000097414

24. Rheault MN, Kren SM, Hartich LA, Wall M, Thomas W, Mesa HA, et al. X-inactivation modifies disease severity in female carriers of murine X-linked Alport syndrome. *Nephrol Dial Transplant.* (2010) 25:764–9. doi: 10.1093/ndt/gfp551

25. Levey AS, Stevens LA, Schmid CH, Zhang YL, Castro AF III, Feldman HI, et al. A new equation to estimate glomerular filtration rate. *Ann Intern Med.* (2009) 150:604–12. doi: 10.7326/0003-4819-150-9-200905050-00006

26. Schwartz GJ, Muñoz A, Schneider MF, Mak RH, Kaskel F, Warady BA, et al. New equations to estimate GFR in children with CKD. *J Am Soc Nephrol.* (2009) 20:629–37. doi: 10.1681/ASN.2008030287

27. Archer H, Evans J, Leonard H, Colvin L, Ravine D, Christodoulou J, et al. Correlation between clinical severity in patients with Rett syndrome with a p.R168X or p.T158M MECP2 mutation, and the direction and degree of skewing of X-chromosome inactivation. *J Med Genet.* (2007) 44:148–52. doi: 10.1136/jmg.2006.045260

28. Mengel-From J, Lindahl-Jacobsen R, Nygaard M, Soerensen M, Ørstavik KH, Hertz JM, et al. Skewness of X-chromosome inactivation increases with age and varies across birth cohorts in elderly Danish women. *Sci Rep.* (2021) 11:4326. doi: 10.1038/s41598-021-83702-2

29. Hatakeyama C, Anderson CL, Beever CL, Penaherrera MS, Brown CJ, Robinson WP. The dynamics of X-inactivation skewing as women age. *Clin Genet.* (2004) 66:327–32. doi: 10.1111/j.1399-0004.2004.00310.x

30. Puck JM, Nussbaum RL, Conley ME. Carrier detection in X-linked severe combined immunodeficiency based on patterns of X chromosome inactivation. *J Clin Invest.* (1987) 79:1395–400. doi: 10.1172/JCI112967

31. Plenge RM, Stevenson RA, Lubs HA, Schwartz CE, Willard HF. Skewed X-chromosome inactivation is a common feature of X-linked mental retardation disorders. *Am J Hum Genet.* (2002) 71:168–73. doi: 10.1086/341123

32. Takemon Y, Wright V, Davenport B, Gatti DM, Sheehan SM, Letson K, et al. Uncovering modifier genes of X-linked Alport syndrome using a novel multiparent mouse model. *J Am Soc Nephrol.* (2021) 32:1961–73. doi: 10.1681/ASN.2020060777

Frontiers in Medicine

Translating medical research and innovation into improved patient care

A multidisciplinary journal which advances our medical knowledge. It supports the translation of scientific advances into new therapies and diagnostic tools that will improve patient care.

Discover the latest Research Topics

See more →

Frontiers

Avenue du Tribunal-Fédéral 34
1005 Lausanne, Switzerland
frontiersin.org

Contact us

+41 (0)21 510 17 00
frontiersin.org/about/contact